Dissertation zur Erlangung des Doktorgrades
der Fakultät für Chemie und Pharmazie
der Ludwig-Maximilians-Universität München

Hemithioindigos for cellular tubulin photopharmacology: From proof of concept to near-quantitatively photoswitchable tools with single-cell precision

Alexander Sailer
aus
Forchheim, Deutschland

2022

Erklärung

Diese Dissertation wurde im Sinne von § 7 der Promotionsordnung vom 28. November 2011 von Herrn Dr. Oliver Thorn-Seshold betreut.

Eidesstattliche Versicherung

Diese Dissertation wurde eigenständig und ohne unerlaubte Hilfe erarbeitet.

München, den 11. August 2022

.....
Alexander Sailer

Dissertation eingereicht am: 16.08.2022

1. Gutachter: Dr. Oliver Thorn-Seshold

2. Gutachter: Prof. Dr. Franz Bracher

Mündliche Prüfung am: 18.10.2022

For Erich Leo Sailer

And if you listen very hard
The tune will come to you at last
When all are one, and one is all
To be a rock and not to roll

ROBERT PLANT

Parts of this work have been published in peer-reviewed journals:

Alexander Sailer[#], Franziska Ermer[#], Yvonne Kraus[#], Ferdinand H. Lutter, Carsten Donau, Maximilian Bremerich, Julia Ahlfeld, and Oliver Thorn-Seshold; Hemithioindigos for Cellular Photopharmacology: Desymmetrised Molecular Switch Scaffolds Enabling Design Control over the Isomer-Dependency of Potent Antimitotic Bioactivity, *ChemBioChem* **2019**, *20*, 1305 – 1314.

Alexander Sailer, Franziska Ermer, Yvonne Kraus, Rebekkah Bingham, Ferdinand H. Lutter, Julia Ahlfeld, and Oliver Thorn-Seshold; Potent hemithioindigo-based antimitotics photocontrol the microtubule cytoskeleton in cellulo, *Beilstein J. Org. Chem*. **2020**, *16*, 125–134.

Alexander Sailer, Joyce C.M. Meiring, Constanze Heise, Linda N. Pettersson, Anna Akhmanova, Julia Thorn-Seshold, and Oliver Thorn-Seshold; Pyrrole Hemithioindigo Antimitotics with Near-Quantitative Bidirectional Photoswitching that Photocontrol Cellular Microtubule Dynamics with Single-Cell Precision, *Angew. Chem. Int. Ed*. **2021**, *60*, 23695–23704.

#: These authors contributed equally to this work.

Other works in preparation from this PhD:

Alexander Sailer, Nicole Urban, Xiao-ning Chai, Johannes Broichhagen, Kerstin Hill, Michael Schäfer, and Oliver Thorn-Seshold; Optical control over the activity of TRPC6 using a photoswitchable derivative of larixol, *manuscript in preparation (aim: ACS ChemBio)*

Alexander Sailer, Ferdinand H. Lutter, Maximilian Bremerich, Małgorzata Borowiak, Luis de la Osa de la Rosa, Constanze Heise, Julia Thorn-Seshold, and Oliver Thorn-Seshold; Structural tuning of bioactive hemithioindigos enabling *in vivo* photocontrol of microtubule-dependent processes, *manuscript in preparation (aim: ChemBioChem)*

1. Abstract

1.1 On the search for hemithioindigo-based tubulin photopharmaceuticals: Overcoming some weaknesses and breaking the spell of azobenzenes

Microtubules (MTs) are hollow polymeric tubes formed of α/β-tubulin heterodimers that are in a constant dynamic equilibrium between growth and shrinkage. MTs are an essential constituent of the cytoskeleton and so are critical in many cellular processes, such as mitosis, cargo trafficking and cell migration.

Consequentially, modulation of MT dynamics is a promising objective in the development of biological research tools, as well as therapeutic drugs. However, since MTs fulfil many *different* physiological roles at the *same* time, global manipulation of the MT network often causes serious off-site effects. This poses a major challenge in MT biology research. A major goal is thus to develop MT-targeting research tools whose activity can be precisely controlled: in terms of location (spatial) to selectively address the area under study, and at a given time point (temporal).

Owing to its unrivalled precision, non-invasiveness, and reversibility, light is an almost ideal stimulus for such spatiotemporally precise modulation of bioactivity. Photopharmacology harnesses these unique features of light to create high-precision photopharmaceuticals. Reversible photopharmaceuticals are bioactive small molecules derivatized with a molecular photoswitch that has two photoisomers that differ in binding affinity towards the biological target. Driven by light, these two isomers are interconverted between each other, thus enabling optical control over protein activity.

Previous approaches towards optical control over MT dynamics have mainly been based on azobenzene-derived photopharmaceuticals. However, azobenzenes are by no means ideal photoswitches, in that they suffer from the need of potentially phototoxic UV light, incomplete photoisomerization, incompatibility with certain functional groups and metabolic lability, among others.

Therefore, this thesis aims at the development of MT photopharmaceuticals that overcome some of the limitations and weaknesses of azobenzene-based approaches. These photopharmaceuticals are based on hemithioindigo (HTI), an emerging photoswitch with various beneficial properties, whose use in photopharmacology has however been scarce and far from systematical. In the following, I describe the development of hemithioindigo-based photopharmaceuticals for MT biology.

Paper One demonstrates the first use of HTIs in cellular photopharmacology (**HOTubs**). We showcase their potential for long-term photocontrol over the MT network, and their suitability for photopharmacology in general. We show in live cells that these HTIs light-

dependently induce cytotoxicity, disruption of the MT network and mitotic cell cycle arrest. They also bring unique possibilities: for most photoswitches including azobenzenes, isomerization is accompanied by large changes in sterics and consequentially it is often the sterics of the protein binding site that decides which photoisomer is the stronger binding one; but since both HTI isomers are nearly planar, we could use rational design rather than protein sterics to control which of the two **HOTub** isomers was the more bioactive. Taken together with the absence of unspecific toxicity and the avoidance of potentially phototoxic UV light, our findings strongly recommend HTIs as general and cell-compatible scaffolds for photopharmacology.

Paper Two aims at increasing the cellular potency of our HTI-based tubulin photopharmaceuticals. I design a SAR study and outline how the structural similarity of a highly potent indanone and hemithioindigo can be harnessed to create research tools (**HITubs**) exceeding the potency of all MT photopharmaceuticals known at the time. Another key aspect of this paper is to show that, unlike azobenzenes, the metastable isomer of HTI photopharmaceuticals has slow enough relaxation even with a strongly electron-donating, tautomerizable -OH group in the *para*-position, to allow its use as a bistable photoswitch. This substantially widens the chemical scope of photopharmaceuticals and thus expands the range of biological targets addressable by photopharmacology.

Paper Three describes how structural finetuning of the photoswitch scaffold yields MT photopharmaceuticals with near-quantitative photoisomerization (**PHTubs**). This enables studies void of undesired background of bioactivity which would stem from incomplete photoisomerization. For this purpose, I design a SAR study and synthesize tools based on pyrrole hemithioindigo (PHT), a photoswitch closely related to HTI. We further show that our **PHTubs** are sturdy photopharmaceuticals, that unlike azobenzenes, resist glutathione-mediated degradation in both isomeric states. This is an important prerequisite for more advanced studies, and we illustrate how PHTs can be implemented to light-dependently modulate the MT network in living cells and with single-cell precision.

Beside these topics, I briefly present my unpublished work on two other projects. The first aims for optical control over γ-tubulin, an isoform involved in cellular MT nucleation. Taking advantage of the similarity between an isoflavone-based γ-tubulin specific inhibitor and HTI, I design an HTI-based photopharmaceutical thought to target MT nucleation (**phatastatin**). We are currently optimizing a key step en route to **phatastatin**. The second project aims towards optical control over proteasomal degradation of tubulin. In the context of a research stay in the Trauner lab at New York University (NYU), I designed and synthesized a series of photoswitchable tubulin degraders (**TubPHOTACs**), and we are currently evaluating two promising compounds for their cellular mechanism.

In summary, this work contributes to light-dependent modulation of MT dynamics and introduces indigoid photoswitches (HTI and PHT) as sturdy photoswitches allowing for visible-light powered, reversible and highly precise studies in photopharmacology.

1.2 Auf der Suche nach Hemithioindigo-basierten Tubulin-Photopharmazeutika: Überwinden einiger Schwächen und der Dominanz von Azobenzolen

Mikrotubuli (MTs) sind hohle röhrenartige, polymere Strukturen, die aus Heterodimeren von α/β-Tubulin bestehen und sich in einem konstanten, dynamischen Gleichgewicht aus Wachstum und Schrumpfung befinden. MTs sind essenzieller Bestandteil des Zytoskeletts and als solche von entscheidender Bedeutung in vielen zellulären Prozessen, wie der Mitose, dem Transport von großen Biomolekülen und der Zellbewegung.

Folglich ist die Modulation der Dynamik von Mikrotubuli ein vielversprechendes Ziel für die Entwicklung von biologischen Forschungsinstrumenten und letztlich Pharmazeutika. Da MTs jedoch viele verschiedene physiologische Funktionen gleichzeitig erfüllen, führt eine globale Manipulation des MT-Netzwerks häufig dazu, dass Effekte an ungewünschten Orten eingeleitet werden. Dies stellt eine große Herausforderung für die Mikrotubuli-Forschung dar. Ein Hauptziel ist daher die Entwicklung von MT-adressierenden Forschungsinstrumenten, deren Aktivität äußert präzise gesteuert werden kann. Diese Steuerung soll örtlich (räumlich), um den zu untersuchenden Bereich selektiv anzusprechen, und zeitlich präzise sein.

Licht ist ein besonders geeigneter Stimulus für derartige räumlich und zeitlich aufgelöste Aktivierungen, da es mit hoher Präzison und nicht-invasiv wie reversibel dosiert werden kann. Diese Eigenschaften macht sich das Forschungsfeld der Photopharmakologie zunutze, um hoch präzise Photopharmazeutika zu entwickeln. Reversible Photopharmazeutika sind biologisch aktive Verbindungen, die einen Photoschalter enthalten, welcher zwei isomere Zustände besitzt. Diese Isomere unterscheiden sich in der Bindungsaffinität zum Zielprotein und können durch Belichtung ineinander überführt werden. Folglich lässt sich durch Belichtung eine optische Kontrolle über die Aktivität des adressierten Proteins erzielen.

Bisherige Strategien zur optischen Kontrolle über die Dynamik von Mikrotubuli beruhten häufig auf Photopharmazeutika, die mit einem Azobenzol als Photoschalter funktionalisiert waren. Diese Azobenzole sind allerdings keineswegs ideale Photoschalter, da sie unter anderem potenziell schädliches UV-Licht zur Isomerisierung benötigen, inkomaptibel mit gewissen funktionellen Gruppen und labil gegenüber metabolischen Enzymen sind und die Isomerisierung häufig nicht quantitativ abläuft.

Das Ziel dieser Doktorarbeit ist daher die Entwicklung von Photopharmazeutika für Anwendungen in der MT-Biologie, die einige der Schwächen und Anwendungsgrenzen von Azobenzol-basierten Strategien überkommen. Diese Photopharmazeutika basieren auf

Hemithioindigo (HTI), einem Photoschalter, der sich zwar durch vorteilhafte Eigenschaften auszeichnet, jedoch bislang in der Photopharmakologie nur äußert spärlich und wenig systematisch eingesetzt wurde. Im Folgenden werde ich die Entwicklung von derartigen HTI-basierten Photopharmazeutika für die MT-Biologie beschreiben.

Die **erste Publikation** stellt die erstmalige Verwendung von HTIs in zellulärer Photopharmakologie dar (**HOTubs**). Wir zeigen auf, welches Potenzial HTIs in Bezug auf die Photokontrolle über das MT-Netzwerk besitzen und dass sie generell für Anwendungen in der Photopharmakologie äußert geeignet sind. Wir zeigen, dass diese HTIs lichtabhängig zytotoxisch sind, das MT-Netzwerk beeinträchtigen und Zellen an der Mitose hindern. HTIs sind dabei einzigartig in der Hinsicht, dass die beiden Photoisomere, anders als bei den meisten Photoschalter, nur geringe Unterschiede in der Geometrie aufweisen. Während für die meisten klassischen Photoschalter (Azobenzole eingeschlossen) daher die Sterik der Bindetasche diskriminiert, welches Isomer das bioaktive ist, ist es für HTIs über rationales Design möglich, im Voraus zu planen, welches Isomer bioaktiv ist. Da HTIs außerdem keine unspezifische Zytotoxizität aufweisen und ohne potenziell phototoxisches UV-Licht betrieben werden können, schließen wir, dass HTIs generell für Anwendungen in der zellulären Photopharmakologie geeignet sind.

Die **zweite Publikation** zielt darauf ab, die zelluläre Potenz von HTI-basierten Tubulin-Photopharmazeutika zu erhöhen. Ich nutze die strukturelle Ähnlichkeit zwischen HTI und einem hochpotenten Indanon-basiertem Tubulininhibitor und identifiziere im Rahmen einer Studie zur Struktur-Aktivitätsbeziehung photoschaltbare Tubulininhibitoren (**HITubs**), deren Aktivität höher ist als alle bisherigen Vorgänger. Ein weiterer wichtiger Aspekt dieser Arbeit ist es zu zeigen, dass das metastabile Isomer von HTI-Photopharmazeutika selbst mit einer stark elektronenschiebenden, tautomerisierbaren -OH- Gruppe in *para*-Position eine ausreichend langsame thermische Relaxation aufweist, um als bistabiler Photoschalter eingesetzt werden zu können. Dies zeichnet HTIs gegenüber Azobenzolen aus und erweitert daher den chemischen Anwendungsbereich von Photopharmazeutika und damit auch die Palette der biologischen Ziele, die durch die Photopharmakologie angesprochen werden können.

Die **dritte Publikation** befasst sich mit der Optimierung der optischen Eigenschaften von MT-Photopharmazeutika. Zu diesem Zweck nutze ich Pyrrolhemithioindigo (PHT), einen Photoschalter mit großer Ähnlichkeit zu HTI, um eine Reihe von **PHTubs** zu synthetisieren. Diese ermöglichen nahezu quantitative Photoisomerisierung, wodurch **PHTubs** ohne latente “Hintergrundaktivität” eingesetzt werden können. Des Weiteren zeigen wir, dass **PHTubs** robuste Photopharmazeutika sind, die, anders als Azobenzole, in beiden isomeren Zuständen gegenüber dem Abbau durch Glutathion resistent sind. Dies ist eine wichtige Voraussetzung für fortgeschrittenere Anwendungen und daher können wir außerdem zeigen, dass **PHTubs**

in lebenden Zellen und mit der Auflösung auf der Ebene von einzelnen Zellen eingesetzt werden können.

Neben diesen Themen beschreibe ich meine bislang unveröffentlichte Arbeit an zwei weiteren Projekten. Das erste Projekt zielt auf die optische Kontrolle über γ-Tubulin ab, einer an der Nukleation beteiligte Isoform von Tubulin. Ich nutze die strukturelle Ähnlichkeit zwischen HTI und einem Isoflavon, das spezifisch γ-Tubulin inhibiert, um ein Photopharmazeutikum (**Phatastatin**) zu entwickeln, das die Nukleation von Mikrotubuli inhibieren soll. Momentan arbeiten wir an der Optimierung eines synthetischen Schlüsselschritts auf dem Weg zu **Phatastatin.** Das zweite Projekt zielt auf die optische Kontrolle über den proteasomalen Abbau von Tubulin ab. Im Rahmen eines Aufenthalts in der Gruppe von Dirk Trauner an der New York University (NYU) konzeptionierte und synthetisierte ich eine Reihe von photoschaltbaren Verbindungen für den Abbau von Tubulin (**TubPHOTACs**). Derzeit evaluieren wir den zellulären Wirkungsmechanismus von zwei vielversprechenden Verbindungen.

Diese Arbeit leistet Beiträge zur lichtabhängigen Modulierung der MT-Dynamik und hebt indigoide Photoschalter (HTI und PHT) als robuste Photoschalter für Anwendungen in der Photopharmakologie hervor. Diese können bidirektional mit sichtbarem Licht betrieben werden und ermöglichen reversible und hochgradig präzise Studien im Feld der Photopharmakologie.

1. Abstract **2**
1.1 On the search for hemithioindigo-based tubulin photopharmaceuticals: Overcoming some weaknesses and breaking the spell of azobenzenes 2
1.2 Auf der Suche nach Hemithioindigo-basierten Tubulin-Photopharmazeutika: Überwinden einiger Schwächen und der Dominanz von Azobenzolen 4
2. Light enables precise remote control over the activity of a biological target **9**
2.1 Optogenetics and the use of photoresponsive proteins 9
2.2 Photopharmacology and the use of photoresponsive ligands 11
2.2.1 Photocages irreversibly release small molecules 11
2.2.2 Photoswitches are reversibly toggled between active and inactive states 12
2.2.2.1 Design logic and requirements for an ideal reversible photopharmaceutical 13
2.2.2.2 Azobenzene is the benchmark scaffold for photopharmacology 15
2.2.2.3 Hemithioindigo is an emerging photoswitch 17
2.2.2.4 Other relevant photoswitches 19
2.3 The microtubule network is a pivotal part of the cytoskeleton 20
2.3.1 Inhibition of tubulin 21
2.3.1.1 Relevance and challenges at hand 21
2.3.1.2 Classification of stabilizing and destabilizing tubulin inhibitors 22
2.3.1.3 The colchicine binding site 22
2.3.2 Optical control of the MT network 24
2.3.2.1 Photopharmaceuticals targeting the colchicine binding site 25
2.3.2.2 Challenges for tubulin photopharmacology 27
3. Aims of the doctoral thesis **29**
4. Author contributions **30**
5. Paper One: HOTubs offer rational design control over the bioactive isomer **30**
6. Paper Two: HITubs are highly potent photoswitchable tubulin inhibitors **81**
7. Paper Three: PHTubs are near-quantitative tubulin photopharmaceuticals suitable for live-cell imaging **129**
8. Ongoing Research **207**
8.1 Towards a γ-tubulin specific photopharmaceutical 207
8.2 Phototargeted degradation of tubulin 209
9. Conclusion and Outlook **215**
9.1 Conclusion 215
9.1.1 Research Summary 215
9.1.2 General Conclusion 216
9.2 Outlook 216
9.2.1 Towards HTI-based MT photopharmaceuticals for *in vivo* applications 216
9.2.2 Tethered tubulin photopharmacology using hemiindigos 218
9.2.3 Isomer-specific coordinative bonds for sign inversion in PHTs 219
9.2.4 Indigoid switches for other targets: Optical control over RNA degradation 221

9.2.5 Photopharmacology towards *in vivo* drug applications 223
9.2.6 General Outlook 223
10. Acknowledgements 225
11. Appendix 226
11.1 Supporting information to chapter 8.1 226
11.2 Supporting information to chapter 8.2 236
11.3 List of abbreviations 255
11.4 Bibliography 257

2. Light enables precise remote control over the activity of a biological target

Biology heavily relies on small-molecule tools or genetic engineering to study protein function, by testing the effects of modulating the activity of a given target protein. However, a cell is a finely arranged entity in which many different processes take place at the same time; and some targets even fulfill different functions at different locations and different time points. The cytoskeletal protein tubulin, for instance, is involved in separation of the chromosomes during mitosis[1], neuronal trafficking,[2] among many other vital processes. To study specific roles of tubulin in these processes without interfering with its other simultaneous processes (i.e., avoiding off-site effects), the activity of a modulator must be controlled with highly precise spatial and temporal localization. The resulting challenge at hand is to conceive strategies, and identify stimuli, suitable for precise modulation of the activity of a given biological target.

In nature, many important processes are fueled or enabled by light, such as photosynthesis, the circadian cycle or vision. Following nature's blueprint of using light as an external stimulus for molecular motion has revolutionized supramolecular chemistry and culminated with the 2016 Nobel Prize jointly awarded to Ben Feringa. For biological research, light appears to be a privileged source for modulation of a bioactivity as well since it offers many beneficial features:

1) Light is non-invasive and visible light is non-toxic. While UV light might induce some phototoxic effects and does not penetrate biological tissue sufficiently[3], visible light is considered to be compatible with biological applications.[4]
2) Light can be applied very precisely: with single cell resolution, and usually even below. Current confocal microscopes enable ca. 200 and 500 nm of lateral and axial resolution of light application in live cells, respectively. Comparing this to the size of a human cell (10 – 100 µm in diameter) underscores the enormous potential for high-precision studies that light uniquely offers.
3) Light does not influence other cellular processes and does not interfere with cellular homeostasis (such as heat or changes of pH or redox states would).

There are two possible approaches to precisely control the activity of a biological target by light. One aims to render the target protein itself photoresponsive (optogenetics), while the other focuses on the development of photoresponsive ligands for that protein (photopharmacology).

2.1 Optogenetics and the use of photoresponsive proteins

Optogenetics[5] uses genetic engineering to render a protein of interest (POI) photoresponsive. The underlying concept is to introduce a structural motif to the POI that

undergoes a light-driven conformational change that triggers a downstream effect. Perhaps the most prominent photoresponsive motifs in optogenetics are rhodopsins.[6] A major hallmark in the physiology of vision, rhodopsins are proteins that rely on the isomerization of retinal (Fig. 1a): absorption of a photon induces isomerization of all-*E* retinal. This isomerization, which occurs at C11 in animal and C13 in microbial rhodopsins[7], results in a change of protein conformation which in turn triggers a biological response, for instance the opening of an ion channel.

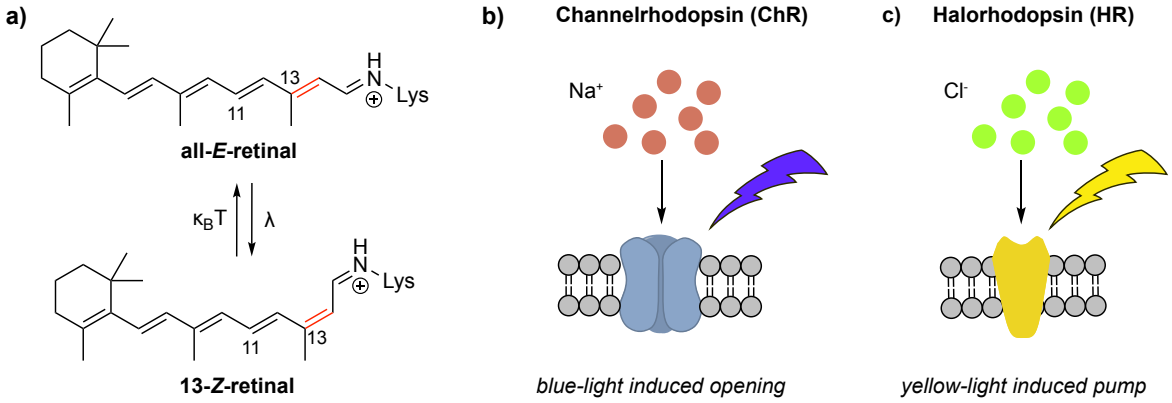

Fig. 1: Rhodopsins and optogenetics. a) In rhodopsins, all-*E*-retinal is attached to a lysine (Lys) residue of the protein as protonated Schiff base and undergoes a light-triggered isomerization to 13-*Z*-retinal (microbes) or 11-*Z*-retinal (animals). The conformational change involved results in downstream signaling. b) Channelrhodopsins are blue-light activated ion channels and c) halorhodopsins are yellow-light activated inward anion pumps.

In optogenetics, the naturally occurring channelrhodopsin (ChR, Fig. 1b)[8] and halorhodopsin (HR, Fig. 1c)[9] are some of the most common constructs for optical control over membrane potentials. While ChR is an unselective ion channel that can be activated by blue light[10], HR is a yellow-light activatable chloride-specific inward pump.[11] In a landmark paper, Boyden and coworkers used lentiviral transfection to introduce a ChR gene to mammalian neurons allowing optical control over excitatory and inhibitory synaptic transmission.[12] Since then, other optogenetical systems to modulate protein function have been developed. One notable example is the flavin-dependent **l**ight **o**xygen **v**oltage (LOV) domain.[1314] While rhodopsins control the influx or efflux of ions, LOV domains function via modulation of protein-protein interactions.[13]

Optogenetics has been successfully applied to many scientific fields, including neuroscience[15] and cell biology (for instance, optical control of microtubule severing[16]) and has very recently enabled partial restoration of vision in a blind patient.[17] Despite these ground breaking advances, the challenge for optogenetics is that every application needs to be tailored (genetically engineered) to the model organism. This is not only time consuming but also hampers the facile transition to other model systems. Instead of rendering the target

photoresponsive, it thus seems reasonable to focus on ligands whose activity can be controlled by light.

2.2 Photopharmacology and the use of photoresponsive ligands

Photopharmacology uses small drug-like molecules whose bioactivity can be activated or deactivated by light. In 1969, Erlanger and coworkers demonstrated a differential in activity between the two photoisomers of azobenzene-derived inhibitors of the acetylcholine receptor.[18] Since then, photopharmaceuticals have greatly contributed to the advances in biology and biochemistry. Successful applications range from optical modulation of ion channels[19], G-protein coupled receptors (GPCRs)[20], lipids[21], enzymes[22,23] and cytoskeletal constituents[24,25] (Fig. 2).

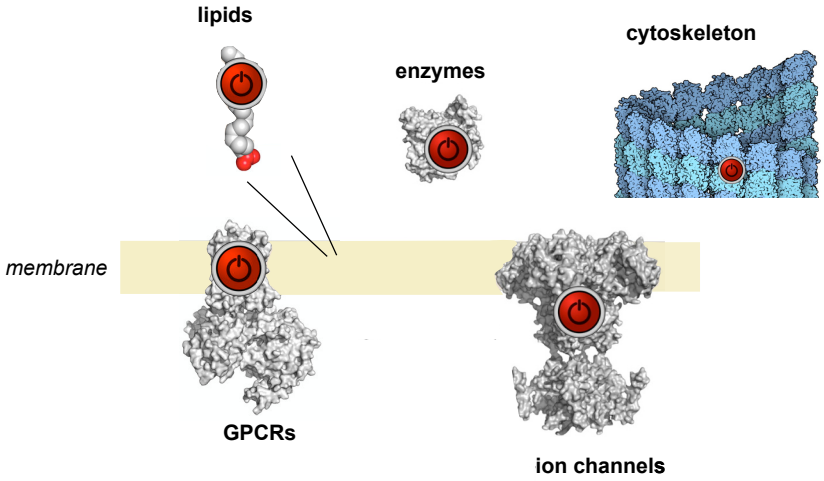

Fig. 2: The scope of photopharmacology (adapted from Trauner et al.[26]). Photopharmaceuticals have been used to modulate GPCRs, lipids, enzymes, ion channels, the cytoskeleton, and various other cellular targets.

Based on the mechanism by which photopharmaceuticals are activated, two different approaches are distinguished: irreversible photocages and reversible photoswitches.

2.2.1 Photocages irreversibly release small molecules

Photocages are ligands bearing a photolabile group that masks key pharmacophoric features.[27] Therefore, the affinity towards its target is dramatically reduced compared to the free (uncaged) compound. Illumination with light of an appropriate wavelength results in *irreversible* cleavage of the cage and release of the active ligand (Fig. 3a). The ligand then binds its target resulting in the desired downstream effects (Fig. 3b). Photocages are thus *a priori lit*-active, though irreversible, photopharmaceuticals; and can be considered as light-triggered prodrugs. The most frequently used photocages are *ortho*-nitrobenzyl derivatives. Drugs featuring esters, thiols, and phosphates are typical structures amenable to caging with the *ortho*-nitrobenzyl group. Illumination of these cages with UV light ($\lambda > 300$ nm) leads to a Norrish-like reaction[28] releasing the free ligand along with a nitrosobenzaldehyde (Fig. 3c).

Two features of this reaction seem problematic: firstly, the application of potentially phototoxic UV light and secondly the stoichiometric amounts of the toxic and highly-absorbing nitroso by-product[29]. While the toxicity of this nitrosobenzaldehyde can be shut down by intramolecular Diels-Alder reaction (after incorporation of a diene into the photocage[30]), the absorption maxima can only slightly be redshifted (by methoxylation, ~ 50 nm[29]). Therefore, substituted coumarins (λ_{max} ~ 400 nm[29]), BODIPYs (λ_{max} ~ 520 nm[31,32]) and π-extended BODIPYs (λ_{max} > 630 nm[33]) were developed as alternative scaffolds to avoid the use of UV light.

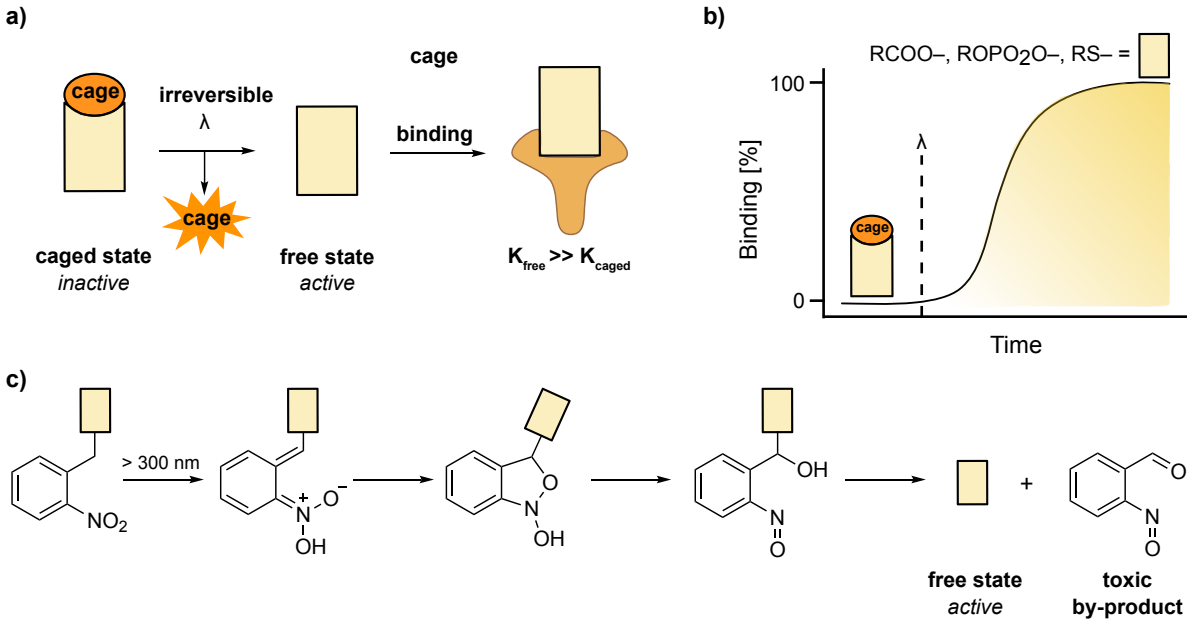

Fig. 3.: Photocages are irreversible photopharmaceuticals. a) A photocaged photopharmaceutical bears a photolabile group (cage) that masks its key pharmacophoric features. Illumination removes the cage and releases the active pharmaceutical. b) Upon illumination, a photocaged compound binds its target with the same kinetics as the parent compound. c) The widely used *ortho*-nitrobenzyl photocage is cleaved in an irreversible Norrish-like reaction forming a toxic and highly absorbing nitrosobenzaldehde.

The first application of photouncaging in biochemistry dates back to 1977 when Engels and Schläger used this strategy to release the second messenger cyclic adenosine monophosphate (cAMP).[34] One year later, Kaplan and coworkers[35] would report the release of adenosine triphosphate (ATP) in a very similar approach and coin the term 'photocage'. Since these pioneering studies, photocages have been successfully used to precisely release neurotransmitters, such as glutamate[36] and dopamine[37], nucleobases for DNA[38] or RNA[39] synthesis, calcium cations[40] or cytotoxic drugs.[41]

2.2.2 Photoswitches are reversibly toggled between active and inactive states

Unlike photocages, photoswitches undergo a *reversible* activation process (Fig. 4a). Illumination with light (λ_1) induces the formation of a metastable isomer that can either be actively converted back to the thermodynamic isomer by illumination with a second wavelength (λ_2) or passively by thermal relaxation (k_BT, Fig. 4a). The two isomers differ in

structure, geometry, polarity and often solubility[42] resulting in differences in binding affinity towards the biological target. Due to their reversible mode of activation, photoswitchable tools can be cycled between their respective on- and off-states multiple times (Fig. 4b). This is a desirable feature for applications where a certain biological response needs to be generated repeatedly (for instance, triggering of action potentials in neuroscience[43]). Compared to photocaging strategies which are based on the release of ligands that are often highly optimized for high binding affinity, photoswitching strategies imply permanent modifications of the applied drug. While this often leads to a reduction in bioactivity and thus certainly poses a drawback to some extent, it also offers the possibility to locally restrain the induced biological effect. This again is contingent on the different activation mechanisms: After activation of a photocage, the released active compound underlies diffusion leading to free distribution of the compound and thus induces undesired off-site activity.

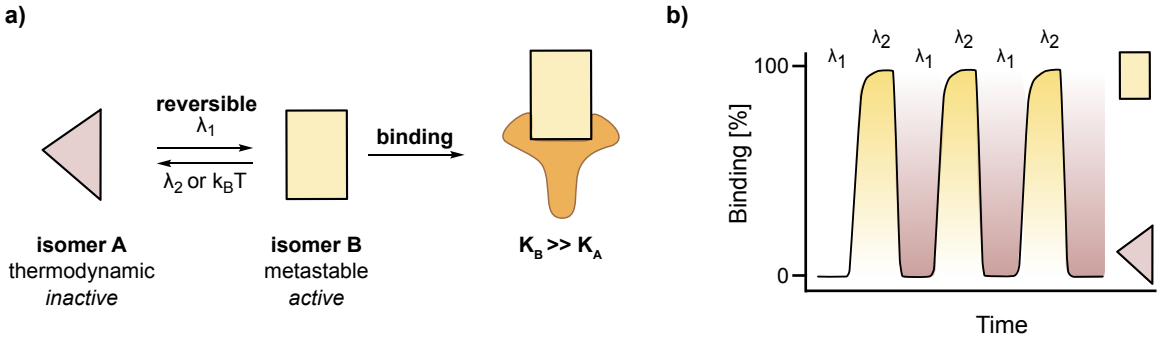

Fig. 4: Photoswitches are reversible photopharmaceuticals (shown: a *lit-state active* photoswitch). a) Illumination (λ_1) isomerizes the inactive **isomer A** to active **isomer B** which has a higher affinity for the target. Illumination with a second wavelength (λ_2), or thermal relaxation (k_BT), leads to back-isomerization to **isomer A**. b) Only **isomer B** binds the target, so the resulting downstream effect can be reversibly toggled on/off by λ_1/λ_2.

A *lit-state active* photoswitch with finely tuned half-life of its active isomer, however, relaxes back to its inactive state upon diffusion or can be photochemically deactivated[24]. Moreover, photoswitchable tools do not release toxic or highly absorbing cleavage products, and thereby enable high-quality experiments without interfering with biochemistry or imaging techniques. All these points highlight the importance and suitability of photoswitchable tools in chemical biology.

2.2.2.1 Design logic and requirements for an ideal reversible photopharmaceutical

In a best-case scenario, photopharmaceuticals with no basal (background) activity are applied *globally* and yet get activated only *locally*. However, designing such a photopharmaceutical is not a trivial endeavor and to reach this ambitious goal, an ideal photopharmaceutical must meet some important requirements (Fig. 5a-c):

1) ***Isomer-dependent activity**:* One isomer should be virtually inactive on its target, while the other should have as high binding affinity, and induce as strong a biological response, as possible.

2) ***Lit-state-activity***: To avoid background activity (induced by residual **isomer A**), it is generally desirable that the metastable isomer is the bioactive one.

3) ***Optical band separation**:* The absorption spectra of the two photoisomers should differ significantly. In an ideal case, light of one wavelength (λ_1) is only absorbed by **isomer A** inducing the forward isomerization while only **isomer B** absorbs light of another wavelength (λ_2) driving the backreaction. Thereby, it is possible to achieve equilibria (photostationary states, PSS) comprised of 100% **A** or **B**, respectively (bidirectional quantitative isomerization). Illumination with a wavelength which both isomers absorb (λ_{mix}) results in PSSs comprised of a mixture of isomers and reduces the photoswitchability of activity.

4) ***Wavelength dependency**:* Absorption maxima should lie in the visible part of the spectrum to circumvent phototoxicity and low penetration depths.[3] For cell culture applications, compatibility with the wavelengths of standard microscopy lasers (fixed wavelengths in the range 405 – 647 nm) are desirable. For true *in vivo* applications in animals, the optimal range lies between approximately 600 and 1200 nm to reduce optical scatter and filtering effects by biomolecules, such as hemoglobin.[3]

5) ***Orthogonality to standard imaging conditions:*** Cell biology often uses fluorescent proteins (GFP, YFP, etc.) for readout. An ideal photopharmaceutical for cell biology has no absorption bands interfering with the excitation of these fluorophores, to prevent isomerization during imaging.

6) ***Fatigue resistance and reversibility***: A useful photopharmaceutical must have the ability to be fully reversibly cycled between the two isomers without degradation (photobleaching) for several cycles. This is the rule for most (not all) photoswitches.

7) ***Thermal relaxation**:* Thermal relaxation of the metastable isomers should be slow enough to allow for sufficient binding after photoactivation, but fast enough to avoid substantial diffusion of the photoactivated isomer. Appropriate half-lives are highly dependent on the application and for instance may lie around 0.1 – 10 s for cerebrovascular applications.[44]

8) ***Metabolic stability***: Photopharmaceuticals should sufficiently resist metabolic enzymes, and cellular reductants, such as glutathione (GSH) which is known to metabolically clear electrophiles including N=N double bonds in azobenzenes.[45]

9) ***Solubility and Potency***: Most photoswitches are planar π-systems that tend to aggregate and have low aqueous solubility.[46] To reduce the necessary concentration of photopharmaceutical and cosolvent (high amounts of DMSO are cytotoxic[47]), sufficient high potency of the photopharmaceutical or prodrug strategies (phosphates[24,48] or amino acid conjugation[49]) are desirable.

10) ***Functional group tolerance***: A photopharmaceutical is only as good as the variety of different structural motifs it can be equipped with. Often electron-donating tautomerizable groups (e.g., hydroxy, or amino groups) in *ortho* or *para*-position to the isomerizable double bond induce fast relaxation of the metastable isomer limiting the applicability of the photopharmaceutical. Since these groups are often involved in polar interactions with the POI, an ideal photopharmaceutical should also tolerate these functional groups.

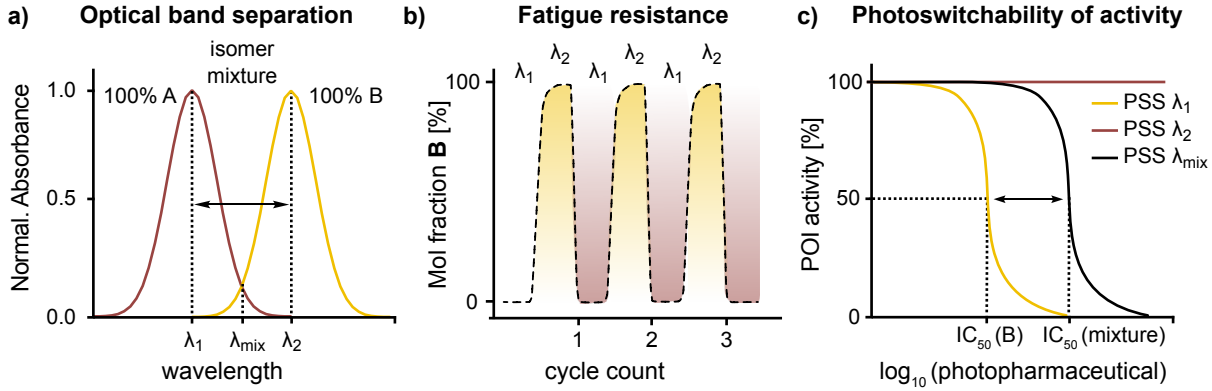

Fig. 5: Requirements for an ideal reversible photopharmaceutical. a) High optical band separations enable isomer-selective absorption and bidirectionally quantitative photoswitching (100% **A** or **B** at PSS). b) A photopharmaceutical needs to be isomerized from its inactive to its active form multiple times without degradation (high fatigue resistance). c) An ideal photopharmaceutical has one highly active and one completely inactive isomer. Illumination with λ_1 generates 100% of the active form (**B**), while λ_2 gives 100% of the inactive form (**A**). A wavelength where both isomers absorb (λ_{mix}) results in a mixture of isomers. Note that this panel represents the case of a *lit*-active inhibitor.

A variety of scaffolds have been applied to photopharmacology, including azobenzenes[50], stilbenes[51], styrylbenzothiazoles (SBTs)[48,52,53] hemithioindigos (HTIs)[54,55], diarylethenes[56] and spiropyran-merocyanin (SPMC) switches.[57] None of these scaffolds are ideal: each come with their respective limitations and challenges. Thus, choosing the 'right' photoswitch for a given application is often difficult and needs careful examination of the target and the research question to be answered.

2.2.2.2 Azobenzene is the benchmark scaffold for photopharmacology

In the overwhelming majority of cases, azobenzenes are the scaffold of choice (Fig. 6a).[50] This is in part because of the synthetic accessibility of azobenzenes but also because of their mostly beneficial optical and geometrical properties: UV light (λ = 320 – 370 nm)[42] predominantly excites the π-π* transition of the thermodynamically favored *E*-isomer and therefore induces the isomerization to the metastable *Z*-isomer with good photochemical

completeness (Fig. 6b). The back-isomerization occurs either thermally, or by illumination with visible light (λ = 420 – 480 nm)[42] that targets the n-π* transition, predominantly of the *Z*-isomer. In azobenzenes, isomerization is accompanied by a drastic change in geometry and polarity (Fig. 6c). While the *E*-isomer is nearly planar and has no dipole moment, the *Z*-isomer is bent and polar (change of dipole moment ~ 3D).[3] These large changes in molecular structure often lead to big differentials in bioactivity for the two isomers explaining the popularity of azobenzenes in photopharmacology. Azobenzenes can either be attached to the periphery of a biologically active compound (azoextension, Fig. 6d) or be embedded within in the pharmacophore (azologization, Fig. 6e). The former approach comes with design challenges: attaching a lipophilic molecule, like a photoswitch, to a ligand changes its overall mass, structure, polarity, and lipophilicity. These changes often result in less potent photopharmaceuticals.[3] The attachment site of the photoswitch must hence be evaluated carefully (for example, by analysis of X-ray structures of the parent ligand bound to the target or guided by known structure-activity relationships). Thus, azologization seems to be the more elegant strategy. Structures amenable to azologization include a variety of important functional groups in medicinal chemistry including ethers, thioethers, amines, benzamides and stilbenes (Fig. 6f).[58] Due to the often *trans*-like orientation of these structures, many azologs tend to be active in their *E*-isomer (*dark*-state activity).[58] This, however, is an inherent limitation of this approach and the azobenzene scaffold itself since in most cases *lit*-active compounds are preferred to avoid backgrounds of bioactivity due to incomplete photoisomerization (see chapter 2.2.2.1).

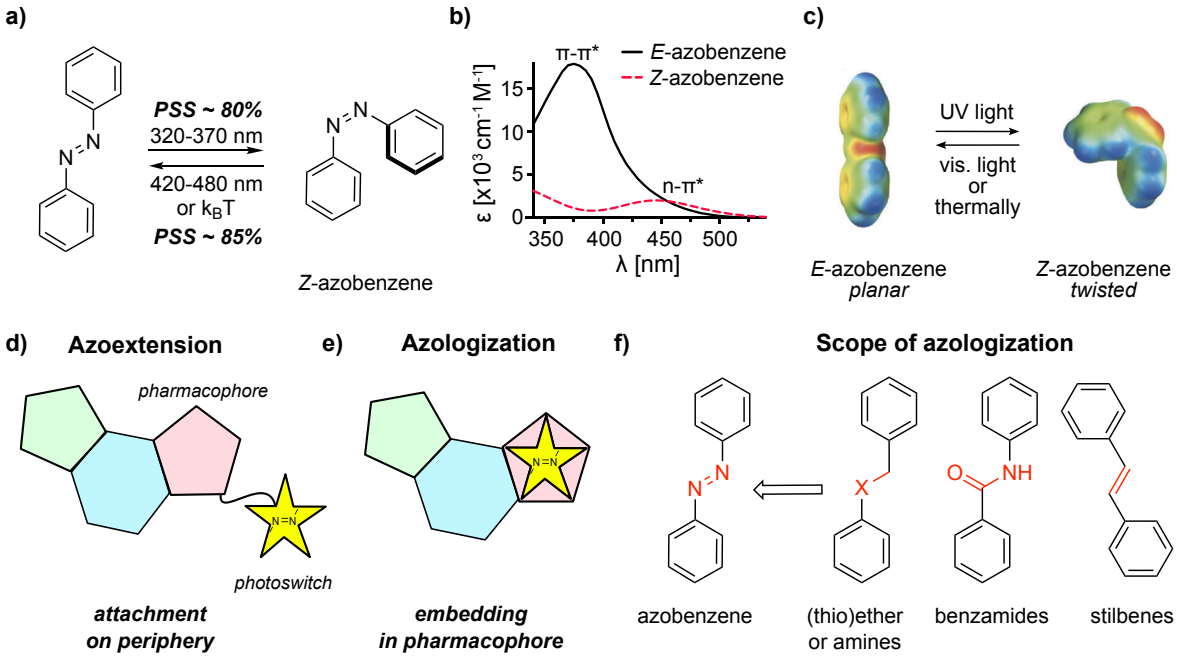

Fig. 6. Azobenzenes are the most widely used photoswitch. a) UV light induces isomerization of *E*-azobenzene to its *Z*-isomer while the backreaction can be partially triggered by visible light partially or completely by thermal relaxation. b) The isomerization processes are enabled by illuminating into the π-π* (*E-Z*) or n-π* (*Z-E*) absorption band (adapted from Trauner et al.[24]). c) Isomerization is accompanied by

large geometrical and polarity changes (adapted from Beharry and Woolley[59]). d) – e) Azobenzenes can be attached on the periphery of the pharmacophore (azoextension, d) or incorporated within the pharmacophore (azologization, e). f) Many structures present in medicinal chemistry can be azologed creating mostly *dark*-active photopharmaceuticals.

Other concerns associated with azobenzenes are the usage of UV light (albeit red-shifting is possible[44,60]), the incompleteness of switching (albeit improvements are reported[61]) and the lability towards cellular reductants, such as GSH.[62] Additionally, highly electron-donating groups at the *para*-position of azobenzenes lead to negligible half-lives of the *Z*-isomer in aqueous media (µs).[63,64] However, functional groups like hydroxy groups often form important protein-ligand interactions. The incompatibility of the azobenzene scaffold with these pharmacophores in the *para*-position is a serious limitation for its use in photopharmacology. All of the above points showcase the necessity for development of alternative photoswitches for photopharmacology.

2.2.2.3 Hemithioindigo is an emerging photoswitch

Hemithioindigo (HTI) is a photoswitch comprised of a thioindigo and a stilbene half (Fig. 7a). Despite its first report by Friedländer[65] dating back to 1906 and its extensive use in supramolecular chemistry[66] as well as molecular motor scaffold[67], HTI is an underdeveloped scaffold in photopharmacology compared to azobenzenes. This underrepresentation, however, contrasts with the beneficial characteristics of this scaffold. HTIs are fully reversible and highly fatigue resistant photoswitches.[68] Unlike for azobenzenes or stilbenes, both isomers absorb in the visible part of the spectrum (Fig. 7b): blue light induces isomerization from the thermodynamically favored *Z* to the metastable *E*-isomer while illumination with green light or thermal relaxation drives the back-isomerization.[69,70] However, due to small differences in the spectral bands of the two isomers (~ 20 nm for HTI)[71], their photochromicity is usually low posing a conceptual challenge for their application.[71]

While their application in photomodulation of lipids[54] and small peptides[72] are reported, their most biochemically-advanced use at the time this PhD began, was a simple HTI (**BODTCM**, Fig. 7c) reported to give isomer-specific inhibition of the 12/15-lipoxygenase (LOX) pathway.[55] However, (1) solubility of HTIs in purely aqueous medium and high µM concentrations seems questionable[46], (2) no quantification of PSS composition or relaxation kinetics of the *E*-isomer were given, and (3) for cellular studies, HPLC-separated isomers were applied instead of *in situ* generated isomers. These apparent weaknesses of this paper highlighted the need for more sophisticated and thorough studies of HTIs as scaffolds in photopharmacology.

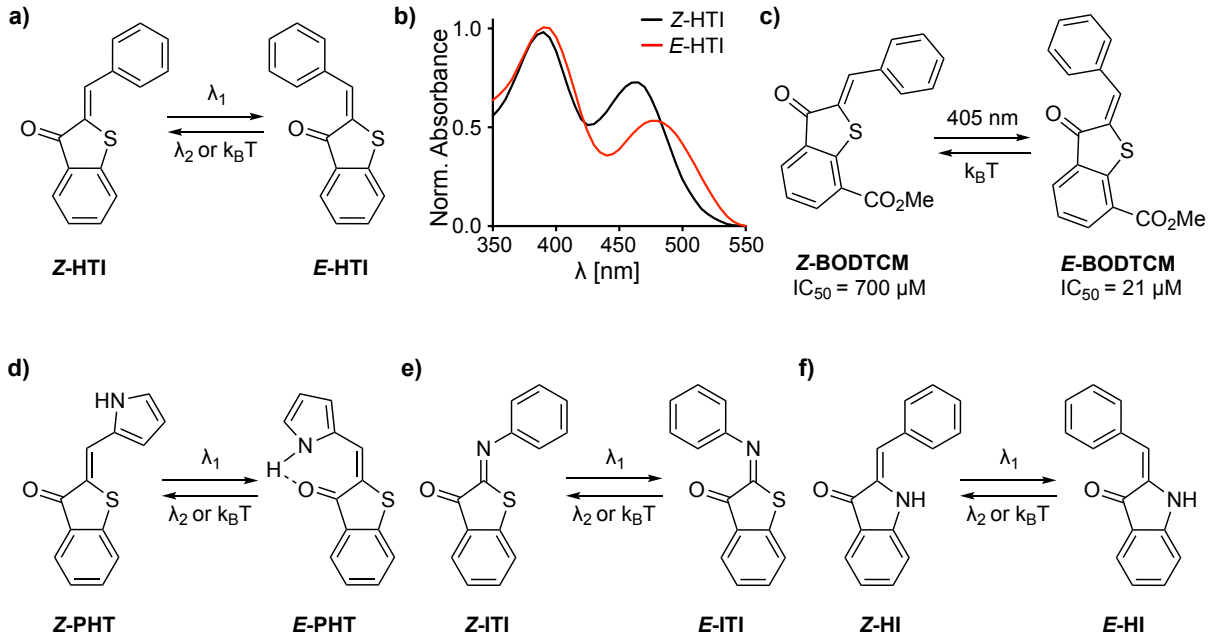

Fig. 7: Hemithioindigos and other indigoid photoswitches. a) HTIs can be switched between their *Z* and *E*-isomers. b) Both isomers absorb in the visible part of the spectrum allowing all-visible light powered photoswitching. c) **BODTCM** was the first HTI-based photopharmaceutical. d) Isomer-specific H-bonding decouples the absorption spectra of PHTs allowing (near)-quantitative photoswitching. e) ITIs have high optical band separations and can be photoswitched in water. f) HIs are less studied, but promising isosteres to HTIs.

Indigoid photoswitches are HTIs that were (isosterically) modified to tune their optical properties. Replacement of the stilbene with a pyrrole half gives pyrrole hemithioindigos (PHTs, Fig 7d) where *E*-isomer specific H-bonding leads to efficient spectral band separation of the isomers and thus permits near-quantitative bidirectional photoswitching.[73] Extending the π-system of the pyrrole with electron-rich arenes can be used to redshift the absorption maxima.[74]

Iminothioindoxyls (ITIs)[75] consist of a thioindigo and an azobenzene half (Fig 7e). They are characterized by high optical band separation (~ 100 nm), resistance to reducing glutathione and importantly can be operated in aqueous media. However, relaxation in the ms range has hampered its use in photopharmacology despite the fact that protonation of the bridging N atom was found to increase the thermal half-life of the *E*-isomer by three orders of magnitude.[76]

Hemiindigos (HI) are isosteres to HTIs in which the thioindigo is replaced by an indigo fragment (Fig. 7f).[77] Their photochromism is generally less-studied but promising: For instance, HIs with electron-donating groups in 4-position are efficiently isomerized with blue (*Z*-*E*, > 80%) and red-orange (*E*-*Z*, > 95%) light.[77] In photopharmacology, water-soluble HIs were used as photoswitchable binders of human HIV-1 RNA.[78]

2.2.2.4 Other relevant photoswitches

Apart from azobenzene and indigoid switches, a few other scaffolds are of interest in photopharmacology. These can be categorized according to their type of isomerization, namely double bond isomerization (such as stilbenes), or (electro)cyclization (such as DTEs, Fig. 8).

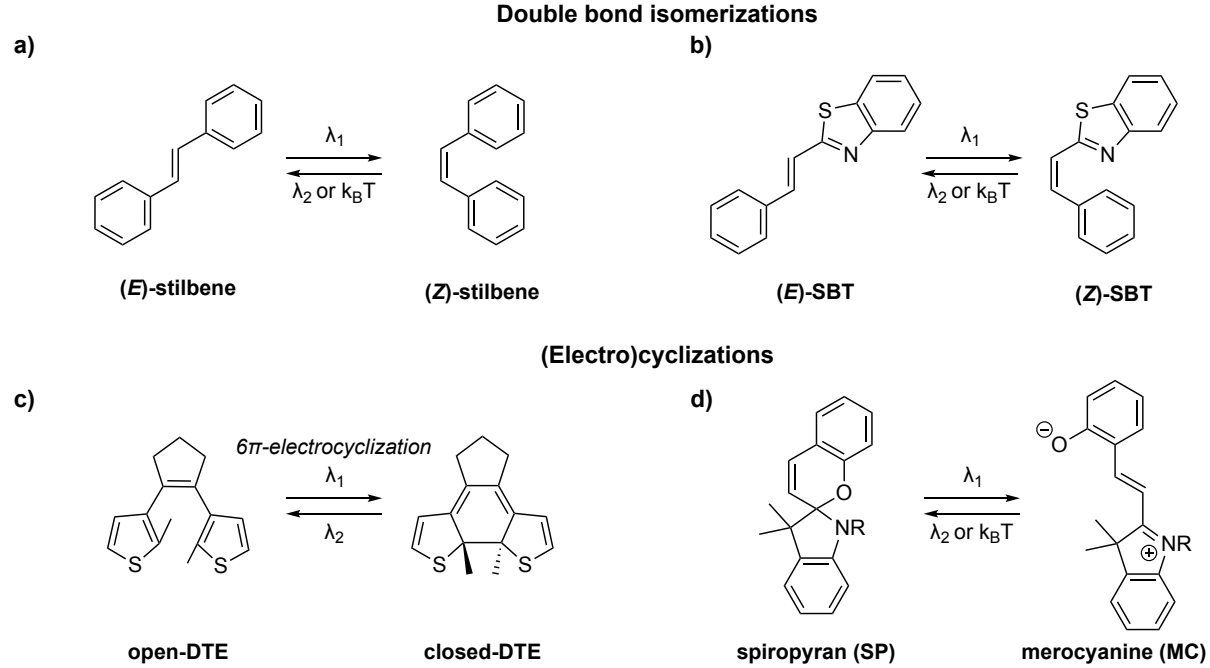

Fig. 8: Other relevant photoswitches in photopharmacology. a) – b) Stilbenes and SBTs can be isomerized with UV light to give a majority of *Z*-isomer. c) DTEs undergo a thermally irreversible (but photochemically reversible) 6π-electrocylization. d) SPs can be opened to their colored merocyanine (MC) isomers by UV light and back-isomerized photochemically or thermally.

Stilbenes are isomerized from their thermodynamically favored *E*-isomer to the metastable *Z*-isomer with low UV-A light (λ < 350 nm, Fig. 8a). Due to blue-shifted and hypochromic absorption maxima of the *Z*-isomers[79], photochemical back-isomerization is possible only under harsh conditions. Additionally, thermal relaxation is usually slow even at elevated temperatures[79] and stilbenes undergo a couple of side reactions, including [2+2]-cycloadditions[79] and formation of dihydrophenanthrenes.[80,81] Nonetheless, stilbenes have found some use in photopharmacology.[51,82]

Styrylbenzothiazoles (SBTs)[83] are derivatives of stilbenes with red-shifted absorption bands allowing *E*-*Z* isomerization with longer wavelengths (λ = 360 – 405 nm, Fig. 8b).[52] In addition, SBTs are less prone to side reactions[80,84], compatible with common imaging techniques[52] and metabolically stable[52] making this scaffold an interesting addition to the toolbox of photopharmacology.[48,52,53]

DTEs are very fatigue resistant photoswitches[80] that undergo a 6π-electrocyclization upon irradiation with UV light (Fig. 8c).[49] The closed form is thermally stable since the ring-opening process is forbidden (Woodward-Hoffmann rules[85]) making DTEs bistable photoswitches.[86]

However, the closed isomer absorbs strongly in the visible part of the spectrum often allowing for quantitative photoswitching.[49] DTEs were used as photochromic dopamine receptor ligands[56], in optical control over inhibition of a kinase[87] or modulation of coenzyme Q.[88] Fulgides[56] and fulgimides[89] are mechanistically similar to DTEs, albeit less used in photopharmacology.

Spiropyrans (SPs) can be opened to their merocyanine (MC) isomer by UV light (Fig. 8d).[90] The highly colored open form can be converted back to the closed form by visible light or thermal relaxation.[90] While regular SPMCs suffer from fast hydrolysis in aqueous media (similar time scale than thermal relaxation)[91], pyridine-substituted SPMCs are more stable.[92] Due to large polarity changes upon isomerization (polarity switches), SPMCs can be used for cellular localization.[57]

2.3 The microtubule network is a pivotal part of the cytoskeleton

Photoswitchable photopharmaceuticals enable highly precise remote control over the activity of a POI, that is unrivaled by classical small-molecule research drugs. This precision proves to be especially practical when the POI is a dynamic structure involved in many different cellular settings, such as the microtubule (MT) network.

The MT network is an essential constituent of the cytoskeleton and as such found in all eukaryotic cells.[93] Structurally, MTs are hollow polymeric tubes with a diameter of ~ 25 µm which are formed by lateral alignment of usually thirteen protofilaments (Fig. 9).[93] These protofilaments, in turn, result from polymerization of soluble α/β-tubulin heterodimers in a head-to-tail manner.[93,94] Thus, MTs are intrinsically polar structures whose polarity is an important prerequisite for many of its functions[93] and used to distinguish the two ends of the polymer, the faster growing (+) and the slower growing (-)-end.

Monomeric free tubulin heterodimers are bound to guanosine triphosphate (GTP). Upon polymerization and incorporation into the lattice, GTP gets hydrolyzed to guanosine diphosphate (GDP) inducing a conformational change (straightening of the slightly curved tubulin).[94] Noteworthily, hydrolysis only takes place on the faster growing (+)-end where β-tubulin is exposed. As a result of this site-specific hydrolysis, most of the lattice consists of GDP-tubulin while only at the (+)-end of the growing MT a cap of GTP-tubulin remains that is thought to stabilize the whole MT (GTP cap model).[95]

MTs are dynamic structures and in a constant state of flux oscillating between growth (‘rescue’) and shrinkage (‘catastrophe’). This process of tubulin polymerizing to and depolymerizing from MTs is termed dynamic instability[95] and is an important requirement for the many vital physiological roles of MTs.[93]

MTs are involved in a plethora of processes ranging from cell homeostasis (such as positioning of organelles during interphase[94] and maintenance of cell morphology through pushing forces of growing MTs[96]) to cell migration.[93]

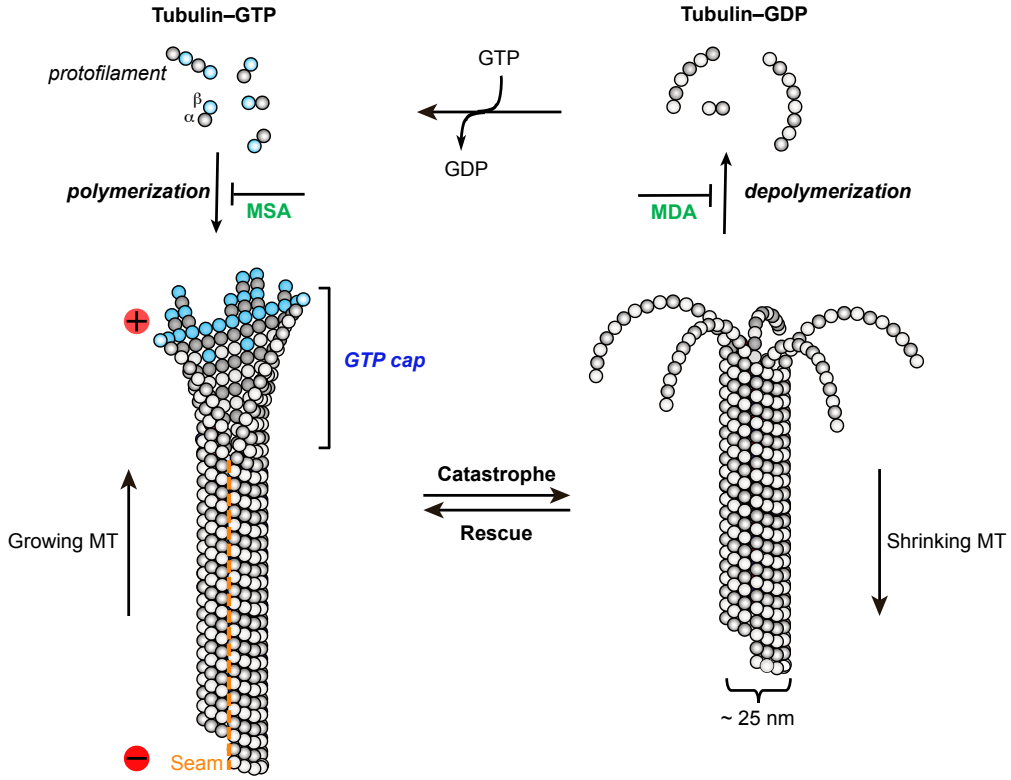

Fig. 9: Dynamic instability of MTs. MTs are in a constant state of flux between growth and shrinkage (adapted from Steinmetz and Prota[94]).

Additionally, MTs serve as scaffolding for the motor proteins dynein and kinesin.[97] Perhaps most importantly for pharmaceutical industry, MTs are involved in formation of the spindle apparatus where depolymerizing MTs drive the separation of chromosomes.[1,98]

2.3.1 Inhibition of tubulin

2.3.1.1 Relevance and challenges at hand

During mitosis, MT dynamics increase 20-100 fold.[97] Inhibition of MT dynamics therefore leads to severe interference with the spindle apparatus, mitotic cell cycle (G2/M) arrest and ultimately apoptosis.[99] Due to this pronounced role during cell division, inhibition of tubulin is an important approach in cancer treatment.[100] In fact, before targeted therapy[101] (monoclonal antibodies or small-molecule inhibitors of oncogenic kinases) was available, tubulin had been the only alternative to DNA as cellular target.[102]

In addition and despite the critical role of MTs in nearly all cellular settings, there remains a significant research gap in tubulin biology (for instance, cellular tubulin degradation pathways remain unclear to this date[103]). This gap partially arises from the fact that genetic manipulations (mutations or knockouts) of tubulin are often lethal.[104–106] Additionally, small-

molecule tubulin inhibitors are usually highly cytotoxic compounds. This poses the risk of inducing cell death when tubulin inhibitors are applied to study tubulin-specific processes. Thus, highly site-selective, precise, and dynamic research tools are needed to study this fascinating scaffold protein.

2.3.1.2 Classification of stabilizing and destabilizing tubulin inhibitors

Mechanistically, tubulin inhibitors impact the dynamic instability of MTs and are thus often referred to as microtubule targeting agents (MTAs). Owing to their effect at high concentrations, they are classified as microtubule disrupting agents (MDAs) and microtubule stabilizing agents (MSAs, Fig.9).[94,102] MDAs reduce the MT polymer mass by preventing the polymerization of soluble heterodimers, while MSAs increase the polymer mass by preventing depolymerization of existing MTs.[102] Most MTAs are marine or botanical natural products produced to avoid predation.[102] While their evolutionary role is vastly conserved, MTs structurally comprise a heterogenous group including but not limited to alkaloids, steroids and (depsi)peptides.[102]

2.3.1.3 The colchicine binding site

Despite the structural diversity within this class, most MTAs exert their biological activity upon binding at distinct regions of tubulin. Until 2013, only three of these binding sites (vinca, taxane and colchicine sites) had been characterized.[94]

However, advances in structural biology, enabled by X-ray crystallography and cryo-electron microscopy (cryo-EM), led to the discovery of three previously unknown sites which were termed the maytansine, pironetin and laulimalide/peloruside sites (Fig. 10a). Very recently, cevipabulin (a vinca-site binding MTA) was discovered to also occupy a hitherto unknown binding site at tubulin.[107] Upon binding at this, yet unnamed, seventh binding site, the αT5 loop undergoes a structural change exposing α-tubulin bound GTP to hydrolysis which leads to destabilization and ultimately degradation of tubulin.[107] This is a significant finding since (1) most of the tubulin binding sites are located at the β subunit of the heterodimer (Fig. 10a) and (2) α-tubulin bound GTP had previously been deemed nonexchangeable[94] (see chapter 2.3).

The colchicine binding site is named after its first identified ligand, the tropolone alkaloid colchicine. This natural product was first isolated from *Colchicum autumnale*, a plant already known to the ancient Romans.[108] The colchicine binding site is deeply buried inside the protein at the interface between the α- and β-subunit and mostly comprised of hydrophobic interactions of β-tubulin with the respective ligands (**c**olchicine **d**omain **i**nhibitors: CDIs, Fig. 10b).[94]

The promiscuous binding site accommodates a great variety of structures, including alkaloids (colchicine), stilbenes (combretastatins)[109], steroids (2-methoxyestradiol)[110] and indoles (nocodazole).[111] Nevertheless, extensive SAR studies for colchicine identified important pharmacophoric motifs for colchicinoid CDIs (Fig. 10c):

1) ***A ring:*** The polymethoxy pattern on the A ring is essential.[112]
2) ***B ring:*** The B ring is not involved in binding but mainly acts as conformational lock of the blade-like ('*cisoid*') structure.[108] This gets reinforced by the fact that introduction of unsaturation to the B ring and simultaneous removal of the acetamide results in potency enhancement.[113]
3) ***C ring:*** Swapping positions of the ketone and the methoxy group in the C ring is not well tolerated[113] while complete replacement of the tropolone with isovanillin is.[108]

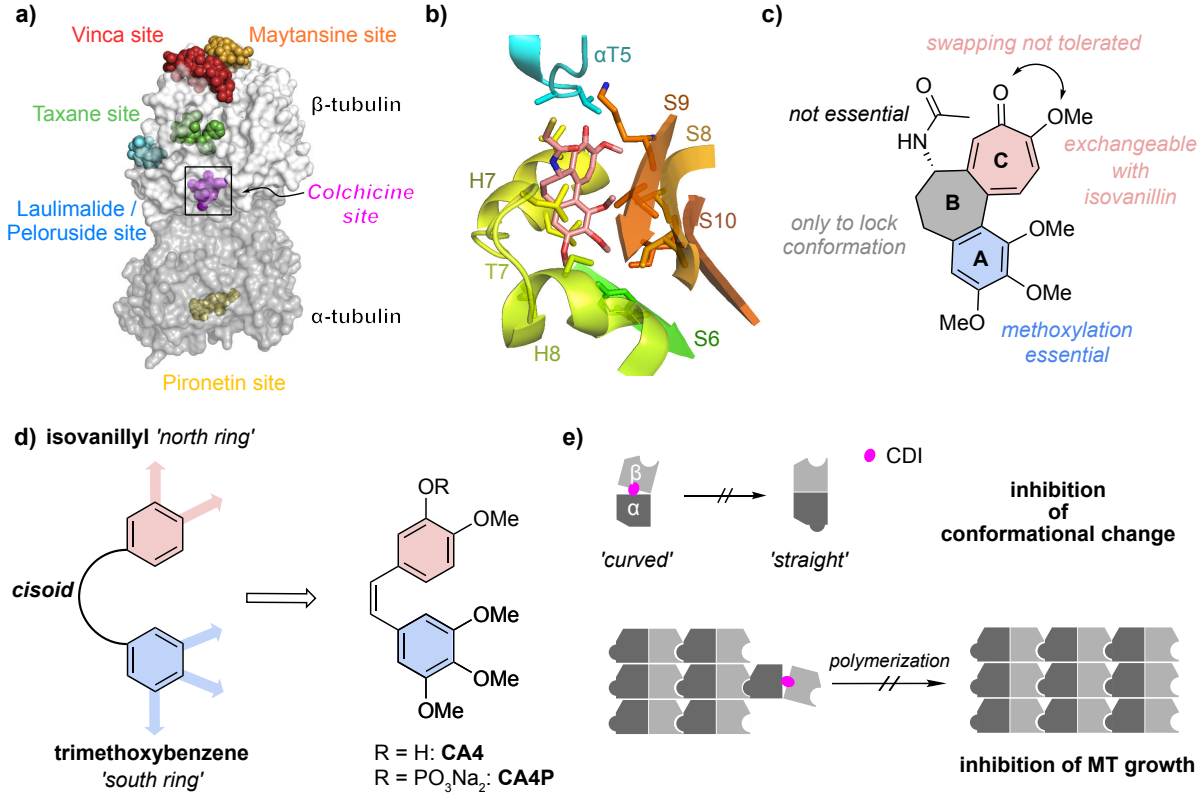

Fig. 10: Tubulin, the colchicine binding site, SAR for colchicine site binders and their mechanism of action. a) Cryo-EM structure of tubulin (taken and adapted from Steinmetz and Prota[94]), b) X-ray crystal structure of DAMA-colchicine bound tubulin (taken from Thorn-Seshold et al.[114]), c) Structure-activity relationship of colchicine and d) a simplified pharmacophore model for colchicine domain inhibitors (CDIs), e) CDIs inhibit a conformational change of tubulin heterodimers preventing incorporation in the lattice and therefore MT polymerization (taken and adapted from Steinmetz and Prota[94]).

From these findings, a simplified pharmacophore model for colchicinoid CDIs can be derived (Fig. 10d): In its most fundamental form, an isovanillyl top ('north') ring is attached to a 3,4,5-trimethoxybenzene bottom ('south') ring. The important '*cisoid*' nature of the molecule[115] is ensured via a *cis*-configured double bond, a ketone or a heterocycle connecting the two halves of the molecule.[116] **Combretastatin A-4** (**CA4**[117], due to limited aqueous

solubility often used as its phosphate prodrug, **CA4P**[109]) is a potent MDA which follows this model and has been extensively utilized as lead structure for the development of CDIs (Fig. 10d).

Mechanistically, CDIs inhibit the conformational change of slightly curved (as found in the soluble heterodimer) to straight tubulin (as found in the MT lattice, Fig. 10e)[94]. As a result of this, tubulin polymerization and microtubule growth are prevented inducing a plethora of downstream effects.

Apart from exerting antimitotic effects, many CDIs also act as vascular-disrupting agents (VDAs)[118] of which some have been translated to clinical trials for cancer treatment.[102]

While colchicine has been long known to disrupt the microtubule network and has been indicated for the treatment of gout[119], it remained the only CDI used in the clinic for a long time. This was until in 2021 tirbanibulin was the first CDI to be approved for the treatment of actinic keratosis, a pre-cancerous skin condition.[120] The very limited medical use of CDIs still stands in contrast to their strong tubulin inhibition and the importance of tubulin as potential drug target. This paradox mainly stems from the high toxicity[121] of colchicine derivatives – potentially, of all CDIs – which narrows the therapeutic window and causes side effects during pharmacotherapy. In other words, toxicity poses a major obstacle for the clinical use of CDIs and calls for strategies to control their bioactivity with high-site selectivity and temporal resolution.

2.3.2 Optical control of the MT network

Microtubules play key roles in many *different* cellular processes at *different* locations of the cell at the *same* time. Given the usually high toxicity of MTAs, *global* (i.e., systemic) administration of MTAs often leads to *global* cell death instead of *local* manipulation of the microtubule network. Therefore, strategies for site-specific activation and temporal resolution (to compensate for diffusion or drug distribution effects) of the activity of tubulin inhibitors are needed. In cancer treatment, where death of cancerous cells is desired, antibody-drug conjugates (ADCs) carrying antimitotic payloads are interesting strategies for targeted therapy. In fact, a few tubulin-targeting ADCs have already been approved in cancer treatment and many more have entered clinical trials.[122]

In biological research, however, where the focus is on studying MT-dependent processes instead of inducing cell death, tools are required whose activity can be reversibly controlled on the single cell level (or beneath).

In other words, a dynamic target like tubulin calls for dynamically controllable tools. Photoswitchable tools using light for remote control over drug activity with its unrivaled

precision and reversibility fulfil this requirement. This renders photopharmacology a privileged and promising strategy for microtubule biology.

2.3.2.1 Photopharmaceuticals targeting the colchicine binding site

Compared to MTAs targeting other binding sites, CDIs are often simple molecules (few if any chiral centers, low molecular mass, and synthetically well accessible). Taken together with the simplistic and yet powerful pharmacophore model available (see chapter 2.3.1.3), CDIs are an interesting starting point for the development of tubulin photopharmaceuticals.

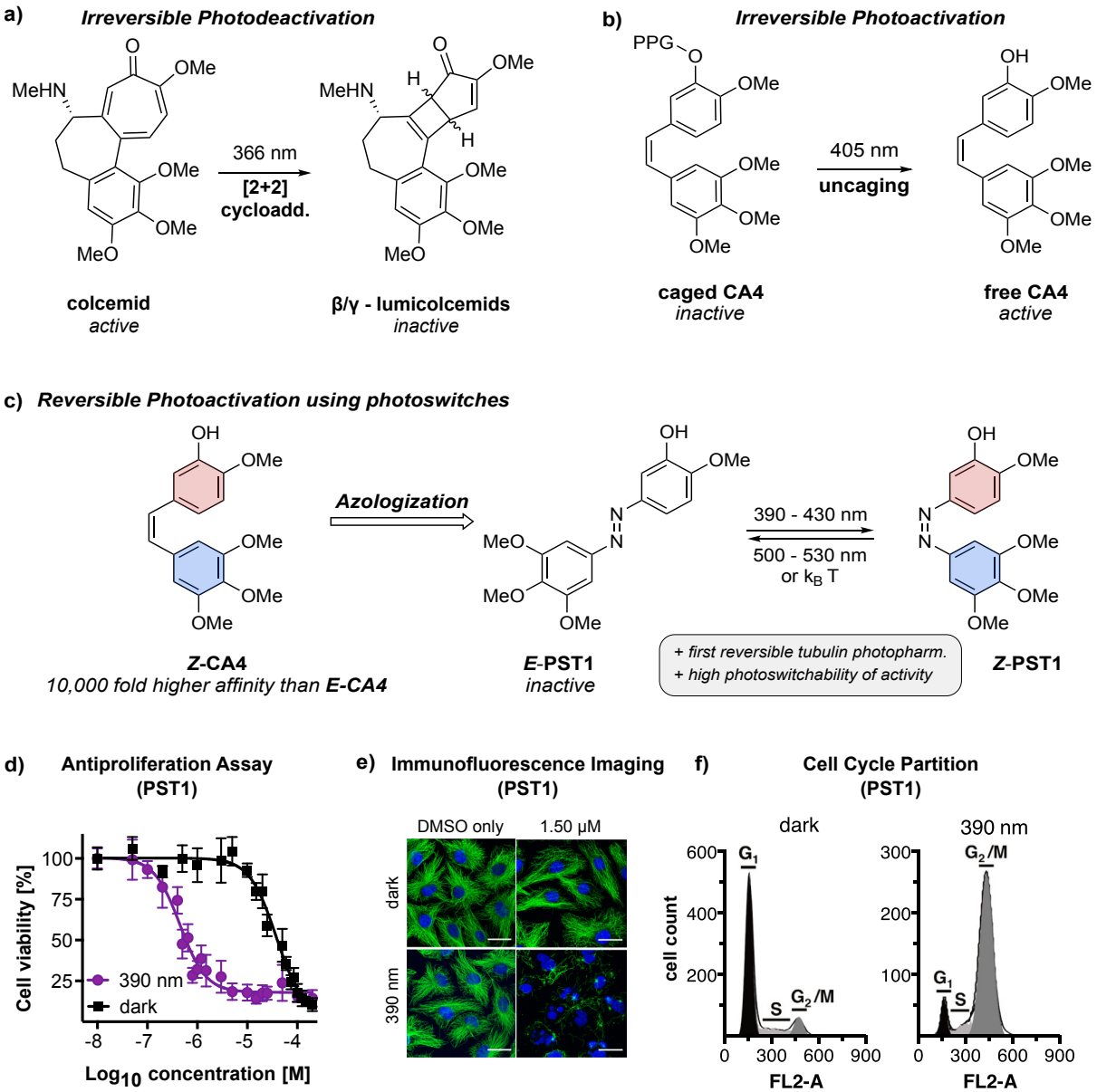

Fig. 11: Colchicine site targeting photopharmaceuticals. a) Illumination of **colcemid** results in formation of less potent **lumicolcemids** (Note: it was not distinguished between **β/γ- lumicolcemid** (endo/exo products) and **α-lumicolcemid** (dimer of **β/γ- lumicolcemid**). b) Irradiation of inactivated (photocaged) **CA4** releases the active CDI (PPG: photolabile protecting group). c) Azologization of **CA4** leads to the photostatins (**PST**), the first reversible tubulin photopharmaceuticals. **PSTs** were expected to be more active as their respective *Z*-isomers similar to **CA4** (10,000 fold higher affinity)[123]**.** d) – f) **PST1** is a potent *lit*-active cytotoxin leading to MT disruption and G2/M arrest (adapted from Trauner et al.[24]).

In 1970, Aronson[124] reported the photodeactivation of colcemid (Fig. 11a). It was found that colcemid inhibited cleavage (division of cells in the early embryonic stage) in fertilized sea urchin eggs and blackworms and that this process could be reversed by illumination with UV light.[124] It was reasoned that colcemid undergoes an irreversible [2+2] cycloaddition leading to inactive lumicolcemid.

Although this work was pioneering, an apparent drawback is the constant background of activity resulting from unreacted colcemid (since the photoreaction is most likely not quantitative). Constant illumination, however, would probably cause phototoxicity to some extent.

To circumvent the issue of background activity, Mitchison and coworkers[125] used a photocaged (6-nitroveratryl ether), photoactivatable derivative of **CA4** (Fig. 11b). Illumination with 405 nm resulted in cleavage of the photocage and release of the active inhibitor which was used to study asters and cleavage planes in amphibian and fish embryos.

In 2015, Trauner and Thorn-Seshold[24] reported the first tubulin inhibitor whose activity can *reversibly* switched on and off (**PST1**). Chemically, **PST1** is an analogue of **CA4** in which the stilbene double bond is isosterically replaced with a diazene (azologization, Fig. 11c). This enables *E*-*Z* isomerization with wavelengths more suitable for cell culture applications than those necessary for isomerizing **CA4**.[82] ***Z*-PST1** is a potent antimitotic (IC_{50} = 500 nM)[24] that leads to G2/M arrest and ultimately cell death while ***E*-PST1** is essentially inactive (at least 200-fold less potent[126] , Fig. 11d-f). **PST1** has enabled non-invasive, reversible and light-dependent modulation of the MT network and was successfully applied in neuroscience[127], to study cellular shape and coherence in migrating amoeboid cells[128] and embryonic development in mice.[129]

A scaffold-inherent limitation for the use of **PSTs**, however, is their susceptibility to GSH degradation with the *Z*-isomer being more labile.[130] This conceptual limitation can, however, be overcome by replacement of the azobenzene with a styrylbenzothiazole (Fig. 12).

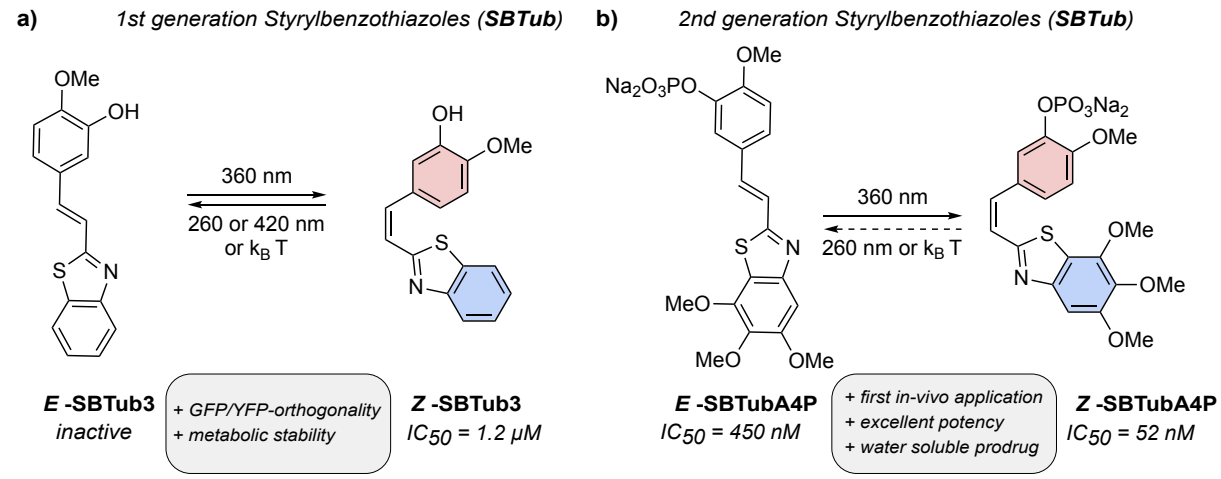

Fig. 12: SBTubs are styrylbenzothiazole derivatives of CA4. a) First-generation **SBTubs** are metabolically stable and GFP/YFP- orthogonal photoswitchable MDAs. b) Second-generation **SBTubs** are highly potent and as their phosphate prodrug water-soluble MTAs which were applied *in vivo*.

The resulting first-generation **SBTubs** (Fig. 12a) were shown to isomer-dependently inhibit cell division and sub-cellularly modulate MT dynamics but, in contrast to **PST1,** resisted GSH-mediated degradation in both isomeric states. Additionally, **SBTubs** show no absorption bands > 470 nm and thereby enable experiments without interfering with imaging techniques using fluorescent protein tags, such as GFP or YFP. However, drawbacks of the first-generation **SBTubs** were unidirectionality of their photoactivation under cellular conditions and low potency.[52] In a follow-up study, Gao, Thorn-Seshold and coworkers performed SAR studies, thereby identified highly potent inhibitors and synthesized a water-soluble prodrug of one of their lead compounds (Fig. 12b).[48] These second-generation **SBTubs** are photoswitchable MDAs that were successfully applied in cell culture (2D and 3D), in fly brain explants and early-stage animals (clawed frog and zebrafish). This is a significant contribution to the field and a milestone towards *in vivo* photopharmacology since before no photopharmaceuticals had been available for which global administrations (i.e., in the whole animal) and local activations were achieved.

2.3.2.2 Challenges for tubulin photopharmacology

Despite these impressive advances, some challenges for tubulin photopharmacology still remain.

1) ***Visible-light powered optical control over the MT network:*** As outlined earlier, UV light comes with the drawbacks of potential phototoxicity and low penetration depths into biological tissue. For tubulin photopharmaceuticals to advance to *in vivo* applications for animals (like mice), it would be desirable to have tools at hand which can be completely operated with visible light.
2) ***Design control over the bioactive isomer:*** Most photoswitches undergo large changes in geometry and sterics upon isomerization. While this is desired in many

cases, it is often the sterics of the protein's binding site rather than rational design that decides whether a tool is *lit* or *dark*-active. It would therefore be a valuable addition to photopharmacology in general to have scaffolds which can be designed at will to be active as one or the other isomer.

3) ***High-potency photoswitchable tubulin inhibitors:*** Tubulin inhibitors are cytotoxic compounds with several side effects and photoswitchable tubulin inhibitors are no exception to this. Additionally, photoswitches often suffer from low aqueous solubility (and thus also in cell culture media). Having highly potent inhibitors at hand, would reduce the necessary concentration in experiments. This would be beneficial in both reducing off-site activity and overcoming solubility issues.
4) ***Expanding the functional group tolerance of tubulin photopharmaceuticals:*** As outlined earlier, substitution of azobenzenes with electron-donating, tautomerizable groups in *para*-position leads to negligibly short half-lives of the metastable isomer. This hampers the application of azologization strategies to some tubulin inhibitors, like indanocine.[131] It would be therefore a valuable addition to the 'toolbox of tubulin photopharmacology' to have a scaffold amenable to this substitution pattern.
5) ***Avoiding background activity by near-quantitative photoswitches:*** Photoisomerization is rarely quantitative. For a *lit*-active compound, this would mean that, even in the best-case isomerization, a considerable portion of inactive isomer remains which leads to higher IC_{50} and thus lower photoswitchability of activity. This is even more problematic for a *dark*-active compound. Incomplete photoisomerization only partially inactivates the inhibitor leading to substantial undesired background activity. In both cases, genuine improvements would be possible by photoswitches with bidirectional near-quantitative isomerization.
6) ***Developing tools for live-cell imaging***. Microtubules are highly dynamic structures. To study their involvement in cellular processes, it would be highly desirable to develop compounds suitable for live-cell imaging.

3. Aims of the doctoral thesis

As outlined earlier, azobenzenes have been the benchmark photoswitch in photopharmacology and have enabled the optical control over a huge variety of targets.[20,21,24,25,132]

However, despite their impressive performance, especially in modulation of membrane-localized targets (GPCRs[20], ion channels[19], and lipids[21]), azobenzenes are by no means ideal photoswitches. Scaffold-inherent limitations of azobenzene photopharmaceuticals include the need for potentially phototoxic UV light, incomplete photoisomerization, incompatibility with certain functional groups, and metabolic lability.

The main aim of this doctoral thesis is therefore the development of photoswitchable tubulin inhibitors that overcome some of the limitations associated with azobenzene photoswitches. For this purpose, HTIs were chosen as alternative scaffold. HTIs are emerging photoswitches with a set of promising features (see chapter 2.2.2.3) but have previously been used only very scarcely in photopharmacology.[54,55]

This thesis aims at the transition of HTI-based tubulin photopharmaceuticals from first proof-of-concept studies to successful application in live-cell imaging.

Key emphasis was put on tools which can be operated by visible light and for which design control over the bioactive isomer (*lit* vs. *dark*-active compounds) was possible (**HOTubs**). Then focus was placed on potency enhancement (**HITub**), and finally on development of bidirectionally near-quantitative tools that could be applied with single-cell precision (**PHTubs**).

Additionally, all hitherto known tubulin targeting photopharmaceuticals[24,48,52,53,130,133] were classical orthosteric inhibitors of the α/β-tubulin heterodimer. To expand the scope of tubulin photopharmacology, I also performed one side project directed towards optical control over γ-tubulin (**phatastatin**), an isoform involved in nucleation of microtubules.[134,135] A separate approach tackled in another side project was to modulate the activity of MTs not by orthosteric inhibition, but by targeted protein degradation of the tubulin protein itself. For this, I also included optical control elements in order to avoid global toxicity, so synthesizing photochemically targeted proteasomal degraders of tubulin (**TubPHOTACs**). This project was conducted in the context of an exchange at New York University in the group of Dirk Trauner.

In the following chapters, I will present my work on HTI-based α/β-tubulin addressing photopharmaceuticals (**Papers One**, **Two** and **Three**), towards γ-tubulin specific photopharmaceuticals (**phatastatin**), and towards optical control over the proteasomal degradation of tubulin (**TubPHOTACs**).

4. Author contributions

The following section covers my personal contribution to the three published papers.

Paper One: HOTubs offer rational design control over the bioactive isomer

I performed parts of the chemical syntheses and chemical characterizations, and all photocharacterizations (PSS and reversibility spectra). I determined PSS composition using NMR spectroscopy, assembled the data, and prepared parts of the figures. I contributed to writing the manuscript.

Paper Two: HITubs are highly potent photoswitchable tubulin inhibitors

I performed most of the chemical syntheses and chemical characterizations. I performed all photocharacterizations (PSS, reversibility, and relaxation spectra). I coordinated data assembly, prepared parts of the figures and contributed to writing the manuscript.

Paper Three: PHTubs are near-quantitative photoswitchable tubulin inhibitors suitable for live-cell imaging

I proposed the PHT photoswitch and designed the SAR study and performed all chemical syntheses and characterizations. I performed all photocharacterizations (PSS, reversibility, and relaxation spectra). I also determined PSS compositions and GSH stability and assisted in performing *in vitro* tubulin polymerization assays. I advised collaboration partners, coordinated data assembly and I contributed to writing the manuscript.

5. Paper One: HOTubs offer rational design control over the bioactive isomer

We started our investigations towards HTI-based photoswitchable tubulin inhibitors by applying the SAR requirements of a CDI to the HTI scaffold, in an approach similar to the azologization strategy used for **PSTs** (see chapter 2.2.2.2). The distance between the two aromatic rings is larger for HTIs than it would be for stilbenes or azobenzenes. It is, however, known that a variety of inter-ring bridges, including heterocycles, are tolerated without loss of potency as long as the correct substitution pattern and the '*cisoid'* connection are followed (see chapter 2.3.1.3).[116] We thus reasoned that insertion of additional distance would not substantially alter tubulin binding.

Importantly, HTIs are almost completely planar in both isomers[136] which differentiates them from azobenzenes where isomerization induces large changes in geometry. This enables only one azobenzene isomer to occupy the POI binding site. As a result, it is often the sterics of

the binding site rather than rational design that decides which isomer is the bioactive one. The difference to HTIs is essential: both HTIs isomers could bind the POI as long as their substitution pattern is in line with the SAR requirements, while isomer-intrinsic steric effects on binding can be neglected. We therefore anticipated that it was possible to decorate either the *E* or the *Z*-isomer of an HTI with the SAR motif and thus create either *lit*- or *dark*-active compounds (Fig. 13). Such a strategy would permit rational design control over the isomer-bioactivity relationship.

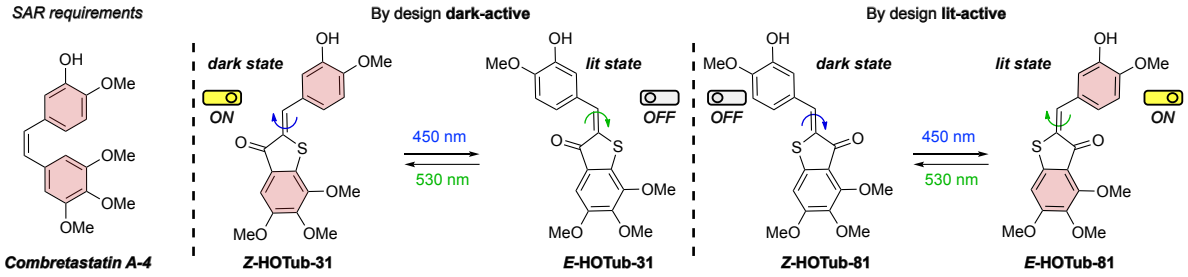

Fig. 13: Design logics of HOTubs. Planarity of both photoisomers allows for rational design control over the bioactive isomer. Matching design goals, **HOTub-31** and **HOTub-81** were active in the dark and after illumination, respectively.

Based on these assumptions, we designed a study consisting of seven compounds (**HOTubs**) of which four were expected to be active in either of their two isomers. The remaining three compounds intentionally violated the pharmacophore model and were used to control for unspecific toxicity of the HTI scaffold (permutation controls).

For the potentially active compounds, we found that it was more practical to map the trimethoxybenzene substitution onto the stilbene and the isovanillyl motif onto the thioindigo half. This resulted in **HOTub-31** (obeying the SAR as its *Z*-isomer) and **HOTub-81** (obeying the SAR as its *E*-isomer). To our delight and in accordance with our design, we found **HOTub-31** to be more cytotoxic in the dark (IC_{50} = 1 µM in the dark vs. IC_{50} = 4 µM after illumination with 450 nm). In line with our understanding of **HOTubs** as MDAs, we additionally observed that **HOTub-31** led to disruption of the MT network and G2/M arrest in the dark. Pleasingly and following our design goals, **HOTub-81** was more potent after illumination with 450 nm (IC_{50} = 2 µM, majority of *E*-isomer after illumination with 450 nm, vs. IC_{50} = 4 µM in the dark).

Our findings confirmed our initial hypothesis that HTIs are a valuable scaffold for photopharmacology, and this study was the first real application of HTIs in long-term cellular assays. Furthermore, we could solve two of the challenges for tubulin photopharmacology (see chapter 2.3.2.2), namely the design control over the bioactive isomer and the creation of tools that are entirely powered by visible light.

ChemPubSoc Europe

DOI: 10.1002/cbic.201800752

CHEMBIOCHEM Full Papers

Hemithioindigos for Cellular Photopharmacology: Desymmetrised Molecular Switch Scaffolds Enabling Design Control over the Isomer-Dependency of Potent Antimitotic Bioactivity

Alexander Sailer[+], Franziska Ermer[+], Yvonne Kraus[+], Ferdinand H. Lutter, Carsten Donau, Maximilian Bremerich, Julia Ahlfeld, and Oliver Thorn-Seshold*[a]

Dedicated to G. R. "Bob" Pettit on the occasion of his 90th birthday

Druglike small molecules with photoswitchable bioactivity—photopharmaceuticals—allow biologists to perform studies with exquisitely precise and reversible, spatial and temporal control over critical biological systems inaccessible to genetic manipulation. The photoresponsive pharmacophores disclosed have been almost exclusively azobenzenes, which has limited the structural and substituent scope of photopharmacology. More detrimentally, for azobenzene reagents, it is not researchers' needs for adapted experimental tools, but rather protein binding site sterics, that typically force whether the *trans* (dark) or *cis* (lit) isomer is the more bioactive. We now present the rational design of HOTubs, the first hemithioindigo-based pharmacophores enabling photoswitchable control over endogenous biological activity in cellulo. HOTubs optically control microtubule depolymerisation and cell death in unmodified mammalian cells. Notably, we show how the asymmetry of hemithioindigos allows a priori design of either *Z*- or *E*- (dark- or lit)-toxic antimitotics, whereas the corresponding azobenzenes are exclusively lit-toxic. We thus demonstrate that hemithioindigos enable an important expansion of the substituent and design scope of photopharmacological interventions for biological systems.

Introduction

Druglike small molecules with photoswitchable bioactivity—photopharmaceuticals—can deliver outstandingly precise spatial and temporal control over critically important biological systems.[1] Photopharmacology has been applied to a range of studies from cell-surface-acting ligands actuating ion channels[2] and GPCRs[3] in neuroscience, to intracellular ligands modulating metabolic[4] and epigenetic[5] enzymes, as well as the cytoskeletal scaffolding protein tubulin.[6] In all these applications, it is the ability to reversibly and noninvasively modulate biological functions independently of drug biodistribution and with high spatiotemporal precision, that brings the key conceptual advantages of photoswitch pharmacology, as against irreversible (uncaging) or slowly-reversible (wash-in/wash-out) methods.

Photopharmacology's most advanced applications are probably in transmembrane receptors, where photoswitches that trigger action potential firing upon photoisomerization to the metastable (lit) state, but relax rapidly to a non-triggering, thermodynamic (dark) state when illumination is removed, have been developed to photosensitise otherwise non-responsive neurons in the retina and restore visual response in blind animals.[7] The approximately millisecond timescale of these photoswitches' spontaneous relaxation perfectly matches the temporal scale of the desired biological control, so combatting spatial diffusion of the isomer patterning established by photoswitching is not needed and unidirectional photocontrol suffices for performance.

However, in intracellular applications, longer-timescale phenomena often associated to downstream pathways are more typically of interest, such as the biological consequences of enzymatic activity or protein relocalisation. Therefore, greater longevity of the metastable isomer is usually desirable to maintain isomer patterning over the experimental time course without repeated illuminations that cause intracellular photodamage to the system under study and/or imaging marker. The conceptually unique biological research applications of such photopharmaceuticals (especially in multicellular systems) then typically involve patterning the isomers in space and/or over time, by two-colour illuminations. Such spatiotemporally reversible two-colour patterning has notably allowed complex studies in em-

[a] *A. Sailer,[+] F. Ermer,[+] Y. Kraus,[+] F. H. Lutter, C. Donau, M. Bremerich, Dr. J. Ahlfeld, Dr. O. Thorn-Seshold*
Department of Pharmacy, Ludwig-Maximilians University Munich
Butenandtstrasse 5–13, Munich 81377 (Germany)
E-mail: oliver.thorn-seshold@cup.lmu.de

[+] *These authors contributed equally to this work.*

Supporting information and the ORCID identification numbers for the authors of this article can be found under https://doi.org/10.1002/cbic.201800752.

This article is part of the young researchers' issue ChemBioTalents. To view the complete issue, visit http://chembiochem.org/chembiotalents

bryology and development, where precise bidirectional switching was employed to subcellularly resolve the organisation of tubulin[8] and its interplay with the actin cytoskeleton[9] in early mouse embryos. In such bidirectional-switching applications, it is crucial for practical success that the metastable isomer be designed to be the more bioactive form, so that maintaining a "non-inhibited" background of activity in the organism does not require repeated illuminations scanning through the entire sample (but only localised illuminations in the area to be affected), and so that moderate spontaneous relaxation rates can help to suppress the accumulation of background levels of the active isomer.

However, no method yet exists for researchers to force the lit state of a photoswitchable ligand to be bioactive and avoid a background of bioactivity from its dark state, or vice versa, at will. We have addressed this conceptual gap by developing photopharmaceuticals around a relatively untried scaffold, with the purpose of delivering both dark- and lit-active compounds against the same protein target following rational design, and evaluating their photocontrol over endogenous biological function in cellulo.

The progress, and the definition, of photopharmacological research have expanded greatly in recent years and the field has been multiply reviewed.[10] In this work, we concentrate on photopharmacological design principles promoting translation through in cellulo to in vivo applications and enabling conceptually novel biological research on a range of extra- and intracellular targets. For this we define "narrow" photopharmacology as: druglike small molecules obeying the Lipinski rules, whose bioactivity can be reversibly modulated to a significant degree through bidirectionally photoreversible isomerisation. Although this definition excludes several noteworthy strategies, such as ligand bioactivity photoswitching that depends on modulating secondary structure elements in larger constructs,[11] we feel it usefully restricts the discussion to a major research area that faces common challenges.

Two main approaches have been used to deliver isomerically dependent changes of protein affinity in "narrow" photopharmacology: 1) The photoswitch is directly appended onto a druglike pharmacophore with the aim that isomerisation impacts the steric access of the pharmacophore to its binding partner,[12] which in the context of azobenzenes is called "azo-extension"; 2) The photoswitch is embedded entirely inside the most critical part of the pharmacophore, which in the context of azobenzenes is called "azologization".[1b] As far as possible, embedding approaches would seem the more rational design, and have been shown to deliver significant differences between the potencies of the more- and less-bioactive isomers ("photoswitchability of bioactivity") in a variety of cellular and organism-based settings.[6]

The repertoire of molecular photoswitches is large, and many have been reported as photoswitch concepts (especially for cell-free in vitro studies); for example, photoswitch concepts depending on fulgides,[13] stilbenes,[14] and diarylethenes[15] have been reported for an interesting range of biological targets. However, azobenzenes remain essentially the only photoswitch to have been validated as a photopharmacological scaffold through multiple in cellulo to in vivo biological applications. The reasons for azobenzenes' reliable performance are well known,[10] but the lack of alternative scaffolds has hampered progress in the field in several ways. Principally, although the large differences between *cis* and *trans* azobenzene sterics have allowed impressive photoswitchability of bioactivity in some endogenous cellular systems (up to >250-fold[6]), it also has the consequence that if a given binding site significantly better accommodates one isomer than the other, it is unlikely that redesigning the substituent pattern on the azobenzene will allow a reversal of isomer preference. Since the drugs that are basis scaffolds for azologization are often "med chem"-like substructures which mainly bind their targets in *trans*-like states (e.g., benzanilide, stilbene or benzyl phenyl ether-type scaffolds), many of the resulting azologues are therefore *trans*- (that is, dark-) active; and even azo-extension approaches often result in *trans*-active compounds.[16] Yet dark-active compounds face severe disadvantages as photopharmaceutical tools for intracellular research applications, principally due to their permanent background of activity despite partial photoswitching to the metastable state, as well as handling difficulties. Recently, ethylene-bridged azobenzenes (diazocines)[17] which feature a *cis*-like dark state and a *trans*-like lit state have made much synthetic progress; but while their potential to act as lit-active alternative scaffolds where linear azobenzenes are *trans*-active is tantalising, their cellular potential has not yet been demonstrated.

We reasoned that if a single isomerisable scaffold is intended to support the design of embedded-pharmacophore ligands with *either* lit- or dark-state bioactivity according to taste, its isomers must offer a nearly superimposable pattern of sites for attaching substituents, and so should be nearly flat in both isomeric states. We therefore selected the hemithioindigo (HTI) photoswitch as a robust, optically well-characterised, photostable and photoreversible molecular switch[18] in which the relative positions of the centroids of the two aryl rings are nearly identical in the *Z* (dark) and *E* (lit) isomers due to the near-planarity of both forms. HTIs bear four potential substituent sites on the thioindoxyl motif and five on the hemistilbene, so we considered it potentially adapted for pharmacophore embedding in most situations where azobenzenes also suc-

Oliver Thorn-Seshold studied chemistry at the University of Sydney and did his PhD in bioorganic chemistry of enzyme-responsive probes with Prof. Jens Hasserodt at the ENS Lyon. In 2013, he joined Prof. Dirk Trauner's lab at LMU Munich where he developed azobenzene-based photoswitchable inhibitors for cytoskeleton research. Since 2016, he has been an independent research group leader at the LMU Munich. His research interests include cellular and in vivo applications of photopharmacology, and tools to study and respond to cellular redox biology.

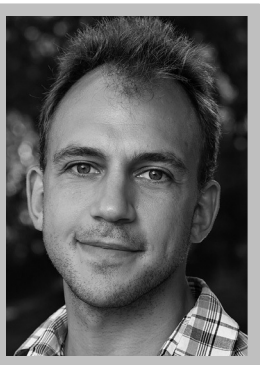

ceed. Hemithioindigos oriented towards chemical biology applications (rather than in lipid physical chemistry[19]) have mainly been employed as photoswitchable bridges or cross-linkers for conformational photoswitching of peptides;[18,20] some designs for photoswitch-appended polypeptides have also been reported.[21] To our knowledge, only one druglike application of HTIs has been reported, where Kühn and co-workers[22] performed a short-term test comparison of the HPLC-separated *E* and *Z* isomers of a carboxylate-bearing HTI for their capacity to inhibit oxidation of linoleic acid in human monocytes transfected to express rabbit 12/15-lipoxygenase, with assays run over 15 min. Their reports showed an assay readout differential of about 1.3- to 1.7-fold between *E* and *Z* isomers, although the compound could not be applied above 4 μM. We considered that this state of the art left much to be done towards the rational design and long-term, in situ-photoswitched biological evaluation of HTIs for cellular photopharmacology.

We therefore desired to test whether the hemithioindigo scaffold could be applied to create potent, reversibly photoswitchable, bioactive compounds for the challenging scenario of intracellular biological applications to endogenously expressed proteins, and we selected tubulin as our target. Cellular tubulin is in a constant state of flux, being continually (non-covalently) polymerised into and depolymerised from microtubules. These critical structures are tightly spatially and temporally coordinated, to drive a variety of anisotropic cellular scaffolding roles, from continual intracellular cargo trafficking, to cell migration in motile cells, through to separation of chromatids and daughter cells during cell division.[23] The requirement for correctly functional microtubule dynamics during mitosis has driven extensive work on targeted and selective microtubule-binding agents as "antimitotic" cancer chemotherapeutics, including paclitaxel, epothilone and vinca alkaloids.[24] In research, the sheer breadth and spatiotemporal complexity of microtubule-dependent biological roles presents an excellent opportunity for photopharmacological intervention, and microtubule-targeting photopharmaceuticals such as PST-1[6] have quickly moved on from chemical proof-of-concept[25] to find diverse cellular[26] and animal research applications.[8,9,27] Due to the massive clinical utility of microtubule-binding agents in cancer therapy, as well as the systemic side-effects of conventional antimitotics, it is also of extensive interest to find more potent photoswitchable microtubule inhibitors[28] and evaluate whether they can be guided by localised tumour illumination to act as tumour-specific antimitotics that spare healthy tissues from chemotherapeutic damage. Successful HTI-based antimitotics could therefore find applications as tools for the cytoskeleton research field, but the opportunity to scaffold-hop from known PST azobenzenes while retaining photoswitchable bioactivity was also of interest for translational applications.

Results

Design and rationale

Extensive structure–activity relationship (SAR) studies across a range of chemotypes[29] as well as recent progress in X-ray crystallography[30] have clarified the structural requirements for tubulin inhibitors binding at the colchicine site (Figure 1 A), and this recommended it to us as a target for the development of HTI-based inhibitors. Prototypically, the important interactions of the colchicinoid pharmacophore (Figure 1 B) are established from a trimethoxyphenyl "south" ring and a methoxyphenyl "north" ring; all contacts involve the β-tubulin subunit except for one contact from the north ring to flexible

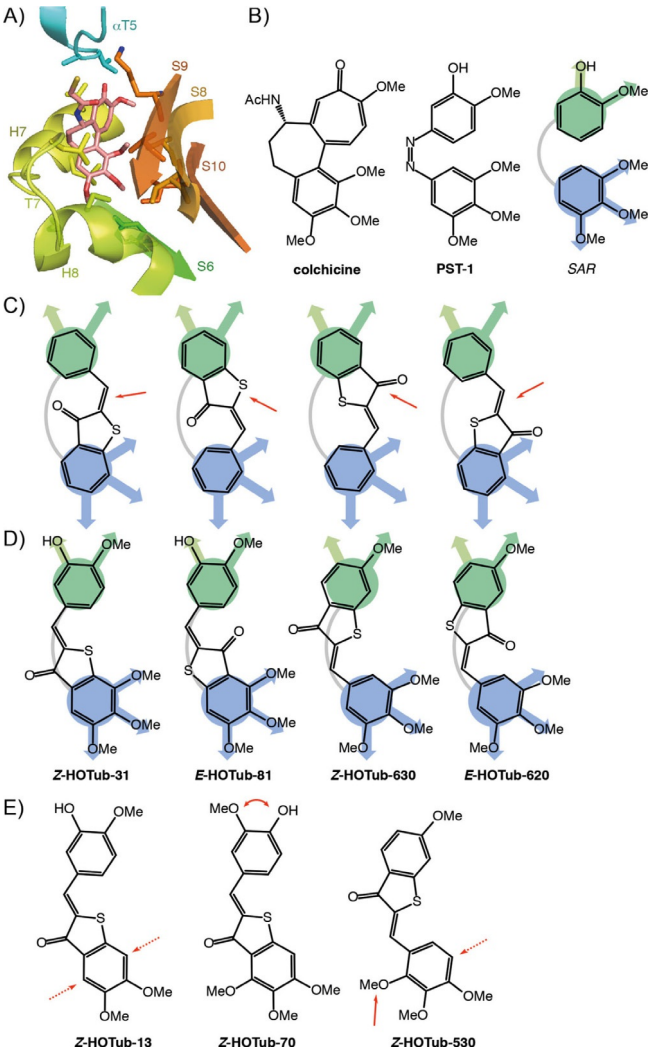

Figure 1. A) *N*-deacetyl-*N*-(2-mercaptoacetyl)-colchicine (DAMA-colchicine) in its binding site on α/β-tubulin with local secondary structure elements annotated and close-contact amino acids depicted (PDB ID: 1SA0[35]). B) Colchicine, PST-1, and a simplistic pharmacophore model. C) The four rejected orientations of HTI mapping onto the colchicine site pharmacophore, with red arrows highlighting the steric clashes anticipated to be detrimental for binding. D) The four HTI mappings remaining were decorated with substituents to match the SAR, giving HOTubs. E) Control structures designed to show no isomer-dependent binding (or no binding), with predicted detrimental groups indicated with red arrows.

loop T5 on the α-subunit. Notably, for our designs the rings can be linked with molecular bridges ranging from the very short (biaryls like colchicine or single atom bridges such as a carbonyl group[31]) through to sizable *cis*-C=C double bonds[32] or even small heterocycles[29] without substantial impact on potency, as long as no atoms of the bridge abut the rigid wall formed by β-sheet strands S8/S9. The only general potency-enhancing substitution is to add a small electronegative substituent (OH, F, NH_2) in *ortho* to the methoxy group on the north ring, pointing away from the S8/S9 wall. Noteworthily, the south ring tolerates neither the introduction, removal, nor permutation of a substituent from the 3,4,5-trisubstituted template; the north ring is slightly more tolerant of changes but introducing groups abutting into S8/S9 essentially abolishes binding. This preferred substituent pattern for close colchicine analogues is shown simplified in Figure 1B; but the binding domain is highly plastic, and accommodates a surprising range of structurally distinct small molecules whose interactions can be difficult to predict.[33] Colchicine domain binders display a limited range of tubulin-disrupting IC_{50} values as determined against purified enzyme in vitro, with only around a fivefold difference apparent between potent binders such as combretastatin A-4 (CA4, IC_{50} ~2 μM) and binders considered weak; yet their EC_{50} values for antiproliferative/cytotoxic activity in cell culture span many orders of magnitude (typically ~10 nM for CA4 and up to 5 μM for colchicine in the same human cell line).[29] A likely explanation is that, as is known for CA4, variable but potentially strong cellular bioconcentration from the extracellular medium as well as sensitive biolocalisation effects within the cell, are substantially more important for observed cell culture potencies in these agents than their K_i against purified enzyme.[34]

To embed HTIs into this pharmacophore, we hypothesised that the relatively long "bridge" between the two phenyl rings would be accepted if the substituent pattern SAR for colchicinoid binders was respected. Without using exact bond geometries, we naively examined the eight potential mappings of the HTI scaffold's lit and dark isomers onto this pattern, and eliminated those which projected the bridging double bond towards the S8/S9 wall and/or did not allow us to map the correct trisubstituted geometry on the south ring (Figure 1C). This left two mappings in the *E* state and two in the *Z* state: that is, two potential lit-state and two potential dark-state bioactives, of which one each was in the "top-down" and one each in the "bottom-up" configuration. We named these HOTubs (Hemithioindigo-cOlchicinoid Tubulin binders).

We expected that orienting the carbonyl group towards the S8/S9 wall (e.g., *E*-HOTub-81) might slightly reduce potency compared to orienting it away (*Z*-HOTub-31), but were hopeful of observing bioactivity nonetheless. We considered the "bottom-up" orientation fixing the hemistilbene motif (easier to diversify) as the north ring (more tolerant) to be particularly desirable for synthesis. For the initial study, we decided to simplify the "top-down" scaffolds by deleting the optional hydroxy group on the north ring, since we anticipated that the relatively vigorous conditions needed for ring closure of the thioindoxyl, plus the sensitivity of HTIs towards nucleophilic attack, would otherwise make the choice of a protecting group to carry through the synthesis difficult. This simplified the "top-down" targets to HOTub-620 and HOTub-630; the "bottom-up" targets HOTub-31 and HOTub-81 were retained with the OH group in the expectation of improved water solubility and potency (Figure 1D). We also designed three "intentional negative control" compounds by molecularly small permutations which according to our SAR understanding ought to abolish specific on-target bioactivity (Figure 1E). We believe this is a valuable general concept for reliable photopharmacology. In the case of HOTubs, as tubulin is critical for cell survival it is impossible to create a "tubulin knock-out" with which to confirm that photoswitching in the absence of the intended target has no biological effect. We instead wished to use these negative control compounds to estimate whether our SAR understanding was correct, in that these key substituent changes would abolish tubulin-specific bioactivity; if so, it would also support that our rational design approach is valid for installing tubulin-specificity. It is important that the changes are small—ideally only regioisomeric permutations—since the resulting close regioisomers could then be expected to show near-identical cellular accumulation and biolocalisation. In this way, the control can then be used as a quick assessment for whether aggregation, membrane-modulation, phototoxicity inside cellular reservoirs where the compounds can be expected to accumulate (e.g., in lipid vesicles), or other confounding effects (such as CALI-type photodamage[36]) are potential problems. Accordingly, HOTub-13 was designed relative to HOTub-31 and HOTub-81 by removing one of the three south ring methoxy groups we estimated necessary for potent binding, which still could permit docking of the compound and then photoreactivity with the protein if that were problematic. HOTub-530 was designed as a single permutation regioisomer of HOTub-630 and a double permutation regioisomer of HOTub-620, allowing it to have similar solubility and biodistribution but intended to abolish tubulin binding; we viewed HOTub-70 not only as a regioisomer of HOTub-31 but also as a control that the orientation in which we mapped the HTI scaffold was appropriate.

Synthesis and photocharacterisations

HTIs are conveniently synthesised by aldol condensation of the corresponding thioindoxyls and benzaldehydes.[37] We first explored the synthesis of our thioindoxyls by intramolecular acylation of the phenyl ring in 2-(phenylthio)acetic acid derivatives. Although preparation of 2-(phenylthio)acetic acids is facile, common cyclisation methods (Friedel–Crafts acylation of the acid chloride, or dehydrative cyclisation with Eaton's reagent) gave only poor yields in our hands. We therefore explored thioindoxyl synthesis by deprotonation of the acidic *S*-methyl group in methyl phenyl sulfides bearing *ortho*-carboxylate derivatives by using lithium diisopropylamide (LDA) followed by intramolecular acylation of the carbanion,[38] which we found to give drastically better yields and easier workup. We typically synthesised the deprotonation–cyclisation precursors by magnesium–halogen exchange on iodophenyl deriva-

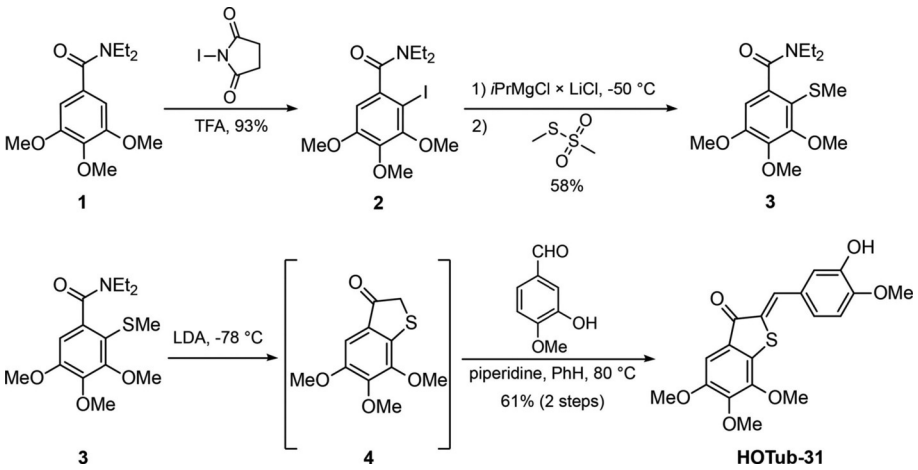

Scheme 1. Synthesis of representative compound HOTub-31 (see also Supporting Information).

tives with Turbo-Grignard,[39] followed by electrophilic quenching with methyl chloroformate (for *ortho*-iodophenyl methyl sulfides) or with $MeSSO_2Me$ (for *ortho*-iodobenzoic acid derivatives).

We tested several condensation reaction conditions, including 1) condensation with amphoteric dehydrating catalysis using aluminium oxide in dry chlorinated solvents, 2) condensation in dry refluxing benzene with piperidine catalysis, and 3) condensation in refluxing NaOH/*t*BuOH.[37] Of these, the benzene/piperidine conditions typically gave the highest isolated yields. Some HTIs decomposed on silica, but we found their relatively low water solubility could be harnessed for purification, by precipitating them from DMSO solutions of crude material. All HOTubs were reached typically on 100 mg scale (see the Supporting Information); a representative synthesis is shown in Scheme 1.

The typical photochemical behaviour of hemithioindigos has been reviewed by Dube and co-workers.[18] We did not expect unusual performance for the polymethoxylated HOTubs so we photocharacterised them pragmatically to qualitatively estimate parameters for later biological applications. Primarily we wished to determine their photostationary state (PSS) compositions—the equilibrium proportion of *E* and *Z* isomers established under saturating illumination at specified wavelengths—to select optimal switching wavelengths for cellular work. For PSS quantification, we initially illuminated samples at various wavelengths then separated the *E* and *Z* isomers by analytical HPLC, quantifying their proportions with an inline diode array detection at an isosbestic point wavelength. However, we determined that UV/Vis spectrophotometry was substantially more accurate in repeatably (<1% deviation) determining small changes to the *E*/*Z* ratios in samples. Determining PSS by spectrophotometry required HOTub solution concentrations well above their aqueous solubility limit (as do NMR measurements), so we constrained our measurements to water-cosolvent mixtures. We do not assume that the average cellular PSS or relaxation rates for HTIs will be identical to those determined in cuvette measurements, as in cellulo HTIs will be in heterogenous environments depending on cellular biolocalisation (e.g., into lipid membranes or aqueous cytosol) and the absorption band intensities and positions, quantum yields of photoisomerisations, and the thermal *E* to *Z* relaxation rate are all known to be solvent dependent.[40] However, we expected that the trends of PSS wavelength dependency as measured in UV/Vis would reasonably correspond to those in the cellular context. We therefore acquired PSS spectra by UV/Vis spectrophotometry (Figure 2 A), and using NMR reference measurements we calibrated and compared PSSs in the visible region

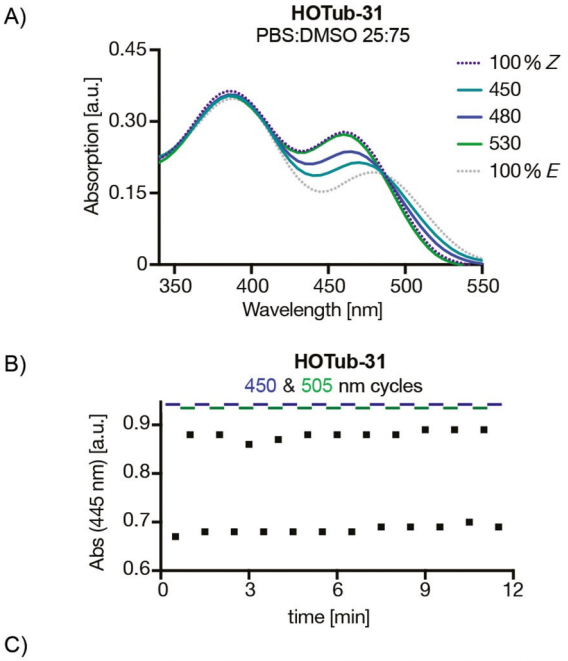

λ [nm]	385	420	445	450	470	480	490	505	530
PSS %Z	62	53	41	35	51	62	68	77	97

Figure 2. A) Typical PSS spectra of HOTub-31 measured in PBS:DMSO 25:75, under saturating 450 nm, 480 nm, and 530 nm illumination, with back-inferred 100% *Z* and 100% *E* spectra. B) Photoreversible switching measured by UV/Vis spectrophotometry, under alternating 450 nm and 505 nm illuminations. No photobleaching was observed after 285 switching cycles. C) Measured PSSs over 385–530 nm, in PBS/DMSO 25:75.

(420–530 nm) to find optimal wavelengths for biological photoswitching applications (Figure 2C).

Rather than highly monochromatic light, we used LEDs with about 15 nm FWHM emission bandwidth for these measurements, similarly to how we intended to perform long-term biological assays. The ratio of the two isomers' photoisomerisation quantum yields, Φ, depends on which band is excited, and rough calculations from PSS spectra show that in the $S_0 \rightarrow S_1$ band (covering ~430–540 nm) the ratio $\Phi_{E\rightarrow Z}/\Phi_{Z\rightarrow E}$ is approximately 1.6, and in the $S_0 \rightarrow S_2$ band (~340–430 nm) the $\Phi_{E\rightarrow Z}/\Phi_{Z\rightarrow E}$ ratio is about 0.9. According to calculations from the 75:25 DMSO/PBS solution measurements (Figure 2A), illumination with 450 nm gave the highest PSS content of metastable *E* isomer (65% *E*) and illumination at 530 nm reached a PSS of ~97% *Z*, both within 30 s illumination. In this solvent mix at 37 °C, the spontaneous relaxation half life of *E*-HOTub-31 was approximately 30 min. We also performed extended tests of photoreversible photoswitching in 75:25 DMSO/PBS in a non-degassed solution open to air, as one method to examine whether photodegradation could be problematic for in cellulo biology. Under these conditions we observed highly repeatable photoreversible switching (Figure 2B) that encouraged us to begin cell culture photoswitching applications.

A)

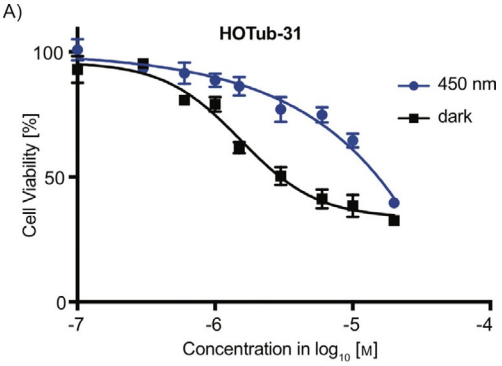

B)

compound	450 nm EC_{50} [μM]	dark EC_{50} [μM]	lit-dark ratio
HOTub-31	4.0	1.0	4.0
HOTub-81	2.1	3.9	0.5
HOTub-620	n.d. (>10)	n.d. (>10)	n.d.
HOTub-630	11	4.5	2.4
HOTub-70	n.d. (>20)	n.d. (>20)	n.d.
HOTub-530	n.d. (>10)	n.d. (>10)	n.d.
HOTub-13	7.3	7.9	0.9

Figure 3. A) Representative MTT antiproliferation assay in HeLa cell line, for HOTub-31, showing the strong difference between antimitotic potencies under 450 nm and dark conditions. B) Cellular antiproliferation EC_{50} values for the HOTubs under 450 nm and dark conditions, with the ratio of lit to dark EC_{50} values calculated, to highlight the fold change of photoswitchable bioactivity.

Photoswitchability of bioactivity in cellulo

Inhibitors of tubulin dynamics act as antimitotic cytotoxins in cell culture, allowing cell viability to serve as a proxy readout for their antitubulin potency in the cellular context. To evaluate the isomer dependency of in cellulo bioactivity of HOTubs we therefore began by assaying their cellular antiproliferative activity, under repeated in situ photoswitching conditions. We used HeLa cervical cancer cells as a cell line representative of the general responses of mammalian cells to tubulin inhibitors. We used self-built arrays of low-intensity LEDs[6] to deliver illuminations with relatively narrow spectral bandwidth, pulsing them once per minute during the entire experimental timeframe to maintain PSS equilibria in cellulo. We initially compared illumination responses under a range of wavelengths from 380–530 nm and dark conditions, and observed that, as expected from the PSS determinations, 450 nm and dark (or, equivalently, 530 nm) illuminations delivered the greatest differences in potency. We therefore concentrated on comparing 450 nm and dark results. We were delighted to observe that the "bottom-up" oriented, hydroxyl-bearing HOTub-31 and HOTub-81 showed potent and repeatable cellular cytotoxicity well below their precipitation threshold, but with sign inversion: HOTub-31 was "dark-toxic" with fourfold photoswitchability of bioactivity (Figure 3A) while HOTub-81 was "lit-toxic", which matched our molecular design goals. Importantly, the permutation control compound HOTub-70 was completely inactive below 20 μM under 450 nm and dark conditions, suggesting that the scaffold design has no significant nonspecific toxic effects as either isomer or in response to illumination. The methoxy-group deletion control compound HOTub-13 was observed to aggregate out of solution at 10 μM, and showed an only gently sloping cytotoxic response (low Hill coefficient) at higher concentrations which we suggest is due to aggregation toxicity not specific binding; we have previously observed that, as compared to 1,2-dimethoxy or 1,2,4-trimethoxy motifs, 1,2,3-trimethoxyaryl compounds have surprisingly greater aqueous solubility, which may be attributed to the out-of-plane orientation of the middle methoxy group that disrupts π-stacking.

Some abrogation of potency had been expected for HOTub-620 and HOTub-630 due to the absence of an orienting hydroxyl group, and they did not prove as potent as the hydroxylated "bottom-up" compounds. Despite showing a lower potency than HOTub-31, we were pleased to observe that "top-down" HOTub-630 also gave the dark-specificity for which it was designed. However, HOTub-620 did not display strong antiproliferative effects below 10 μM under either illumination condition. Again, the permutation control HOTub-530 displayed only weak antiproliferative effects and these were entirely independent of illumination conditions (see the Supporting Information for full data).

We found many aspects of these results exciting. The minimal-permutation controls showed substantially weaker as well totally non-photoswitchable toxicity, thus suggesting that HTI photoswitches with appropriate properties (especially solubility) can be cellularly tolerated at mid-micromolar concentrations and do not necessarily cause phototoxicity under repeated illumination conditions. This opens broader opportunities for their photopharmaceutical exploitation; and is particularly pleasing because the possibility to near-quantitatively photoisomerise HTIs from the metastable to the stable isomer (here,

~97%) differentiates them from the performance of the azobenzene scaffold, where the typically far less complete nature of this photoprocess (~80%) depresses the maximum achievable dynamic range of photoswitching. The robust and repeatable cytotoxicity of the active compounds represents the first demonstration of HTI-based "narrow" (druglike) photopharmaceuticals designed for an endogenous protein target, and an intracellular target at that. Most pleasingly, the rationally designed isomer-specific cytotoxicity in the active compounds supported that our design procedure for "mapping" the *E*- or *Z*-state HTI isomers into the colchicinoid pharmacophore to create lit- or dark-state toxins at will, despite potential preferences of the protein binding site, could indeed be robustly achieved on the desymmetrised HTI scaffold, in accordance with our design aims.

However, cytotoxicity assays do not provide mechanistic information about the most relevant in cellulo target or targets of a compound over a long-term assay (neither do in vitro assays against purified enzyme). Therefore, we wished to answer the question of whether isomer-dependent modulation of tubulin polymerisation dynamics is the major in cellulo bioactivity mechanism of the HOTubs, across both lit- and dark-active designs. We focussed on "bottom-up" HOTub-31 and HOTub-81, anticipating that their greater solubility compared to the non-hydroxylated "top-down" compounds would deliver a cleaner pharmacological profile.

Firstly, we examined directly their capacity to photomodulate microtubule network structure within cells in long-term illuminations. The direct mechanism of action of colchicine-site binding drugs is to reduce tubulin polymerisation dynamics, but after long-term exposure to the more potent inhibitors in this class, microtubule network structures become disorganised and then progressively depolymerised (although effective inhibitors of polymerisation dynamics that produce antimitotic effects but do not reduce polymer mass are also known[41]). We accordingly performed immunofluorescence staining and confocal microscopy of the polymer microtubule network of cells treated for 24 h (Figure 4).

Dark-toxic HOTub-31 gave strong photoswitchability of microtubule structure disruption, with the greatest difference in effect visible around 1.5 μM. At this concentration, lit cells featured nearly normal microtubule networks whereas dark-treated cells had almost entirely depolymerised structures. Incubations at higher concentrations confirmed the dark-toxicity of this compound (Figure S5). Lit-toxic HOTub-81 required higher concentrations to see substantial effects, but whereas lit cells treated at 10 μM were substantially found in an entirely microtubule-depolymerised state, cells could be treated at up to 20 μM under dark conditions with only a smaller fraction of cells (that were apparently arrested in mitosis, when cells have preemptively depolymerised most of their microtubules) showing substantial network depolymerisation. Although there is residual disruption of microtubule structure and mass with both compounds in their less active states (compare to negative control image), our strategy towards forcing both isomer specificities of microtubule disrupting activity seemed supported by this direct biological visualisation (Figure 4).

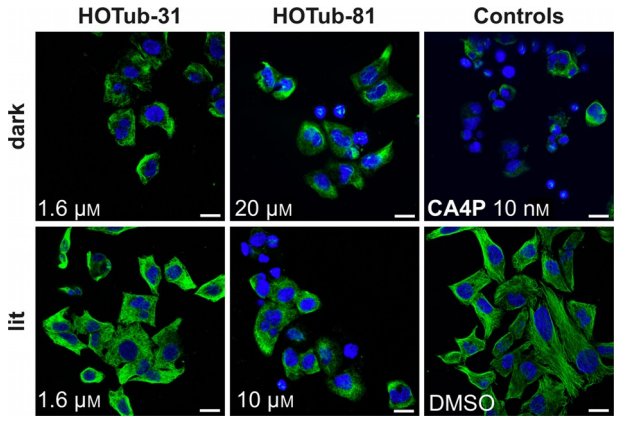

Figure 4. Confocal microscopy of immunofluorescently stained microtubule networks after 24 h lit- or dark-treatment with HOTubs shows illumination-specific antimicrotubule effects that match the sign and the potency of their cellular cytotoxicity. HOTub-31 at 1.6 μM, with the lit treatment at 410 nm; HOTub-81 at 10 μM under the lit treatment (450 nm) but 20 μM under dark treatment; negative control image: 1% DMSO cosolvent-treated cells under 450 nm; positive control image: CA4 phosphate (MTT EC_{50} = 5 nM) at 10 nM. Scale bars: 20 μm. DAPI nuclear stain shown in blue, immunostained tubulin shown in green; for details, see the Supporting Information and Figure S5.

Lastly, we analysed cell cycle perturbation, as an orthogonal method to test whether tubulin binding in cellulo is the likely long-term mechanism of action of these compounds. Tubulin-binding agents, whose major cellular mechanism of toxicity is the disruption of microtubule dynamics or structure, should show cell cycle arrest in G_2/M phase.[24b] Compounds with other toxic mechanisms, such as nonspecific photodamage, should not significantly impact the cell cycle; and even cell-cycle-affecting compounds that may confound immunofluorescence assessment of microtubule polymer structure can be filtered out if they have a different profile of cell cycle effects (e.g., doxorubucin can reduce microtubules seen in microscopy, but does not cause G_2/M arrest). We therefore used flow cytometry to analyse cell cycle repartition in cells treated for 24 h. HOTub-31 showed strongly illumination-dependent bioactivity, provoking almost total G_2/M arrest at 3 μM under dark conditions, but with no visible cell cycle perturbation at this concentration under 450 nm illumination (Figure 5).

Discussion

Taken together, our biological cross-evaluations support that the HOTubs' relevant cellular target is tubulin, that the hemithioindigo scaffold can serve as a basis for cell-compatible and potent photopharmaceuticals according to the "narrow" druglike definition, and that the molecular asymmetry of the HTI can be used to rationally design photopharmaceuticals that, according to taste, feature either lit-activity or dark-activity against the same endogenous intracellular target protein.

That HOTubs could successfully be designed for tubulin offers several perspectives for their unique, practical applications. Tubulin is one of many survival-critical intracellular proteins whose activity it has not been possible to regulate directly by genetic methods, such as by the creation of optogenetic tubulin constructs, that would give the experimenter biologi-

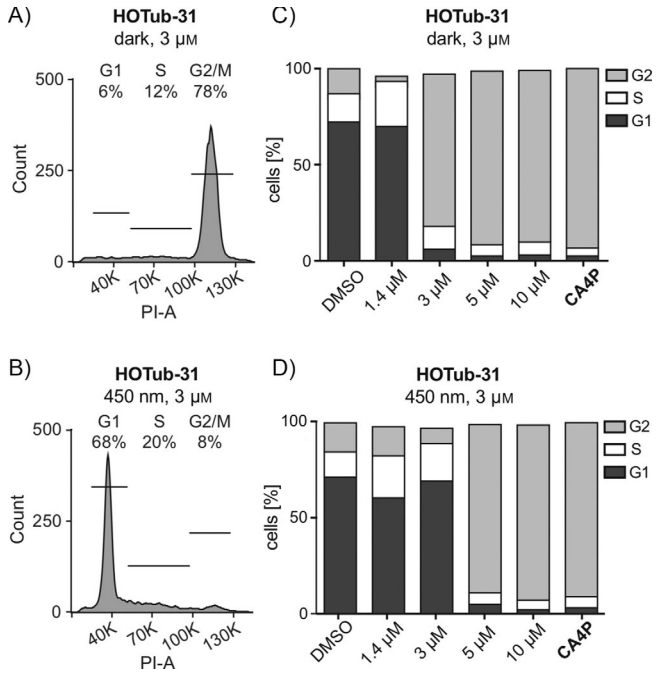

Figure 5. Cell cycle analysis of HOTub-31-treated cells. A, B) Representative histograms showing light-dependency of cell cycle arrest, with population binning indicated. C, D) HOTub-31 causes dose- and light-dependent cell cycle arrest. All experiments contained DMSO at 1% *v/v*; CA4P was used at 10 nM (further details in Supporting Information).

cally meaningful (spatiotemporally precise) control over microtubule structure and biology. In this context, by enabling such previously impossible studies, the azobenzene-based photopharmaceutical PST-1 (azocombretastatin) has already achieved significant applications, leveraging the spatially and temporally precise photoreversible switching of its bioactivity.[8,9,27] Alternative photoswitchable scaffolds for tubulin photocontrol that could expand the chemical substituent tolerance of practical tubulin photopharmaceuticals, as well as enable the opposite photoresponse (dark-active) from PST-1 and so access conceptually distinct applications, would also be of extensive interest to the cytoskeleton research community.

Towards more general photopharmaceutical applications of HTIs, it is noteworthy that the metastable isomers of HTIs bearing mesomerically stabilising or tautomerisable substituents in *para* on the hemistilbene are not necessarily "fast-relaxing" (half-lives below ~1 ms) in aqueous environments, unlike what is seen for azobenzenes (probably the same is true on all positions of the thioindoxyl, explorations are ongoing by other groups[42]). Azobenzenes face other common challenges in cellular environments, including thiol addition into the photoswitchable N=N double bond that can lead to compound degradation, sequestration, or off-target effects; we expect that the C=C photoswitchable bond in HTIs will have a different and overall diminished profile of thiol sensitivity. The cellular applicability we now show for "narrow" HTI photopharmaceuticals (where the ability to decorate the photoswitch with arbitrary substituents is particularly important) argues this photoswitch scaffold may now prove important in opening new chemical space in photopharmacology.

The cytotoxic potencies of HOTub-31 (ca. fourfold change between dark and 450 nm treatments) suggest that the PSS values measurable in DMSO or 75:25 DMSO/PBS do not apply to the "average" PSS established in the cellular situation. Even were its *E* isomer essentially inactive, the change of potency to be expected between dark and lit treatments in the MTT assay would otherwise be only threefold (35% *Z* at 450 nm) according to the PSS in 75:25 DMSO/PBS. We believe that one factor behind this observation will prove to be that the relatively lipophilic HOTubs might be extensively localised in lipid environments (potentially with different partition coefficients in the *Z* and *E* forms), and that this modifies the effective cellular PSSs. While in the case of HOTub-31 this may work in favour of the photoswitchability of its apparent potency, we anticipate that installing still better aqueous solubility in HTIs will prove important for their reliability in general cellular applications, for predictability of photoswitching and biodistribution as well as to avoid potential [2+2] photocycloadditions[43] in aggregated HTIs (we also believe the importance of solubility is reflected in the weaker photoswitchability of potency of the non-hydroxylated HOTubs). Current advances in HTI photoswitch design are also leading to photoswitches with extremely high photoswitchability of isomer ratios,[44] which if applied to HOTub derivatives could offer perspectives for even dark-state-active HTIs to be photopatterned with yet higher photoswitchability of bioactivity.

Conclusions

This study has demonstrated the first uses of pharmacophore-embedded hemithioindigos as cell-compatible photopharmaceuticals enabling long-term in situ photocontrol of an endogenous intracellular biological target. The match of our compounds' photodependent bioactivities to the predictions from SAR mapping, as well as the inactivity of the intentional negative controls, argues that off-target bioactivity including aggregation toxicity and photodamage effects are not problematic with the scaffolds and concentrations employed. In particular, we consider the ability to rationally embed the HTI scaffold in such a way as to show either lit- or dark-state bioactivity, to hold much potential for photopharmacology applications, where typically lit-active compounds are desirable. In the present case, we have shown the ability of the HTI scaffold to be used as an effective asymmetric mimic for a pharmacophore mapping onto a *cis*-azobenzene, which due to the difference in torsion angles (~60° for *cis*-azobenzene and nearly planar for either HTI isomer) was not immediately obvious, but which probably relies on binding site plasticity. We fully expect however that the HTI can also be mapped asymmetrically onto (geometrically more similar) *trans*-azobenzene-like pharmacophores, and that HTIs can therefore be used to "rework" especially dark-active azobenzene photopharmaceuticals into conceptually more valuable lit-active HTI analogues (or, also, dark-actives if so desired).

Despite the attractiveness of tubulin as a target for continued development of in cellulo- (and ultimately in vivo-) appropriate photopharmaceuticals with diverse properties, we now

believe that the most straightforwardly rewarding applications of such molecular reworking will be in the creation of lit-active HTI-type photopharmaceuticals for situations where azobenzene reagents have hitherto been *trans*-active. By "inverting the sign" of photoresponse, such reagents could avoid the major problems associated with *trans*-active azobenzenes, that is, spontaneous generation of, and incomplete photoisomerisation away from, the more bioactive isomer. These problems typically act in concert to limit the photoswitchability of bioactivity that can be applied in cellular contexts. We therefore hope that, by enabling free design of lit- or dark-state activity, the present work will open new horizons for robust photopharmacological applications against a variety of targets.

Experimental Section

Materials: Chemistry building blocks and biology reagents were obtained from commercial sources as described in the Supporting Information.

General synthesis: Typical synthetic strategies are summarised as follows. Hemithioindigos were synthesised by aldol condensation of the corresponding thioindoxyls and benzaldehydes. Diverse condensation reaction conditions were trialled, including 1) room temperature condensation on neutral, basic, or acidic aluminium oxide under dry chlorinated solvents, 2) condensation in dry refluxing benzene with piperidine catalysis, and 3) condensation in refluxing NaOH/*t*BuOH; of these, the benzene/piperidine conditions typically gave highest isolated yields. One-pot procedures without intermediate purification of the thioindoxyls typically resulted in tedious workups and low yields. In our hands, some hemithioindigos decomposed significantly during normal phase silica gel column chromatography despite precautions to deactivate the gel, generating a plethora of decomposition products. Purification through precipitating the hemithioindigo out of concentrated DMSO solution by adding water, often proved a better alternative. Thioindoxyls were synthesised by intramolecular cyclisation, either of the 2-(phenylthio)acetyl chloride with $AlCl_3$ in chlorinated solvents, of the 2-(phenylthio)acetic acid with Eaton's reagent, or with exposure of 2-(methylthio)benzoic esters or amides to LDA in THF; of these, the LDA/THF conditions typically gave highest isolated yields when alternative routes could practicably be compared. Despite literature reports of the instability of thioindoxyls, in our hands these electron-rich thioindoxyls showed no significant degradation upon long-term storage at −20 °C, and generally tolerated workups and ordinary bench handling without decomposition (high pH should be avoided however). Towards 2-(methylthio)benzoate derivatives, we first attempted directed *ortho*-metalations of, for example, methyl(3,4,5-trimethoxyphenyl)sulfide with *s*BuLi/TMEDA, but this instead deprotonated the *S*-methyl group, leading to undesired 2-(3,4,5-trimethoxyphenylthio)acetic acids upon quenching with CO_2. The cyclisation precursors were therefore typically synthesised by magnesium–halogen exchange on *ortho*-iodobenzene derivatives with turbo-Grignard,[39] followed by electrophilic quenching with methyl chloroformate (for phenyl methyl thioethers) or with $MeSSO_2Me$ (for benzoate derivatives). All syntheses are fully described in the Supporting Information.

Photoisomerisation: reference photostationary states were determined by NMR spectroscopy of DMSO solutions of HOTubs at 1 mM, that had been 1) kept dark at 60 °C overnight (all-*Z*), or else 2) irradiated with a 3 W Epistar LED driven at 350 mA and placed directly under a stirred vial of HOTub solution (1 cm diameter, height < 0.4 cm) for 2 min and for 5 min before solution transfer to the NMR tube and its loading into the spectrometer were performed rapidly under dark conditions. NMR acquisition was started immediately (total delay time ~1 min). That PSS had been reached was confirmed by the equivalence of the 2 min and 5 min illumination measured PSSs; that thermal relaxation during delay time did not significantly affect the measured PSSs was confirmed by the equivalence of a single representative PSS measurement with an analogous measurement where an additional 20 min delay was introduced. These were taken to define the PSSs of 100 μM HOTub solutions in 75:25 DMSO/PBS mixture at 25 °C that had been photoequilibrated with the same LEDs, the absorption spectra of which were measured by UV/Vis spectroscopy. UV/Vis was then used to scan sequentially through a range of PSSs established under varying LED wavelengths, to show the repeatability of photoswitching as well as to characterise intermediate PSSs between the reference PSSs determined from NMR spectroscopy (450 nm and dark (all-*Z*) conditions as cross-checked to 505 nm). Full descriptions are given in the Supporting Information.

Cell biology: studies were performed as previously described.[6] In brief, HeLa human cervical cancer cell line sourced from the ATCC was used for all studies; all treatments were performed in triplicate; results are only reported when three independent experiments returned quantitatively similar results within acceptable error ranges; experiments were typically conducted using combretastatin A-4 phosphate as a highly potent, positive control reference compound with the same binding site and bioactivity as was desired to for the HOTubs. Antiproliferative or cytotoxic potencies were determined by MTT assay of cells seeded at ~5000 cells/well in 96-well microtitre plates and left to adhere for 24 h before treatment with HOTub for 48 h, under pulsed in situ illuminations typically at 450 nm (typical timing: 100 ms ON per 60 s OFF) delivered from self-built LED plates containing ~10 mW LEDs (Roithner Lasertechnik) as compared to cells incubated under dark conditions, as previously described.[6] Immunofluorescence staining of cellular microtubule networks was performed after 24 h treatment of cells with HOTubs under pulse-illuminated or dark conditions; removal of monomeric tubulin with extraction buffer was followed by fixation with methanol or glutaraldehyde, and immunostaining using rabbit anti-α-tubulin primary antibody and donkey anti-rabbit Alexa Fluor 488 secondary antibody, mounted in presence of DAPI nuclear stain; imaging was typically conducted on a Zeiss LSM710 confocal microscope (Zen Black software 2009) and images were processed with FIJI/ImageJ software (NIH); for full details see the Supporting Information. Flow cytometric cell cycle analysis was performed after 24 h of HOTub treatments as per previous experiments, with cell permeabilization then chromatin staining using propidium iodide (both in fixed and in non-fixed cells, identical results were observed by these methods); flow cytometric analysis for cell cycle repartition was conducted with standard gating for intact PI-positive cells, partitioning events into sub-G_1, G_1, S, or G_2/M bins by using either FlowJo or FlowingSoftware (with qualitatively identical results). See the Supporting Information for full details.

Acknowledgements

This project was funded by the Deutsche Forschungsgemeinschaft (DFG, German Research Foundation) (SFB 1032 project B09; TRR 152, project P24 number 239283807; and Emmy Noether grant TH 2231/1-1). We thank Irina Solovei (CALM microscopy platform,

LMU) and Christophe Jung (Gene Centre, LMU) for access to and assistance with confocal imaging; Neda Tafrishi for access to and assistance with FACS (FACS Core Facility, Gene Centre, LMU Munich); Luis de la Osa de la Rosa, Malgorzata Borowiak, Ruben Sachsse and Niklas Peters for trialling cellular toxicity assay parameters; Herbert Bachmeier and Axel Gersdorf for LED arrays (LMU); Peter Gänsheimer, Patricia Schuerle and Sophia Schwarz for advice on synthetic routes; and colleagues at the International Symposia on Photopharmacology for productive discussions.

Conflict of Interest

The authors declare no conflict of interest.

Keywords: antiproliferation · cytoskeleton · drug design · hemithioindigo · photochromism · photopharmacology

[1] a) A. A. Beharry, G. A. Woolley, *Chem. Soc. Rev.* **2011**, *40*, 4422 – 4437; b) K. Hüll, J. Morstein, D. Trauner, *Chem. Rev.* **2018**, *118*, 10710 – 10747; c) W. A. Velema, W. Szymanski, B. L. Feringa, *J. Am. Chem. Soc.* **2014**, *136*, 2178 – 2191.

[2] A. Bautista-Barrufet, M. Izquierdo-Serra, P. Gorostiza, in *Novel Approaches for Single Molecule Activation and Detection* (Eds.: F. Benfenati, E. Di Fabrizio, V. Torre), Springer, Berlin, **2014**, pp. 169 – 188.

[3] a) A. Rullo, A. Reiner, A. Reiter, D. Trauner, E. Y. Isacoff, G. A. Woolley, *Chem. Commun.* **2014**, *50*, 14613 – 14615; b) X. Gómez-Santacana, S. Pittolo, X. Rovira, M. Lopez, C. Zussy, J. A. R. Dalton, A. Faucherre, C. Jopling, J.-P. Pin, F. Ciruela, C. Goudet, J. Giraldo, P. Gorostiza, A. Llebaria, *ACS Cent. Sci.* **2017**, *3*, 81 – 91.

[4] W. A. Velema, J. P. van der Berg, M. J. Hansen, W. Szymanski, A. J. M. Driessen, B. L. Feringa, *Nat. Chem.* **2013**, *5*, 924 – 928.

[5] W. Szymanski, M. E. Ourailidou, W. A. Velema, F. J. Dekker, B. L. Feringa, *Chem. Eur. J.* **2015**, *21*, 16517 – 16524.

[6] M. Borowiak, W. Nahaboo, M. Reynders, K. Nekolla, P. Jalinot, J. Hasserodt, M. Rehberg, M. Delattre, S. Zahler, A. Vollmar, D. Trauner, O. Thorn-Seshold, *Cell* **2015**, *162*, 403 – 411.

[7] A. Polosukhina, J. Litt, I. Tochitsky, J. Nemargut, Y. Sychev, I. De Kouchkovsky, T. Huang, K. Borges, D. Trauner, R. N. Van Gelder, R. H. Kramer, *Neuron* **2012**, *75*, 271 – 282.

[8] J. Zenker, M. D. White, R. M. Templin, R. G. Parton, O. Thorn-Seshold, S. Bissiere, N. Plachta, *Science* **2017**, *357*, 925 – 928.

[9] J. Zenker, M. D. White, M. Gasnier, Y. D. Alvarez, H. Y. G. Lim, S. Bissiere, M. Biro, N. Plachta, *Cell* **2018**, *173*, 776 – 791.

[10] M. M. Lerch, M. J. Hansen, G. M. van Dam, W. Szymanski, B. L. Feringa, *Angew. Chem. Int. Ed.* **2016**, *55*, 10978 – 10999; *Angew. Chem.* **2016**, *128*, 11140 – 11163.

[11] a) O. Babii, S. Afonin, M. Berditsch, S. Reiβer, P. K. Mykhailiuk, V. S. Kubyshkin, T. Steinbrecher, A. S. Ulrich, I. V. Komarov, *Angew. Chem. Int. Ed.* **2014**, *53*, 3392 – 3395; *Angew. Chem.* **2014**, *126*, 3460 – 3463; b) C. J. Stankovic, S. H. Heinemann, S. L. Schreiber, *Biochim. Biophys. Acta* **1991**, *1061*, 163 – 170.

[12] a) W. A. Velema, M. J. Hansen, M. M. Lerch, A. J. M. Driessen, W. Szymanski, B. L. Feringa, *Bioconjugate Chem.* **2015**, *26*, 2592 – 2597; b) M. Wegener, M. J. Hansen, A. J. M. Driessen, W. Szymanski, B. L. Feringa, *J. Am. Chem. Soc.* **2017**, *139*, 17979 – 17986.

[13] D. Lachmann, C. Studte, B. Männel, H. Hübner, P. Gmeiner, B. König, *Chem. Eur. J.* **2017**, *23*, 13423 – 13434.

[14] D. Schmidt, T. Rodat, L. Heintze, J. Weber, R. Horbert, U. Girreser, T. Raeker, L. Bußmann, M. Kriegs, B. Hartke, C. Peifer, *ChemMedChem* **2018**, *13*, 2415 – 2426.

[15] a) D. Wilson, J. W. Li, N. R. Branda, *ChemMedChem* **2017**, *12*, 284 – 287; b) N. A. Simeth, A. C. Kneuttinger, R. Sterner, B. König, *Chem. Sci.* **2017**, *8*, 6474 – 6483.

[16] a) A. Mourot, T. Fehrentz, Y. Le Feuvre, C. M. Smith, C. Herold, D. Dalkara, F. Nagy, D. Trauner, R. H. Kramer, *Nat. Methods* **2012**, *9*, 396; b) B. Eisel, F. W. W. Hartrampf, T. Meier, D. Trauner, *FEBS Lett.* **2018**, *592*, 343 – 355.

[17] a) M. Schehr, D. Hugenbusch, T. Moje, C. Näther, R. Herges, *Beilstein J. Org. Chem.* **2018**, *14*, 2799 – 2804; b) R. Siewertsen, H. Neumann, B. Buchheim-Stehn, R. Herges, C. Näther, F. Renth, F. Temps, *J. Am. Chem. Soc.* **2009**, *131*, 15594 – 15595.

[18] S. Wiedbrauk, H. Dube, *Tetrahedron Lett.* **2015**, *56*, 4266 – 4274.

[19] a) T. Seki, T. Tamaki, T. Yamaguchi, K. Ichimura, *Bull. Chem. Soc. Jpn.* **1992**, *65*, 657 – 663; b) K. Eggers, T. M. Fyles, P. J. Montoya-Pelaez, *J. Org. Chem.* **2001**, *66*, 2966 – 2977.

[20] N. Regner, T. T. Herzog, K. Haiser, C. Hoppmann, M. Beyermann, J. Sauermann, M. Engelhard, T. Cordes, K. Rück-Braun, W. Zinth, *J. Phys. Chem. B* **2012**, *116*, 4181 – 4191.

[21] T. Lougheed, V. Borisenko, T. Hennig, K. Rück-Braun, G. A. Woolley, *Org. Biomol. Chem.* **2004**, *2*, 2798 – 2801.

[22] S. Herre, T. Schadendorf, I. Ivanov, C. Herrberger, W. Steinle, K. Rück-Braun, R. Preissner, H. Kuhn, *ChemBioChem* **2006**, *7*, 1089 – 1095.

[23] C. Dumontet, M. A. Jordan, *Nat. Rev. Drug Discovery* **2010**, *9*, 790 – 803.

[24] a) T. J. Mitchison, *Mol. Biol. Cell* **2012**, *23*, 1 – 6; b) J. R. Peterson, T. J. Mitchison, *Chem. Biol.* **2002**, *9*, 1275 – 1285.

[25] a) J. E. Sheldon, M. M. Dcona, C. E. Lyons, J. C. Hackett, M. C. T. Hartman, *Org. Biomol. Chem.* **2016**, *14*, 40 – 49; b) A. J. Engdahl, E. A. Torres, S. E. Lock, T. B. Engdahl, P. S. Mertz, C. N. Streu, *Org. Lett.* **2015**, *17*, 4546 – 4549.

[26] K. Eguchi, Z. Taoufiq, O. Thorn-Seshold, D. Trauner, M. Hasegawa, T. Takahashi, *J. Neurosci.* **2017**, *37*, 6043 – 6052.

[27] A. Singh, T. Saha, I. Begemann, A. Ricker, H. Nüsse, O. Thorn-Seshold, J. Klingauf, M. Galic, M. Matis, *Nat. Cell Biol.* **2018**, *20*, 1126 – 1133.

[28] S. K. Rastogi, Z. Zhao, S. L. Barrett, S. D. Shelton, M. Zafferani, H. E. Anderson, M. O. Blumenthal, L. R. Jones, L. Wang, X. Li, C. N. Streu, L. Du, W. J. Brittain, *Eur. J. Med. Chem.* **2018**, *143*, 1 – 7.

[29] G. C. Tron, T. Pirali, G. Sorba, F. Pagliai, S. Busacca, A. A. Genazzani, *J. Med. Chem.* **2006**, *49*, 3033 – 3044.

[30] R. Gaspari, A. E. Prota, K. Bargsten, A. Cavalli, M. O. Steinmetz, *Chem.* **2017**, *2*, 102 – 113.

[31] G. R. Pettit, B. Toki, D. L. Herald, P. Verdier-Pinard, M. R. Boyd, E. Hamel, R. K. Pettit, *J. Med. Chem.* **1998**, *41*, 1688 – 1695.

[32] G. R. Pettit, S. B. Singh, E. Hamel, C. M. Lin, D. S. Alberts, D. Garcia-Kendal, *Experientia* **1989**, *45*, 209 – 211.

[33] Y. Wang, H. Zhang, B. Gigant, Y. Yu, Y. Wu, X. Chen, Q. Lai, Z. Yang, Q. Chen, J. Yang, *FEBS J.* **2016**, *283*, 102 – 111.

[34] R. H. Bisby, S. W. Botchway, J. A. Hadfield, A. T. McGown, A. W. Parker, K. M. Scherer, *Eur. J. Cancer* **2012**, *48*, 1896 – 1903.

[35] R. B. Ravelli, B. Gigant, P. A. Curmi, I. Jourdain, S. Lachkar, A. Sobel, M. Knossow, *Nature* **2004**, *428*, 198 – 202.

[36] K. Jacobson, Z. Rajfur, E. Vitriol, K. Hahn, *Trends Cell Biol.* **2008**, *18*, 443 – 450.

[37] M. T. Konieczny, W. Konieczny, S. Okabe, H. Tsujimoto, Y. Suda, K. Wierzba, *Chem. Pharm. Bull.* **2006**, *54*, 350 – 353.

[38] C. Mukherjee, S. Kamila, A. De, *Tetrahedron* **2003**, *59*, 4767 – 4774.

[39] A. Krasovskiy, P. Knochel, *Angew. Chem. Int. Ed.* **2004**, *43*, 3333 – 3336; *Angew. Chem.* **2004**, *116*, 3396 – 3399.

[40] J. Wang, K. Rueck-Braun, *ChemPhotoChem* **2017**, *1*, 493 – 498.

[41] J. Zhou, D. Panda, J. W. Landen, L. Wilson, H. C. Joshi, *J. Biol. Chem.* **2002**, *277*, 17200 – 17208.

[42] F. Kink, M. P. Collado, S. Wiedbrauk, P. Mayer, H. Dube, *Chem. Eur. J.* **2017**, *23*, 6237 – 6243.

[43] J. D. Harris, M. J. Moran, I. Aprahamian, *Proc. Natl. Acad. Sci. USA* **2018**, *115*, 9414.

[44] J. E. Zweig, T. R. Newhouse, *J. Am. Chem. Soc.* **2017**, *139*, 10956 – 10959.

Manuscript received: November 30, 2018

Accepted manuscript online: January 11, 2019

Version of record online: April 12, 2019

CHEMBIOCHEM

Supporting Information

Hemithioindigos for Cellular Photopharmacology: Desymmetrised Molecular Switch Scaffolds Enabling Design Control over the Isomer-Dependency of Potent Antimitotic Bioactivity

Alexander Sailer[+], Franziska Ermer[+], Yvonne Kraus[+], Ferdinand H. Lutter, Carsten Donau, Maximilian Bremerich, Julia Ahlfeld, and Oliver Thorn-Seshold*[a]

cbic_201800752_sm_miscellaneous_information.pdf

Author Contributions

Following ICMJE guidelines, the authors declare their roles as follows: AS: performed chemical synthesis and photocharacterisations; FE: performed viability screening, immunostaining, and cell cycle analysis; YK: performed viability screening and immunostaining; FHL, CD, MB: performed chemical synthesis; JA: performed confocal imaging, cell cycle analysis, and data analysis; OTS: conceived and supervised the study, wrote the manuscript with support from all authors.

Table of Contents

Conventions 3
Standard Procedures 4
Synthesis of **HOTub-13** 4
Synthesis of **HOTub-31** 6
Synthesis of **HOTub-620** 9
Synthesis of **HOTub-630** 11
Synthesis of 4,5,6-trimethoxybenzo[*b*]thiophen-3(2*H*)-one (**S15**) 13
Synthesis of **HOTub-70** 17
Synthesis of **HOTub-81** 17
Determination of the E/Z-ratio in the photostationary state 18
in cellulo biology assays 20
Supplemental References 23
NMR spectra 23

Conventions

Hemithioindigo geometry and nomenclature: Hemithioindigos (HTIs) are drawn by default in their Z-isomeric form, however, both E & Z forms will constitute a given sample depending on light exposure so they are named without E/Z-designations.

Abbreviations: The following abbreviations are used: Hex – distilled isohexanes, cHex – cyclohexane, EA – ethyl acetate, HRMS – high-resolution mass spectrometry, DCM – dichloromethane, LDA – lithium diisopropylamide, TFA – 2,2,2-trifluoroacetic acid, THF – tetrahydrofuran, Me – methyl, Et – ethyl, MeCN – acetonitrile, MS – molecular sieves, *i*Pr – *iso*propyl, Bu – butyl.

Reagents and Conditions: Unless stated otherwise: (1) all reactions and characterisations were performed with unpurified, undried, non-degassed solvents and reagents, used as obtained, under closed air atmosphere without special precautions; (2) "hexane" used for chromatography was distilled from commercial crude isohexane fraction on rotavap; (3) when not specified, "column" and "chromatography" refer to flash column chromatography performed on Merck silica gel Si-60 (40-63 μm); (4) procedures and yields are unoptimised; (5) yields refer to isolated spectroscopically pure materials, corrected for residual solvent content; (6) all eluent and solvent mixtures are given as volume ratios unless otherwise specified, thus "1:1 EA:Hex" indicates a 1:1 mixture (by volume) of ethyl acetate and hexanes.

Thin-layer chromatography (TLC) was run on 0.25 mm Merck silica gel plates (60, F-254). UV light (254 nm) was used as a visualising agent. R_f values were usually determined in ethyl acetate : hexane (EA:Hex) eluents. TLC characterisations are thus abbreviated as per (R_f = 0.09 on 6:1 EA:Hex).

NMR: Standard NMR characterisation was by 1D ^{1}H- and ^{13}C-NMR spectra, with COSY, HSQC, HMBC or heteronuclear NMR performed as needed. Known compounds were checked against literature data and their spectral analysis is not detailed unless necessary. The default spectrometer used was a Bruker Ascend 400 (400 MHz & 100 MHz for ^{1}H and ^{13}C respectively); NMR solvents are given individually for each compound. For determination of the composition of the photostationary states (450 and 505 nm), a Bruker Avance III HD (500 MHz) equipped with CryoProbe™ Prodigy broadband probe was used. Chemical shifts (δ) are reported in ppm calibrated to residual non-perdeuterated solvent as an internal reference[1]. The following peak descriptions are used: singlet (s), doublet (d), triplet (t), quartet (q), multiplet (m), broad (br) and doublet of doublets (dd).

Mass Spectra: HRMS was carried out by the Zentrale Analytik of the LMU, Munich using ESI or EI ionisation as specified.

UV-Vis Spectra: UV-vis spectra were recorded on an Agilent Cary 60 UV-vis spectrophotometer.

Standard Procedures

Where Standard Procedures were used in synthesis, unless stated otherwise, the amounts of reactants/reagents employed were implicitly adjusted to maintain the same molar ratios as in the given Procedure, and no other alterations from the Standard Procedure (eg. reaction time, extraction solvent, temperature) were made, unless stated otherwise.

Standard Procedure: Formation of HTIs *via* Piperidine Catalysed Aldol Condensations

An oven dried Schlenk flask was charged with the thioindoxyl (1.00 eq.), the aldehyde (equivalents are given individually) and molecular sieves (4 Å) under an atmosphere of nitrogen. Dry benzene (5 – 10 mL) and piperidine (0.1 mL) were added and the solution was heated to reflux for the time indicated individually. After cooling to room temperature, a saturated aqueous solution of NH_4Cl (5 – 15 mL) was added, the phases were separated and the aqueous layer was extracted with DCM (3 x 50 mL), dried over Na_2SO_4 or $MgSO_4$ and evaporated. Purification was accomplished as indicated individually.

Synthesis of HOTub-13

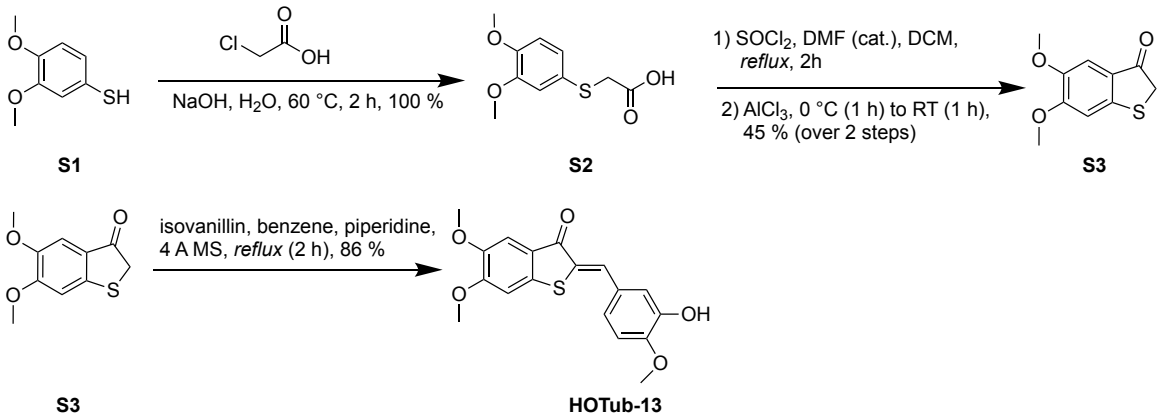

Scheme **S1**: Synthesis of **HOTub-13**

2-((3,4-dimethoxyphenyl)thio)acetic acid (S2)

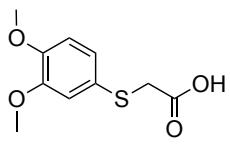

To a suspension of 3,4-dimethoxythiophenol (1.97 g, 11.6 mmol, 1.00 eq) in an aqueous sodium hydroxide solution (2 M, 46 mL) was added a solution of chloroacetic acid (1.27 g, 13.4 mmol, 1.16 eq) in water (8 mL) at room temperature. The resulting reaction mixture was heated to 60 °C for 2 h. Concentrated hydrochloric acid was added to the clear solution until

pH = 1. The yellow suspension was extracted with ethyl acetate (3 × 15 mL) and the combined organic extracts were washed with brine and dried over Na_2SO_4. The solvent was removed under reduced pressure affording **S2** as a pale yellow solid (2.64 g, 11.6 mmol, 100 %).

^{1}H-NMR (DMSO-d_6, 400 MHz): δ (ppm) = 12.67 (s, 1H), 7.00 (d, *J* = 1.7 Hz, 1H), 6.94 (dd, *J* = 1.7 / 8.3 Hz, 1H), 6.90 (d, *J* = 8.3 Hz, 1H), 3.74 (s, 3H), 3.73 (s, 3H), 3.67 (s, 2H,); **^{13}C-NMR** (DMSO-d_6, 100 MHz): δ (ppm) = 161.3, 139.2, 138.5, 116.2, 112.9, 104.2, 102.6, 45.9, 45.8, 27.3; **HRMS** (ESI$^-$) for $C_{10}H_{11}O_4S^-$ [M-H$^+$]: calcd. m/z 227.03780, found m/z 227.03844.

5,6-Dimethoxybenzo[*b*]thiophen-3(2*H*)-one (S3)

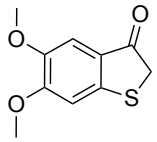

To a solution of **S2** (500 mg, 2.19 mmol, 1.00 eq.) in dry DCM (10 mL) was added $SOCl_2$ (339 mg, 2.85 mmol, 0.21 mL, 1.30 eq.) and dry DMF (0.1 mL) and the reaction mixture was heated to reflux for 2 h after which time the volatiles were removed *in vacuo* using an external cooling trap. The remaining orange crude product was dissolved in dry DCM (10 mL), cooled to 0 °C and $AlCl_3$ (730 mg, 5.48 mmol, 2.50 eq.) was carefully added portion wise under a stream of nitrogen. The solution was stirred at 0 °C for 30 min, then allowed to reach room temperature and stirred for 1 h. The solution was carefully quenched by the addition of water (15 mL), the phases were separated, and the aqueous layer was extracted with DCM (3 x 20 mL). The combined organic extracts were dried over Na_2SO_4, evaporated and the crude was purified by column chromatography (EA:Hex, 1:4) affording **S3** as an orange crystalline solid (207 mg, 0.98 mmol, 45 %). After isolation, the product was frozen and stored under an atmosphere of nitrogen.

^{1}H-NMR ($CDCl_3$, 400 MHz): δ (ppm) = 7.19 (s, 1H), 6.83 (s, 1H), 3.95 (s, 3H), 3.88 (s, 3H), 3.80 (s, 2H); **^{13}C-NMR** ($CDCl_3$, 100 MHz): δ (ppm) = 198.6, 156.6, 149.6, 148.0, 123.8, 107.0, 105.6, 56.6, 56.3, 40.1; **R_f** = 0.36 on 1:4 EA:Hx (blue fluorescence upon illumination with 254/366 nm); **HRMS** (ESI$^+$) for $C_{10}H_{11}O_3S^+$ [M+H$^+$]: calcd. m/z 211.04289, found m/z 211.04237.

2-(3-Hydroxy-4-methoxybenzylidene)-5,6-dimethoxybenzo[*b*]thiophen-3(2*H*)-one (HOTub-13)

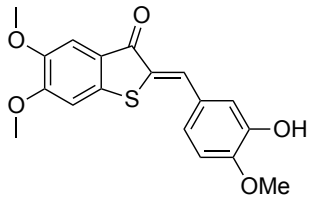

By Standard Procedure, commercial 3-hydroxy-4-methoxybenzaldehyde (80 mg, 0.52 mmol, 1.10 eq.) was reacted with **S3** (100 mg, 0.48 mmol, 1.00 eq.) for 2 h. Precipitation by addition of distilled water to a concentrated solution of the crude in DMSO (repeated once) yielded **HOTub-13** as a red solid (141 mg, 0.41 mmol, 86 %).

^{1}H-NMR ($CDCl_3$, 400 MHz): δ (ppm) = 7.83 (s, 1H), 7.34 (s, 1H), 7.29 (d, *J* = 2.1 Hz, 1H), 7.21 (dd, *J* = 2.1 / 8.4 Hz, 1H), 6.92 (d, *J* = 8.4 Hz), 6.89 (s, 1H), 5.85 (s, 1H), 3.97 (s, 3H), 3.93 (s, 3H), 3.91 (s, 3H); **^{13}C-NMR** ($CDCl_3$, 100 MHz): δ (ppm) = 187.6, 155.9, 148.5, 148.3, 146.0, 141.0, 133.4 , 129.5, 128.1, 125.0, 123.6, 116.3, 110.9, 107.8, 105.3, 56.6, 56.4, 56.2; **R_f** = 0.33 on 1:1 EA:Hx; **HRMS** (ESI $^+$) for $C_{18}H_{17}O_5S^+$ [M+H$^+$]: calcd. m/z 345.07967, found m/z 345.07902; **HRMS** (ESI$^-$) for $C_{18}H_{15}O_5S^-$ [M-H$^+$]: calcd. m/z 343.06457, found m/z 343.06485.

Synthesis of HOTub-31

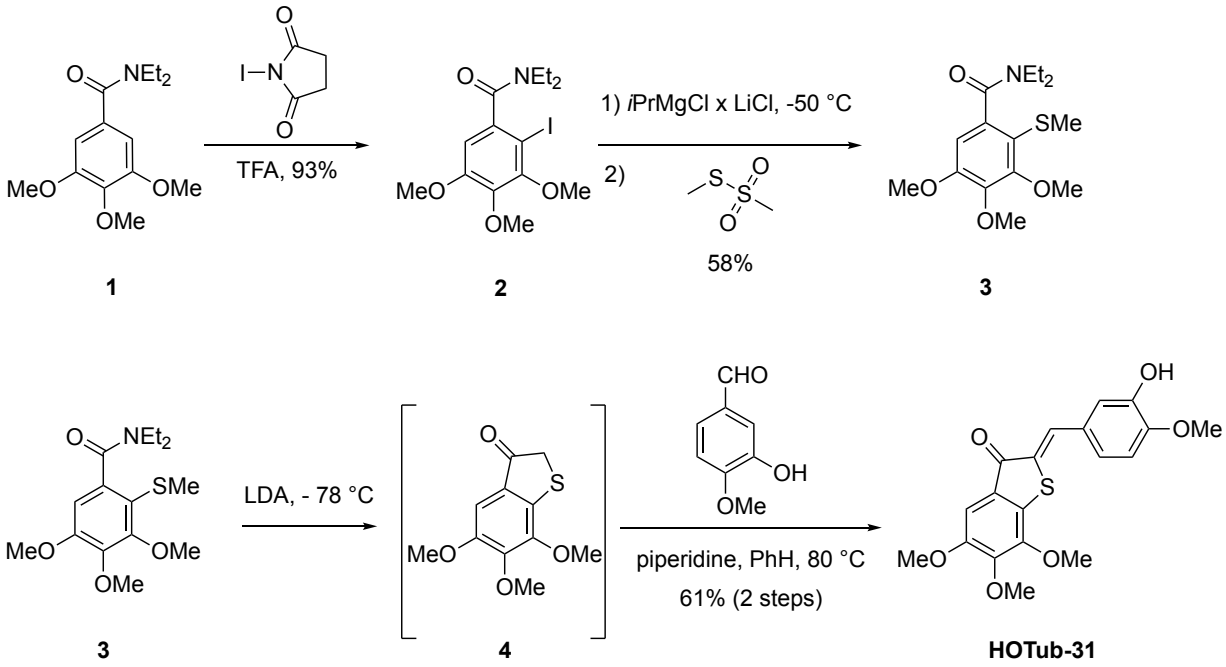

Scheme S2: Synthesis of **HOTub-31**

N,N -Diethyl-2-iodo-3,4,5-trimethoxybenzamide (2)

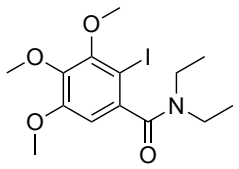

To a solution of *N*,*N*-diethyl-3,4,5-trimethoxybenzamide (763 mg, 2.85 mmol, 1.00 eq.) in acetonitrile (40 mL) was added *N*-iodosuccinimide (728 mg, 3.14 mmol, 1.10 eq) and 2,2,2-trifluoroacetic acid (114 mg, 1.00 mmol, 0.08 mL, 0.35 eq.) at room temperature and the reaction mixture was stirred for 2.5 h. The reaction mixture was extracted with Et_2O (3 × 60 mL) and the combined organic extracts were washed with brine, dried over Na_2SO_4, filtered and concentrated under reduced pressure. The crude was purified by column chromatography (EA:Hex, 2:3) to give **2** (1.04 g, 2.65 mmol, 93 %) as a yellow solid.

^{1}H-NMR ($CDCl_3$, 400 MHz): δ (ppm) = 6.60 (s, 1H), 3.87 (s, 3H), 3.86 (s, 3H), 3.83 (s, 3H), 3.30 – 3.10 (m, 4H), 1.28 (t, *J* = 7.1 Hz, 3H), 1.08 (t, *J* = 7.1 Hz, 3H); **^{13}C-NMR** ($CDCl_3$, 100 MHz): δ (ppm) = 169.9, 154.5, 153.6, 142.2, 138.4, 106.6, 80.9, 61.2, 61.1, 56.4, 42.9, 39.0, 14.1, 12.5; **R_f** = 0.17 on 2:3 EA:Hx; **HRMS** (EI^+) for $C_{14}H_{20}INO_4$ [M^+]: calcd. m/z 393.0437; found m/z 393.0426.

***N*,*N*-Diethyl-3,4,5-trimethoxy-2-(methylthio)benzamide (3)**

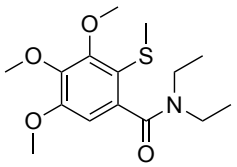

To a solution of **2** (0.27 g, 0.70 mmol, 1.00 eq.) in THF (2 mL) was added Turbo-Grignard (1.1 M in THF, 0.81 mL, 0.91 mmol, 1.30 eq.) dropwise at − 50 °C under an atmosphere of nitrogen. After 5 min, S-methyl methanethiosulfonate (215 mg, 1.70 mmol, 0.16 mL, 2.50 eq.) was added at − 50 °C and the yellow reaction mixture was allowed to warm to −30 °C. After 1 h, the yellow/red reaction mixture was allowed to warm to room temperature, quenched with saturated aqueous NH_4Cl solution and extracted with ethyl acetate. After washing with brine, drying over Na_2SO_4, filtering and concentration under reduced pressure, the crude product was purified by column chromatography (EA:Hx, 2:3) to give **3** (125 mg, 0.40 mmol, 58 %) as a pale yellow solid.

^{1}H-NMR ($CDCl_3$, 400 MHz): δ (ppm) = 6.52 (s, 1H), 3.95 (s, 3H), 3.85 (s, 3H), 3.83 (s, 3H), 3.79 (m, 1H), 3.34 (dq, *J* = 14.1 / 7.1Hz, 1H), 3.11 (q, *J* = 7.2 Hz, 2H), 2.35 (s, 3H), 1.26 (t, *J* = 7.1

Hz, 3H), 1.05 (t, J = 7.1 Hz, 3H); **^{13}C-NMR** ($CDCl_3$, 100 MHz): δ (ppm) = 169.3, 155.6, 154.5, 142.9, 138.1, 118.2, 105.3, 61.4, 61.1, 56.3, 43.0, 39.0, 19.5, 14.1, 12.6; **R_f** = 0.23 on 1:1 EA:Hx; **HRMS** (EI^+) for $C_{15}H_{23}NO_4S$ [M^+]: calcd. m/z 313.1348; found m/z 313.1343.

(3-Hydroxy-4-methoxybenzylidene)-4,5,6-trimethoxybenzo[*b*]thiophen-3(2*H*)-one (HOTub-31)

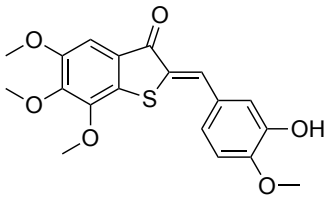

To a solution of *n*BuLi (1.6 M in hexanes, 153 mg, 1.50 mL, 2.39 mmol, 1.50 eq.) in dry THF was added *N*,*N*-diisopropylamine (403 mg, 3.99 mmol, 0.56 mL, 2.50 eq.) dropwise at - 78 °C. The resulting reaction mixture was allowed to warm to -30 °C and stirred for 45 min. prior to the addition of a solution of **3** (500 mg, 1.60 mmol, 1.00 eq.) in THF in the range of - 78 to – 30 °C. The resulting yellow solution was allowed to warm to room temperature. After 14 h, the reaction mixture was quenched with saturated aqueous NH_4Cl solution and extracted with ethyl acetate. After washing with brine, drying over Na_2SO_4, filtering and concentration under reduced pressure, the crude product was used without further purification.

The crude thioindoxyl was reacted with commercial isovanillin (170 mg, 1.12 mmol, 0.70 eq.) according to Standard Procedure for 16 h. Purification was accomplished by MPLC (EA:Hx, 2 %:98 %) giving **HO-Tub 31** as a red/brown solid (255 mg, 0.98 mmol, 61 %).

^{1}H-NMR ($CDCl_3$, 400 MHz): δ (ppm) = 7.86 (s, 1H), 7.36 (d, *J* = 2.2 Hz, 1H), 7.30 – 7.26 (m, 1H), 7.24 (s, 1H), 6.94 (d, *J* = 8.4 Hz, 1H), 5.76 (s, 1H), 4.01 (s, 3H), 4.00 (s, 3H), 3.96 (s, 3H), 3.91 (s, 3H); **^{13}C-NMR** ($CDCl_3$, 100 MHz): δ (ppm) = 188.0, 153.1, 148.6, 148.3, 147.6, 146.1, 134.1, 133.1, 129.2, 128.1, 126.0, 125.2, 116.5, 110.9, 104.4, 61.4, 61.1, 56.6, 56.2; **R_f** = 0.35 on 1:1 EA:Hx; **HRMS** (ESI^+) for $C_{19}H_{19}O_6S$ [$M+H^+$]: calcd. m/z 375.0896, found m/z 375.0897.

Synthesis of HOTub-620

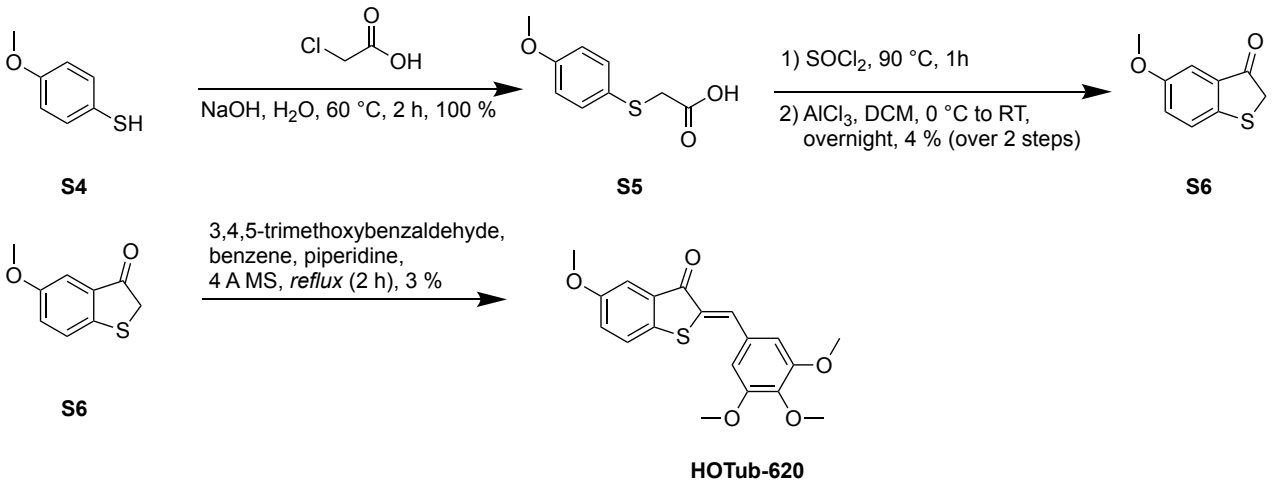

Scheme S3: Synthesis of **HOTub-620**

2-((4-Methoxyphenyl)thio)acetic acid (S5)

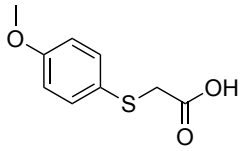

4-methoxythiophenol (213 mg, 1.52 mmol, 1.00 eq.) was suspended in NaOH (2 M, 5 mL). A solution of chloroacetic acid (179 mg, 1.81 mmol, 1.19 eq.) in water (0.5 mL) was added and the mixture was stirred for 2 h at 60 °C. $Na_2S_2O_3$ solution (1 M, 2 mL) was added, and the mixture was stirred for another hour at 60 °C. After acidifying with concentrated HCl to pH 1, it was extracted with EtOAc (3 × 25 mL), the organic layer was washed with brine, dried over Na_2SO_4 and the solvent was removed under reduced pressure giving **S5** as a yellow solid (302 mg, 1.52 mmol, 100 %).

^{1}H-NMR (400 MHz, $CDCl_3$): δ (ppm) = 10.80 (br. s, 1H), 7.29 (d, *J* = 8.8 Hz, 2H), 6.70 (d, *J* = 8.8 Hz, 2H), 3.62 (s, 3H), 3.40 (s, 2H) ppm.; **^{13}C-NMR** (100 MHz, $CDCl_3$): δ (ppm) = 175.8, 159.9, 134.3, 124.4, 114.8, 55.4, 38.6 ppm; **HRMS** (ESI^-) for $C_9H_9O_3S^-$ = $[M–H^+]$: calcd. m/z 197.02779, found m/z 197.02756.

5-Methoxybenzo[*b*]thiophen-3(2*H*)-one (S6)

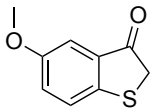

A solution of **S5** (1.34 g, 6.74 mmol, 1.00 eq.) in an excess of $SOCl_2$ (7 mL) was heated to 90 °C for 1 h. After cooling to room temperature, the solvent was removed under reduced pressure and the residue was dried in high vacuum. The remaining oil was dissolved in DCM (15 ml) and $AlCl_3$ (1.20 g, 7.50 mmol, 1.11 eq.) was added slowly under cooling. The mixture was stirred overnight at room temperature and then poured into ice water, basified using 2 M NaOH and extracted with EtOAc. After acidifying the solution with conc. HCl it was extracted again with EtOAc. The combined organic extracts were washed with brine, dried over $MgSO_4$ and the solvent was removed under reduced pressure. The crude product was purified by chromatography (EA:Hx, 1:5→1:2) to yield **S6** (43 mg, 0.24 mmol, 4 %). This product can be further purified by crystallization from absolute EtOH.

^{1}H-NMR (400 MHz, $CDCl_3$): δ (ppm) = 7.25 (dd, *J* = 8.6 / 0.6 Hz, 1H), 7.17 (d, *J* = 2.6 Hz, 1H), 7.13 (dd, *J* = 8.6 / 2.7 Hz, 1H), 3.78 (s, 2H), 3.76 (s, 3H); **^{13}C-NMR** (100 MHz, $CDCl_3$): δ (ppm) = 200.0, 157.7, 146.3, 131.9, 125.6, 125.2, 107.9, 55.7, 40.1; $\mathbf{R_f}$ = 0.46 on 1:2 EA:Hx, (blue fluorescence upon illumination with 366 nm).

5-Methoxy-2-(3,4,5-trimethoxybenzylidene)benzo[*b*]thiophen-3(2*H*)-one (HOTub-620)

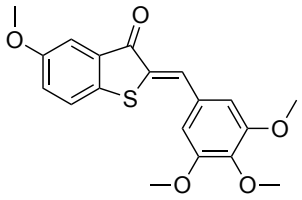

By Standard Procedure, commercial 3,4,5-trimethoxybenzaldehyde (7 mg, 33.3 μmol, 1.00 eq.) was reacted with **S6** (6 mg, 33.3 μmol, 1.00 eq.) and piperidine (0.05 mL) in dry benzene (3 mL) for 2 h at *reflux* and 4 h at room temperature. The crude product was purified by column chromatography (EA:Hx, 1:10 →1:4) and automated flash chromatography (9 %:91 %, EA:Hx) giving **HOTub-620** as orange crystals (0.4 mg, 1,12 μmol, 3 %).

^{1}H-NMR (400 MHz, $CDCl_3$): δ (ppm) = 7.88 (s, 1H), 7.41 (d, *J* = 2.7 Hz, 1H), 7.38 (d, *J* = 8.6 Hz, 1H), 7.20 (dd, *J* = 8.6 / 2.7 Hz, 1H), 6.95 (s, 2H), 3.94 (s, 6H), 3.92 (s, 3H), 3.86 (s, 3H);

^{13}C-NMR (100 MHz, $CDCl_3$): δ (ppm) = 188.6, 158.5, 153.6, 140.1, 137.7, 134.1, 131.7, 130.6, 129.9, 124.8, 124.6, 109.1, 108.3, 61.2, 56.3, 55.9; **R_f** = 0.47 on 1:2 EA:Hx; **HRMS** (ESI^+) for $C_{19}H_{18}O_5S$ = [M]: calcd. m/z 358.0875, found m/z 358.0852.

Synthesis of HOTub-630

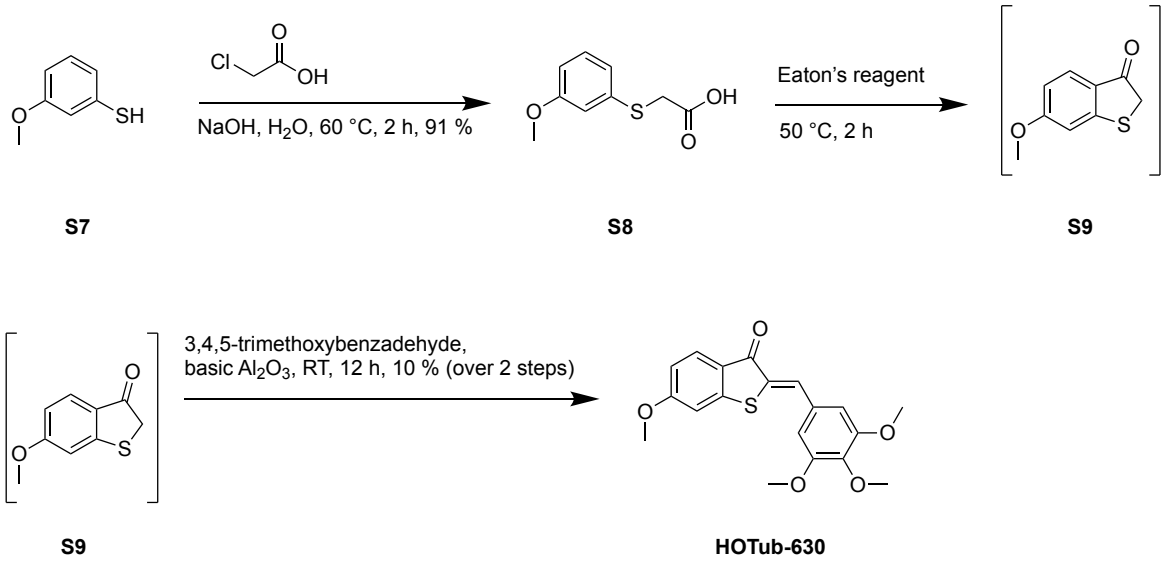

Scheme S4: Synthesis of **HOTub-630**

2-((3-Methoxyphenyl)thio)acetic acid (S8)

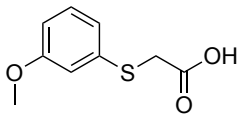

To a suspension of 3-methoxythiophenol (250 mg, 1.79 mmol, 1.00 eq.) in aqueous NaOH (2 M, 5 mL) was added a solution of chloroacetic acid (201 mg, 2.13 mmol, 1.19 eq.) in water (0.5 mL) and the mixture was stirred for 2 h at 60 °C. Aqueous $Na_2S_2O_3$ solution (1 M, 2 mL) was added, and the mixture was stirred for another hour at 60 °C. After acidifying with concentrated HCl to pH 1, the mixture was extracted with EtOAc (3 × 25 mL), the organic layer was washed with brine, dried over Na_2SO_4 and the solvent was removed under reduced pressure giving **S8** as a colourless oil (321 mg, 1.62 mmol, 91 %).

^{1}H-NMR (400 MHz, $CDCl_3$): δ (ppm) = 12.80 (br. s, 1H), 7.22 (t, *J* = 8.2 Hz, 1H), 6.88 (d, *J* = 7.1 Hz, 2H), 6.80 – 6.70 (m, 1H), 3.81 (s, 2H), 3.74 (s, 3H), 3.68 (s, 3H); **^{13}C-NMR** (100 MHz,

$CDCl_3$): δ (ppm) = 170.9, 148.9, 148.1, 125.8, 122.6, 113.9, 112.3, 55.6, 36.9; **HRMS** (ESI^-) for $C_9H_9O_3S$ [M-H^+]: calcd m/z 197.02779, found m/z 197.02756.

6-Methoxy-2-(3,4,5-trimethoxybenzylidene)benzo[*b*]thiophen-3(2*H*)-one (HOTub-630)

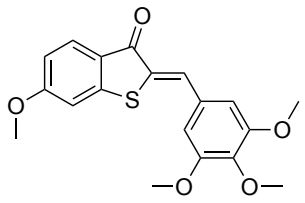

S8 (109 mg, 0.55 mmol, 1.00 eq.) was covered with Eaton's reagent and stirred for 2 h at 50 °C. The reaction was quenched by addition of water and the mixture was extracted with DCM (3 × 25 mL). The combined organic layers were washed with a saturated aqueous $NaHCO_3$ solution (3 × 25 mL) and brine (3 x 25 mL), dried over Na_2SO_4 and the volume was reduced to 5 – 6 mL. To this solution of the crude thioindoxyl **S9**, basic Al_2O_3 (200 mg) and 3,4,5-trimethoxybenzaldehyde (22 mg, 0.11 mmol, 0.20 eq.) were added, and the mixture was stirred at room temperature for 12 h after which time the mixture was filtered through a silica gel pad on 1:1 EA:Hx. The solvent was removed under reduced pressure and the crude product was purified by column chromatography (EA:Hx, 1:10 →1:1.5) and preparative TLC (cHx:$CHCl_3$:MeOH, 1:1:0.08) followed by precipitation with water from a solution in acetone (water:acetone, 3:1). After centrifugation, **HOTub-630** was separated mechanically as a pale yellow solid (4 mg, 0.01 mmol, 10 %).

^{1}H-NMR (400 MHz, 400 MHz): δ (ppm) = 7.88 (d, *J* = 8.6 Hz, 1H), 7.83 (s, 1H), 6.97 (d, *J* = 2.1 Hz, 1H), 6.94 (s, 2H), 6.84 (dd, *J* = 8.6 / 2.1 Hz, 1H), 3.95 (s, 6H), 3.92 (s, 6H); **^{13}C-NMR** (100 MHz, $CDCl_3$): δ (ppm) = 187.0, 165.8, 153.6 ('2), 148.8, 139.9, 132.9, 130.1, 130.0, 128.7, 124.1, 113.6, 108.1 ('2), 107.7, 61.2, 56.3 ('2), 56.0; **R_f** = 0.43 on 1:2.4, EA:Hx; **HRMS** (EI^+) for $C_{19}H_{18}O_5S$ = [M]: calcd. m/z 358.4080, found m/z 358.0864.

Synthesis of 4,5,6-trimethoxybenzo[*b*]thiophen-3(2*H*)-one (S15)

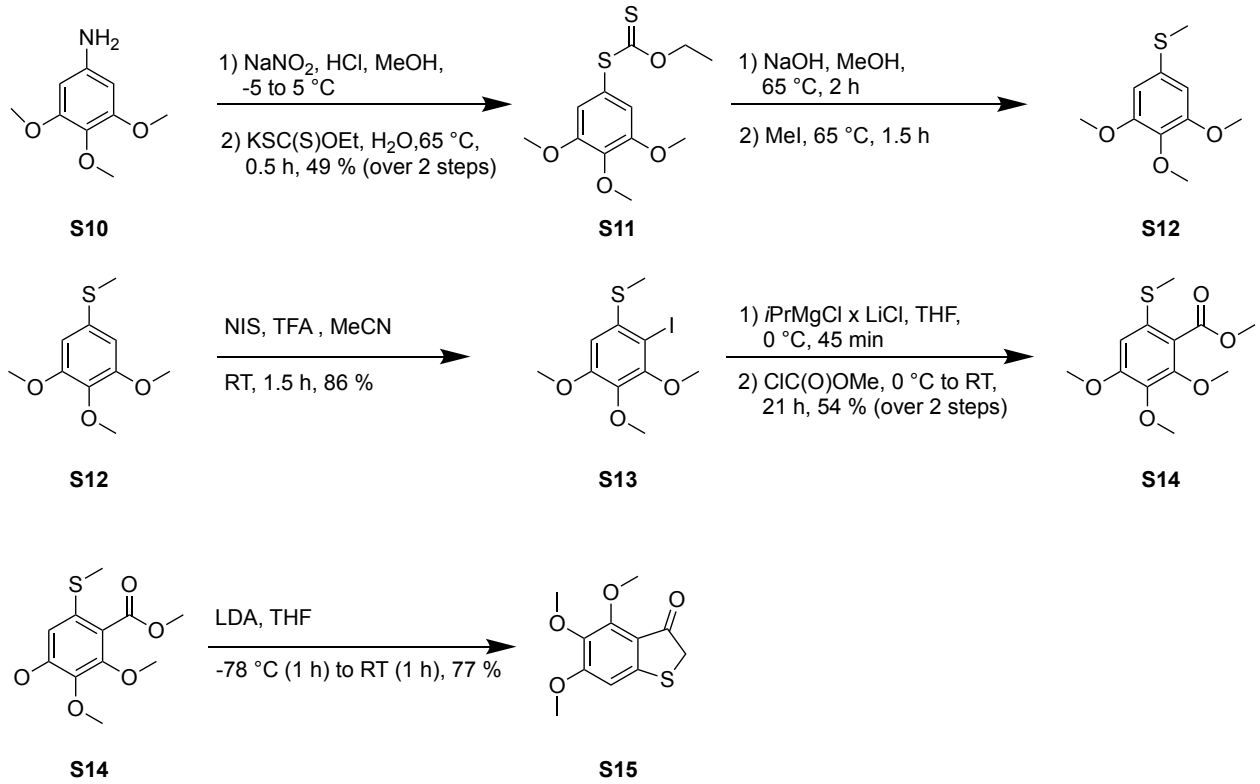

Scheme S5: Synthesis of **S15**

O-ethyl S-(3,4,5-trimethoxyphenyl) carbonodithioate (S11)

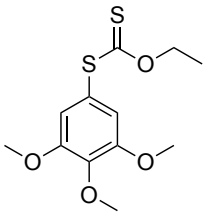

3,4,5-trimethoxyaniline (750 mg, 4.09 mmol, 1.00 eq.) was dissolved in MeOH (20 mL) and cooled to - 5 °C. An aqueous solution of $NaNO_2$ (333 mg, 4.83 mmol, 2M, 2.4 mL, 1.18 eq.) and HCl (900 mg, 24.7 mmol, 12M, 0.75 mL, 6.04 eq.) were added keeping the temperature below 5 °C. The reaction mixture was then slowly added to a solution of potassium ethyl xanthogenate (1.97 g, 12.3 mmol, 3.00 eq.) in water (15 mL) and heated to 65 °C for 0.5 h. The aqueous layer was then extracted with EtOAc (3 x 30 mL) and the combined organic extracts were evaporated. The crude was purified by means of column chromatography (EA:Hex, 1:8). The product can be further purified by recrystallization from *n*-pentane giving

S11 as a slightly yellow solid (575 mg, 2.00 mmol, 49 %). The experimental data is in full accordance with literature.[2]

^{1}H-NMR ($CDCl_3$, 400 MHz): δ (ppm) = 6.72 (s, 2H), 4.61 (q, *J* = 7.1 Hz, 2H), 3.87 (s, 3H), 3.84 (s, 6H), 1.33 (t, *J* = 7.1 Hz, 3H, H**1**); **^{13}C-NMR** ($CDCl_3$, 100 MHz): δ (ppm) = 213.4, 153.5, 139.7, 124.7, 112.3, 70.5, 61.1, 56.4, 13.8; $\mathbf{R_f}$ = 0.58 on 1:4 EA:Hex ; **HRMS** (EI^+) for $C_{12}H_{17}O_4S_2^+$ = [M^+]: calcd. m/z 288.0490, found 288.0486, for $C_9H_{11}O_3S$ = [M-$C_3H_5OS^+$]: calcd. m/z 199.0428, found m/z 199.0424.

Methyl(3,4,5-trimethoxyphenyl) sulfane (S12)

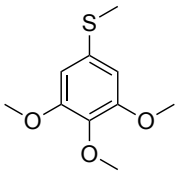

To a solution of **S11** (2.96 g, 10.3 mmol, 1.00 eq.) in MeOH (30 mL) was added a solution of NaOH (4.42 g, 111 mmol, 10.8 eq.) in water (30 mL) at room temperature. The suspension was heated to 65 °C for 2 h after which time MeI (2.19 g, 15.4 mmol, 0.96 mL, 1.50 eq.) was added dropwise. The reaction mixture was heated to 65 °C for 1.5 h and the solvents were removed under reduced pressure. The residue was treated with water (50 mL) and EtOAc (50 mL), the remaining solid was filtered off and the aqueous phase was extracted with EtOAc (2 x 50 mL). After drying the combined organic extracts over Na_2SO_4, the volatiles were removed yielding **S12** as an off-white solid (1.77 g, 8.26 mmol, 80 %), which was pure enough to be used in the next steps without further purification.**^{1}H-NMR** ($CDCl_3$, 400 MHz): δ (ppm) = 6.50 (s, 2H), 3.83 (s, 6H), 3.79 (s, 3H) ,2.46 (s, 3H); **^{13}C-NMR** ($CDCl_3$, 100 MHz): δ (ppm) = 153.6, 136.4, 133.4, 104.9, 61.1, 56.4, 17.2; $\mathbf{R_f}$ = 0.50 on 1:4 EA:Hex; **HRMS** (EI^+) for $C_{10}H_{14}O_3S^+$ = [M^+]: calcd. m/z 214.0667, found m/z 214.0643, for $C_9H_{11}O_3S^+$ = [M-CH_3^+]: calcd. m/z 199.0428, found m/z 199.0423.

(2-Iodo-3,4,5-trimethoxyphenyl)(methyl)sulfane (S13)

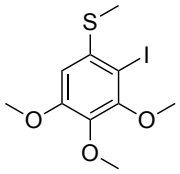

To a solution of **S12** (1.82 g, 8.48 mmol, 1.00 eq.) in acetonitrile (90 mL) were added *N*-iodosuccinimide (2.10 g, 9.33 mmol, 1.10 eq.) and 2,2,2-trifluoroacetic acid (338 mg, 2.97 mmol, 0.23 mL, 0.35 eq.) at room temperature. The reaction mixture was stirred for 1.5 h in the dark before a saturated aqueous solution of $Na_2S_2O_3$ (90 mL) was added. The solids were filtered off, the acetonitrile was removed under reduced pressure and the remaining aqueous layer was extracted with DCM (3 x 90 mL). The combined organic extracts were dried over Na_2SO_4, filtered, and evaporated. The crude product was purified by column chromatography (EA:Hx, 1:1) giving **S13** as an off-white solid (2.76 g, 7.26 mmol, 86 %).

^{1}H-NMR ($CDCl_3$, 400 MHz): δ (ppm) = 6.56 (s, 1H), 3.87 (s, 3H), 3.86 (s, 3H), 3.83 (s, 3H), 2.44 (s, 3H); **^{13}C-NMR** ($CDCl_3$, 100 MHz): δ (ppm) = 154.3, 153.7, 139.8, 138.0, 106.0, 85.9, 61.2, 60.9, 56.4, 18.0; **R_f** = 0.48 on 1:1 EA:Hex; **HRMS** (EI^+) for $C_{10}H_{13}IO_3S^+ = [M^+]$: calcd. m/z 339.9630, found m/z 339.9610.

Methyl 2,3,4-trimethoxy-6-(methylthio)benzoate (S14)

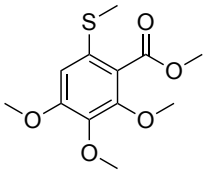

A solution of **S13** (340 mg, 1.00 mmol, 1.00 eq.) in dry THF (2 mL) was added to Turbo-Grignard (1.3 M in THF, 1.05 mmol, 0.77 mL, 1.05 eq.) at 0 °C under nitrogen. After complete magnesiation (as indicated *via* LC-MS, 45 min.), freshly distilled methyl chloroformate (bp. 69 °C, 243 mg, 2.50 mmol, 0.20 mL, 2.50 eq.) was added. The ice bath was removed and the reaction mixture was stirred for 21 h at room temperature. A saturated aqueous solution of NH_4Cl (5 mL) was added and the phases were separated. The aqueous layer was extracted with DCM (3 x 10 mL), dried over Na_2SO_4, and evaporated. Purification by column chromatography (EA:Hex, 1:10) gave **S14** as an off-white solid (147 mg, 0.54 mmol, 54 %). **S12** was isolated as a side-product (14 mg, 0.07 mmol, 7 %).

^{1}H-NMR ($CDCl_3$, 400 MHz): δ (ppm) = 6.63 (s, 1H), 3.86 (s, 3H), 3.84 (s, 3H), 3.83 (s, 3H), 3.79 (s, 3H) 2.39 (s, 3H); **^{13}C-NMR** ($CDCl_3$, 100 MHz): δ (ppm) = 166.9, 154.7, 151.2, 140.7, 130.9, 123.2, 108.6, 61.8, 60.9, 56.2, 52.3, 18.3; **R_f** = 0.10 on 1:10 EA:Hex; **HRMS** (ESI^+) for $C_{11}H_{13}O_4S^+ = [M\text{-}CH_3O^+]$: calcd. m/z 241.05291, found m/z 241.05284, for $C_{12}H_{16}O_5NaS^+ = [M+Na^+]$ calcd. m/z 295.06107, found m/z 295.06111.

4,5,6-Trimethoxybenzo[*b*]thiophen-3(2*H*)-one (S15)

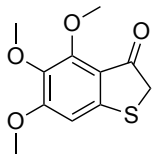

To a freshly prepared solution of LDA in THF was added a solution of **S14** (164 mg, 0.60 mmol, 1.00 eq.) in dry THF (3 mL) at - 78 °C and the reaction mixture was stirred for 1 h, then allowed to reach room temperature and stirred at room temperature for 1 h. The reaction was quenched by the addition of a saturated aqueous solution of NH_4Cl (15 mL), the phases were separated, and the aqueous phase was extracted with DCM (4 x 10 mL). The combined organic extracts were dried over Na_2SO_4, evaporated and the crude product was purified by column chromatography (EA:Hex, 1:4) yielding **S15** as a yellow solid (111 mg, 0.46 mmol, 77 %). After isolation, the product was frozen and stored under an atmosphere of nitrogen.

LDA was prepared by adding *n*BuLi (2.5 M in THF, 596 mg, 0.80 mL, 1.99 mmol, 3.31 eq.) to a solution of freshly distilled DIPA (219 mg, 0.31 mL, 2.17 mmol, 3.60 eq.) in dry THF (3 mL) at - 78 °C and stirring the solution for 15 min.

^{1}H-NMR ($CDCl_3$, 400 MHz): δ (ppm) = 6.59 (s, 1H), 3.97 (s, 3H), 3.89 (s, 3H), 3.79 (s, 3H), 3.74 (s, 2H); **^{13}C-NMR** ($CDCl_3$, 100 MHz): δ (ppm) = 196.5, 160.6, 154.0, 152.4, 139.3, 117.2, 101.9, 62.0, 61.5, 56.5, 40.3; **R_f** = 0.32 on 1:4 EA:Hex (blue fluorescence upon illumination with 254 nm); **HRMS** (ESI^+) for $C_{11}H_{13}O_4S^+$ $[M+H^+]$: calcd. m/z 241.05291, found m/z 241.05281, for $C_{11}H_{12}O_4NaS^+ = [M+Na^+]$: calcd. m/z 263.03485, found m/z 263.03485.

Synthesis of HOTub-70

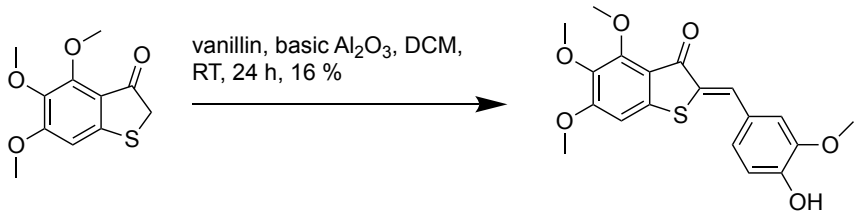

S15 **HOTub-70**

Scheme **S6**: Synthesis of **HOTub-70**

S15 (46 mg, 0.19 mmol, 1.00 eq.) was dissolved in DCM (5 mL), then vanillin (23 mg, 0.15 mmol, 0.80 eq.) and basic aluminium oxide (200 mg) were added. After stirring at room temperature for one day, the formation of yellow hemithioindigo could be observed. The suspension was filled into a narrow, sand filled column, and the hemithioindigo was desorbed by rinsing the aluminium oxide with acetone, DCM and MeOH, until the solvents were colourless. The mixture was then dried over Na_2SO_4 and evaporated. The crude product was dissolved in $CHCl_3$ and washed with a saturated solution of Na_2SO_3 in 50 % EtOH (3 x 10 mL), 50 % EtOH (2 x 10 mL) and brine (1 x 10 mL) to remove residual aldehyde. After drying over Na_2SO_4, the product was purified via column chromatography yielding **HOTub-70** as yellow crystals (11 mg, 0.03 mmol, 16 %).

^{1}**H NMR** (400 MHz, $CDCl_3$): δ (ppm) = 7.72 (s, 1H), 7.18 (dd, *J* = 8.3 / 2.0 Hz, 2H), 7.11 (d, *J* = 2.0 Hz, 1H), 6.94 (d, *J* = 8.3 Hz, 1H), 6.67 (s, 1H), 5.90 (s, 1H), 4.00 (s, 3H), 3.91 (s, 3H), 3.90 (s, 3H), 3.80 (s, 3H); ^{13}**C NMR** (101 MHz, $CDCl_3$): δ (ppm) = 185.5, 159.9, 154.7, 147.5, 146.7, 143.7, 140.1, 132.4, 128.5, 127.1, 125.7, 117.2, 115.1, 112.7, 101.7, 62.2, 61.6, 56.5, 56.0; **HRMS** (ESI^+) for $C_{19}H_{19}O_6S^+$ = [M+H$^+$]: calcd m/z 375.08969, found m/z 375.08930.

Synthesis of HOTub-81

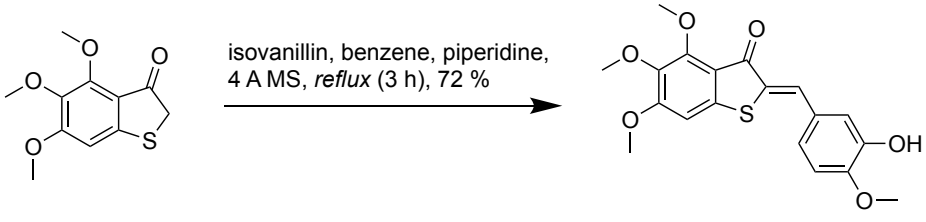

S15 **HOTub-81**

Scheme **S7**: Synthesis of **HOTub-81**

By Standard Procedure, commercial 3-hydroxy-4-methoxybenzaldehyde (44 mg, 0.29 mmol, 0.87 eq.) was reacted with **S15** (80 mg, 0.33 mmol, 1.00 eq.) for 3 h. The crude was purified by column chromatography (EA:Hx, 1:2 →3:1) giving **HOTub-81** as a red solid (78 mg, 0.21 mmol, 72 %).

^{1}H-NMR ($CDCl_3$, 400 MHz): δ (ppm) = 7.75 (s, 1H), 7.27 (d, *J* = 2.1 Hz, 1H), 7.18 (dd, *J* = 2.1 / 8.0 Hz, 1H), 6.91 (d, *J* = 8.4 Hz, 1H), 6.70 (s, 1H), 5.69 (s, 1H), 4.04 (s, 3H), 3.94 (s, 3H), 3.93 (s, 3H), 3.85 (s, 3H); **^{13}C-NMR** ($CDCl_3$, 100 MHz): δ (ppm) = 185.7, 160.0, 154.8, 148.2, 146.0, 144.0, 140.2, 132.2, 129.3, 128.2, 124.8, 117.2, 116.1, 110.9, 101.8, 62.3, 61.7, 56.6, 56.2; **R_f** = 0.24 on 1:2 EA:Hx; **HRMS** (ESI^+) for $C_{19}H_{19}O_6S^+$ [$M+H^+$]: calcd. m/z 375.08969, found m/z 375.09004; **HRMS** (ESI^-) for $C_{19}H_{17}O_6S^-$ [$M-H^+$]: calcd. m/z 373.07513, found m/z 373.07548.

Determination of the E/Z-ratio in the photostationary state

For the determination of *E*/*Z* ratio in the photostationary state, solutions of **HOTub-31** (1 mM, 0.65 mL in d_6-DMSO) were prepared. To adapt the dark state, the vials were wrapped with aluminum foil and kept at 60 °C for 14 h. After cooling to room temperature, a ^{1}H-NMR spectrum (500 MHz, 32 scans) was recorded. Subsequently, the samples were transferred to a wide-necked vial, illuminated with a 450 nm LED for 2 min and a second ^{1}H-NMR spectrum was recorded. This procedure was repeated with a 505 nm LED. The ratio of the two photoisomers was determined by comparison of the integrals at 3.89 ppm (Z- isomer) and 3.90 ppm (E- isomer). At 450 nm, the PSS is comprised of 65 % E-isomer and 35 % Z-isomer, while at 505 nm the Z-isomer (74 %) is the dominating species.

In order to assess the influence of thermal relaxation under these measurement conditions, a sample was irradiated with 450 nm for 5 min and then split into two separate NMR tubes. The first tube was measured subsequently after irradiation, while the second tube was wrapped with aluminum foil and kept at room temperature for 20 min and a ^{1}H-NMR spectrum was recorded. No significant differences were observed and we concluded that relaxation under these conditions was negligeable.

UV-vis spectra were recorded in mixtures of DMSO and PBS (3:1 v:v) at 150 µM, covering the range from 340 to 600 nm. The samples were illuminated with 3 W (350 mA) Epistar LEDs (eBay *suiyanr*) shining through the optical beam of a quartz microcuvette, with second illumination periods at the same wavelength used to verify that PSS had indeed been reached (no evolution of the spectrum). Less than 30 s illumination was required to reach PSSs.

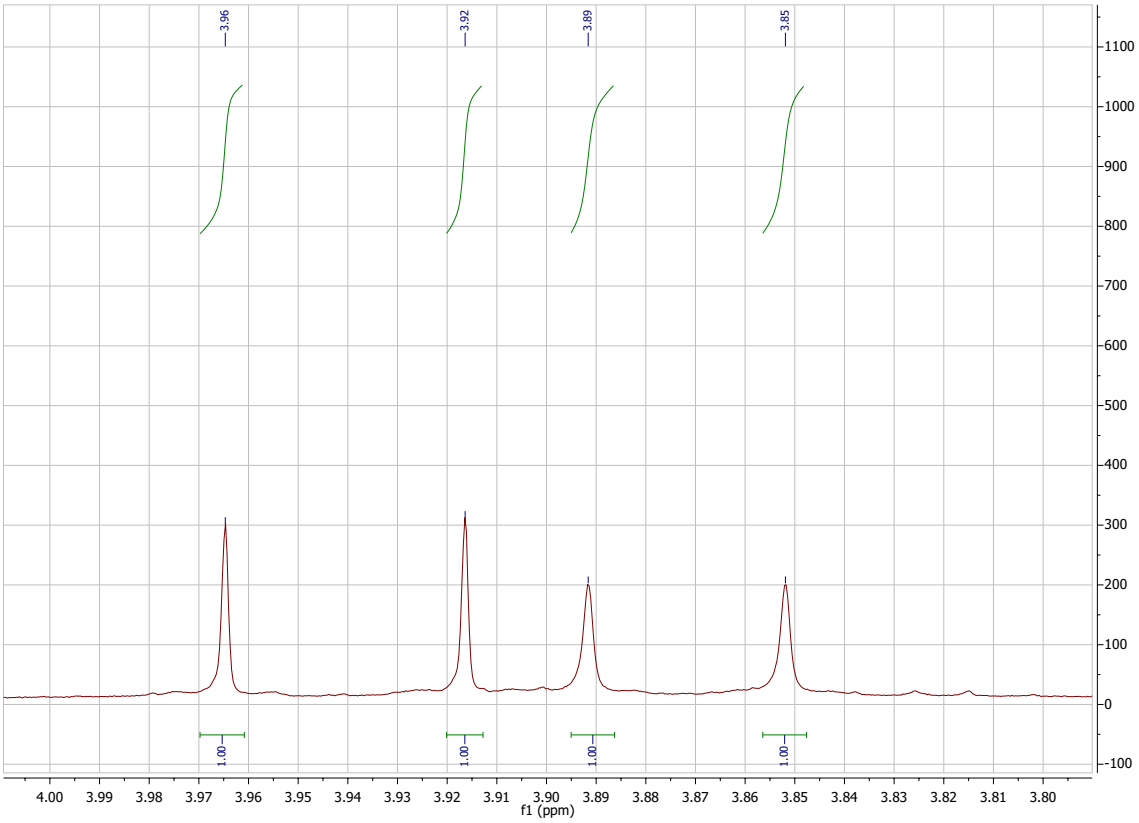

Figure S1: Section of the ^{1}H-NMR spectrum of **(all-*Z*)-HOTub-31** in the dark adapted state. Note that for easier comparison each signal of the methoxy groups is calibrated to 1.

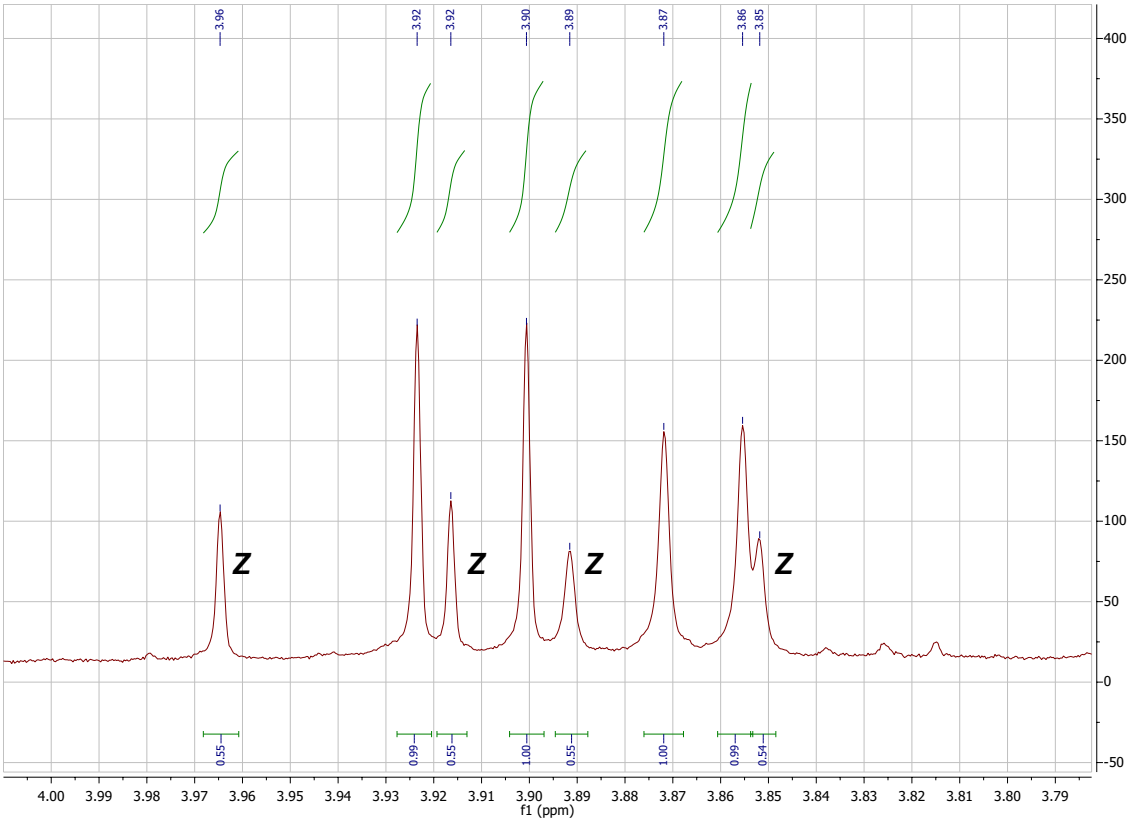

Figure S2: Section of the ^{1}H.NMR spectrum of **HOTub-31** in the PSS at 450 nm

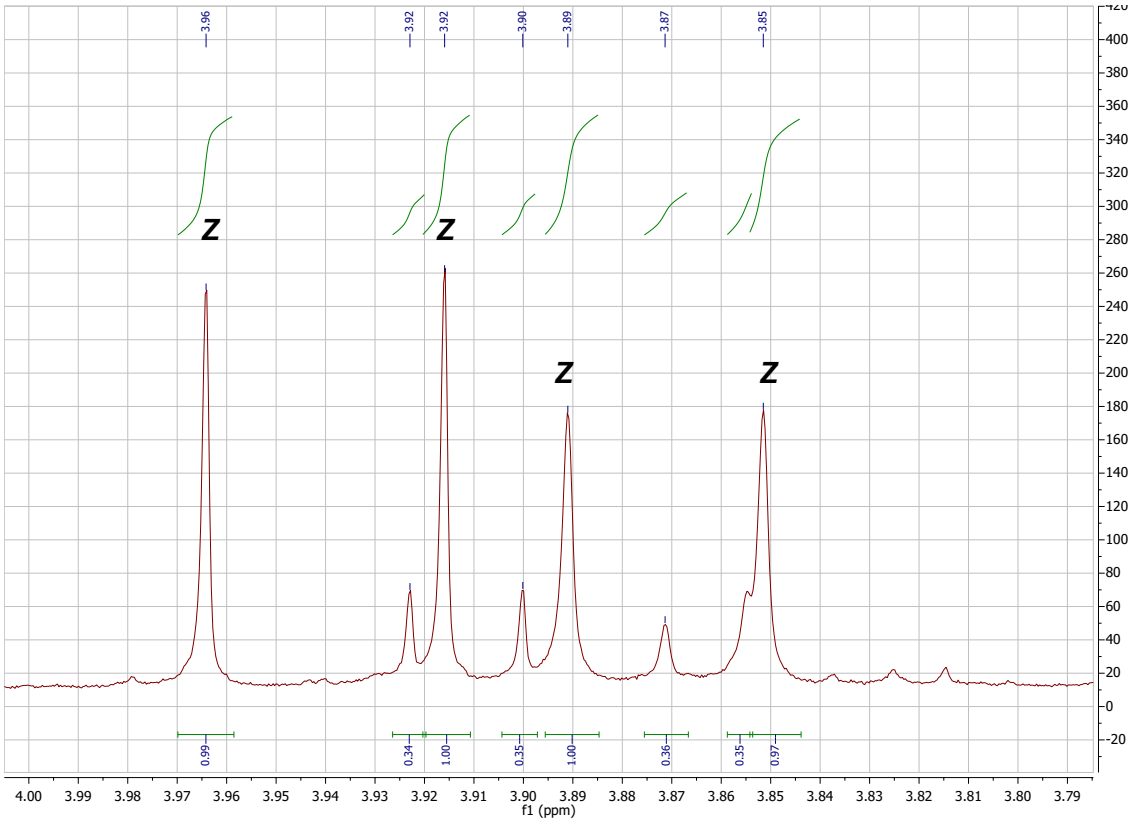

Figure S3: ^{1}H.NMR spectrum of **HOTub-31** in the PSS at 505 nm

in cellulo biology assays

General Cell Culture: HeLa cells were maintained under standard cell culture conditions. Compounds were applied using a minimum of co-solvent, typically 1 % DMSO. Cells were incubated in lightproof boxes or under pulsed illumination using a home-made LED lighting system as described before[3].

MTT assay: Mitochondrial dehydrogenase activity in HeLa cell lines was quantified by spectrophotometrically measuring the reduction of 3-(4,5-dimethylthiazol-2-yl)-2,5-diphenyl tetrazolium bromide (MTT) to formazan, as previously described.[3] Cells were seeded on 96-well microtitre plates. After 24 h, cells were treated with **HOTubs**, shielded from ambient light with light-proof boxes, and exposed to the appropriate light regimes (100 ms on every 60 s). Following 48 h of treatment, cells were incubated with 0.5 mg/mL MTT for 3 hours at 37 °C. The formazan crystals were dissolved in DMSO, and absorbance at 570 nm was measured using a FLUOstar Omega microplate reader (BMG Labtech). Results represent mean and SD, which are proportional to the cell number.

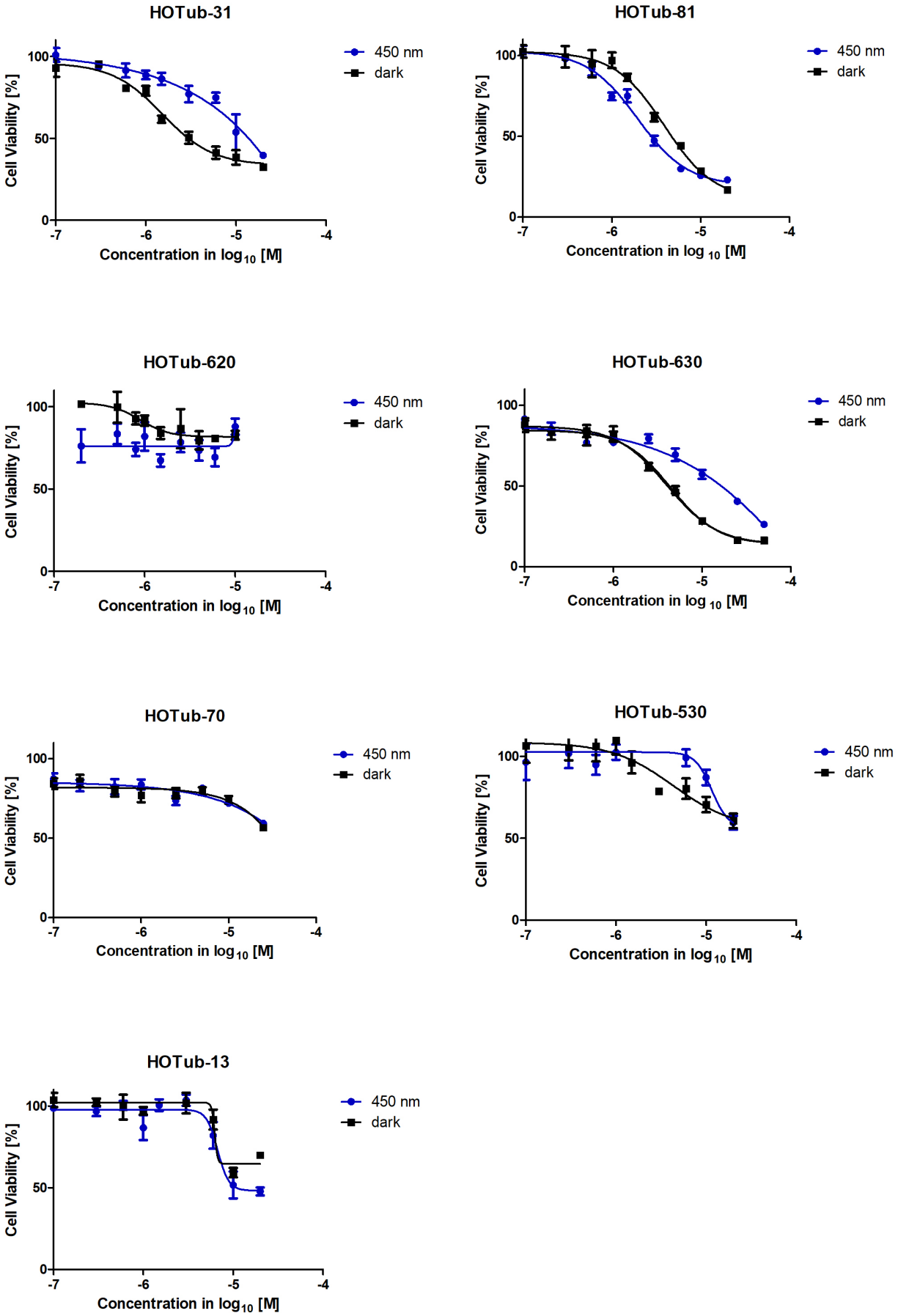

Figure S4: Representative results from MTT assays for **HOTubs**

Cell cycle analysis: Following treatment with **HOTubs** under the indicated light regime, cells were harvested and fixed in 70 % ethanol on ice and incubated in a staining solution [2 % DNase-free RNase A 10 mg/mL, 0.1 % Triton X-100 and 1 mg/mL propidium iodide (PI)] for 15 min at 37 °C. Following the PI staining cells were analysed by flow cytometry using a LSR Fortessa- BD company (FACS Core Facility – Gene Centre Munich, Munich, Germany) run by BD FACSDiva 8.0.1 software. The cell cycle analysis was subsequently performed using FlowJo-V10 software (Tree Star Inc., Ashland, OR, USA). Cells with subdiploid DNA content (inferior to G1 phase content) were considered as apoptotic in accordance with *Nicoletti et al*.[4] Results represent mean and SD calculated for triplicates from one representative experiment.

Fixed cell imaging by confocal microscopy: For fixed cell imaging, HeLa cells were seeded directly on glass coverslips in 24-well plates and treated with **HOTub**, either in the dark or under illumination by the LED array system using 410 nm or 450 nm LEDs and pulsing of 75 ms every 15 s or 100 ms every 60 s for 24 hours. Then the coverslips were washed with extraction buffer (80 mM PIPES pH 6.8; 1 mM $MgCl_2$, 5 mM ethylene glycol tetra-acetic acid (EGTA) dipotassium salt and 0.5 % Triton X- 100) for 30 s at 37 °C to remove monomeric and dimeric tubulin subunits and fixed for 10 min with a final concentration of 0.5 % glutaraldehyde or else 6 min in ice-cold methanol; the glutaraldehyde-fixed cells were then quenched for 7 min with 0.1 % $NaBH_4$ in PBS. Coverslips were washed with PBS twice and then blocked with PBS containing 10 % FCS and 0.3% Tween 20 for 30 min at room temperature. For immunofluorescence staining of microtubules, the cells were treated with primary antibody (rabbit alpha-tubulin AB (Abcam ab18251), 1:400 dilution in PBS/10 %FCS) for one hour and then washed with PBS before application of the secondary antibody (donkey anti-rabbit Alexa Fluor 488 (Abcam ab150073), 1:400 dilution in PBS/10 %FCS) for one hour. The coverslips were mounted on microscopy glass slides using Roti®-Mount FluorCare DAPI (Carl Roth) and then imaged with a Zeiss LSM 510, LSM 710 or SP5 confocal microscope.

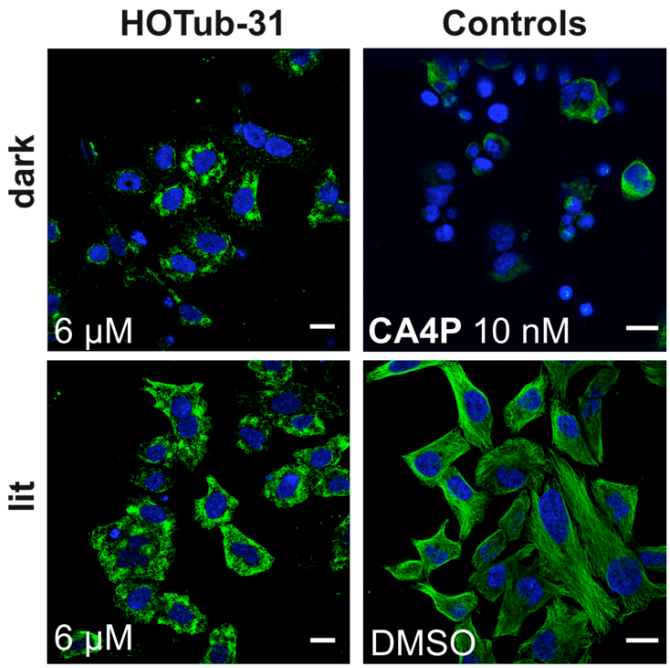

Figure S5: Extended immunofluorescence results from **HOTub-31** shows the dark-activity of this compound in more detail**.** Substantially greater microtubule depolymerisation is evident under dark conditions as compared to lit incubation, despite the lit condition's disruption of network integrity due to residual inhibition (likely from residual *Z*-**HOTub-31**).

Supplemental References

[1] H. E. Gottlieb, V. Kotlyar, A. Nudelman, *J. Org. Chem.* **1997**, *62*, 7512-7515.
[2] S. Kitzig, K. Ruck-Braun, *J Pept Sci* **2017**, *23*, 567-573.
[3] M. Borowiak, W. Nahaboo, M. Reynders, K. Nekolla, P. Jalinot, J. Hasserodt, M. Rehberg, M. Delattre, S. Zahler, A. Vollmar, D. Trauner, O. Thorn-Seshold, *Cell* **2015**, *162*, 403-411.
[4] I. Nicoletti, G. Migliorati, M. C. Pagliacci, F. Grignani, C. Riccardi, *J Immunol Methods* **1991**, *139*, 271-279.

NMR spectra

On the following pages, NMR spectra of intermediates towards and final products of the most bioactive compounds **HOTub-81** and **HOTub-81** are shown, as representative examples for all **HOTub** syntheses.

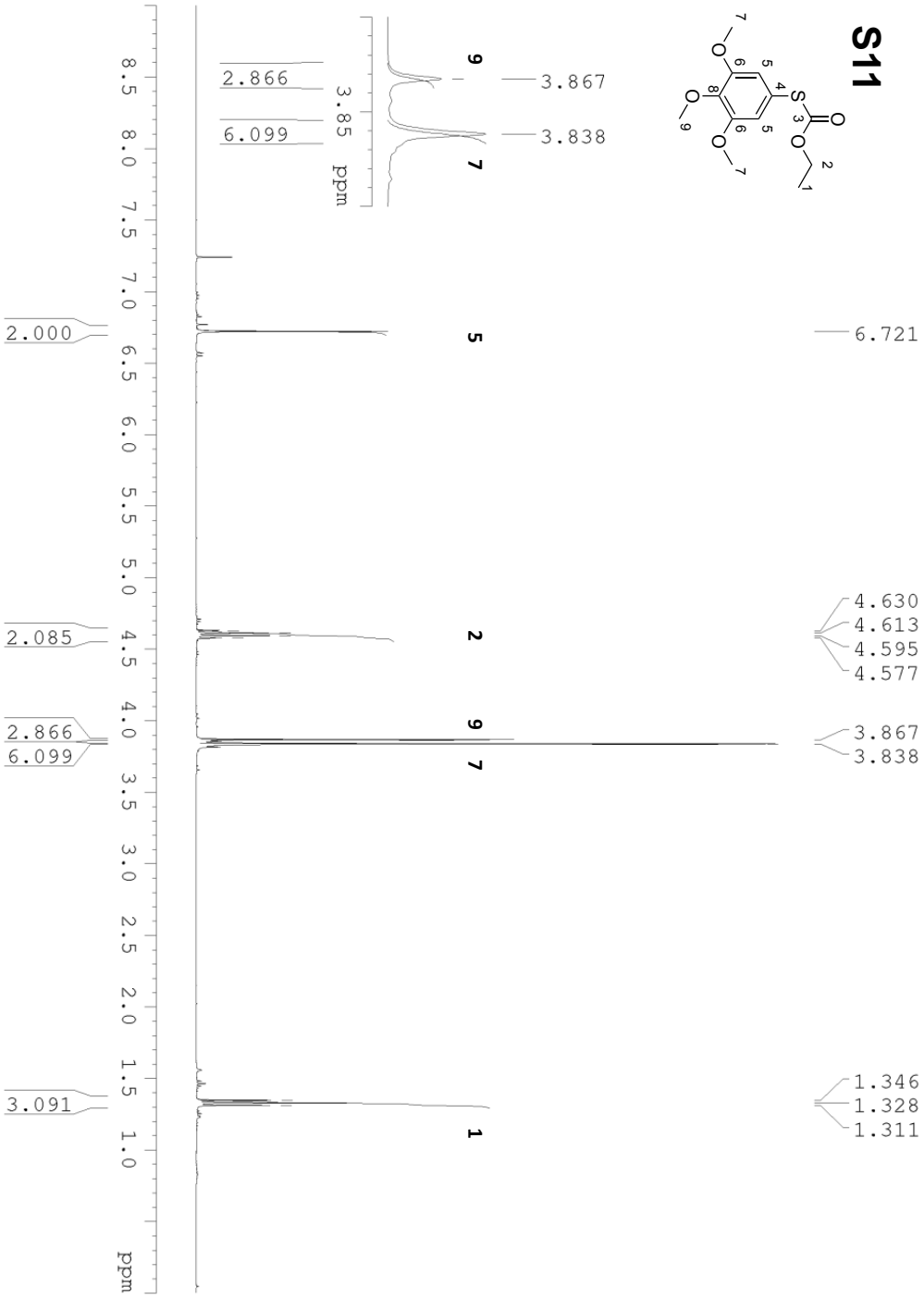
S11
2.866
6.099
3.85
ppm
3.867
3.838
2.000
2.085
2.866
6.099
3.091
6.721
4.630
4.613
4.595
4.577
3.867
3.838
1.346
1.328
1.311
ppm

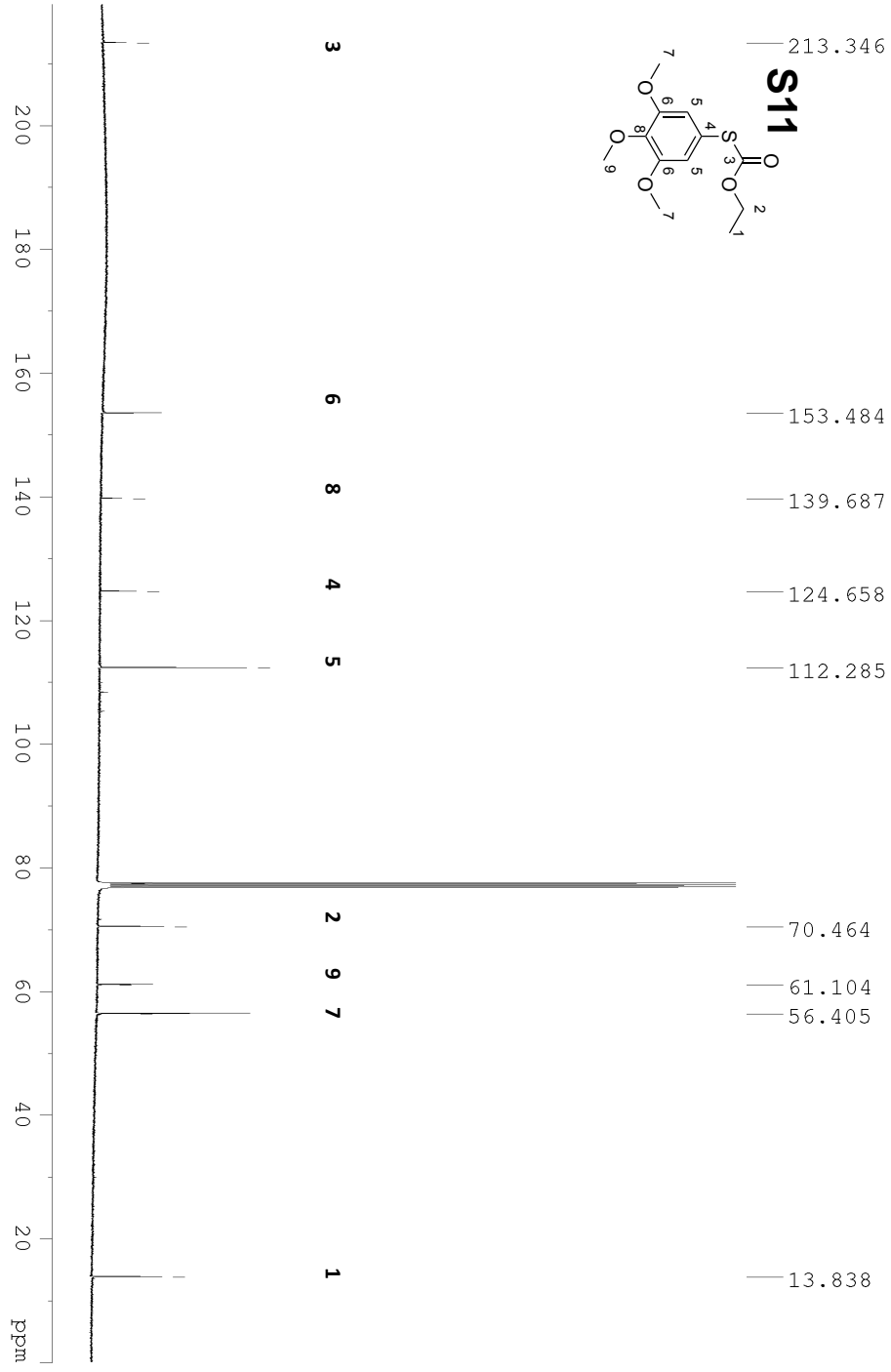
S11
213.346
153.484
139.687
124.658
112.285
70.464
61.104
56.405
13.838
ppm

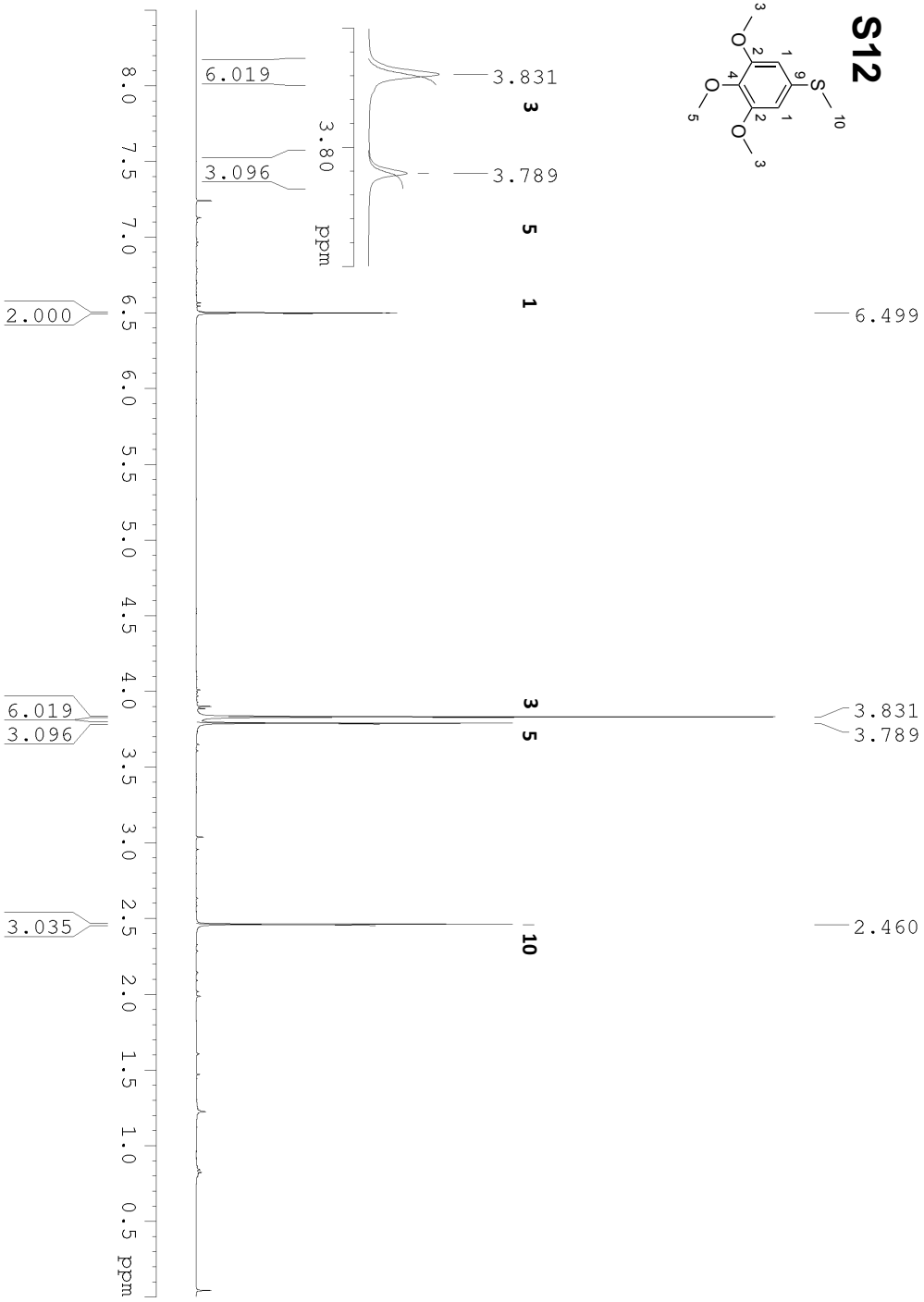
S12
6.019
3.096
3.80
ppm
3.831
3.789
2.000
6.499
6.019
3.096
3.831
3.789
3.035
2.460
8.0
7.5
7.0
6.5
6.0
5.5
5.0
4.5
4.0
3.5
3.0
2.5
2.0
1.5
1.0
0.5
ppm

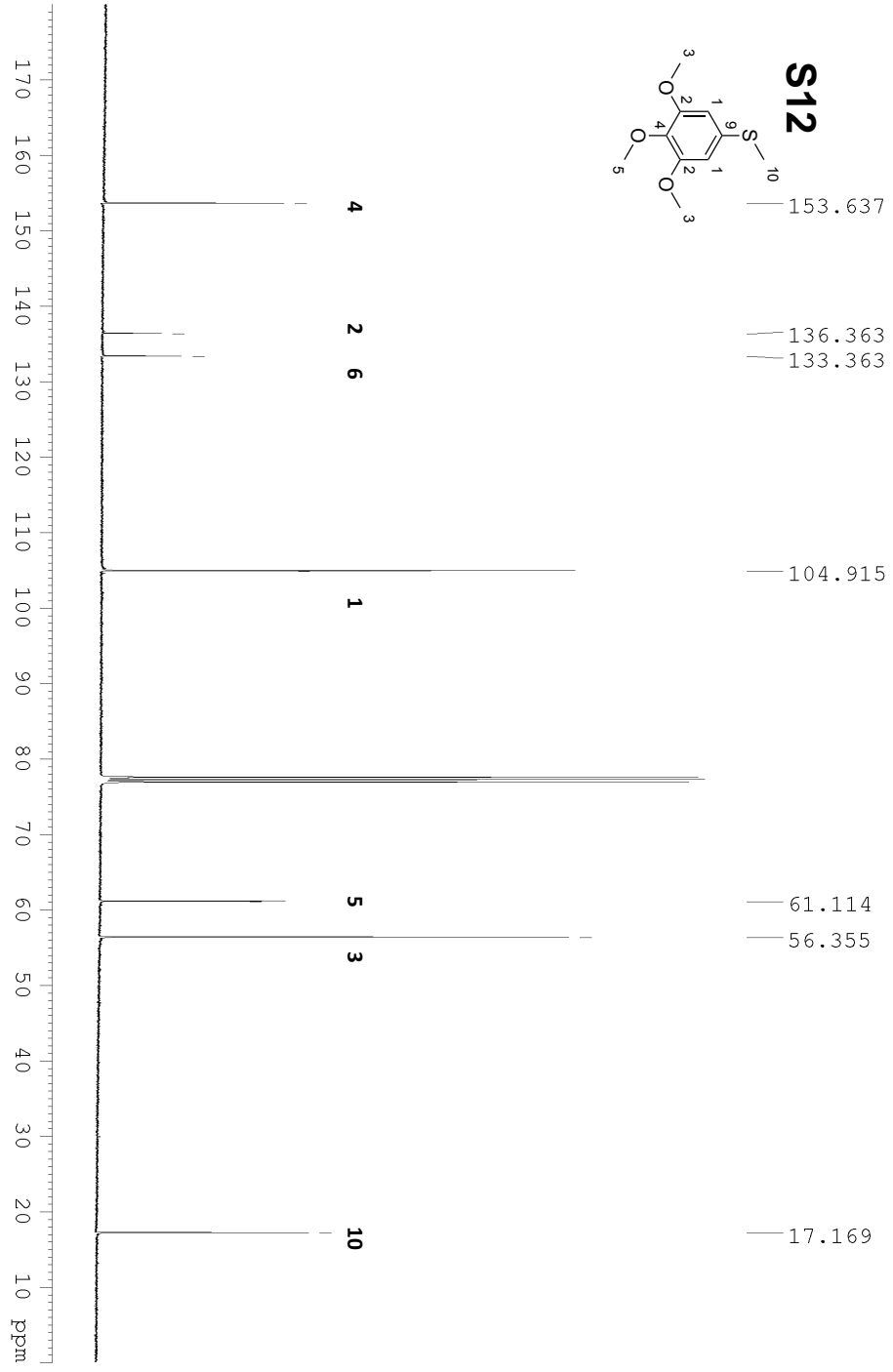
S12
153.637
136.363
133.363
104.915
61.114
56.355
17.169
4
2
6
1
5
3
10
170 160 150 140 130 120 110 100 90 80 70 60 50 40 30 20 10 ppm

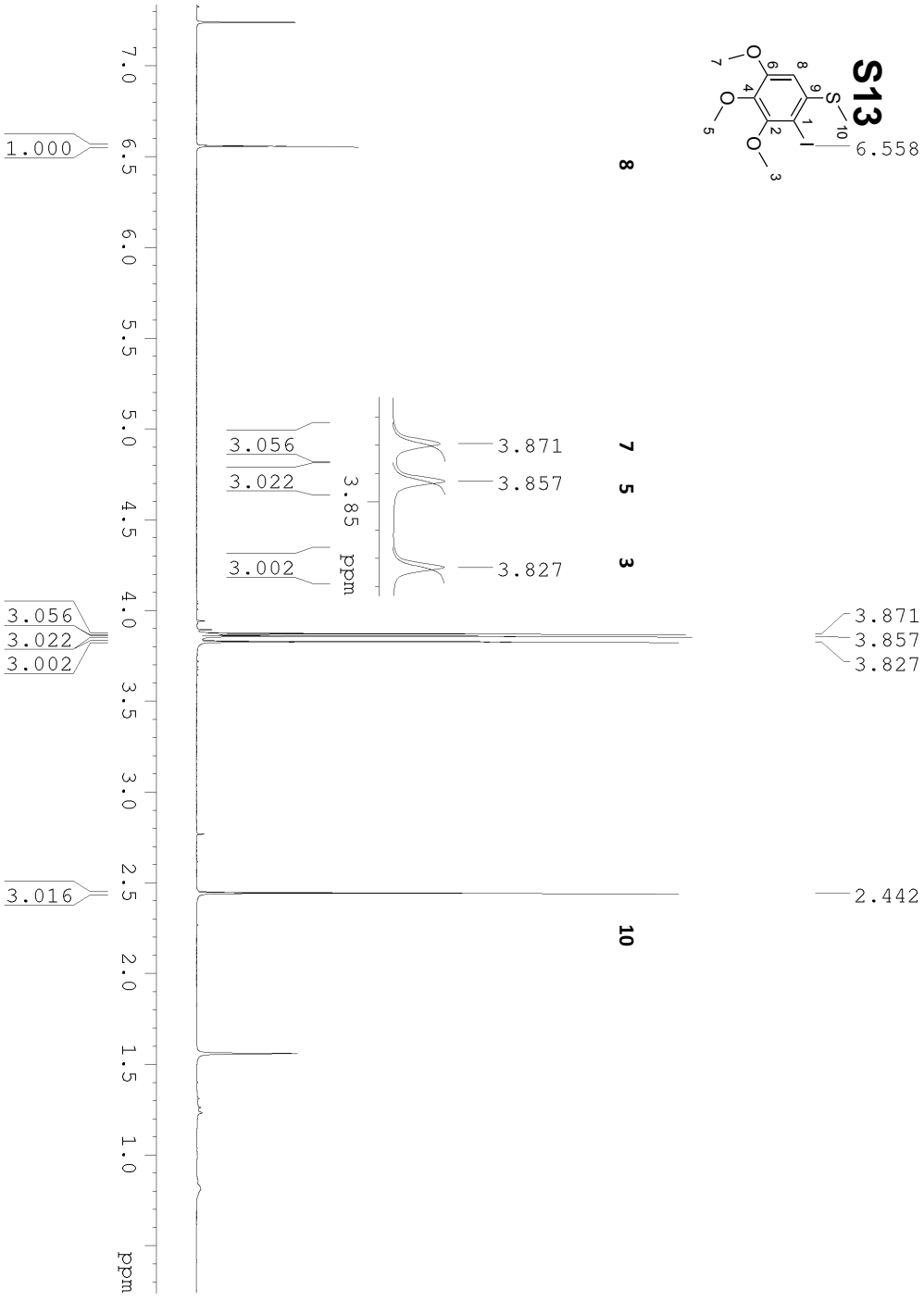
S13
6.558
1.000
3.056
3.022
3.002
3.016
3.871
3.857
3.827
2.442
8
7
5
3
10
3.85 ppm
ppm

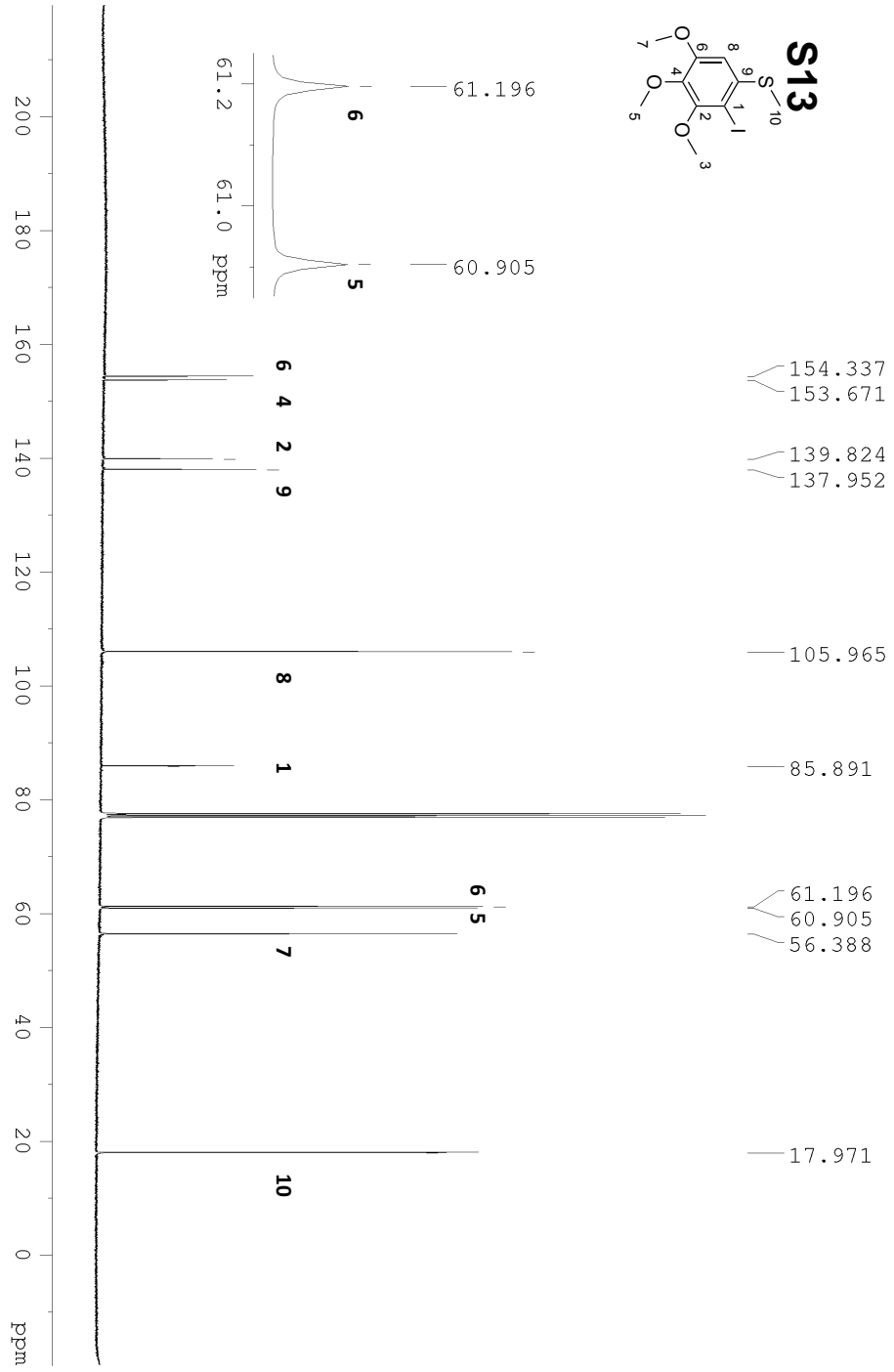
S13
61.196
60.905
61.2
61.0
ppm
154.337
153.671
139.824
137.952
105.965
85.891
61.196
60.905
56.388
17.971
200
180
160
140
120
100
80
60
40
20
0
ppm

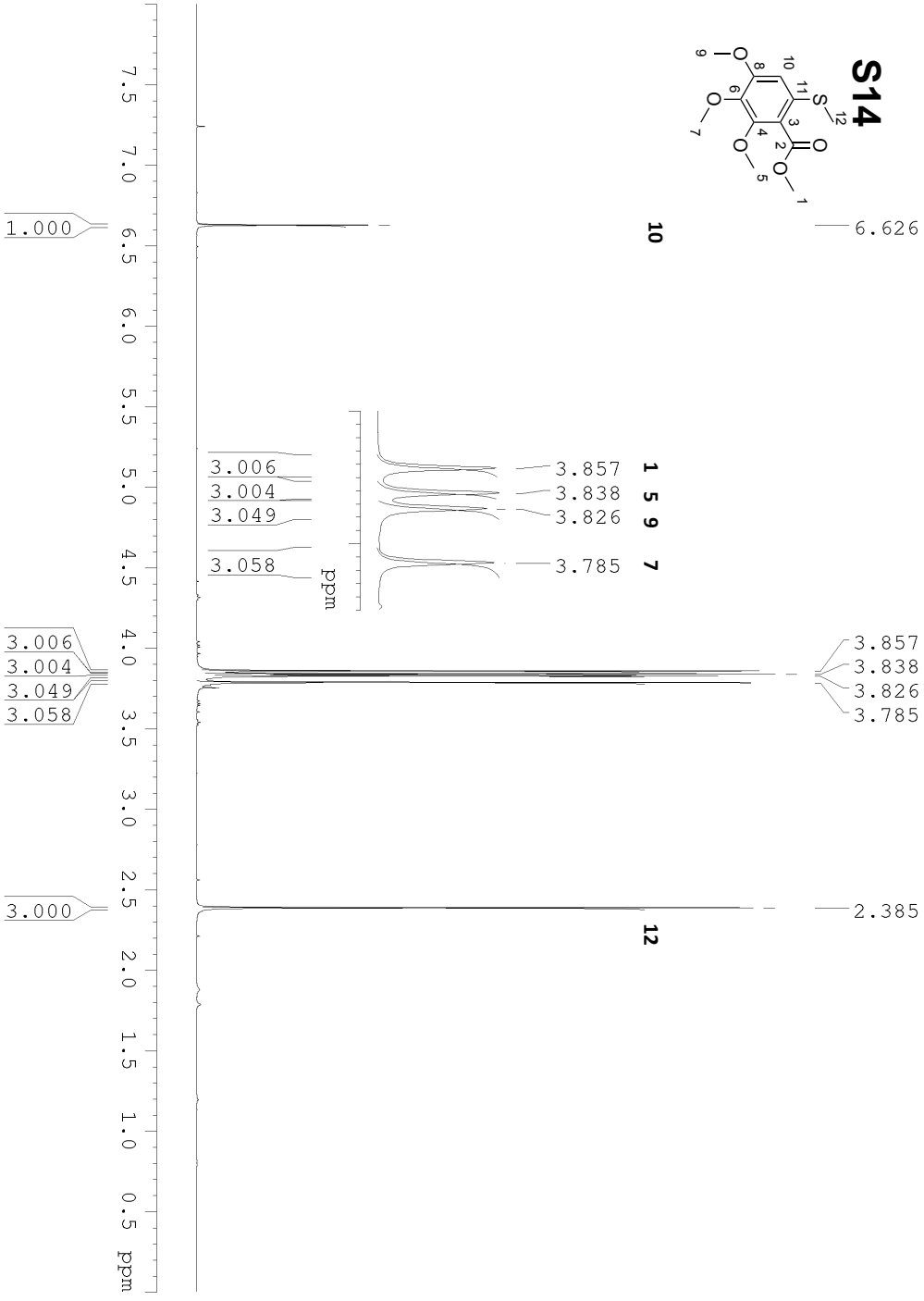
S14
1.000
3.000
6.626
2.385
3.857
3.838
3.826
3.785
3.006
3.004
3.049
3.058
10
1 5 9 7
12
ppm

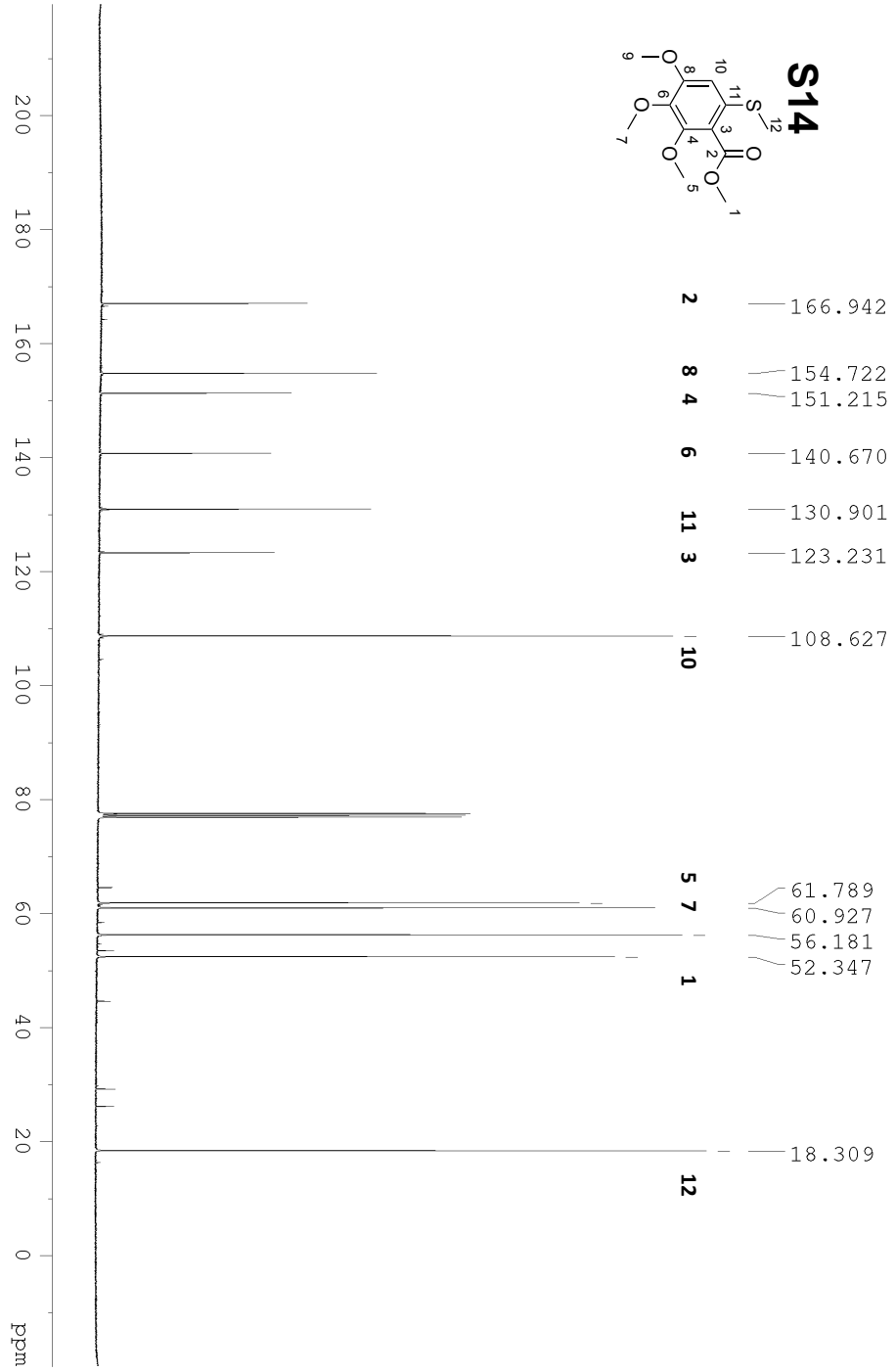
S14
200
180
160
140
120
100
80
60
40
20
0
ppm
2
8
4
6
11
3
10
5
7
1
12
166.942
154.722
151.215
140.670
130.901
123.231
108.627
61.789
60.927
56.181
52.347
18.309

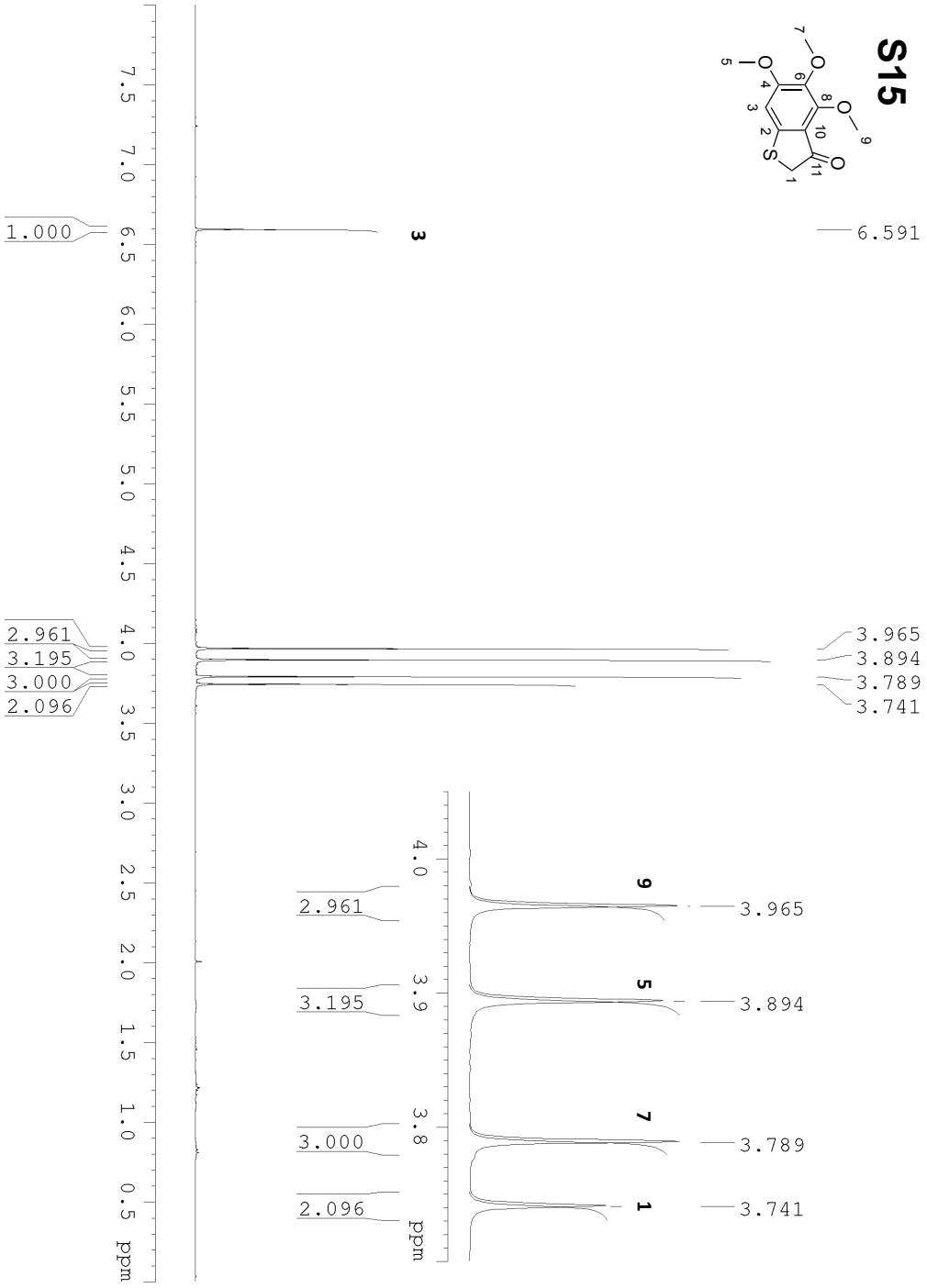
S15
1.000
2.961
3.195
3.000
2.096
3
6.591
3.965
3.894
3.789
3.741
9
5
7
1
ppm

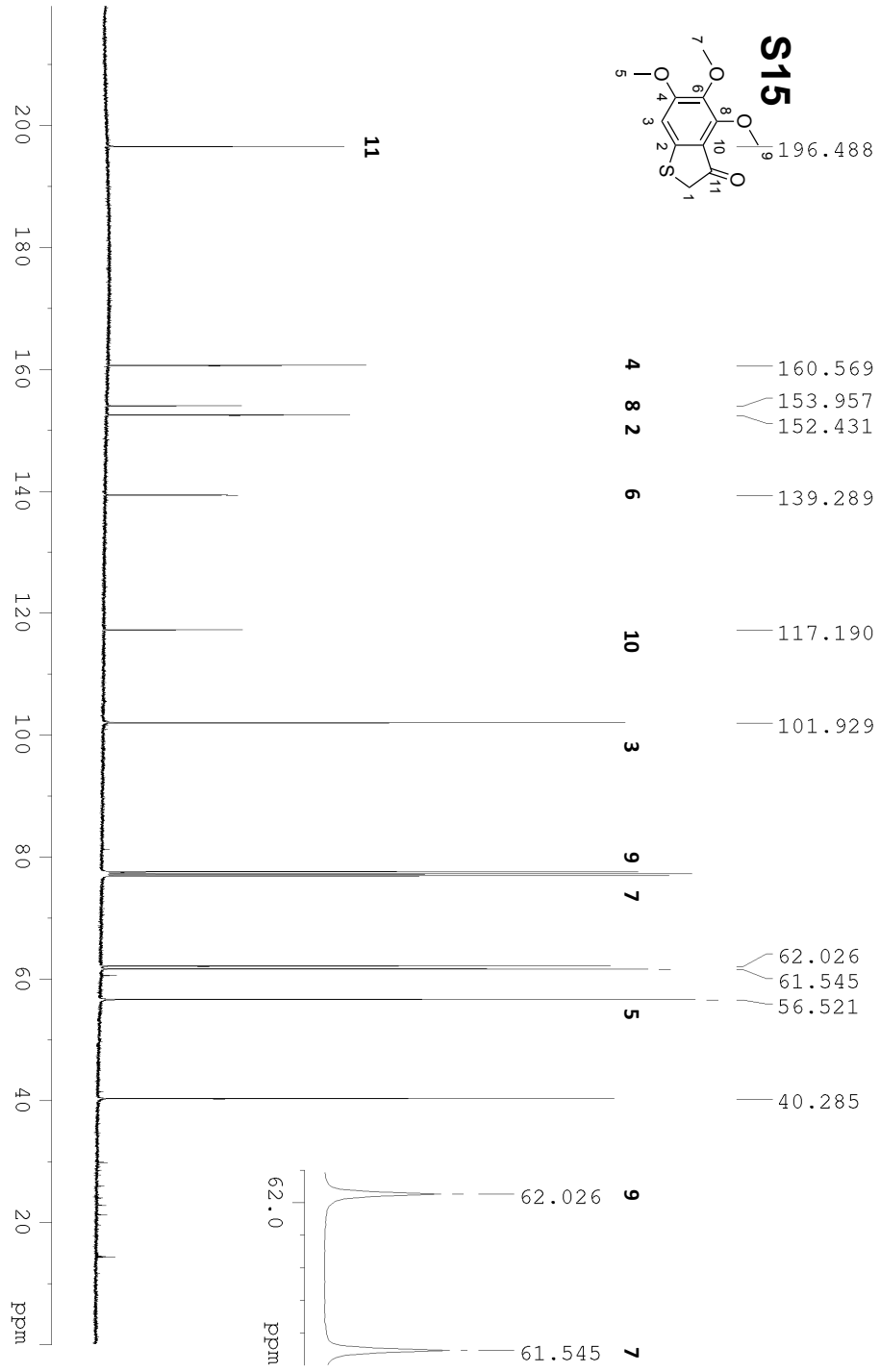
S15
196.488
160.569
153.957
152.431
139.289
117.190
101.929
62.026
61.545
56.521
40.285
11
4
8
2
6
10
3
9
7
5
62.026
61.545
ppm
200
180
160
140
120
100
80
60
40
20
62.0

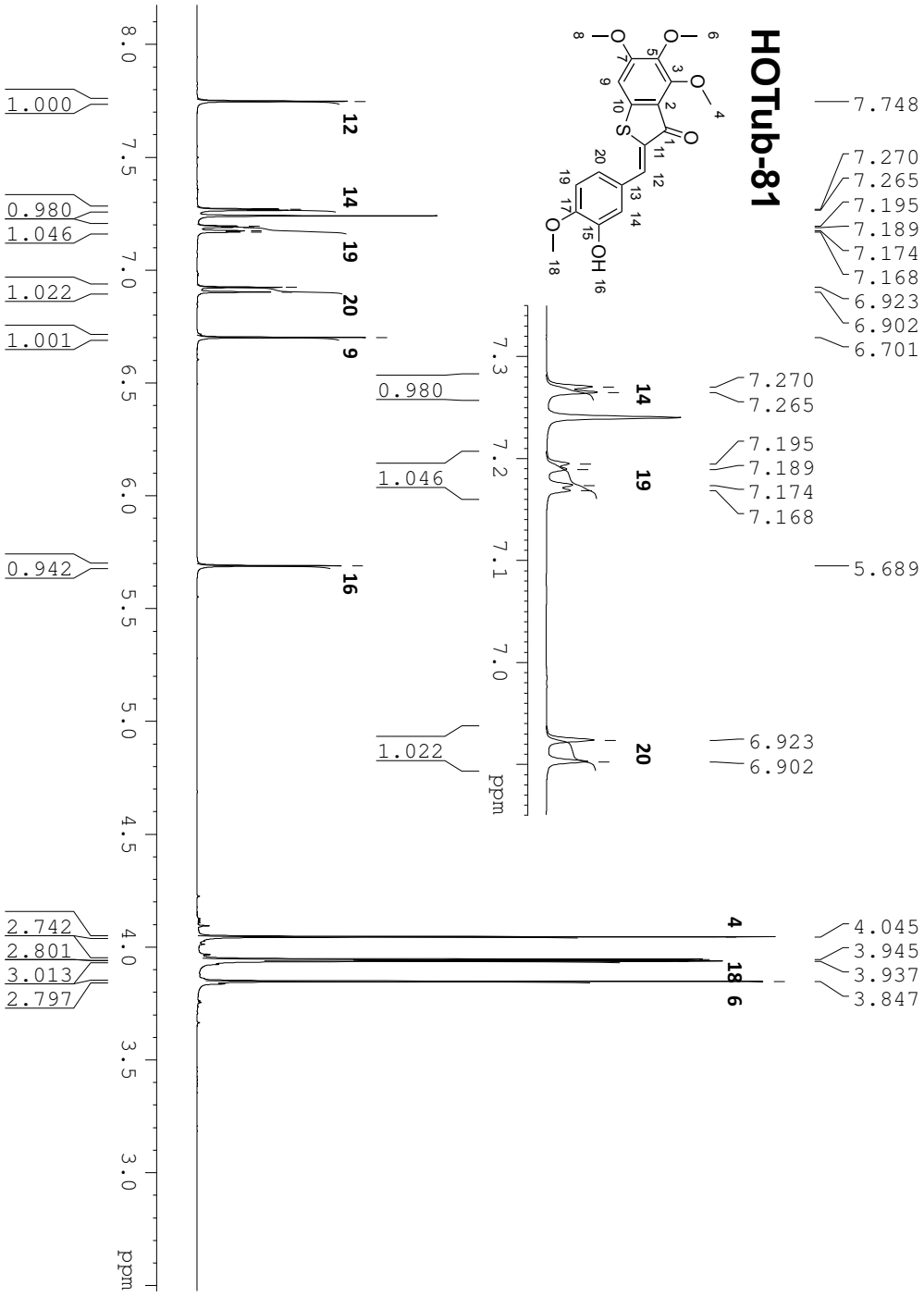
HOTub-81
7.748
7.270
7.265
7.195
7.189
7.174
7.168
6.923
6.902
6.701
5.689
4.045
3.945
3.937
3.847
1.000
0.980
1.046
1.022
1.001
0.942
2.742
2.801
3.013
2.797
ppm

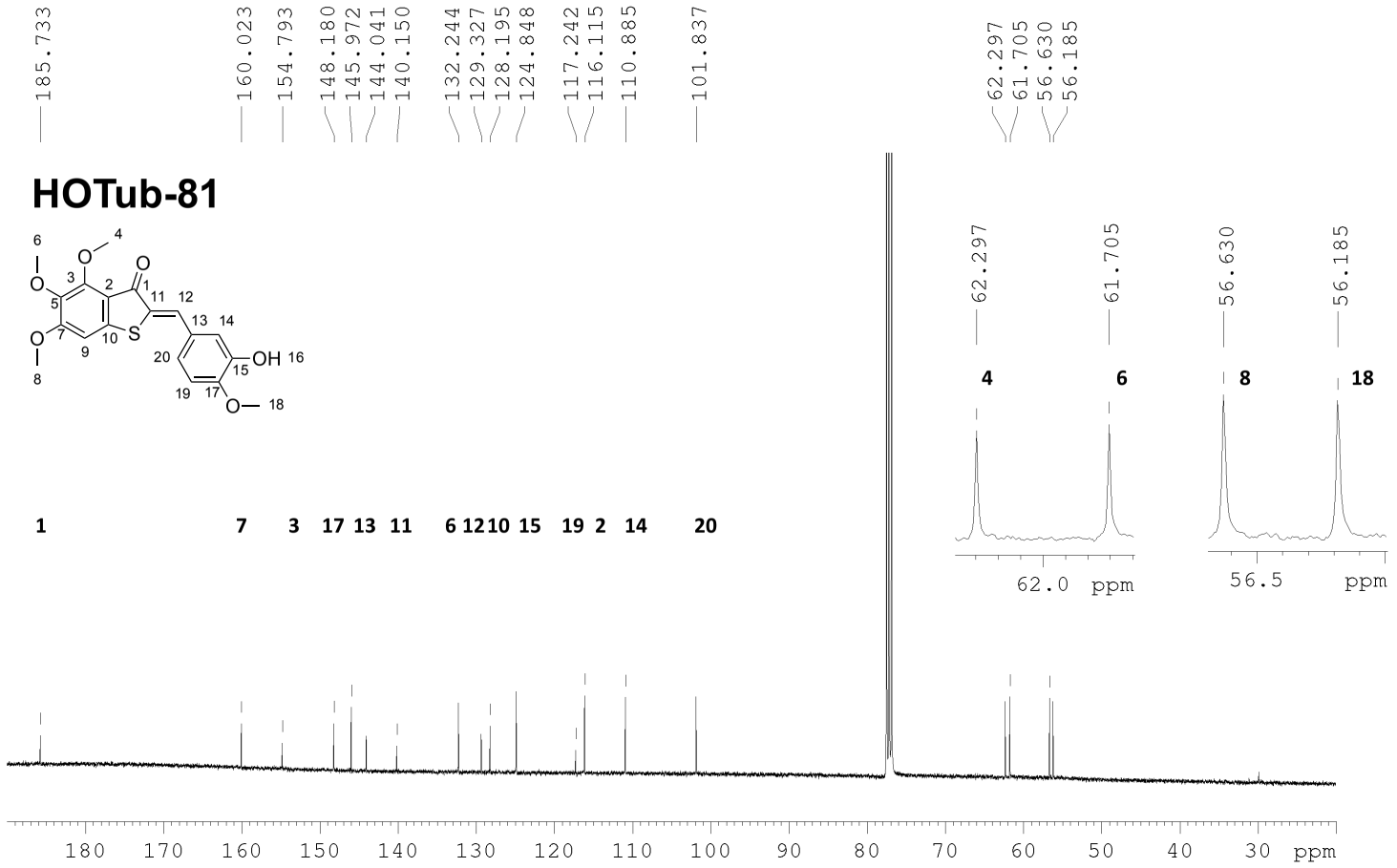
185.733
160.023
154.793
148.180
145.972
144.041
140.150
132.244
129.327
128.195
124.848
117.242
116.115
110.885
101.837
62.297
61.705
56.630
56.185
HOTub-81
1 7 3 17 13 11 6 12 10 15 19 2 14 20
4 6 8 18
62.0 ppm
56.5 ppm
180 170 160 150 140 130 120 110 100 90 80 70 60 50 40 30 ppm

2

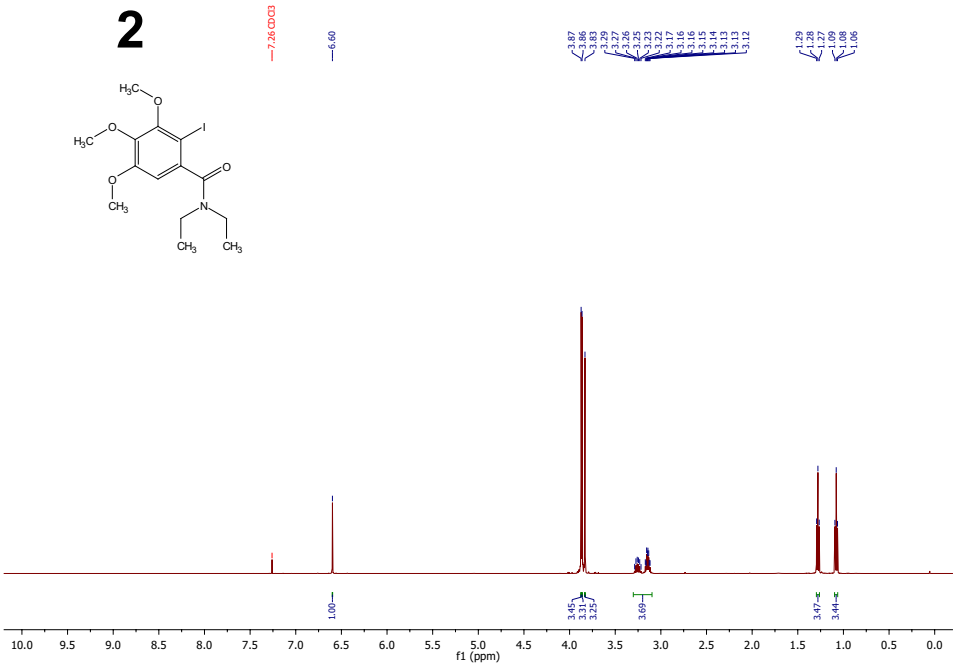
7.26 CDCl3
6.60
3.87
3.86
3.83
3.29
3.27
3.26
3.25
3.23
3.22
3.17
3.16
3.15
3.14
3.13
3.12
1.29
1.28
1.27
1.09
1.08
1.06
1.00
3.45
3.31
3.25
3.69
3.47
3.44
f1 (ppm)

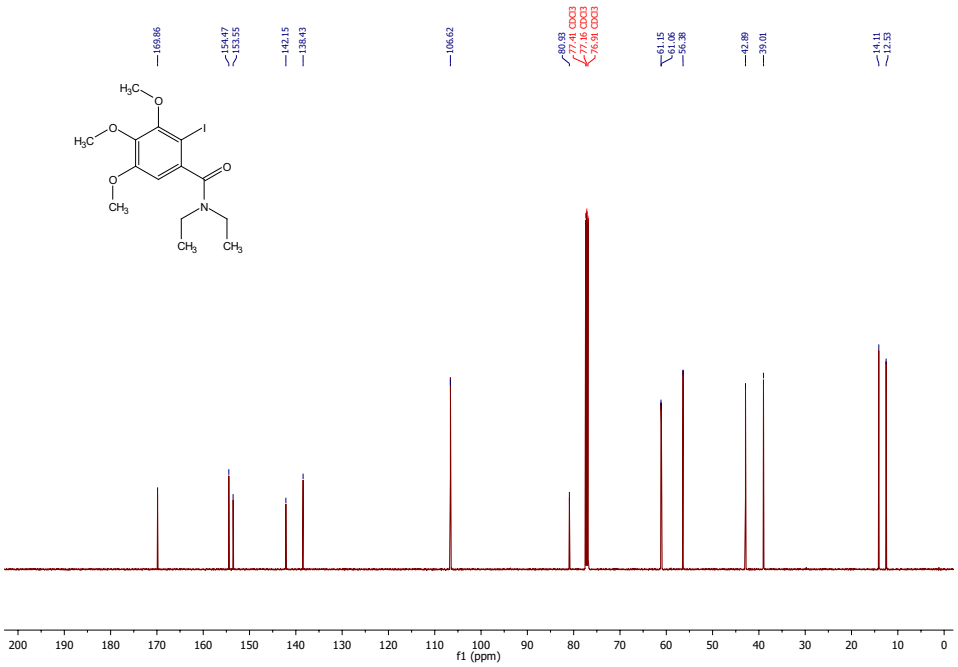
169.86
154.47
153.55
142.15
138.43
106.62
80.93
77.41 CDCl3
77.16 CDCl3
76.91 CDCl3
61.15
61.06
56.38
42.89
39.01
14.11
12.53
f1 (ppm)

3

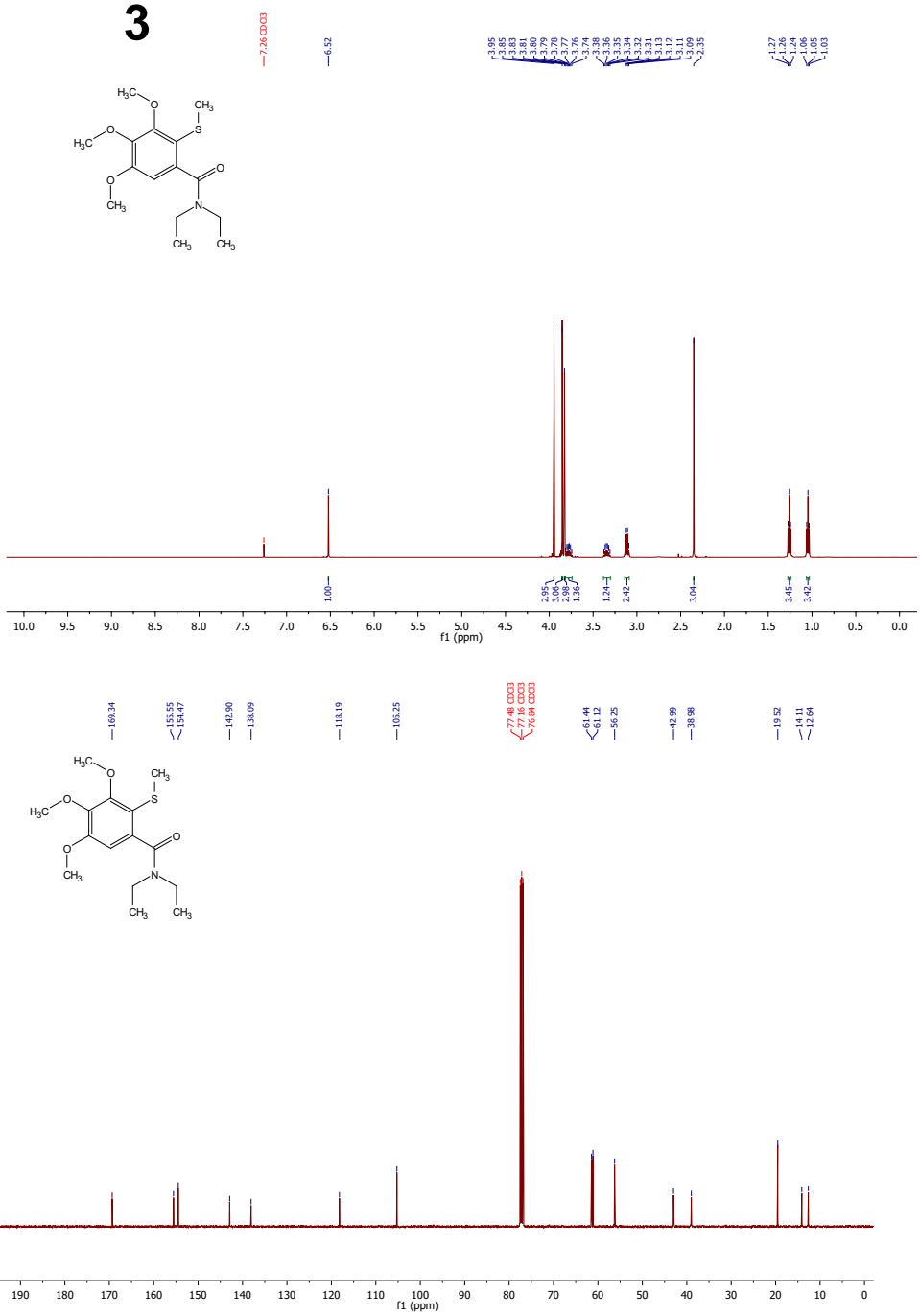
7.26 CDCl3
6.52
3.95
3.85
3.83
3.81
3.80
3.79
3.78
3.77
3.76
3.74
3.38
3.36
3.35
3.34
3.33
3.31
3.13
3.12
3.11
3.09
2.35
1.27
1.26
1.24
1.06
1.05
1.03
1.00
2.05
3.05
2.98
1.36
1.24
2.42
3.04
3.45
3.42
f1 (ppm)
169.34
155.55
154.47
142.90
138.09
118.19
105.25
77.48 CDCl3
77.16 CDCl3
76.84 CDCl3
61.44
61.12
56.25
42.99
38.98
19.52
14.11
12.64
f1 (ppm)

HOTub-31

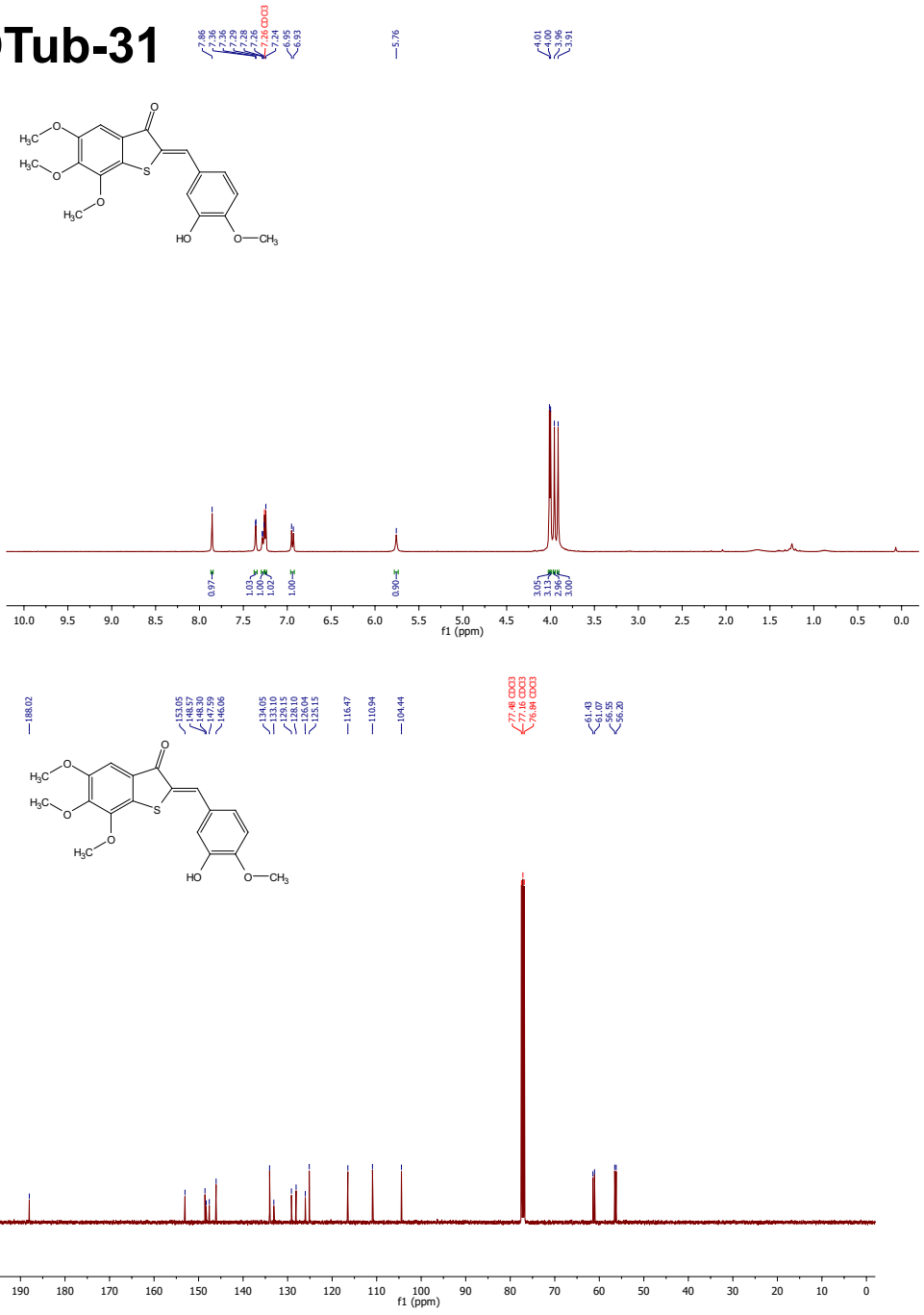
7.86
7.36
7.35
7.29
7.28
7.26
7.26 CDCl3
7.24
6.95
6.93
5.76
4.01
4.00
3.96
3.91
0.97
1.03
1.00
1.02
1.00
0.90
3.05
3.13
2.96
3.00
f1 (ppm)
188.02
153.05
148.57
148.30
147.59
146.66
134.05
133.10
129.15
128.10
126.04
125.15
116.47
110.94
104.44
77.48 CDCl3
77.16 CDCl3
76.84 CDCl3
61.43
61.07
56.55
56.20
f1 (ppm)

6. Paper Two: HITubs are highly potent photoswitchable tubulin inhibitors

Although **HOTubs** were successful in the first proof-of-concept study, they suffered from relatively low potency. In order to enhance the cellular potency of HTI-based tubulin photopharmaceuticals, we intentionally moved away from **CA4** as lead structure, and towards the highly potent synthetic indanone-derivative **indanocine**[131] (Fig. 14).

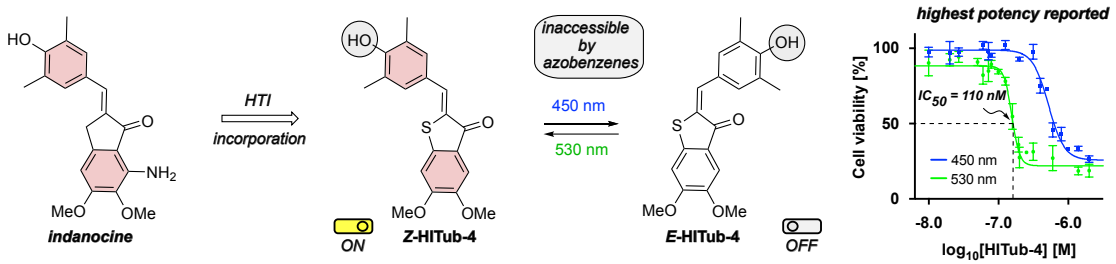

Fig. 14: HITubs are highly potent MT photopharmaceuticals bearing a substitution pattern that is not exploitable by azobenzene-based approaches (*p*-hydroxy arene).

We were also interested in the photochemistry of these *para*-hydroxylated hemithioindigos: While reports on the synthesis of similar compounds existed[54], no characterization of their photoproperties had been available. Since *para*-hydroxylated azobenzenes have negligibly short half-lives of the metastable isomers[63,64], we were particularly interested in the thermal relaxation rates and the pH-dependency of photoswitching. We found that in polar-protic organic solvents at neutral or acidic pH, bistable bulk photoswitching was confirmed, whereas increasing the pH resulted in complete loss of photoswitchability along with a bathochromic and hyperchromic shift of the absorption band. We reasoned that this was due to the formation of a quinoidal structure that resulted from deprotonation of the phenol. In such a structure, the connecting bond between the thioindigo and the stilbene fragment would be freely rotatable explaining the loss of photoswitchability. Oddly enough, bulk photoswitching could not be observed in neutral environment once aqueous buffer was introduced (DMSO with 25% buffer) where the formation of a quinoidal structure could be ruled out by UV-Vis. We assumed that this was most likely due to fast thermal relaxation of the metastable *E*-isomer. Thermal relaxation in polar-aprotic solvents occurs in the second range and decreases to milliseconds in ethanol which is still substantially slower than reported for similar azobenzenes.[63]

Despite the loss of photoswitchability observed in cell-free aqueous media and rather fast thermal relaxation, we assessed the cytotoxic effects of **HITubs**. Interestingly and to our delight, we noticed that these compounds were highly cytotoxic, and their bioactivity was photoswitchable under cellular conditions. We attributed this seemingly paradox finding to biolocalization of the **HITubs** in lipophilic compartments of the cell where their photoisomerization could proceed efficiently and their metastable isomers had sufficiently high half-lives.

We synthesized seven HTI analogs of indanocine and varied the methoxylation pattern of the bottom ring as well as the *para*-substituent and the methylation pattern of the top ring. Increasing the steric demand of the top ring (through exchange of the methyl with methoxy groups or alkylation of the phenol) abolished tubulin binding. On the other hand, removal of the phenolic hydroxyl gave a potent compound (IC_{50} = 400 nM) that, however, lacked photoswitchability of its bioactivity. Interestingly, we found the amino group present in **indanocine** not to be essential for potent cytotoxicity and in fact translating all features except for this amino group onto the HTI scaffold gave the most potent compound of the series, **HITub-4**.

Matching our expectations, all active compounds were more potent in their *Z*-isomer (*dark*-state activity). **Z-HITub-4** was the most potent photoswitchable tubulin inhibitor (IC_{50} = 110 nM, fourfold photoswitchability of activity) reported to that date with its activity being ten-fold higher than its predecessors **HOTubs**[114] and Gao's first-generation **SBTubs**[52] and five-fold enhanced compared to azocombretastatins.[24,130] In the dark (100% *Z*-isomer), **HITub-4** inhibited tubulin polymerization *in vitro*, induced MT disruption and mitotic cell cycle arrest. These findings reinforced our understanding of **HITubs** as photoswitchable MDAs.

In summary, we presented the most potent photoswitchable tubulin inhibitor to that date. We also elucidated the pH- and solvent-dependency on photoisomerization of HTIs with an electron-donating group in *para*-position and showcased that these compounds can indeed be a valuable tool for photopharmacology in cases where azobenzenes cannot be applied. Our results also corroborate that differentials in cellular bioactivity can be observed despite high thermal relaxation obtained *in vitro* experiments. This might be due to biolocalization in hydrophobic compartments of the cell. We believe that this is a finding which is of general interest in photopharmacology.

BEILSTEIN JOURNAL OF ORGANIC CHEMISTRY

Potent hemithioindigo-based antimitotics photocontrol the microtubule cytoskeleton in cellulo

Alexander Sailer, Franziska Ermer, Yvonne Kraus, Rebekkah Bingham, Ferdinand H. Lutter, Julia Ahlfeld and Oliver Thorn-Seshold*

Full Research Paper

Open Access

Address:
Department of Pharmacy, Ludwig Maximilian University of Munich, Butenandtstraße 5-13, Munich 81377, Germany

Email:
Oliver Thorn-Seshold* - oliver.thorn-seshold@cup.lmu.de

* Corresponding author

Keywords:
antimitotics; cytoskeleton; hemithioindigo; photopharmacology; photoswitch

Beilstein J. Org. Chem. **2020,** *16,* 125–134.
doi:10.3762/bjoc.16.14

Received: 31 July 2019
Accepted: 13 November 2019
Published: 27 January 2020

This article is part of the thematic issue "Molecular switches".

Guest Editor: W. Szymanski

Abstract

Background: Hemithioindigo is a promising molecular photoswitch that has only recently been applied as a photoswitchable pharmacophore for control over bioactivity in cellulo. Uniquely, in contrast to other photoswitches that have been applied to biology, the pseudosymmetric hemithioindigo scaffold has allowed the creation of both dark-active and lit-active photopharmaceuticals for the same binding site by a priori design. However, the potency of previous hemithioindigo photopharmaceuticals has not been optimal for their translation to other biological models.

Results: Inspired by the structure of tubulin-inhibiting indanones, we created hemithioindigo-based indanone-like tubulin inhibitors (**HITubs**) and optimised their cellular potency as antimitotic photopharmaceuticals. These **HITubs** feature reliable and robust visible-light photoswitching and high fatigue resistance. The use of the hemithioindigo scaffold also permitted us to employ a *para*-hydroxyhemistilbene motif, a structural feature which is denied to most azobenzenes due to the negligibly short lifetimes of their metastable *Z*-isomers, which proved crucial to enhancing the potency and photoswitchability. The **HITubs** were ten times more potent than previously reported hemithioindigo photopharmaceutical antimitotics in a series of cell-free and cellular assays, and allowed robust photocontrol over tubulin polymerisation, microtubule (MT) network structure, cell cycle, and cell survival.

Conclusions: HITubs represent a powerful addition to the growing toolbox of photopharmaceutical reagents for MT cytoskeleton research. Additionally, as the hemithioindigo scaffold allows photoswitchable bioactivity for substituent patterns inaccessible to the majority of current photopharmaceuticals, wider adoption of the hemithioindigo scaffold may significantly expand the scope of cellular and in vivo targets addressable by photopharmacology.

Introduction

The cytoskeletal scaffolding protein tubulin, a heterodimer consisting of α and β subunits, each of various isotypes, reversibly assembles into giant non-covalent polymeric microtubules (MTs), which play a pivotal role as a dynamic scaffold for a multitude of cellular processes. These include mechanostasis, the completion of mitosis, cell motility, and cargo trafficking in all cell types, as well as cell-type-specific roles, such as polarization, cargo sorting, and trafficking in neurons; the regulation and functioning of these processes is still not satisfactorily understood [1-4]. The MT cytoskeleton is a finely tuned complex system that is highly conserved through evolution. Direct genetic modifications of tubulin that affect its functions risk causing a diversity of effects, due to its many survival-critical roles, as well as non-functionality of the modified tubulin product. For example, knockout approaches have only been described for single isoforms of α/β-tubulin, and these cannot deliver the dynamic reversibility and effect-specificity that is required for understanding MT biology; and optogenetic modifications of tubulin have never succeeded. Instead, studies of the roles of MTs in these processes overwhelmingly rely on small molecule tubulin inhibitors [1].

Due to the non-invasiveness and high spatiotemporal precision with which optical stimulation can be applied, photopharmacology has drawn great interest for studies of crucial biological processes in a range of fields, from neuroscience [5,6] and G-protein-coupled receptor (GPCR) function [7,8] to antibiotic research [9]. Particularly in the context of MT biology, photopharmacology is an attractive development beyond classical small molecule inhibitors; since the spatiotemporal complexity inherent to the diversity of tubulin-dependent cellular processes may finally yield to studies that can leverage high-spatiotemporal-specificity optical control to deliver cell-specific, time-reversible modulation of native cytoskeleton function.

We and others have reported on photoswitchable azobenzene-based inhibitors of tubulin polymerisation [10-13] that have since been used in studies of neuronal trafficking [14] and embryonic development [15,16], and we have recently reported biologically robust heterostilbenes that deliver green fluorescent protein (GFP)-orthogonal MT photocontrol [17]. However, in both azobenzene and heterostilbene scaffolds, the steric properties of the *E*- and *Z*-isomer are so different that the protein binding site shape determines that the *Z*-isomer (the lit-form) is the more bioactive one, without the possibility of sign inversion by substituent shifts. To overcome this conceptual limitation, we recently reported on the first use of hemithioindigos (HTIs) as photoswitchable pharmacophores for optical control of tubulin dynamics in vitro (cell-free) and MT-dependent processes in cellulo [18]. We showed for the first time that the pseudosymmetry of hemithioindigos can be used to enable a priori design of HTI-based pharmacophores for a single binding site, with higher bioactivity as either the lit-form *E*- or the dark-

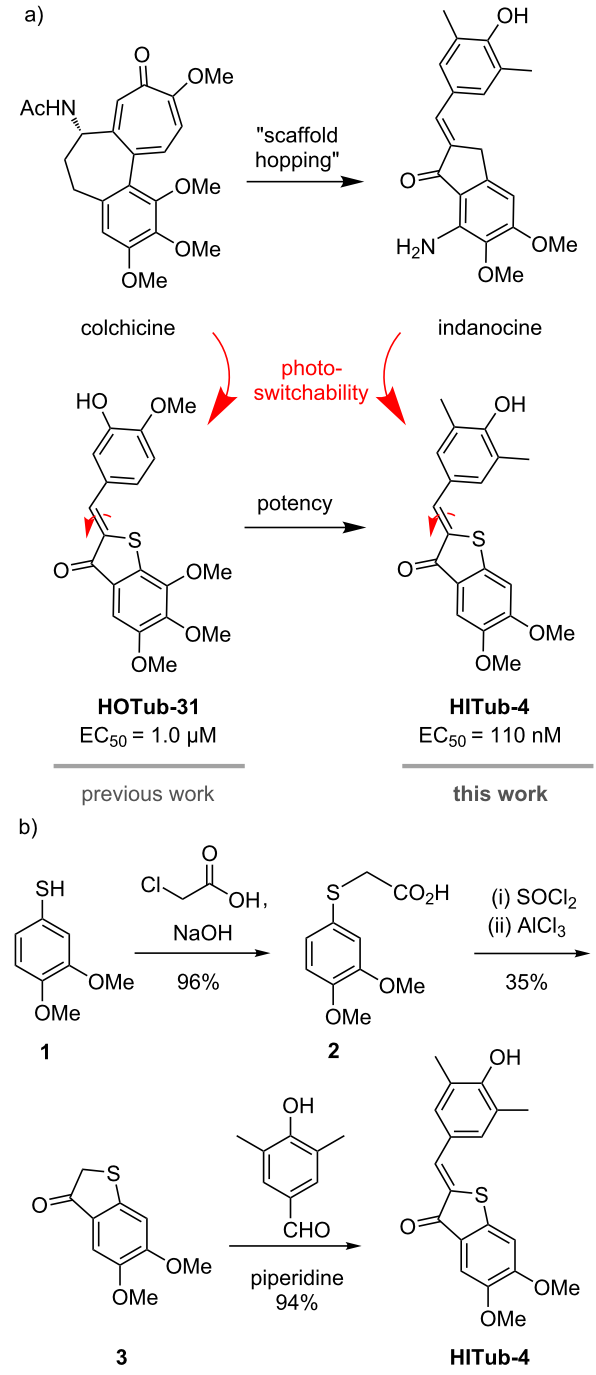

Figure 1: a) The potent tubulin inhibitor colchicine as a lead scaffold led to the development of the **HOTub** generation of HTI-based antimitotics (e.g., **HOTub-31**). Changing the lead scaffold to indanocine led to the development of up to ten times more potent **HITubs** (e.g., **HITub-4**). b) Straightforward, short, and high-yielding synthesis of **HITub-4**.

form *Z*-isomer, just by changing substituent patterns, and developed HTI-based antimitotics with cytotoxic potencies in the low micromolar range (Figure 1a) [18].

In this work, we wished to enhance the bioactivity of the distinctive dark-active HTI-based tubulin-binding antimitotics while retaining the benefits of the HTI scaffold, namely robust, fatigue-resistant, all-visible-light photoswitching.

Results and Discussion

Design strategy for HTIs

The HTI-based colchicinoid **HOTubs** (e.g., **HOTub-31**) that we previously explored had the HTI photoswitch embedded inside a methoxylation pattern, such that one isomer obeyed the structure–activity relationship (SAR) of colchicine or its analogue combretastatin A-4 and was bioactive, while the other isomer clashed with their SAR and was less active [18]. That approach of directly embedding a photoswitch motif inside the pharmacophore seemed to be more promising for photopharmacology than the synthetically more straightforward attachment of photoswitches on the pharmacophore periphery. We expected that embedding (which is referred to as azologization in the case of azobenzene-based photopharmaceuticals [19]) should in general lead to more significant alterations of the binding-relevant structure, and increase the differential potency between isomers of the resulting photopharmaceutical, than peripheral attachment (referred to as azo-extension in the case of azobenzenes [18]). We therefore desired to maintain the embedding strategy, yet to improve potency we chose to break with substitution patterns strictly based on colchicine. It is not the case that colchicine (or any other small-molecule inhibitor) represents an ideal structure that colchicine domain inhibitors (CDIs) should reproduce. Thus, our design focus was to introduce reversible photoresponse to a CDI rather than developing compounds with high similarity to colchicine per se, aiming at compounds where one isomer would be almost biologically inactive such that light can be used to effect a photoisomerisation-based switch-on/switch-off of bioactivity. The end-to-end distance of the HTI scaffold is significantly longer than that in either the biaryl colchicine or the stilbene combretastatin, and the torsion angle between the aryl blades of the HTI is nearly planar (up to 4°), while that between the rings of (*Z*)-combretastatin or colchicine is approximately 50–60° [20]. Thus, we assumed that the length and the near-planarity of the HTI could suit it to different substituent patterns to those of colchicine, and attempted to rationally determine these.

Firstly, since the HTI scaffold is longer than a biaryl motif but should occupy a similar volume in the pocket, we assumed that we would have to reduce the substituent bulk present on colchicine/combretastatin A-4. The middle methoxy group of colchicine's trimethoxy-substituted "south ring" (Figure 1a) makes a beneficial polar contact in the binding pocket via the oxygen atom, but upon demethylation, the potency is much reduced, presumably from insufficient desolvation in the colchicine site (which is known from work on podophyllotoxin derivatives [20]). We therefore chose to keep that methoxy group intact. However, colchicine's methoxy group on the "north ring" establishes a non-polar spacefilling interaction, which can be replaced equipotently by an ethyl group. Thus, we considered that the HTI scaffold could best be reduced in volume by "shortening" this substituent, maintaining the above-mentioned non-polar interaction.

Secondly, since the torsion angle of the HTI is far lower than that of (*Z*)-stilbenes or biaryl compounds, we considered that even with shortening, their SARs might not directly match. Mainly, we assumed that re-orientation of the substituent pattern on one or both rings (e.g., re-orientation of the archetypal 3,4,5-trimethoxyphenyl south ring pattern to a 4,5,6-trimethoxyaryl pattern) might be needed to occupy a similar space.

A wealth of CDIs have been reported, including scaffolds such as aurones that apparently reproduce the substituent pattern SAR of combretastatins [21] while having closely similar scaffold steric properties to HTIs. However, in light of the considerations above, we rather selected indanocine as a starting point for alternative substituent patterning (Figure 1a). Indanocine is a cytotoxic indanone-based CDI (EC_{50} ≈ 10–40 nM) [22] with similar cell culture potency to colchicine (EC_{50} ≈ 3–20 nM) [23] that likewise disrupts MTs, arrests cells in the G2/M phase, and induces apoptosis. Although the size and geometry of thioindoxyl and indanone rings differ because of the S/CH_2 replacement, we assumed that "mapping" the substitution pattern of indanocine onto a hemithioindigo core should result in a lead structure for tubulin-binding (*Z*)-HTIs, namely the class of **HITubs**.

The *para*-hydroxy substitution of indanocine suggested that HTI might be a more desirable photopharmaceutical scaffold than the widely used azobenzene motif. While *para*-hydroxyazobenzenes feature negligibly short *cis*-to-*trans* thermal relaxation half- lives in aqueous media in the range of µs [24,25], probably making them unsuitable for robust photoswitching applications against intracellular targets, data for *para*-hydroxy HTIs have not been reported so far. We considered that if the *para*-hydroxy-**HITubs** featured photoswitchable bioactivity in cellulo, implying suitable (*E*)-HTI stability under cellular conditions, this would more generally commend them as a scaffold of choice for cellular photo-

pharmaceutical use with strong electron-donating substituents, such as amino or hydroxy groups in *ortho*- or *para*-position, aiming at intracellular targets. This is an important scope of substituents to address, since these small polar groups often establish high-affinity ligand–target interactions, but otherwise represent an obstacle to photoswitchability with azobenzene compounds.

Preview: design of target **HITubs**

Our SAR-driven compound development path is described in full later in the section on bioactivity, but in brief, we began the series of indanocine-inspired HTI designs by replacing the south ring amino unit of indanocine (which is attached in *ortho*-position to the key south ring methoxy group) by a hydroxy function, giving **HITub-1** (Figure 2).

When **HITub-1** later proved less bioactive than we had wished, we explored steric and polarity changes to this south ring hydroxy group by methylation (**HITub-2**), methylation and shifting on the ring (**HITub-3**), or even its removal (**HITub-4**). We additionally controlled against our design logic of north ring substituent shortening (**HITub-5**). We also controlled for the SAR observation that CDIs should not tolerate a non-polar central north ring substituent (**HITub-6**), but can support removal of this substituent altogether, with only small potency loss (**HITub-7**) [20]. The progression and results of this SAR study are explained below in the section on bioactivity.

General synthetic access

Synthetic routes to HTIs are well established [26] and typically involve aldol condensation of benzaldehyde onto thioindoxyls. However, the key step is the formation (and where necessary, isolation) of the thioindoxyl species. In our studies, the electron-rich dimethoxy- and trimethoxy-substituted thioindoxyls were noted to be unstable to air, base, and silica gel during chromatography, so it was sought to minimise their exposure to these conditions during synthesis. In the end, we used two routes to the thioindoxyls: either Friedel–Crafts acylation of α-phenylthioacetic acids (which are easily accessible from thiophenols by alkylation using 2-chloroacetic acid, Figure 1b) or else, lithium diisopropylamide (LDA)-mediated cyclisation of 2-(methylthio)benzamides, which were obtained by directed *ortho*-metalation of the respective benzamides followed by quenching with dimethyl disulfide [27] (Supporting Information File 1, Scheme S1). In general, we found the LDA-mediated cyclisation more convenient, as it generated fewer side products and enabled faster, easier workup and purification. We used these routes to synthesise the **HITubs** typically in good (32% for **HITub-4**, Figure 1b) to excellent (93% for **HITub-7**, Scheme S5) overall yields from commercial building blocks (see Supporting Information File 1).

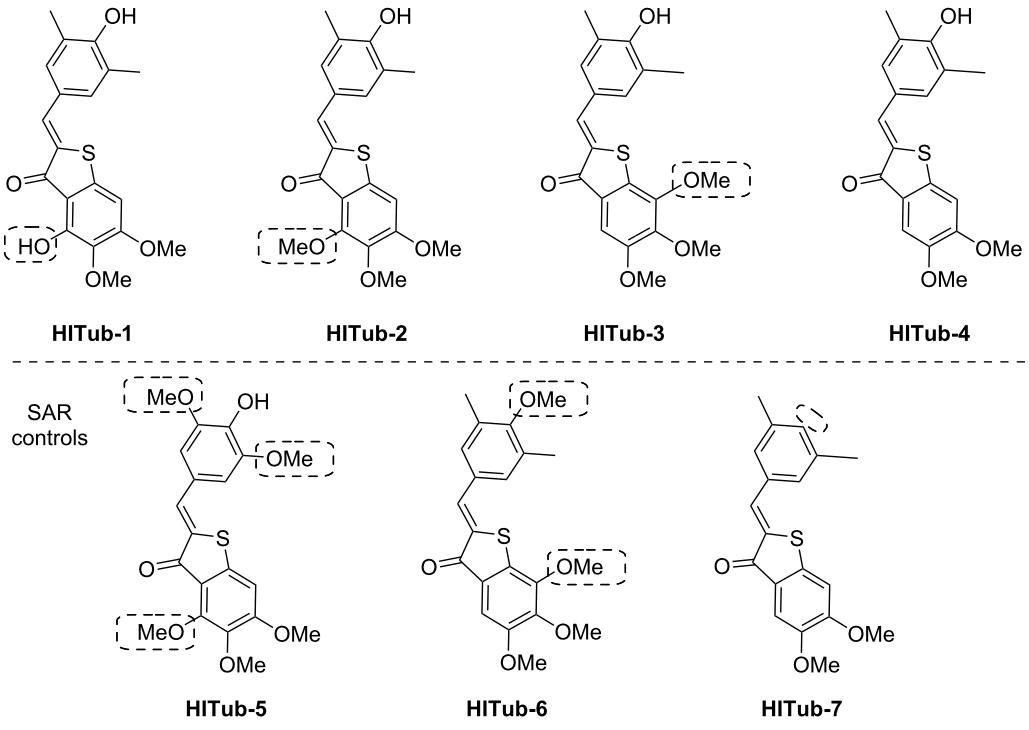

Figure 2: Chemical structures of **HITubs**. Key variations with respect to **HITub-4** are highlighted in dashed boxes.

Photocharacterisation

Although some *para*-hydroxy-substituted HTIs have been described [28,29], we are unaware of any report of the solvent- and pH-dependency of their photochromism and thermal relaxation. Dube and co-workers have reported that in general, increasing the electron-donating strength of groups in the hemistilbene *para*-position of HTIs correlates to (a) a bathochromic shift of the $S_0 \rightarrow S_1$ absorption band (up to $\lambda_{max} \approx 500$ nm with julolidine substitution) and (b) decreased thermal stability of the metastable *E*-isomer, i.e., faster thermal relaxation [30]. However, they also reported that introducing electron-donating groups (methoxy, dimethylamino) in *para*-position to the thioindoxyl sulfur atom restored *E*-stability while maintaining red-shifted absorption maxima. This *para*-position was occupied by the key methoxy group in all our **HITub** designs. With scant information available, we could not predict the thermal stability of (*E*)-**HITubs** in cellular conditions, so we turned to experimental measurement.

Since we found no substantial differences between the photochemical properties of the *para*-hydroxylated compounds (Figure 3 and Supporting Information File 1, Figure S1), we here describe the photocharacterisation of **HITub-4** as a representative example of the photoswitchable bioactive compounds (for more detailed analysis see Supporting Information File 1). In polar aprotic solvents, the **HITub-4** *Z*-isomer ($\lambda_{max} \approx 380$, 460 nm) showed robust, reliable, and fully reversible photoswitching (λ = 450 nm for $Z \rightarrow E$ and 530 nm for $E \rightarrow Z$ switching), with the high fatigue resistance characteristic of HTIs. The *E*-isomer's thermal half-life in EtOAc or DMSO was ca. 40 s (Figure 3 and Supporting Information File 1, Figure S3). Its absorption spectra and photoswitchability were unaltered by the addition of acid, however, addition of base led to a remarkable bathochromic and hyperchromic shifts of the absorption band at ca. 550 nm, and no observed photoswitchability (Supporting Information File 1, Figure S2). We assumed that this spectrum resulted from a quinoidal structure, formed after deprotonation of the hydroxy group, and that the lack of observable photoswitchability arose due to fast free rotation around the C–C single bond connecting the thioindigo and hemistilbene motifs. Interestingly, in neutral or acidic aqueous media where the quinoidal structure is not present (λ_{max} ca. 370, 480 nm), photoswitching could not be observed either, which we presumed to be due to fast thermal relaxation. However, noting that typical CDIs are substantially biolocalised into lipid environments within cells [31], we decided to explore photoswitching-based cellular assays with these compounds nonetheless (further discussion in Supporting Information File 1).

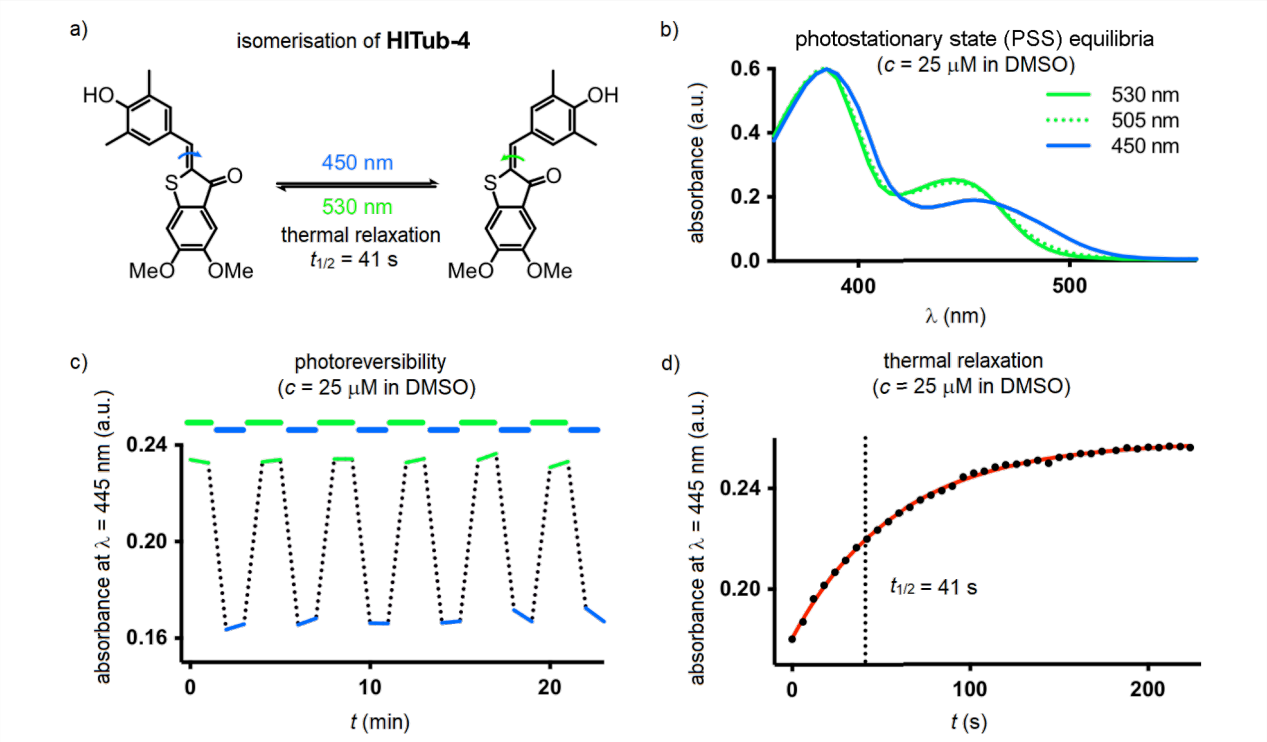

Figure 3: Photocharacterisation of **HITub-4**. a) Photochemical and thermal isomerisation. b) UV–vis spectra after saturating illumination at λ = 450, 505, and 530 nm, respectively. c) Photoreversible switching upon alternating illumination (λ = 450 and 530 nm). d) Thermal relaxation at room temperature after reaching the photostationary state at λ = 450 nm.

We found that the photochemical properties of the non-*para*-hydroxylated control **HITub-6** were similar to those of previously reported non-*para*-hydroxylated **HOTubs** [18], with satisfactory photoswitching in both DMSO and phosphate-buffered saline (PBS)/DMSO mixtures (Figure S1f,g in Supporting Information File 1).

Bioactivity: SAR study of **HITubs** in cellulo

To begin evaluating the isomer-dependent bioactivity of **HITub** photopharmaceuticals in cellulo, we first performed resazurin (resorufin *N*-oxide) antiproliferation assays under different lighting conditions (Figure 4). Inhibitors of tubulin polymerisation act as antimitotic cytotoxins in cell culture by preventing formation of a functional mitotic spindle, resulting in mitotic arrest and eventually cell death. The reduction of resazurin by viable cells serves as a fluorogenic proxy readout for antimitotic potency in cellulo, since the degree of resazurin turnover scales to the number of cells still viable after compound treatment, although the mechanism behind antiproliferative activity must later be determined using more specific assays. We used the HeLa human cervical cancer cell line to assess the biological activity of **HITubs** in all cellular experiments shown in this work. Since tubulin is a highly conserved protein target critical for survival in all cell types, we expected that, as for other colchicine domain tubulin inhibitors, trends in potency and in photoswitchability of potency determined in this representative mammalian cell line can be translated to other cell types, although their specific response (e.g., EC_{50} values) would need individual determination. Nocodazole was used as a benchmarking reference and mechanistic positive control in all in cellulo assays since it is a potent inhibitor of the colchicine binding site (EC_{50} ≈ 40 nM) with both appropriate solubility and straightforward handling.

Self-made low-intensity LED arrays with relatively narrow bandwidth were used for illumination of cells during assays, with a pulsing regime of 75 ms every 15 s to maintain photostationary state equilibria in cellulo [10]. We cross-checked different illumination wavelengths in cellular toxicity assays; in accordance with the DMSO photoswitching studies, we observed that 530 nm (ca. 97% *Z*-configuration, but additionally controls for non-specific phototoxicity) delivered results equivalent to dark conditions (exclusively *Z*-configuration), to which 450 nm (lit conditions, ca. 70% *E*-configuration) gave the greatest difference in antiproliferative potencies.

We began our studies with **HITub-1**. This is a HTI analogue of indanocine in which the indanocine amino function (in *ortho*-position to the key south ring methoxy group) has been replaced by a synthetically more accessible hydroxy group (delivered via demethylation of a trimethoxy precursor through BBr_3). The

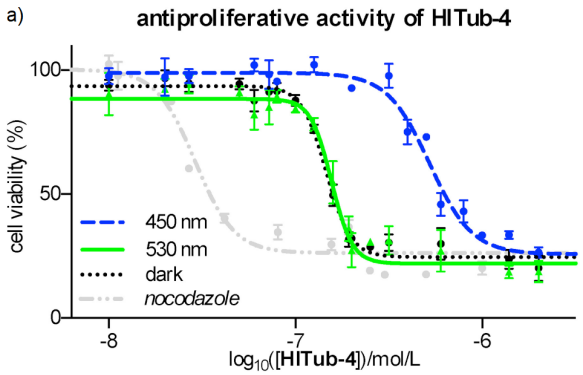

b)

compound	dark EC_{50} (μM)	450 nm EC_{50} (μM)	lit/dark ratio
HITub-1	0.5	1.1	2.2
HITub-2	1.2	3.8	3.2
HITub-3	0.15	0.4	2.7
HITub-4	0.11	0.45	4.1
HITub-5	n.d. (>50)	n.d. (>50)	n.d.
HITub-6	n.d. (>10)	n.d. (>10)	n.d.
HITub-7	0.4	0.4	1.0

Figure 4: a) Resazurin reduction assay for **HITub-4** and nocodazole in HeLa cells (n = 3), demonstrating the difference in antiproliferative potencies at λ = 450 and 530 nm/dark conditions (75 ms pulsing every 15 s). b) EC_{50} values of **HITubs** from cellular antiproliferation assays under dark conditions and at λ = 450 nm. The ratio of lit/dark EC_{50} values shows the fold change in photoswitchable bioactivity.

hydroxy and amino groups have similar size and polarity, and can both act as H-bond donors or acceptors. Therefore, we expected **HITub-1** to allow reliable evaluation of the indanocine substituent pattern. (*Z*)-**HITub-1** was already strongly bioactive (EC_{50} ≈ 500 nM, Figure 4b), although one order of magnitude less so than indanocine (EC_{50} ≈ 10–40 nM, depending on the cell line). Pleasingly, although we had not observed its photoswitching in pure aqueous media, in the heterogeneous cellular environment, we found that its overall toxicity under lit conditions was reliably and reproducibly halved.

We then explored changes to the substituent pattern to determine whether we could improve both *Z*-isomer potency in an absolute sense and the overall photoswitchability of potency comparing *E*- and *Z*-isomers. We began by methylating the south ring hydroxy group (**HITub-2**) to see how changes in size and polarity affect the bioactivity; surprisingly, the potency loss was not dramatic (indicating that this position is not a key determinant of bioactivity), but the photoswitchability increased substantially (3-fold with regard to the lit/dark ratio). We took this as an encouraging indicator of the overall polarity

required for binding, and now examined re-orienting the south ring substituents by shifting the trimethoxy pattern on the ring (**HITub-3**), which improved the potency dramatically (EC_{50} ≈ 150 nM for the *Z*-isomer) while retaining the 3-fold photoswitchability of bioactivity.

Since comparison of **HITub-2** and **HITub-3** showed that the potency can be retained without substituents in *ortho*-position to either the carbonyl group or the sulfur atom, for maximal simplicity, we tested whether both substituents could be deleted simultaneously (**HITub-4**). This proved to be the strongest-performing compound of our studies, with the *Z*-isomer possessing an EC_{50} value of ca. 110 nM and a 4-fold difference of bioactivity between lit and dark conditions (λ = 450 nm). This difference was surprisingly high, given that even in aprotic media (e.g., lipid environment reservoirs within cells), there should be ca. 30% residual *Z*-isomer at photoequilibrium [18], and we had expected that any (*E*)-**HITub** entering the cytosol (aqueous environment) would quickly relax to its more bioactive *Z*-isomer before encountering its cytosolic protein target. We theorised that fast cytosolic relaxation of the *para*-hydroxy **HITubs** to their bioactive *Z*-isomer may actually be a decisive factor in preventing the simple equilibration of the extracellular **HITub** concentration (exclusively *Z*-configuration due to fast relaxation, irrespective of illumination conditions) with the cytosolic (*Z*)-**HITub** concentration available to bind to tubulin (and which all experiments show is reduced under λ = 450 nm illumination). Examining this in detail is beyond the scope of this study, however, see Supporting Information File 1 for a discussion on isomer-dependent subcellular biolocalisation effects.

We first controlled against our design logic of north ring substituent shortening by changing the north ring apolar-contact methyl groups to methoxy groups (**HITub-5**), and were satisfied when this abolished bioactivity. We also controlled for the result, known from extensive SAR work at the colchicine site [18,32], that CDIs should not tolerate a non-polar central north ring substituent (**HITub-6**) but can support removal of this substituent altogether, with only small potency loss (**HITub-7**). We considered that if the screened compounds obeyed this principle, it would reinforce our mechanistic understanding of them as CDIs. Indeed, **HITub-6** proved inactive until it reached its solubility limit, but (*Z*)-**HITub-7** was relatively potent and featured an only 4-fold reduction of bioactivity as compared to its hydroxylated parent (*Z*)-**HITub-4**. Interestingly, however, **HITub-7** displayed no difference between dark (all-*Z*) and lit (mostly *E*) conditions, and we were unable to rationalise this with reference to either polarity or structure, in light of our prior work on apolar **HOTubs** [18] (see also Supporting Information File 1). We were, however, overall satisfied by these findings (Supporting Information File 1, Figure S4), especially by the potency and photoswitchability of **HITub-4**.

These results indicated that indanocine-inspired HTI-based reagents are a potent, cellularly bioactive class of photoswitchably antiproliferative agents, with the most potent light-controlled antimitotic bioactivity reported for photoswitches designed for tubulin: 10-fold enhancement compared to the predecessor HTI generation **HOTubs** [18] and styrylbenzothiazole-based **SBTubs** [17], and 5-fold superior to azocombretastatins [10-12]. In view of the generally limited solubility of photopharmaceuticals (associated with their extended flat aromatic structures), this increase in potency renders the **HITub** compound class a promising addition to the toolbox of photoswitchable antimitotics, which might prove valuable for future in vivo studies.

We also noted that the *para*-hydroxy **HITubs** featured ca. 30% residual (*Z*)-**HITub** at PSS λ = 450 nm in cell-free measurements, and that for **HITub-2**–**4**, the PSS isomer mixture's cellular cytotoxicity at that wavelength was on average 3.3-fold lower than the cytotoxicity of the corresponding (*Z*)-**HITub** (Figure 4). This can be interpreted as indicative that the *E*-isomers are essentially biologically inactive, similar to what has been observed for heterostilbene **SBTubs** [17] and azobenzene photostatins (**PSTs**) [10]. If substantiated, HTI-like analogues for which photostationary state (PSS) with enhanced proportions of *E*-isomer can be photogenerated would represent an exciting advance: they could, in contrast to the other photoswitch types, allow all-visible, photoreversible, high-potency switching while reproducing similarly beneficial photoswitchability of bioactivity.

Mechanistic assessment of **HITub** action

We now determined to confirm the mechanism of action of the **HITub** compounds. To evaluate the biological mechanism of action behind the **HITubs**' photoswitchable antimitotic activity, we first checked their inhibition of polymerisation of purified tubulin in a cell-free assay. The results showed almost identical inhibition potency for **HITub-4** at *c* = 10 μM as for the archetypal CDI colchicine at *c* = 20 μM (Figure S5, Supporting Information File 1), which we took to indicate that (*Z*)-**HITub-4** exerted its bioactivity by specifically binding to tubulin directly in the cell-free system. This suggests that the same specific direct action can be reproduced in cellulo, and that effects on auxiliary cellular systems dependent upon the MT cytoskeleton can likely be downstream effects of MT depolymerisation. We next investigated the **HITubs**' isomer-dependent effects on the MT network inside cells, focusing on the active analogues **HITub-4** and **HITub-2** in comparison with inactive **HITub-5** as a control (Figure 5). By reducing tubulin polymerisation dy-

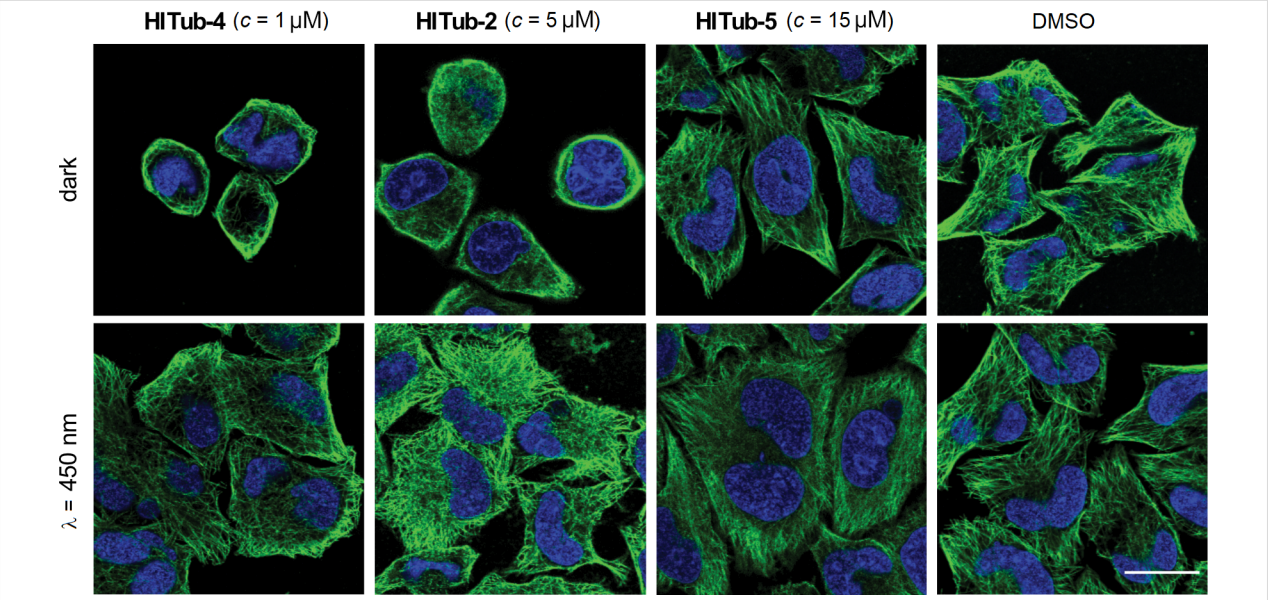

Figure 5: Confocal microscopy images of immunofluorescently labelled MT networks after treatment with **HITubs** for 24 h under lit (λ = 450 nm) and dark conditions. **HITub-4** and **HITub-2** caused light-dependent MT disruption at low concentrations (*c* = 1 and 5 µM, respectively) matching their cytotoxicities (EC_{50} = 1 and 5 µM, respectively). High concentrations of the structurally related negative control **HITub-5**, like the DMSO co-solvent control, produced no effects under either illumination condition. MTs (anti-α-tubulin) are visualized in green while the nuclear stain 4′,6-diamidino-2-phenylindole (DAPI) is visualized in blue. Scale bar length = 20 µm.

namics, CDI treatment should first disorganise and then depolymerise the cellular MT network. We performed immunofluorescence staining of the MT network within cells treated with **HITubs** and documented the resulting disruption of the physiological MT network integrity, and consequently also changes in cell morphology by confocal microscopy. Cells exposed to **HITub-4** (1 µM) in the dark or under λ = 530 nm illumination (to maintain exclusively *Z*-configuration) show near-complete disruption of MT structures after 24 h, while treatment with λ = 450 nm illumination caused no significant disruption of the MT network compared to an untreated dark control (Figure 5). Less potent **HITub-2** also showed similar light dependency of its biological effects at higher concentrations (Supporting Information File 1, Figure S6). Pleasingly, SAR control **HITub-5** showed no impact on MT integrity at the highest tested concentration under lit or dark conditions, which we took as a promising indication for the absence of phototoxicity or of other effects non-specific to tubulin disruption.

Lastly, to substantiate the causative link between the observations on MT disruption and cellular toxicity, we examined the impacts of **HITub-4** on the cell cycle. Tubulin-binding agents whose major cellular mechanism of toxic action is the disruption of MT dynamics or structure should cause cell cycle arrest in the G2/M phase by preventing the completion of mitosis [1]. We examined cell cycle repartition by quantification of cellular DNA content via propidium iodide (PI) incorporation, which was analysed by flow cytometry (Supporting Information File 1, Figure S7). HeLa cells were treated for 24 h with **HITub-4** under λ = 530 and 450 nm irradiation, respectively, with the synthetic tubulin-binding agent nocodazole (Noc) used as a reference. As expected, **HITub-4** showed highly light-dependent bioactivity with near-complete G2/M phase arrest at a concentration of 6 µM and λ = 530 nm irradiation (Figure 6a and Figure 6b), but nearly no cell cycle interference at the same concentration and λ = 450 nm irradiation (Figure 6c and Figure 6d).

Conclusion

Taken together, these results indicate that the **HITubs** had achieved their design aims, being a rationally-designed, potency-enhanced set of HTI-based tubulin-inhibiting photopharmaceuticals with photoswitchable bioactivity across cell biology assays, allowing reliable photocontrol over tubulin polymerisation, MT network structure, cell cycle, and cell survival. They feature mid-nanomolar potency in cellulo, the highest yet reported for photopharmaceutical tubulin inhibitors, as well as satisfactory photoswitchability of potency. We expect that due to the **HITubs**' potency of tubulin inhibition, they will prove a powerful reagent system for biological studies on MT, especially where dark-isomer activity (compared to the currently known, lit-active azobenzenes or styrylbenzothiazoles) is desirable, in particular for cell-free mechanistic studies [33]. More broadly, this work also shows that the HTI scaffold robustly enables the photoswitchable use of resonance-capable substituents that can establish high-affinity interactions (such as *para*-

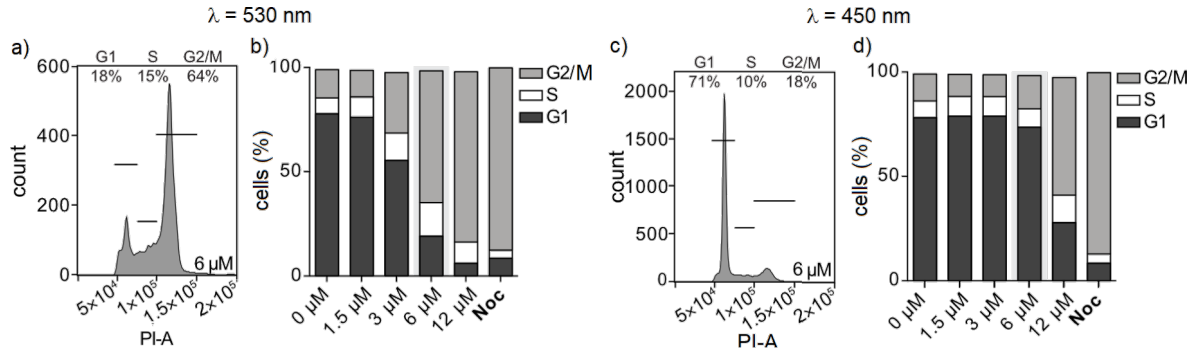

Figure 6: Cell cycle analysis of **HITub-4**-treated cells. a) and b) (*Z*)-**HITub-4** caused significant G2/M arrest already at a concentration of 6 μM (λ = 530 nm). c) and d) Under irradiation at λ = 450 nm, where a majority of (*E*)-**HITub-4** was present, no mitotic arrest could be observed at comparable concentrations. a) and c) Representative histograms showing cell cycle arrest, with population binning as indicated. In b) and d), nocodazole (Noc) was used as a positive control (*c* = 1 μM).

hydroxy groups), which are otherwise problematic for current photopharmaceutical scaffolds to tolerate without loss of photoswitchability. In the broader sense, this is of interest for cell biology and further highlights the potential of HTIs as a pharmacophore scaffold for expanding the scope of cellular photopharmacology.

Supporting Information

Supporting Information File 1

Full experimental protocols for chemical syntheses, photocharacterisation, biochemistry, and cell biology, including NMR spectra.
[https://www.beilstein-journals.org/bjoc/content/supplementary/1860-5397-16-14-S1.pdf]

Acknowledgements

This research was supported by funds from the German Research Foundation (DFG: SFB1032 *Nanoagents for Spatiotemporal Control* project B09, SFB TRR 152 project P24 number 239283807, and an Emmy Noether grant) and the Munich Centre for Nanoscience (CeNS) to O.T.-S. A.S. particularly thanks Linda Pettersson for her great assistance during photocharacterisation.

ORCID® iDs

Alexander Sailer - https://orcid.org/0000-0003-4140-9956
Rebekkah Bingham - https://orcid.org/0000-0001-5740-0353
Julia Ahlfeld - https://orcid.org/0000-0002-4879-4159
Oliver Thorn-Seshold - https://orcid.org/0000-0003-3981-651X

Preprint

A non-peer-reviewed version of this article has been previously published as a preprint doi:10.26434/chemrxiv.9176747

References

1. Peterson, J. R.; Mitchison, T. J. *Chem. Biol.* **2002,** *9,* 1275–1285. doi:10.1016/s1074-5521(02)00284-3
2. Guedes-Dias, P.; Nirschl, J. J.; Abreu, N.; Tokito, M. K.; Janke, C.; Magiera, M. M.; Holzbaur, E. L. F. *Curr. Biol.* **2019,** *29,* 268–282.e8. doi:10.1016/j.cub.2018.11.065
3. Armstrong, M. T.; Armstrong, P. B. *Exp. Cell Res.* **1979,** *120,* 359–364. doi:10.1016/0014-4827(79)90395-1
4. Kelliher, M. T.; Saunders, H. A.; Wildonger, J. *Curr. Opin. Neurobiol.* **2019,** *57,* 39–45. doi:10.1016/j.conb.2019.01.003
5. Banghart, M.; Borges, K.; Isacoff, E.; Trauner, D.; Kramer, R. H. *Nat. Neurosci.* **2004,** *7,* 1381–1386. doi:10.1038/nn1356
6. Caporale, N.; Kolstad, K. D.; Lee, T.; Tochitsky, I.; Dalkara, D.; Trauner, D.; Kramer, R.; Dan, Y.; Isacoff, E. Y.; Flannery, J. G. *Mol. Ther.* **2011,** *19,* 1212–1219. doi:10.1038/mt.2011.103
7. Riefolo, F.; Matera, C.; Garrido-Charles, A.; Gomila, A. M. J.; Sortino, R.; Agnetta, L.; Claro, E.; Masgrau, R.; Holzgrabe, U.; Batlle, M.; Decker, M.; Guasch, E.; Gorostiza, P. *J. Am. Chem. Soc.* **2019,** *141,* 7628–7636. doi:10.1021/jacs.9b03505
8. Agnetta, L.; Kauk, M.; Canizal, M. C. A.; Messerer, R.; Holzgrabe, U.; Hoffmann, C.; Decker, M. *Angew. Chem., Int. Ed.* **2017,** *56,* 7282–7287. doi:10.1002/anie.201701524
9. Velema, W. A.; van der Berg, J. P.; Hansen, M. J.; Szymanski, W.; Driessen, A. J. M.; Feringa, B. L. *Nat. Chem.* **2013,** *5,* 924–928. doi:10.1038/nchem.1750
10. Borowiak, M.; Nahaboo, W.; Reynders, M.; Nekolla, K.; Jalinot, P.; Hasserodt, J.; Rehberg, M.; Delattre, M.; Zahler, S.; Vollmar, A.; Trauner, D.; Thorn-Seshold, O. *Cell* **2015,** *162,* 403–411. doi:10.1016/j.cell.2015.06.049
11. Engdahl, A. J.; Torres, E. A.; Lock, S. E.; Engdahl, T. B.; Mertz, P. S.; Streu, C. N. *Org. Lett.* **2015,** *17,* 4546–4549. doi:10.1021/acs.orglett.5b02262
12. Sheldon, J. E.; Dcona, M. M.; Lyons, C. E.; Hackett, J. C.; Hartman, M. C. T. *Org. Biomol. Chem.* **2016,** *14,* 40–49. doi:10.1039/c5ob02005k
13. Müller-Deku, A.; Loy, K.; Kraus, Y.; Heise, C.; Bingham, R.; Ahlfeld, J.; Trauner, D.; Thorn-Seshold, O. *bioRxiv* **2019,** No. 778993. doi:10.1101/778993
14. Eguchi, K.; Taoufiq, Z.; Thorn-Seshold, O.; Trauner, D.; Hasegawa, M.; Takahashi, T. *J. Neurosci.* **2017,** *37,* 6043–6052. doi:10.1523/jneurosci.0179-17.2017

15. Zenker, J.; White, M. D.; Templin, R. M.; Parton, R. G.; Thorn-Seshold, O.; Bissiere, S.; Plachta, N. *Science* **2017,** *357,* 925–928. doi:10.1126/science.aam9335
16. Singh, A.; Saha, T.; Begemann, I.; Ricker, A.; Nüsse, H.; Thorn-Seshold, O.; Klingauf, J.; Galic, M.; Matis, M. *Nat. Cell Biol.* **2018,** *20,* 1126–1133. doi:10.1038/s41556-018-0193-1
17. Gao, L.; Kraus, Y.; Wranik, M.; Weinert, T.; Pritzl, S. D.; Meiring, J. C. M.; Bingham, R.; Olieric, N.; Akhmanova, A.; Lohmüller, T.; Steinmetz, M. O.; Thorn-Seshold, O. *bioRxiv* **2019,** No. 716233. doi:10.1101/716233
18. Sailer, A.; Ermer, F.; Kraus, Y.; Lutter, F. H.; Donau, C.; Bremerich, M.; Ahlfeld, J.; Thorn-Seshold, O. *ChemBioChem* **2019,** *20,* 1305–1314. doi:10.1002/cbic.201800752
19. Hüll, K.; Morstein, J.; Trauner, D. *Chem. Rev.* **2018,** *118,* 10710–10747. doi:10.1021/acs.chemrev.8b00037
20. Tron, G. C.; Pirali, T.; Sorba, G.; Pagliai, F.; Busacca, S.; Genazzani, A. A. *J. Med. Chem.* **2006,** *49,* 3033–3044. doi:10.1021/jm0512903
21. Lawrence, N. J.; Rennison, D.; McGown, A. T.; Hadfield, J. A. *Bioorg. Med. Chem. Lett.* **2003,** *13,* 3759–3763. doi:10.1016/j.bmcl.2003.07.003
22. Leoni, L. M.; Hamel, E.; Genini, D.; Shih, H.; Carrera, C. J.; Cottam, H. B.; Carson, D. A. *J. Natl. Cancer Inst.* **2000,** *92,* 217–224. doi:10.1093/jnci/92.3.217
23. Dose Response Curves for NSC 757. National Cancer Institute - Developmental Therapeutics Program: Rockville, MD, https://dtp.cancer.gov/services/nci60data/colordoseresponse/pdf/757 (accessed Nov 6, 2019).
24. Garcia-Amorós, J.; Sánchez-Ferrer, A.; Massad, W. A.; Nonell, S.; Velasco, D. *Phys. Chem. Chem. Phys.* **2010,** *12,* 13238–13242. doi:10.1039/c004340k
25. Dunn, N. J.; Humphries, W. H., IV; Offenbacher, A. R.; King, T. L.; Gray, J. A. *J. Phys. Chem. A* **2009,** *113,* 13144–13151. doi:10.1021/jp903102u
26. Wiedbrauk, S.; Dube, H. *Tetrahedron Lett.* **2015,** *56,* 4266–4274. doi:10.1016/j.tetlet.2015.05.022
27. Mukherjee, C.; De, A. *Synlett* **2002,** 325–327. doi:10.1055/s-2002-19752
28. Takeo, Y.; Takahiro, S.; Takashi, T.; Kunihiro, I. *Bull. Chem. Soc. Jpn.* **1992,** *65,* 649–656. doi:10.1246/bcsj.65.649
29. Eggers, K.; Fyles, T. M.; Montoya-Pelaez, P. J. *J. Org. Chem.* **2001,** *66,* 2966–2977. doi:10.1021/jo0056848
30. Kink, F.; Collado, M. P.; Wiedbrauk, S.; Mayer, P.; Dube, H. *Chem. – Eur. J.* **2017,** *23,* 6237–6243. doi:10.1002/chem.201700826
31. Bisby, R. H.; Botchway, S. W.; Hadfield, J. A.; McGown, A. T.; Parker, A. W.; Scherer, K. M. *Eur. J. Cancer* **2012,** *48,* 1896–1903. doi:10.1016/j.ejca.2011.11.025
32. Nguyen, T. L.; McGrath, C.; Hermone, A. R.; Burnett, J. C.; Zaharevitz, D. W.; Day, B. W.; Wipf, P.; Hamel, E.; Gussio, R. *J. Med. Chem.* **2005,** *48,* 6107–6116. doi:10.1021/jm050502t
33. Gaspari, R.; Prota, A. E.; Bargsten, K.; Cavalli, A.; Steinmetz, M. O. *Chem* **2017,** *2,* 102–113. doi:10.1016/j.chempr.2016.12.005

License and Terms

BEILSTEIN JOURNAL OF ORGANIC CHEMISTRY

Supporting Information

for

Potent hemithioindigo-based antimitotics photocontrol the microtubule cytoskeleton in cellulo

Alexander Sailer, Franziska Ermer, Yvonne Kraus, Rebekkah Bingham, Ferdinand H. Lutter, Julia Ahlfeld and Oliver Thorn-Seshold

Beilstein J. Org. Chem. **2020,** *16,* 125–134. doi:10.3762/bjoc.16.14

Full experimental protocols for chemical syntheses, photocharacterisation, biochemistry, and cell biology, including NMR spectra

Authorship Statement: Following the ICMJE guidelines, the authors declare their roles in the present work as follows: A.S. performed chemical synthesis, photocharacterisation and coordinated data assembly, F.E. performed in vitro studies, Y.K. performed in cellulo studies, R.B. performed in vitro tubulin polymerisation assays, F.H.L. performed chemical synthesis, J.A. performed in cellulo studies and coordinated data interpretation and assembly. O.T.-S. designed the concept and experiments, supervised all experiments, coordinated all data and wrote the manuscript with input from all authors.

Table of Contents

Part A: Chemical syntheses S3
Conventions S3
Standard procedures.....S4
Synthesis of HITub-3.....S6
Synthesis of HITub-4.....S8
Synthesis of HITub-2 and HITub-5.....S10
Synthesis of HITub-1.....S11
Synthesis of HITub-7.....S13
Synthesis of HITub-6.....S14
Part B: Photocharacterisation in vitro S17
UV–vis spectrophotometry of bulk samples S17
PSS spectra of the HITubs.....S17
Solvent- and pH-dependency of photoisomerisability and relaxation rate .S18
Part C: Biochemistry and cellular biology S21
Resazurin antiproliferation assays S22
In vitro tubulin polymerisation assay S22
Immunofluorescence imaging of microtubule network structure S23
Cell cycle analysis S24
Supplemental references.....S25
Part D: NMR spectra S26

Part A: Chemical syntheses

Conventions

Hemithioindigo geometry and nomenclature: Hemithioindigos (HTIs) are drawn by default in their *Z*-isomeric form. However, this should be understood to imply either or both of the *E* & *Z* forms constituting a given sample depending on light exposure, therefore by default they are also named without *E*/*Z*-designations.

Abbreviations: The following abbreviations are used: *sec*Bu – *secondary* butyl, Bu – butyl, calcd. – calculated, cHx – cyclohexane, DCM – dichloromethane, DIPA – *N*-(propan-2-yl)propan-2-amine, DMSO – dimethyl sulfoxide, EA / EtOAc – ethyl acetate, EtOH – ethanol, Hx – distilled isohexanes, HRMS – high-resolution mass spectrometry, LDA – lithium diisopropylamide, MeCN – acetonitrile, *n*-Bu – *normal* butyl, MS – molecular sieves, NIS – N-iodosuccinimide, TFA – trifluoroacetic acid, THF – tetrahydrofuran, TMEDA – tetramethylethylendiamine,.

Automated flash chromatography: Automated flash chromatography was performed on a Biotage Isolera One instrument using 254 nm as detection wavelength and eluting with mixtures of ethyl acetate and isohexanes.

Reagents and conditions: Unless stated otherwise: (1) all reactions and characterisations were performed with unpurified, undried, non-degassed solvents and reagents, used as obtained, under closed air atmosphere without special precautions unless stated otherwise. The use of dry solvents in this context is to be understood as using anhydrous solvents bought from Acros Organics which were stored and handled under an atmosphere of nitrogen; (2) “hexane” used for chromatography was distilled from commercial crude isohexane fraction on rotavap; (3) when not specified, “column” and “chromatography” refer to flash column chromatography performed on Merck silica gel Si-60 (40–63 µm); (4) procedures and yields are unoptimised; (5) yields refer to isolated chromatographically and spectroscopically pure materials (6) all eluent and solvent mixtures are given as volume ratios unless otherwise specified, thus “1:1 EA:Hx” indicates a 1:1 mixture (by volume) of ethyl acetate and hexanes.

Thin-layer chromatography (TLC) was run on 0.25 mm Merck silica gel plates (60, F-254). UV light (254 nm) was used as a visualising agent. R_f values were usually determined in ethyl acetate : hexane (EA:Hx) eluents. TLC characterisations are thus abbreviated as per (R_f = 0.09 on EA:Hx, 6:1).

NMR: Standard NMR characterisation was by 1D ^{1}H- and ^{13}C-NMR spectra, with COSY, HSQC, HMBC or heteronuclear NMR performed as needed. Known compounds were checked against literature data and their spectral analysis is not detailed unless necessary. The default spectrometer used was a Bruker Ascend 400 (400 MHz & 100 MHz for ^{1}H and ^{13}C

respectively); NMR solvents are given individually for each compound. For determination of the composition of the photostationary states (450 and 505 nm), a Bruker Avance III HD (500 MHz) equipped with CryoProbe™ Prodigy broadband probe was used.

Chemical shifts (δ) are reported in ppm calibrated to residual non-perdeuterated solvent as an internal reference[1]. The following peak descriptions are used: singlet (s), doublet (d), triplet (t), quartet (q), multiplet (m), broad (br.).

Mass Spectra: HRMS was carried out by the Zentrale Analytik of the LMU, Munich using ESI or EI ionisation as specified.

Standard procedures

Where standard procedures were used in synthesis, unless stated otherwise, the amounts of reactants/reagents employed were implicitly adjusted to maintain the same molar ratios as in the given procedure, and no other alterations from the standard procedure (e.g., reaction time, extraction solvent, temperature) were made, unless stated otherwise.

Standard procedure A: amidation of benzoic acids

The carboxylic acid was dissolved in an excess of thionyl chloride under an atmosphere of nitrogen and heated to reflux for 3 h. The volatiles were removed under reduced pressure using an external cooling trap, the oily residue was dried in high vacuum and dissolved in dry THF. The solution was cooled to 0 °C and diethylamine (3.00 equiv) was added dropwise via syringe under a stream of nitrogen (a second needle was used as overpressure valve to remove HCl). After complete addition, the cooling bath was removed and the reaction mixture was stirred overnight at room temperature. Water was added carefully, the phases were separated and the aqueous phase was extracted with EtOAc. The combined organic extracts were washed with HCl (2 M, 2 times) and NaOH (2 M, 2 times) to remove residual amine and benzoic acid, respectively. After washing with brine (2 times), the combined organic extracts were dried over Na_2SO_4, evaporated and purified by flash chromatography to yield the benzamide.

Standard procedure B: directed *ortho* metalation and thiomethylation

TMEDA was distilled over KOH pellets under an atmosphere of nitrogen (bp. 123 °C; ambient pressure) and stored under nitrogen. To a solution of TMEDA (1.20 or 2.50 equiv) in dry THF was added *sec*BuLi (1.4 M in cyclohexane, 1.2 or 2.5 equiv) at −78 °C and the bright yellow reaction mixture was stirred for 15 min. prior to dropwise addition of a solution of the benzamide (1.00 equiv) in dry THF. The colourless solution was kept at −78 °C for further 15 min. and a solution of dimethyl disulfide (2.00 equiv) in dry THF was added dropwise. After 15 min. the reaction mixture was allowed to warm to room temperature and stirred for the time indicated. The reaction was quenched by the careful addition of a saturated aqueous solution

of NH_4Cl, the phases were separated and the aqueous phase was extracted with EtOAc (3 times). The combined organic extracts were washed with brine (3 times), dried over Na_2SO_4 and evaporated. The crude was purified as stated to yield the *ortho*-thiomethyl benzamide.

Standard procedure C: base-mediated cyclisations of *ortho*-thiomethyl benzamides

LDA was prepared fresh by adding n-BuLi (2.50 M in cyclohexane) to a solution of DIPA in dry THF. To a solution of LDA (1.50–4.30 equiv) in dry THF was added the *ortho*-thiomethyl benzamide (1.00 equiv) at −78 °C and the reaction mixture was stirred at this temperature for 1–1.25 h, then allowed to warm to room temperature and stirred for another hour. The reaction was quenched by the careful addition of a saturated aqueous solution of NH_4Cl, the phases were separated and the aqueous phase was extracted with DCM. The combined organic extracts were dried over Na_2SO_4 and evaporated. Purification was accomplished by (automated) flash chromatography to yield the thioindoxyl.

Standard procedure D: formation of HTIs via piperidine catalysed aldol condensations

An oven dried Schlenk flask was charged with the thioindoxyl (1.00 equiv), the aldehyde (equivalents are given individually) and molecular sieves (4 Å) under an atmosphere of nitrogen. Dry benzene or toluene and piperidine (few drops) were added and the solution was heated to 80 °C for the time indicated individually. After cooling to room temperature, a saturated aqueous solution of NH_4Cl was added, the phases were separated and the aqueous layer was extracted with DCM. The combined organic extracts were dried over Na_2SO_4 and evaporated. Purification was accomplished as stated to yield the hemithioindigo.

Standard procedure E: formation of HTIs via dehydrative ring closure

The (phenylthio)acetic acid (1.00 equiv) was suspended in an excess of Eaton's reagent (P_2O_5 in methanesulfonic acid) and stirred for 2 h at 50 °C. The reaction was quenched by addition of water and the mixture was extracted with DCM. The combined organic layers were washed with a saturated aqueous solution of $NaHCO_3$ (3 times), brine, dried over Na_2SO_4 and the volume was reduced to 5–6 mL. To this solution of thioindoxyl was added basic Al_2O_3 and the corresponding aldehyde (typically 0.25–0.45 equiv; as stated) and the mixture was stirred at ambient temperature. After completion of the reaction (detected by TLC), the mixture was filtered through a silica gel pad on 1:1 EA:Hx and the solvent was removed under reduced pressure. Purification was accomplished by flash chromatography, preparative thin-layer chromatography or precipitation as stated to yield the hemithioindigo.

Synthesis of HITub-3

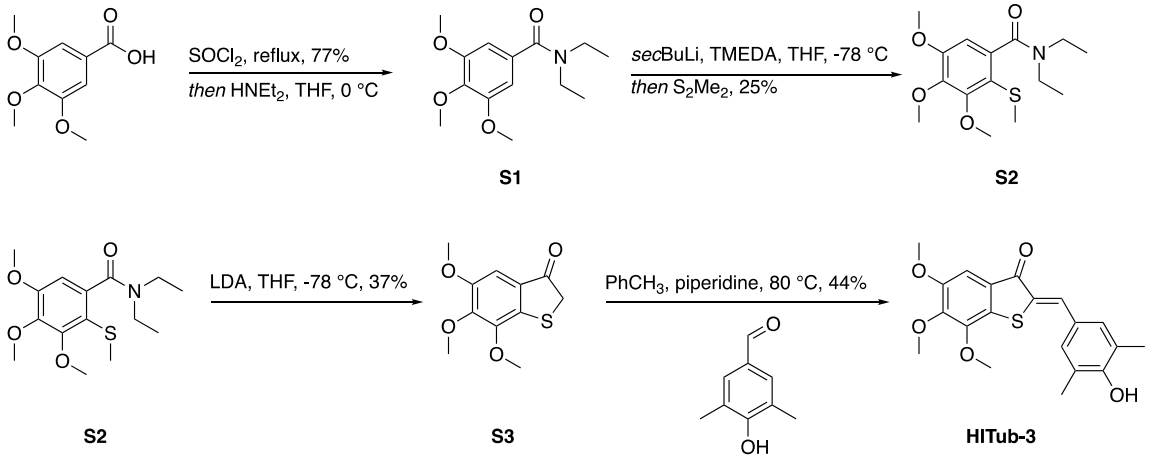

Scheme S1: Synthesis of **HITub-3**.

N,*N*-Diethyl-3,4,5-trimethoxybenzamide (S1)

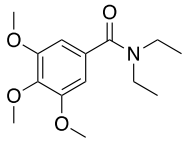

By standard procedure A, reacting commercially available 3,4,5-trimethoxybenzoic acid (1.00 g, 4.71 mmol, 1.00 equiv) with excess thionyl chloride (5 mL) followed by treatment of the acid chloride with diethylamine (1.03 g, 14.1 mmol, 1.46 mL, 3.00 equiv) in dry THF (20 mL). Purification by means of flash chromatography (EA:Hx, 1:1 → 3:1) afforded amide **S1** (969 mg, 3.62 mmol, 77%) as colorless oil that solidified upon standing.

The spectral data match the literature[2].

^{1}H-NMR ($CDCl_3$, 400 MHz): δ (ppm) = 6.56 (pseudo d, 2H), 3.84 (pseudo d, 6H), 3.82 (pseudo d, 3H), 3.50 (br. pseudo s, 2H), 3.27 (br. pseudo s, 2H), 1.20 – 1.13 (br. m, 6H, H); **^{13}C-NMR** ($CDCl_3$, 100 MHz): δ (ppm) = 171.1, 153.4, 138.7, 132.8, 130.0, 103.6, 61.0, 56.3, 43.4, 39.4, 14.5, 13.0; **R_f** = 0.20 on EA:Hx, 1:1; ESI$^+$ **HRMS** for $C_{14}H_{22}NO_4^+$: calcd. m/z 268.15433, found m/z 268.15450; for $C_{14}H_{21}NO_4Na^+$: calcd. m/z 290.13628, found m/z 290.13640.

N,*N*-diethyl-3,4,5-trimethoxy-2-(methylthio)benzamide (S2)

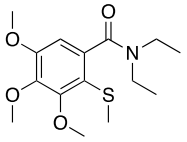

By standard procedure B, reacting amide **S1** (640 mg, 2.39 mmol, 1.00 equiv) with *sec*BuLi (3.21 g, 5.99 mmol, 4.28 mL, 2.50 equiv) and TMEDA (696 mg, 5.99 mmol, 0.90 mmol, 2.50 equiv) followed by quenching with dimethyl disulfide (451 mg, 4.79 mmol, 0.43 mL,

2.00 equiv) in dry THF (20 mL) overnight. Purification was accomplished by flash chromatography (EA:Hx, 1:1) and automated flash chromatography (EA:Hx, 5 → 60%) affording **S2** as a colorless oil (184 mg, 0.59 mmol, 25%).

The analytical data is in good agreement with our previously published data[3].

^{1}H-NMR ($CDCl_3$, 400 MHz): δ (ppm) = 6.39 (s, 1H), 3.81 (s, 3H), 3.72 (s, 3H), 3.70 (s, 3H), 3.66 – 3.59 (m, 1H), 3.25 – 3.17 (m, 1H), 3.01 – 2.96 (q, *J* = 7.1 Hz, 2H), 2.21 (s, 3H), 1.12 (t, *J* = 7.1 Hz, 3H), 0.92 (t, *J* = 7.1 Hz, 3H); **^{13}C-NMR** ($CDCl_3$, 100 MHz): δ (ppm) = 168.8, 155.1, 154.1, 142.4, 138.0, 117.7, 104.8, 61.0, 60.7, 55.9, 42.6, 38.5, 19.1, 13.8, 12.3; **R_f** = 0.36 on EA:Hx, 1:1; ESI$^+$ **HRMS** for $C_{15}H_{23}NO_4SNa^+$: calcd. m/z 336.12400, found m/z 336.12402.

5,6,7-Trimethoxybenzo[*b*]thiophen-3(2*H*)-one (S3)

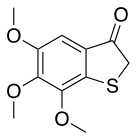

By standard procedure C, **S2** (25 mg, 79.8 µmol, 1.00 equiv) was reacted with LDA (prepared from *n*-BuLi (36 mg, 120 µmol, 0.05 mL, 1.50 equiv) and DIPA (20 mg, 200 µmol, 0.03 mL, 2.50 equiv)). After stirring for 1 h at −78 °C and 1 h at ambient temperature, the mixture was worked up and the crude product was purified by automated flash chromatography (EA:Hx, 5 → 40%) affording thioindoxyl **S3** (7 mg, 29.1 µmol, 37%) as a pale yellow crystalline solid. Due to limited chemical stability of electron-rich thioindoxyls under air, the product was immediately condensed with the respective aldehyde after spectroscopic characterisation.

^{1}H-NMR ($CDCl_3$, 400 MHz): δ (ppm) = 7.05 (s, 1H), 3.97 (s, 3H), 3.95 (s, 3H), 3.86 (s, 3H), 3.75 (s, 2H); **^{13}C-NMR** ($CDCl_3$, 100 MHz): δ (ppm) = 199.3, 152.6, 148.9, 147.8, 141.7, 126.2, 103.4, 61.4, 60.8, 56.5, 39.5; **R_f** = 0.36 (blue fluorescence under illumination with 366 nm) on EA:Hx, 1:4.

2-(4-Hydroxy-3,5-dimethylbenzylidene)-5,6,7-trimethoxybenzo[*b*]thiophen-3(2*H*)-one (HITub-3)

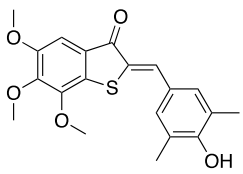

By standard procedure D, thioindoxyl **S3** (5 mg, 20.8 µmol, 1.00 equiv) was reacted with commercially available 3,5-dimethyl-4-hydroxybenzaldehyde (4 mg, 27.1 µmol, 1.30 equiv) in

dry toluene (3 mL) for 2.5 h at 80 °C then 1 h at 25 °C. Automated flash chromatography (EA:Hx, 5 → 40%) yielded **HITub-3** as an orange solid (3.4 mg, 9.1 µmol, 44%).

^{1}H-NMR ($CDCl_3$, 400 MHz): δ (ppm) = 7.84 (s, 1H), 7.38 (s, 2H), 7.23 (s, 1H), 5.08 (br. s, 1H), 4.01 (s, 3H), 3.98 (s, 3H), 3.90 (s, 3H), 2.30 (s, 6H); **^{13}C-NMR** ($CDCl_3$, 100 MHz): δ (ppm) = 188.1, 154.7, 153.0, 148.1, 147.6, 134.6, 133.0, 132.3, 128.0, 126.7, 126.2, 124.0, 104.4, 61.4, 61.2, 56.5, 16.1; **R_f** = 0.27 on EA:Hx, 1:4; ESI$^+$ **HRMS** for $C_{21}H_{23}O_5S^+$: calcd. m/z 373.11042, found m/z 373.11008; ESI$^-$ **HRMS** for $C_{21}H_{22}O_5S^-$: calcd. m/z 371.09587, found m/z 371.09597.

Synthesis of HITub-4

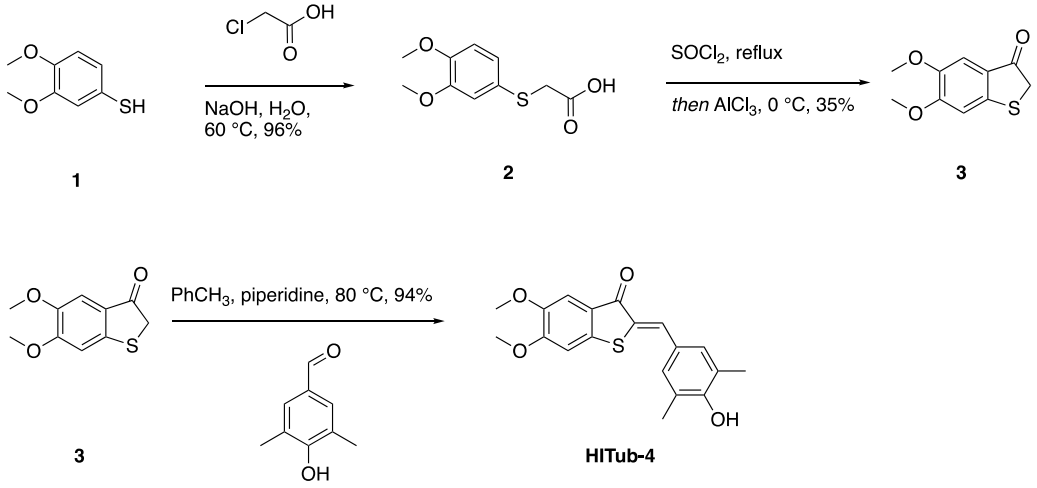

Scheme S2: Synthesis of **HITub-4**.

2-((3,4-Dimethoxyphenyl)thio)acetic acid (2)

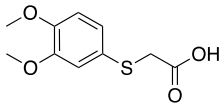

Acetic acid derivative **2** was prepared starting from commercially available thiol **1** following our previously published procedure; spectral data are in good agreement with our previously published data[3].

^{1}H-NMR (DMSO-d_6, 400 MHz): δ (ppm) = 12.67 (s, 1H), 7.00 (d, *J* = 1.7 Hz, 1H), 6.94 (dd, *J* = 1.7 & 8.3 Hz, 1H), 6.90 (d, *J* = 8.3 Hz, 1H), 3.74 (s, 3H), 3.73 (s, 3H), 3.67 (s, 2H); **^{13}C-NMR** (DMSO-d_6, 100 MHz): δ (ppm) = 161.3, 139.2, 138.5, 116.2, 112.9, 104.2, 102.6, 45.9, 45.8, 27.3; ESI$^-$ **HRMS** for $C_{10}H_{11}O_4S^-$: calcd. m/z 227.03780, found m/z 227.03844.

5,6-Dimethoxybenzo[*b*]thiophen-3(2*H*)-one (3)

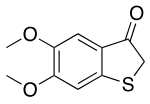

Thioindoxyl **3** was prepared following our previously reported procedure and all spectral data are in good agreement with our previously published data[3].

^{1}H-NMR ($CDCl_3$, 400 MHz): δ (ppm) = 7.17 (s, 1H), 6.82 (s, 1H), 3.94 (s, 3H), 3.87 (s, 3H), 3.79 (s, 2H); **^{13}C-NMR** ($CDCl_3$, 100 MHz): δ (ppm) = 198.6, 156.5, 149.6, 147.9, 123.7, 106.9, 105.6, 56.6, 56.3, 40.1; $\mathbf{R_f}$ = 0.33 on EA:Hx, 1:4 (blue fluorescence under illumination with 254 / 366 nm); EI **HRMS** for $C_{10}H_{10}O_3S$: calcd. m/z 210.0345, found m/z 210.1287.

2-(4-Hydroxy-3,5-dimethylbenzylidene)-5,6-dimethoxybenzo[*b*]thiophen-3(2*H*)-one (HITub-4)

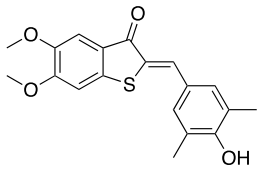

By standard procedure D, reacting thioindoxyl **3** (325 mg, 1.55 mmol, 1.00 equiv) with commercially available 3,5-dimethyl-4-hydroxybenzaldehyde (255 mg, 1.70 mmol, 1.10 equiv) in dry toluene (20 mL) for 2 h at 80 °C and overnight at room temperature. The crude product was dissolved in DMSO, water was added, the suspension was centrifuged and the supernatant was pipetted off (repeated once). The residue was dissolved in DCM, washed with water and dried over Na_2SO_4. The volatiles were removed in vacuo and the remaining solid was lyophilised to yield **HITub-4** as red solid (500 mg, 1.46 mmol, 94%).

^{1}H-NMR (DMSO-d_6, 400 MHz): δ (ppm) = 9.19 (s, 1H), 7.71 (s, 1H), 7.40 (s, 1H), 7.38 (s, 2H), 7.27 (s, 1H), 3.90 (s, 3H), 3.83 (s, 3H), 2.23 (s, 6H); **^{13}C-NMR** (DMSO-d_6, 100 MHz): δ (ppm) = 186.0, 156.2, 155.8, 148.1, 139.7, 132.9, 131.8, 127.1, 125.1, 124.9, 122.5, 107.2, 106.4, 56.4, 55.8, 16.8; $\mathbf{R_f}$ = 0.41 on EA:Hx, 1:2; ESI$^-$ **HRMS** for $C_{19}H_{17}O_4S^-$: calcd. m/z 341.08530, found m/z 341.08545.

Synthesis of HITub-2 and HITub-5

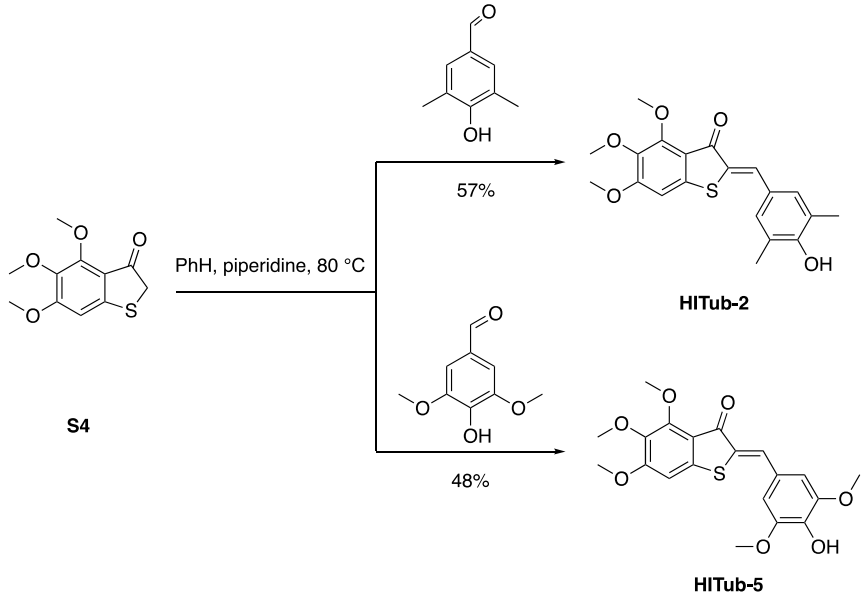

Scheme S3: Synthesis of **HITub-2** and **HITub-5**.

4,5,6-Trimethoxybenzo[*b*]thiophen-3(2*H*)-one (S4)

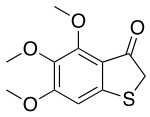

S4 was prepared following our previously reported procedure and all spectral data are in good agreement with our previously published data[3].

^{1}H-NMR ($CDCl_3$, 400 MHz): δ (ppm) = 6.59 (s, 1H), 3.97 (s, 3H), 3.89 (s, 3H), 3.79 (s, 3H), 3.74 (s, 2H); **^{13}C-NMR** ($CDCl_3$, 100 MHz): δ (ppm) = 196.5, 160.6, 154.0, 152.4, 139.3, 117.2, 101.9, 62.0, 61.5, 56.5, 40.3; **R_f** = 0.32 on EA:Hx, 1:4 (blue fluorescence under illumination with 254 nm); ESI$^+$ **HRMS** for $C_{11}H_{13}O_4S^+$: calcd. m/z 241.05291, found m/z 241.05281, for $C_{11}H_{12}O_4NaS^+$: calcd. m/z 263.03485, found m/z 263.03485.

2-(4-Hydroxy-3,5-dimethylbenzylidene)-4,5,6-trimethoxybenzo[*b*]thiophen-3(2*H*)-one (HITub-2)

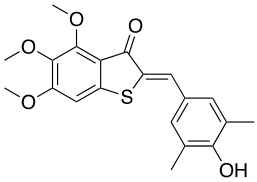

By standard procedure D, thioindoxyl **S5** (50 mg, 0.21 mmol, 1.00 equiv) was reacted with commercially available 3,5-dimethyl-4-hydroxybenzaldehyde (31 mg, 0.21 mmol, 1.00 equiv)

in dry benzene (20 mL) for 2 h at 80 °C. The crude product was dissolved in DMSO, water was added, the suspension was centrifuged and the supernatant was pipetted off (repeated once) yielding **HITub-2** as orange solid (44 mg, 0.12 mmol, 57%).

^{1}H-NMR ($CDCl_3$, 400 MHz): δ (ppm) = 7.74 (s, 1H), 7.31 (s, 2H), 6.71 (s, 1H), 5.05 (br. s, 1H), 4.05 (s, 3H), 3.94 (s, 3H), 3.85 (s, 3H), 2.29 (s, 6H); **^{13}C-NMR** ($CDCl_3$, 100 MHz): δ (ppm) = 185.8, 159.9, 154.7, 154.3, 144.0, 140.1, 132.7, 132.0, 128.3, 126.8, 123.9, 117.4, 101.7, 62.3, 61.7, 56.6, 16.1; **R_f** = 0.39 on Hx:DCM:MeOH, 1:1:0.04; ESI^+ **HRMS** for $C_{20}H_{21}O_5S^+$: calcd. m/z 373.11042, found m/z 373.11050, ESI^- **HRMS** for $C_{20}H_{19}O_7S^-$: calcd. m/z 371.09587, found m/z 371.09634.

2-(4-Hydroxy-3,5-dimethoxybenzylidene)-4,5,6-trimethoxybenzo[*b*]thiophen-3(2*H*)-one (HITub-5)

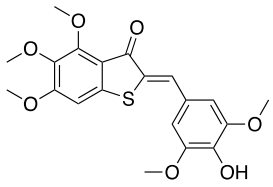

By standard procedure D, thioindoxyl **S5** (15 mg, 0.06 mmol, 1.00 equiv) was reacted with commercially available 3,5-dimethoxy-4-hydroxybenzaldehyde (14 mg, 0.07 mmol, 1.2 equiv) in dry benzene (5 mL) for 3.5 h at 80 °C. The crude was purified by flash chromatography (Hx:DCM:MeOH, 1:1:0.04) to give **HITub-5** (12 mg, 0.03 mmol, 48%).

^{1}H-NMR ($CDCl_3$, 400 MHz): δ (ppm) = 7.75 (s, 1H), 6.91 (s, 2H), 6.72 (s, 1H), 5.83 (s, 1H), 4.06 (s, 3H), 3.95 (s, 6H), 3.94 (s, 3H), 3.85 (s, 3H); **^{13}C-NMR** ($CDCl_3$, 100 MHz): δ (ppm) = 185.5, 160.1, 154.8, 147.4, 143.7, 140.2, 136.9, 132.7, 129.0, 126.2, 117.3, 108.0, 101.8, 62.3, 61.7, 56.6, 56.5; **R_f** = 0.39 on Hx:DCM:MeOH, 1:1:0.04; ESI^+ **HRMS** for $C_{20}H_{21}O_7S^+$: calcd. m/z 405.10080, found m/z 405.10015; ESI^- **HRMS** for $C_{20}H_{19}O_7S^-$: calcd. m/z 403.08570, found m/z 403.08616.

Synthesis of HITub-1

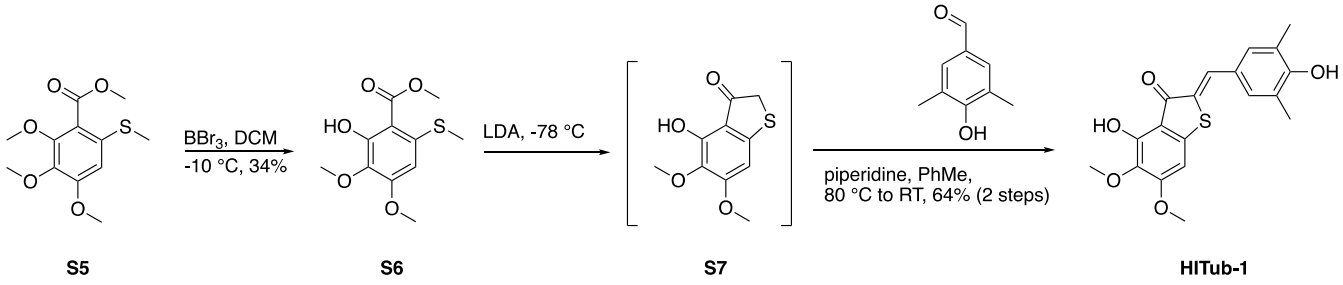

Scheme S4: Synthesis of **HITub-1**.

Methyl 2,3,4-trimethoxy-6-(methylthio)benzoate (S5)

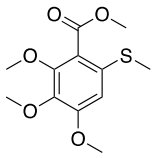

S5 was prepared following our previously reported procedure with all spectroscopical data matching the literature.[3]

Methyl 2-hydroxy-3,4-dimethoxy-6-(methylthio)benzoate (S6)

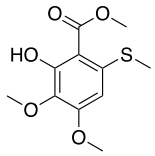

To a solution of **S5** (50 mg, 0.18 mmol, 1.00 equiv) in dry DCM (2 mL) was added BBr_3 (1 M in DCM, 0.20 mmol, 0.20 mL, 1.10 equiv) at −10 °C and the mixture was stirred for 30 min prior to quenching by the addition of an aqueous saturated solution of $NaHCO_3$. After acidification with HCl (2 M) the layers were separated and the aqueous phase was extracted with DCM. The combined organic layers were dried over Na_2SO_4 and evaporated. The crude was purified by flash chromatography (EA:Hx, 1:4) giving pure **S6** as a white solid (16 mg, 0.06 mmol, 34%).

^{1}H-NMR ($CDCl_3$, 400 MHz): δ (ppm) = 11.61 (s, 1H), 6.23 (s, 1H), 3.96 (s, 3H), 3.92 (s, 3H), 3.82 (s, 3H), 2.41 (s, 3H); **^{13}C-NMR** ($CDCl_3$, 100 MHz): δ (ppm) = 170.9, 157.8, 156.7, 139.8, 133.6, 105.0, 99.9, 60.8, 56.0, 52.1, 16.6; **R_f** = 0.34 on EA:Hx, 1:4; ESI^+ **HRMS** for $C_{11}H_{13}O_5S^-$: calcd. m/z 257.04892, found m/z 257.04937.

4-Hydroxy-2-(4-hydroxy-3,5-dimethylbenzylidene)-5,6-dimethoxybenzo[b]thiophen-3(2H)-one (HITub-1)

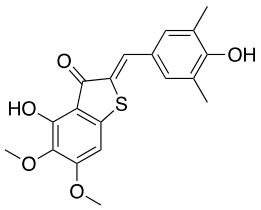

By standard procedure C, **S6** (18 mg, 0.07 mmol, 1.00 equiv) was reacted with LDA (prepared from *n*-BuLi ((2.5 M in hexane, 19 mg, 0.30 mmol, 0.12 mL, 4.33 equiv) and DIPA (32 mg, 0.32

mmol, 0.04 mL, 4.60 equiv)). After stirring for 1 h at −78 °C and 1 h at 25 °C, the mixture was worked up yielding crude **S7**.

An analytically pure sample of thioindoxyl **S7** can be obtained by purification of the crude by automated flash chromatography (EA:Hx, 5 → 100%) and was characterised as follows: **^{1}H-NMR** ($CDCl_3$, 400 MHz): δ (ppm) = 9.81 (s, 1H), 6.46 (s, 1H), 3.92 (s, 3H), 3.85 (s, 2H), 3.84 (s, 3H); **^{13}C-NMR** ($CDCl_3$, 100 MHz): δ (ppm) = 201.8, 161.7, 153.0, 150.5, 132.9, 112.4, 98.7, 61.1, 56.7, 40.5; **R_f** = 0.37 on EA:Hx, 1:4; ESI^+ **HRMS** for $C_{10}H_{11}O_4S^+$: calcd. m/z 227.03726, found m/z 227.03743; ESI^- **HRMS** for $C_{10}H_9O_4S^-$: calcd. m/z 225.02270, found m/z 225.02256.

Due to partial decomposition during chromatography it is however more practical to use crude **S7** in the following step. By standard procedure D, crude **S7** was reacted with commercially available 3,5-dimethyl-4-hydroxybenzaldehyde (11 mg, 0.07 mmol, 1.00 equiv) in dry toluene (5 mL) for 1h at 80 °C and overnight at room temperature. After work-up, the crude product was purified by precipitation with water from a concentrated DMSO solution (repeated once) to afford **HITub-1** as an orange-brown solid (16 mg, 0.04 mmol, 64% over two steps).

^{1}H-NMR (DMSO-d_6, 400 MHz): δ (ppm) = 10.14 (s, 1H), 9.22 (s, 1H), 7.65 (s, 1H), 7.36 (s, 2H), 7.00 (s, 1H), 3.90 (s, 3H), 3.70 (s, 3H), 2.23 (s, 6H); **^{13}C-NMR** (DMSO-d_6, 100 MHz): δ (ppm) = 187.8, 170.6, 170.2, 160.5, 156.7, 152.8, 141.8, 133.8, 132.7, 132.2, 127.4, 125.6, 125.2, 111.9, 99.9, 60.8, 57.1, 17.2; **R_f** = 0.35 on DCM + 1% MeOH; **HRMS** for $C_{19}H_{19}O_5S^+$: calcd. m/z 359.09477, found m/z 359.09522; **HRMS** for $C_{19}H_{17}O_5S^-$: calcd. m/z 357.08022, found m/z 357.08054.

Synthesis of HITub-7

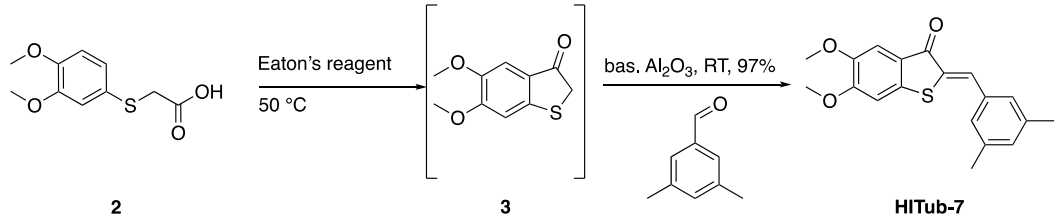

Scheme S5: Synthesis of **HITub-7**.

2-(3,5-Dimethylbenzylidene)-5,6-dimethoxybenzo[*b*]thiophen-3(2*H*)-one (HITub-7)

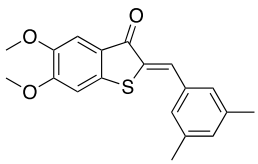

By standard procedure E, **2** (300 mg, 1.31 mmol, 4.00 equiv) was stirred with Eaton's reagent for 2 h. After extraction, commercially available 3,5-dimethylbenzaldehyde (44 mg, 0.33 mmol, 1.00 equiv) and basic Al_2O_3 were added to crude **3**. The mixture was stirred for 12 h and after work-up the crude product was purified by chromatography (EA:Hx, 1:10 → 1:4) to yield **HITub-7** (104 mg, 0.32 mmol, 97%).

^{1}H-NMR ($CDCl_3$, 400 MHz): δ (ppm) = 7.86 (s, 1H), 7.36 (s, 1H), 7.30 (s, 2H), 7.03 (s, 1H), 6.91 (s, 1H), 3.97 (s, 3H), 3.92 (s, 3H), 2.36 (s, 6H); **^{13}C-NMR** ($CDCl_3$, 100 MHz): δ (ppm) = 187.6, 156.1, 148.4, 141.2, 138.7, 134.4, 133.6, 132.1, 130.9, 128.9, 123.5, 107.9, 105.3, 56.6, 56.4, 21.5; **R_f** = 0.38 on EA:Hx, 1:2.4; EI **HRMS** for $C_{19}H_{18}O_3S$: calcd. m/z 326.4100, found m/z 326.0966.

Synthesis of HITub-6

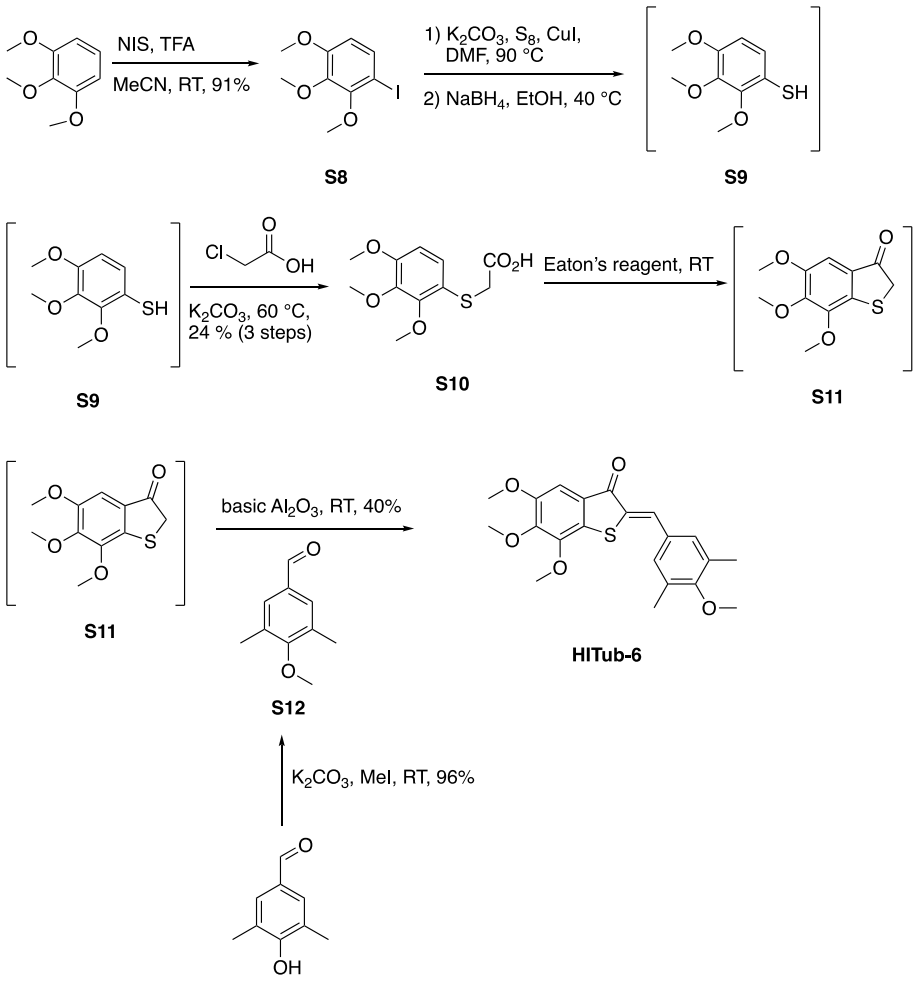

Scheme S6: Synthesis of **HITub-6**.

1-Iodo-2,3,4-trimethoxybenzene (S8)

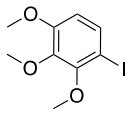

The compound was prepared following a procedure published by Castanet et al.[4] and the spectral data are in good agreement with literature.[5]

^{1}H-NMR ($CDCl_3$, 400 MHz): δ (ppm) = 7.42 (d, *J* = 8.8 Hz, 1H), 6.50 (d, *J* = 8.8 Hz, 1H), 3.88 (s, 3H), 3.86 (s, 3H), 3.87 (s, 3H) 3.85 (s, 3H); **^{13}C-NMR** ($CDCl_3$, 100 MHz): δ (ppm) = 154.5, 153.5, 142.8, 132.7, 109.9, 81.5, 61.2, 61.0, 56.3; $\mathbf{R_f}$ = 0.52 on EA:Hx, 1:5.

2-((2,3,4-Trimethoxyphenyl)thio)acetic acid (S10)

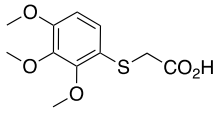

An oven-dried Schlenk tube was filled with **S8** (1.95 g, 6.61 mmol, 1.00 equiv), sulphur powder (701 mg, 21.9 mmol, 3.31 equiv), CuI (136 mg, 0.72 mmol, 0.11 equiv) and K_2CO_3 (1.80 g, 13.0 mmol, 1.97 equiv). After addition of DMF (15 mL), the tube was evacuated carefully and refilled with nitrogen. The mixture was stirred for 12 h at 90 °C. Under cooling with ice-water, ground $NaBH_4$ (891 mg, 23.6 mmol, 3.57 equiv) was added and the mixture was stirred for 5 h at 40 °C. After addition of EtOH (5 mL), the mixture was stirred for another 4 h at this temperature. Chloroacetic acid (1.50 g, 15.9 mmol, 2.41 equiv) and K_2CO_3 (0.51 g, 3.69 mmol, 0.56 equiv) were added and the reaction mixture was heated up to 60 °C for 5 h. After addition of water (5 mL), the reaction mixture was stirred for 4 d at ambient temperature. Water (400 mL) was added and it was extracted with EtOAc (3 × 50 mL). The combined organic layers were washed with $Na_2S_2O_3$ solution (1 M, 3 × 25 mL), brine (25 mL) and dried over Na_2SO_4. The solvent was evaporated under reduced pressure to yield 1.49 g of crude acid **S10**. By checking with LC–MS, desired product **S10** as well as the corresponding thiol **S9** were detected. Therefore, the alkylation procedure was repeated. The crude product was suspended in NaOH (2 M, 30 mL) and a solution of chloroacetic acid (813 mg, 8.60 mmol) in water (3 mL) was added and the reaction mixture was stirred at 60 °C for 2 h. $Na_2S_2O_3$ solution (1 M, 2 mL) was added and the mixture was stirred for another hour at 60 °C. After acidifying with concentrated HCl to pH 1, it was extracted with EtOAc (3 × 25 mL), the organic layer was washed with brine, dried over Na_2SO_4 and the solvent was removed under reduced pressure. The residue was purified by chromatography (EA:Hx:MeOH, 1:1:0 → 1:1:1) to yield **S10** as a pale yellow oil (413 mg, 1.60 mmol, 24% over 3 steps).

^{1}H-NMR ($CDCl_3$, 400 MHz): δ (ppm) = 7.14 (d, *J* = 8.7 Hz, 1H), 6.63 (d, *J* = 8.7 Hz, 1H), 3.94 (s, 3H), 3.86 (s, 3H), 3.85 (s, 3H), 3.59 (s, 2H); **^{13}C-NMR** ($CDCl_3$, 100 MHz): δ (ppm) = 175.3,

154.5, 153.6, 142.8, 128.0, 119.0, 107.8, 61.3, 61.1, 56.2, 37.0; **R_f** = 0.68 on EA:Hx:MeOH, 1:1:1; ESI^+ **HRMS** for $C_{11}H_{15}O_5S^+$: calcd. m/z 259.29545, found m/z 259.06355.

4-Methoxy-3,5-dimethylbenzaldehyde (S12)

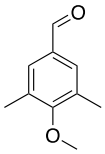

4-Hydroxy-3,5-dimethylbenzaldehyde (600 mg, 3.99 mmol, 1.00 equiv) and an excess of K_2CO_3 were suspended in dry acetone. Iodomethane (1 mL, 16.00 mmol, 4.01 equiv) was added and the reaction mixture was stirred for 12 h at ambient temperature. The solvent was removed under reduced pressure. After addition of water (20 mL), the mixture was extracted with ethyl acetate (3 × 30mL), the combined organic layers were washed with brine, dried over Na_2SO_4 and the solvent was removed under reduced pressure to yield **S12** as a colourless oil (630 mg, 3.84 mmol, 96%)

The spectral data match the literature.[5]

^{1}H-NMR ($CDCl_3$, 400 MHz): δ (ppm) = 9.87 (s, 1H), 7.55 (s, 2H), 3.77 (s, 3H), 2.34 (s, 6H); **^{13}C-NMR** ($CDCl_3$, 100 MHz): δ (ppm) = 191.8, 162.5, 132.2, 132.1, 130.8, 59.8; **R_f** = 0.29 on EA:Hx, 1:2.4.

5,6,7-Trimethoxy-2-(4-methoxy-3,5-dimethylbenzylidene)benzo[*b*]thiophen-3(2*H*)-one (HITub-6)

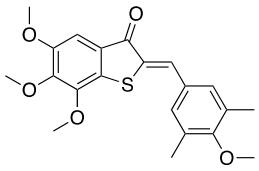

By Standard Procedure E, acid **S10** (75 mg, 0.29 mmol, 4.75 equiv) was stirred with Eaton's reagent for 1 h. After extraction, aldehyde **S12** (10.0 mg, 0. 06 mmol, 1.00 equiv) was added to crude **S11**. The mixture was stirred for 12 h. The crude product was purified by chromatography (EA:Hx, 1:10 → 1:2.4) to yield **HITub-6** as a yellow solid (8.8 mg, 0.02 mmol, 40%).

^{1}H-NMR ($CDCl_3$, 400 MHz): δ (ppm) = 7.84 (s, 1H), 7.39 (s, 2H), 7.23 (s, 1H), 4.01 (s, 3H), 3.99 (s, 3H), 3.90 (s, 3H), 3.75 (s, 3H), 2.34 (s, 6H); **^{13}C-NMR** ($CDCl_3$, 100 MHz): δ (ppm) = 188.1, 159.1, 153.1, 148.3, 147.6, 134.0, 133.1, 132.1, 132.0, 130.1, 129.5, 126.0, 104.4, 61.4, 61.2, 59.9, 56.6, 16.4; **R_f** = 0.36 on EA:Hx, 1:2.4; EI **HRMS** for $C_{21}H_{22}O_5S$: calcd. m/z 386.4620 m/z, found m/z 386.1187.

Part B: photocharacterisation in vitro

UV–vis spectrophotometry of bulk samples

Absorption spectra in cuvette ("UV–vis") were acquired on a Varian CaryScan 60 (1 cm pathlength). For photoisomerisation measurements, Hellma microcuvettes (108-002-10-40) taking 500 µL volume to top of optical window were used with test solution such that the vertical pathlength of the isomerisation light is less than 7 mm to the bottom of the cuvette window. Measurements were performed as stated individually. All photoisomerisations and relaxation rate measurements were performed at room temperature. "Star" LEDs (H2A1-models at 375, 450, 505, 515 and 530 nm from Roithner Lasertechnik) were used for photoisomerisations in the cuvette that were also predictive of what would be obtained in LED-illuminated cell culture. For all photoswitching studies the samples were illuminated by shining through the optical beam of the microcuvette, with additional illumination periods at the same wavelength used to verify that PSS had indeed been reached (no further evolution of the spectrum).

PSS spectra of the HITubs

HITubs show reliable and robust reversible switching in polar aprotic solvents. Samples containing 100% *Z* isomer (from incubation in the dark at 60 °C, Figures S1 and 3) are photoswitched to a PSS with a majority of *E* isomer after saturating illumination with 450 nm; subsequent illumination with 530 nm photoisomerizes back to a PSS favouring the *Z* isomer (typically almost 100% reached). We observed that **HITub-1** could be photoswitched in slightly acidified DMSO (Figure S1a) but did not show bulk photoswitching in neutral DMSO presumably due to pH-dependent fast relaxation as discussed below.

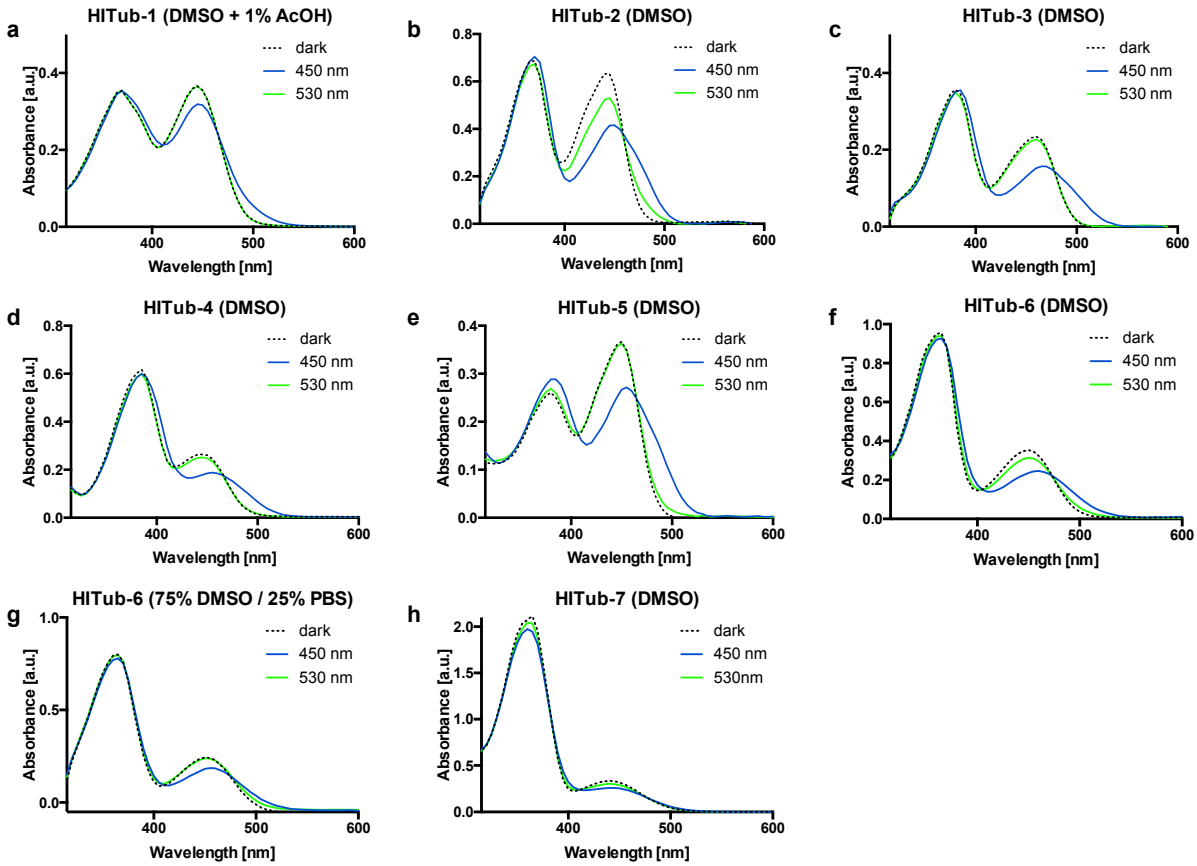

Figure S1: PSS absorption spectra of the **HITubs** at a concentration of 25 µM after incubation at 60 °C in the dark and after saturating illumination with 450 and 530 nm, respectively. All spectra in DMSO unless stated otherwise.

Solvent- and pH-dependency of photoisomerisability and relaxation rate

Addition of acid does not alter the absorption spectra or photoswitchability of **HITub-4** (Figure S2a,b). Under basic conditions however a significant hyperchromic and bathochromic shift of the absorption maximum (and to abolition of photoswitchability) is observed (Figure S2c,d). This is equally true for all **HITubs** bearing a *para*-hydroxy group on the stilbene moiety (data only shown for **HITub-4**; Figure S2c,d).We presume this results from deprotonation of the *p*-hydroxy group and resonance that substantially favours a quinoidal species, in which the photoswitchable C=C double bond of the hemithioindigo form is now tautomerised to a single bond, leading to free rotation and preventing photoswitchability. In neutral or acidic aqueous media, where the presumed quinoidal form is not present (Figure S2e-f), still no bulk photoisomerisation was observed under the applied conditions, which we presume is caused by very fast relaxation to the thermodynamically preferred *Z* isomer in aqueous media.[6]

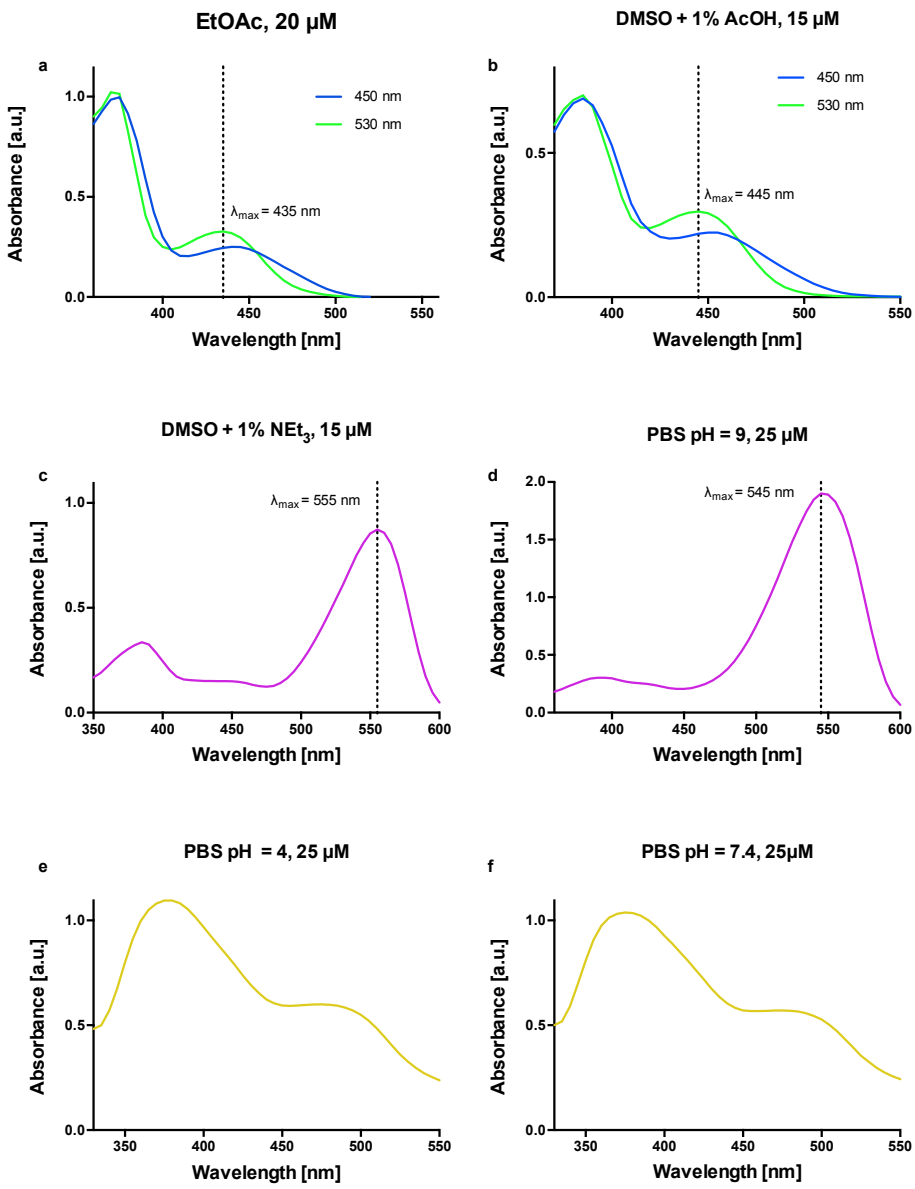

Figure S2: (**a**, **b**) Absorption spectra of **HITub-4** after saturating illumination with 450 (blue) and 530 nm (green) in neutral or acidified polar aprotic solvents, see also Fig S1d. (**c**) **HITub-4** photoswitchability could not be observed in basified aprotic media. (**d** – **f**) **HITub-4** photoswitchability could not be observed in aqueous media mixtures (75% DMSO / 25% PBS at the indicated pH).

The thermal relaxation half-life of **HITub-4** was measured at around 40 s in neutral polar aprotic solvents DMSO and EtOAc (Figure 3d and S3a) and was only slightly faster in acidified DMSO (Figure S3b). To bridge the gap towards determining a halflife in aqueous media, we measured relaxation in polar protic EtOH (Figure S3c) where the *E*-**HITub-4** thermal half-life is decreased to around 800 ms. In order to compare its performance to that of a similar *para*-hydroxy-substituted azobenzene, we attempted cuvette measurements of the thermal half-life of 4'-hydroxy-3,4,5-trimethoxyazobenzene (prepared according to literature [7]). However, neither in water nor even in DMSO could we observe that azobenzene's bulk photoisomerisation in cuvette, i.e. any spectral reversion was complete in < 12.5 ms (data not

shown) although we presume its half-life is orders of magnitude smaller as literature suggests [8]. Therefore, we concluded that the use of the HTI scaffold in this way can significantly slows spontaneous relaxation of resonance- or tautomerism-capable substituents as compared to cognate azobenzenes, and we considered there would be a chance to observe HTI isomer-dependent bioactivity in the heterogeneous cellular milieu when we applied photoswitching pulses faster than the timescale of spontaneous relaxation in aprotic media.

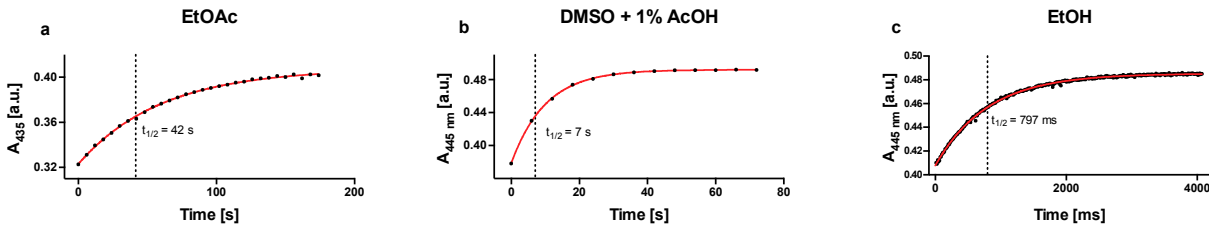

Figure S3: Thermal relaxation of **HITub-4** at 25 °C (**a**) in EtOAc, (**b**) in acidified DMSO and (**c**) in EtOH.

In these experiments, the bulk photoswitchability of *para*-hydroxy **HITub-4** was therefore confirmed in aprotic media, although not observed in protic cosolvent-aqueous media. This later seemed paradoxical when faced with its clearly photoswitchable cellular bioactivity profile. However, we note that (1) the ca. 3–4 fold biological photoswitchability index (difference between 450 nm-lit and dark-state bioactivity) of **HITub-4** and of other *para*-hydroxy **HITubs** matches closely the ca. 3.3-fold cell-free change of bioactive *Z*-isomer concentration going from dark/530 nm (100% / > 98% *Z*) to 450 nm (ca. 32% *E*) conditions, seen in PSS measurements in aprotic media; (2) these biological and concentration indices are identical to those measured for non-*para*-hydroxy **HOTubs**[3] that *are* metastable in aqueous media; (3) the solubility of **HITub-4** in pure water is very low (approx. 60 nM in distilled water, unpublished data) and it is rapidly extracted from aqueous phase into organic solvent (the limitations associated to hydrophobicity / poor solubility for further studies, such as in vivo work, are common for the vast majority of microtubule modulators of this binding site class and can be overcome by introducing water-soluble prodrug designs as we have previously shown for azocombretastatins [9]).

We theorise therefore that (a) *para*-hydroxy **HITubs** are *not* photoswitched in extracellular aqueous solution but remain as *Z* isomers there; (b) **HITubs** accumulate mainly in aprotic environments in the cell, presumably lipid membranes and vesicles, slowly exchanging across intervening (unfavoured) aqueous environments and thereby also partitioning onto hydrophobic domains of carrier protein (including binding to the colchicine site of tubulin, for active compounds); (c) under biological assay conditions the overall (*Z* + *E*) **HITub** concentration in cellular lipid environments reaches equilibrium with the extracellular applied concentration, and due to the unfavoured partitioning into water, the lipid cellular environments act as a barrier to isomer-specific equilibration of *Z*-**HITub** concentration across the membrane

between extracellular and intracellular aqueous environments; therefore (d) the *para*-hydroxy **HITub** located in aprotic environments can be photoswitched to reach its PSS there (e.g., 70:30 *E:Z* under 450 nm) while the aqueous intracellular *Z*-**HITub** concentration quickly equilibrates with this new reservoir concentration of *Z*-**HITub**. Thereby changes to the lipid reservoir *E:Z* ratio of the **HITub** (by photoequilibration) modify the intracellularly-available *Z*-**HITub** concentration that can bind tubulin, independent of the speed of *E* to *Z* relaxation in aqueous media. We have not found similar analyses in the literature of photopharmaceuticals, but we believe this principle may be found to apply in the case of other stable-isomer-active fast-relaxing photopharmaceuticals.[10]

Part C: Biochemistry and cellular biology

General cell culture: HeLa cells were maintained under standard cell culture conditions in Dulbecco's modified Eagle's medium (DMEM; PAN-Biotech: P04-035550) supplemented with 10% fetal calf serum (FCS), 100 U/mL penicillin and 100 U/mL streptomycin. Cells were grown and incubated at 37 °C in a 5% CO_2 atmosphere. Cells were typically transferred to phenol red free medium prior to assays (DMEM; PAN-Biotech: P04-03591). Compounds were applied using a minimum of co-solvent, typically 1% DMSO and were added via a D300e digital dispenser (Tecan). For assays, cells were either incubated under dark conditions (indicating that compounds were set to the all-*Z* state by thermal relaxation of the DMSO stocks at 60 °C overnight, applied while working under red-light conditions and then incubated in lightproof boxes) or lit conditions (under pulsed illumination at 450 or 530 nm using a home-made LED lighting system). "Lit" timing conditions were 75 ms pulses applied every 15 s. We controlled for unspecific phototoxicity induced by the illumination setup by including an untreated and illuminated sample in every cellular assay.

Resazurin assay: Mitochondrial diaphorase activity in HeLa cell lines was quantified by spectrophotometrically measuring the reduction of resazurin (7-hydroxy-3*H*-phenoxazin-3-one 10-oxide) to resorufin. 5,000 cells/well were seeded on 96-well microtitre plates. After 24 h, cells were treated with **HITubs**, shielded from ambient light with light-proof boxes, and exposed to the appropriate light regimes. Following 45 h of treatment, cells were incubated with 20 µL of 0.15 mg/mL resazurin per well for 3 hours at 37°C. The resorufin fluorescence (excitation 544 nm, emission 590 nm) was measured using a FLUOstar Omega microplate reader (BMG Labtech). Results are represented as percent of untreated control (reading zero was assumed to correspond to zero viable cells) and represented as mean of at least three independent experiments with SD.

Cell cycle analysis: Following 24 h of treatment with **HITubs** under the indicated light regime, cells were harvested and fixed in ice-cold 70% ethanol and incubated in a staining solution [2% DNase-free RNase A 10 mg/mL, 0.1 % Triton X-100 and 2 mg/mL propidium iodide (PI)]

for 30 min at 37 °C. Following the PI staining, cells were analyzed by flow cytometry using an LSR Fortessa (Becton Dickinson) run by BD FACSDiva 8.0.1 software. The cell cycle analysis was subsequently performed using FlowJo-V10 software (Tree Star Inc.). Results from one representative experiment are shown as a histogram. Quantification from gating on the respective histograms is shown as percent of live/singlet/PI-positive parent population per cell cycle phase across different concentrations of the compound. Every experiment was performed independently and in technical triplicates at least three times with a mean of 14,000 PI-positive singlet cells analyzed per replicate.

Resazurin antiproliferation assays

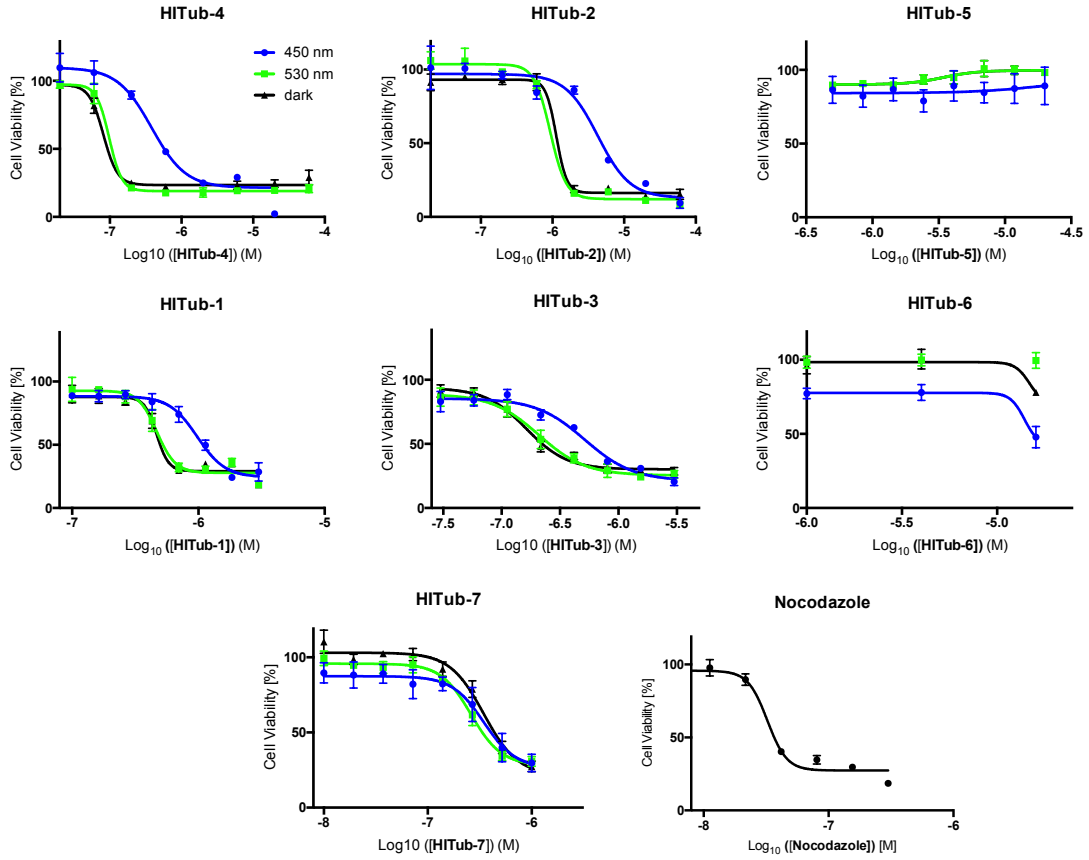

Figure S4: Representative results from Resazurin assays for **HITubs**. HeLa cells were treated with the compounds for 48 h under dark or lit (530 nm, 450 nm) conditions. Nocodazole was used as a positive reference to show antiproliferative effect in cells via microtubule depolymerisation leading towards cell death.

In vitro tubulin polymerisation assay

A **HITub-4** DMSO stock was diluted using 10% DMSO in BRB80 to reach 0.5 mM. This was mixed 1:1 with 100 mM GTP solution (in water) at room temperature. 4 µL of this mixture were spiked into ice-cold MAP-rich tubulin in BRB80 buffer (96 µL, 2 mg/mL). The sample was transferred to a quartz microcuvette held at 37 ºC in a UV–vis spectrophotometer, and was then monitored for absorbance (= turbidity) changes due to polymerisation over 20 min. A Cary 60 UV–vis spectrophotometer (Agilent Technologies) run by Cary WinUV software (version 5.0.0.999, Agilent Technologies) was used with temperature control achieved by a Cary single

cell Peltier accessory (Agilent Technologies). Absorbance data were acquired every 15 s. Generated data were processed and visualised using GraphPad Prism 6 software. Curve heights were adjusted to 0 at time zero, to account for differences in sample preparation. Since **HITub-4** cannot be isomerised in this monophasic cell-free solvent system, we did not expect to be able to observe a difference between **HITub-4** antipolymerisation activity in the dark or after 450 nm illumination, and indeed this was shown experimentally; therefore, only dark data (indicating strong polymerisation inhibition) are shown (Figure S5). We left it to cellular assays (complex multiphasic environment) to test isomer-dependent differences in bioactivity.

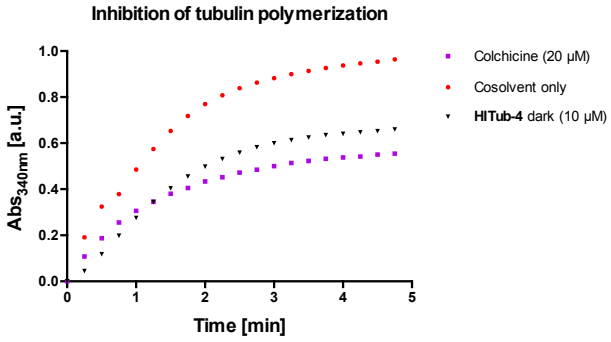

Figure S5: **HITub-4** shows *in vitro* inhibition of tubulin polymerisation (black triangle). Turbidimetric *in vitro* polymerisation assay; greater absorbance corresponds to a greater degree of polymerisation.

Immunofluorescence imaging of microtubule network structure

For fixed cell imaging (Figure 5, Figure S6), HeLa cells were seeded directly on glass coverslips in 24-well plates and treated with **HITubs**, either in the dark (all-*Z*) or under illumination by the LED array system using 450 nm LEDs (max. 70% *E*) pulsed at 75 ms "on" every 15 s, for 24 h. Then the coverslips were washed with extraction buffer (80 mM PIPES pH 6.8; 1 mM $MgCl_2$, 5 mM ethylene glycol tetra-acetic acid (EGTA) dipotassium salt and 0.5% Triton X-100) for 30 s at 37°C to remove monomeric and dimeric tubulin subunits and fixed for 10 min with a final concentration of 0.5% glutaraldehyde or else 6 min in ice-cold methanol; the glutaraldehyde-fixed cells were then quenched for 7 min with 0.1% $NaBH_4$ in PBS. Coverslips were washed with PBS twice and then blocked with PBS containing 10% FCS and 0.3% Tween-20 for 30 min at room temperature. For immunofluorescence staining of microtubules, the cells were treated with primary antibody (rabbit anti-alpha-tubulin; abcam ab18251; 1:400 in blocking buffer) for 1 h and then washed with PBS before application of the secondary antibody (donkey anti-rabbit Alexa Fluor 488; abcam ab150073; 1:400 in blocking buffer) for 1 h. The coverslips were mounted on microscopy glass slides using Roti®-Mount FluorCare DAPI (Carl Roth) and imaged with a Zeiss LSM 510, LSM 710 or SP5 confocal microscope. Image processing was performed using FIJI image analysis platform[11].

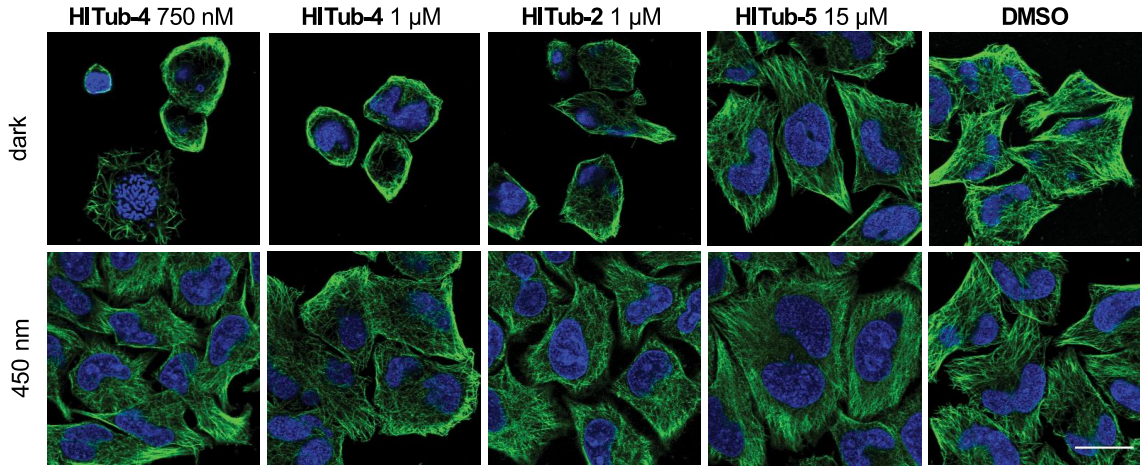

Figure S6: Immunofluorescence imaging of cells treated under lit/dark conditions with **HITub-4**, **HITub-2** and **HITub-5**, or the corresponding DMSO cosolvent controls. Microtubules of HeLa cells were immunostained with anti-α-tubulin (green), nuclei stained with DAPI (blue), scale bar = 20 μm; some images were shown in Figure **5**.

Cell cycle analysis

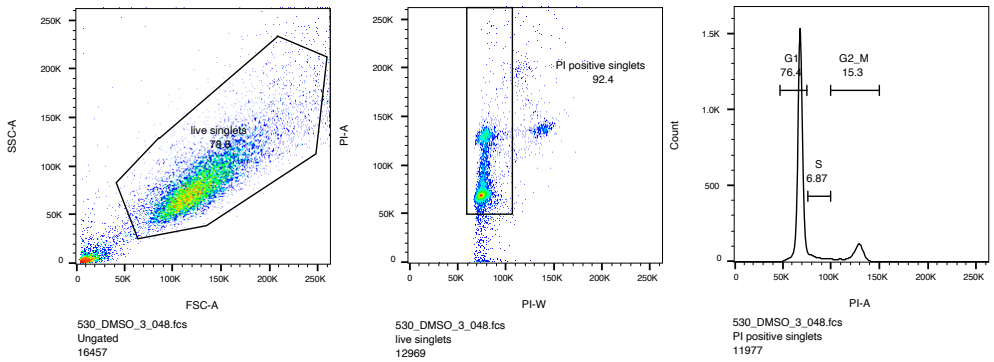

Figure S7: Representative gating strategy applied to all datasets from flow cytometric cell cycle analysis. Live singlets were determined from SSC/FSC plot, PI-positive singlets (mean of 14,000 per replicate) were then plotted as histogram and cell cycle phase gates were set to accommodate for minimal peak shifts across all samples.

Supplemental references

1. Gottlieb, H. E.; Kotlyar, V.; Nudelman, A. *J. Org. Chem.* **1997**, *62* (21), 7512-7515.
2. Suresh Kumar, A.; Thulasiram, B.; Bala Laxmi, S.; Rawat, V. S.; Sreedhar, B. *Tetrahedron* **2014**, *70* (36), 6059-6067.
3. Sailer, A.; Ermer, F.; Kraus, Y.; Lutter, F. H.; Donau, C.; Bremerich, M.; Ahlfeld, J.; Thorn-Seshold, O. *Chembiochem* **2019**, *20* (10), 1305-1314.
4. Castanet, A.-S.; Colobert, F.; Broutin, P.-E. *Tetrahedron Lett.* **2002**, *43* (29), 5047-5048.
5. Orito, K.; Hatakeyama, T.; Takeo, M.; Suginome, H. *Synthesis* **1995**, *1995* (10), 1273-1277.
6. Kink, F.; Collado, M. P.; Wiedbrauk, S.; Mayer, P.; Dube, H. *Chemistry* **2017**, *23* (26), 6237-6243.
7. Sutariya, P. G.; Modi, N. R.; Pandya, A.; Rana, V. A.; Menon, S. K. *RSC Advances* **2013**, *3* (13).
8. Garcia-Amorós, J.; Sánchez-Ferrer, A.; Massad, W. A.; Nonell, S.; Velasco, D. *Phys. Chem. Chem. Phys.* **2010**, *12* (40), 13238-13242, 10.1039/C004340K.
9. Borowiak, M.; Nahaboo, W.; Reynders, M.; Nekolla, K.; Jalinot, P.; Hasserodt, J.; Rehberg, M.; Delattre, M.; Zahler, S.; Vollmar, A.; Trauner, D.; Thorn-Seshold, O. *Cell* **2015**, *162* (2), 403-411.
10. Eisel, B.; Hartrampf, F. W. W.; Meier, T.; Trauner, D. *FEBS Lett* **2018**, *592* (3), 343-355.
11. Schindelin, J.; Arganda-Carreras, I.; Frise, E.; Kaynig, V.; Longair, M.; Pietzsch, T.; Preibisch, S.; Rueden, C.; Saalfeld, S.; Schmid, B.; Tinevez, J. Y.; White, D. J.; Hartenstein, V.; Eliceiri, K.; Tomancak, P.; Cardona, A. *Nat Methods* **2012**, *9* (7), 676-82.

Part D: NMR spectra

5,6,7-Trimethoxybenzo[*b*]thiophen-3(2*H*)-one (S3)

^{1}H-NMR spectrum

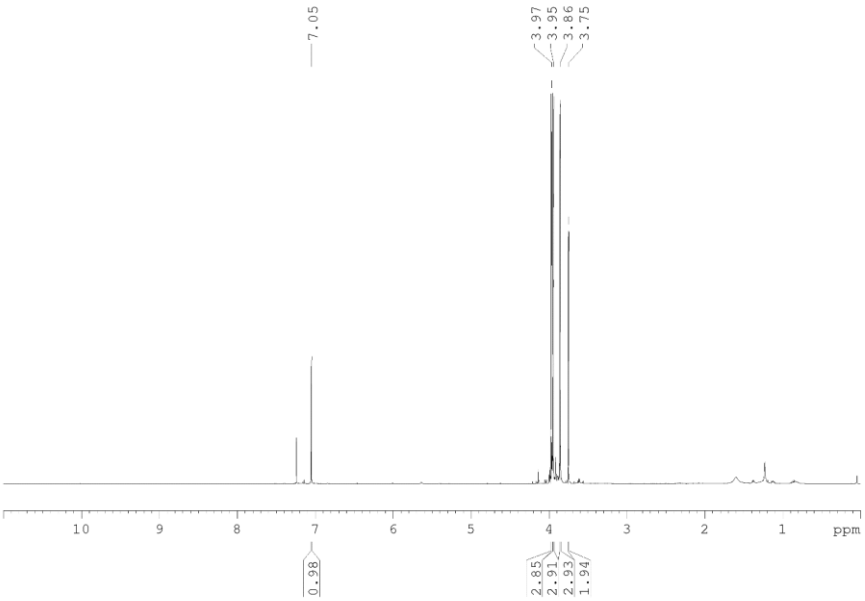

^{13}C NMR spectrum

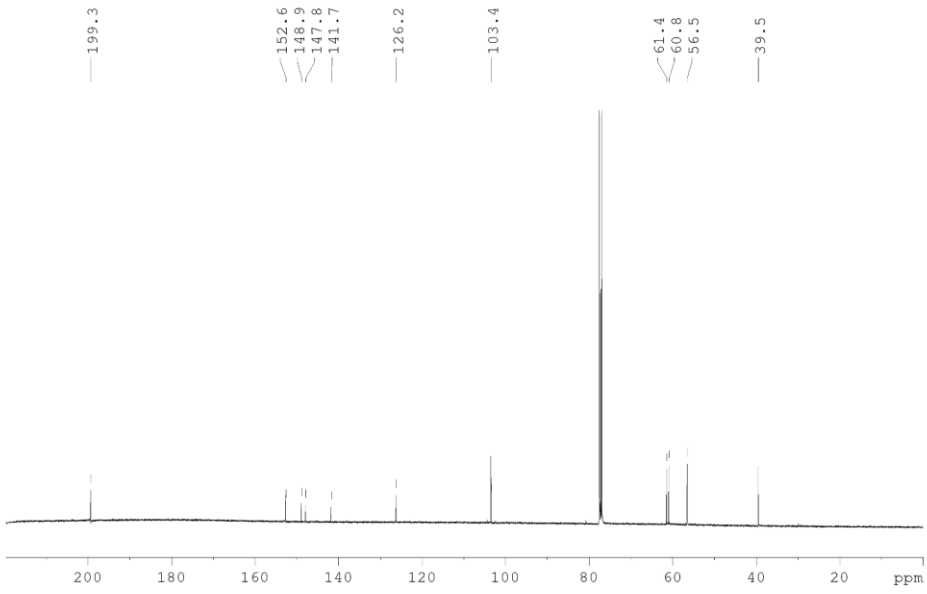

Methyl 2-hydroxy-3,4-dimethoxy-6-(methylthio)benzoate (S6)

^{1}H NMR spectrum

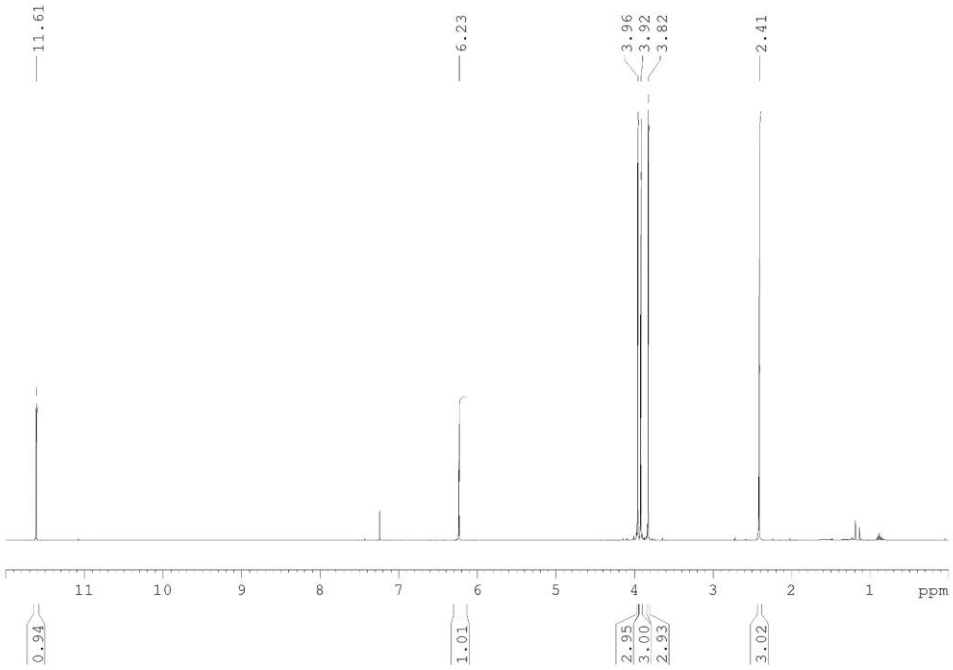

^{13}C NMR spectrum

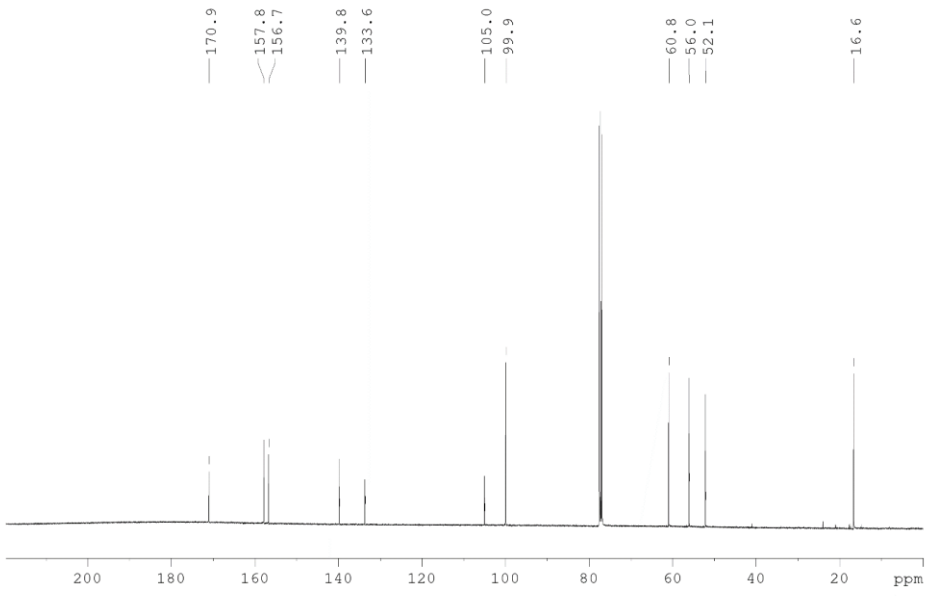

4-Hydroxy-5,6-dimethoxybenzo[*b*]thiophen-3(2*H*)-one (S7)

^{1}H NMR spectrum

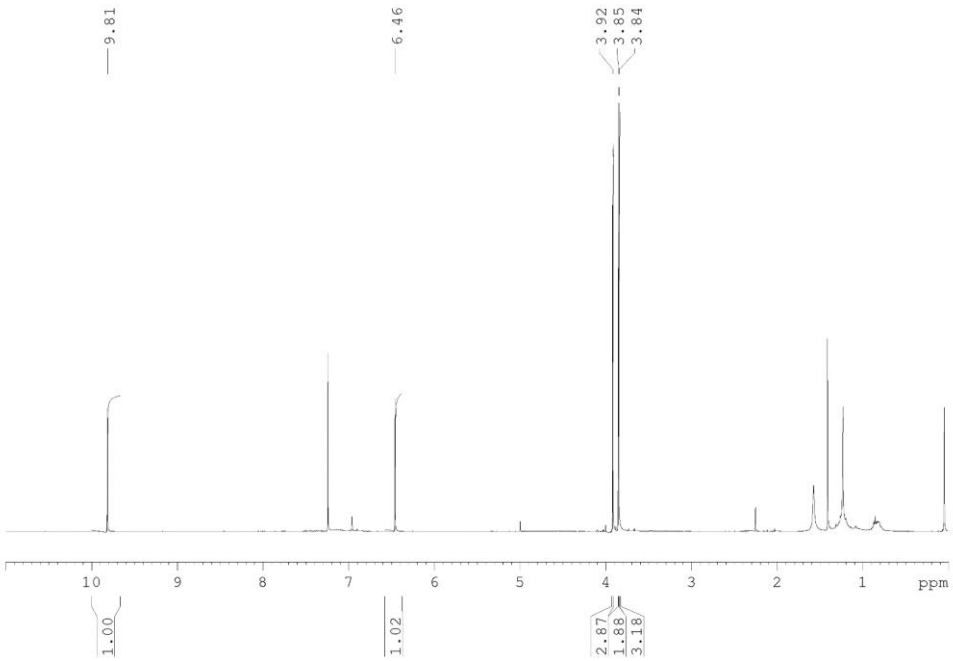

^{13}C NMR spectrum

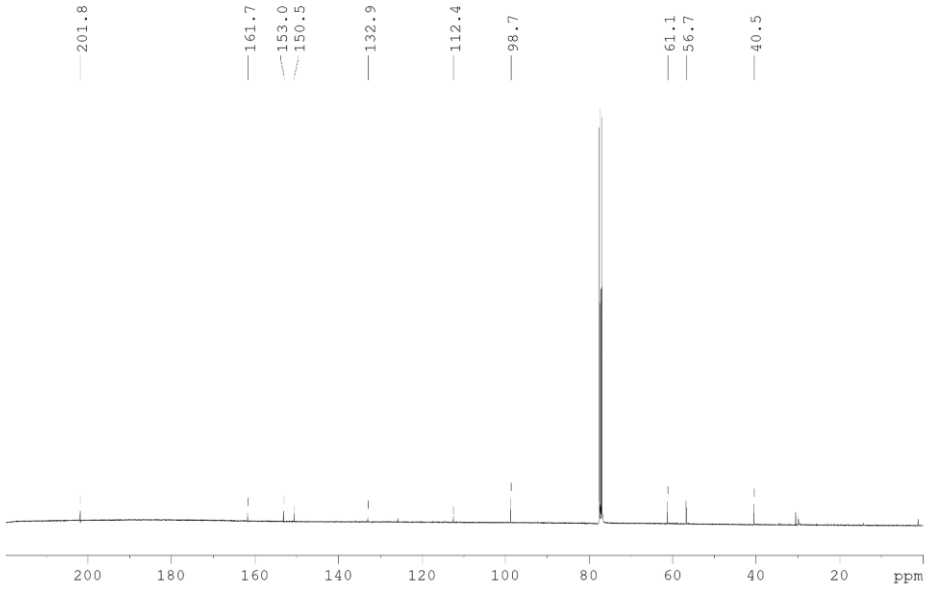

4-Hydroxy-2-(4-hydroxy-3,5-dimethylbenzylidene)-5,6-dimethoxybenzo[b]thiophen-3(2*H*)-one (HITub-1)

^{1}H NMR spectrum

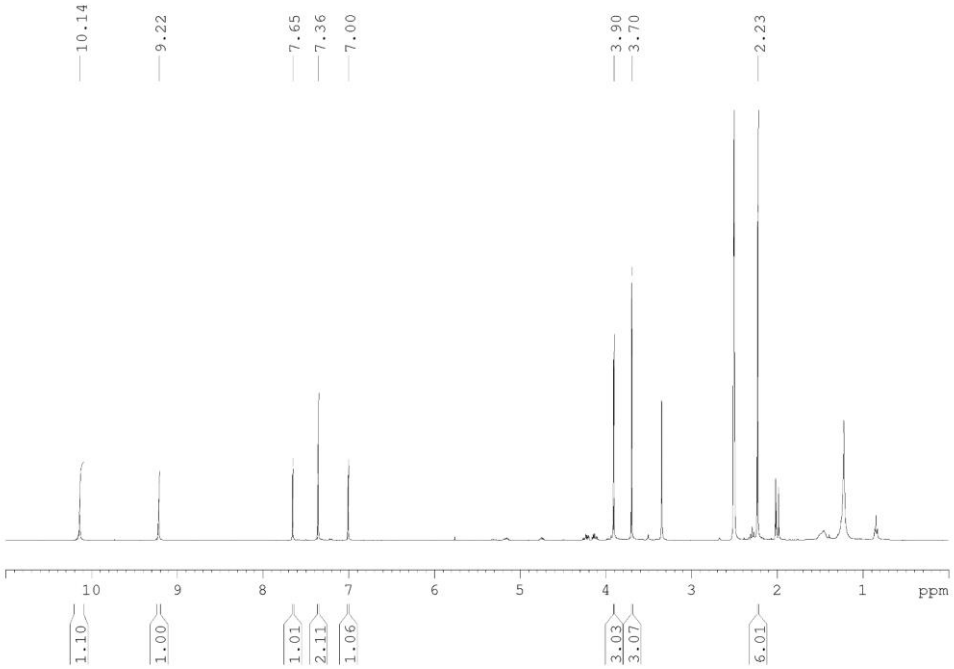

^{13}C NMR spectrum

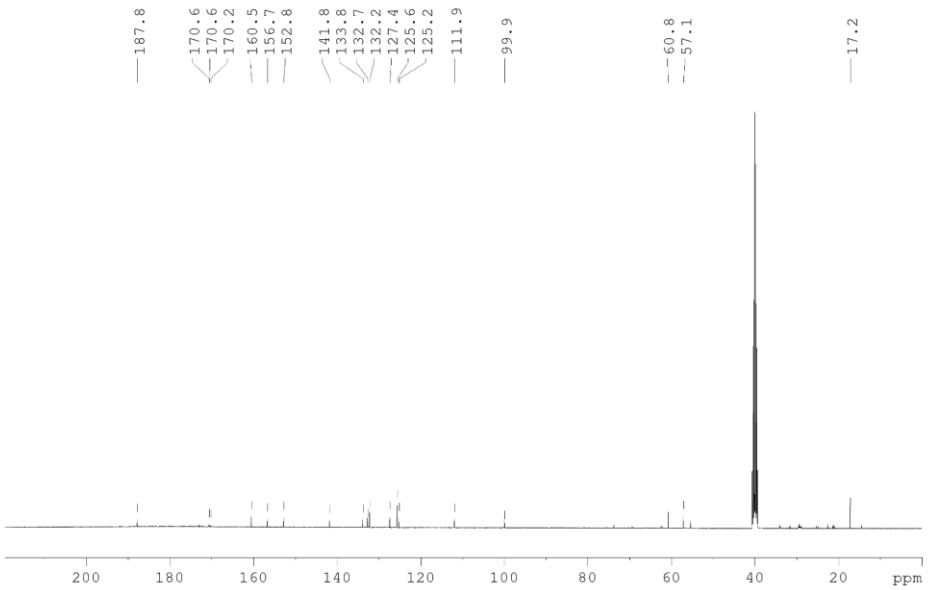

2-(4-Hydroxy-3,5-dimethylbenzylidene)-4,5,6-trimethoxybenzo[*b*]thiophen-3(2*H*)-one (HITub-2)

^{1}H NMR spectrum

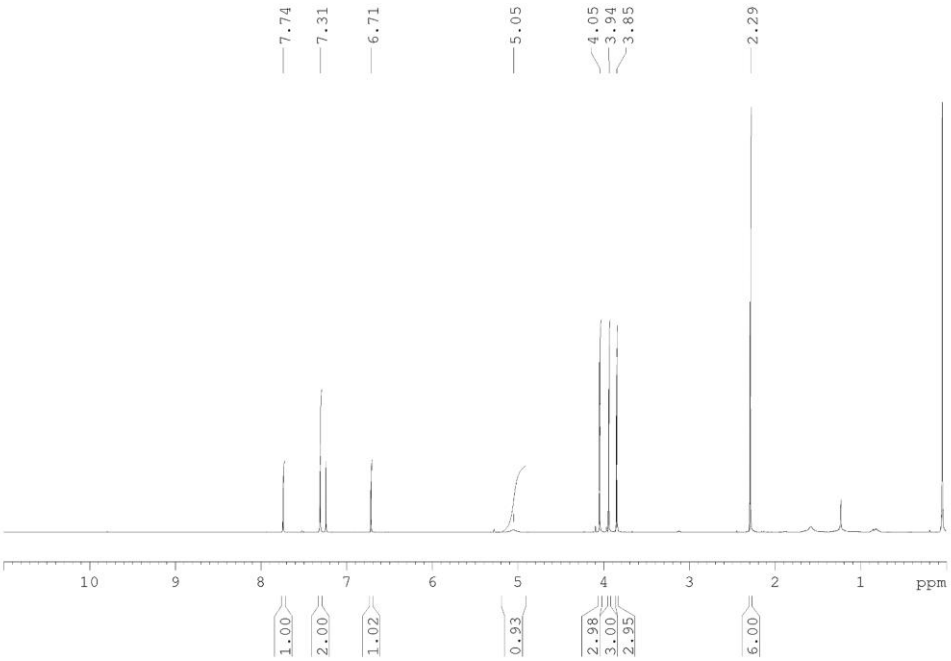

^{13}C NMR spectrum

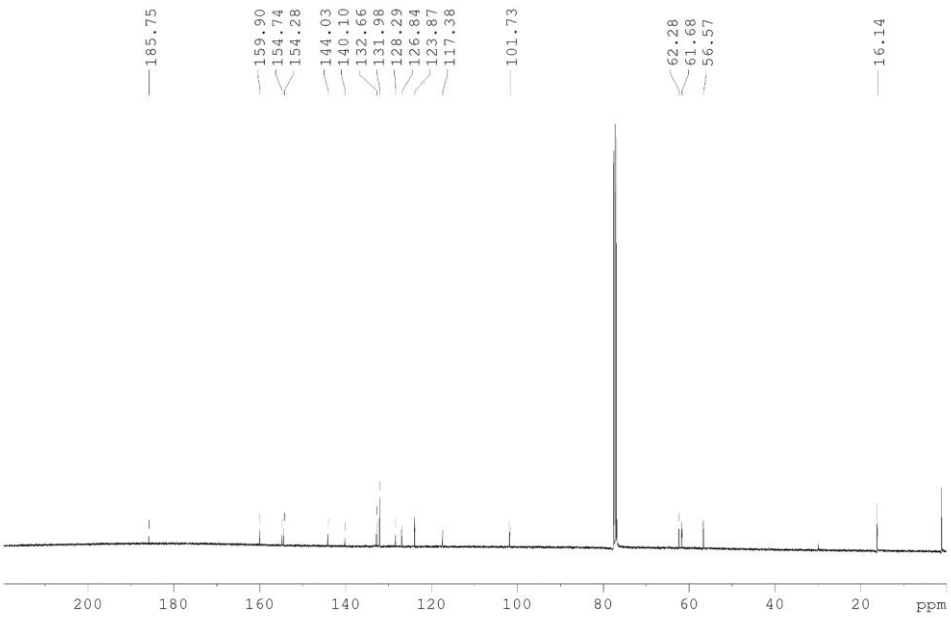

2-(4-Hydroxy-3,5-dimethylbenzylidene)-5,6,7-trimethoxybenzo[*b*]thiophen-3(2*H*)-one (HlTub-3)

^{1}H NMR spectrum

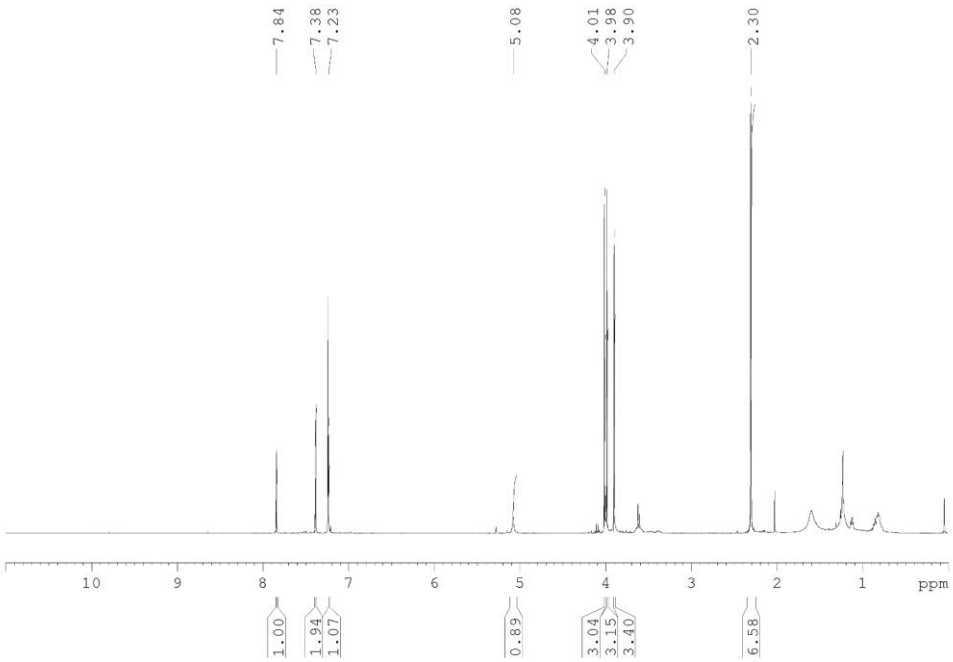

^{13}C NMR spectrum

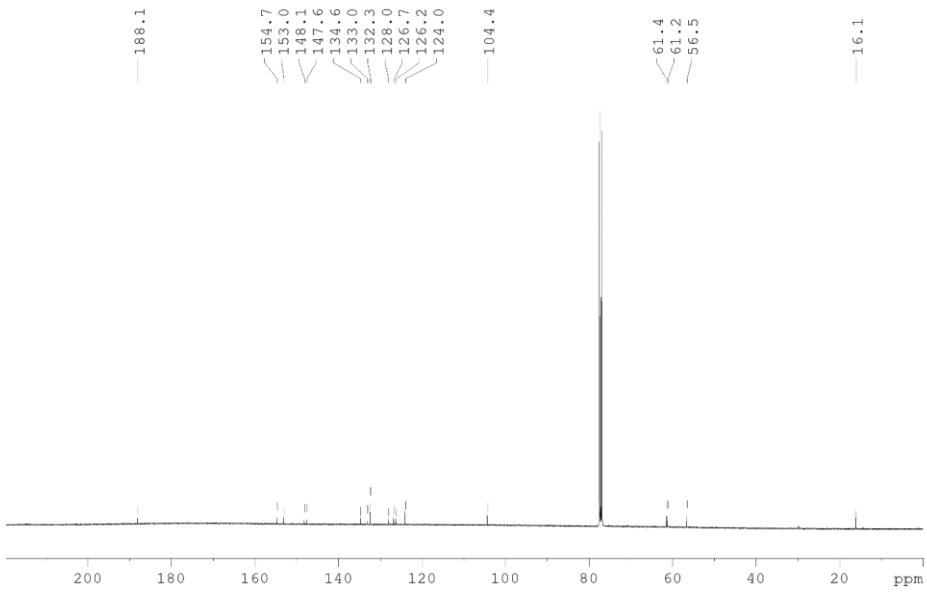

2-(4-Hydroxy-3,5-dimethylbenzylidene)-5,6-dimethoxybenzo[*b*]thiophen-3(2*H*)-one (HlTub-4)

^{1}H NMR spectrum

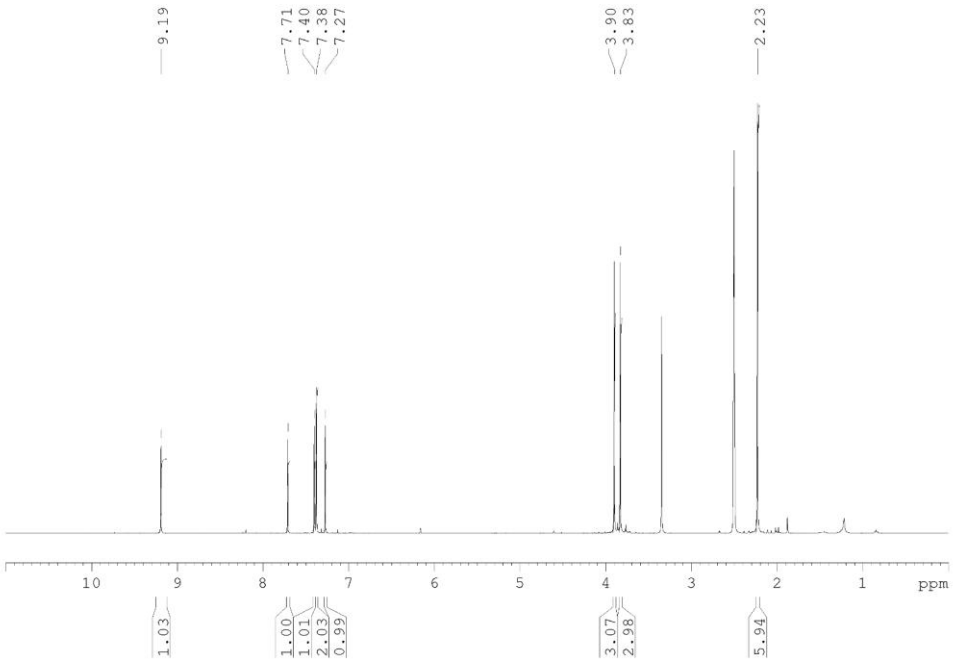

^{13}C NMR spectrum

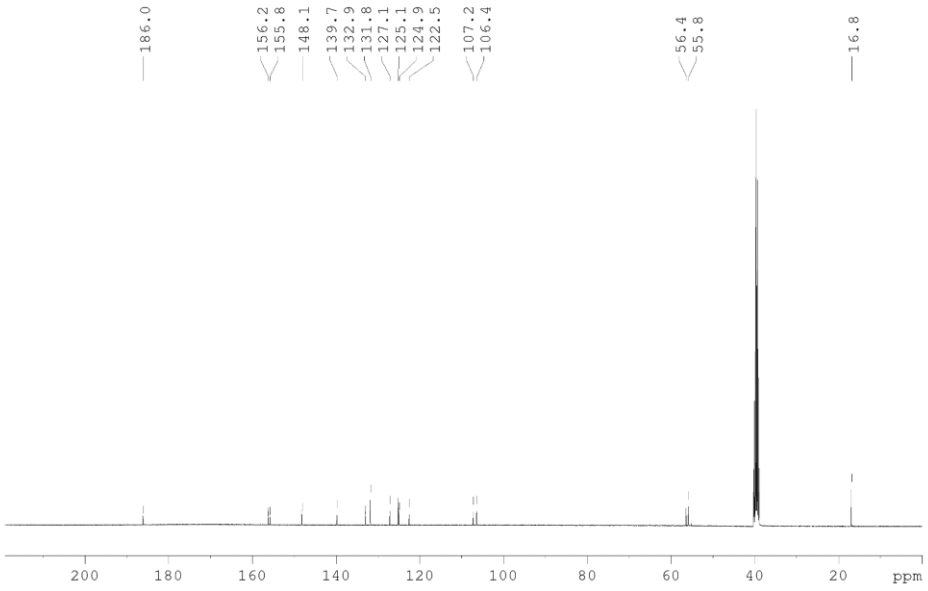

2-(4-Hydroxy-3,5-dimethoxybenzylidene)-4,5,6-trimethoxybenzo[*b*]thiophen-3(2*H*)-one (HlTub-5)

^{1}H NMR spectrum

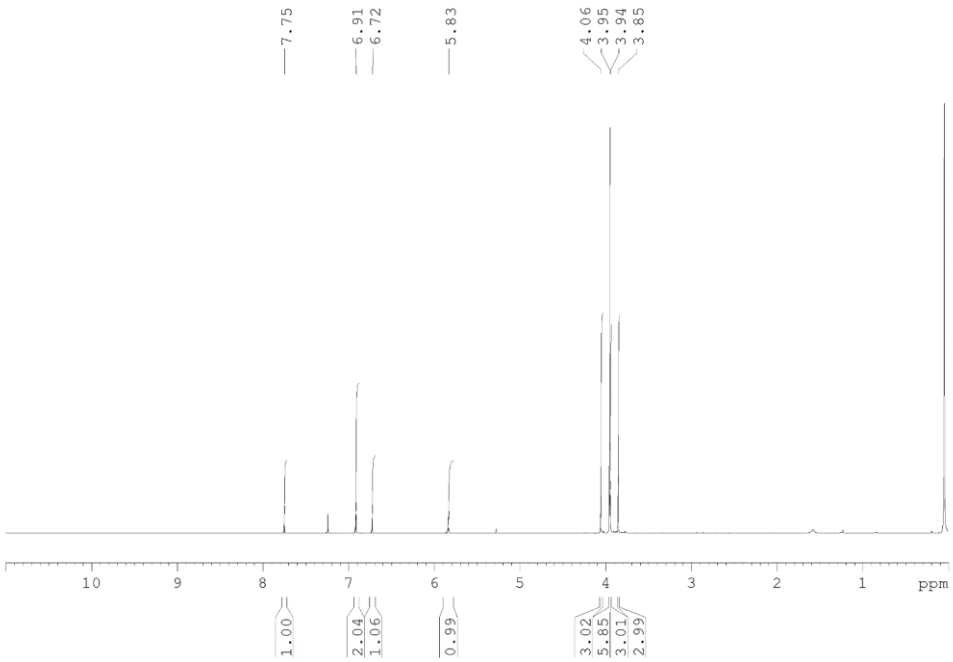

^{13}C NMR spectrum

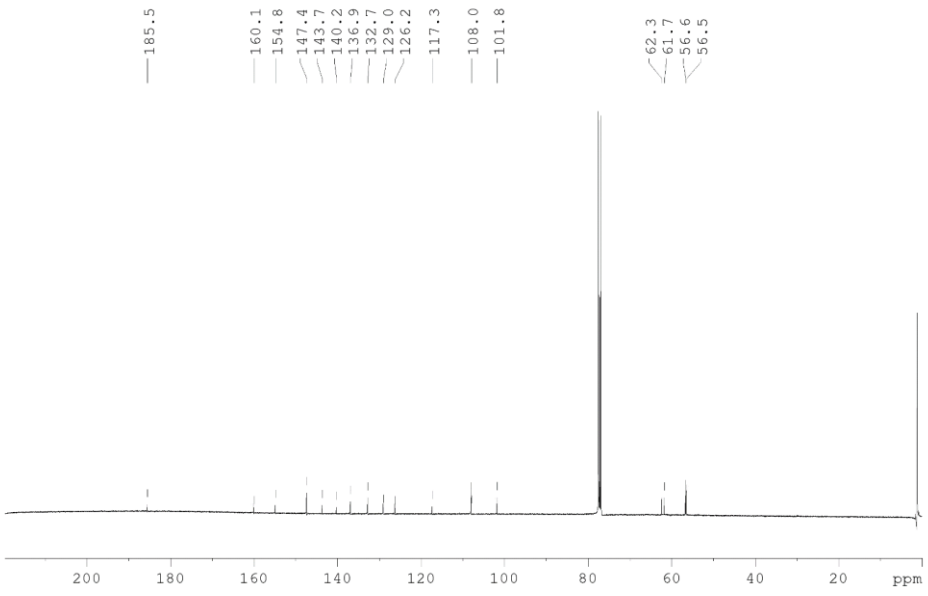

5,6,7-Trimethoxy-2-(4-methoxy-3,5-dimethylbenzylidene)benzo[*b*]thiophen-3(2*H*)-one (HlTub-6)

^{1}H NMR spectrum

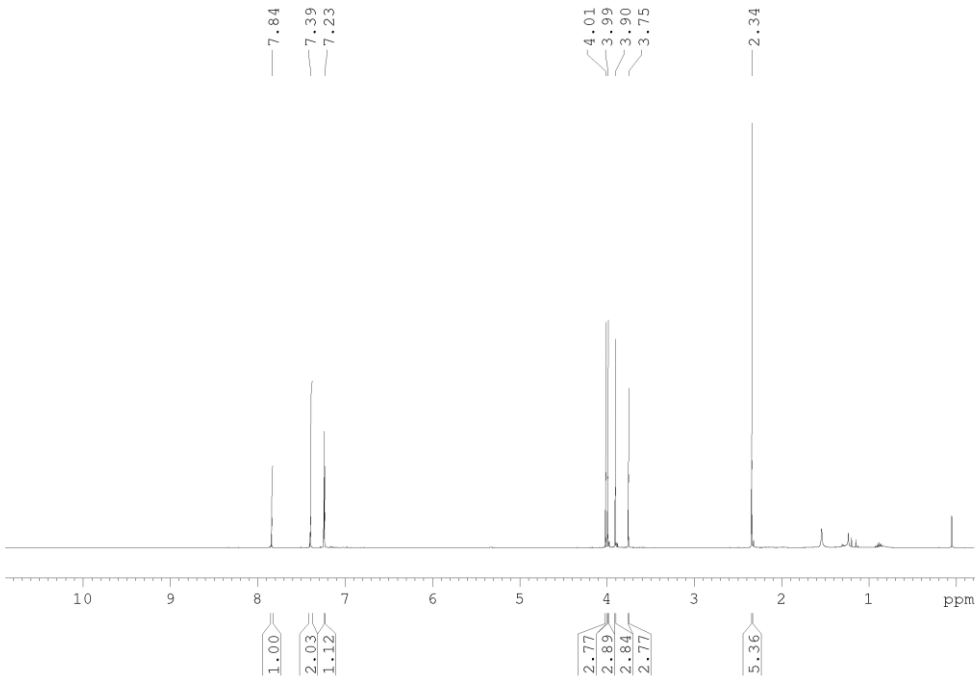

^{13}C NMR spectrum

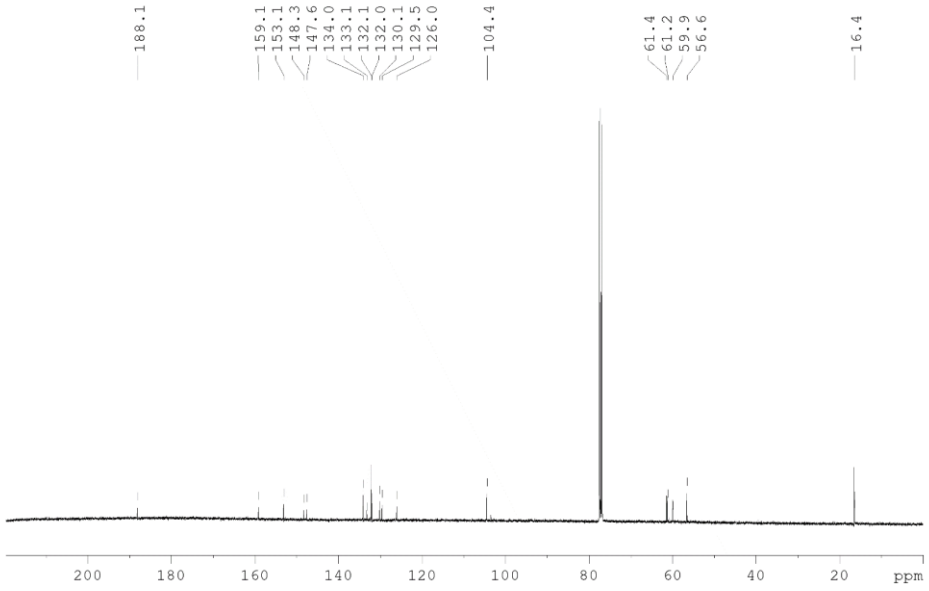

2-(3,5-Dimethylbenzylidene)-5,6-dimethoxybenzo[*b*]thiophen-3(2*H*)-one (HITub-7)

^{1}H NMR spectrum

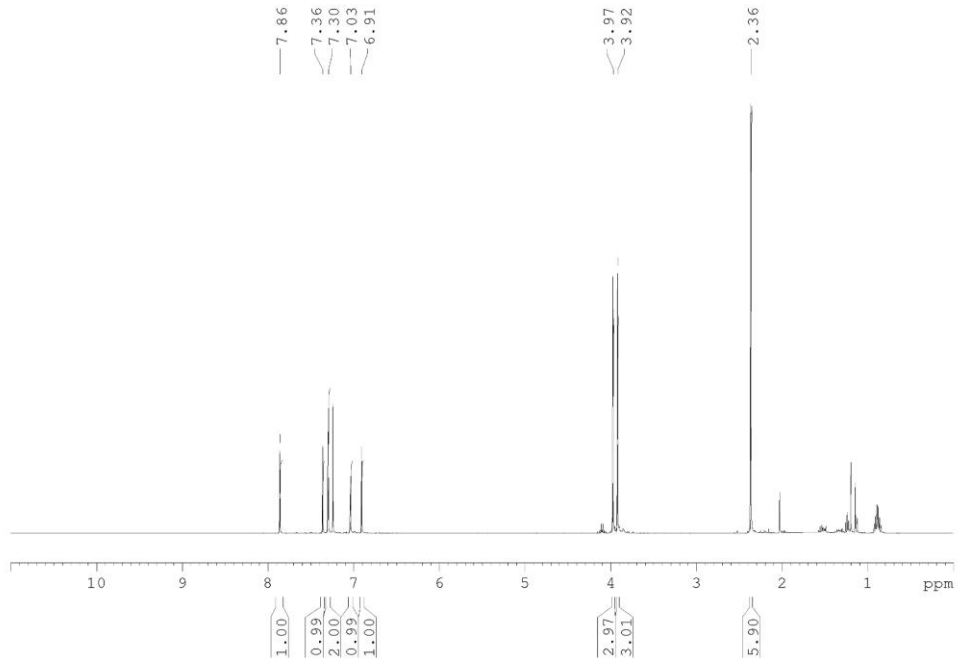

^{13}C NMR spectrum

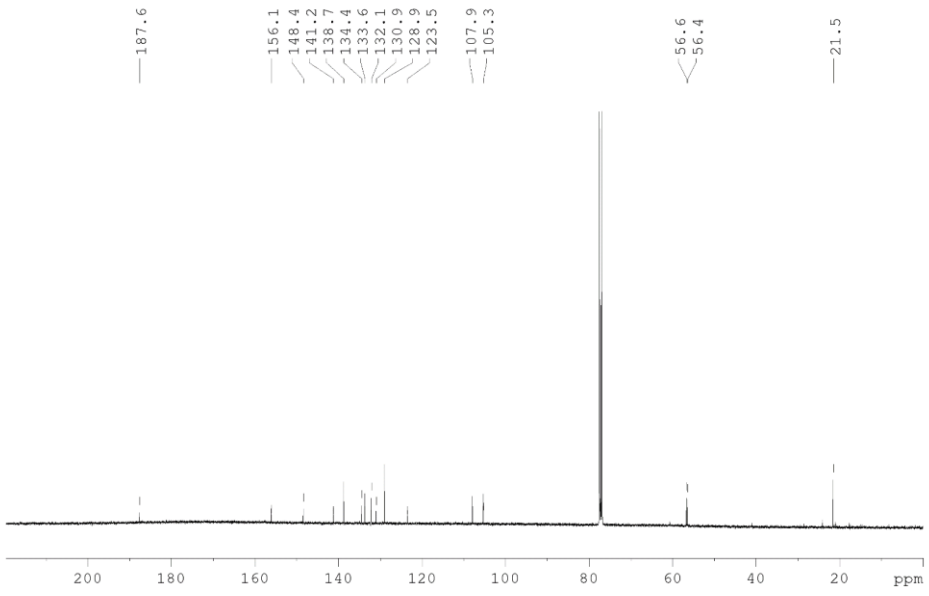

7. Paper Three: PHTubs are near-quantitative tubulin photopharmaceuticals suitable for live-cell imaging

Both first-generation **HOTubs** and second-generation **HITubs** suffered from unfavorable PSS compositions (~ 65 – 70% *E*-isomer after illumination with blue light). This posed a serious drawback for *dark*-active compounds **HOTub-31** and **HITub-4** as incomplete photoisomerization leaves a background of bioactivity likely to interfere with MT-dependent processes.

We therefore sought to create photoswitchable tubulin inhibitors which kept their beneficial features inherent to HTIs (all-visible light powered, reversible, and robust switching) but at the same time could be isomerized near-quantitatively (Fig. 15).

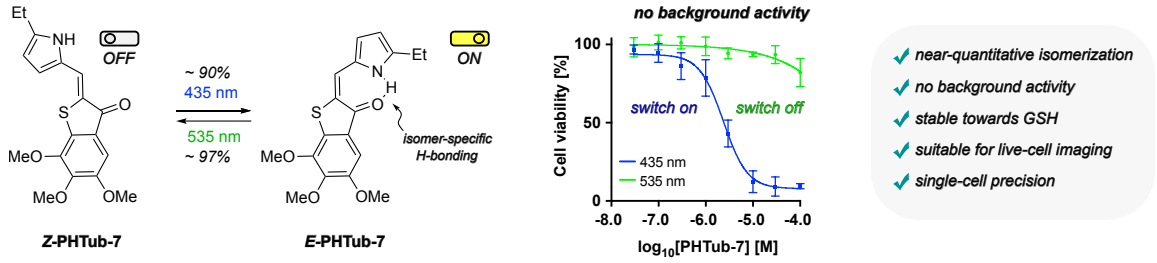

Fig. 15: PHTubs are metabolically stable tubulin photopharmaceuticals, void of background activity and suitable for live-cell imaging.

We based our investigations on the PHT scaffold (see chapter 2.2.2.3) and set out to synthesize a series of PHTs (**PHTubs**) in which we varied the pattern of methoxylation of the bottom ring and the position of an ethyl group on the pyrrole ring. For synthetic ease, we decided for this ethyl group substitution on the pyrrole ring which is a known isosteric and equally potent replacement of the 'north ring' methoxy group of CDIs.[137]

We thoroughly characterized the photoproperties of these six **PHTubs** and a conceptual *N*-methylated negative control we synthesized for comparison. We found the **PHTubs**, in line with previous reports of PHTs[73,74], to be fully reversible and fatigue resistant photoswitches with high optical band separations of the isomers (up to 45 nm, compare to ~ 20 nm for 'regular' HTIs[71]) and bidirectional near-quantitative isomerization in polar-aprotic media. To simulate more physiological conditions, we assessed the photoproperties in mixtures of DMSO and buffer. We found the band separation and the thermal stability of the *E*-isomer to decline with increasing proportion of water matching Newhouse's early reports on PHTs.[73] We assumed this correlation to result from solvent-induced hydrolysis of the hydrogen bonding in more aqueous environment. We also assessed the GSH stability of **PHTubs** and found no sign of degradation for both isomers.

We proceeded with the assessment of isomer-dependent cytotoxicity and identified two highly interesting compounds.

PHTub-8 was a very potent *dark*-active agent (IC_{50} = 30 nM, Jurkat cell line) whose photoswitchability of activity was however very modest.

PHTub-7 was a *lit*-active compound with fair potency after illumination with 450 nm (IC_{50} = 3.5 µM, Jurkat cell line). Importantly, under dark conditions **PHTub-7** produced no visible cytotoxicity resulting in very high photoswitchability of activity. We confirmed that tubulin was indeed the cellular target by *in vitro* tubulin polymerization assays, analysis of the cell cycle partition and confocal microscopy of immunofluorescently labeled MTs in fixed cells.

Encouraged by the overall performance of our **PHTubs**, we applied **PHTub-7/8** in live cell imaging experiments. Our experiments were based on studying MT dynamics in HeLa cells that were transfected to express fluorescently labeled end binding (EB) proteins. EBs bind the growing end of MTs and imaging EBs results in dynamic comets that are indicative of MT dynamics.[52,133,138] The readout can be understood as reduced comet counts result from reduced MT dynamics. For *dark*-active **PHTub-8**, we observed that illumination with blue light increased the comet count which is in line with deactivation of the compound. On the other hand, **PHTub-7** led to substantial decrease of comet counts after illumination with blue light again matching our isomer-activity relationship obtained from cytotoxicity assays.

Taken together, our results are significant for tubulin photopharmacology since we demonstrated that (1) it is possible to entirely switch on/off the bioactivity of a photopharmaceutical in cells, (2) PHTs are suitable for live cell imaging applications and (3) PHTs can be photoisomerized with standard lasers of confocal microscopes. Our findings also recommend the PHT scaffold for general applications in photopharmacology.

How to cite: *Angew. Chem. Int. Ed.* **2021**, *60*, 23695 – 23704
International Edition: doi.org/10.1002/anie.202104794
German Edition: doi.org/10.1002/ange.202104794

Photoswitches

Pyrrole Hemithioindigo Antimitotics with Near-Quantitative Bidirectional Photoswitching that Photocontrol Cellular Microtubule Dynamics with Single-Cell Precision**

*Alexander Sailer, Joyce C. M. Meiring, Constanze Heise, Linda N. Pettersson, Anna Akhmanova, Julia Thorn-Seshold, and Oliver Thorn-Seshold**

Abstract: *We report the first cellular application of the emerging near-quantitative photoswitch pyrrole hemithioindigo, by rationally designing photopharmaceutical* ***PHTub*** *inhibitors of the cytoskeletal protein tubulin.* ***PHTub****s allow simultaneous visible-light imaging and photoswitching in live cells, delivering cell-precise photomodulation of microtubule dynamics, and photocontrol over cell cycle progression and cell death. This is the first acute use of a hemithioindigo photopharmaceutical for high-spatiotemporal-resolution biological control in live cells. It additionally demonstrates the utility of near-quantitative photoswitches, by enabling a dark-active design to overcome residual background activity during cellular photopatterning. This work opens up new horizons for high-precision microtubule research using* ***PHTub****s and shows the cellular applicability of pyrrole hemithioindigo as a valuable scaffold for photocontrol of a range of other biological targets.*

Introduction

Optically targeted approaches to manipulate biological systems have revolutionised diverse research fields, by enabling the non-invasive patterning of protein activity with resolution on the spatial and temporal scales inherent to cellular functions. The high-precision studies that optical approaches allow have particular promise for systems whose spatiotemporal regulation is key to their functions: such as action potential firing in neuroscience, or cytoskeleton structure and dynamics in cell biology.[1–3] The major optical approaches are optogenetics,[4] photouncaging,[5] and photopharmacology.[6] Photopharmacology offers both distinct performance and a unique application space. Unlike photouncaging, photopharmaceuticals can be modulated reversibly, to avoid a build-up of background bioactivity that could compromise biological readout; their photoresponse is near-instantaneous and does not generate toxic uncaging by-products; and their photoresponse wavelengths are often more biologically compatible and more tunable than those of caging groups.[7,8] Unlike optogenetics, photopharmaceuticals do not need genetic engineering, so they transition easily between biological models; and they can target proteins which do not allow functional photocontrol by fusion constructs, such as the cytoskeletal scaffolds tubulin and actin.[3,8,9] Since the spatiotemporally precise orchestration of cytoskeleton structure and dynamics is critically important to hundreds of biological processes, cytoskeleton photopharmaceuticals have emerged as a valuable goal of research in recent years.[10,11] They hold promise for basic research into anisotropic processes, for example, in intracellular transport, mechanostasis and cell motility, as well as for applied research on, for example, anti-invasive strategies in cancer therapy.[10,12,13]

The development of photopharmaceuticals has however been held back by the limited space of photoswitch scaffolds shown to permit bioactivity photoswitching in cells, and by their drawbacks. An "ideal" photoswitch scaffold would permit near-complete, bidirectional photoisomerisations in situ in live cells under practical conditions, to allow efficient and precise photopatterning of its photoisomers. An ideal photopharmaceutical would further decorate this scaffold to create a ligand with near-zero bioactivity as one isomer, and potent bioactivity as the other isomer. The vast majority of cellularly applicable photopharmaceuticals rely on azobenzene scaffolds, with diarylethenes, fulgides and hemithioindigos as minor players (Figure 1a); yet these scaffolds are far from ideal. Here we expand the space of cellular photoswitch scaffolds, tackling two performance problems that azobenzenes in particular fail to address. In doing so we provide both a useful new reagent for photocontrol of the microtubule (MT) cytoskeleton, and general advances for practical photopharmacology.

The first disadvantage of current photoswitches that we focus on, is that, typically, they cannot be quantitatively bidirectionally photoisomerised with biologically compatible

[*] A. Sailer, C. Heise, L. N. Pettersson, Dr. J. Thorn-Seshold, Dr. O. Thorn-Seshold
Department of Pharmacy
Ludwig-Maximilians University of Munich
Butenandtstrasse 7, 81377 Munich (Germany)
E-mail: oliver.thorn-seshold@cup.lmu.de
Dr. J. C. M. Meiring, Prof. Dr. A. Akhmanova
Department of Biology, Utrecht University
Padualaan 8, 3584 Utrecht (The Netherlands)

[**] A previous version of this manuscript has been deposited on a preprint server (https://doi.org/10.26434/chemrxiv.14130107.v1).
Supporting information and the ORCID identification number(s) for the author(s) of this article can be found under: https://doi.org/10.1002/anie.202104794.

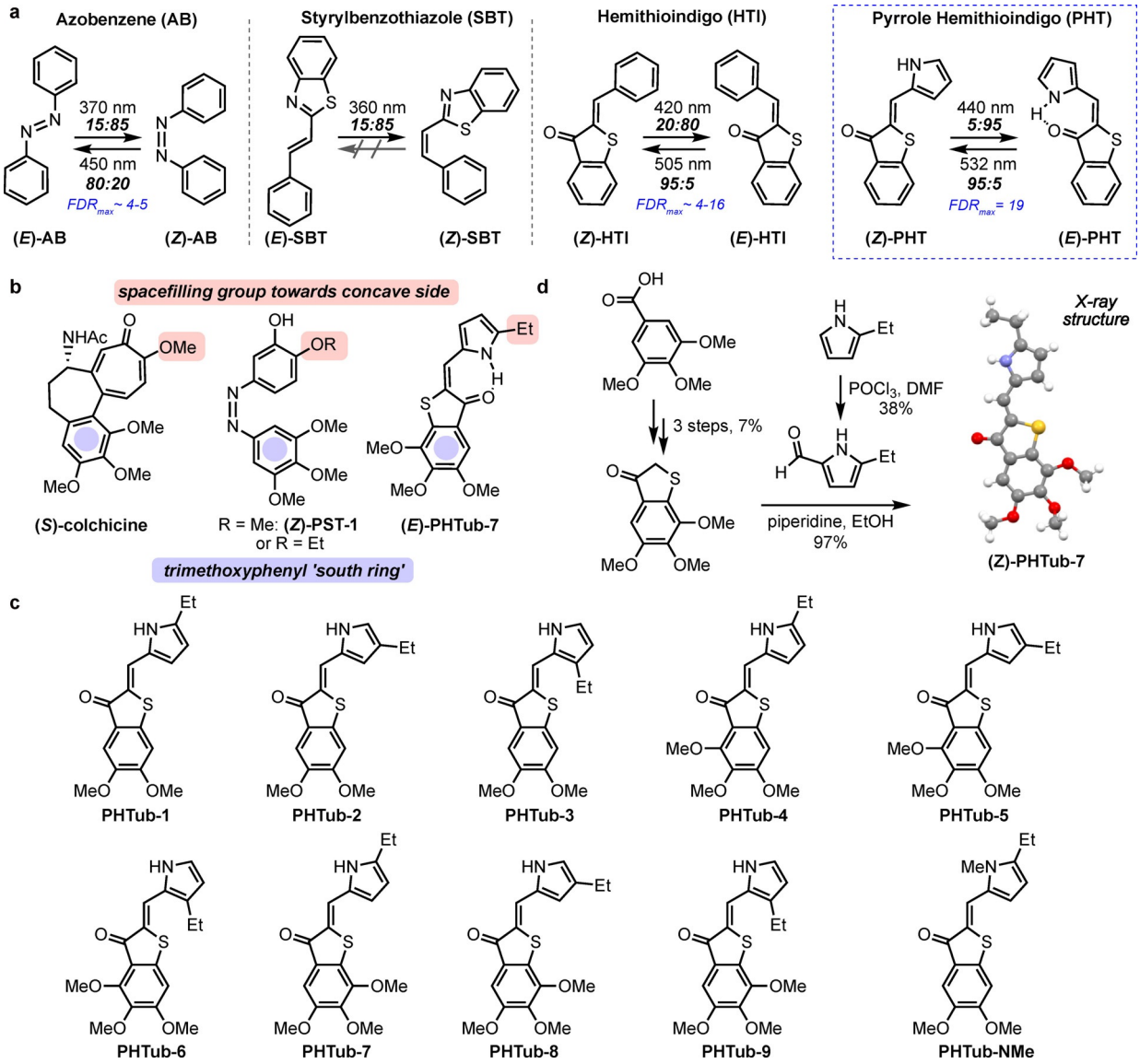

Figure 1. Design and synthesis of **PHTub**s: a) Photoswitchable scaffolds azobenzene, styrylbenzothiazole, hemithioindigo, and pyrrole hemithioindigo, with typical best photostationary state isomer ratios achieved under photoswitching in the biologically compatible wavelength range, and corresponding FDR_{max} values. b) **PHTub**s designed by derivatising PHT towards the pharmacophore requirements of the colchicine binding site on tubulin. c) Structures of **PHTub**s synthesised and tested in this study. d) Summary synthesis of representative reagent, **PHTub-7**, by piperidine-catalysed aldol condensation of the corresponding thioindoxyl and pyrrole carboxaldehyde; **PHTub-7** is depicted using its X-ray crystal structure (*Z* isomer).

wavelengths, which limits their power to photopattern biological activity. Using azobenzene as the most important example, its largest typical change of photostationary state (PSS) composition is around 4–5-fold (between ca. 15:85 *trans*:*cis* under 370 nm and ca. 80:20 *trans*:*cis* under 450 nm, though new polysubstituted or heteroaromatic azobenzenes can perform better).[1,14–16] Thus, even if only one of an azobenzene's two isomers is biologically active, photoswitching with cell-compatible wavelengths (>360 nm) can, in a best-case scenario, achieve just 4–5-fold photocontrol over the concentration patterning of the bioactive species. We define this useful quantity of the photoswitch scaffold as its maximum functional dynamic range, FDR_{max} [Eq. (1)], where

$$FDR_{max} = \frac{\phi_F}{\phi_B} \quad (1)$$

ϕ_F is the fraction of the biologically more active isomer after the most complete "forwards" photoisomerisation (PSS with the highest content of this isomer), and ϕ_B is the remaining fraction of that isomer after the most complete back-isomerisation. Note however, that typical photopharmaceuticals have substantial residual bioactivity in the less active isomer: so their actual functional dynamic range of bioactivity (FDR) cannot approach the FDR_{max}, which only reflects scaffold isomerisation (Figure 1 a).

The second disadvantage we focus on, is that the fixed-wavelength lasers available to biologists cannot deliver these "best-case" isomerisations, since typical confocal microscopes

only have a subset of the 405, 442, 488, 514, 561, and 647 nm laser lines.

These disadvantages can combine to ruin the performance of even biologically well-designed photopharmaceuticals. For example, the MT-inhibiting azobenzene **PST-1** (Figure 1b),[3,17–19] designed towards an exceptional 10000-fold difference of tubulin-binding affinity between the photoisomers,[20] has a FDR_{max} of just 9-fold with "best-case" photoisomerisations (380/525 nm). This is still comparatively high for azobenzenes; but with biologically available laser lines, the practical FDR that can be reached is just 3-fold (405/514 nm): a sharp loss of potential for an otherwise excellent photopharmaceutical.[3]

To create practical MT cytoskeleton photopharmaceuticals, we therefore focussed on photoswitch scaffolds with high FDR_{max} that also match to biologically accessible visible-light lasers. Previous explorations of C=C-based photoswitches (405 nm-switchable styrylbenzothiazole[21] as well as visible-light-switchable hemithioindigos;[22–26] Figure 1a) have highlighted their robustness to glutathione (GSH)[27] as well as their tolerance of tautomerisable polar functional groups (e.g. *para*-hydroxy groups) that are important for ligand–target interactions. These features make C=C-based photoswitches attractive for further research, particularly compared to azobenzenes, which are known to suffer GSH lability, and where tautomerisable functional groups counteract their photoisomer patterning.[28,29]

Newhouse and Zweig recently developed the C=C-based photoswitch pyrrole hemithioindigo (PHT, Figure 1a), which has an outstanding FDR_{max} of ca. 40 in organic media, due to band separation between the groundstate *Z* and metastable *E* isomers, driven by the *E* isomer's intramolecular pyrrole NH···O=C carbonyl hydrogen bond.[27,30] While the photostability and GSH resistance of PHT encourage biological use, their report described insolubility and poor/zero photoswitching in increasingly aqueous media.[27] However, we previously observed that polymethoxylated derivatives of otherwise low-solubility scaffolds can be photoswitched repeatedly in situ in cells, to photopattern bioactivity with performance recalling that seen in apolar media.[31] We attributed this to cellular sequestration of the hydrophobic photoswitches primarily in water-excluded/lipid environments that do allow photoswitching, giving comparatively slow cell-averaged rates of spontaneous *E*-to-*Z* relaxation, yet with rapid exchange from the aprotic environment supplying the photopatterned isomer ratio to the cytosol.[31] We therefore reasoned that a sufficiently soluble pyrrole hemithioindigo photopharmaceutical might apply a cellular FDR approaching this high FDR_{max}, as its photostationary state equilibria (PSSs) could reflect those of apolar media.

This we determined to test experimentally, evaluating the PHT scaffold in the biological context through proof-of-concept applications photocontrolling the dynamics of the MT cytoskeleton. This led us to design **PHTub**s, PHT-based photopharmaceuticals intended to isomer-dependently bind tubulin at the colchicine site, for cellular use as photoswitchable antimitotics and cytoskeleton inhibitors aiming at high-FDR and high-spatiotemporal-resolution photocontrol of cell cycle, cell viability, and cellular MT dynamics.

Results

Design and Synthesis

We designed **PHTub**s as PHT-based close steric analogues of the MT inhibitor colchicine. The colchicine pharmacophore consists of two aryl blades: a "southern" di- or tri-methoxyaryl ring, fixed close to a "northern" ring projecting a methoxy or ethyl spacefilling group (Figure 1b).[32] We chose the thioindoxyl to replace the southern ring to permit flexible substitution, leaving the pyrrole ring to bear the single ethyl group. We created nine **PHTub**s to scan orientations of the di/trimethoxy and ethyl substituents seeking both potency and isomer-dependency of bioactivity.

Of these, we expected that the 3′-ethyl **PHTub-3/6/9** would not bind tubulin with high affinity in either isomer due to the misoriented projection of the ethyl group (Figure 1b). We therefore expected **PHTub-3/6/9** would serve as useful regioisomeric controls, mismatching the SAR understood for the desired biological target. We and others[33] use regioisomeric controls to test for nonspecific bioactivity: both the classic effects of pan-assay interference compounds (PAINS) that must be anticipated for hydrophobic photoswitches (e.g., promiscuous binding, aggregation on proteins, or membrane disruption);[34] as well as nonspecific scaffold toxicity or phototoxicity under illumination.[22] By excluding such activity, regioisomeric controls can support that other compounds designed to match the target SAR act isomer-dependently and target-specifically (see Supporting Note 1). We also synthesised an N-methylated control **PHTub-NMe** that we expected to be inactive due to a steric clash (of the N-methyl group with the binding pocket wall),[21] but we were interested to study the effects of suppressing the NH···O=C hydrogen bond upon its photochemistry and, potentially, bioactivity (Figure 1c).

These **PHTub**s were synthesised in four to eight steps, assembling the PHT cores by piperidine-catalysed aldol condensation of ethylpyrrole-2-carbaldehydes onto methoxylated thioindoxyls (Figure 1d, Scheme S2, see Supporting Information).

Photoswitching

The **PHTub**s could be photoswitched in dry or in 25% aqueous polar media, under air, over multiple cycles without degradation (Figure 2a, Figure S2–S5). We would expect these lipophilic **PHTub**s to concentrate in water-excluded environments in cells, and so to display good cellular photoswitchability at 430–450 nm (giving ca. 90% *E*) vs. 515–530 nm (giving ca. 95% *Z*; Figure 2b, Figure S8, Table S4). By low photoresponse to > 550 nm we also expected that they could permit orthogonal imaging in the red fluorescent protein (RFP) channel at 561 nm.

Matching expectations from Newhouse and Zweig,[27] the band separation of PHT isomers (and thus the FDR_{max}) depended on the solvent's capacity to interrupt the internal H-bond, with ca. 45 nm separation in aprotic dry MeCN (FDR_{max} ca. 20-fold at 440/525 nm for all compounds)

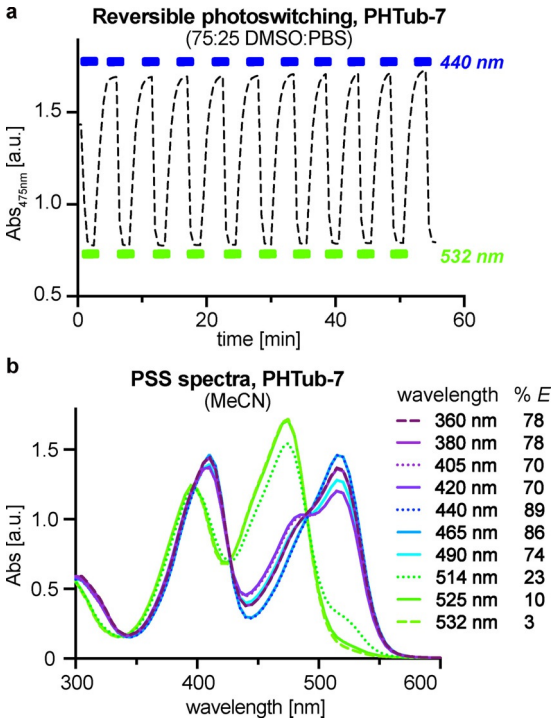

Figure 2. Photoswitching: a) **PHTub-7** is robustly and reversibly photoswitched from a majority-*Z* to a majority-*E* photostationary state (PSS) at 440 nm, and back to majority-*Z* with 532 nm. b) **PHTub-7** PSS absorbance spectra (UV/Vis spectroscopy) and composition (HPLC analysis) when illuminated with biocompatible wavelengths.

decreasing to ca. 30 nm in 75:25 DMSO:PBS (FDR_{max} below 10-fold, Table S2). N-methylated **PHTub-NMe** had similar photoswitching as phenyl hemithioindigo in both apolar solvents and DMSO:PBS, highlighting the role of the NH···O=C hydrogen bond in reaching high FDR. While the 3′/4′-ethylated PHTs had all-*Z* dark-adapted states, 5′-ethylated **PHTub-3/6/9** seemed to have nonzero *E* isomer proportion in the dark-adapted state (Figure S5 and discussion in the Supporting Information). Typical *E*-to-*Z* relaxation half-lives were in the hours to minutes range, being fastest in hydrogen-bond-disrupting polar solvents (Figure S6,7). **PHTub**s withstood challenge by 10 mM GSH over hours, and during repeated cycles of *Z*–*E* isomerization and thermal relaxation (Figure S9). This contrasts favourably to similarly polymethoxylated *Z*-azobenzenes that are destroyed by thiols.[21]

We therefore began exploring the applicability of PHT as an in situ-photoswitchable scaffold for cell biology through the use of **PHTub**s as photoswitchable MT inhibitors.

Structure-and-Photoisomer-Activity Relationship

Microtubule inhibition blocks cell proliferation, ultimately inducing cell death.[35] Therefore, we initially assessed the cellular bioactivity of the **PHTub**s by assaying their antiproliferative activity, in 44 hour assays in both HeLa cervical cancer and Jurkat T-cell leukaemia cell lines, under regularly pulsed illuminations designed to test both *E* and *Z* PHT isomers (Table 1).[3]

Table 1: IC_{50} values of all **PHTub**s in HeLa and Jurkat cell lines as *majority-*Z* and *majority-*E* isomer mixtures.[a]

	IC_{50} HeLa [μM]		IC_{50} Jurkat [μM]	
compound	*Z*-PHTub*	*E*-PHTub*	*Z*-PHTub*	*E*-PHTub*
PHTub-1	> 30 (n.sol.)	1.8	10	2
PHTub-2	0.2	0.4	0.1	0.3
PHTub-3	13	3.2	9	3.5
PHTub-4	> 100	ca. 9	4	ca. 20
PHTub-5	> 100	11	> 100	3
PHTub-6	> 20 (n.sol.)	ca. 20 (n.sol.)	> 20 (n.sol.)	> 20 (n.sol.)
PHTub-7	> 50 (n.sol.)	4.5	> 50 (n.sol.)	3.5
PHTub-8	0.07	0.12	0.03	0.05
PHTub-9	6.3	5.5	4.5	4.3
PHTub-NMe	> 20 (n.sol.)	ca. 20 (n.sol.)	> 20 (n.sol.)	ca. 20 (n.sol.)

[a] *Majority-*Z* by illumination at 525–535 nm or by dark conditions; *majority-*E* by illumination at 435–450 nm; 44 h incubation; illuminations pulsed at 75 ms per 15 s with $< 3\ mW cm^{-2}$; three independent experiments; n.sol. indicates apparent bioactivity near the solubility limit, which we attribute to aggregation; see Supporting Information for details.

PHTub-4/5/6 gave low-potency effects that match expectations for weak, nonspecific toxicity of low-solubility compounds near their aggregation threshold. We interpret this as a lack of tubulin binding, due to a steric clash of their south ring's outer methoxy group with the T7 loop of the colchicine site.[20,22] Yet, as both di- and tri-methoxyaryl rings can be tolerated in the southern binding lobe,[32] we expected that deleting the outer methoxy (**PHTub-1/2/3**) or shifting it around the ring (**PHTub-7/8/9**) could permit cytotoxicity, and both were confirmed. In these series, the position of the northern ethyl group was the major determinant of both isomers' bioactivity, which corresponded between the sets (e.g. **PHTub-1** corresponding to **PHTub-7**).

4′-Ethyl **PHTub-2/8** achieved excellent potency: superior to all photoswitchable tubulin binders yet reported[3,21,31] and near to colchicine site binders used as drugs (**PHTub-8** $IC_{50}s \leq$ 120 nM, colchicine ca. 20 nM), although their bioactivity was only slightly photoswitchable (*Z*-**PHTub2/8** ca. 2× as potent as the *E* isomers).

Shifting to a 5′-ethyl group in **PHTub-1/7** sacrificed potency, but greatly improved the photoswitchability of bioactivity: a necessary compromise for effective photopharmaceuticals. *E*-**PHTub-1** had good potency (mostly-*E*-**PHTub-1** IC_{50} ca. 2 μM in Jurkat and HeLa), while *Z*-**PHTub-1** gave only weak irreproducible bioactivity above 10 μM, which we attributed to its aggregation rather than to tubulin binding. We have observed elsewhere that the out-of-plane middle methoxy group of a 3,4,5-trimethoxyphenyl motif brings significant solubility benefits compared to dimethoxyphenyl, which can suppress aggregation effects and so increase the photoswitchability of bioactivity.[3] We were delighted to see this in **PHTub-7**, which retained similarly good potency under blue illumination (mostly-*E*-**PHTub-7** IC_{50} ca. 3–5 μM in Jurkat and HeLa), yet gave no visible effects as the *Z* isomer at even 10–17-fold higher concentrations (< 10% antiproliferative effect up to 50 μM; Figure 3a,b).

Shifting instead to a 3′-ethyl group showed that **PHTub-1/7** are at a local optimum for the photoswitchability of bioactivity. **PHTub-3** was active (*E*-$IC_{50} = 3$ μM) but had only

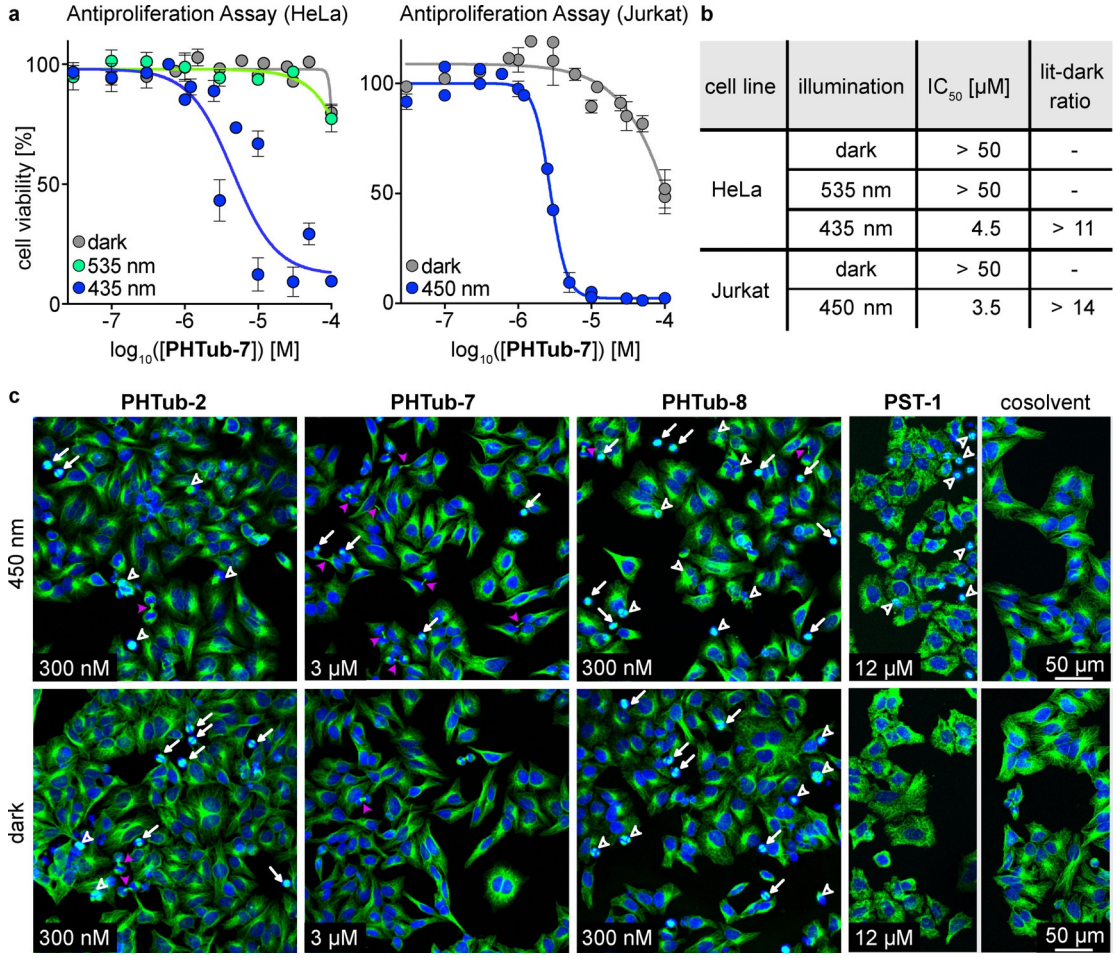

cell line	illumination	IC_{50} [µM]	lit-dark ratio
HeLa	dark	> 50	-
	535 nm	> 50	-
	435 nm	4.5	> 11
Jurkat	dark	> 50	-
	450 nm	3.5	> 14

Figure 3. **PHTub** bioactivity is light-specific and tubulin-mediated. a,b) **PHTub-7** gave strong light-specific antiproliferative effects with wavelength-dependency aligning to cell-free PSS measurements (HeLa and Jurkat cells; where for comparison, **PST-1** IC_{50}s: HeLa 1 µM (435 nm), 40 µM (dark); Jurkat 80 nM (435 nm), 20 µM (dark)). c) Immunofluorescence imaging of microtubule network architecture in HeLa cells treated with **PHTub-2**/**7**/**8** or cosolvent only, under pulsed 450 nm illumination or dark conditions. White arrows indicate mitotic arrests, hollow white arrowheads indicate multipolar spindles and other mitotic failures, filled pink arrowheads indicate remnant cytokinetic bridges (12 h incubation; α-tubulin in green, DNA stained with DAPI in blue).

mediocre photoswitchability of bioactivity (3-fold), while **PHTub-9** was similarly and not strongly active as both isomers. **PHTub-NMe**, whose *N*-methyl group similarly acts a spacefilling group adjacent to the double bond, was fully inactive as both isomers (Table 1).

Taken together, the ordered structure–activity relationships of the **PHTub**s (trimethoxy orientation and spacefill location) are consistent with those expected for colchicine site binders.[32] The demonstration of weakly potent light-independent regioisomer controls, for example, **PHTub-6**/**9**, and highly-potent but nearly-light-independently active **PHTub-2**/**8**, argues that phototoxicity or other nonspecific toxicities are not relevant for the **PHTub**s or the PHT scaffold. Due to its excellent photoswitchability of bioactivity, we proceeded into further biological testing with **PHTub-7** as our lead PHT photopharmaceutical. In parallel, we used **PHTub-2**/**8** interchangeably as low-photoswitchability but highly bioactive controls likely to share *E*-**PHTub-7**'s mechanism of action.

Tubulin-Specific Mechanism of Action in Cells

To test the tubulin-specificity of their light-dependent cytotoxicity, we first imaged the endogenous microtubule (MT) network architecture in cells incubated with **PHTub**s, to observe direct effects on their desired target protein. The nanomolar-potent **PHTub-2**/**8** caused a high proportion of mitotic arrests (arrows) and multipolar spindles or other mitotic failures (hollow arrowheads) under both illumination conditions (Figure 3c), reflecting expectations from their cytotoxicity assays. **PHTub-7** was less potent in its effects, matching the cytotoxicity results: but the 450 nm-specific accumulation of mitotic arrests and of abnormal remnant cytokinetic bridges (filled arrowheads)—a hallmark of perturbed mitosis[36]—was notable, whereas this was almost not seen in dark conditions (Figure 3c). Cell-free assays testing inhibition of the polymerisation of purified tubulin protein supported a direct tubulin-binding mechanism of action for the **PHTub**s, with **PHTub-7** and **PHTub-8** displaying comparable potency as the reference colchicine site inhibitors,

nocodazole and colchicine, yet with isomer-dependent bioactivity matching, respectively the lit-activity and dark-activity of the cellular assays (Figure S10). We concluded that **PHTub**s were supported as cellularly active inhibitors binding tubulin.

To crosscheck if the major cellular bioactivity mechanism of the **PHTub**s is MT inhibition, we examined their induction of light-dependent G_2/M-phase cell cycle arrest at their antiproliferative concentrations, which is a hallmark of microtubule inhibitors.[32] Using flow cytometric analysis we observed, as expected, induction of G_2/M arrest for *E*-**PHTub-7** but not for *Z*-**PHTub-7** (Figure 4), while **PHTub-2** gave potent but nearly light-independent cell cycle arrest (Figure S12). This further supports that *E*-**PHTub-7** potently inhibits MT function while *Z*-**PHTub-7** does not, suiting it to photoswitching-based control of MT-dependent processes.

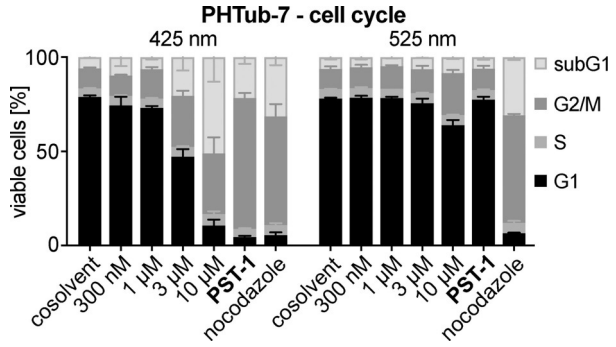

Figure 4. Cell cycle photocontrol. Cells treated with **PHTub-7** under 425 nm pulsing show significant G2/M arrest and cell death (sub-G1 phase cells), similar to that seen with reference MT inhibitor **PST-1** (12 µM) and light-independently with nocodazole (300 nM); but **PHTub-7** has no effects under 525 nm pulsing (compare to DMSO cosolvent-only controls).

Live Cell Photocontrol of Microtubule Dynamics by In Situ PHTub Photoswitching

We next tested the suitability of **PHTub**s (and by extension, the PHT scaffold) for spatially and temporally precise live cell photoswitching uses in confocal microscopy. This is a significant advance for photopharmacology, since as far as we know, no hemithioindigo derivatives have yet been demonstrated in temporally resolved live cell studies with spatially resolved in situ photoswitching. To do so, we imaged microtubule dynamics in HeLa cells transfected with fluorescently labelled end binding proteins (EBs). EBs mark the GTP cap regions of polymerising MTs. Thus, imaging EBs reveals the plus ends of polymerising MTs as dynamic comets;[37] and imaging during photoswitching is a spatiotemporally resolved readout for isomerisation-dependent inhibition of MT dynamics by photoswitchable inhibitors.[3,38]

We first confirmed that *Z*-**PHTub-7** (dark state) has no significant residual effects on MT dynamics by imaging tdTomato-EB3 at 561 nm; *Z*-**PHTub-7** caused no significant change of MT dynamics compared to DMSO controls (Figure 5).

Next, we applied 442 nm laser pulses to photoisomerise **PHTub-7** in situ to the *E* isomer throughout the field of view. This drastically suppressed cellular MT dynamics with high temporal precision (Figure 5a,b). MT dynamics did not recover over minutes; in light of further experiments, we believe this indicates that *E*-**PHTub-7** does not rapidly diffuse out of cells because it is lipophilic (intracellular "sinks";[39] see below).

442 nm is nearly an ideal photoactivation wavelength for PHTs (Table S4), but it is not a very common laser line on the confocal microscopes where MT research is performed. However, GFP-exciting lasers (typically 487, 488, or 491 nm) are standard on all confocal microscopes. We therefore tested whether GFP lasers are suitable for cellular photoactivation of **PHTub-7**. Indeed, 487 nm illumination also caused reproducible inhibition of MT dynamics (Figure 5c,d; Movie S1), although with slower response than 442 nm. These useful results show that PHT-based photopharmaceuticals can be photoisomerised using standard blue or cyan confocal microscope lasers, that have low potential for phototoxicity in cell research (see also Supporting Note 2). This contrasts favourably to most photocages and to most other photopharmaceuticals that require UV (355 nm laser) or near-UV (405 nm laser) photoactivations.

To crosscheck the mechanism of action of **PHTub-7**, we also imaged its potent congener **PHTub-8**, which had appeared more active as its dark (*Z*) isomer than in its lit state. Encouragingly, we observed both that *Z*-**PHTub-8** suppresses MT dynamics and that in situ 442 or 487 nm illumination caused drastic acceleration of MT polymerisation for a short while. Photoaccelerations could typically be performed at least three times before their magnitude became less impressive (Figure 5e,f; Movie S3; see Discussion). These results match the dark-activity of its cytotoxicity and immunofluorescence assays, so supporting that both **PHTub7/8** directly and photoswitchably inhibit tubulin.

Lastly, we performed cell-precise photoisomerisations of **PHTub-7** in single selected cells, hoping to temporally precisely block MT dynamics in those cells, without affecting their neighbour cells. In cells targeted with 442 nm laser regions (ROIs), EB3 comet counts dropped even below what had been seen with full field of view photoactivations, and did not recover over minutes, while neighbour cells remained unaffected as in non-treated and non-illuminated cosolvent controls (Figure 5g,h; Movie S4). By excluding bulk photoisomerisation in the medium, this supports the idea of intracellular sinks[39] of slowly diffusing **PHTub** being responsible for cell-persistent effects. (It also contrasts to diffusional recovery (approx. 30 s) observed for other scaffolds, such as the styrylbenzothiazole *Z*-**SBTub3**[21]).

Thus, **PHTub-7** can inhibit MT dynamics of target cells with temporal precision on the scale of seconds and spatial precision on the single-cell level. Taken together, these experiments also demonstrate that the PHT scaffold may more generally be uniquely suited for in situ photoswitching use in live cells with standard confocal microscope lasers, as part of both dark- or lit-active photopharmaceuticals, also against other protein targets.

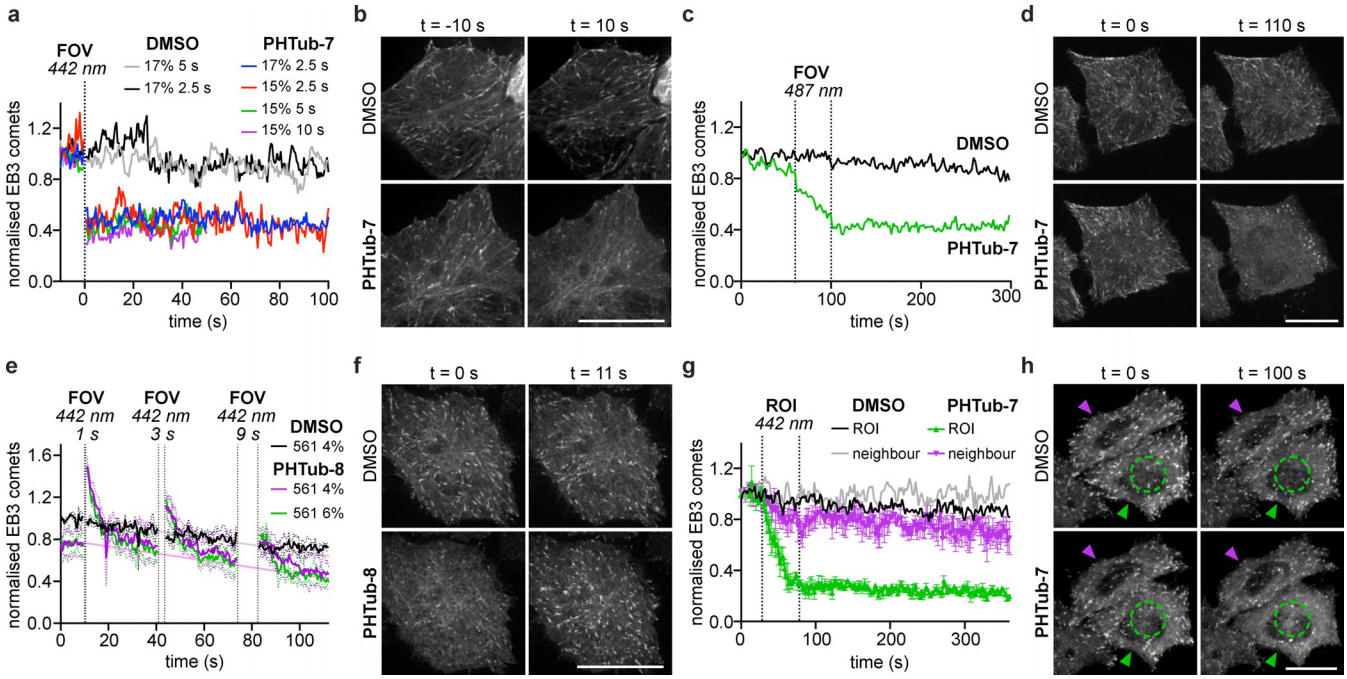

Figure 5. **PHTub**s enable in situ photoswitching of MT dynamics in live cells. a–d) MT dynamics are temporally precisely suppressed when cells treated with lit-active ***Z*-PHTub-7** (2 μM) are illuminated within the field of view (FOV) at a,b) 442 nm or at c,d) 487 nm (related to Movie S1). e,f) Cells treated with dark-active ***Z*-PHTub-8** (0.5 μM) have suppressed MT dynamics, which can be repeatedly accelerated by illuminations at 442 nm (related to Movie S3). Photobleaching background rate fits (grey: DMSO, pink: treated) are guides to the eye to distinguish accelerations. g,h) Cell-precise MT dynamics suppression is caused by 442 nm photoactivation of ***Z*-PHTub-7** (2 μM) within a subcellular region of interest (shown by green circle) in a target "ROI" cell (green arrowhead), while adjacent "neighbour" cells without photoactivation (pink arrowhead) do not show altered MT dynamics (related to Movie S4; EB3-tdTomato-transfected HeLa cells; tdTomato imaged at 561 nm; normalised EB3 "comet" counts quantify dynamic MTs; b/d/f/h: scale bars indicate 20 μm; for full caption and details see Supporting Information).

Discussion

Photopharmacological approaches to high-spatiotemporal-precision manipulation of endogenous proteins have progressed significantly, enabling biological application to membranes, ion channels, and the cytoskeleton.[1,9,40] Photopharmaceuticals for the cytoskeleton have transitioned rapidly beyond their cellular proofs of concept showing non-invasive, reversible, cellularly resolved optical control over MT dynamics and network structure.[41] For example, despite the relatively poor functional dynamic range of the azobenzene **PST**s (3-fold at 405/514 nm), they have found high-precision uses in embryonic fruit fly *D. melanogaster*,[42] worm *C. elegans*,[3] zebrafish *D. rerio*,[43] and mouse *M. musculus*,[44] where they have helped to resolve questions in development and in neuroscience.[45,46] Such uses illustrate the power of photopharmacology to enable previously inaccessible studies of spatiotemporally complex processes.

However, the scope of photopharmacology remains restricted by the photochemical and biochemical limitations of its photoswitch scaffold repertoire.[47] Several limitations of the major scaffold azobenzene, including the diazene's susceptibility to thiol-mediated degradation and its restricted scope of substituents compatible with bistable photoswitch performance, are well-known.[21] Non-azobenzene photoswitches that avoid these drawbacks, such as dithienylethenes, hemithioindigos, and heterostilbenes, have only recently begun to be used in bioactive pharmacophores validated in cellular studies;[21,22,48] and the development of new photoswitch scaffolds is a valuable research goal in general.[49] Yet, while some recently developed scaffolds have approached near-quantitative bidirectional photoswitching in physiological media,[50] there is still no clear choice of scaffold that can robustly ensure this performance in cells using the light sources that are actually available in biological research.

Here we show that PHT may be a general photopharmaceutical alternative to azobenzenes, offering comparable size and chemical simplicity, but better GSH resistance, more cell-compatible photoisomerisation wavelengths, and a better match of its optimum photoisomerisation wavelengths to those available on all confocal microscopes.

We had particularly sought to develop a photopharmaceutical with a high functional dynamic range (FDR). Towards this end, we hoped that with the **PHTub**s' hydrophobicity favouring biolocalisation in water-excluded environments, their cellular photoswitching could approach the excellent PSSs that PHT shows in organic media.[27] This is not yet generally recognised as a design opportunity for photopharmacology, but we believe it is an important one. Tuning photochemistry dependent on cellular/local environment has long been exploited in fluorescence microscopy[51] and its applications are advancing rapidly;[52] and environment-dependency has been observed experimentally for photoswitches (e.g. hypsochromic shifts of optimum *E*-to-*Z* isomer-

isation wavelength in membranes;[53] 60 nm bathochromic shifts upon protein binding[54]). The photoswitchability of bioactivity observed with **PHTub-7** in this work suggests that PHT's favourable organic-media photochemistry can indeed be harnessed for cellular applications. This suggests new design opportunities for photopharmaceuticals to bring high functional dynamic range photoswitching to bear in biology.

Additionally, through **PHTub-8**, we have given the first demonstration of time-resolved live cell photocontrol of a dark-active cytoskeleton photopharmaceutical. Though its reversibility was limited, this achievement is conceptually significant: because reversible dark-active photocontrol over biological processes using stoichiometric inhibitors is more challenging to achieve than with highly nonlinearly acting modulators (as have been used to control, for example, excitable cell firing[55]). Reversible stoichiometric control requires (i) high in situ photoconversion to the less bioactive metastable isomer (i.e. high practical FDR), which is typically problematic for photoswitch scaffolds (other than PHTs); and (ii) high isomer specificity of bioactivity, which is typically problematic for their bioactive derivatives (other than some colchicinoids). Although *E*-**PHTub-8** had significant residual bioactivity, its high FDR—achieved by matching the PHT scaffold's peak isomerisation efficiency to the GFP laser—was crucial for its success in achieving photoaccelerations. We also believe that enhanced dark-active compounds based on **PHTub-8** can be useful tools for localised induction of MT polymerisation in biology, which remains a high-value goal of reagent development.[40,56]

It was interesting that **PHTub-8** appeared somewhat reversible while **PHTub-7** did not (Figure 5e,g). We discount three suggestions for reversibility that are usually significant for photopharmacology (diffusion into/out of cells; spontaneous *E*-to-*Z* relaxation; and *E*-to-*Z* photoreversion of **PHTub8** by 561 nm imaging) due to the results of control experiments (see Supporting Note 3). We propose instead that **PHTub-8** reversibility arises since upon each 442/487 nm photoisomerisation, partial *E*-**PHTub-8** unbinding from tubulin monomers "injects" tubulin into the polymerisable pool, so polymerisation rate and comet count transiently increase. This excess is then "used up" by addition to MT polymer; and over ca. 10 s the cell returns to steady state MT dynamics. Thus at each subsequent 442/487 nm photoisomerisation pulse, there is less tubulin monomer that can be injected, and rate enhancements become smaller. These considerations can have general interest for photopharmacology.

Conclusion

In this work we have applied the pyrrole hemithioindigo (PHT) photoswitch scaffold to develop a rationally designed series of photopharmaceutical reagents for in situ-photoswitching-based optical control over the cellular microtubule (MT) cytoskeleton: a critical biological target in urgent need of reagents enabling high-resolution modulation assays.[41] The choice of the PHT scaffold was driven by its superior photoswitching performance at microscopy laser lines. We have demonstrated these **PHTub** reagents' capacity to apply optical control over MT network integrity, cell division, and cell death in long-term assays. In short-term assays, they achieve temporally resolved, cell-specific, optical modulation of MT dynamics in live cells. To our knowledge this is the first high-resolution live cell application of any hemithioindigo as a photopharmaceutical pharmacophore; and its success highlights both the **PHTub**s' and the PHT scaffold's promise for a range of high-spatiotemporal-precision biological studies. We therefore believe that **PHTub-7** in particular will be a valuable photopharmaceutical for high-precision cytoskeleton research, with promising applications in the fields of cellular transport, mechanostasis, migration, cell division, and embryonic development.

This research also suggests that the PHT scaffold too will find a broad range of applications to biological targets that are poorly addressed by current photopharmaceuticals. These targets may be located both cytosolically, as well as in water-excluded environments where the PHT scaffold may be even more advantageously applicable. Novel photoswitches that can be introduced into known photopharmaceutical designs to retain their on-target bioactivity while accessing new photochemical performance are rightly recognised as high-value targets in photopharmacology (e.g. spectrally shifted diazocines,[57,58] tetra-*ortho*-substituted azobenzenes,[15,59] and azoniums[60]). Therefore it is broadly significant that the similar molecular design of **PHTub-7** compared to its azobenzene analogues (**PST**s) ensured similar isomer-dependent bioactivity. Our work thus suggests that Zweig and Newhouse's pyrrole hemithioindigos[27] may be generally useful as a straightforward alternative to azobenzenes in photopharmacology, for powerful photopharmaceuticals with higher functional dynamic ranges under standard microscopy lasers, useful against a range of biological targets.

Acknowledgements

We are grateful to Henrietta Lacks, now deceased, and to her surviving family members for their contributions to biomedical research. We thank E. Fajardo-Ruiz (LMU) for tubulin polymerisation assays; D. Lonken (LMU) for early PHTub viability testing; and Marie Delattre (ENS Lyon, FR) and Wallis Nahaboo (University of Brussels, BE) for early development of cellular photoswitchability of hemithioindigos. We thank Peter Mayer (LMU) for X-ray data and Werner Spahl (LMU) for mass spectra. Deposition Number 2089743 contains the supplementary crystallographic data for this paper. These data are provided free of charge by the joint Cambridge Crystallographic Data Centre and Fachinformationszentrum Karlsruhe Access Structures service www.ccdc.cam.ac.uk/structures. J.T.-S. thanks the Joachim Herz foundation for grant support. O.T.-S. thanks the German Research Foundation (DFG: Emmy Noether grant number 400324123, SFB 1032 project B09 number 201269156, SFB TRR 152 project P24 number 239283807, SPP 1926 project XVIII number 426018126) and the Munich Centre for NanoScience initiative (CeNS) for funding. J.C.M.M. acknowledges sup-

port from an EMBO Long Term Fellowship. Open Access funding enabled and organized by Projekt DEAL.

Conflict of Interest

The authors declare no conflict of interest.

Keywords: cytotoxicity · hemithioindigo · microtubule dynamics · photopharmacology · photoswitch

[1] A. Rullo, A. Reiner, A. Reiter, D. Trauner, E. Y. Isacoff, G. A. Woolley, *Chem. Commun.* **2014**, *50*, 14613 – 14615.
[2] L. Agnetta, M. Kauk, M. C. A. Canizal, R. Messerer, U. Holzgrabe, C. Hoffmann, M. Decker, *Angew. Chem. Int. Ed.* **2017**, *56*, 7282 – 7287; *Angew. Chem.* **2017**, *129*, 7388 – 7393.
[3] M. Borowiak, W. Nahaboo, M. Reynders, K. Nekolla, P. Jalinot, J. Hasserodt, M. Rehberg, M. Delattre, S. Zahler, A. Vollmar, D. Trauner, O. Thorn-Seshold, *Cell* **2015**, *162*, 403 – 411.
[4] J. Joshi, M. Rubart, W. Zhu, *Front. Bioeng. Biotechnol.* **2020**, *7*, 466.
[5] R. Weinstain, T. Slanina, D. Kand, P. Klán, *Chem. Rev.* **2020**, *120*, 13135 – 13272.
[6] M. J. Fuchter, *J. Med. Chem.* **2020**, *63*, 11436 – 11447.
[7] P. Klán, T. Šolomek, C. G. Bochet, A. Blanc, R. Givens, M. Rubina, V. Popik, A. Kostikov, J. Wirz, *Chem. Rev.* **2013**, *113*, 119 – 191.
[8] K. Hüll, J. Morstein, D. Trauner, *Chem. Rev.* **2018**, *118*, 10710 – 10747.
[9] M. Borowiak, F. Küllmer, F. Gegenfurtner, S. Peil, V. Nasufovic, S. Zahler, O. Thorn-Seshold, D. Trauner, H.-D. Arndt, *J. Am. Chem. Soc.* **2020**, *142*, 9240 – 9249.
[10] B. T. Castle, D. J. Odde, *Cell* **2015**, *162*, 243 – 245.
[11] T. Wittmann, A. Dema, J. van Haren, *Curr. Opin. Cell Biol.* **2020**, *66*, 1 – 10.
[12] S. Florian, T. J. Mitchison in *The Mitotic Spindle: Methods and Protocols* (Eds.: P. Chang, R. Ohi), Springer New York, New York, **2016**, pp. 403 – 421.
[13] J. R. Peterson, T. J. Mitchison, *Chem. Biol.* **2002**, *9*, 1275 – 1285.
[14] M. J. Fuchter, *J. Med. Chem.* **2020**, *63*, 11436—11447.
[15] D. B. Konrad, G. Savasci, L. Allmendinger, D. Trauner, C. Ochsenfeld, A. M. Ali, *J. Am. Chem. Soc.* **2020**, *142*, 6538—6547.
[16] C. E. Weston, R. D. Richardson, P. R. Haycock, A. J. P. White, M. J. Fuchter, *J. Am. Chem. Soc.* **2014**, *136*, 11878 – 11881.
[17] A. J. Engdahl, E. A. Torres, S. E. Lock, T. B. Engdahl, P. S. Mertz, C. N. Streu, *Org. Lett.* **2015**, *17*, 4546 – 4549.
[18] J. E. Sheldon, M. M. Dcona, C. E. Lyons, J. C. Hackett, M. C. T. Hartman, *Org. Biomol. Chem.* **2016**, *14*, 40 – 49.
[19] S. K. Rastogi, Z. Zhao, S. L. Barrett, S. D. Shelton, M. Zafferani, H. E. Anderson, M. O. Blumenthal, L. R. Jones, L. Wang, X. Li, C. N. Streu, L. Du, W. J. Brittain, *Eur. J. Med. Chem.* **2018**, *143*, 1 – 7.
[20] R. Gaspari, A. E. Prota, K. Bargsten, A. Cavalli, M. O. Steinmetz, *Chem* **2017**, *2*, 102 – 113.
[21] L. Gao, J. C. M. Meiring, Y. Kraus, M. Wranik, T. Weinert, S. D. Pritzl, R. Bingham, E. Ntouliou, K. I. Jansen, N. Olieric, J. Standfuss, L. C. Kapitein, T. Lohmüller, J. Ahlfeld, A. Akhmanova, M. O. Steinmetz, O. Thorn-Seshold, *Cell Chem. Biol.* **2021**, *28*, 228 – 241.
[22] A. Sailer, F. Ermer, Y. Kraus, F. Lutter, C. Donau, M. Bremerich, J. Ahlfeld, O. Thorn-Seshold, *ChemBioChem* **2019**, *20*, 1305 – 1314.
[23] N. Regner, T. T. Herzog, K. Haiser, C. Hoppmann, M. Beyermann, J. Sauermann, M. Engelhard, T. Cordes, K. Rück-Braun, W. Zinth, *J. Phys. Chem. B* **2012**, *116*, 4181 – 4191.
[24] S. Kitzig, M. Thilemann, T. Cordes, K. Rück-Braun, *ChemPhysChem* **2016**, *17*, 1252 – 1263.
[25] F. Kink, M. P. Collado, S. Wiedbrauk, P. Mayer, H. Dube, *Chem. Eur. J.* **2017**, *23*, 6237 – 6243.
[26] K. Stallhofer, M. Nuber, F. Schüppel, S. Thumser, H. Iglev, R. de Vivie-Riedle, W. Zinth, H. Dube, *J. Phys. Chem. A* **2021**, *125*, 4390 – 4400.
[27] J. E. Zweig, T. R. Newhouse, *J. Am. Chem. Soc.* **2017**, *139*, 10956 – 10959.
[28] J. Gavin, J. F. M. Ruiz, K. Kedziora, H. Windle, D. P. Kelleher, J. F. Gilmer, *Bioorg. Med. Chem. Lett.* **2012**, *22*, 7647 – 7652.
[29] D. M. Nikolaev, M. S. Panov, A. A. Shtyrov, V. M. Boitsov, S. Yu. Vyazmin, O. B. Chakchir, I. P. Yakovlev, M. N. Ryazantsev in *Progress in Photon Science: Recent Advances* (Eds.: K. Yamanouchi, S. Tunik, V. Makarov), Springer International Publishing, Cham, **2019**, pp. 139 – 172.
[30] J. E. Zweig, T. A. Ko, J. Huang, T. R. Newhouse, *Tetrahedron* **2019**, *75*, 130466.
[31] A. Sailer, F. Ermer, Y. Kraus, R. Bingham, F. H. Lutter, J. Ahlfeld, O. Thorn-Seshold, *Beilstein J. Org. Chem.* **2020**, *16*, 125 – 134.
[32] G. C. Tron, T. Pirali, G. Sorba, F. Pagliai, S. Busacca, A. A. Genazzani, *J. Med. Chem.* **2006**, *49*, 3033 – 3044.
[33] J. Lee, M. Schapira, *ACS Chem. Biol.* **2021**, *16*, 579 – 585.
[34] J. B. Baell, J. W. M. Nissink, *ACS Chem. Biol.* **2018**, *13*, 36 – 44.
[35] M. A. Jordan, K. Wendell, S. Gardiner, W. B. Derry, H. Copp, L. Wilson, *Cancer Res.* **1996**, *56*, 816 – 825.
[36] G. Normand, R. W. King in *Polyploidization and Cancer* (Ed.: R. Y. C. Poon), Springer New York, New York, **2010**, pp. 27 – 55.
[37] J. Roostalu, C. Thomas, N. I. Cade, S. Kunzelmann, I. A. Taylor, T. Surrey, *eLife* **2020**, *9*, e51992.
[38] A. Müller-Deku, J. C. M. Meiring, K. Loy, Y. Kraus, C. Heise, R. Bingham, K. I. Jansen, X. Qu, F. Bartolini, L. C. Kapitein, A. Akhmanova, J. Ahlfeld, D. Trauner, O. Thorn-Seshold, *Nat. Commun.* **2020**, *11*, 4640.
[39] K. Scherer, R. Bisby, S. Botchway, J. Hadfield, A. Parker, *J. Biomed. Opt.* **2014**, *20*, 051004.
[40] S. D. Pritzl, P. Urban, A. Prasselsperger, D. B. Konrad, J. A. Frank, D. Trauner, T. Lohmüller, *Langmuir* **2020**, *36*, 13509—13515.
[41] O. Thorn-Seshold, J. Meiring, *ChemRxiv* **2021**, https://doi.org/10.26434/chemrxiv.14424176.v1.
[42] A. Singh, T. Saha, I. Begemann, A. Ricker, H. Nüsse, O. Thorn-Seshold, J. Klingauf, M. Galic, M. Matis, *Nat. Cell Biol.* **2018**, *20*, 1126 – 1133.
[43] C. Vandestadt, G. C. Vanwalleghem, H. A. Castillo, M. Li, K. Schulze, M. Khabooshan, E. Don, M.-L. Anko, E. K. Scott, J. Kaslin, *bioRxiv* **2019**, 539940.
[44] J. Zenker, M. D. White, R. M. Templin, R. G. Parton, O. Thorn-Seshold, S. Bissiere, N. Plachta, *Science* **2017**, *357*, 925 – 928.
[45] J. Zenker, M. D. White, M. Gasnier, Y. D. Alvarez, H. Y. G. Lim, S. Bissiere, M. Biro, N. Plachta, *Cell* **2018**, *173*, 776 – 791.
[46] K. Eguchi, Z. Taoufiq, O. Thorn-Seshold, D. Trauner, M. Hasegawa, T. Takahashi, *J. Neurosci.* **2017**, *37*, 6043 – 6052.
[47] V. A. Gutzeit, A. Acosta-Ruiz, H. Munguba, S. Häfner, A. Landra-Willm, B. Mathes, J. Mony, D. Yarotski, K. Börjesson, C. Liston, G. Sandoz, J. Levitz, J. Broichhagen, *Cell Chem. Biol.* **2021**, https://doi.org/10.1016/j.chembiol.2021.02.020.
[48] N. A. Simeth, A. C. Kneuttinger, R. Sterner, B. König, *Chem. Sci.* **2017**, *8*, 6474 – 6483.
[49] M. W. H. Hoorens, M. Medved", A. D. Laurent, M. Di Donato, S. Fanetti, L. Slappendel, M. Hilbers, B. L. Feringa, W. Jan Buma, W. Szymanski, *Nat. Commun.* **2019**, *10*, 2390.
[50] M. P. O'Hagan, J. Ramos-Soriano, S. Haldar, S. Sheikh, J. C. Morales, A. J. Mulholland, M. C. Galan, *Chem. Commun.* **2020**, *56*, 5186 – 5189.

[51] J. Kapuscinski, *Biotechnic & Histochemistry* **1995**, *70*, 220 – 233; Histochemistry **1995**, 70, 220 – 233.
[52] L. Wang, J. Hiblot, C. Popp, L. Xue, K. Johnsson, *Angew. Chem. Int. Ed.* **2020**, *59*, 21880 – 21884; *Angew. Chem.* **2020**, *132*, 22064 – 22068.
[53] P. Urban, S. D. Pritzl, D. B. Konrad, J. A. Frank, C. Pernpeintner, C. R. Roeske, D. Trauner, T. Lohmüller, *Langmuir* **2018**, *34*, 13368 – 13374.
[54] D. M. Barber, S.-A. Liu, K. Gottschling, M. Sumser, M. Hollmann, D. Trauner, *Chem. Sci.* **2017**, *8*, 611 – 615.
[55] P. Stawski, M. Sumser, D. Trauner, *Angew. Chem. Int. Ed.* **2012**, *51*, 5748 – 5751; *Angew. Chem.* **2012**, *124*, 5847 – 5850.
[56] K. B. Buck, J. Q. Zheng, *J. Neurosci.* **2002**, *22*, 9358 – 9367.
[57] M. S. Maier, K. Hüll, M. Reynders, B. S. Matsuura, P. Leippe, T. Ko, L. Schäffer, D. Trauner, *J. Am. Chem. Soc.* **2019**, *141*, 17295 – 17304.
[58] R. Siewertsen, H. Neumann, B. Buchheim-Stehn, R. Herges, C. Näther, F. Renth, F. Temps, *J. Am. Chem. Soc.* **2009**, *131*, 15594 – 15595.
[59] D. Bléger, J. Schwarz, A. M. Brouwer, S. Hecht, *J. Am. Chem. Soc.* **2012**, *134*, 20597 – 20600.
[60] S. Samanta, A. Babalhavaeji, M. Dong, G. A. Woolley, *Angew. Chem. Int. Ed.* **2013**, *52*, 14127 – 14130; *Angew. Chem.* **2013**, *125*, 14377 – 14380.

Manuscript received: April 7, 2021
Revised manuscript received: July 23, 2021
Accepted manuscript online: August 30, 2021
Version of record online: October 1, 2021

Angewandte Chemie
Eine Zeitschrift der Gesellschaft Deutscher Chemiker

Supporting Information

Pyrrole Hemithioindigo Antimitotics with Near-Quantitative Bidirectional Photoswitching that Photocontrol Cellular Microtubule Dynamics with Single-Cell Precision**

*Alexander Sailer, Joyce C. M. Meiring, Constanze Heise, Linda N. Pettersson, Anna Akhmanova, Julia Thorn-Seshold, and Oliver Thorn-Seshold**

anie_202104794_sm_miscellaneous_information.pdf
anie_202104794_sm_Movie_S1.mp4
anie_202104794_sm_Movie_S2.mp4
anie_202104794_sm_Movie_S3.mp4
anie_202104794_sm_Movie_S4.mp4

Author Contributions

A.S. Conceptualization: Supporting; Data curation: Lead; Investigation: Lead; Supervision: Supporting
J.M. Data curation: Equal; Investigation: Supporting; Writing—review & editing: Supporting
C.H. Investigation: Supporting
L.P. Investigation: Supporting
A.A. Funding acquisition: Supporting; Supervision: Supporting; Writing—review & editing: Supporting
J.T. Data curation: Supporting; Formal analysis: Supporting; Supervision: Supporting
O.T. Conceptualization: Lead; Funding acquisition: Lead; Methodology: Lead; Project administration: Lead; Resources: Lead; Supervision: Lead; Writing—original draft: Lead; Writing—review & editing: Lead.

***Supporting Information to*:**

Pyrrole hemithioindigo antimitotics with near-quantitative bidirectional photoswitching that photocontrol cellular microtubule dynamics with single-cell precision

Supporting Notes 1-3 ..... ***2***

Chemical Synthesis ***4***

Conventions **4**

General procedures **6**

Synthesis of precursors **7**

Synthesis of PHTubs **12**

X-ray crystallography data of PHTub-7 ..... **17**

Photochemical Characterisation ***18***

UV-Vis spectrophotometry of bulk samples **18**

PSS spectra of PHTubs **18**

PSS spectra in aqueous media **22**

Solvent effects on photoswitching **23**

General trends in thermal relaxation **23**

Thermal relaxation of PHTub-7 at 37 °C **24**

Absorption spectra of separated isomers and comparison to PSS spectra **25**

Determination of the PSS composition **26**

Stability of PHTub-7 against reduced glutathione (GSH) **26**

Photoproperties of PHTub-3/6/9 ..... **27**

Biological Applications ***28***

General cell culture **28**

Resazurin assays **28**

***In vitro* tubulin polymerisation** **29**

Cell cycle analysis **30**

Immunofluorescence imaging of microtubule network structure **31**

Live Cell Imaging **31**

Full caption to Figure 5 ..... **32**

Illumination-(in)dependency and off- and on-target bioactivity **33**

Supplemental References ***34***

HRMS spectra ***37***

NMR spectra ***47***

Supporting Notes 1-3

(1) Regioisomeric Controls: We expected that the 3'-ethyl **PHTub-3/6/9** would not bind tubulin efficiently as either isomer, due to the misoriented projection of the ethyl group (**Fig 1b**) into the binding lobe wall. We therefore expected **PHTub-3/6/9** would serve as useful *regioisomeric controls,* by intentionally mismatching to the SAR understood for our desired biological target. We and others[1] use regioisomeric controls to test for nonspecific bioactivity: both the classic effects of pan-assay interference compounds (PAINS) that must be anticipated for hydrophobic photoswitches (e.g., promiscuous binding, aggregation on proteins, or membrane disruption);[2] as well as nonspecific scaffold toxicity or phototoxicity under illumination.[3] Ideally, one or more close regioisomeric controls can be shown to have biological effects that are weak, and are independent of the applied isomer, and independent of the illumination protocol, and ideally to be inactive against the biological target of the study. Such observations can support that, for those other compounds designed to match SAR, illumination-dependent bioactivity *is* isomer-specific and does not involve nonspecific PAINS-like effects; when reinforced by other evidence, this can provide good support that designed-active compounds are also target-specific. (In lucky cases, such a regioisomeric control could be found that is biologically inactive against "all" targets, so providing still stronger evidence: although clearly this is *not* required in order for a designed-active compound to be active on their desired target).
The results arising from these regioisomeric controls are discussed throughout the main text as appropriate, with an extra section in the Supporting Information accompanying **Fig S13** ("**Illumination-(in)dependency and off- and on-target bioactivity**").

(2) Wavelength response of PHTubs: We had observed that **PHTub-7** appeared not to undergo *Z* to *E* isomerisation during 561 nm imaging (e.g. **Fig 5a** before 442 nm pulse), which matches expectations from the cell-free photoswitching study. Somewhat surprisingly we also found that cellular MT dynamics were unaffected by illuminations with the 405 nm laser, at least under a restriction of flux to avoid photobleaching (**PHTub-7/8**, **Movie S2**). These results suggest that the cell-free measurement in homogenous media (in DMSO/PBS, reversible PHT isomerisations with no observed losses, over all wavelengths from 360 to ca. 550 nm; c.f. **Fig 2b**) does not necessarily capture the photoswitching behaviour reflected in short- or long-term cellular experiments (good isomerisation to *E* at 440/490 nm, but no obvious effects at 405 nm at least in our trials).

(3) Photoreversibility? Though at first glance it might seem paradoxical that **PHTub-8** was temporally reversible while **PHTub-7** was not (**Fig 5e,g**), we believe this has a consistent explanation. We propose that this arises since upon 442/487 nm photoisomerisation, partial *E*-**PHTub-8** unbinding from tubulin monomers "injects" tubulin into the polymerisable pool, so polymerisation rate and comet count increase. This excess is then 'used up' by addition to MT polymer; and over ca. 10 s the cell returns to steady state dynamics. Thus at each subsequent 442/487 nm photoisomerisation pulse, there is less tubulin monomer that can be injected, and rate enhancements become smaller. We stated that typically three cycles could be performed where accelerations are obvious; but note that this limit is not only biological - it partially arises since accelerations must be distinguished against a continuous background

of comet decrease from marker photobleaching during imaging (pink fit in **Fig 5e**) as has also previously been described,[4] and this bleaching restricts the potential for imaging the system. We have discounted three alternative suggestions for reversibility that are usually significant for photopharmacology: (1) due to the results of e.g. **Fig 5g** we proposed that **PHTub**s do not rapidly diffuse out of cells; under equilibrated conditions we assume that diffusion into cells is also relatively slow; therefore we do not assign the fast reversibility only of **PHTub-8** to diffusion. (2) We believe that spontaneous relaxation is too slow to be involved ($t_{½}$ probably >> 15 min in primarily water-excluded environments), and see no reasons that it would be so rapid for **PHTub8** while being insignificant for **PHTub7**. (3) We excluded photoreversion of **PHTub8** by experiments where we increased imaging laser power but saw no rate change (**Fig 5e**; **Movie S3**). These considerations can have general interest for photopharmacology.

Chemical Synthesis

Conventions

Hemithioindigo geometry and nomenclature:

Hemithioindigos (HTIs) are drawn by default in their *Z*-isomeric form. However, this should be understood to imply either or both of the *E* & *Z* forms constituting a given sample depending on light exposure, therefore by default they are also named without *E*/*Z*-designations.

Abbreviations:

The following abbreviations are used: Ac_2O – acetic anhydride, calcd. – calculated, DCM – dichloromethane, DMF – dimethylformamide, DMSO – dimethyl sulfoxide, EA / EtOAc – ethyl acetate, EI – electron impact, ESI – electrospray ionisation, Et_2O – diethyl ether, Hx – distilled isohexanes, HRMS – high-resolution mass spectrometry, iPrOH – isopropanol, MeCN – acetonitrile, R_f – retention factor, THF – tetrahydrofuran, t_R – retention time, λ_{max} – wavelength corresponding to maximal absorption.

Automated Flash Chromatography:

Automated Flash Chromatography was performed on a Biotage Isolera One instrument using 254 nm as detection wavelength and eluting with mixtures of ethyl acetate and isohexanes.

Reagents and Conditions:

Unless stated otherwise: (1) all reactions and characterisations were performed with unpurified, undried, non-degassed solvents and reagents, used as obtained, under closed air atmosphere without special precautions. The use of dry solvents in this context is to be understood as using anhydrous solvents bought from Acros Organics which were stored and handled under an atmosphere of nitrogen; (2) “hexane” used for chromatography was distilled from commercial crude isohexane fraction on rotavap; (3) when not specified, “column” and “chromatography” refer to flash column chromatography performed on Merck silica gel Si-60 (40-63 µm); (4) procedures and yields are unoptimised; (5) yields refer to isolated chromatographically and spectroscopically pure materials (6) all eluent and solvent mixtures are given as volume ratios unless otherwise specified, thus “1:1 EA:Hx” indicates a 1:1 mixture (by volume) of ethyl acetate and hexanes.

Thin-layer chromatography (TLC):

TLC was run on 0.25 mm Merck silica gel plates (60, F-254). UV light (254 nm) was used as a visualising agent. R_f values were usually determined in ethyl acetate : hexane (EA:Hx) eluents. TLC characterisations are thus abbreviated as per R_f = 0.09 (EA:Hx, 6:1).

High-performance liquid chromatography coupled to mass spectrometry (LCMS):

Analytical high-performance liquid chromatography (HPLC) was performed on an Agilent 1100 SL coupled HPLC system with (a) a binary pump to deliver H2O:MeCN eluent mixtures containing 0.1% formic acid at a 0.4 mL/min flow rate, (b) Thermo Scientific Hypersil GOLDTM C18 column (1.9 µm; 3 × 50 mm) maintained at 25 °C, whereby the solvent front eluted at t_{ret} = 0.5 min, (c) an Agilent 1100 series diode array detector, (d) a Bruker HCT Ultra mass spectrometer. Typical run conditions were a linear gradient of H2O:MeCN eluent composition from 90:10 through to 1:99, applied during the separation phase (first 5 min), then 0:100 for 2 min for flushing; the column was (re)equilibrated with 90:10 eluent mixture for 2 min before each run. Thus, **LC-MS**: t_R (**Z isomer**) = 6.50 min, λ_{max} (**Z isomer**) = 408, 466 nm

indicates detection of the *Z* isomer eluting at 6.50 min and showing absorption maxima at 408 and 466 nm, respectively.

Nuclear magnetic resonance (NMR) spectroscopy:

Standard NMR characterisation was performed by 1D ^{1}H- and ^{13}C-NMR spectra with NOESYx as needed. Known compounds were checked against literature data. The default spectrometer used was a Bruker Ascend 400 (400 MHz & 100 MHz for ^{1}H and ^{13}C respectively); NMR solvents are given individually for each compound. Chemical shifts (δ) are reported in ppm calibrated to residual non-perdeuterated solvent as an internal reference.[5] The following peak descriptions are used: singlet (s), doublet (d), triplet (t), quartet (q), multiplet (m), broad (br.), pseudotriplet (~t).

High-resolution mass spectrometry (HRMS)

Electron impact (EI) ionisation was performed on a Thermo Q Exactive GC Orbitrap or Finnigan MAT 95 sector field mass spectrometer. The resolution was set to approximately 5000 (MAT95) or 50 000 (at m/z 200, Q Exactive GC). Depending on the used method, a span from 40 to 1040 u was detected. Ionisation was performed at 250 °C source temperature and 70 eV electron energy.

Electrospray ionisation (ESI) was performed on a Thermo Finnigan LTQ FT Ultra Fourier Transform Ion Cyclotron Resonance Spectrometer. The resolution was set to 100 000 at m/z 400. Depending on the used method, a span from 50 to 2000 u was detected. The current of the spray capillary at the IonMax ESI probe head was 4 kV, the temperature of the heating capillary 250 °C, N_2 flow of sheath gas 20 and the sweep gas flow 5 units.

X-ray crystallography

X-ray intensity data of **PHTub-7** were measured on a Bruker D8 Venture TXS system equipped with a multilayer mirror monochromator and a Mo Kα rotating anode X-ray tube (λ = 0.71073 Å). The frames were integrated with the Bruker SAINT software package.[6] Data were corrected for absorption effects using the Multi-Scan method (SADABS).[7] The structure was solved and refined using the Bruker SHELXTL Software Package.[8] All C-bound hydrogen atoms have been calculated in ideal geometry riding on their parent atoms, the N-bound one has been refined freely. The disorder of the ethyl moiety over three sites (site occupation factors 0.55, 0.33, 0.12) has been described by a split model. All split atoms have been refined isotropically. The C-C bonds have been restrained to be equal within a standard deviation of 0.01 Å. The SIMU restraint has been applied for split atoms. The figures have been drawn at the 50% ellipsoid probability level.[9] In the case of disorder the less-occupied parts have been neglected for the figures.

General procedures

NB: The literature-known thioindoxyls were accessed either by base treatment of 2-(methylthio)benzamides[10], or by intramolecular Friedel-Crafts acylation of the 2-(phenylthio)acetic acids[11] (which although convenient usually gave lower yields).

***General Procedure A (GP A)**: Reduction of acetyl pyrroles*

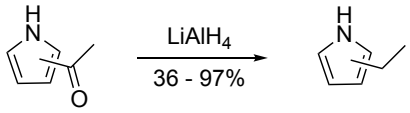

S1 / S6

Scheme S1: Reduction of acetyl pyrroles.

This procedure is a modified literature procedure.[12]

To a cold (0 °C) solution of the respective acetylpyrrole (1.0 eq.) in dry THF (0.68 – 1.15 M) was added $LiAlH_4$ (1 M in THF, 2.0 eq.) dropwise. After complete addition, the cooling bath was removed and the mixture was heated to reflux overnight. It was diluted with Et_2O and the reaction was quenched by the **careful** addition of water followed by an aqueous solution NaOH (2 M) and water. The mixture was stirred for 15 min, anhydrous Na_2SO_4 was added, the solids were filtered off, the filter cake was washed with DCM and the yellow filtrate was carefully evaporated (**product is volatile**). Purification can either be achieved by *vacuum* distillation or silica gel column chromatography with chromatography regularly giving higher yields of product with similar purity.

***General Procedure B (GP B)**: Formation of HTIs via piperidine catalysed aldol condensations*

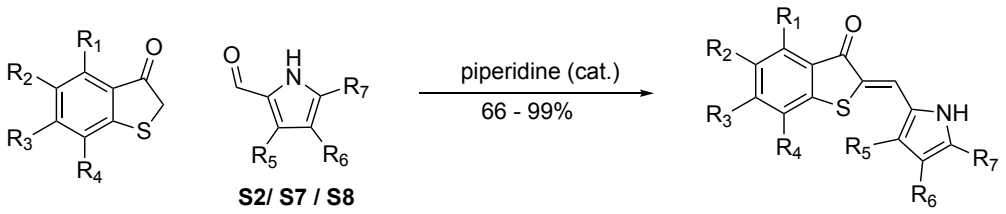

S2/ S7 / S8

$R_1 = R_4 = H$, $R_2 = R_3 = OMe$, $R_5 = R_6 = H$, $R_7 = Et$ **PHTub-1**
$R_1 = R_4 = H$, $R_2 = R_3 = OMe$, $R_5 = R_7 = H$, $R_6 = Et$ **PHTub-2**
$R_1 = R_4 = H$, $R_2 = R_3 = OMe$, $R_6 = R_7 = H$, $R_5 = Et$ **PHTub-3**
$R_1 = R_2 = R_3 = OMe$, $R_4 = H$, $R_5 = R_6 = H$, $R_7 = Et$ **PHTub-4**
$R_1 = R_2 = R_3 = OMe$, $R_4 = H$, $R_5 = R_7 = H$, $R_6 = Et$ **PHTub-5**
$R_1 = R_2 = R_3 = OMe$, $R_4 = H$, $R_6 = R_7 = H$, $R_5 = Et$ **PHTub-6**
$R_1 = H$, $R_2 = R_3 = R_4 = OMe$, $R_5 = R_6 = H$, $R_7 = Et$ **PHTub-7**
$R_1 = H$, $R_2 = R_3 = R_4 = OMe$, $R_5 = R_7 = H$, $R_6 = Et$ **PHTub-8**
$R_1 = H$, $R_2 = R_3 = R_4 = OMe$, $R_6 = R_7 = H$, $R_5 = Et$ **PHTub-9**

Scheme S2: Formation of HTIs via piperidine catalysed aldol condensations

This procedure is a modified literature procedure.[13]

To a concentrated solution (0.14 – 0.30 M) of the respective thioindoxyls (1.2 eq.) and aldehydes (1.0 eq.) in dry EtOH was added piperidine (catalytic amounts). The reaction mixture was stirred at room temperature under nitrogen (usually 15 – 18 h) after which time the volatiles were removed under reduced pressure. The crude products were dissolved in minimal volumes of DMSO and precipitated with water. After centrifugation (10 min, 15 000 rpm), the supernatant was pipetted off and the procedure was repeated. The residue was partitioned between DCM and water, the phases were separated and

the organic layer was thoroughly washed with water and brine, dried over Na_2SO_4 and evaporated yielding the **PHTubs** as orange, red, brown or black solids.

Synthesis of precursors

5-ethylpyrrole-2-carbaldehyde was obtained by reduction of 2-acetylpyrrole followed by Vilsmaier-Hack formylation (**Scheme S1**). 3- and 4-ethylpyrrole-2-carbaldehydes were prepared from 3-ethylpyrrole, whose formylation gave a separable mixture of 3- and 4-ethylpyrrole-2-carbaldehydes (**Scheme S3**).

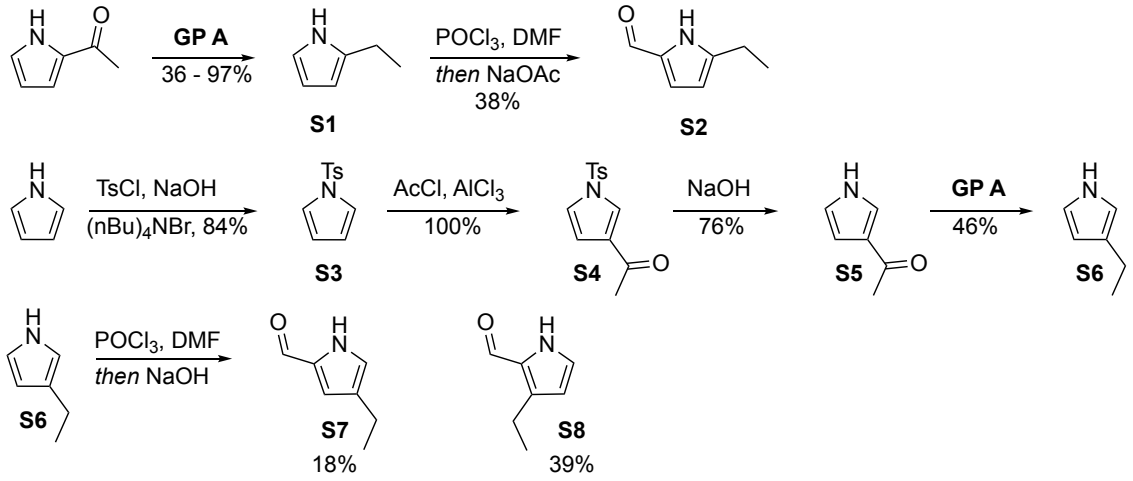

Scheme S3: Synthesis of precursors.

2-Ethyl-1*H*-pyrrole (S1)

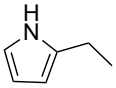

The compound was prepared from commercial 2-acetylpyrrole (1.00 g, 9.16 mmol, 1.0 eq.) and $LiAlH_4$ (1M in THF, 18.30 mL, 18.30 mmol, 2.0 eq.) in dry THF (8 mL) according to **GP A**. Purification can either be achieved by vacuum distillation (bp. 59 °C, 15 mbar, 36% yield) or silica gel column chromatography (Et_2O:Hx, 15:85, 97% yield).

The spectral data match literature.[14]

^{1}H-NMR ($CDCl_3$, 400 MHz):δ = 7.92 (br. s, 1H), 6.67 (q, *J* = 2.2 Hz, 1H), 6.13 (q, *J* = 2.8 Hz, 1H), 5.92 (~q, 1H), 2.63 (q, *J* = 7.6 Hz, 2H), 1.24 (t, *J* = 7.6 Hz, 3H); **^{13}C-NMR** ($CDCl_3$, 100 MHz): δ = 134.3, 116.2, 108.4, 104.3, 20.9, 13.7; **R_f** = 0.64 (Et_2O:Hx, 15:85); EI$^+$ **HRMS** for $C_6H_9N^+$ = $[M]^+$: calcd. m/z 95.0735, found m/z 95.0729, for $C_5H_6N^+$ = $[M\text{-}CH_3]^+$: calcd. m/z 80.0494, found m/z 80.0494.

5-Ethyl-1*H*-pyrrole-2-carbaldehyde (S2)

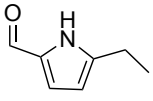

The compound was synthesised according to a modified literature procedure.[15]

An oven-dried Schlenk flask was charged with dry DCM (5 mL) and dry DMF (277 mg, 3.78 mmol, 0.29 mL, 1.2 eq.) cooled to 0 °C and $POCl_3$ (586 mg, 3.78 mmol, 0.36 mL, 1.2 eq.) was added dropwise. After complete addition, the mixture was allowed to reach room temperature and stirred for 15 min. The reaction mixture was cooled again to 0 °C and a solution of the pyrrole (300 mg, 3.15 mmol, 1.0 eq.) in

dry DCM (3 mL) was added dropwise. After complete addition, the reaction was heated to reflux for 2 h, cooled to room temperature, a solution of NaOAc (1.42 g, 17.30 mmol, 5.5 eq.) in water (8 mL) was added and it was again refluxed for 30 minutes. The mixture was diluted with DCM (10 mL), washed with water (10 mL), saturated Na_2CO_3 solution (2 x 10 mL) and brine (5 mL). The combined organic extracts were dried over Na_2SO_4 and evaporated. The oily red crude product was purified by flash chromatography (EA:Hx, 1:4) yielding the desired aldehyde as yellow oil that solidified after freezing and thawing (147 mg, 1.19 mmol, 38%).

The spectral data match literature.[15]

^{1}H-NMR ($CDCl_3$, 400 MHz): δ = 9.65 (br. s, 1H), 9.35 (s, 1H), 6.88 (m, 1H), 6.07 (m, 1H), 2.69 (q, *J* = 7.6 Hz, 2H), 1.27 (t, *J* = 7.6 Hz, 3H); **^{13}C-NMR** ($CDCl_3$, 100 MHz): δ = 178.4, 145.4, 131.9, 123.5, 109.0, 21.2, 13.3; **R_f** = 0.43 (EA:Hx, 1:4); ESI$^+$ **HRMS** for $C_7H_{10}ON^+ = [M+H]^+$: calcd. m/z 124.07569, found m/z 124.07570.

1-Tosyl-1*H*-pyrrole (S3)

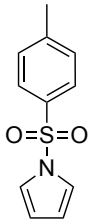

The compound was synthesised following a modified literature procedure.[16]

To a suspension of pyrrole (5.00 g, 74.5 mmol, 5.21 mL, 1.0 eq.) in DCM (100 mL), tetrabutylammonium bromide (2.40 g, 7.45 mmol, 0.1 eq.) and NaOH (50 wt%, 65 mL) was added a solution of tosyl chloride (21.3 g, 112 mmol, 1.5 eq.) in DCM (50 mL). The mixture was stirred for 48 h at room temperature after which time it was filtered over a pad of celite. The filtrate was washed with brine (50 mL) and the organic phase was dried over Na_2SO_4 and evaporated. The crude product was recrystallised from iPrOH yielding the desired product as an off-white solid (13.9 g, 62.6 mmol, 84%).

The spectral data for ^{1}H-NMR vary slightly from literature but match the desired molecule.[17]

^{1}H-NMR ($CDCl_3$, 400 MHz): δ = 7.72 (d, *J* = 8.4 Hz, 2H), 7.26 (d, *J* = 8.2 Hz, 2H), 7.13 (t, *J* = 2.3 Hz, 2H), 6.26 (t, *J* = 2.3 Hz, 2H), 2.38 (s, 3H); **^{13}C-NMR** ($CDCl_3$, 400 MHz): δ = 145.1, 136.2, 130.1, 126.9, 120.8, 113.6, 21.7; R_f = 0.56 (EA:Hx, 1:4); EI$^+$ **HRMS** for $C_{11}H_{11}NO_2S^+ = [M]^+$: calcd. m/z 221.0510, found m/z 221.0504, EI$^+$ **HRMS** for $C_7H_7O_2S^+ = [M-C_4H_4N]^+$: calcd. m/z 155.0161, found m/z 155.0160.

1-(1-Tosyl-1*H*-pyrrol-3-yl)ethan-1-one (S4)

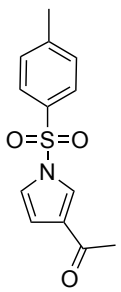

The compound was synthesised following a modified literature procedure.[18]

To a suspension of $AlCl_3$ (14.5 g, 108 mmol, 6.0 eq.) in dry DCM (200 mL) was added Ac_2O (5.53 g, 54.2 mmol, 3.0 eq.) at room temperature. After 10 min, a solution of *N*-tosyl pyrrole **S3** (4.00 g, 18.1 mmol, 1.0 eq.) in dry DCM (15 mL) was added and the mixture was stirred at room temperature for 2 h. Water (100 mL) was added and the phases were separated. The aqueous phase was extracted with DCM (3 x 100 mL) and the combined organic extracts were dried over Na_2SO_4 and evaporated yielding the desired product as an off-white solid (4.76 g, 18.1 mmol, 100%) that was used without further purification. The spectral data match literature.[19]

^{1}H-NMR ($CDCl_3$, 400 MHz): δ = 7.78 (d, *J* = 8.4 Hz, 2H), 7.69 (t, *J* = 1.9 Hz, 1H), 7.32 (d, *J* = 8.1 Hz, 2H), 7.11 (dd, *J* = 3.3 / 2.2 Hz, 1H), 6.66 (dd, *J* = 3.3 / 1.6 Hz, 1H), 2.41 (s, 3H), 2.39 (s, 3H); **^{13}C-NMR** ($CDCl_3$, 100 MHz): δ = 193.1, 146.1, 135.2, 130.5, 129.4, 127.4, 124.7, 121.7, 112.5, 27.4, 21.9; ; **R_f** = 0.30 (EA:Hx, 1:3); ESI$^+$ **HRMS** for $C_{13}H_{14}NO_3S^+$ = $[M+H]^+$: calcd. m/z 264.06889, found m/z 264.06874; ESI$^-$ **HRMS** for $C_{13}H_{12}NO_3S^-$ = $[M-H]^-$: calcd. m/z 262.05434, found m/z 262.05431.

1-(1*H*-Pyrrol-3-yl)ethan-1-one (S5)

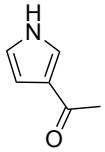

The compound was synthesised following a literature procedure.[18]

To a solution of **S4** (4.76 g, 18.1 mmol, 1.00 eq.) in 1,4-dioxane (50 mL) was added aq. NaOH (2M, 100 mL) and the mixture was stirred at room temperature overnight. EtOAc (25 mL) was added, the phases were separated and the aqueous phase was extracted with EtOAc (25 mL). The combined organic extracts were washed with brine (2 x 25 mL), dried over Na_2SO_4 and evaporated to yield a beige flaky solid (1.50 g, 13.7 mmol, 76%) that was used without further purification.

The spectral data match literature.[20,21]

^{1}H-NMR ($CDCl_3$, 400 MHz): δ = 9.91 (br. s, 1H), 7.42 (m, 1H), 6.76 (m, 1H), 6.61 (m, 1H), 2.42 (s, 3H); **^{13}C-NMR** ($CDCl_3$, 100 MHz): δ = 195.0, 125.9, 124.3, 120.0, 108.6, 27.3; **R_f** = 0.30 (EA:Hx, 1:1); EI$^+$ **HRMS** for $C_6H_7NO^+$ = $[M]^+$: calcd. m/z 109.0527, found m/z 109.0523, EI$^+$ **HRMS** for $C_5H_4NO^+$= $[M-CH_3]^+$: calcd. m/z 94.0287, found m/z 94.0288.

3-Ethyl-1*H*-pyrrole (S6)

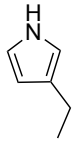

This compound was prepared from 3-acetylpyrrole (1.48 g, 13.6 mmol, 1.0 eq. mmol) and $LiAlH_4$ (1M in THF, 27.1 mL, 27.1 mmol, 2.0 eq.) in dry THF (20 mL) according to **GP A**. The product was purified by silica gel column chromatography (Et_2O:Hx, 15:85) as a colourless volatile liquid (596 mg, 6.26 mmol, 46%). The spectral data vary slightly from literature but match the desired product.[20,21]

^{1}H-NMR ($CDCl_3$, 400 MHz): δ = 7.98 (br. s, 1H), 6.73 (m, 1H), 6.59 (m, 1H), 6.12 (m, 1H), 2.54 (q, *J* = 7.5 Hz, 2H), 1.21 (t, *J* = 7.5 Hz, 3H); **^{13}C-NMR** ($CDCl_3$, 100 MHz): δ = 126.3, 117.8, 114.5, 108.3, 20.1, 15.5; **R_f** = 0.40 (Et_2O:Hx, 15:85); EI^+ **HRMS** for $C_6H_9N^+ = [M]^+$: calcd. m/z 95.0735, found m/z 95.0729, EI^+ **HRMS** for $C_5H_6N^+ = [M\text{-}CH_3]^+$: calcd. m/z 80.0495, found m/z 80.0494.

Formylation of 3-Ethyl-1*H*-pyrrole (S6)

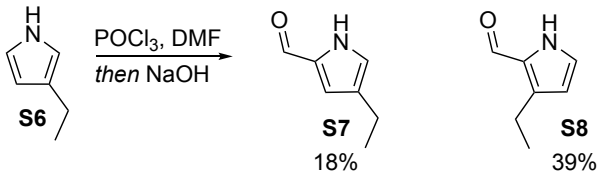

Scheme S4: Formylation of 3-Ethyl-1*H*-pyrrole.

Formylation was accomplished following a modified literature procedure.[22]

$POCl_3$ (1.91 g, 12.3 mmol, 1.16 mL, 2.0 eq.) was added dropwise to dry DMF (0.99 g, 13.5 mmol, 1.05 mL, 2.2 eq.) at 0 °C. The solution was stirred until the formation of the Vilsmeier reagent as solid material was complete. The material was dried in high vacuum for 20 min prior to again cooling to 0 °C and addition of dry DCM (6 mL). To this mixture was added a solution of pyrrole **S6** (585 mg, 6.15 mmol, 1.0 eq.) in dry DCM (10 mL) at 0 °C . After complete addition, the cooling bath was removed and the mixture was allowed to stir at room temperature overnight. The volatiles were removed under reduced pressure, water (15 mL) was added carefully (cooling) to the residue followed by NaOH pellets (1.97 g, 49.2 mmol, 8.0 eq.) and the mixture was stirred at room temperature for 6 h, heated to reflux for 30 min and stirred overnight at room temperature. EtOAc (40 mL) was added, the phases were separated and the aqueous layer was extracted with EtOAc (2 x 10 mL). The combined organic extracts were dried over Na_2SO_4 and evaporated. The crude was purified by automated flash chromatography (EA:Hx, 0 → 10% EA) with 4-ethyl-1*H*-pyrrole-2-carbaldehyde (**S7**) eluting at 8% EA (yellow-brownish oil (139 mg, 1.13 mmol, 18%)) and 3-ethyl-1*H*-pyrrole-2-carbaldehyde (**S8**) eluting at 10% EA (faintly yellow oil (295 mg, 2.40 mmol, 39%)):

4-Ethyl-1*H*-pyrrole-2-carbaldehyde (S7)

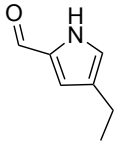

The spectral data vary from literature but match the desired molecule.[22]

^{1}H-NMR ($CDCl_3$, 400 MHz): δ = 9.43 (s, 1H), 9.13 (br. s, 1H), 6.90 (~t, 1H), 6.80 (~t, 1H), 2.51 (q, *J* = 7.6 Hz, 2H), 1.19 (t, *J* = 7.6 Hz, 3H); **^{13}C-NMR** ($CDCl_3$, 100 MHz): δ = 179.2, 132.7, 129.4, 124.3, 120.7, 19.8, 15.2; **R_f** = 0.20 (EA:Hx, 15:85); EI^+ **HRMS** for $C_7H_9NO^+ = [M]^+$: calcd. m/z 123.0641, found m/z 123.0679; EI^+ **HRMS** for $C_6H_6NO^+ = [M\text{-}CH_3]^+$: calcd. m/z 108.0444, found m/z 108.0445.

3-Ethyl-1*H*-pyrrole-2-carbaldehyde (S8)

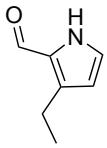

The spectral data vary from literature but match the desired molecule.[22]
^{1}H-NMR ($CDCl_3$, 400 MHz): δ = 9.61 (s, 1H), 9.50 (br. s, 1H), 7.00 (~t, 1H), 6.17 (t, *J* = 2.5 Hz, 1H), 2.79 (q, *J* = 7.6 Hz, 2H), 1.26 (t, *J* = 7.6 Hz); **^{13}C-NMR** ($CDCl_3$, 100 MHz): δ = 177.6, 139.8, 128.9, 126.1, 111.2, 18.7, 16.2; **R_f** = 0.20 (EA:Hx, 15:85); EI^+ **HRMS** for $C_7H_9NO^+ = [M]^+$: calcd. m/z 123.0641, found m/z 123.0679; EI^+ **HRMS** for $C_6H_6NO^+ = [M\text{-}CH_3]^+$: calcd. m/z 108.0444, found m/z 108.0445.

The assignment of the regioisomers **S7** and **S8** was confirmed by 1D-NOESY experiments (**Fig. S1**).

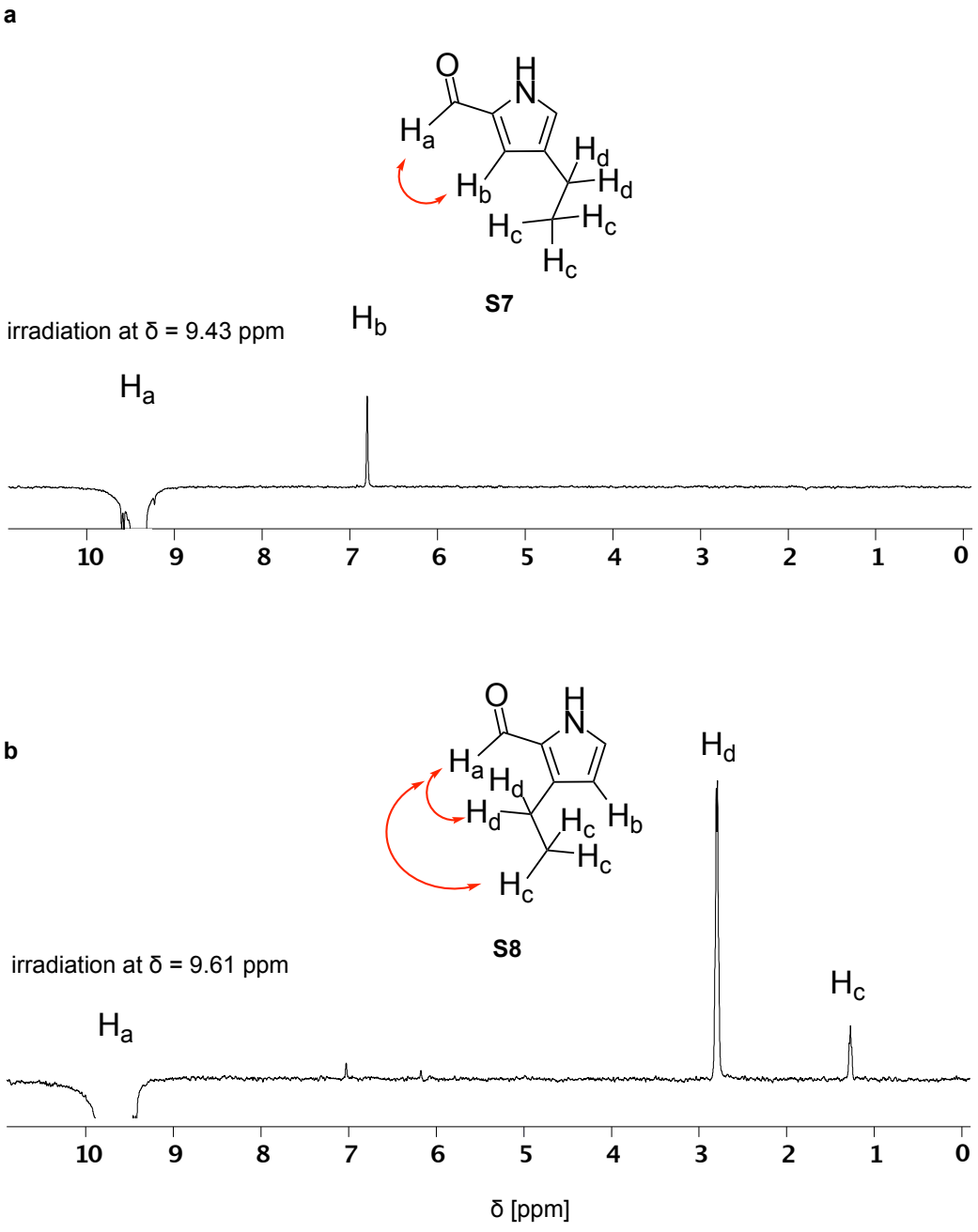

Fig. S1: NOESY interactions (red arrows) indicative of the two regioisomers were used to assign the isomers.

Synthesis of PHTubs

2-((5-Ethyl-1*H*-pyrrol-2-yl)methylene)-5,6-dimethoxybenzo[*b*]thiophen-3(2*H*)-one (PHTub-1)

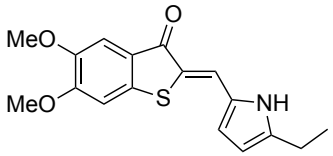

PHTub-1 was prepared by reacting 5,6-dimethoxybenzo[*b*]thiophen-3(2*H*)-one[23] (127 mg, 0.60 mmol) with respective aldehyde **S2** (62 mg, 0.50 mmol) in dry EtOH (2 mL) according to **GP B** as brown solid (152 mg, 0.48 mmol, 96%).

^{1}H-NMR (DMSO-D_6, 400 MHz) δ = 11.57 (s, 1H), 7.72 (s, 1H), 7.34 (s, 1H), 7.23 (s, 1H), 6.62 (~t, *J* = 2.9 Hz, 1H), 6.18 (~t, *J* = 2.8 Hz, 1H), 3.89 (s, 3H), 3.82 (s, 3H), 2.64 (q, *J* = 7.6 Hz, 2H), 1.21 (t, *J* = 7.6 Hz, 3H); **^{13}C-NMR** (DMSO-D_6, 100 MHz): δ = 183.6, 155.1, 148.1, 143.9, 140.4, 130.3, 129.0, 126.7, 122.2, 121.3, 111.0, 106.8, 104.6, 56.5, 56.3, 21.9, 13.0; **LC-MS**: t_R (***Z* isomer**) = 6.44 min, λ_{max} (***Z* isomer**) = 416, 476 nm; ESI$^+$ **HRMS** for $C_{17}H_{18}NO_3S^+$ = $[M+H]^+$: calcd. m/z 316.10019, found m/z 316.09975, ESI$^-$ **HRMS** for $C_{17}H_{16}NO_3S^-$ = $[M-H]^-$: calcd. m/z 314.08564, found m/z 314.08571, ESI$^-$ **HRMS** for $C_{16}H_{14}NO_3S^-$ = $[M-CH_3]^-$: calcd. m/z 300.06999, found m/z 300.07003.

2-((4-Ethyl-1*H*-pyrrol-2-yl)methylene)-5,6-dimethoxybenzo[*b*]thiophen-3(2*H*)-one (PHTub-2)

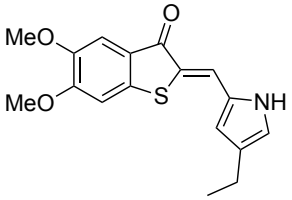

PHTub-2 was prepared by reacting 5,6-dimethoxybenzo[*b*]thiophen-3(2*H*)-one[23] (98 mg, 0.46 mmol) with respective aldehyde **S7** (53 mg, 0.39 mmol) in EtOH (1.6 mL) according to **GP B** as brown solid (84 mg, 0.27 mmol, 69%).

^{1}H-NMR (D_3COD, 400 MHz): δ = 7.74 (s, 1H), 7.31 (s, 1H), 7.17 (s, 1H), 6.97 (s, 1H), 6.69 (s, 1H), 3.95 (s, 3H), 3.88 (s, 3H), 2.56 (q, *J* = 7.6 Hz, 2H), 1.24 (t, *J* = 7.6 Hz, 3H); **^{13}C-NMR** (DMSO-D_6, 400 MHz): δ = 185.9, 155.8, 148.4, 139.1, 130.1, 128.4, 123.9 (two signals), 123.2, 123.0, 114.2, 107.5, 106.8, 56.7, 56.2, 20.0, 15.6; **LC-MS**: t_R (**Z isomer**) = 6.50 min, λ_{max} (**Z isomer**) = 408, 466 nm; ESI$^+$ **HRMS** for $C_{17}H_{18}NO_3S^+$ = $[M+H]^+$: calcd. m/z 316.10019, found m/z 316.09976, ESI$^-$ **HRMS** for $C_{17}H_{16}NO_3S^-$ = $[M-H]^-$: calcd. m/z 314.08564, found m/z 314.08570.

2-((3-Ethyl-1*H*-pyrrol-2-yl)methylene)-5,6-dimethoxybenzo[*b*]thiophen-3(2*H*)-one (PHTub-3)

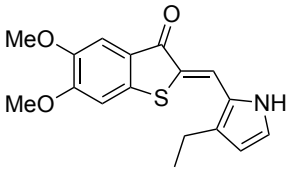

PHTub-3 was prepared by reacting 5,6-dimethoxybenzo[*b*]thiophen-3(2*H*)-one[23] (29 mg, 0.14 mmol) with respective aldehyde **S8** (14 mg, 0.12 mmol) in dry EtOH (1 mL) according to **GP B** as black solid (24 mg, 0.08 mmol, 66%).

^{1}H-NMR (D_3COD, 400 MHz), mixture of the two photoisomers (~63% ***Z* isomer** and ~37% ***E* isomer**) : δ = 7.90 (s, 1H, ***Z* isomer**), 7.38 (s, 1H, ***E* isomer**), 7.37 (s, 1H, ***Z* isomer 1**), 7.31 (s, 1H, ***E* isomer**), 7.22 (d, *J* = 2.3 Hz, 1H, ***E* isomer**), 7.19 (s, 1H, ***Z* isomer**), 7.18 (d, *J* = 2.5 Hz, 1H, ***Z* isomer**), 7.14 (s, 1H, ***E* isomer**), 6.32 (d, *J* = 2.3 Hz, 1H, ***E* isomer**), 6.26 (d, *J* = 2.5 Hz, 1H, ***Z* isomer**), 3.97 (s, 3H, ***Z* isomer**), 3.95 (s, 3H, ***E* isomer**), 3.90 (s, 3H, ***E* isomer**), 3.89 (s, 3H, ***Z* isomer**), 2.73 (q, *J* = 7.6 Hz, 4H, 2 H ***Z* isomer** & 2 H ***E* isomer**), 1.26 (t, *J* = 7.6 Hz, 6H, 3H ***Z* isomer** & 3H ***E* isomer**); **^{13}C-NMR** (DMSO-D_6, 400 MHz): δ = 185.2, 183.1, 155.3 (two signals), 148.0, 147.8, 139.9, 138.7, 137.4, 136.7, 127.3, 127.1, 126.6, 125.5, 125.3, 123.5, 123.2, 121.6, 121.0, 120.4, 111.7, 110.9, 107.0, 106.6, 106.2, 105.5, 56.3 (two signals), 55.7, 55.6, 19.0, 18.6, 15.9, 15.8; **LC-MS**: t_R (***Z* isomer**) = 6.23 min, λ_{max} (***Z* isomer**) = 402, 468 nm; t_R (***E* isomer**) = 7.04 min, λ_{max} (***E* isomer**) = 414, 502 nm; ESI^+ **HRMS** for $C_{17}H_{18}NO_3S^+ = [M+H]^+$: calcd. m/z 316.10019, found m/z 316.09994, ESI^- **HRMS** for $C_{17}H_{16}NO_3S^- = [M-H]^-$: calcd. m/z 314.08564, found m/z 314.08572.

2-((5-Ethyl-1*H*-pyrrol-2-yl)methylene)-4,5,6-trimethoxybenzo[*b*]thiophen-3(2*H*)-one (PHTub-4)

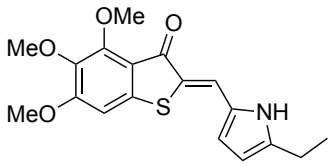

PHTub-4 was prepared by reacting 4,5,6-trimethoxybenzo[*b*]thiophen-3(2*H*)-one[23,24] (35 mg, 0.14 mmol) with respective aldehyde **S2** (15 mg, 0.12 mmol) in dry EtOH (1 mL) according to **GP B** as orange solid (34 mg, 0.10 mmol, 71%).

^{1}H-NMR (DMSO-D_6, 400 MHz): δ = 11.57 (s, 1H), 7.62 (s, 1H), 7.18 (s, 1H), 6.56 (s, 1H), 6.16 (s, 1H), 3.91 (s, 3H), 3.89 (s, 3H), 3.72 (s, 3H), 2.63 (q, *J* = 7.6 Hz, 2H), 1.21 (t, *J* = 7.6 Hz, 3H); **^{13}C-NMR** (DMSO-D_6, 100 MHz): δ = 184.1, 159.7, 153.8, 142.4, 141.8, 139.9, 127.5, 122.9, 122.0, 117.7, 115.4, 110.2, 103.5, 62.3, 61.4, 57.1, 21.0, 13.8; **LC-MS**: t_R (***Z* isomer**) = 6.49 min, λ_{max} (***Z* isomer**) = 390, 472 nm; ESI^+ **HRMS** for $C_{18}H_{20}NO_4S^+ = [M+H]^+$: calcd. m/z 346.11076, found m/z 346.11072, ESI^- **HRMS** for $C_{18}H_{18}NO_4S^- = [M-H]^-$: calcd. m/z 344.09620, found m/z 344.09625.

2-((4-Ethyl-1*H*-pyrrol-2-yl)methylene)-4,5,6-trimethoxybenzo[*b*]thiophen-3(2*H*)-one (PHTub-5)

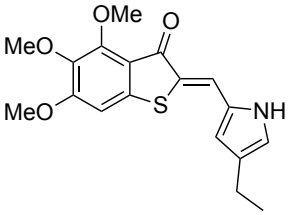

PHTub-5 was prepared by reacting 4,5,6-trimethoxybenzo[*b*]thiophen-3(2*H*)-one[23,24] (40 mg, 0.17 mmol) with respective aldehyde **S7** (17 mg, 0.14 mmol) in dry EtOH (1 mL) according to **GP B** as orange solid (38 mg, 0.11 mmol, 79%).

^{1}H-NMR (D_3COD, 400 MHz): δ = 7.68 (s, 1H), 7.02 (s, 1H), 6.94 (~t, 1H), 6.64 (~t, 1H), 4.00 (s, 3H), 3.97 (s, 3H), 3.82 (s, 3H), 2.56 (q, *J* = 7.6 Hz, 2H), 1.23 (t, *J* = 7.6 Hz, 3H); **^{13}C-NMR** (DMSO-D_6, 100 MHz): δ = 183.7, 159.3, 153.4, 142.1, 139.5, 129.4, 127.9, 123.2, 122.2, 121.6, 117.1, 113.4, 103.0, 61.8, 61.0, 56.6, 19.5, 15.1; **LC-MS**: t_R (***Z* isomer**) = 6.52 min, λ_{max} (***Z* isomer**) = 384, 462 nm, t_R

(***E* isomer**) = 7.20 min, λ_{max} (***E* isomer**) = 390, 496 nm; ESI$^+$ **HRMS** for $C_{18}H_{20}NO_4S^+$ = $[M+H]^+$: calcd. m/z 346.11076, found m/z 346.11064, ESI$^-$ **HRMS** for $C_{18}H_{18}NO_4S^-$ = $[M-H]^-$: calcd. m/z 344.09620, found m/z 344.09638.

2-((3-Ethyl-1*H*-pyrrol-2-yl)methylene)-4,5,6-trimethoxybenzo[*b*]thiophen-3(2*H*)-one (PHTub-6)

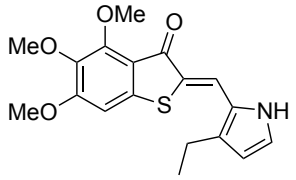

PHTub-6 was prepared by reacting 4,5,6-trimethoxybenzo[*b*]thiophen-3(2*H*)-one[23,24] (34 mg, 0.14 mmol) with respective aldehyde **S8** (15 mg, 0.12 mmol) in dry EtOH (1 mL) according to **GP B** as black solid (25 mg, 0.07 mmol, 75%).

^{1}H-NMR (D_3COD, 400 MHz), mixture of the two photoisomers (~69% ***Z* isomer** and ~31% ***E* isomer**) : δ = 7.81 (s, 1H, ***Z* isomer**), 7.25 (s, 1H, ***E* isomer**), 7.18 (d, *J* = 2.4 Hz, 1H, ***E* isomer**), 7.14 (d, *J* = 2.6 Hz, 1H, ***Z* isomer**), 7.01 (s, 1H, ***Z* isomer**), 6.96 (s, 1H, ***E* isomer**), 6.30 (d, *J* = 2.4 Hz, 1H, ***E* isomer**), 6.25 (d, *J* = 2.6 Hz, 1H, ***Z* isomer**), 4.02 (s, 1H, ***E* isomer**), 4.01 (s, 1H, ***Z* isomer**), 3.97 (s, 3H, ***Z* isomer**), 3.95 (s, 3H, ***E* isomer**), 3.83 (s, 3H, ***E* isomer**), 3.82 (s, 3H, ***Z* isomer**), 2.71 (q, *J* = 7.6 Hz, 4H, 2H ***Z* isomer** & 2H ***E* isomer**), 1.25 (t, *J* = 7.6 Hz, 6H, 3H ***Z* isomer** & 3H ***E* isomer**); **^{13}C-NMR** (DMSO-D_6, 100 MHz): δ = 183.6, 182.6, 159.3, 159.2, 153.5, 153.4, 143.2, 142.1, 139.5, 139.2, 136.9, 136.2, 126.8, 126.7, 125.4, 125.1, 123.4, 121.4, 120.8, 119.6, 118.9, 116.9, 111.5, 110.8, 102.8, 102.1, 61.9, 61.8, 61.7, 61.0, 56.7, 56.6, 19.0, 18.6, 15.9, 15.8; **LC-MS**: t_R (***Z* isomer**) = 6.35 min, λ_{max} (***Z* isomer**) = 378, 464 nm, t_R (***E* isomer**) = 7.13 min, λ_{max} (***E* isomer**) = 390, 498 nm; ESI$^+$ **HRMS** for $C_{18}H_{20}NO_4S^+$ = $[M+H]^+$: calcd. m/z 346.11076, found m/z 346.11058, ESI$^-$ **HRMS** for $C_{18}H_{18}NO_4S^-$ = $[M-H]^-$: calcd. m/z 344.09620, found m/z 344.09614.

2-((5-Ethyl-1*H*-pyrrol-2-yl)methylene)-5,6,7-trimethoxybenzo[*b*]thiophen-3(2*H*)-one (PHTub-7)

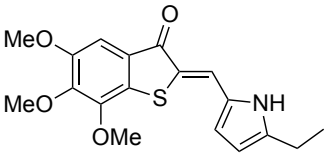

PHTub-7 was prepared by reacting 5,6,7-trimethoxybenzo[*b*]thiophen-3(2*H*)-one[23] (68 mg, 0.28 mmol) with respective aldehyde **S2** (29 mg, 0.24 mmol) in dry EtOH (1.7 mL) according to **GP B** as orange solid (79 mg, 0.23 mmol, 97%).

A crystal suitable for X-ray diffraction was obtained by layering a solution of **PHTub-7** in DCM with Et_2O.

^{1}H-NMR (DMSO-D_6, 400 MHz): δ = 11.62 (s, 1H), 7.76 (s, 1H), 7.16 (s, 1H), 6.72 (~t, 1H), 6.20 (~t, 1H), 3.95 (s, 3H), 3.89 (s, 3H), 3.87 (s, 3H), 2.65 (q, *J* = 7.6 Hz, 2H), 1.21 (t, *J* = 7.6 Hz); **^{13}C-NMR** (DMSO-D_6, 100 MHz): δ = 185.4, 152.8, 147.1, 146.9, 142.5, 129.9, 127.0, 126.5, 123.5, 121.4, 116.3, 110.3, 103.7, 60.9, 60.7, 56.2, 20.6, 13.3, **LC-MS**: t_R (***Z* isomer**) = 6.79 min, λ_{max} (***Z* isomer**) = 408, 486 nm; ESI$^+$ **HRMS** for $C_{18}H_{20}NO_4S^+$ = $[M+H]^+$: calcd. m/z 346.11076, found m/z 346.11036, ESI$^-$ **HRMS** for $C_{18}H_{18}NO_4S^-$ = $[M-H]^-$: calcd. m/z 344.09620, found m/z 344.09606.

2-((4-Ethyl-1*H*-pyrrol-2-yl)methylene)-5,6,7-trimethoxybenzo[*b*]thiophen-3(2*H*)-one (PHTub-8)

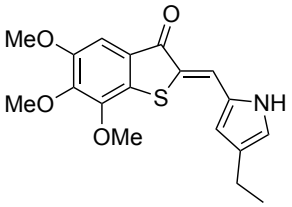

PHTub-8 was prepared by reacting 5,6,7-trimethoxybenzo[*b*]thiophen-3(2*H*)-one[23] (56 mg, 0.23 mmol) with respective aldehyde **S7** (24 mg, 0.20 mmol) in dry EtOH (1.5 mL) according to **GP B** as orange solid (67 mg, 0.19 mmol, 97%).

^{1}H-NMR (D_3COD, 400 MHz): δ = 7.78 (s, 1H), 7.23 (s, 1H), 7.00 (m, 1H), 6.75 (m, 1H), 4.02 (s, 3H), 3.96 (s, 3H), 3.91 (s, 3H), 2.58 (q, *J* = 7.6 Hz, 2H), 1.25 (t, *J* = 7.6 Hz, 3H); **^{13}C-NMR** (DMSO-D_6, 400 MHz): δ = 185.6, 152.8, 147.1 (two signals), 130.1, 130.0, 127.8, 126.3, 123.7, 123.4, 122.2, 114.6, 103.8, 60.9, 60.8, 56.3, 19.5, 15.2; **LC-MS**: t_R (***Z* isomer**) = 6.77 min, λ_{max} (***Z* isomer**) = 404, 478 nm, t_R (***E* isomer**) = 7.45 min, λ_{max} (***E* isomer**) = 408, 510 nm; ESI$^+$ **HRMS** for $C_{18}H_{20}NO_4S^+$ = $[M+H]^+$: calcd. m/z 346.11076, found m/z 346.11040, ESI$^-$ **HRMS** for $C_{18}H_{18}NO_4S^-$ = $[M-H]^-$: calcd. m/z 344.09620, found m/z 344.09597.

2-((3-Ethyl-1*H*-pyrrol-2-yl)methylene)-5,6,7-trimethoxybenzo[*b*]thiophen-3(2*H*)-one (PHTub-9)

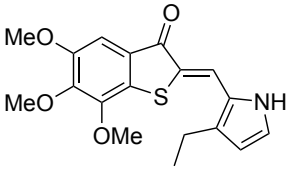

PHTub-9 was prepared by reacting 5,6,7-trimethoxybenzo[*b*]thiophen-3(2*H*)-one[23] (61 mg, 0.25 mmol) with respective aldehyde **S8** (26 mg, 0.21 mmol) in dry EtOH (1.5 mL) according to **GP B** as black solid (72 mg, 0.21 mmol, 99%).

^{1}H-NMR (D_3COD, 400 MHz), mixture of the two photoisomers (~63% ***Z* isomer** and ~37% ***E* isomer**): δ = 7.85 (s, 1H, ***Z* isomer**), 7.30 (s, 1H, ***E* isomer**), 7.19 (s, 3H, 1H **isomer 1** & 2H ***E* isomer**), 7.16 (~d, 1H, ***Z* isomer**), 6.29 (~d, 1H, ***E* isomer**), 6.24 (d, *J* = 2.1 Hz, 1H, ***Z* isomer**), 3.99 (s, 3H, ***Z* isomer**), 3.97 (s, 3H, ***E* isomer**), 3.94 (s, 3H, ***Z* isomer**), 3.93 (s, 3H, ***E* isomer**), 3.88 (s, 6H, 3H ***Z* isomer** & 3H ***E* isomer**), 2.70 (m, 4H, 2H ***Z* isomer** & 2H ***E* isomer**), 1.24 (t, *J* = 7.6 Hz, 6H, 3H ***Z* isomer** & 3H ***E* isomer**); **^{13}C-NMR** (DMSO-D_6, 400 MHz): δ = 185.4, 183.2, 152.8, 152.5, 147.0, 146.9, 146.6, 146.5, 138.4, 137.8, 131.5, 130.2, 128.0, 127.9, 127.6, 127.5, 126.3, 126.2, 123.5, 121.1, 120.3, 120.2, 112.1, 111.0, 103.8, 103.3, 61.0, 61.0, 60.7, 60.6, 56.3, 56.2, 19.0, 18.6, 15.8, 15.7; **LC-MS**: t_R (***Z* isomer**) = 6.68 min, λ_{max} (***Z* isomer**) = 398, 476 nm, t_R (***E* isomer**) = 7.34 min, λ_{max} (***E* isomer**) = 408, 514 nm; ESI$^+$ **HRMS** for $C_{18}H_{20}NO_4S^+$ = $[M+H]^+$: calcd. m/z 346.11076, found m/z 346.11054, ESI$^-$ **HRMS** for $C_{18}H_{18}NO_4S^-$ = $[M-H]^-$: calcd. m/z 344.09620, found m/z 344.09613.

2-((4-Ethyl-1-methyl-1*H*-pyrrol-2-yl)methylene)-5,6-dimethoxybenzo[*b*]thiophen-3(2*H*)-one (PHTub-NMe)

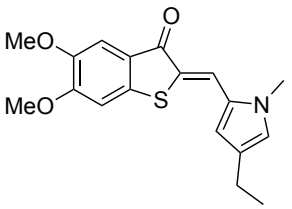

To a suspension of NaH (60 wt% dispersion in mineral oil, 2.8 mg, 0.07 mmol, 2.3 eq.) in dry THF (1 mL) was slowly added a solution of **PHTub-2** (10 mg, 0.03 mmol, 1.0 eq.) in dry THF (3 mL) at 0 °C. After complete addition, the deep red solution was allowed to reach room temperature and stirred for 15 min prior to cooling again to 0 °C and addition of MeI (228 mg, 1.61 mmol, 0.10 mL, excess). The orange reaction mixture was warmed to room temperature and stirred for 5 h, aqueous NH_4Cl (5 mL) was added and the phases were separated. The aqueous layer was then extracted with DCM (3 x 10 mL), the combined organic layer was dried over Na_2SO_4 and evaporated. The crude product was subjected to automated flash chromatography (EA:Hx, 10 → 100%), product containing fractions were evaporated and further purified as stated for **other PHTubs** (precipitation from a concentrated solution in DMSO). **PHTub-NMe** was obtained as orange solid (5 mg, 0.02 mmol, 52%).

^{1}H-NMR (D_3COD, 400 MHz): δ = 7.78 (s, 1H), 7.28 (s, 2H), 7.12 (s, 1H), 6.67 (s, 1H), 3.91 (s, 3H), 3.87 (s, 3H), 3.76 (s, 3H), 2.51 (q, *J* = 7.6 Hz, 2H), 1.22 (t, *J* = 7.6 Hz, 3H); **^{13}C-NMR** (DMSO-D_6, 400 MHz): δ = 185.4, 155.4, 148.0, 138.6, 128.3, 127.7, 127.7, 124.1, 123.4, 119.8, 114.9, 107.0, 106.4, 56.3, 55.8, 33.8, 19.4, 15.1; **LC-MS**: t_R (**Z isomer**) = 6.77 min, λ_{max} (***Z* isomer**) = 412, 472 nm; ESI^+ **HRMS** for $C_{18}H_{20}NO_3S^+ = [M+H]^+$: calcd. m/z 330.11584, found m/z 330.11569.

X-ray crystallography data of PHTub-7

CCDC Deposition Number 2089743 contains the supplementary crystallographic data for this paper.

M [gmol^{-1}]	345.40
crystal size [mm]	0.120 × 0.080 × 0.050
T [K]	173.(2)
radiation	MoKα
crystal system	monoclinic
space group	'P 1 21/c 1'
a [Å]	6.7271(14)
b [Å]	30.531(6)
c [Å]	7.8581(17)
α [°]	90
β [°]	93.992(7)
γ [°]	90
V [Å^3]	1610.0(6)
Z	4
calc. density [gcm^{-3}]	1.425
M [mm^{-1}]	0.224
absorption correction	Multi-Scan
transmission factor range	0.94 – 0.99
refls. measured	38420
R_{int}	0.0475
mean σ(*I*) [I]	0.0259
θ range	3.035 – 28.281
observed refls.	3757
x, y (weighting scheme)	0.0475, 0.9936
hydrogen refinement	mixed
Flack parameter	?
refls in refinement	3985
parameters	266
restraints	46
R(F_{obs})	0.0442
$R_w(F^2)$	0.1175
S	1.140
shift/error$_{max}$	0.001
max electron density [e Å^{-3}]	0.390
min electron density [e Å^{-3}]	−0.276

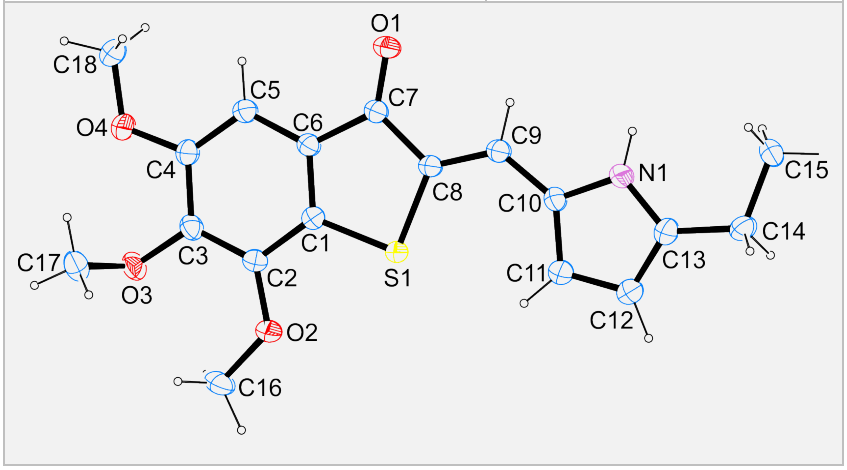

Table S1: X-ray crystallographic data and thermal ellipsoid structure of PHTub-7

Photochemical Characterisation

UV-Vis spectrophotometry of bulk samples

Absorption spectra in cuvette ("UV-Vis") were acquired on a Varian CaryScan 60 (1 cm pathlength). For photoisomerisation measurements, quartz or disposable plastic microcuvettes were used with test solution such that the vertical pathlength of the isomerisation light is less than 7 mm to the bottom of the optical window. Measurements were performed as stated individually. All photoisomerisations and relaxation rate measurements were performed at room temperature in non-degassed solvents unless stated differently. "Star" LEDs (H2A1-models - typically 410, 440, 470, 490, 505 and 525 nm - from Roithner Lasertechnik) or a V5 monochromator (TILL Photonics, Gräfelfing, Germany) were used for photoisomerisations in the cuvette that were also predictive of what would be obtained in LED-illuminated cell culture. For all photoswitching studies the samples were illuminated by shining from top of the cuvette, with additional illumination periods at the same wavelength used to verify that PSS had indeed been reached (no further evolution of the spectrum). Unless stated differently, all measurements were performed at a default concentration of 50 µM. Stocks in DMSO were kept at 60 °C for 14 h prior to measurements to account for a maximum ratio of *Z* isomer in the dark adapted state.

PSS spectra of PHTubs

PHTubs show reversible photoisomerisation with 440 nm illumination most efficient for *Z* → *E* and 525 or 532 nm for *E* → *Z*. In accordance with literature[13], the S0 → S1 absorption maxima of the isomers are well separated (~ 40 – 45 nm) in polar aprotic solvents such as acetonitrile (MeCN, **Fig. S2**) or dichloromethane (DCM). Compared to similarly-substituted phenyl hemithioindigos such as the **HOTubs**[23] (or **HITubs**[24]), the absorption maxima of the *E*-**PHTub** isomers are strongly redshifted.

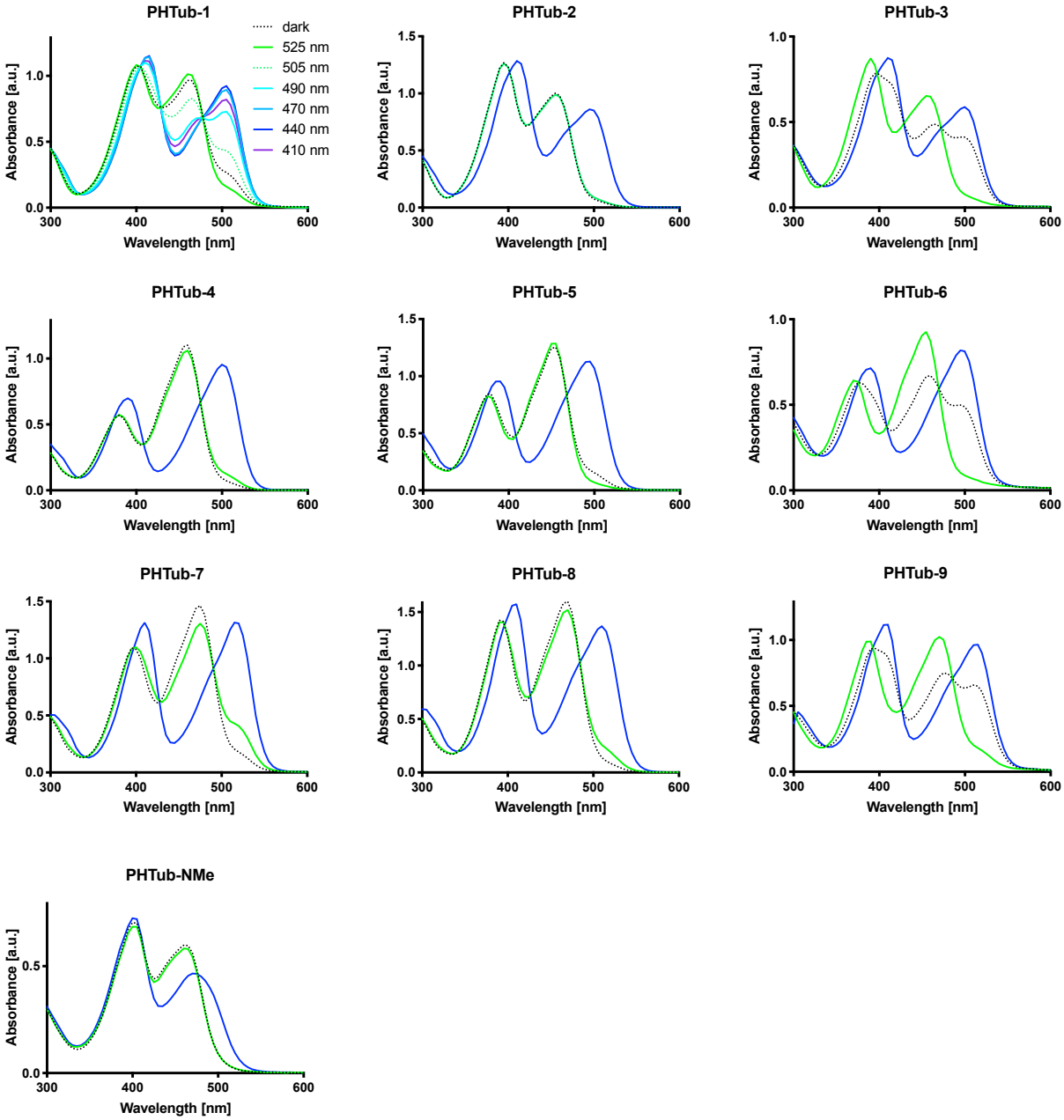

Fig. S2: Absorption spectra of PHTubs in the dark adapted state and after saturating illumination with 440 nm (blue) and 525 nm (green) in MeCN.

The conceptual negative control **PHTub-NMe** in which the pyrrole core was *N*-methylated showed the characteristics of a conventional HTI[23] and could be photoisomerised by illumination with 440 and 525 nm in both 'dry' organic solvents and DMSO/PBS mixtures which is in contrast to literature where loss of photoswitching upon N-methylation is reported.[13]

Similar trends were observed in DCM (**Fig. S3**) suggesting that polar-aprotic solvents have positive effects on photoswitching of **PHTubs**.

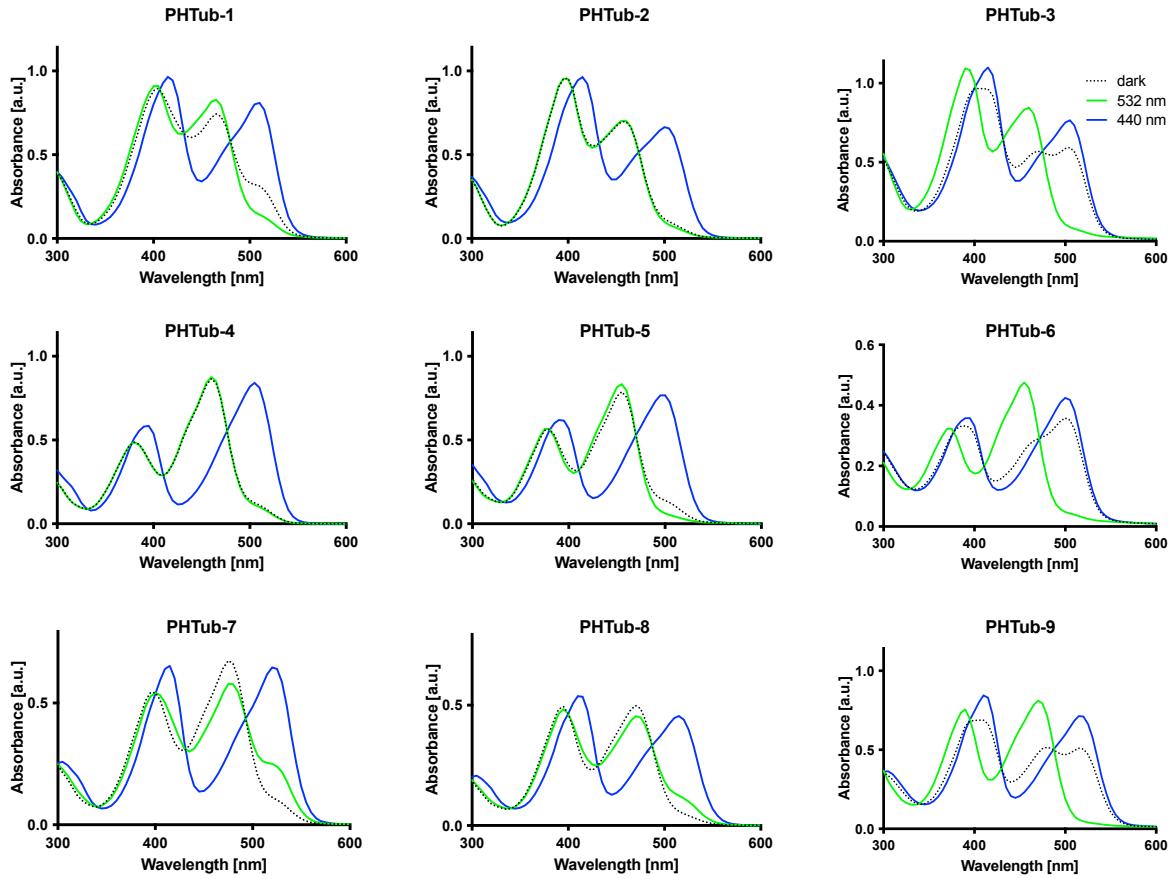

Fig. S3: Absorption spectra of PHTubs in the dark adapted state and after saturating illumination with 440 nm (blue) and 525 or 532 nm (green) in DCM.

In DMSO the band separation between the two isomers' spectra was still present albeit smaller than compared to DCM or MeCN (**Fig. S4**). This might reflect more tendency towards intermolecular rather than intramolecular H-bonds for the *E*-**PHTubs** (see **solvent effects on photoswitching, Table S2**).

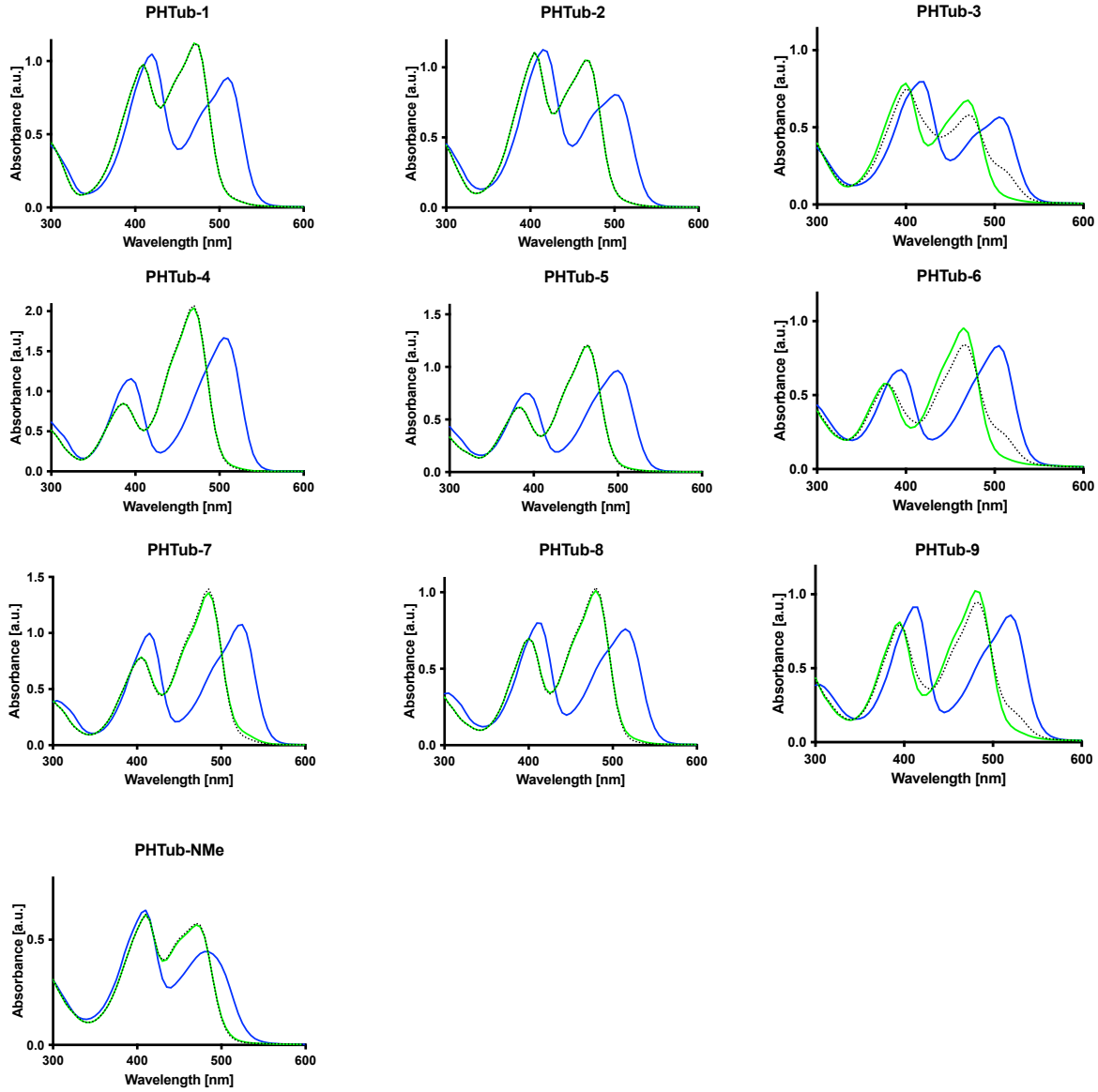

Fig. S4: Absorption spectra of PHTubs in the dark adapted state and after saturating illumination with 440 nm (blue) and 525 or 532 nm (green) in DMSO.

PSS spectra in aqueous media

To simulate a more physiological environment, we measured absorption spectra in more aqueous media (25% PBS in DMSO, **Fig. S5**). We observed a severe decrease in band separation in the spectra of the two photoisomers. This finding will be discussed in the following section.

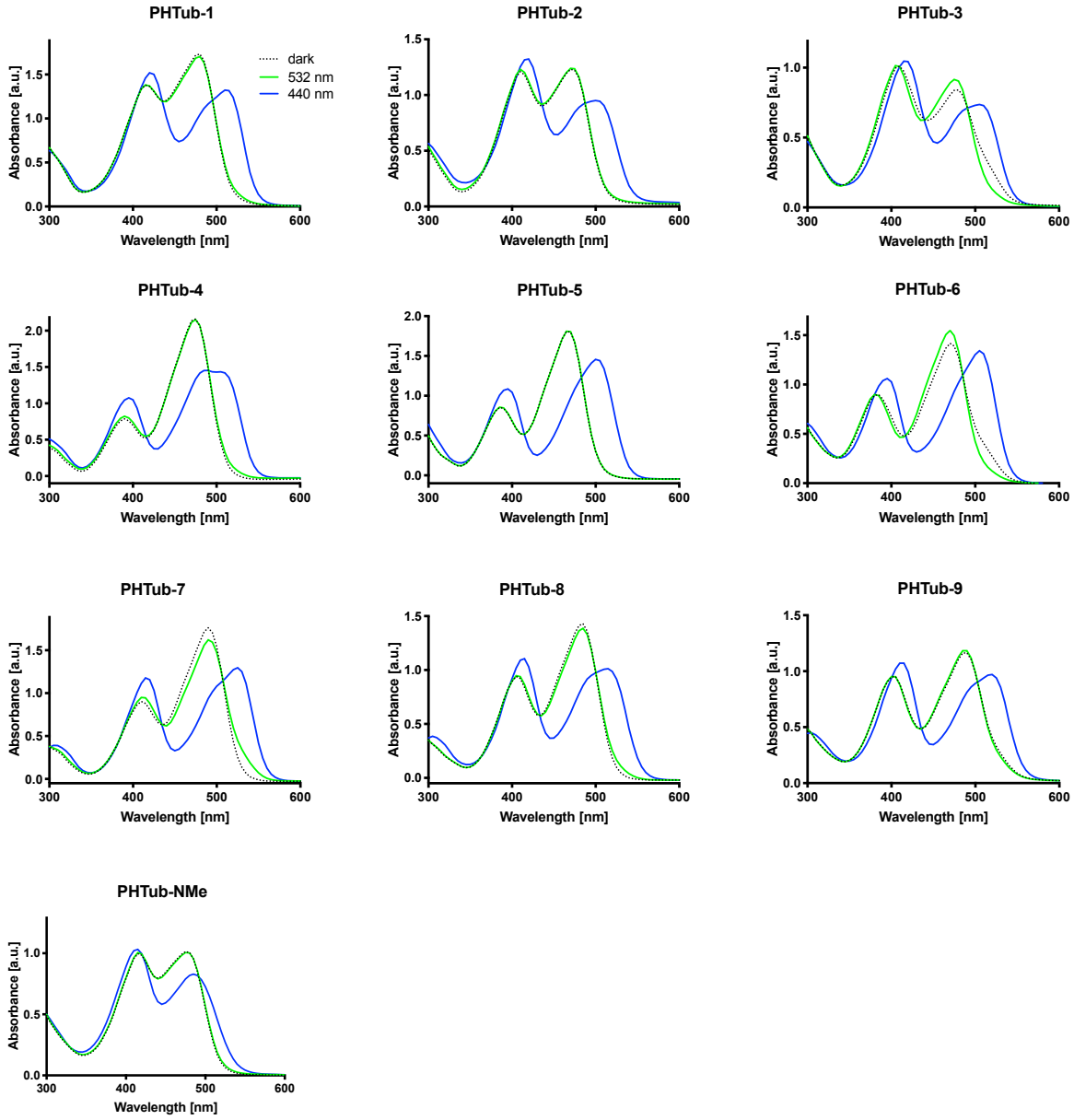

Fig. S5: Dark-adapted and PSS spectra of PHTubs in 25% PBS in DMSO.

Solvent effects on photoswitching

While retaining their properties with respect to isomerisation and reversibility, we observed that the separation between the isomers' absorption maxima decrease with the solvent's ability to form H-bonds (**Table S2**).

	Band separation [nm]			
Compound	DCM	MeCN	DMSO	25% PBS in DMSO
PHTub-1	45	45	40	30
PHTub-2	40	40	35	30
PHTub-3	45	45	35	25
PHTub-4	45	45	35	30
PHTub-5	45	40	40	35
PHTub-6	45	40	40	35
PHTub-7	45	40	40	35
PHTub-8	45	40	35	30
PHTub-9	45	40	35	30
PHTub-NMe	n.d.	10	10	10

Table S2: Quantification of isomer band separation of PHTubs with respect to solvents (values rounded to nearest 5 nm).

This finding is in line with literature for similar compounds, where solvents with increasing hydrogen bonding ability were correlated to less efficient photoisomerisation.[13] We presume this to be a result of competition between *intramolecular* (between C=O and NH functionality) and *intermolecular* (between solvent and NH functionality) interactions. *N*-methylated **PHTub-NMe** were observed to exhibit less pronounced band separation independently of the solvent, which would be expected for a regular HTI.

General trends in thermal relaxation

Thermal relaxation was measured by observing the recovery of absorbance at the absorption maximum of the redshifted band (typically 460 – 490 nm) of the *Z* isomer after saturating illumination with 440 nm. These experiments were conducted at a default concentration of 50 µM at room temperature.

The previously mentioned solvent effect affects thermal relaxation rates in a similar fashion and are exemplarily shown for **PHTub-1** (**Fig. S6**). In polar aprotic solvents like DCM the half-life of the *E* isomer lies in the hour to day range and decreases with increasing solvent polarity to the minute range.

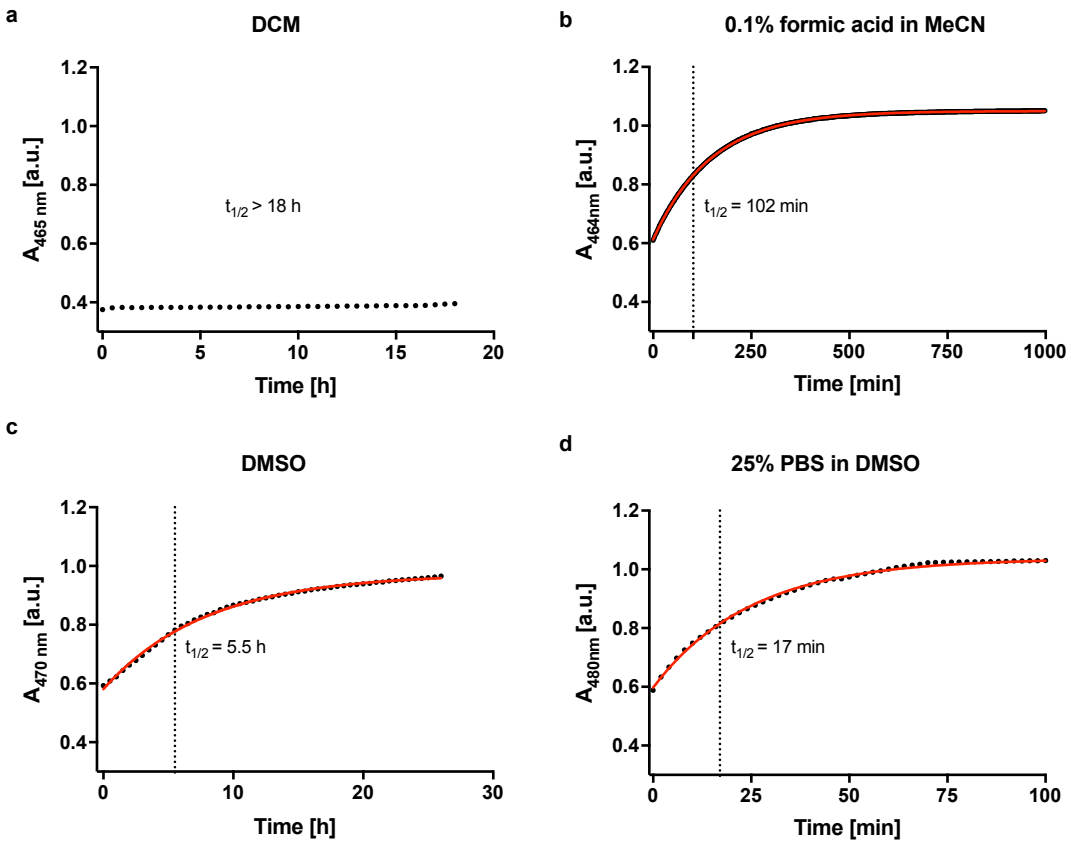

Fig. S6. Solvent-dependent thermal relaxation PHTub-1.

Thermal relaxation of PHTub-7 at 37 °C

To simulate more physiological conditions, thermal relaxation of **PHTub-7** was measured in aqueous DMSO at 37 °C (**Fig. S7**). For this purpose, the aforementioned procedure was repeated while keeping the cuvette at 37 °C (temperature maintenance by Peltier device).

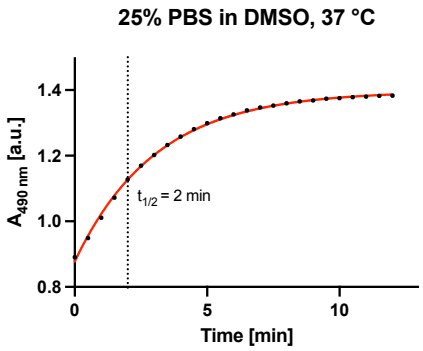

Fig. S7: Thermal relaxation of PHTub-7 at 37 °C.

Absorption spectra of separated isomers and comparison to PSS spectra

Isomer separation was accomplished by analytical HPLC-UV injecting stock solutions (5 mM, MeCN; 10 µL) of the respective **PHTubs** using the following set-up (**Table S3**).

Column	Thermo Scientific Hypersil GOLD™ C18 (1.9 µm; 3 x 50 mm)
Gradient	isocratic
Solvent	0.1% formic acid in MeCN
Run time	7 min.
Retention times t_R	t_R (*Z*) ~ 3 min., t_R (*E*) ~ 4 min.

Table S3: Conditions for HPLC separation of photoisomers.

The spectra of the separated isomers were exported and compared to the normalised spectra obtained from measurements in cuvette in the same solvent (**Fig S8**). In general, a good agreement between spectra of the pure *Z* isomer (HPLC) and the *E/Z* mixture after saturating illumination with 525 nm light (UV-Vis); and between spectra of the pure *E* isomer (HPLC) and the *E/Z* mixture after saturating illumination with blue light (440 nm) can be observed. These qualitative data hint at near-complete photoswitching at these wavelengths; for a quantitative analysis we however focussed on HPLC (see following section).

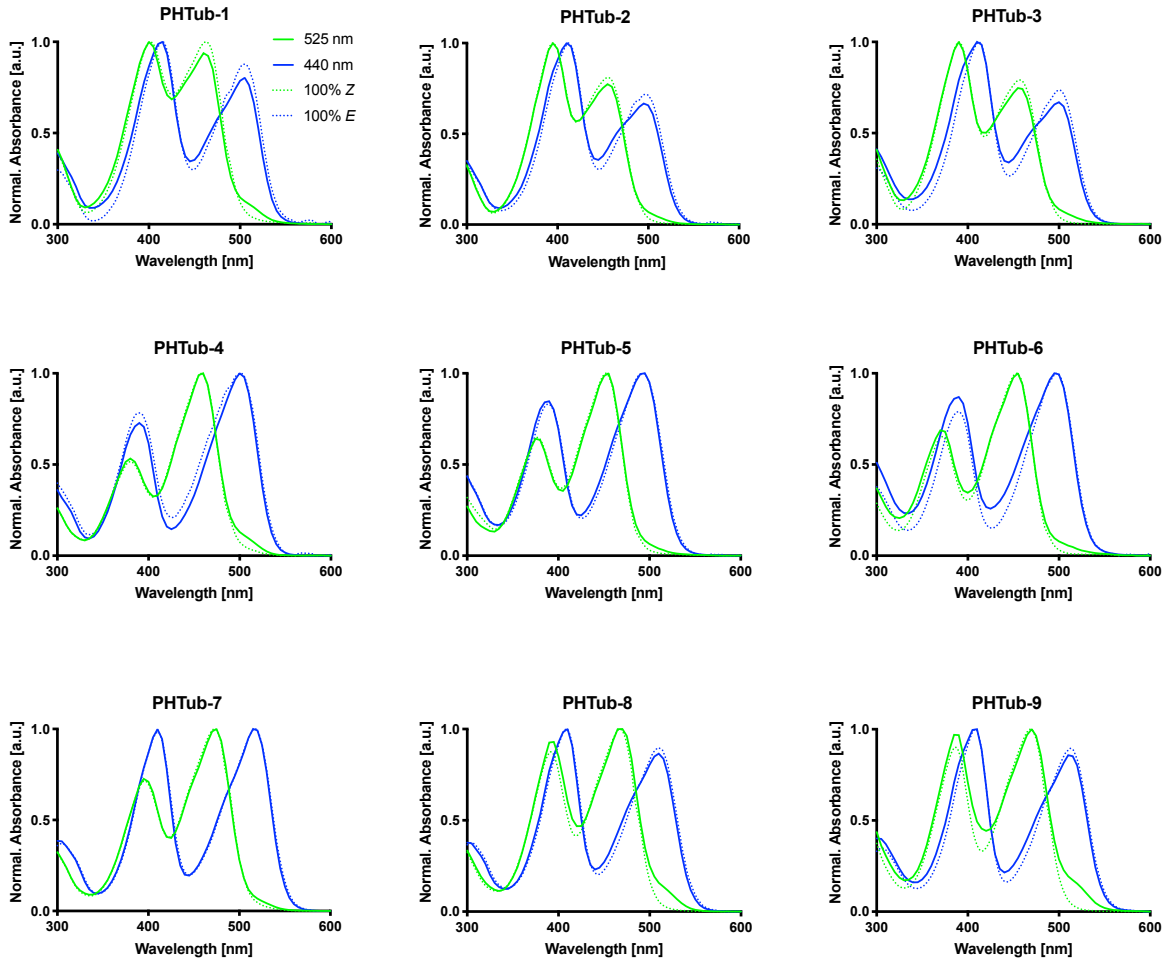

Fig. S8: Normalised absorption spectra of PHTubs after illuminations at 440 and 525 nm (blue and green solid lines, respectively) in HPLC solvent (0.1% formic acid in acetonitrile) plotted against HPLC inline DAD spectra of pure *E* and *Z* isomers (dotted blue and green lines, respectively).

Determination of the PSS composition

The PSS composition was determined by analytical HPLC-UV (conditions as shown in **Table S3**). Firstly, absorption spectra of the **PHTubs** in the HPLC solvent were recorded, the isosbestic points were determined and used as detecting wavelength for DAD. The thermal relaxation rate of one representative compound in the solvent mixture was determined ($t_{1/2}$ = 102 min., **PHTub-1**, **Fig. S6b**) and allowed us to exclude relaxation effects in this procedure, since the delay between illumination and elution of isomers was only ca. 5 – 6 min. For determination of the PSS composition, a stock solution (5 mM, MeCN) of the respective **PHTub** was diluted to 30 µM with only minimal exposure to light. This sample was run on HPLC and the areas under the curves of the respective peaks were compared to determine the PSS proportions of *E* and *Z* (**Table S4**). The same sample was then irradiated for 15 min. with a 440 nm LED from the bottom of the vial (distance between LED and vial < 1 cm) and subsequently run on HPLC again. This procedure was repeated with a 525 nm LED and with a monochromator (illumination wavelengths: 360, 380, 405, 420, 465, 475, 490, 514 and 532 nm, bandwidth: 10 nm, data shown in **Fig. 1f**) while measuring absorption spectra to check when PSS was reached.

	Z isomer [%]			*E* isomer [%]
Compound	*dark*	*525 nm*	*532 nm*	*440 nm*
PHTub-1	76	90	88	90
PHTub-2	79	92	96	88
PHTub-3	36	91	92	89
PHTub-4	84	91	93	86
PHTub-5	89	95	96	94
PHTub-6	50	95	93	91
PHTub-7	78	90	97	89
PHTub-8	82	85	86	92
PHTub-9	31	80	91	93
PHTub-NMe	n.d.	n.d.	n.d.	n.d.

Table S4: PSS composition in MeCN in the dark and after illumination with 525 nm LED or monochromatic 532 nm (majority-*Z*); and after illumination with 440 nm LED (majority-*E*).

Stability of PHTub-7 against reduced glutathione (GSH)

The stability of similar compounds against the prevalent biological nucleophile and reductant glutathione (ca. 5 mM intracellular concentration) has previously been shown in the literature at room temperature.[13] For application in a more biological context it is however preferable to assess the stability of compounds at more physiological conditions (*i.e.* at 37 °C, pH = 7.4 and 10 mM GSH). In brief, a stock solution of **PHTub-7** in DMSO was diluted with a stock solution of reduced GSH in PBS (final concentrations of **PHTub-7**: 50 µM and GSH: 10 mM, total proportion of PBS: 25%). This solution was then transferred to a cuvette and placed at 37 °C in the spectrophotometer (temperature control was performed by a Peltier device). Spectra were taken immediately after placing the sample inside the photometer and after distinct time intervals. The absorbance at λ = 490 nm was plotted against the time (**Fig S9**). *Z*-**PHTub-7** seems to be stable against GSH for times > 200 min (**Fig S9a**). To assess the stability of the *E* isomer,

the procedure was repeated with repeated illumination with a 440 nm LED to reach a majority of *E*-**PHTub-7**. We found no signs of degradation after 3 consecutive cycles but only consistent thermal relaxations with a half-life of 1.31 ± 0.08 min (mean ± standard deviation) of the metastable *E* isomer (**Fig S9b**) which compares well with thermal relaxation in absence of GSH (**Fig. S7**).

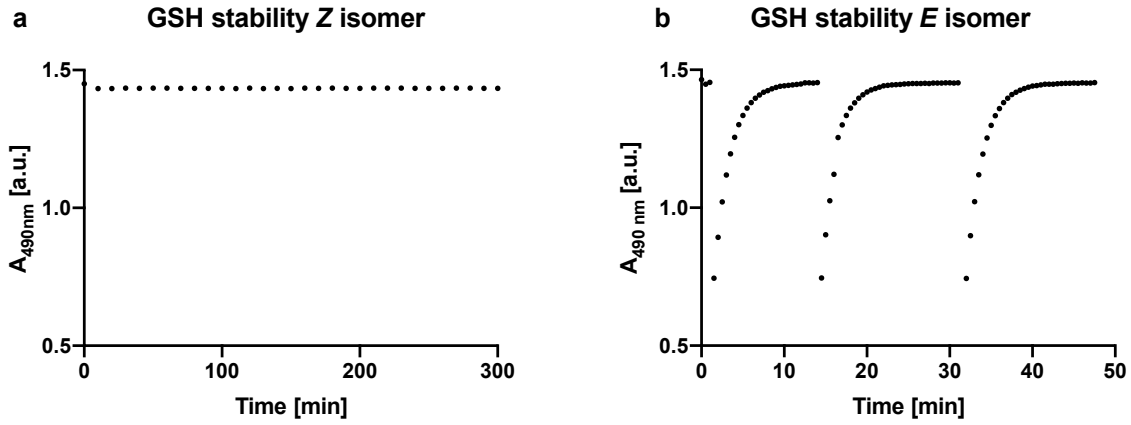

Fig. S9: Stability of a) Z-PHTub-7 (sample treated in the dark) and b) *Z*-and-*E*-PHTub-7 (repeated illuminations with 440 nm then relaxations without 440 nm), both challenged with 10 mM GSH at 37 °C.

Photoproperties of PHTub-3/6/9

(1) *E*-isomer proportion in the dark-adapted state: To our surprise, we found **PHTubs-3/6/9** to exhibit an unusually high proportion of *E* isomer in the thermally-relaxed (60°C overnight) dark-adapted state in MeCN (see PSS spectra in MeCN, **Fig S2**, and Determination of PSS composition); although the *E* proportion of the corresponding DMSO stocks was lower (similar to, but not as low as that shown in **Fig S5**), it was still significant.

(2) TICT states?: Hemithioindigos bearing substituents in the *ortho*-position of the stilbene were studied in detail in the literature.[25,26] It was found that this substitution leads to severe twisting of the stilbene and a second possible deexcitation pathway namely rotation around the single bond rather than double bond isomerisation. While less polar solvents favoured double bond isomerisation leading to unusually high quantum yields for double bond isomerisation (Φ up to 56%), polar solvents favoured rotation around the single bond and so had lower quantum yield of double bond isomerisation. Mechanistically, this was explained by the formation of a highly polar twisted intramolecular charge transfer (TICT) species in polar solvents. The formation of TICT states was proved by high Stokes shifts and a dual behaviour of fluorescence. To assess whether the pyrrole hemithioindigos **PHTub-3/6/9** could form TICT states in polar solvents (MeCN, DMSO), we measured the fluorescence of **PHTub-3/6/9** and compared them to **PHTub-1** and a regular HTI. While the regular HTI showed a stronger fluorescence signal, the fluorescence of all **PHTubs** was very weak and we observed no substantial difference between the potentially twisted **PHTub-3/6/9** and the non-twisted **PHTubs** (data not shown); therefore we do not propose that TICT states in polar solvents are relevant for their photochemistry.

Biological Applications

General cell culture

Cell lines were maintained under standard cell culture conditions at 37 °C in a 5% CO_2 atmosphere. HeLa cells were kept in Dulbecco's modified Eagle's medium (DMEM; PAN-Biotech: P04-035550) supplemented with 10% fetal calf serum (FCS), 100 U/mL penicillin and 100 U/mL streptomycin. Jurkat cells were kept in RPMI with 10% FCS, 100 U/mL penicillin and 100 U/mL streptomycin, 1% glutamine. Cells were typically transferred to phenol red free medium prior to assays (DMEM; PAN-Biotech: P04-03591; RPMI - PAN-Biotech: P04-16515). Compounds were applied using a minimum of co-solvent, typically 1% DMSO and were added via a D300e digital dispenser (Tecan).

For assays, compounds were set to the all-*Z* state by thermal relaxation of the DMSO stocks at 60 °C overnight, then treated cells were either incubated under dark conditions (incubation in lightproof boxes) or lit conditions (incubated under pulsed illumination at typically 435 or 535 nm using a home-made LED lighting system delivering ca. 3 mW / cm^2 optical output to the wells[27], which is a comparatively low intensity). "Lit" timing conditions were 75 ms pulses applied every 15 s. Since the light intensity of this home-made system cannot be reproducibly "dimmed" (whether by current decrease or by increasing the distance from LED to cells), we have found in this work as previously[23,27–29] that the best practical solution for maintaining a consistent near-PSS environment is to apply more light than is strictly needed. Rather than adapting the lighting conditions compound by compound we use this default timing pattern, which is tolerated by all cell lines we have worked with, and which all our studies have confirmed is tolerated *in the presence of* these various photoswitch scaffolds without phototoxic effects. The "75 ms per 15 s" frequency should be favourably compared to e.g. "7.5 s per 1500 s" which would not only (1) overload cells by radiant and convective heating of the LED, as well as by photothermal effects from light absorption by photoswitch chromophores, but also (2) allow compounds with seconds-to-minutes relaxation timescales to revert substantially to the thermodynamic ground state between pulses, therefore making the long-term assay evaluation *not* reflect true isomer-dependency, nor predictive of acute photoswitching effects in short-term culture which is the targeted use-scenario that all such compounds are intended for.

Resazurin assays

Mitochondrial diaphorase activity in HeLa or Jurkat cell lines, as a proxy for viable cell count, was quantified by spectrophotometrically measuring the reduction of resazurin (7-hydroxy-10-oxidophenoxazin-10-ium-3-one) to resorufin (7-hydroxy-3*H*-phenoxazin-3-one). 5,000 HeLa cells/well or 10,000 Jurkat cells were seeded on 96-well microtitre plates. After 24 h, cells were treated with **PHTubs**, shielded from ambient light with light-proof boxes, and exposed to the appropriate light regimes. Following 48 h of treatment, cells were incubated with 20 µL of 0.15 mg/mL resazurin per well for 3 h at 37 °C. The resorufin fluorescence (excitation 544 nm, emission 590 nm) was measured using a FLUOstar Omega microplate reader (BMG Labtech). Results are represented as percent of untreated control and represented as mean of three independent experiments with SD.

In vitro tubulin polymerisation

The aim of this assay was to confirm direct target binding in purified cell-free conditions, in order to complement and confirm the much more powerful and relevant assays of microtubule polymerisation dynamics in live cells (**Fig 5**). Purified tubulin from calf brain was obtained from CSIC (Spain). The polymerisation reaction was performed at 2 mg/mL tubulin, in BRB80 polymerisation buffer (80 mM piperazine-N,N′-bis(2-ethanesulfonic acid) (PIPES), 0.5 mM EGTA, 2 mM $MgCl_2$, pH = 6.9), in a cuvette (100 µL, 1 cm path length) in a Varian CaryScan 60 with Peltier cell temperature control unit maintained at 37 °C, with final concentrations of 3% DMSO and 5% glycerol by volume. Tubulin was incubated for 5 min at 37°C optionally with reference colchicine site inhibitors nocodazole or colchicine, or else with **PHTub**; then, GTP (final concentration 1 mM) was added and the solution mixed by pipetting up and down for 5 s to initiate polymerisation, then absorbance at 340 nm was zeroed; absorbance was then measured every 15 s to monitor polymerisation (since polymerised tubulin scatters light by Rayleigh scattering). Nocodazole/colchicine were not illuminated in the experiment; **PHTub-7/8** were either not illuminated or else were continuously illuminated at 535 nm for all-*Z* measurement; and were continuously illuminated at 440 nm for partial-*E* measurement; using a monochromator-liquid light guide setup (ca. 3 mW/cm^2 with FWHM 10 nm). We expected both tested **PHTubs** to inhibit tubulin polymerisation if they indeed directly bound to tubulin at the colchicine binding site as intended. Cellular bioactivity in the superfamily of colchicine site inhibitors is strongly influenced by bioconcentration and bioavailability (due to their hydrophobic nature, which can even result in >100-fold bioconcentration from extracellular medium into cells - see discussions in e.g. Tron[30] or Bisby[31]). While this prevents simple translation between cell-free and cellular potencies, it would nevertheless have been pleasing to observe **PHTub-8** to be more active in its all-*Z*-state and **PHTub-7** to be more active in its partly-*E*-state, since this would match the ordering of cellular results. We specify "partly-*E*" since this cell-free assay is conducted under essentially homogenous, polar, protic, aqueous conditions (that do not mimic the multiphase cellular setting), so we did not expect to maintain a substantial *E*-isomer proportion under these conditions due to fast relaxation, as indicated above.[13] In the event, **PHTub-7** showed a pleasing increase of inhibitory activity under 440 nm illumination, while **PHTub-8** was more active as the all-*Z* state, matching expectations from cellular studies (**Fig. S10**).

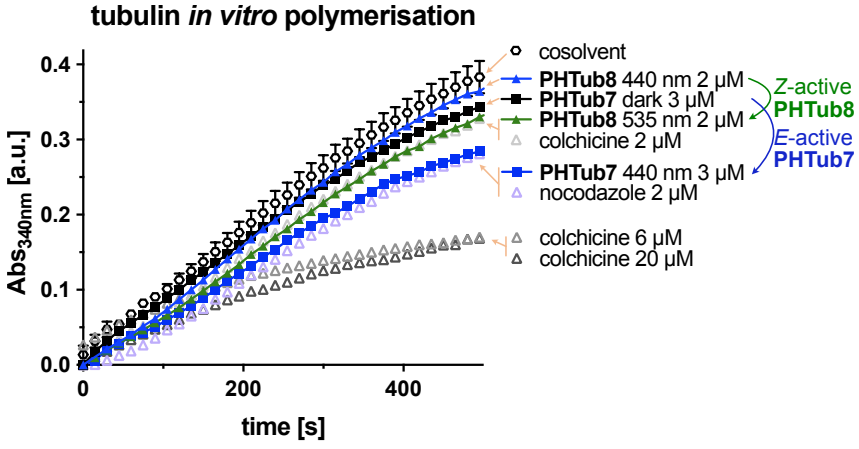

Fig. S10: *In vitro* tubulin polymerisation assay. Higher values in absorbance correspond to greater extent of polymerisation; lower values indicate inhibition of polymerisation.

Cell cycle analysis

Following 24 h of treatment with **PHTubs** under the indicated light regime, cells were harvested and fixed in ice-cold 70% ethanol and incubated in a staining solution [2% DNase-free RNase A 10 mg/mL, 0.1% Triton X-100 and 2 mg/mL propidium iodide (PI)] for 30 min at 37 °C. Following the PI staining, cells were analysed by flow cytometry using an LSR Fortessa (Becton Dickinson) run by BD FACSDiva 8.0.1 software. The cell cycle analysis was subsequently performed using FlowJo-V10 software (Tree Star Inc.). Results from one representative experiment are shown as a histogram (eg. **Fig 3**). Quantification from gating (**Fig S11**) on the respective histograms is shown as percent of live/singlet/PI-positive parent population per cell cycle phase across different concentrations of the compound (**Fig S12**). Every experiment was performed independently and in technical triplicates at least three times with a mean of 14,000 PI-positive singlet cells analyzed per replicate.

Cosolvent treated control

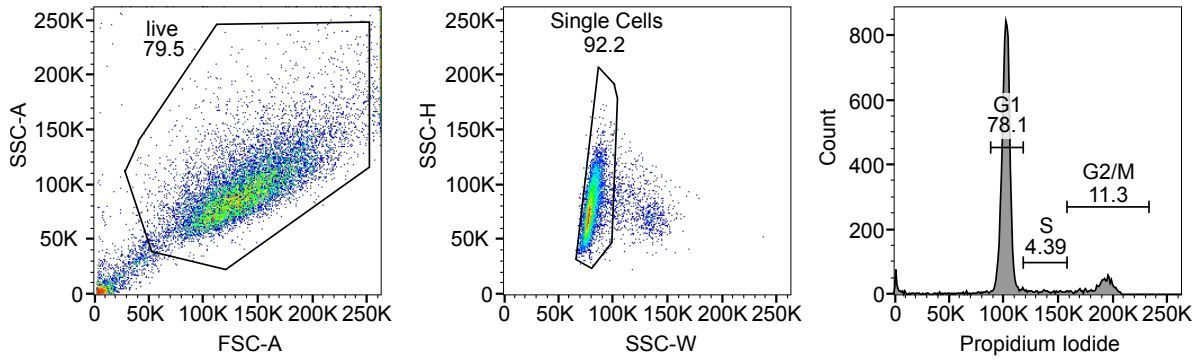

Fig. S11: Representative gating strategy applied to all datasets from flow cytometric cell cycle analysis. Live singlets were determined from SSC/FSC plot, PI-positive singlets (mean of 14,000 per replicate) were then plotted as histogram and cell cycle phase gates were set to accommodate for minimal peak shifts across all samples.

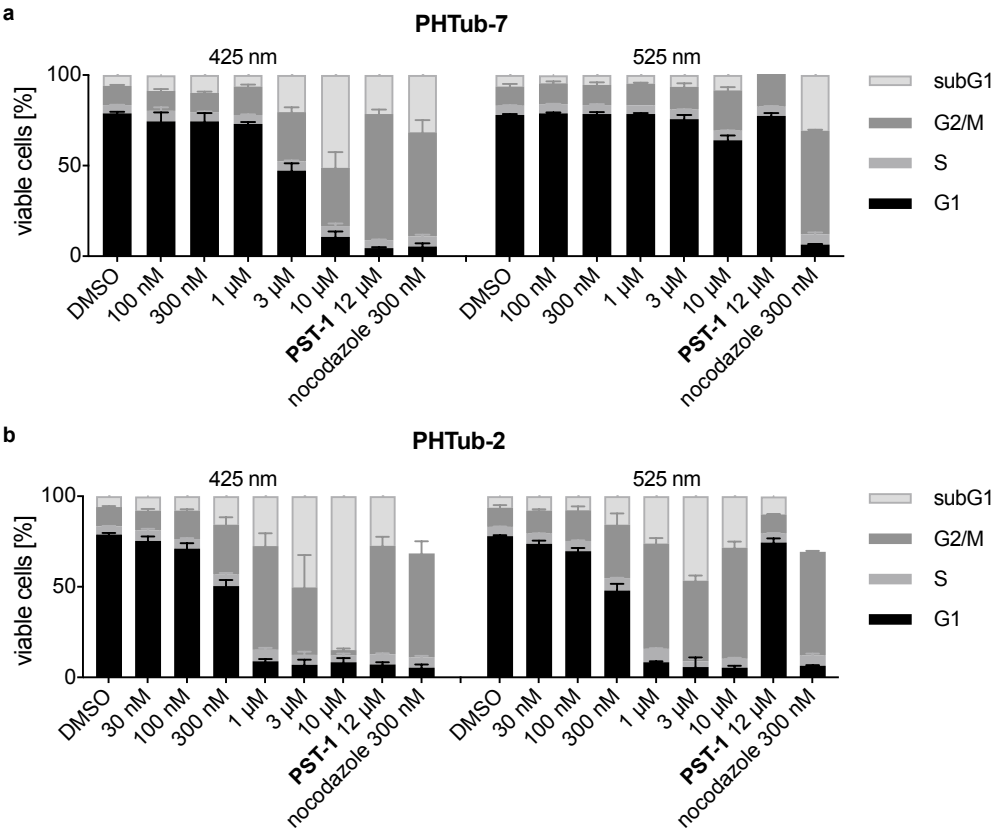

Fig. S12: Cell cycle repartition for cells treated with (a) PHTub-7 and (b) PHTub-2, with light-dependent G2/M-arrest-causing control PST-1 and light-independent G2/M-arrest-causing control nocodazole.

Immunofluorescence imaging of microtubule network structure

For fixed cell imaging, HeLa cells were seeded directly on glass coverslips in 24-well plates and treated with **PHTubs**, either in the dark (all-*Z*; we confirmed separately that 525 nm illumination produced the same outcomes (data not shown)) or under illumination by the LED array system using 425 nm LEDs pulsed at 75 ms “on” every 15 s, for 12 h. Cells were fixed in ice-cold methanol for 5 min. Coverslips were washed with PBS twice, then blocked and permeabilised with PBS containing 10% FCS and 0.1% Triton-100 for 30 min at room temperature. For immunofluorescence staining of microtubules, the cells were treated with primary antibody (rabbit anti-alpha-tubulin; abcam ab18251; 1:200 in blocking buffer) over night at 4 °C; on the next day cover slips were washed with PBS before application of the secondary antibody (donkey anti-rabbit Alexa Fluor 488; abcam ab150073; 1:500 in blocking buffer) for 1 h. The coverslips were mounted on microscopy glass slides using Roti®-Mount FluorCare DAPI (Carl Roth) and imaged with a Zeiss LSM 710 confocal microscope. Image processing was performed using the FIJI image analysis platform.[32]

Live Cell Imaging

For live cell imaging, HeLa cells were transfected with EB3-tdTomato using Fugene6 (Promega) according to manufacturer’s instructions. Cells were imaged 24 hours after transfection in standard cell

culture medium (described above) with 1% DMSO. Cells were imaged on a Nikon Eclipse Ti microscope with Perfect Focus System (Nikon), a spinning disk-based confocal scanner unit (CSUX1-A1, Yokogawa), ILas system (Roper Scientific France/ PICT-IBiSA, Institut Curie) for localized laser control, and an Evolve 512 EMCCD camera (Photometrics) with a stage top incubator INUBG2E-ZILCS (Tokai Hit) and lens heating calibrated for incubation at 37 °C with 5% CO_2. Microscope image acquisition was controlled using MetaMorph 7.7. A 561 nm Cobolt Jive laser was used to image tdTomato; **i**lluminations were performed using Voltran Stradus 405 nm, 442 nm and 487 nm lasers. Images were acquired using Plan Apo VC 100x N.A. 1.40, Plan Apo VC 60x N.A. 1.40 and Plan Fluor 40x N.A. 1.30 oil objectives. Imaging conditions were first optimized to minimize tdTomato bleaching and phototoxicity for cells in 1% DMSO. **For compound-treated acquisitions**, in a dark room with only red ambient light, 2 µM **PHTub-7** or 0.5 µM **PHTub-8** in prewarmed cell medium containing 1% DMSO was applied to cells. Cells were protected from all ambient light after application of drug and pre-incubated for at least 5 minutes before commencing experiments. 561 nm imaging intensities used were 50-160 µW/cm^2, 500 ms per frame, one frame per 2 s. Localized illuminations in ROIs with 442 nm used 5-17 µW/cm^2 intensity with 3 scans of 86 ms per scan repeated every 2 s for 26 frames (52 s). Comet count analysis was performed in ImageJ using the ComDet plugin (E. Katrukha, University of Utrecht, Netherlands, https://github.com/ekatrukha/ComDet).

Full caption to Figure 5

Figure 5 – PHTubs enable *in situ* photoswitching of MT dynamics in live cells. EB3-tdTomato-transfected HeLa cells; tdTomato imaged at 561 nm.

(a-d) Live cell EB3 “comet” counts (which quantify dynamic microtubules) are sharply and temporally precisely suppressed when cells treated with lit-active *Z*-**PHTub-7** (2 µM) are illuminated within the field of view (FOV) (a-b) at 442 nm or (c-d) at 487 nm (data related to Movie S1). Graphs show comet counts normalised to the average of the first 5 frames, n = 1 cell per condition. (b) DMSO-treated and *Z*-**PHTub-7** treated cells, 10 s before (t = -10 s) and 10 s after (t = 10 s) photoactivation with 17% laser power 442 nm for 2.5 s. (d) Still images of a cell analysed in (c), first imaged in DMSO, then after *Z*-**PHTub-7** added, each before (t = 0 s) and 10 s after (t = 110 s) photoactivation phases with 487 nm laser.

(e-f) Cells treated with dark-active *Z*-**PHTub-8** (0.5 µM) have suppressed MT dynamics, which can be repeatedly accelerated by illumination at 487 nm (data related to Movie S3). Pink faded background lines indicate rough fits to background photobleaching rate (same for treated and untreated cells) as a guide to the eye to distinguish accelerations. Cells are first imaged and photoactivated in 1% DMSO, then *Z*-**PHTub-8** (0.5 µM) is added and imaging / photoactivation is repeated. Graph shows mean ± SEM comet counts normalized to the first 5 frames of the DMSO control, n = 3 cells per condition. (f) Representative cell treated with DMSO and later with *Z*-**PHTub-8**, each before initial 1 s FOV 442 nm photoactivation (t = 0 s; MTs suppressed with **PHTub-8**), and directly after it (t = 11 s; MTs active with **PHTub-8**).

(g-h) Cell-precise MT dynamics suppression is caused by 442 nm photoactivation of *Z*-**PHTub-7** (2 µM) within a subcellular region of interest (shown by green circle) in a target "ROI" cell (green arrowhead), while adjacent "neighbour" cells (pink arrowhead) also in *Z*-**PHTub-7** but without

photoactivation, do not show greatly altered MT dynamics (data related to Movie S4). Cells are first imaged and photoactivated in 1% DMSO, then *Z*-**PHTub-7** (2 µM) is added and the imaging / photoactivation is repeated. Graph shows mean ± SEM comet counts normalized to the average cell counts of the first 5 frames, n = 3 cells per condition.

General Remark: (a, c, e, g) DMSO controls illustrate that in the absence of **PHTub**s, comet counts are unaffected by the 442 nm or 487 nm cellular or subcellular photoactivation protocols.

General Conditions: (a) dotted vertical line indicates an inserted 442 nm phase of the indicated laser power and duration (phase duration not represented on timecourse); (c, e, g) dotted vertical lines indicate start and finish of 487 nm or 442 nm phases; (b, d, f, h) scale bars indicate 20 µm.

Illumination-(in)dependency and off- and on-target bioactivity

First, we note that the position of the pyrrole ethyl group dictates *E*- or *Z*- activity of those isomers which have the correct substituent orientations to match the colchicine site pharmacophore: moderately potent *E*-active **PHTub1/7** (5-Et) are distinct from the much more potent and slightly more *Z*-active **PHTub2/8** (4-Et). We do not think that this move of the ethyl group flips whether the *E* or *Z* isomer is the more bioavailable. So we conclude that at least one (and for simplicity, presumably both) compound pairs, display isomer-dependent potency mediated by tubulin binding in cells. Next, we note that the acute in-cell tubulin polymerisation assays (Fig 5) also support this interpretation, by matching to the pattern of *Z*-active **PHTub8** vs *E*-active **PHTub7** seen in longterm assays. Finally, we note that **PHTub9** toxicity is independent of the (non)-illumination conditions (**Fig S13**). Assuming that PHT isomerisation is occurring in cells (as supported by the match of in-cell tubulin polymerisation assays with long-term viability results), the only way that its toxicity can be nearly constant is if the overall toxicity of the compound is truly invariant with isomer status as well as unrelated to phototoxicity - i.e. that **PHTub9** is an ideal control compound for revealing what an absence of isomer-dependent activity should look like. (The same is true for **PHTub6**, but since it is additionally not showing bioactivity, its role as a control is slightly different, i.e. controlling against phototoxicity). Also, since one would expect any biological effects to be dependent on concentration *as potentially modified by isomer-dependent bioavailability*, this suggests bioavailability of **PHTub9** is isomer-independent. In turn this suggests that the biological effects of closely structurally related compounds **PHTub2/7/8** should also not be interpreted as reflecting an isomer-dependency of bioavailability but rather the simplest assumption, of isomer-dependent binding, is preferred. Noting too that **PHTub6/9** are "permuted towards inactivity" against tubulin according to the SAR of the colchicine site, while the designed-for-activity compounds such as **PHTub2/7/8** display more potent as well as mechanistically-indicated tubulin-mediated bioactivity in cell-free and in acute cellular and in long-term cellular assays, we additionally believe it is well-supported that the performance pattern of the **PHTubs** as a set matches the expected SAR, which in itself is an indication of activity on-target against tubulin for the designed-for-activity compounds.

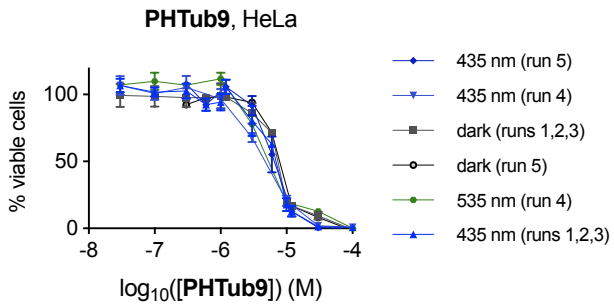

Fig. S13: Dark vs 535 nm illumination does not change assay outcomes, which we interpret as strong proof of the suitability of this compound as a non-tubulin-binding control, which reveals the absence of phototoxicity in this experimental setup, and reveals the absence of any significant isomer-dependency of bioavailability that could otherwise impact the PHTubs in the micromolar range.

Supplemental References

(1) Lee, J.; Schapira, M. The Promise and Peril of Chemical Probe Negative Controls. *ACS Chem. Biol.* **2021**, *16* (4), 579–585. https://doi.org/10.1021/acschembio.1c00036.

(2) Baell, J. B.; Nissink, J. W. M. Seven Year Itch: Pan-Assay Interference Compounds (PAINS) in 2017—Utility and Limitations. *ACS Chem. Biol.* **2018**, *13* (1), 36–44. https://doi.org/10.1021/acschembio.7b00903.

(3) Sailer, A.; Ermer, F.; Kraus, Y.; Lutter, F.; Donau, C.; Bremerich, M.; Ahlfeld, J.; Thorn-Seshold, O. Hemithioindigos as Desymmetrised Molecular Switch Scaffolds: Design Control over the Isomer-Dependency of Potent Photoswitchable Antimitotic Bioactivity in Cellulo. *ChemBioChem* **2019**, *20*, 1305–1314. https://doi.org/10.1002/cbic.201800752.

(4) Borowiak, M.; Nahaboo, W.; Reynders, M.; Nekolla, K.; Jalinot, P.; Hasserodt, J.; Rehberg, M.; Delattre, M.; Zahler, S.; Vollmar, A.; Trauner, D.; Thorn-Seshold, O. Photoswitchable Inhibitors of Microtubule Dynamics Optically Control Mitosis and Cell Death. *Cell* **2015**, *162* (2), 403–411. https://doi.org/10.1016/j.cell.2015.06.049.

(5) Gottlieb, H. E.; Kotlyar, V.; Nudelman, A. NMR Chemical Shifts of Common Laboratory Solvents as Trace Impurities. *J. Org. Chem.* **1997**, *62* (21), 7512–7515. https://doi.org/10.1021/jo971176v.

(6) Bruker. SAINT. Bruker AXS Inc., Madison, Wisconsin, USA. 2012.

(7) Sheldrick. SADABS. University of Göttingen, Germany. 1996.

(8) Sheldrick, G. SHELXT - Integrated Space-Group and Crystal-Structure Determination. *Acta Crystallographica Section A*, 2015, *71*, 3–8.

(9) Farrugia, L. J. *WinGX* and *ORTEP for Windows* : An Update. *J Appl Crystallogr* **2012**, *45* (4), 849–854. https://doi.org/10.1107/S0021889812029111.

(10) Mukherjee, C.; De, A. Application of Directed Metallation in Synthesis, Part 2: An Expedient Synthesis of Methoxybenzo[b]Thiophenes. *Synlett* **2002**, *2002* (02), 0325–0327. https://doi.org/10.1055/s-2002-19752.

(11) Friedländer, P.; Woroshzow, N. Über Thioindigofarbstoffe Der Naphthalinreihe. *Justus Liebigs Annalen der Chemie* **1912**, *388* (1), 1–23. https://doi.org/10.1002/jlac.19123880102.

(12) Kancharla, P.; Kelly, J. X.; Reynolds, K. A. Synthesis and Structure–Activity Relationships of Tambjamines and B-Ring Functionalized Prodiginines as Potent Antimalarials. *J. Med. Chem.* **2015**, *58* (18), 7286–7309. https://doi.org/10.1021/acs.jmedchem.5b00560.

(13) Zweig, J. E.; Newhouse, T. R. Isomer-Specific Hydrogen Bonding as a Design Principle for Bidirectionally Quantitative and Redshifted Hemithioindigo Photoswitches. *J. Am. Chem. Soc.* **2017**, *139* (32), 10956–10959. https://doi.org/10.1021/jacs.7b04448.

(14) Znidar, D.; O'Kearney-McMullan, A.; Munday, R.; Wiles, C.; Poechlauer, P.; Schmoelzer, C.; Dallinger, D.; Kappe, C. O. Scalable Wolff–Kishner Reductions in Extreme Process Windows Using a Silicon Carbide Flow Reactor. *Org. Process Res. Dev.* **2019**, *23* (11), 2445–2455. https://doi.org/10.1021/acs.oprd.9b00336.

(15) Wu, L.; Burgess, K. A New Synthesis of Symmetric Boraindacene (BODIPY) Dyes. *Chem. Commun.* **2008**, No. 40, 4933. https://doi.org/10.1039/b810503k.

(16) Gracia, S.; Schulz, J.; Pellet-Rostaing, S.; Lemaire, M. Synthesis of New Pyrrolobenzazepinesvia Pictet-Spengler Cyclization. *Synlett* **2008**, *2008* (12), 1852–1856. https://doi.org/10.1055/s-2008-1078567.

(17) Heredia, M. D.; Guerra, W. D.; Barolo, S. M.; Fornasier, S. J.; Rossi, R. A.; Budén, M. E. Transition-Metal-Free and Visible-Light-Mediated Desulfonylation and Dehalogenation Reactions: Hantzsch Ester Anion as Electron and Hydrogen Atom Donor. *J. Org. Chem.* **2020**, *85* (21), 13481–13494. https://doi.org/10.1021/acs.joc.0c01523.

(18) Kakushima, M.; Hamel, P.; Frenette, R.; Rokach, J. Regioselective Synthesis of Acylpyrroles. *J. Org. Chem.* **1983**, *48* (19), 3214–3219. https://doi.org/10.1021/jo00167a014.

(19) Huffman, J. W.; Smith, V. J.; Padgett, L. W. Acylation of N-p-Toluenesulfonylpyrrole under Friedel–Crafts Conditions: Evidence for Organoaluminum Intermediates. *Tetrahedron* **2008**, *64* (9), 2104–2112. https://doi.org/10.1016/j.tet.2007.12.043.

(20) He, Y.; Lin, M.; Li, Z.; Liang, X.; Li, G.; Antilla, J. C. Direct Synthesis of Chiral 1,2,3,4-Tetrahydropyrrolo[1,2- *a*]Pyrazines via a Catalytic Asymmetric Intramolecular Aza-Friedel–Crafts Reaction. *Org. Lett.* **2011**, *13* (17), 4490–4493. https://doi.org/10.1021/ol2018328.

(21) Garrido, D. O. A.; Buldain, G.; Ojea, M. I.; Frydman, B. Synthesis of 2-Alkylputrescines from 3-Alkylpyrroles. *J. Org. Chem.* **1988**, *53* (2), 403–407. https://doi.org/10.1021/jo00237a032.

(22) Kancharla, P.; Reynolds, K. A. Synthesis of 2,2′-Bipyrrole-5-Carboxaldehydes and Their Application in the Synthesis of B-Ring Functionalized Prodiginines and Tambjamines. *Tetrahedron* **2013**, *69* (39), 8375–8385. https://doi.org/10.1016/j.tet.2013.07.067.

(23) Sailer, A.; Ermer, F.; Kraus, Y.; Lutter, F. H.; Donau, C.; Bremerich, M.; Ahlfeld, J.; Thorn-Seshold, O. Hemithioindigos for Cellular Photopharmacology: Desymmetrised Molecular Switch Scaffolds Enabling Design Control over the Isomer-Dependency of Potent Antimitotic Bioactivity. *ChemBioChem* **2019**, *20* (10), 1305–1314. https://doi.org/10.1002/cbic.201800752.

(24) Sailer, A.; Ermer, F.; Kraus, Y.; Bingham, R.; Lutter, F. H.; Ahlfeld, J.; Thorn-Seshold, O. Potent Hemithioindigo-Based Antimitotics Photocontrol the Microtubule Cytoskeleton in Cellulo. *Beilstein J. Org. Chem.* **2020**, *16*, 125–134. https://doi.org/10.3762/bjoc.16.14.

(25) Wiedbrauk, S.; Maerz, B.; Samoylova, E.; Reiner, A.; Trommer, F.; Mayer, P.; Zinth, W.; Dube, H. Twisted Hemithioindigo Photoswitches: Solvent Polarity Determines the Type of Light-Induced Rotations. *J. Am. Chem. Soc.* **2016**, *138* (37), 12219–12227. https://doi.org/10.1021/jacs.6b05981.

(26) Wiedbrauk, S.; Maerz, B.; Samoylova, E.; Mayer, P.; Zinth, W.; Dube, H. Ingredients to TICT Formation in Donor Substituted Hemithioindigo. *J. Phys. Chem. Lett.* **2017**, *8* (7), 1585–1592. https://doi.org/10.1021/acs.jpclett.7b00371.

(27) Borowiak, M.; Nahaboo, W.; Reynders, M.; Nekolla, K.; Jalinot, P.; Hasserodt, J.; Rehberg, M.; Delattre, M.; Zahler, S.; Vollmar, A.; Trauner, D.; Thorn-Seshold, O. Photoswitchable Inhibitors of Microtubule Dynamics Optically Control Mitosis and Cell Death. *Cell* **2015**, *162* (2), 403–411. https://doi.org/10.1016/j.cell.2015.06.049.

(28) Gao, L.; Meiring, J. C. M.; Kraus, Y.; Wranik, M.; Weinert, T.; Pritzl, S. D.; Bingham, R.; Ntouliou, E.; Jansen, K. I.; Olieric, N.; Standfuss, J.; Kapitein, L. C.; Lohmüller, T.; Ahlfeld, J.; Akhmanova, A.; Steinmetz, M. O.; Thorn-Seshold, O. A Robust, GFP-Orthogonal Photoswitchable Inhibitor Scaffold Extends Optical Control over the Microtubule Cytoskeleton. *Cell Chemical Biology* **2021**, *28*, 1–14. https://doi.org/10.1016/j.chembiol.2020.11.007.

(29) Müller-Deku, A.; Meiring, J. C. M.; Loy, K.; Kraus, Y.; Heise, C.; Bingham, R.; Jansen, K. I.; Qu, X.; Bartolini, F.; Kapitein, L. C.; Akhmanova, A.; Ahlfeld, J.; Trauner, D.; Thorn-Seshold, O. Photoswitchable Paclitaxel-Based Microtubule Stabilisers Allow Optical Control over the Microtubule Cytoskeleton. *Nature Communications* **2020**, *11* (1), 4640. https://doi.org/10.1038/s41467-020-18389-6.

(30) Tron, G. C.; Pirali, T.; Sorba, G.; Pagliai, F.; Busacca, S.; Genazzani, A. A. Medicinal Chemistry of Combretastatin A4: Present and Future Directions. *J. Med. Chem.* **2006**, *49* (11), 3033–3044. https://doi.org/10.1021/jm0512903.

(31) Bisby, R. H.; Botchway, S. W.; Hadfield, J. A.; McGown, A. T.; Parker, A. W.; Scherer, K. M. Fluorescence Lifetime Imaging of E-Combretastatin Uptake and Distribution in Live Mammalian Cells. *European Journal of Cancer* **2012**, *48* (12), 1896–1903. https://doi.org/10.1016/j.ejca.2011.11.025.

(32) Schindelin, J.; Arganda-Carreras, I.; Frise, E.; Kaynig, V.; Longair, M.; Pietzsch, T.; Preibisch, S.; Rueden, C.; Saalfeld, S.; Schmid, B.; Tinevez, J.-Y.; White, D. J.; Hartenstein, V.; Eliceiri, K.; Tomancak, P.; Cardona, A. Fiji: An Open-Source Platform for Biological-Image Analysis. *Nat Methods* **2012**, *9* (7), 676–682. https://doi.org/10.1038/nmeth.2019.

HRMS spectra

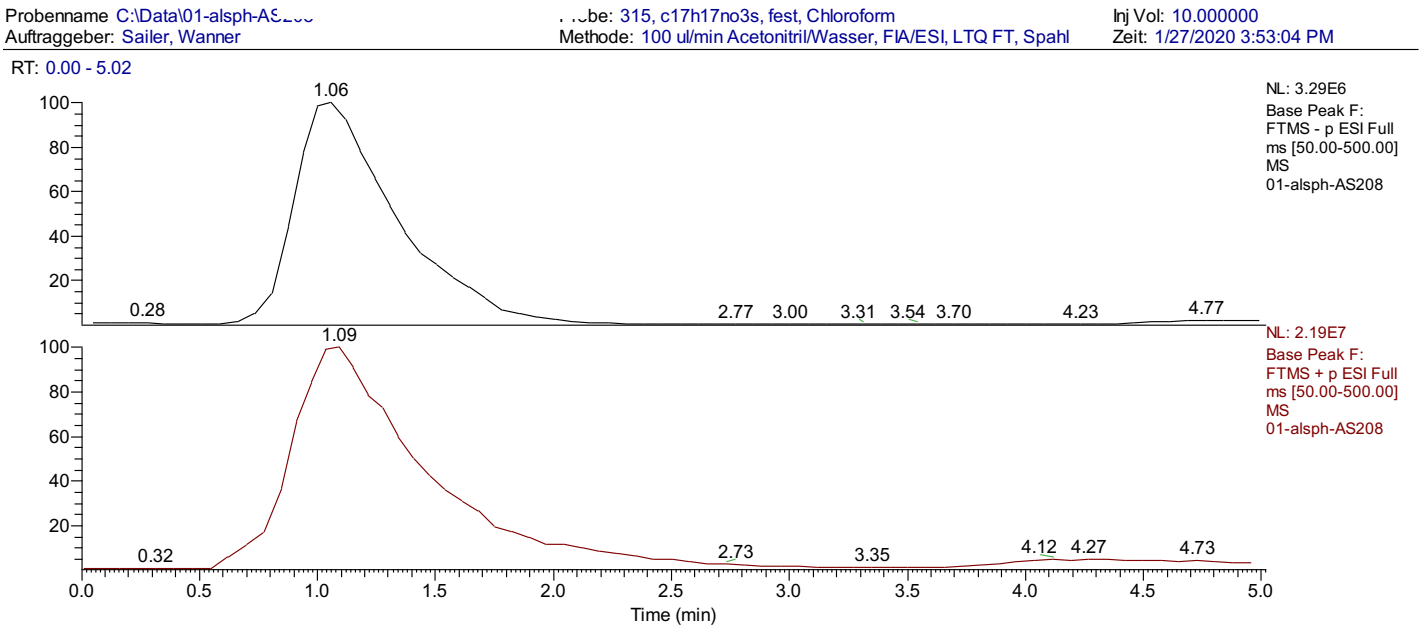

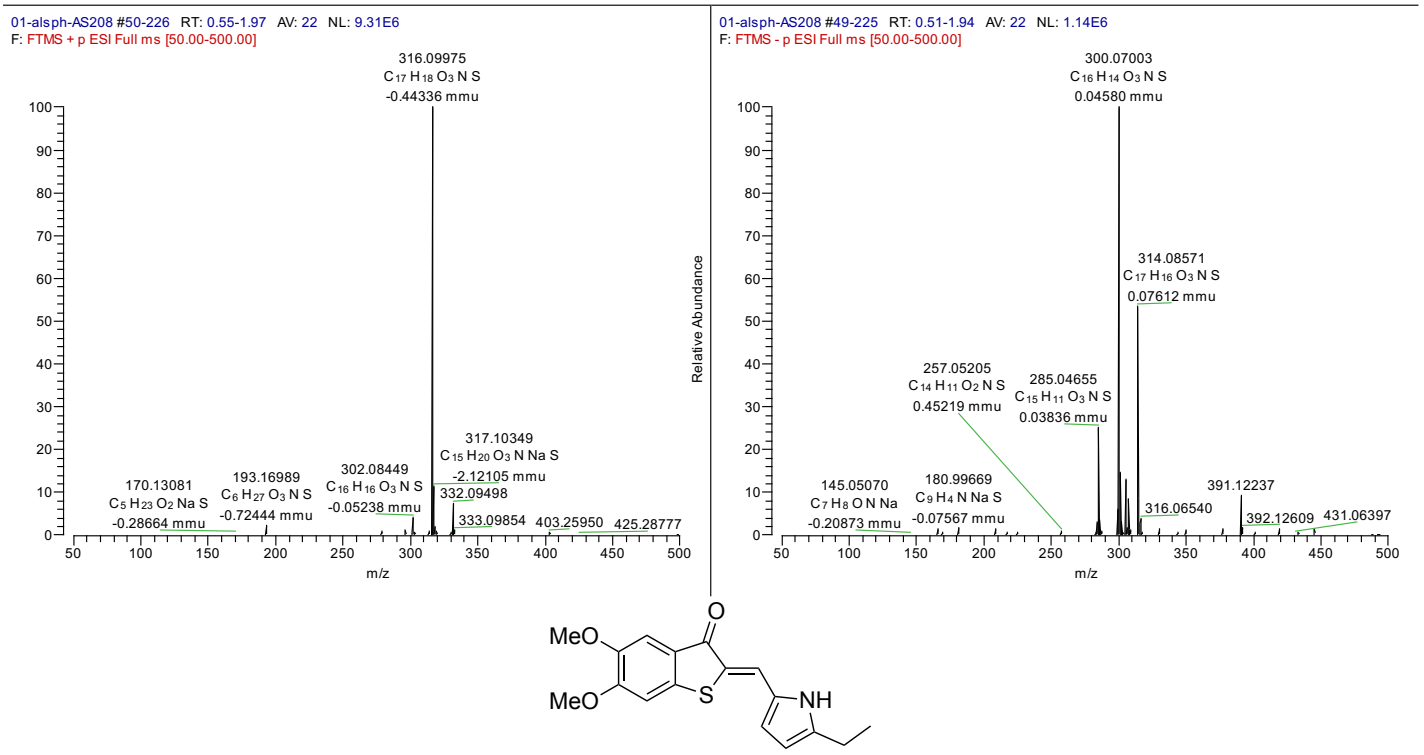

PHTub-1: ESI$^+$ **HRMS** for $C_{17}H_{18}NO_3S^+$ = $[M+H]^+$: calcd. m/z 316.10019, found m/z 316.09975, ESI$^-$ **HRMS** for $C_{17}H_{16}NO_3S^-$ = $[M-H]^-$: calcd. m/z 314.08564, found m/z 314.08571, ESI$^-$ **HRMS** for $C_{16}H_{14}NO_3S^-$ = $[M-CH_3]^-$: calcd. m/z 300.06999, found m/z 300.07003

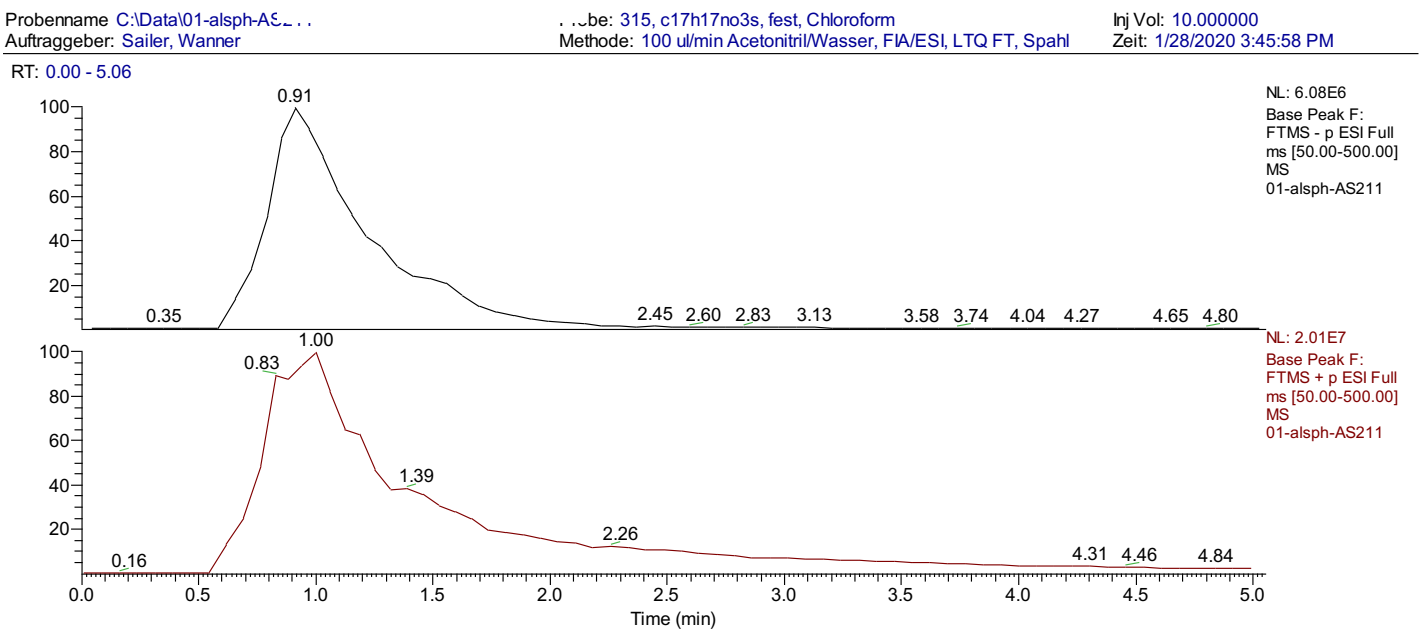

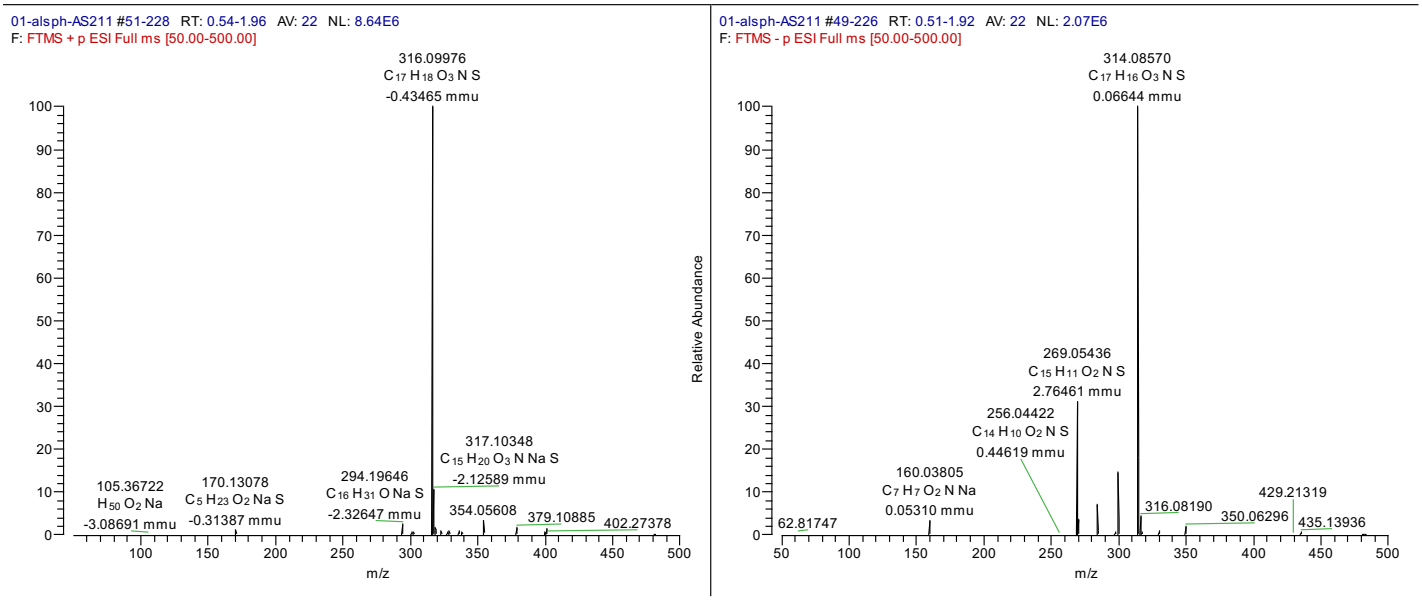

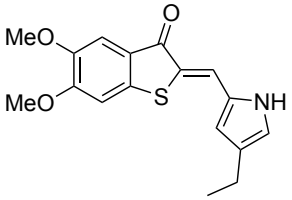

PHTub-2: ESI^+ **HRMS** for $C_{17}H_{18}NO_3S^+ = [M+H]^+$: calcd. m/z 316.10019, found m/z 316.09976, ESI^- **HRMS** for $C_{17}H_{16}NO_3S^- = [M-H]^-$: calcd. m/z 314.08564, found m/z 314.08570.

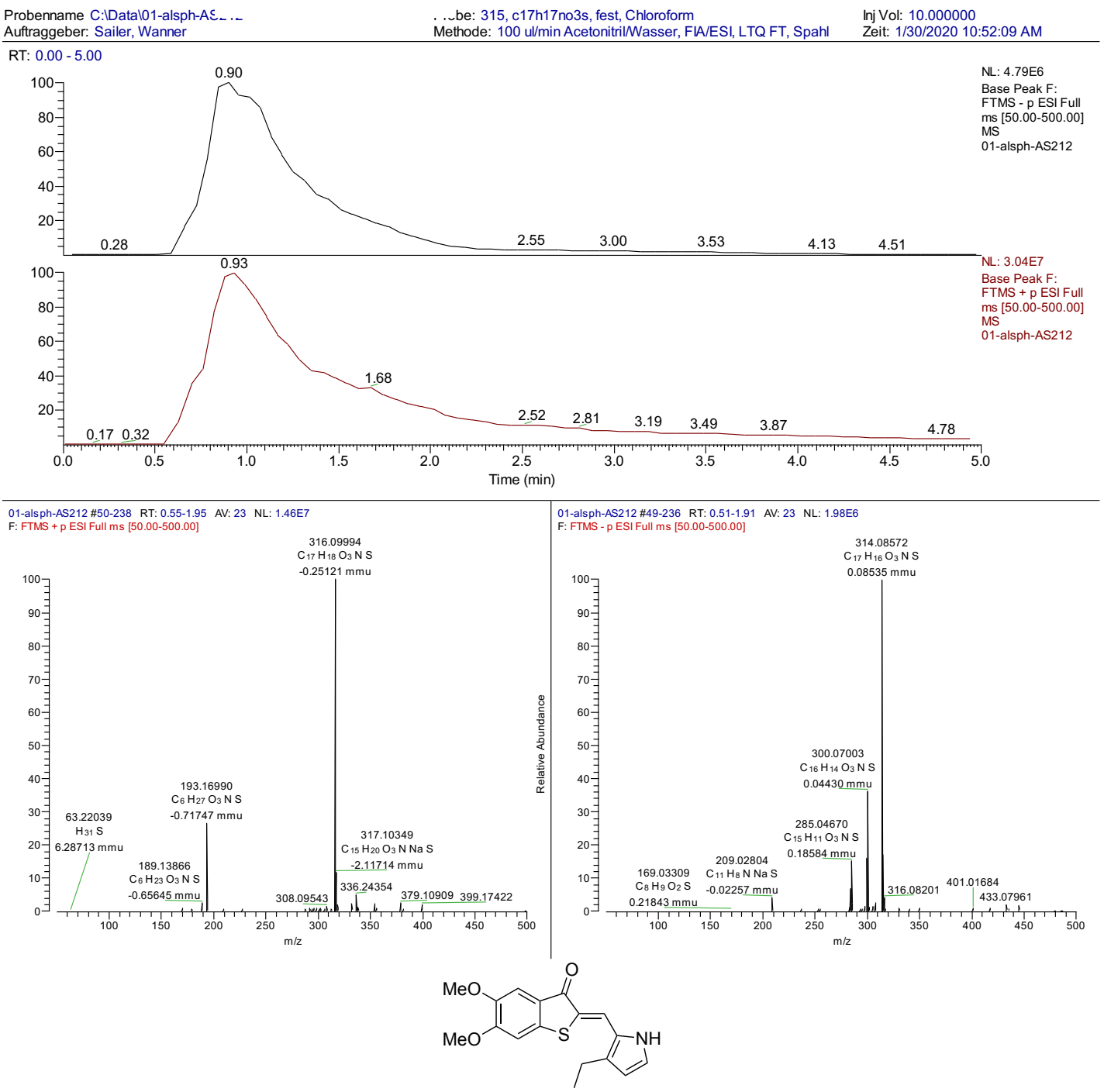

PHTub-3: ESI$^+$ **HRMS** for $C_{17}H_{18}NO_3S^+$ = $[M+H]^+$: calcd. m/z 316.10019, found m/z 316.09994, ESI$^-$ **HRMS** for $C_{17}H_{16}NO_3S^-$ = $[M-H]^-$: calcd. m/z 314.08564, found m/z 314.08572.

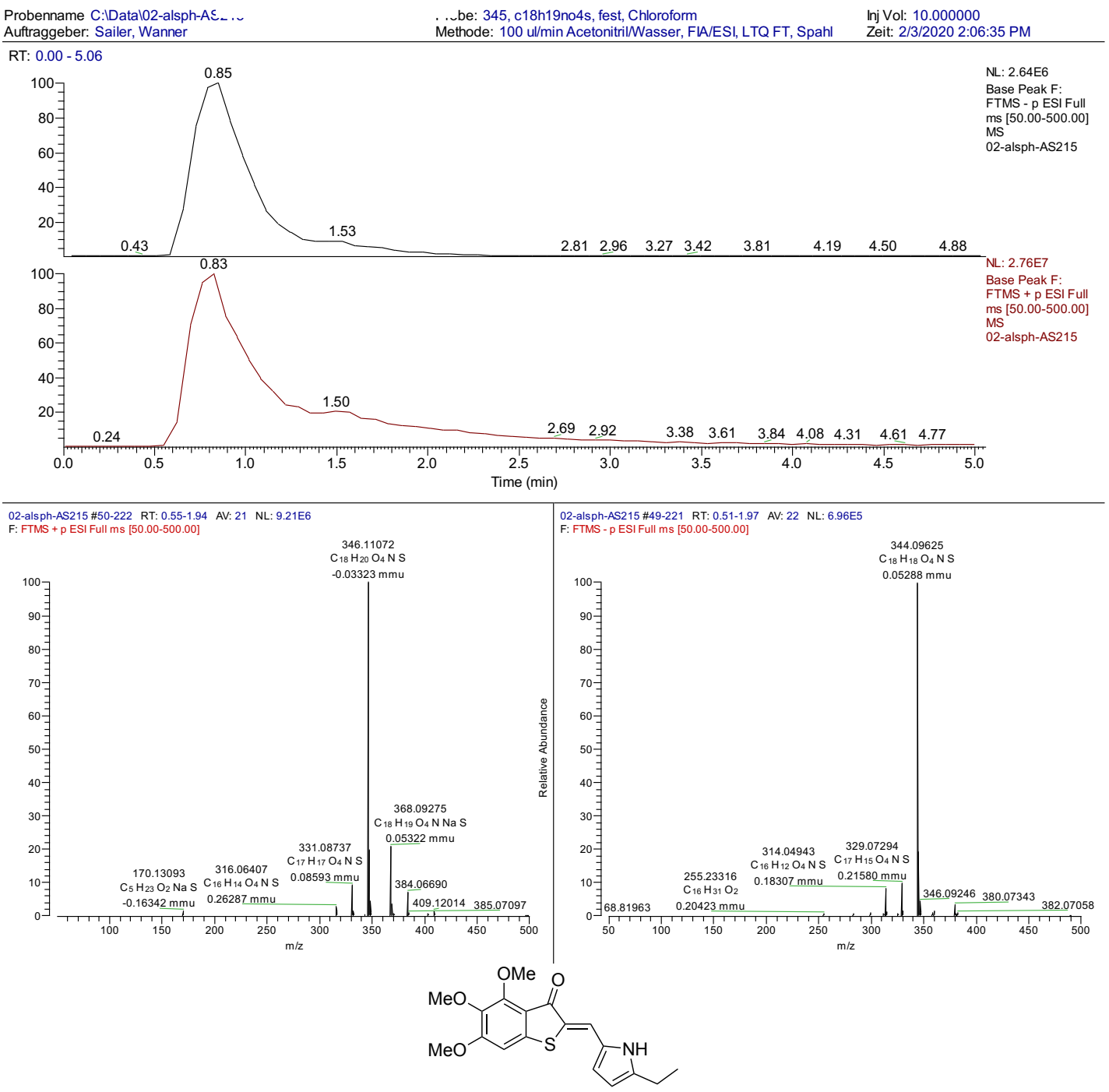

PHTub-4: ESI$^+$ **HRMS** for $C_{18}H_{20}NO_4S^+$= $[M+H]^+$: calcd. m/z 346.11076, found m/z 346.11072, ESI$^-$ **HRMS** for $C_{18}H_{18}NO_4S^-$ = $[M-H]^-$: calcd. m/z 344.09620, found m/z 344.09625.

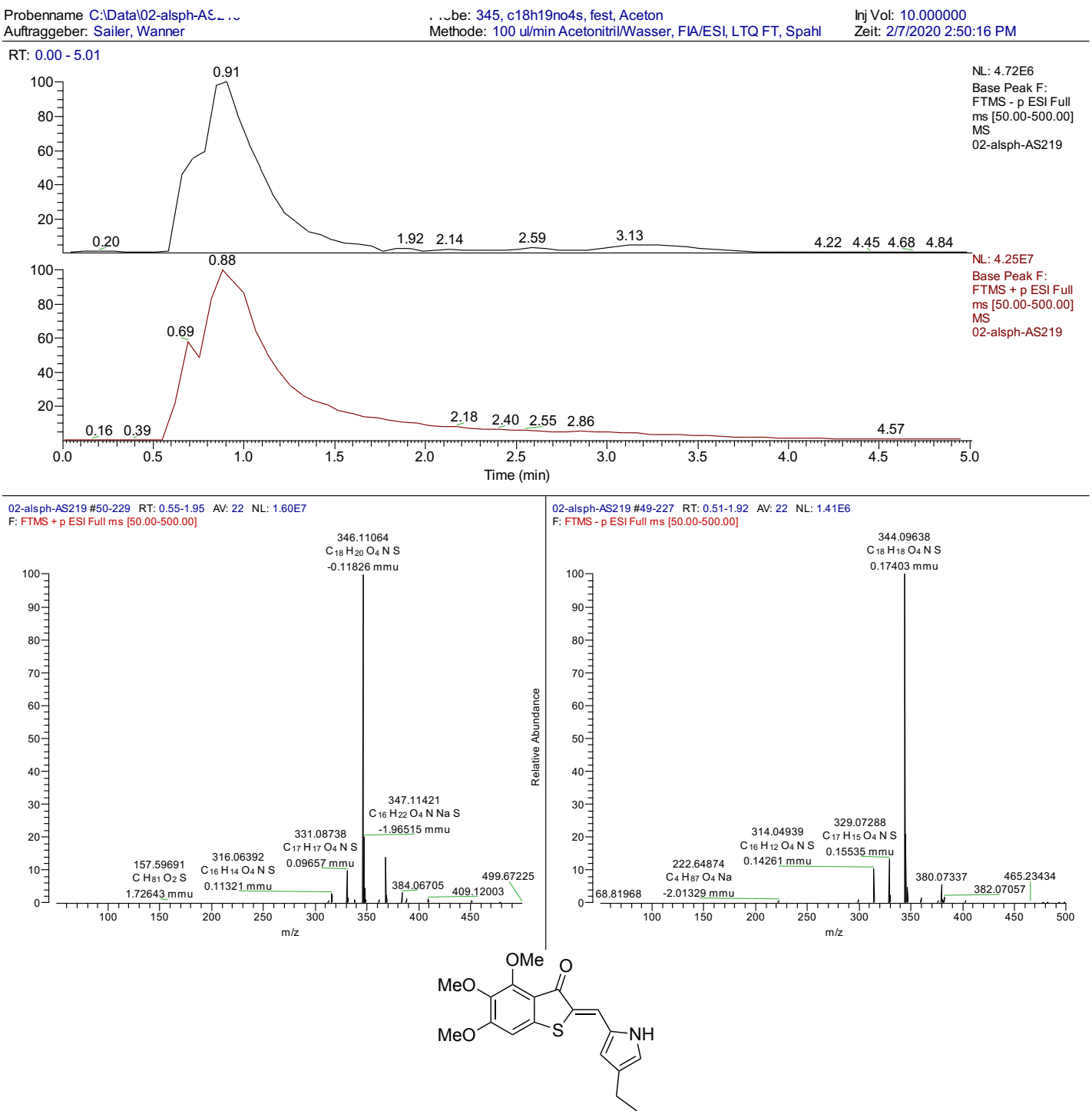

PHTub-5: ESI$^+$ **HRMS** for $C_{18}H_{20}NO_4S^+ = [M+H]^+$: calcd. m/z 346.11076, found m/z 346.11064, ESI$^-$ **HRMS** for $C_{18}H_{18}NO_4S^- = [M-H]^-$: calcd. m/z 344.09620, found m/z 344.09638.

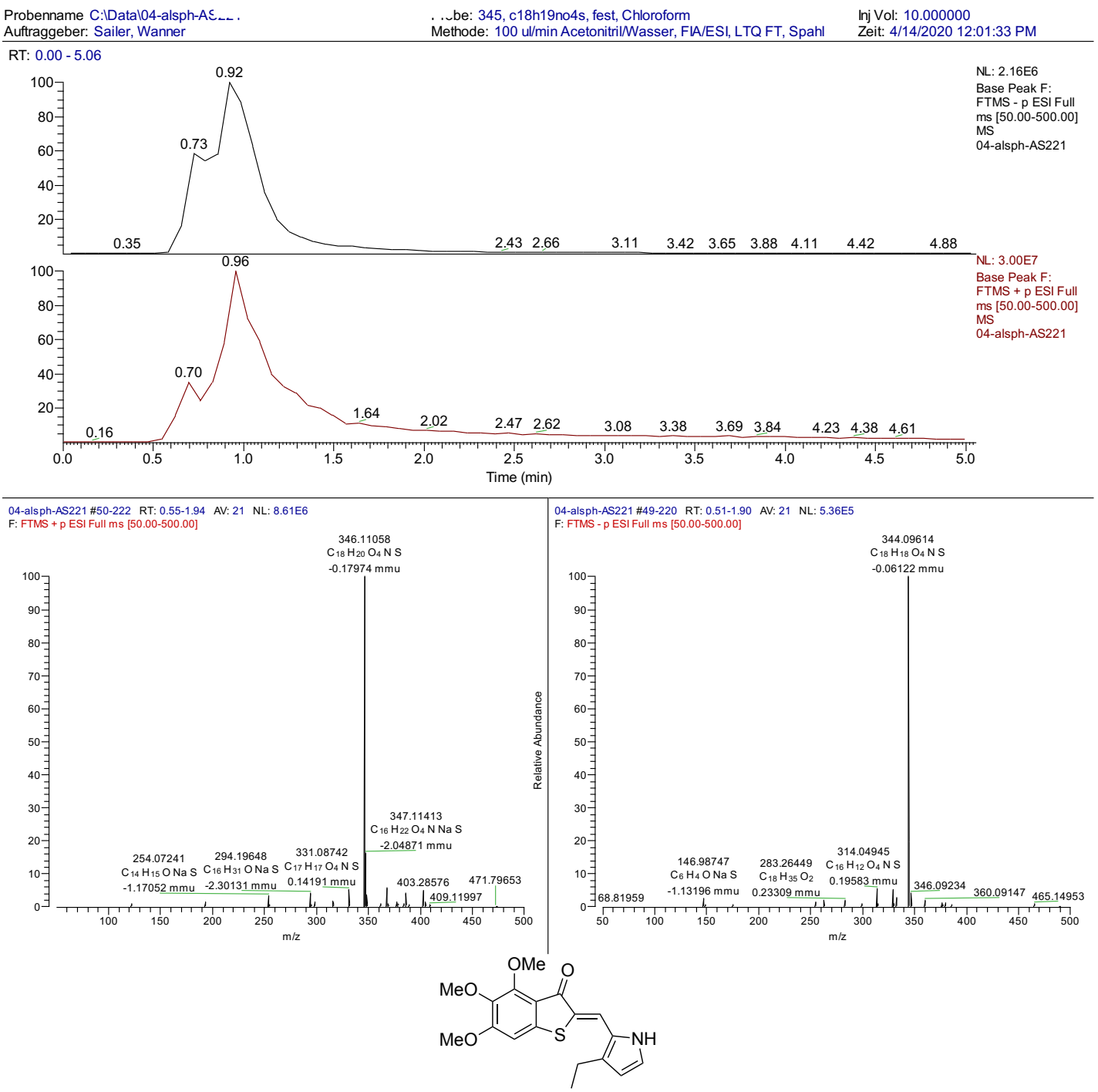

PHTub-6: ESI$^+$ **HRMS** for $C_{18}H_{20}NO_4S^+$ = $[M+H]^+$: calcd. m/z 346.11076, found m/z 346.11058, ESI$^-$ **HRMS** for $C_{18}H_{18}NO_4S^-$ = $[M-H]^-$: calcd. m/z 344.09620, found m/z 344.09614.

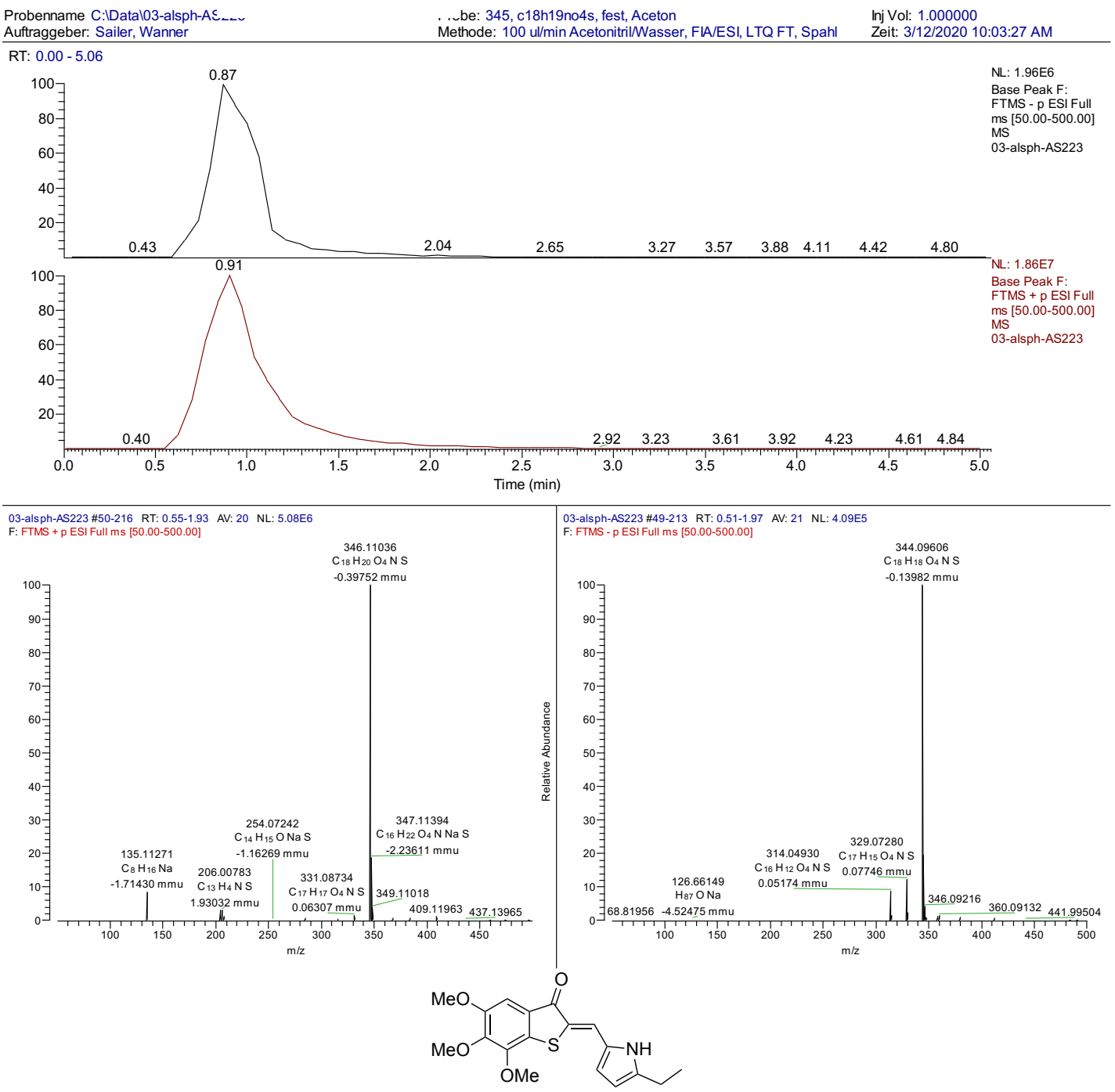

PHTub-7: ESI$^+$ **HRMS** for $C_{18}H_{20}NO_4S^+$ = $[M+H]^+$: calcd. m/z 346.11076, found m/z 346.11036, ESI$^-$ **HRMS** for $C_{18}H_{18}NO_4S^-$ = $[M-H]^-$: calcd. m/z 344.09620, found m/z 344.09606.

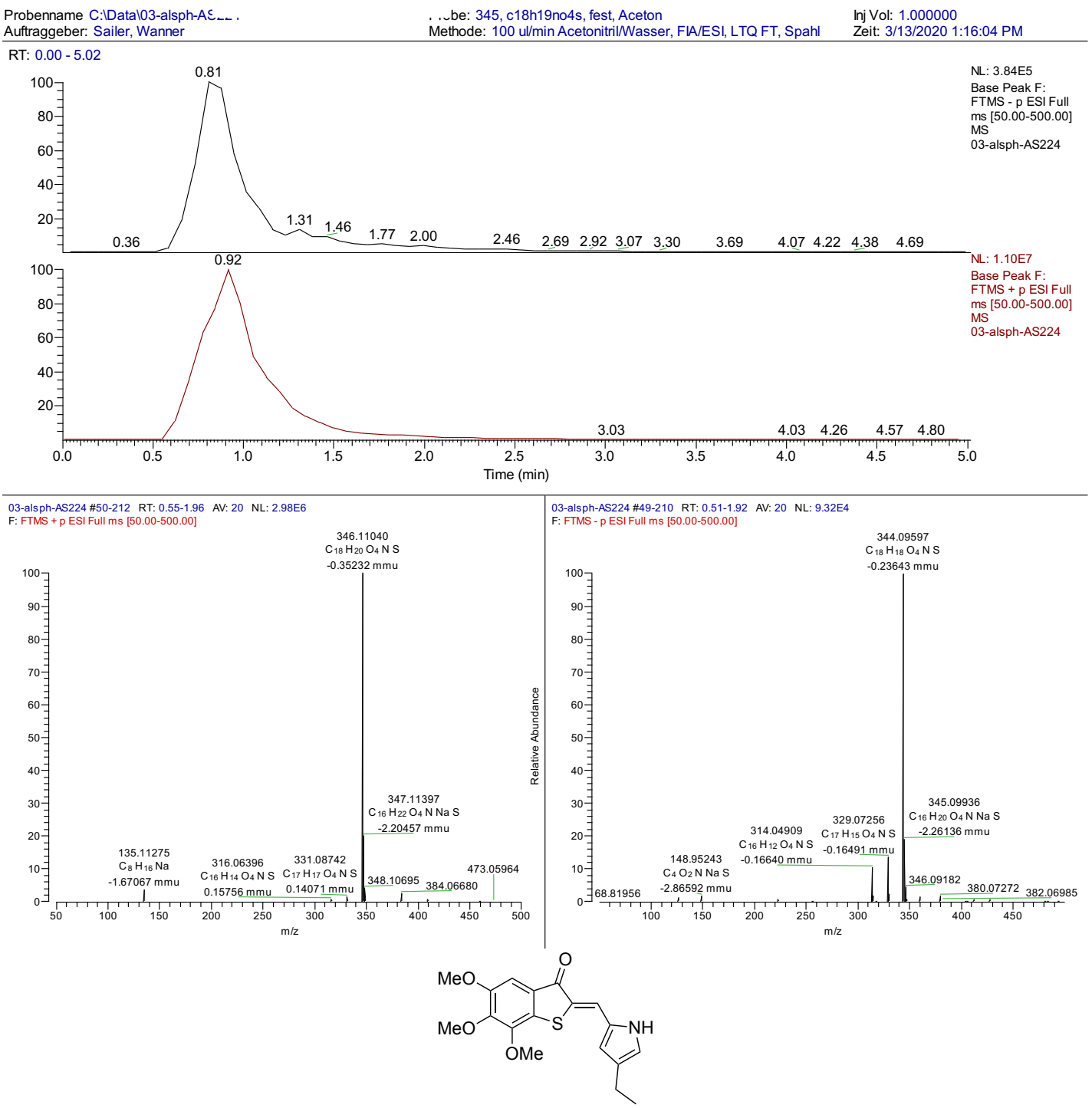

PHTub-8: ESI$^+$ **HRMS** for $C_{18}H_{20}NO_4S^+$ = $[M+H]^+$: calcd. m/z 346.11076, found m/z 346.11040, ESI$^-$ **HRMS** for $C_{18}H_{18}NO_4S^-$ = $[M-H]^-$: calcd. m/z 344.09620, found m/z 344.09597.

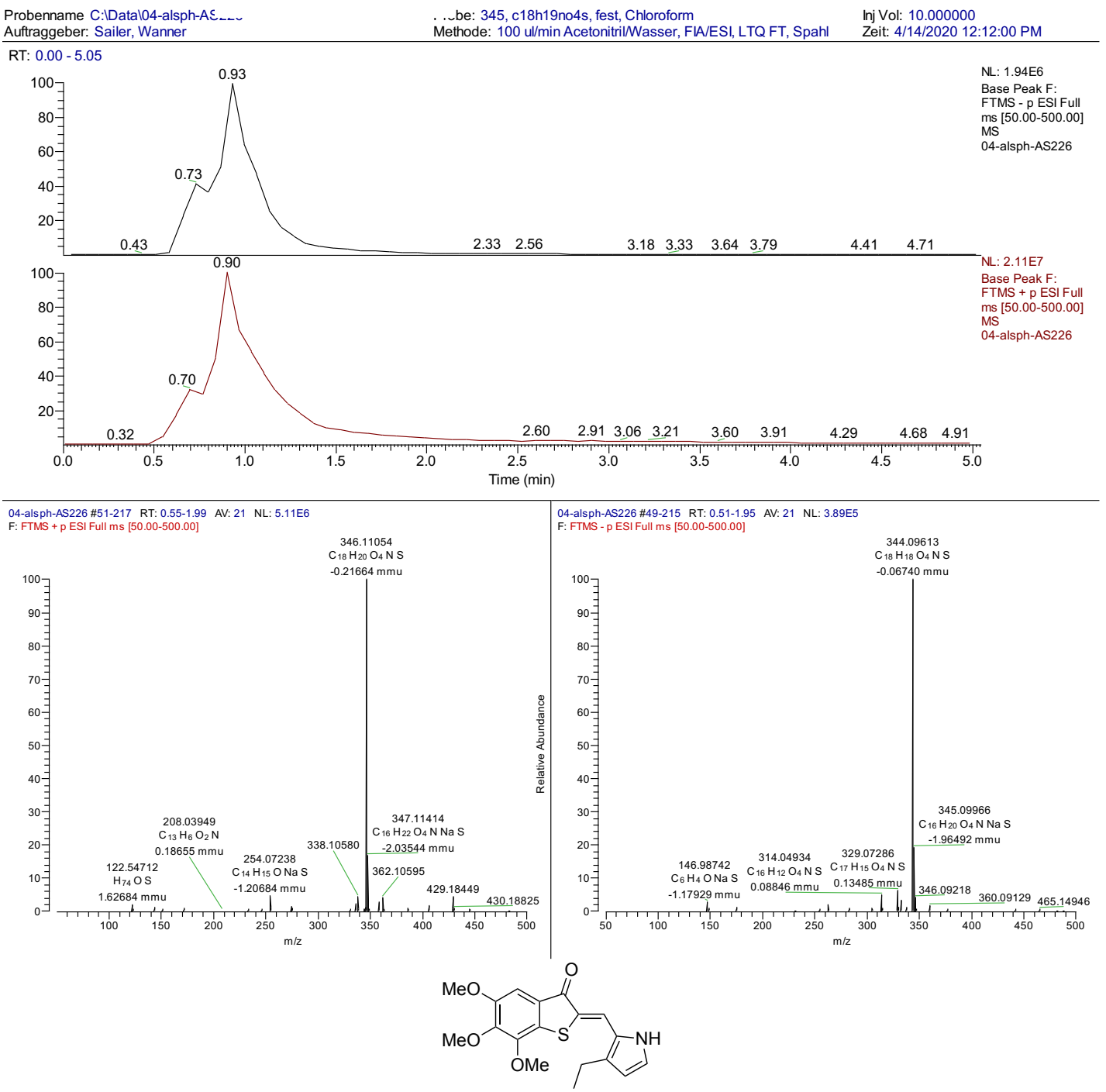

PHTub-9: ESI$^+$ **HRMS** for $C_{18}H_{20}NO_4S^+$ = $[M+H]^+$: calcd. m/z 346.11076, found m/z 346.11054, ESI$^-$ **HRMS** for $C_{18}H_{18}NO_4S^-$ = $[M-H]^-$: calcd. m/z 344.09620, found m/z 344.09613.

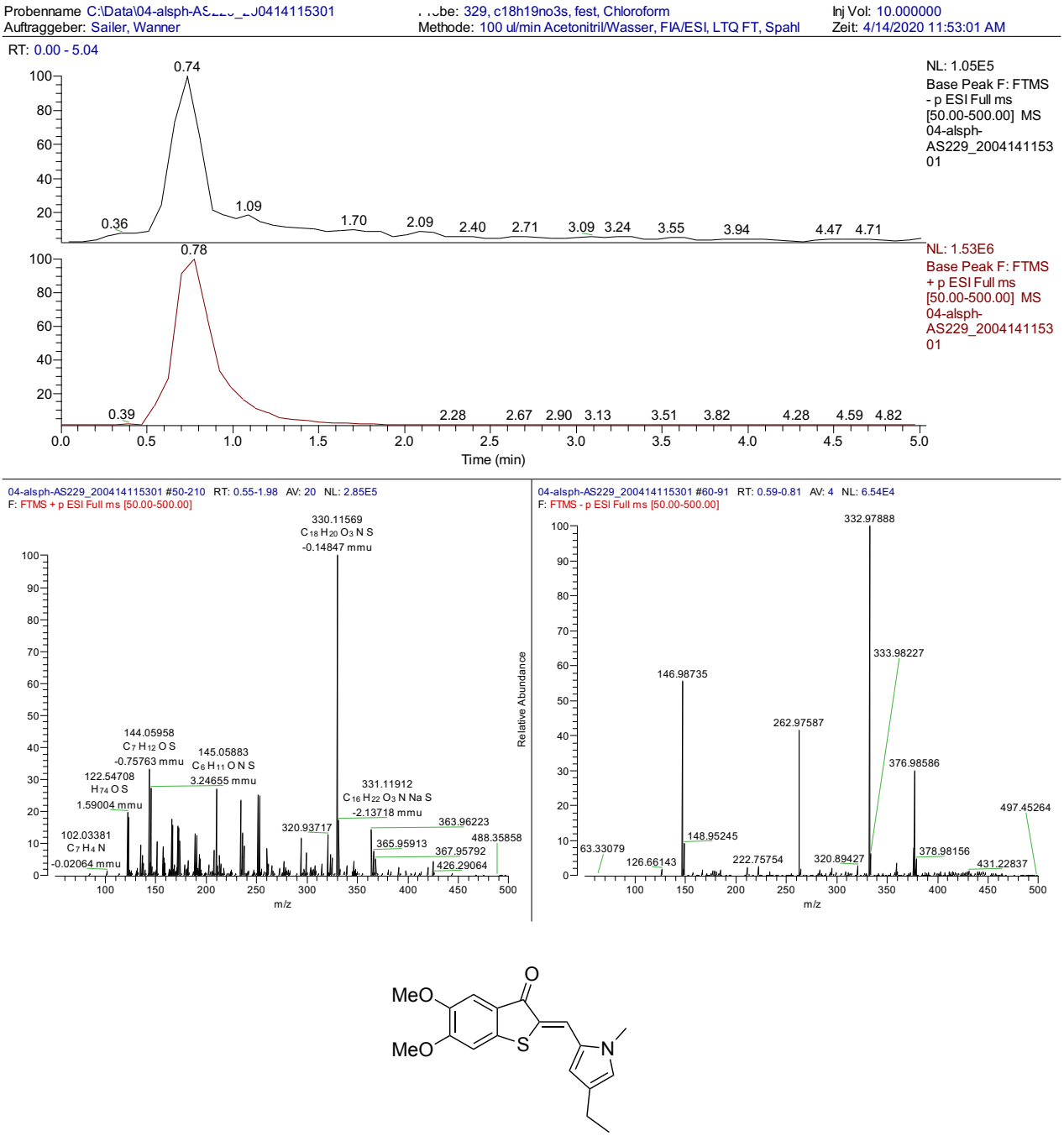

PHTub-NMe: ESI$^+$ **HRMS** for $C_{18}H_{20}NO_3S^+$ = $[M+H]^+$: calcd. m/z 330.11584, found m/z 330.11569.

NMR spectra

2-Ethyl-1*H*-pyrrole (S1)

^{1}H-NMR ($CDCl_3$, 400 MHz)

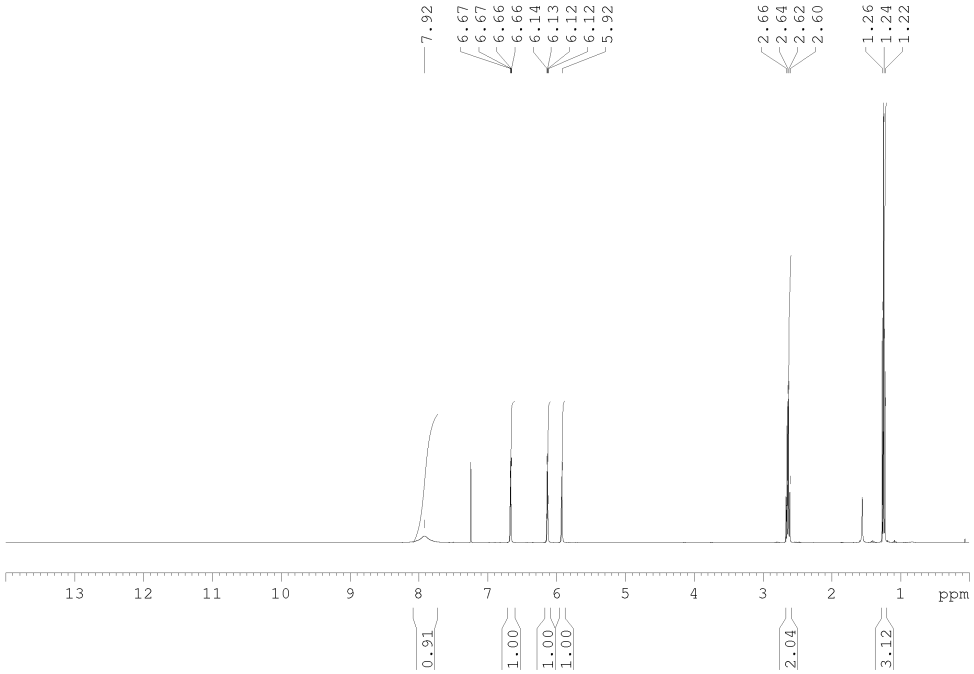

^{13}C-NMR ($CDCl_3$, 100 MHz)

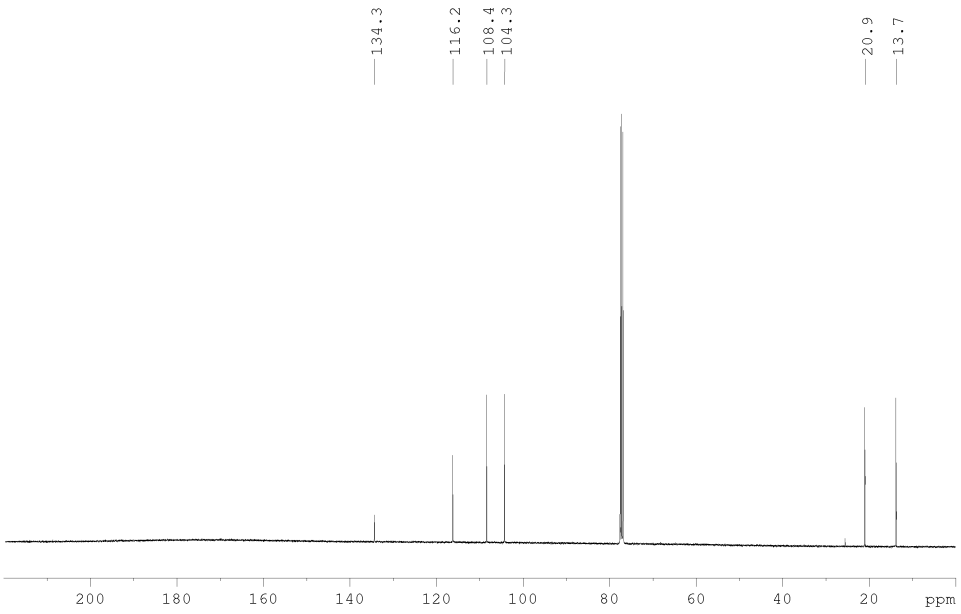

5-Ethyl-1*H*-pyrrole-2-carbaldehyde (S2)

^{1}H-NMR ($CDCl_3$, 400 MHz)

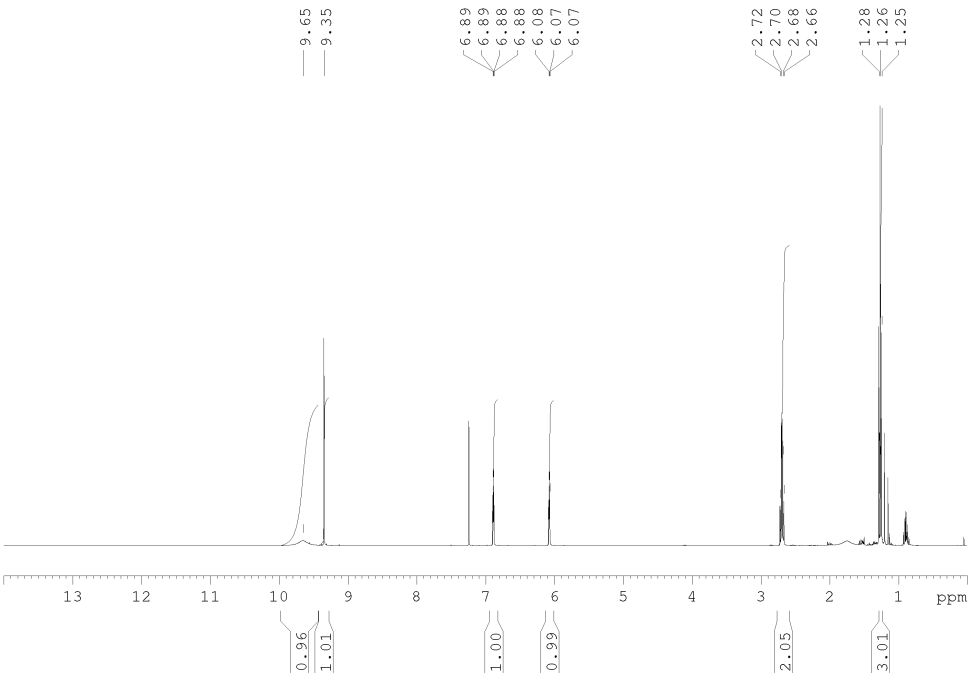

^{13}C-NMR ($CDCl_3$, 100 MHz)

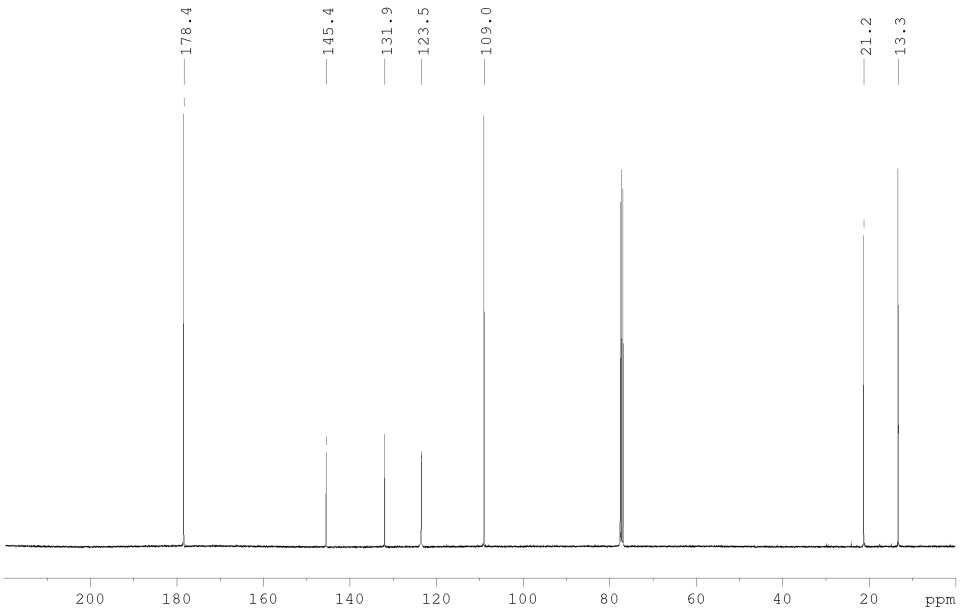

1-Tosyl-1*H*-pyrrole (S3)

^{1}H-NMR ($CDCl_3$, 400 MHz)

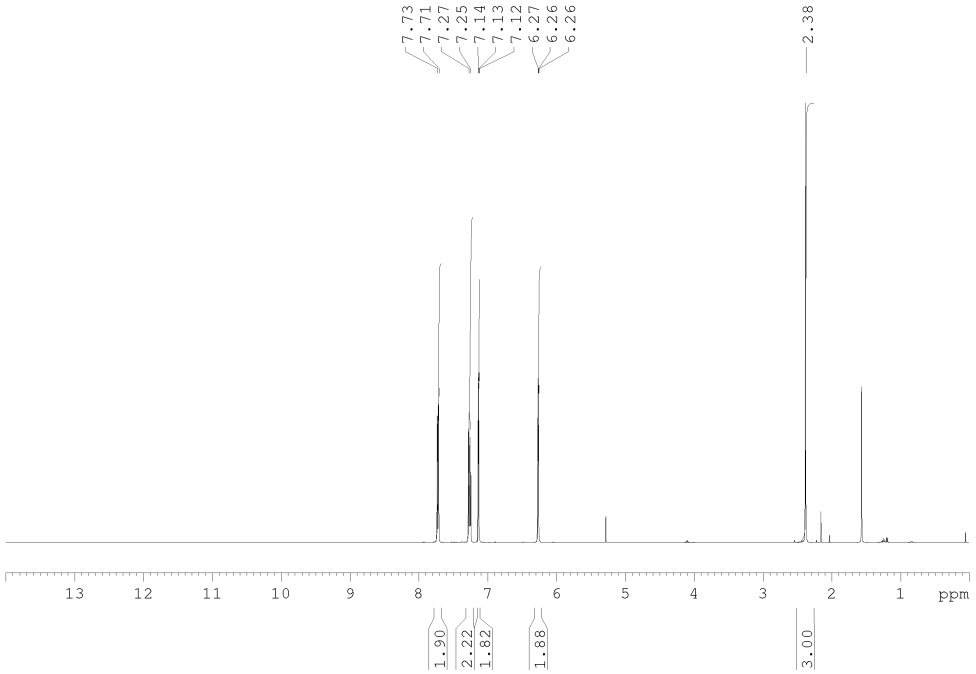

^{13}C-NMR ($CDCl_3$, 100 MHz)

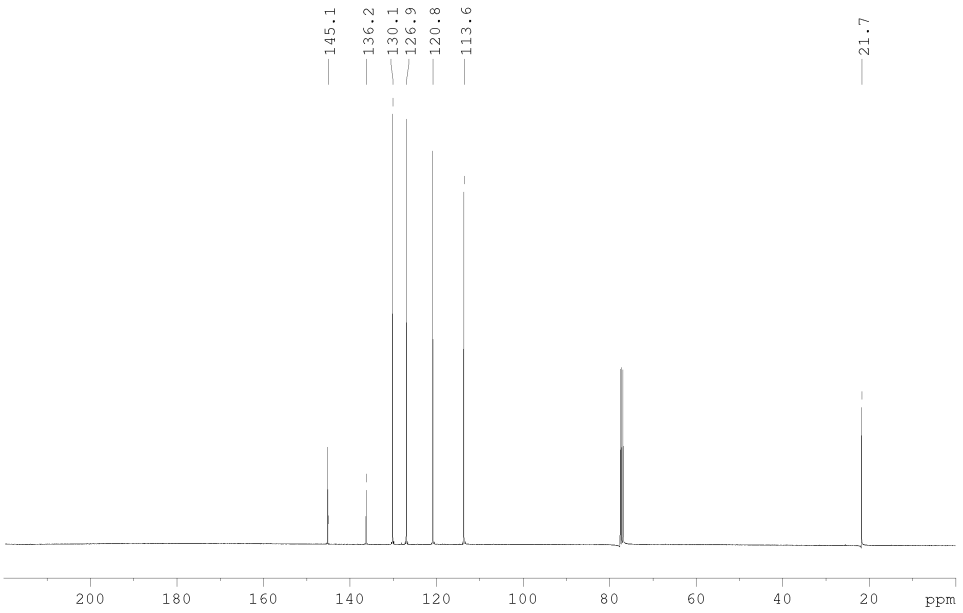

1-(1-Tosyl-1*H*-pyrrol-3-yl)ethan-1-one (S4)

^{1}H-NMR ($CDCl_3$, 400 MHz)

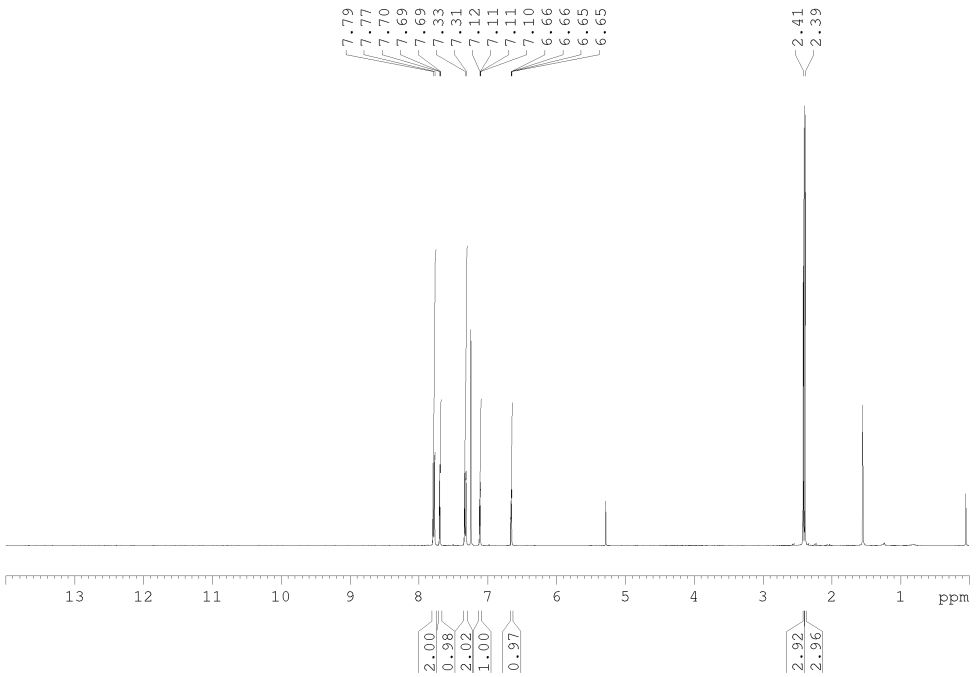

^{13}C-NMR ($CDCl_3$, 100 MHz)

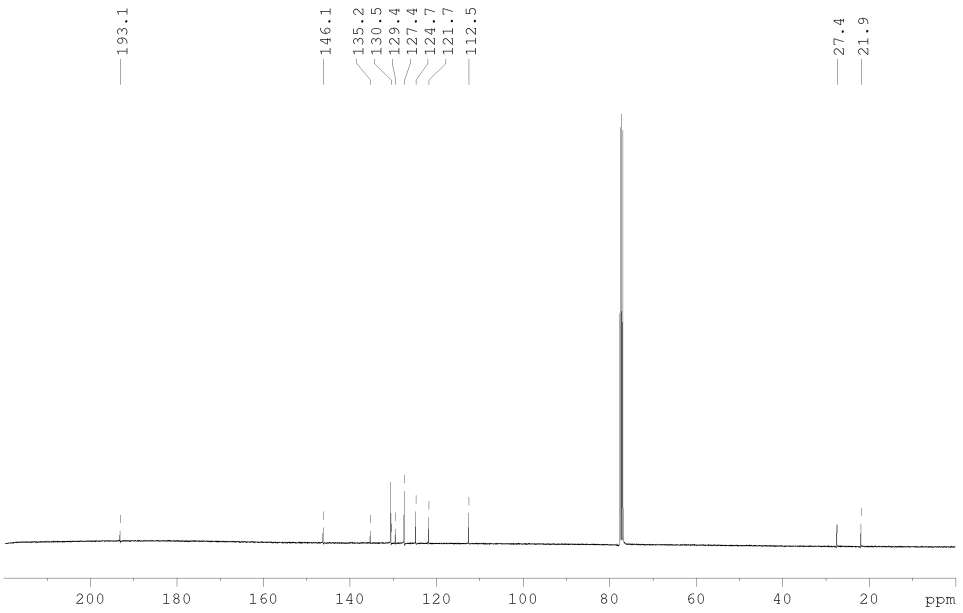

1-(1*H*-pyrrol-3-yl)ethan-1-one (S5)

^{1}H-NMR ($CDCl_3$,400 MHz)

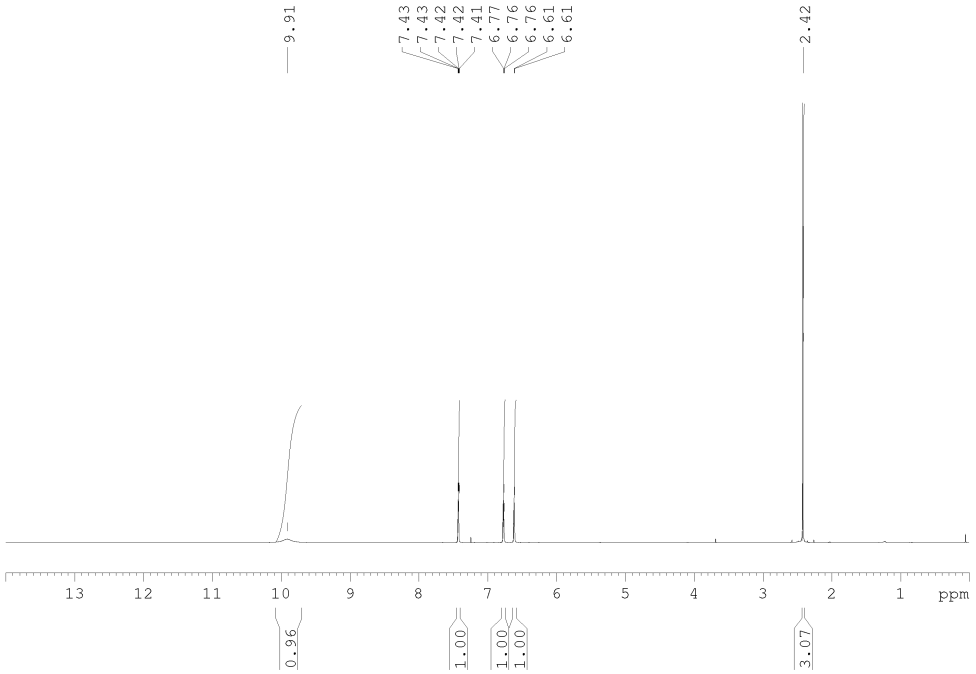

^{13}C-NMR (CDCl3, 100 MHz)

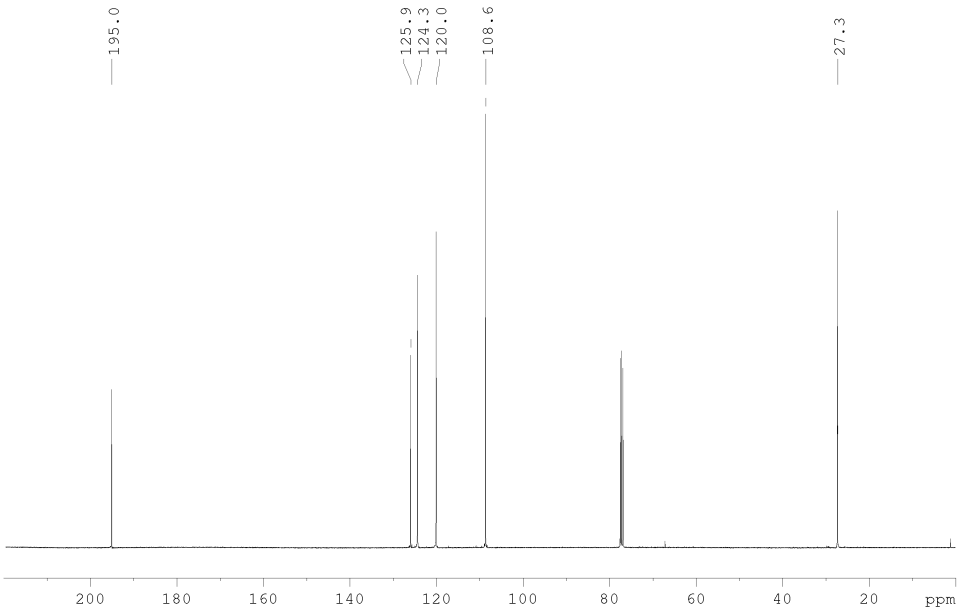

3-Ethyl-1*H*-pyrrole (S6)

^{1}H-NMR ($CDCl_3$, 400 MHz)

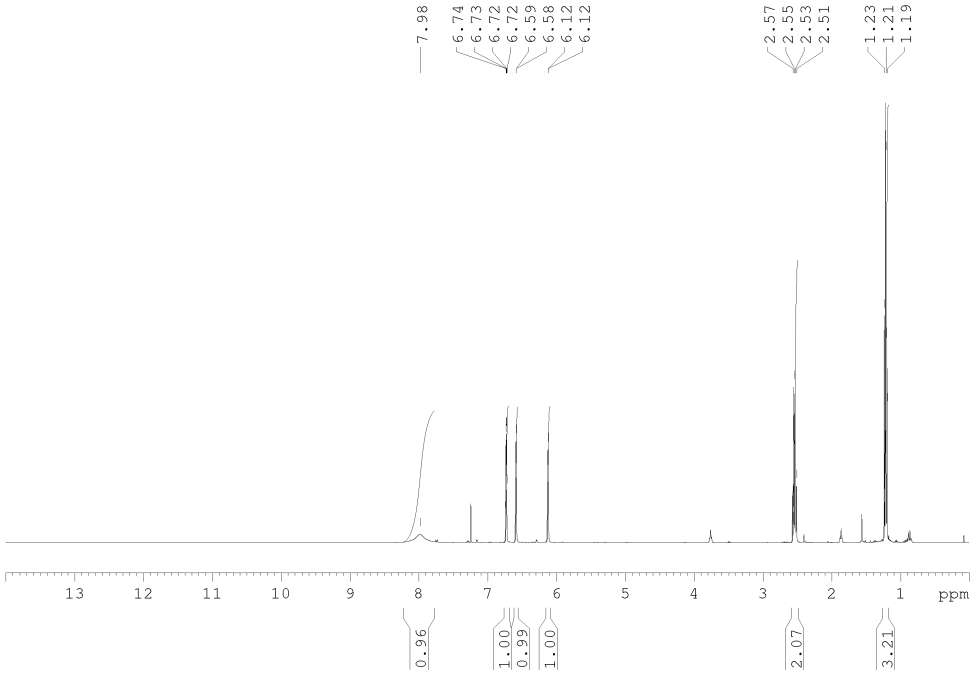

^{13}C-NMR ($CDCl_3$, 100 MHz)

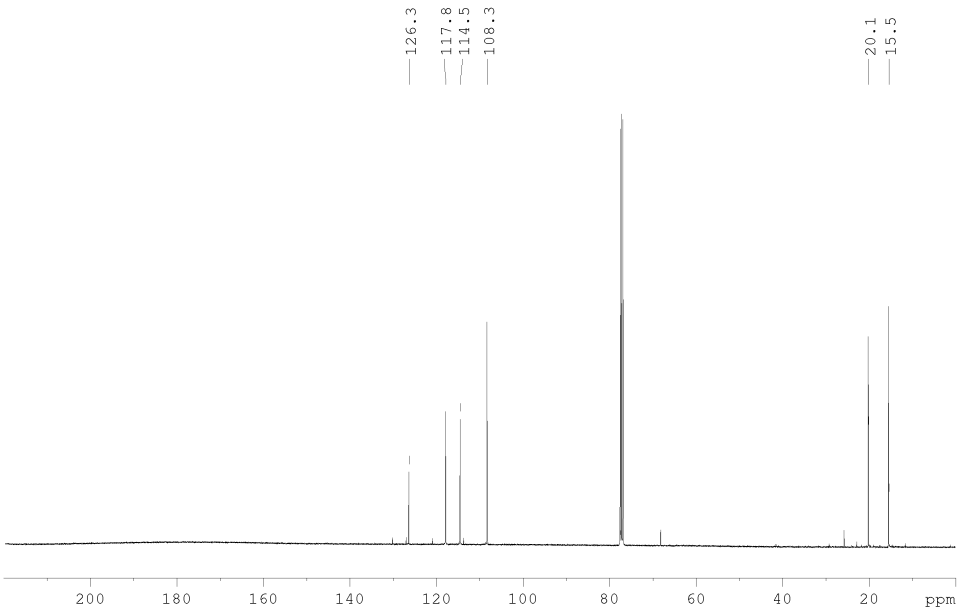

4-Ethyl-1*H*-pyrrole-2-carbaldehyde (S7)

^{1}H-NMR ($CDCl_3$, 400 MHz)

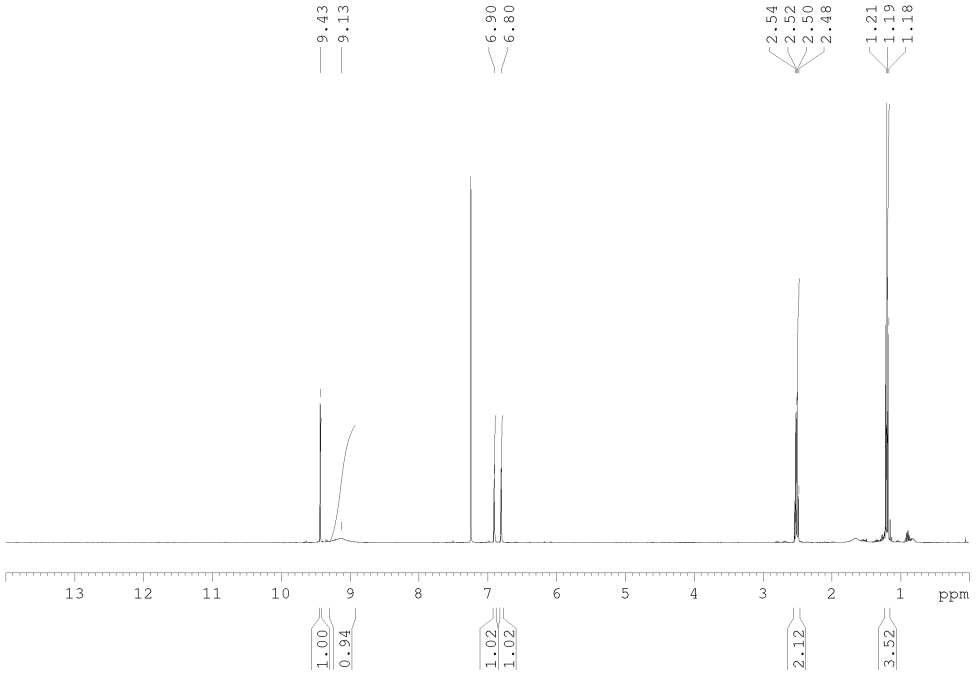

^{13}C-NMR ($CDCl_3$, 100 MHz)

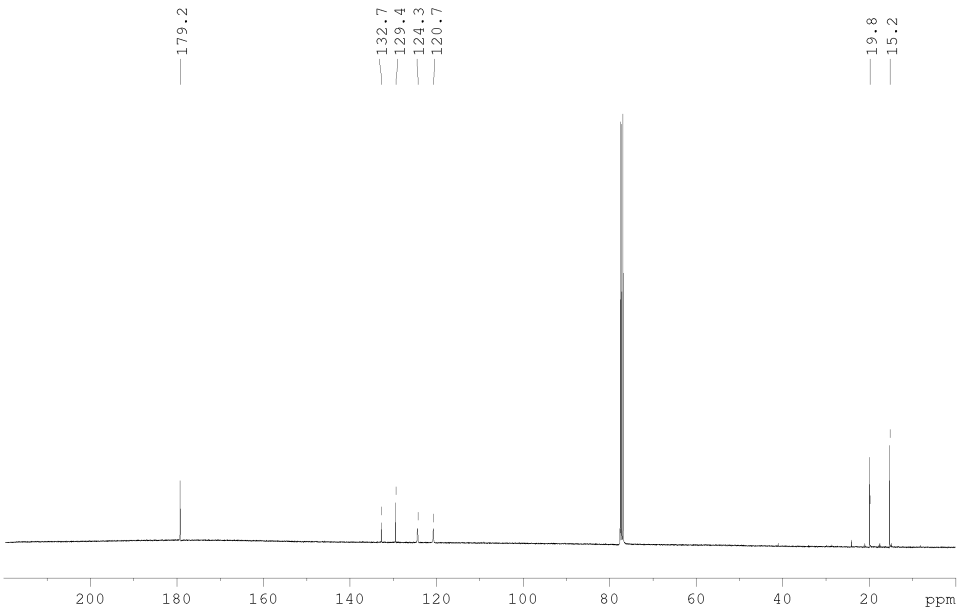

3-Ethyl-1*H*-pyrrole-2-carbaldehyde (S8)

^{1}H-NMR ($CDCl_3$, 400 MHz)

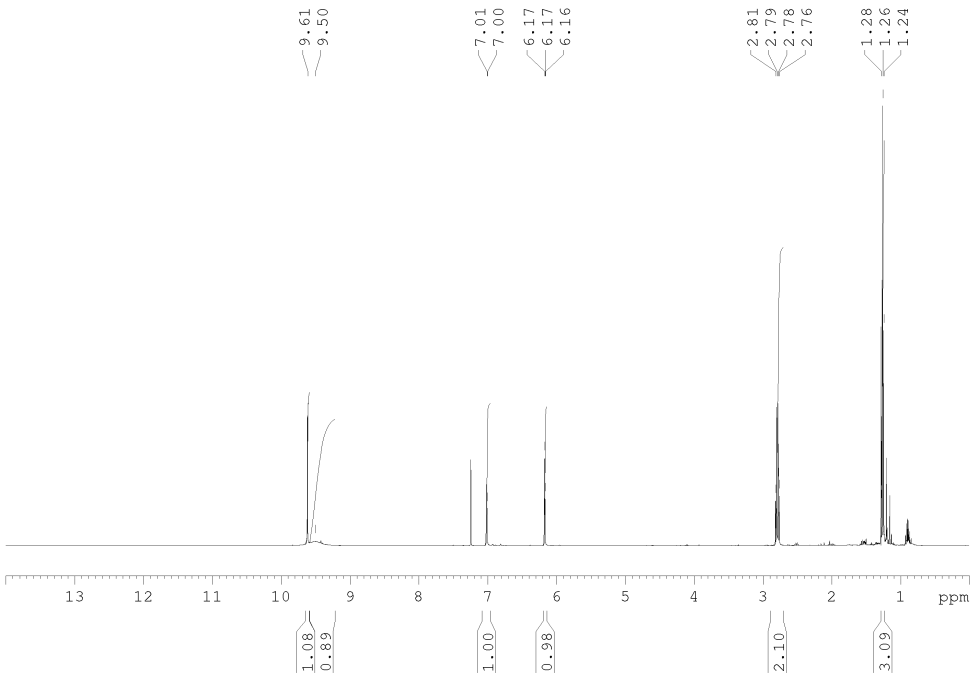

^{13}C-NMR ($CDCl_3$, 100 MHz)

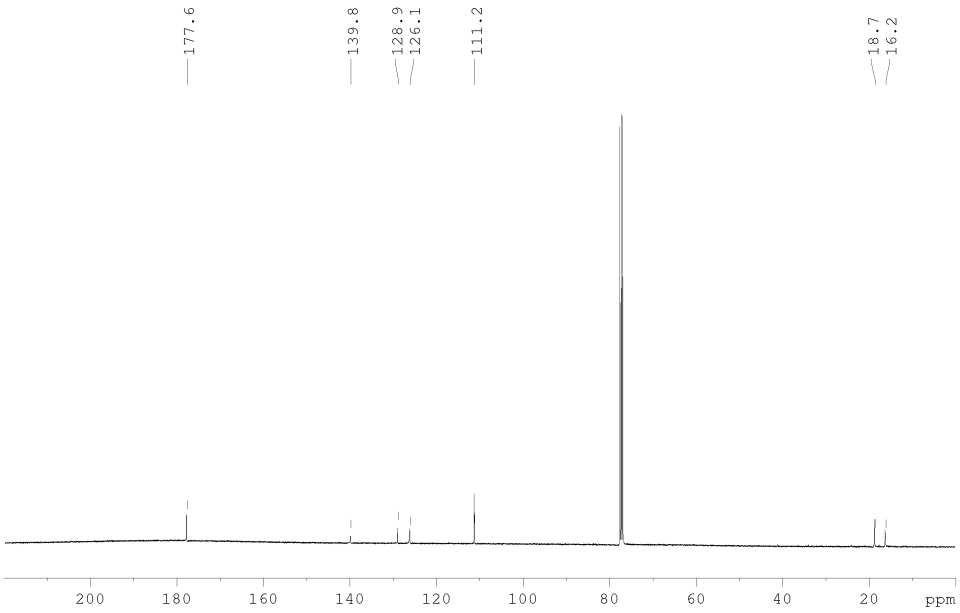

2-((5-ethyl-1*H*-pyrrol-2-yl)methylene)-5,6-dimethoxybenzo[*b*]thiophen-3(2*H*)-one (PHTub-1)

^{1}H-NMR (DMSO-D_6, 400 MHz)

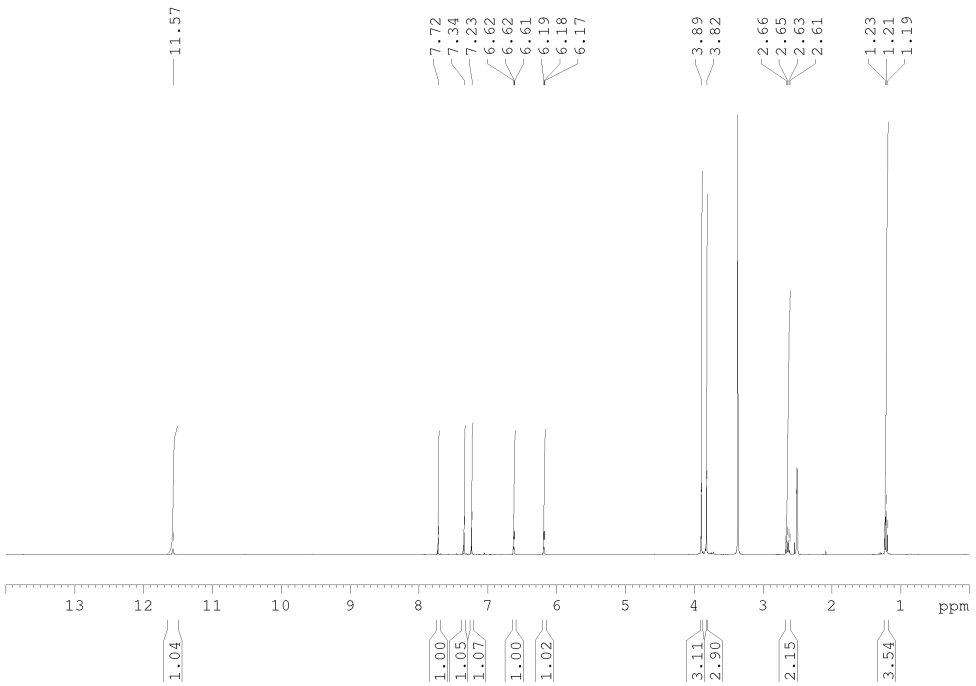

^{13}C-NMR (DMSO-D_6, 100 MHz)

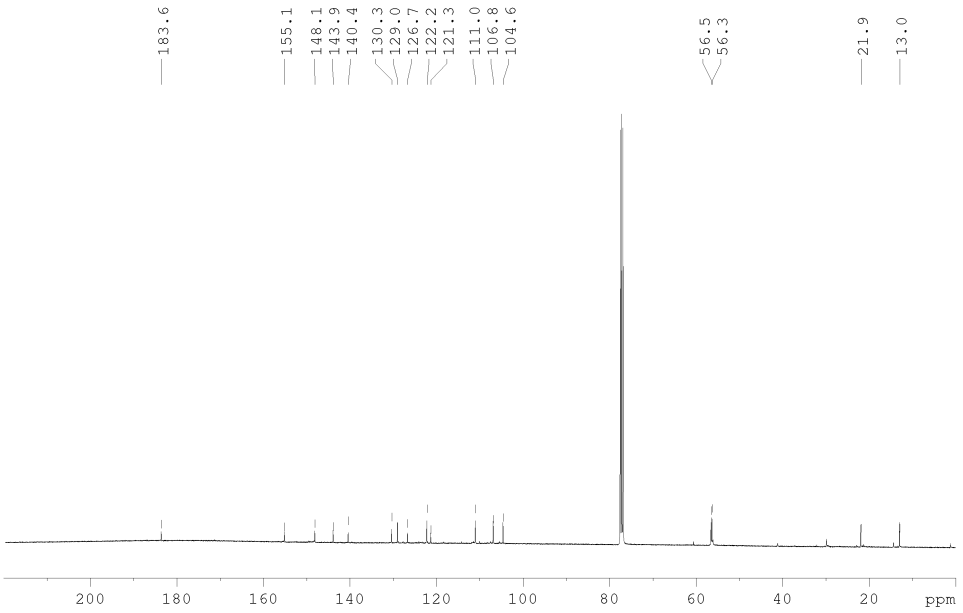

2-((4-Ethyl-1*H*-pyrrol-2-yl)methylene)-5,6-dimethoxybenzo[*b*]thiophen-3(2*H*)-one (PHTub-2)

^{1}H-NMR (MeOD, 400 MHz)

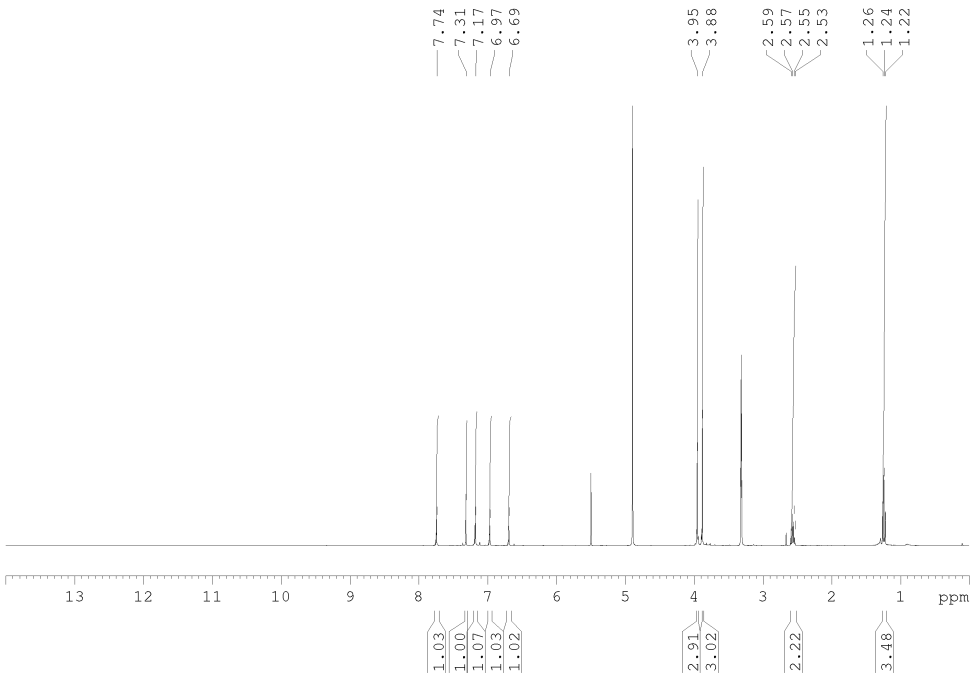

^{13}C-NMR (DMSO-D_6, 100 MHz)

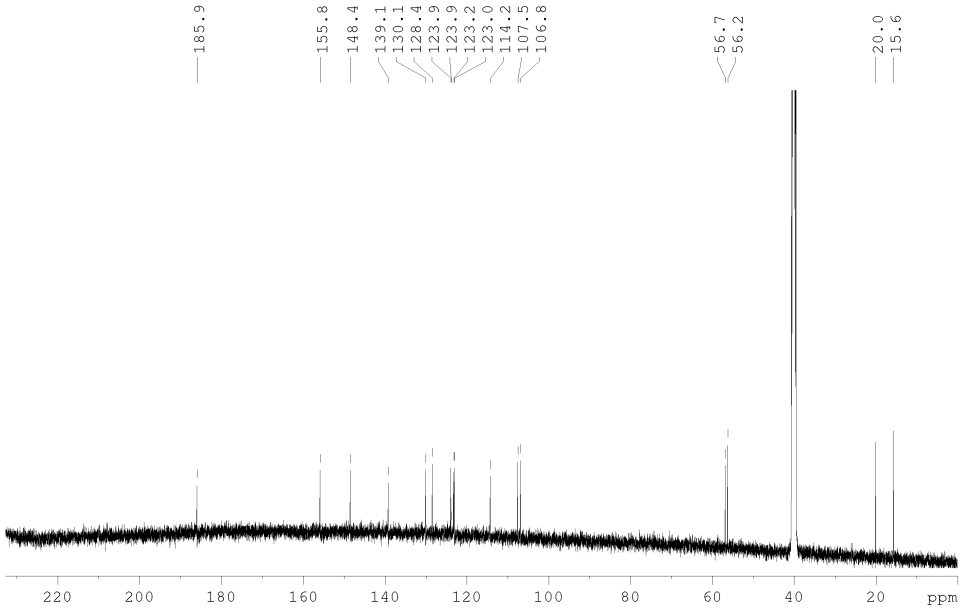

2-((3-ethyl-1*H*-pyrrol-2-yl)methylene)-5,6-dimethoxybenzo[*b*]thiophen-3(2*H*)-one (PHTub-3)

^{1}H-NMR (D_3COD, 400 MHz)

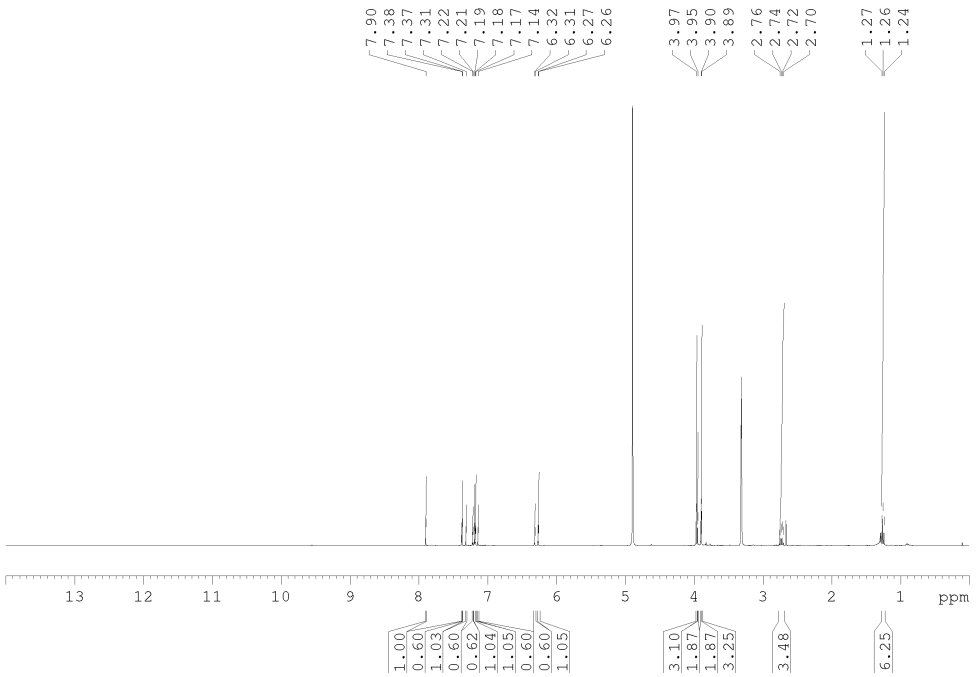

^{13}C-NMR (DMSO-D_6, 100 MHz)

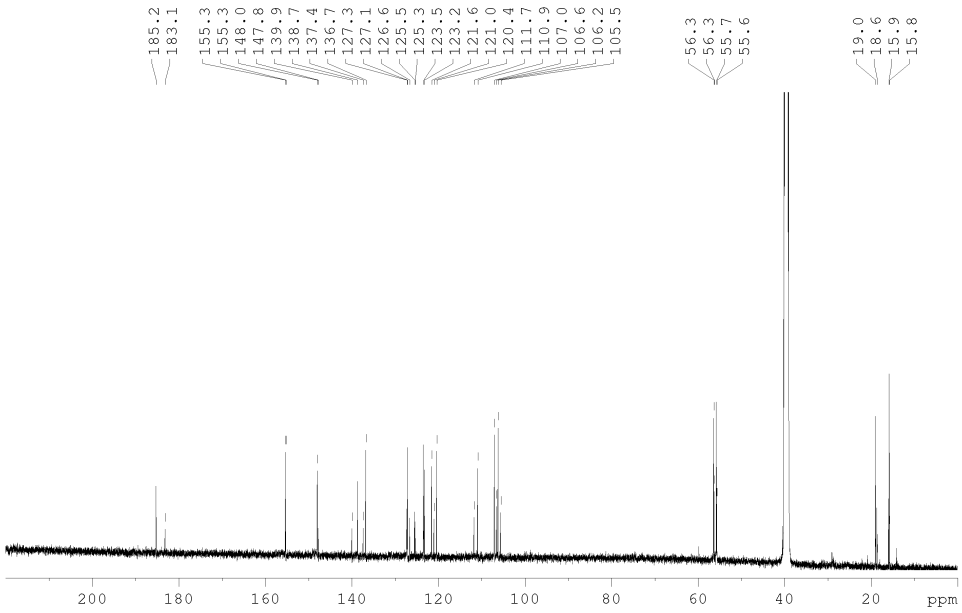

2-((5-Ethyl-1*H*-pyrrol-2-yl)methylene)-4,5,6-trimethoxybenzo[*b*]thiophen-3(2*H*)-one (PHTub-4)

^{1}H-NMR (DMSO-D_6, 400 MHz)

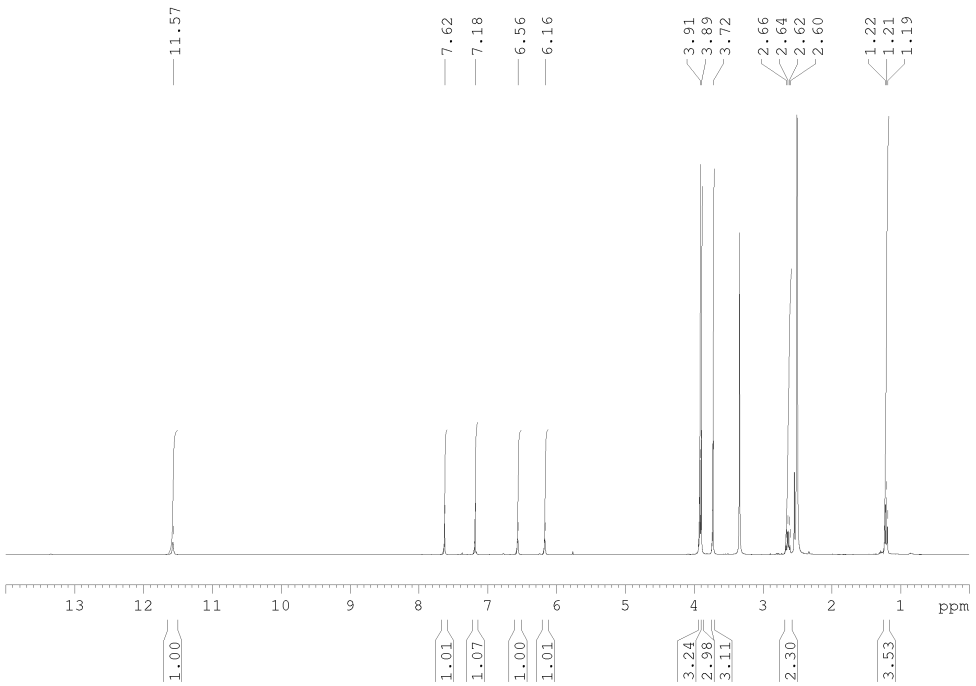

^{13}C-NMR (DMSO-D_6, 100 MHz)

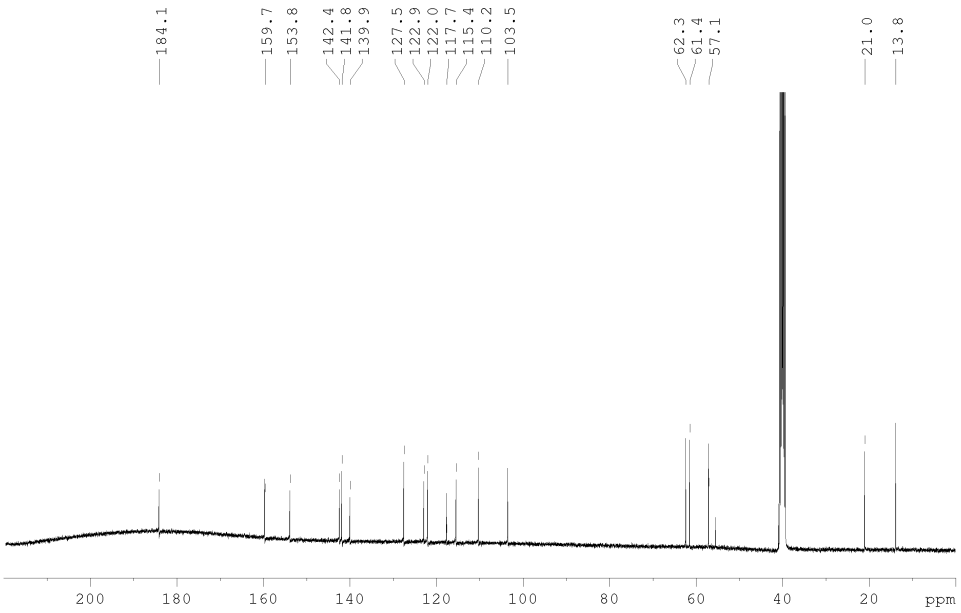

2-((4-Ethyl-1*H*-pyrrol-2-yl)methylene)-4,5,6-trimethoxybenzo[*b*]thiophen-3(2*H*)-one (PHTub-5)

^{1}H-NMR (D_3COD, 400 MHz)

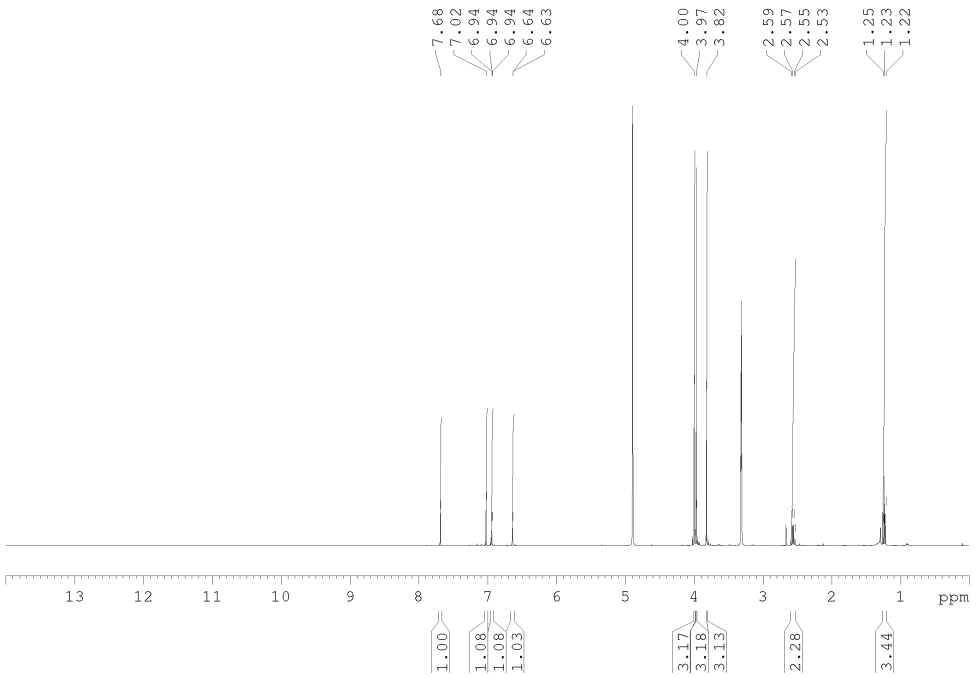

^{13}C-NMR ($DMSO-D_6$, 100 MHz)

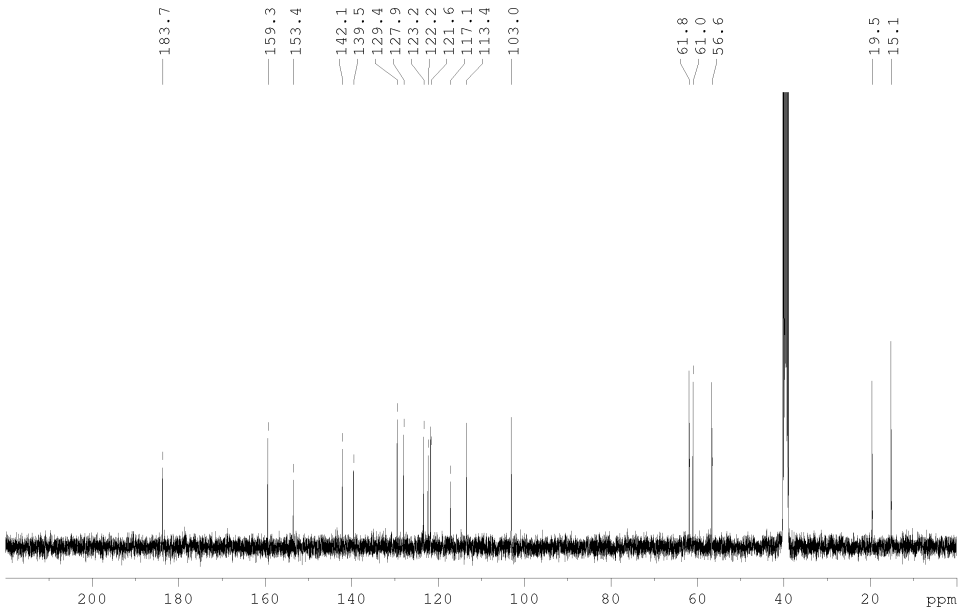

2-((3-Ethyl-1*H*-pyrrol-2-yl)methylene)-4,5,6-trimethoxybenzo[*b*]thiophen-3(2*H*)-one (PHTub-6)

^{1}H-NMR (D_3COD, 400 MHz)

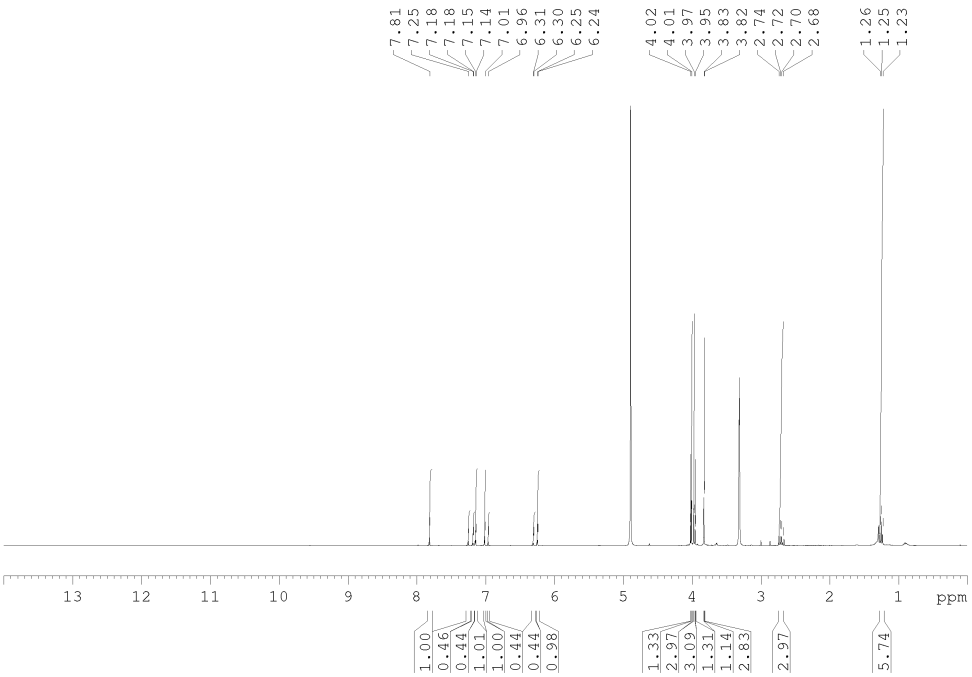

^{13}C-NMR (DMSO-D_6, 100 MHz)

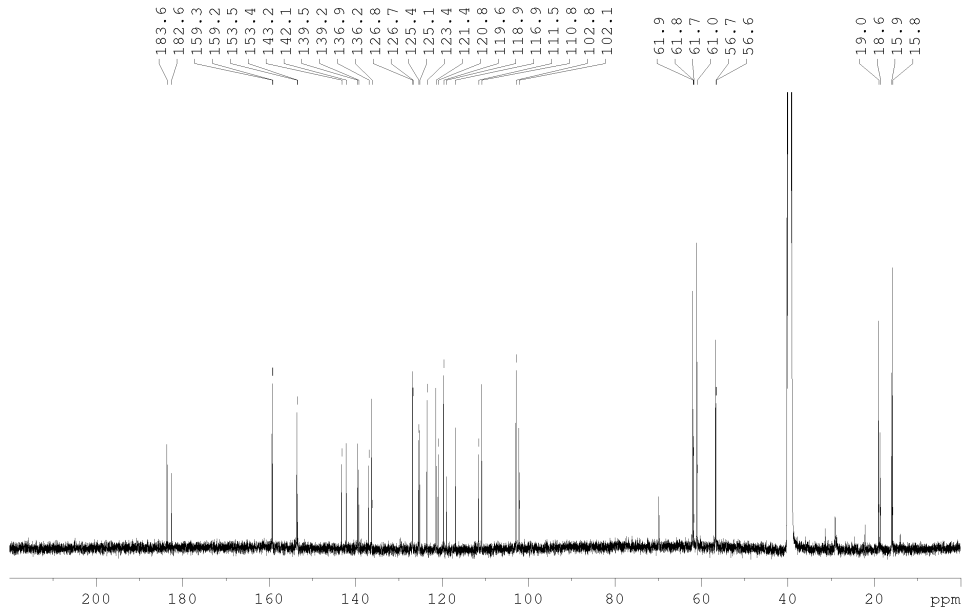

2-((5-Ethyl-1*H*-pyrrol-2-yl)methylene)-5,6,7-trimethoxybenzo[*b*]thiophen-3(2*H*)-one (PHTub-7)
^{1}H-NMR (DMSO-D_6, 400 MHz)

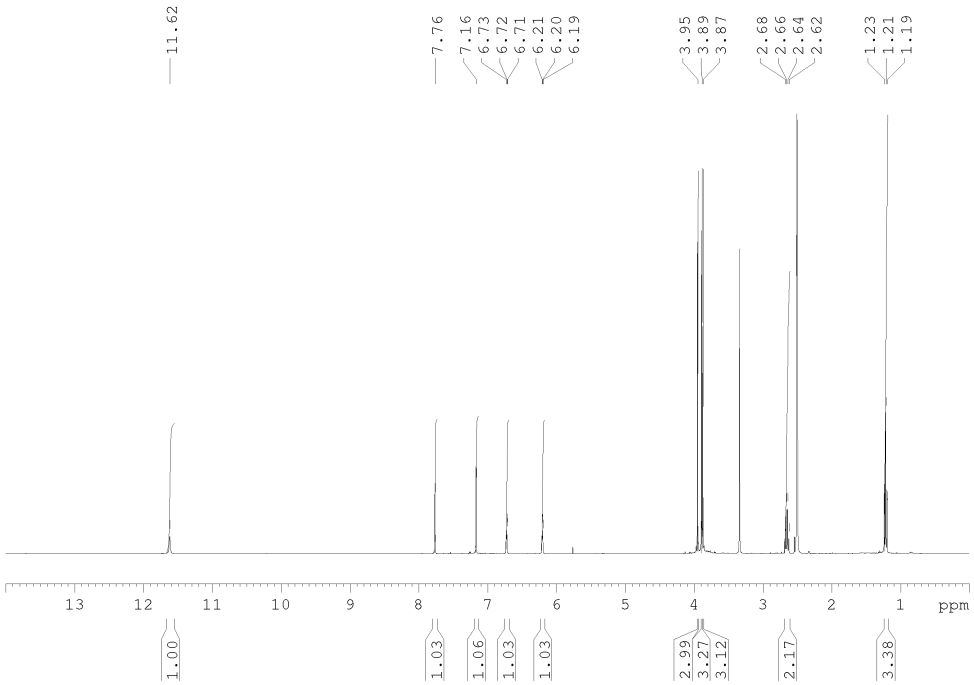

^{13}C-NMR (DMSO-D_6, 100 MHz)

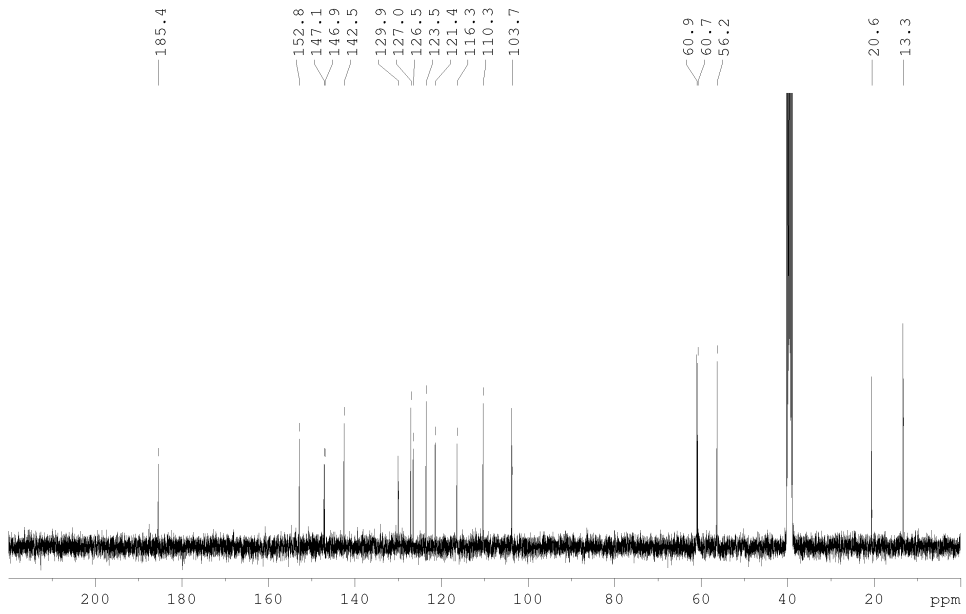

2-((4-Ethyl-1*H*-pyrrol-2-yl)methylene)-5,6,7-trimethoxybenzo[*b*]thiophen-3(2*H*)-one (PHTub-8)

^{1}H-NMR (CD_3OD, 400 MHz)

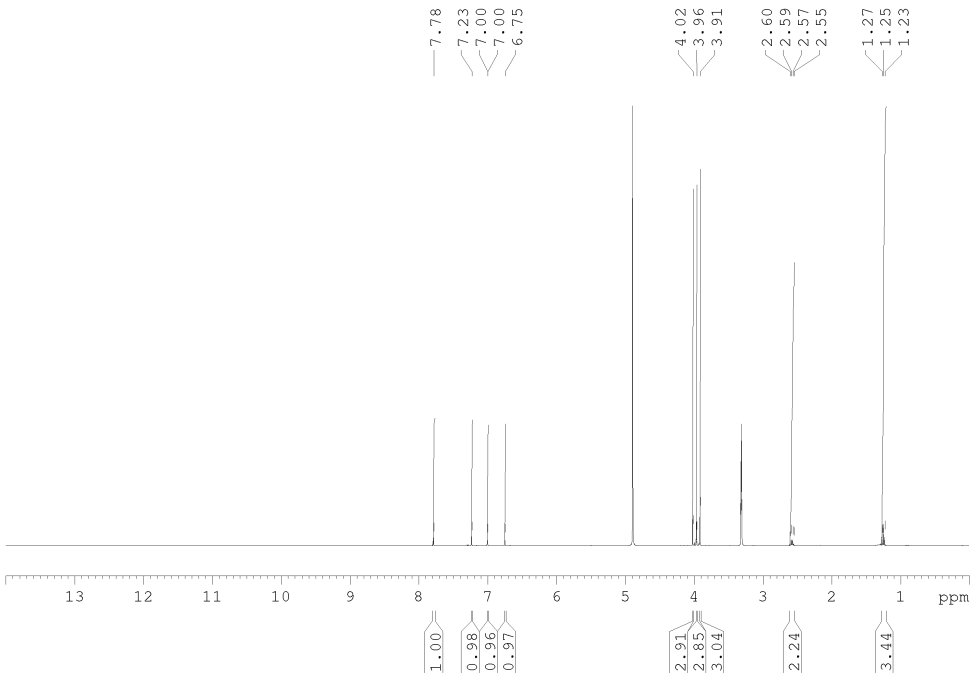

^{13}C-NMR (DMSO-D_6, 100 MHz)

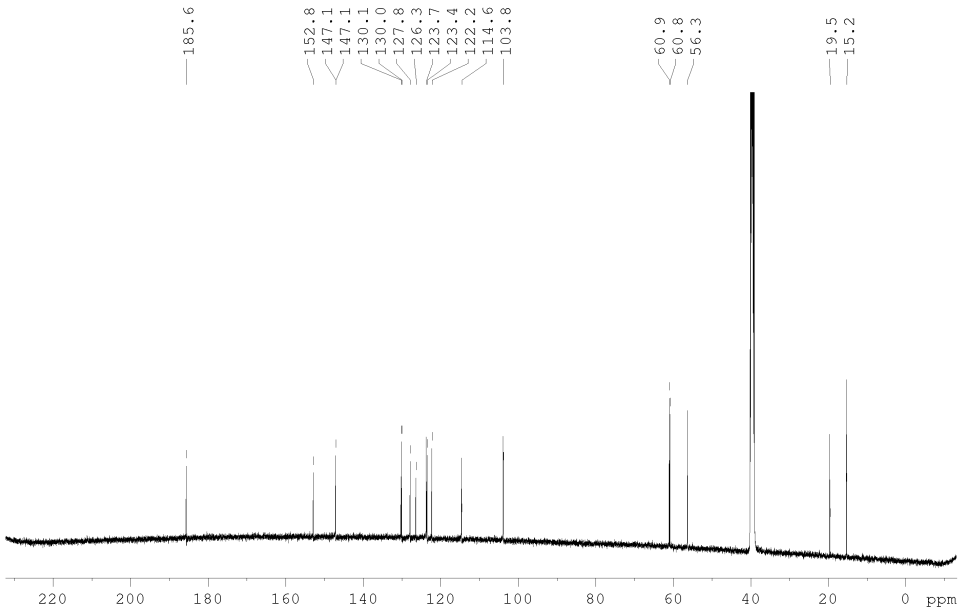

2-((3-Ethyl-1*H*-pyrrol-2-yl)methylene)-5,6,7-trimethoxybenzo[*b*]thiophen-3(2*H*)-one (PHTub-9)

^{1}H-NMR (CD_3OD, 400 MHz)

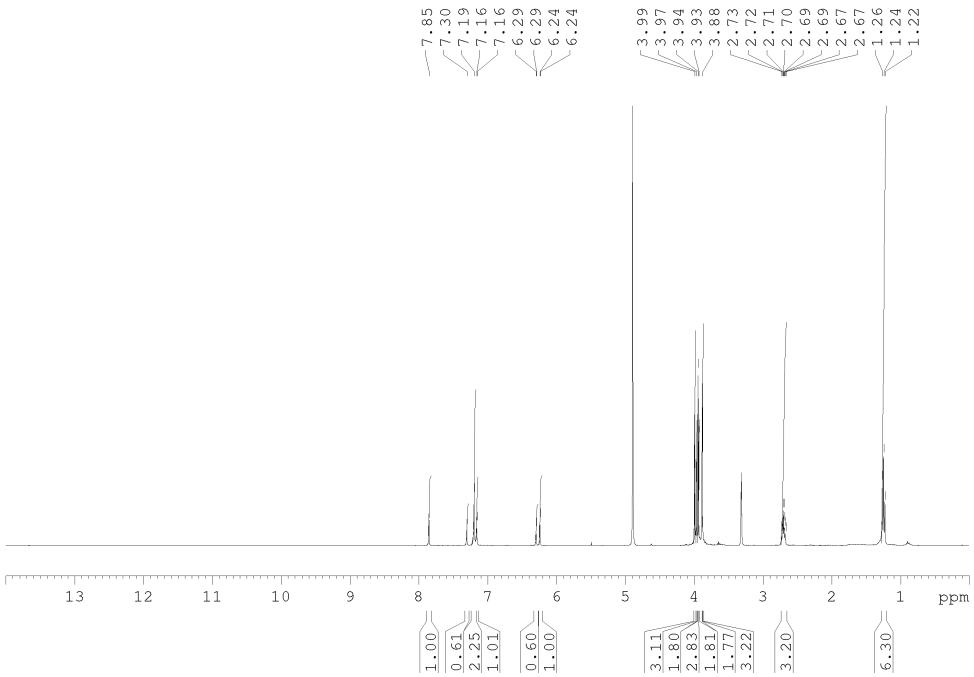

^{13}C-NMR ($DMSO-D_6$, 100 MHz)

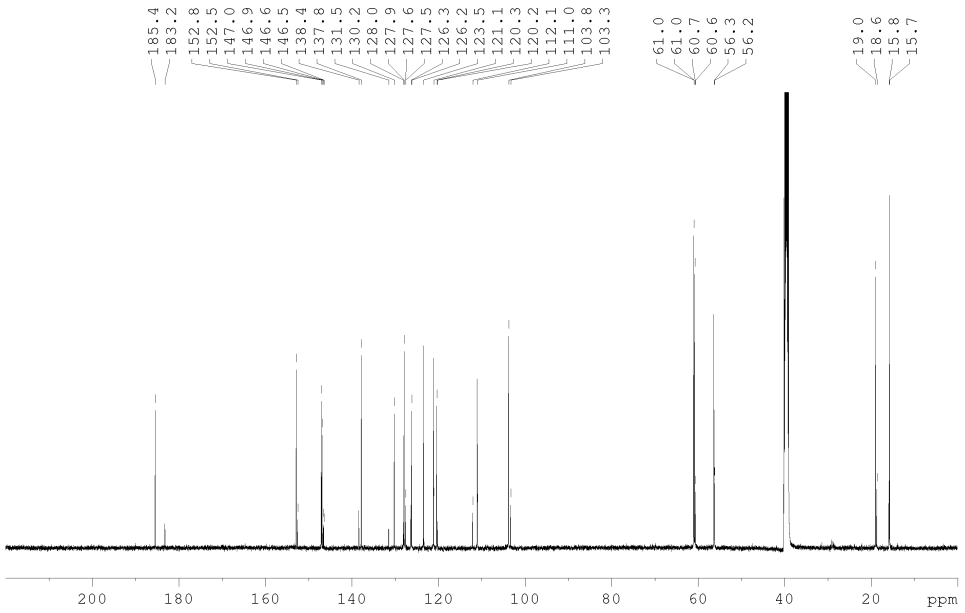

2-((4-Ethyl-1-methyl-1*H*-pyrrol-2-yl)methylene)-5,6-dimethoxybenzo[*b*]thiophen-3(2*H*)-one (PHTub-NMe)

^{1}H-NMR (CD_3OD, 400 MHz)

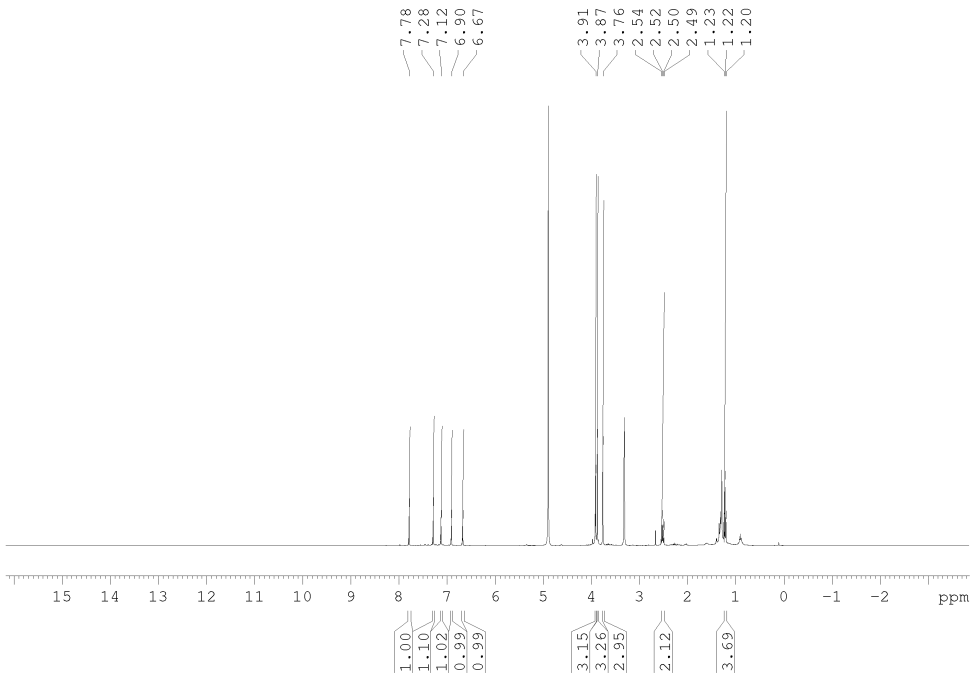

^{13}C-NMR ($DMSO-D_6$, 100 MHz)

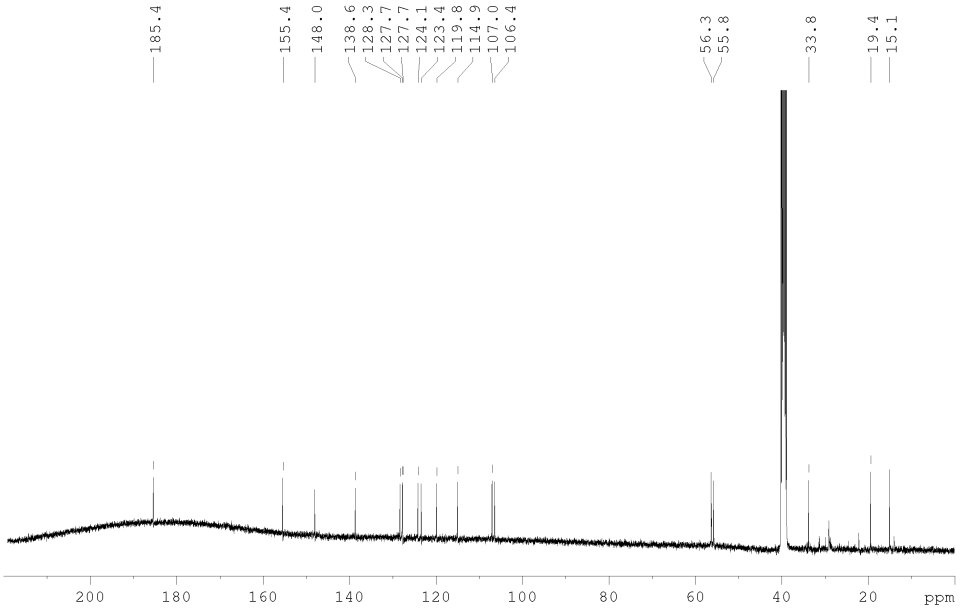

8. Ongoing Research

8.1 Towards a γ-tubulin specific photopharmaceutical

Contribution: I designed and performed the synthesis towards **phatastatin** and characterized all compounds. I was assisted by my intern Fabian Heck.

All hitherto described tubulin photopharmaceuticals targeted the α/β-heterodimer.[24,48,52,53,133] This is not surprising since very few inhibitors of other tubulin isoforms are known. One notable example is **gatastatin**[135] which is reported to be a γ-tubulin specific inhibitor (12-fold selectivity for γ over α/β-tubulin). Unlike α/β-tubulin, the γ-isoform is not involved in the MT lattice. It instead forms the γ-tubulin small ring complex (γTuSC) which is considered to be critical for cellular MT nucleation.[139]

Inspired by the structural similarity of the isoflavone **gatastatin** and hemithioindigo, we hypothesized that decorating an HTI core with the substituent pattern found in **gatastatin** might enable optical control over γ- tubulin inhibition (**phatastatin**, Fig. 16)

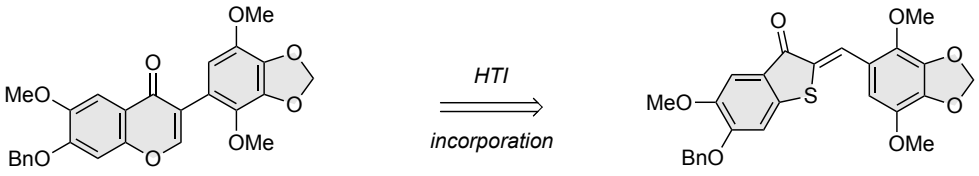

gatastatin **phatastatin**

Fig. 16: Phatastatin is an HTI derivative of the γ-tubulin specific inhibitor gatastatin.

Retrosynthetically, we cut **phatastatin** in two halves: the left half containing the thioindigo and the right half containing the benzodioxole part, respectively (Scheme 1). We began our synthetic endeavor by benzylation of phenol **1** (91% yield). We initially attempted the subsequent reduction with elemental tin and hydrochloric acid but found that substantial debenzylation (presumably through *in situ* generated hydrogen) simultaneously took place. While Na_2S in a mixture of dioxane and water only retained unreacted starting material, $SnCl_2$ as reductant afforded the desired aniline **2** in almost quantitative yield (96%). Aniline **2** was then subjected to a Leuckart-thiophenol cascade[140] consisting of diazotization followed by treatment with potassium ethyl xanthogenate giving an aromatic xanthogenate (23% yield). Hydrolysis of this aromatic xanthogenate then gave the free thiophenol which was subsequently alkylated with chloroacetic acid to give thiophenyl acetic acid **3** in moderate yield (41%). Formation of the acyl chloride followed by a Friedel-Crafts acylation should then deliver the desired thioindoxyl **4**. The formation of a regioisomer in which the ring closure appears *ortho* to the benzyloxy group is possible, but we hypothesize that steric hinderance induced by the benzyloxy group renders **4** the major product.

Key aldehyde **7** is known to literature and we followed the procedure developed by Newson.[141] Briefly, anthraquinone **5** was *bis*-methylated before being subjected to a Baeyer-Villiger oxidation.[142] The resulting eight-membered lactone was hydrolyzed by Cs_2CO_3 and the *in situ* generated catechol was alkylated with CH_2Br_2 to afford benzodioxole **6**.

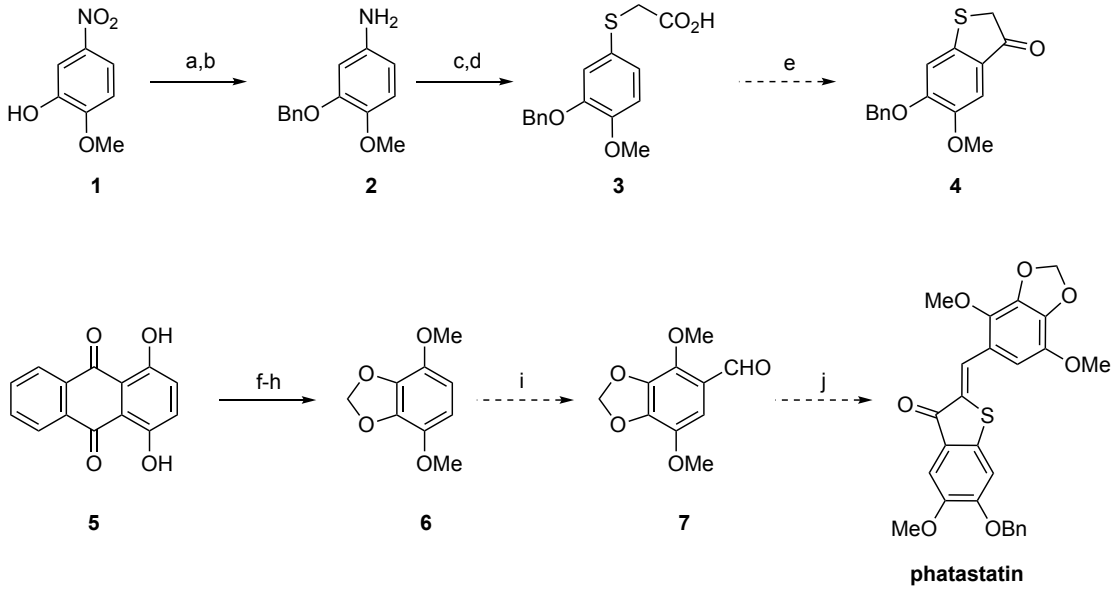

Scheme 1: Synthesis towards phatastatin. a) BnBr, K_2CO_3, acetone, 70°C, 91%, b) $SnCl_2 \cdot 2\ H_2O$, EtOH, 70°C, 96%, c) $NaNO_2$, HCl, MeOH, - 5°C *then* potassium ethyl xanthogenate, 65°C, 23%, d) NaOH, MeOH, 70°C *then* chloroacetic acid, 60°C, 41%, e) $SOCl_2$, 70°C *then* $AlCl_3$, 0°C to RT, f) MeI, K_2CO_3, DMF, 40°C, 81%, g) $NaBO_3 \cdot 4\ H_2O$, TFA, RT, 18%, h) CH_2Br_2, Cs_2CO_3, DMF, 80°C, 36%, i) $POCl_3$, DMF, j) **4**, piperidine, toluene, 80°C. Note that dashed lines indicate that synthesis has not been carried out yet.

In our hands, this step (despite being literature-known) posed some synthetic challenge: while we were able to isolate pure material, the reaction was low-yielding (best case: 36%) and inconsistent. Attempts to improve reaction yields by increasing the reactivity of the methylenating agent (CH_2I_2) did not considerably alter the observed yield (33%). We instead presume that low solubility of **6** might lead to substantial loss of product during work-up. Thus, it might be advantageous to isolate the intermediate catechol and avoid major work-up procedures after methylenation. Formylation of **6** should then yield aldehyde **7** which, in the final step, will be subjected to a piperidine-catalyzed condensation with thioindoxyl **4** to yield **phatastatin**.

In the future, we plan on optimizing the methylenation step in the synthesis of aldehyde **7** and the ring closure reaction of carboxylic acid **3** en route towards **phatastatin**.

We believe that **phatastatin** holds the potential for optical control over the cellular nucleation of microtubules. **Phatastatin** would be the first tubulin photopharmaceutical targeting an isoform other than α/β-tubulin and would open up new exciting possibilities for MT biology.

8.2 Phototargeted degradation of tubulin

Contribution: This project was enabled by a scholarship of the German Academic Exchange Service (DAAD). Research was carried out in the groups of Oliver Thorn-Seshold (LMU) and Dirk Trauner (New York University, NYU). I carried out the entire synthesis and chemical characterization of all compounds. Cytotoxicity assays were performed by Nynke A. Vepřek and Tongil Ko (both NYU).

Silencing the activity of a protein can be achieved using several different approaches: (1) by partial knock-down (by e.g., shRNA[143]) or (2) complete knock-out (by e.g., CRISPR/Cas[144]) of the gene, or (3) by inhibition of its orthosteric or allosteric binding site. Since genetic knock-out of tubulin is often lethal (see chapter 2.3.1.1), tubulin research has mainly relied on the development of inhibitors. However, factors like biolocalization and cellular distribution have so far proven major obstacles in the development of photoswitchable tools for microtubule research.

A fourth potential route towards downregulation of protein activity can be achieved by its selective degradation. In 2001 Sakamoto and Deshaies[145] reported on the development of a catalytic system comprised of a ligand of the POI and a binder of an E3 ligase. These two entities are connected via an aliphatic linker and the resulting bifunctional molecule is called a **pro**teolysis **ta**rgeting **c**himera (**PROTAC**). Upon simultaneous binding to its targets (E3 ligase and POI), ubiquitylation of the POI takes place followed by unbinding and degradation of the ubiquitylated POI by proteolysis.

Changing the mode of action of a compound from mere inhibition of a target's function to regulation of cellular protein levels, is a major leap towards control of proteins that were previously not addressable ('non-druggable 80%').[146] The fact that **PROTAC**s are applied in catalytic quantities display another benefit of this new concept when compared to 'stoichiometric' quantities for classical inhibitors. However, this approach also poses severe risks when applied systematically since it leads to complete and long-lasting absence of the protein and therefore also universal loss of its biological functions.

Precise modulation of **PROTAC** activity is thus of high interest. Only recently, Trauner, Reynders and coworkers[147] reported on an approach towards spatiotemporal control over **PROTAC** activity by making E3 ligase recruitment photoisomer-dependent (Fig. 17). The resulting **pho**tochemically **ta**rgeted **c**himeras (**PHOTAC**s) only led to protein degradation when activated by illumination with blue or UV light while showing almost no **PROTAC**-like activity in the dark, thereby increasing the spatiotemporal resolution of protein degradation.

The strategy of selective degradation has successfully been applied to a variety of proteins ranging from estrogen[148] and androgen receptors[149] to soluble kinases.[150] We wished to expand this concept to tubulin biology in general and colchicine domain inhibitors in particular.

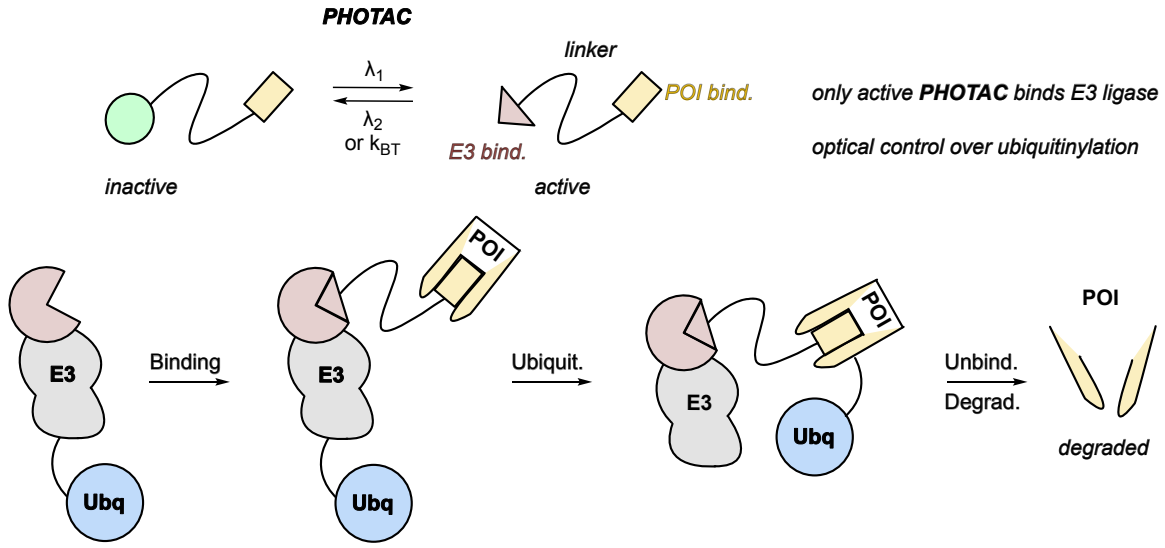

Fig. 17: Schematic depiction of PHOTAC function. Photoisomerization of the inactive **PHOTAC** changes the affinity towards E3 ligase and leaves affinity towards the POI unchanged. The active **PHOTAC** then binds the E3 ligase and the POI simultaneously. After transfer of ubiquitin and unbinding of the **PHOTAC**, the POI gets degraded by the proteasome. E3: E3 ligase binder, POI: protein of interest, Ubq: ubiquitin.

The goal of the project was the development of **tub**ulin-addressing **pho**tochemically **ta**rgeting **c**himeras as research tools for tubulin biology (**TubPHOTACs**). We anticipated to develop tools that would light-dependently transfer ubiquitin onto tubulin. This could provide tools for solving many remaining research questions: for example, whether (poly)ubiquitination of tubulin would even lead to proteasomal degradation (a surprising unknown)[103]; or, which other downstream effects (such as changes of MT polymer mass or dysregulation of the reciprocal interaction of the actin and the microtubule cytoskeleton) would result from a titrated, global degradation of this important 'housekeeping' protein. We were encouraged in our approach by the recent report of a covalent tubulin inhibitor which induces proteasomal degradation of the tubulin heterodimer (due to misfolding recognition).[151] At the time of this project, no **PROTAC** attempts to target cytoskeleton proteins had been made. Later in 2021, Mitchison and coworkers would report their failed attempts towards targeted tubulin degradation.[152] However, we believe that one of their conjugation strategies violated the SAR requirements for the inhibitor employed, and we hope that our **TubPHOTACs** present a viable way of overcoming this design issue.

TubPHOTACs were designed to consist of a photoswitchable E3 ligase binding domain and a CDI which are connected via a short aliphatic linker (Fig. 18). As E3 binders, we employed azobenzene functionalized lenalidomide derivatives that had successfully been used before.[147] Since choice of length and nature of the linker (alkyl or polyethylene glycol) is a crucial factor regarding key parameters like cell permeability, efficacy and biodistribution, it

needs careful examination.[153,154] For synthetic ease, we however started by synthesizing a variety of linkers with small alkyl chains (n = 2, 4, 6).

As tubulin inhibitors, we used combretastatin (**CA-TubPHOTACs**) and colchicine (**Col-TubPHOTACs**) derivatives (Fig. 18). We anticipated modification of **CA4** by branching from the stilbene double bond with an amide, and modification of colchicine either by replacement of the methoxy group in the C ring, or by acylation of the B-ring amine (not pursued).

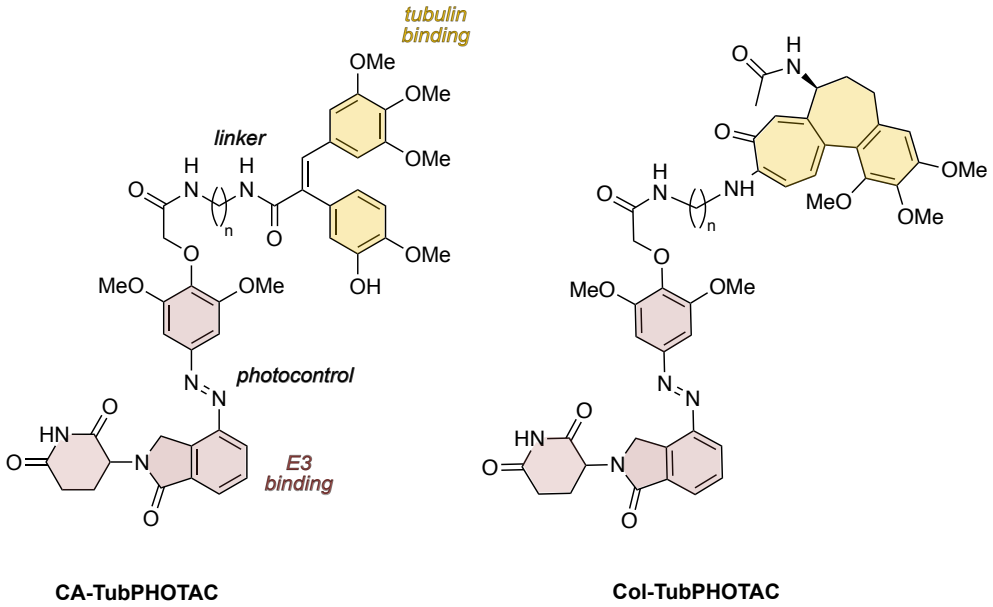

Fig. 18: Design of the synthesized and evaluated TubPHOTACS. TubPHOTACS consist of a photoswitchable E3 ligase recruiting domain (depicted in red) which is covalently linked to a tubulin inhibitor (depicted in yellow) through an alkyl linker.

We set out by synthesizing the photoswitchable E3 ligase binder **2** according to literature[147] (Scheme 2 top). The cereblon-binding **lenalidomide** was reacted with syringol in an azo coupling reaction followed by alkylation with *tert*-butyl bromoacetate to afford azobenzene **S1**. Deprotection with TFA then yielded the desired building block **1**. Starting from this carboxylic acid, we then ventured on to synthesize the E3 binder-linker constructs as described in literature.[147] HATU-mediated peptide coupling with commercially available mono-*Boc*-protected terminal bisamines first gave the desired amides **2-4** which were then deprotected with TFA to give the desired constructs **5-7** as their respective TFA salts. This modular approach allowed facile attachment of combretastatin **8** which was synthesized by Perkin condensation of 2-(3-hydroxy-4-methoxyphenyl) acetic acid with 3,4,5-trimethoxybenzaldehyde[155] (Scheme 2 middle). Attachment to constructs **5-7** was accomplished by HATU-mediated amide coupling affording the desired **CA-TubPHOTAC1-3**. While this reaction proceeded smoothly for C_4-linked **CA-TubPHOTAC2**, purification of the other two target compounds was hampered by the presence of inseparable impurities.

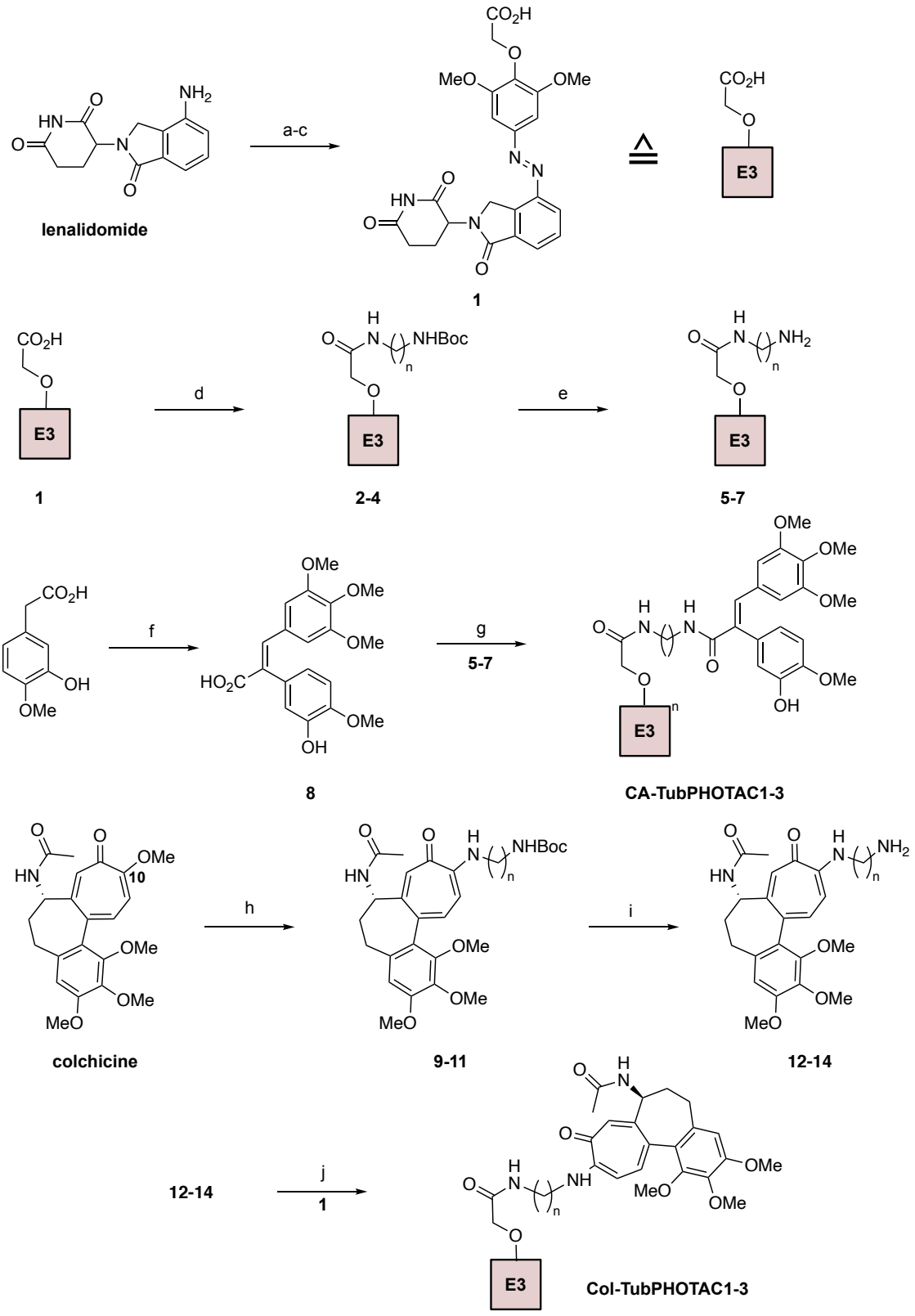

Scheme 2: Synthesis of TubPHOTACs. E3**:** E3 ligase binder, a) $NaNO_2$, HCl, syringol, b) K_2CO_3, *tert*-butyl bromoacetate c) TFA, DCM (9% over three steps), d) $H_2N(CH_2)_nNHBoc$, HATU, DIPEA, DMF; n = 2 (**2**, not isolated), n = 4 (**3**, 78%), n = 6 (**4**, 39%); e) TFA, DCM; n = 2 (**5**, 83% over two steps), n = 4 (**6**, 100%), n = 6 (**7**, 100%), f) 3,4,5-trimethoxybenzaldehyde, Ac_2O, NEt_3, 110°C, 9%, g) HATU, DIPEA, DMF; n = 2 (**CA-TubPHOTAC1-3**, not isolated), n = 4 (**CA-TubPHOTAC2**, 30%), n = 6 (**CA-TubPHOTAC3**, not isolated), h) $H_2N(CH_2)_nNHBoc$, MeOH, RT; n = 2 (**9**, 100%), n = 4 (**10**, 100%), n = 6 (**11**, >99%), i) TFA, DCM; n = 2 (**12**, >99%), n = 4 (**13**, >99%), n = 6 (**14**, >99%), j) HATU, DIPEA, DMF, RT; n = 2 (**Col-TubPHOTAC1**, 70%), n = 4 (**Col-TubPHOTAC2**, 61%), n = 6 (**Col-TubPHOTAC3**, 53%).

We then went on to derivatize colchicine. It is well known that the methoxy group in the tropolone ring at C10 can be replaced, at least by short aliphatic amines, while retaining potency.[108,112,156] Thus, we considered this position as suitable starting point for derivatization. We started by nucleophilic substitution of the methoxy group in the tropolone ring (Scheme 2 bottom).

Introduction of amines at this position is synthetically straightforward[156], and we treated colchicine with an excess of mono-*Boc*-protected terminal bisamines to obtain the desired protected colchicinoid amines **9-11** in quantitative yields and with easy purifications. Deprotection with TFA then gave the desired free amines **12-14** in quantitative yield with traces of residual TFA as the only contaminant. In the last step, the isolated colchicinoid amines **12-14** were linked to carboxylic acid **1** by means of HATU-mediated peptide coupling to give **Col-TubPHOTACs1-3** in mediocre to good yields (53 – 70%).

Initial assessment of the biological activity of **TubPHOTACs** focused on light-dependent cell viability assays since we presumed that degradation of a high-expression housekeeper protein like tubulin should to some extent result in cytotoxicity (Fig. 19).

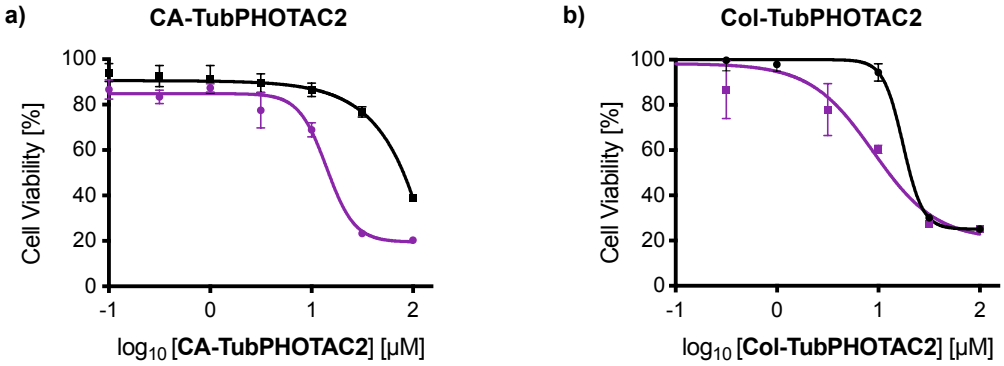

Fig. 19: Light-dependent cytotoxicity assays of CA-TubPHOTAC2 and Col-TubPHOTAC2 in RS4;11 cells. Purple lines indicate illumination with 390 nm, black lines indicate treatment in the dark.

We found a correlation between photoswitchability of cytotoxicity and the cell line under study. While all **PHOTACs** showed some cytotoxic effects in human embryonic kidney cells (HEK-293, IC_{50} in the low µM concentration range), they did so without substantial differences between lit and dark conditions. Due to this low photoswitchability, the observed cytotoxicity could either stem from tubulin degradation as desired or from mere tubulin binding.

However, the case was different for the RS4;11 leukemia cell line: **CA-TubPHOTAC2** and **Col-TubPHOTAC2** again showed micromolar cytotoxicity but this time with a noticeable to moderate difference between lighting conditions (Fig. 19). Since our **PHOTACs** are based on recruitment of the cereblon system, this observation might be due to different cellular cereblon expression levels in these cell lines. It is also worth mentioning that both probes were *dark*-active, which matched our expectations.

Combretastatins can be photoisomerized under UV light[82] which drastically changes their bioactivity (see chapter 2.3.2.1).[123] To rule out that the observed differences in cytotoxicity of **CA-TubPHOTAC2** result from isomerization of the stilbene double bond, we assayed combretastatin derivative **8** for light-dependent cytotoxicity. We found **8** to be cytotoxic (IC_{50} ~ 1 µM) with no apparent difference between the dark or pulsed 390 nm lighting used as standard assay conditions (data not shown). This supports both the initial hypothesis that our modification of **CA4** did not abolish tubulin binding and that the assay set-up was suitable for the stilbene-based **CA-TubPHOTACs**.

In conclusion, I synthesized and isolated a series of three **Col-TubPHOTACs** and one **CA-TubPHOTAC** which we assayed for light-dependent cytotoxicity in different cell lines. In RS4;11 cells, **CA-TubPHOTAC2** and **Col-TubPHOTAC2** showed light-dependent cytotoxicity. The rather small effect on cell survival elicited by **TubPHOTACs** should not be understood as a failure of mechanistic design. In fact, it is known that decreasing the cellular tubulin content by as much as 30 – 40% is not necessarily linked to substantial effects on cell growth or survival.[157]

Although these preliminary findings were promising, confirming the mode of action of **TubPHOTACs** to be degradation of tubulin is not possible by cytotoxicity assays alone. In the future, we will thus perform immunoblotting assays (Western blots) to clarify whether our **TubPHOTACs** are indeed tools for optical control over tubulin degradation. Chemically, a strong focus will be put on the purification of **CA-TubPHOTAC1&2** and the synthesis of derivatives with other linker lengths and nature (for instance, PEG instead of alkyl linkers). Deacetylation of colchicine is well precedented in literature[158] and attachment of different amides is known to be tolerated with respect to tubulin binding.[112] We thus intend to synthesize a different set of colchicine-derived **TubPHOTACs** for which the linker-lenalidomide construct will be attached via an amide bond to colchicine's C ring.

We believe that the development of tubulin targeting **PHOTACs** can have major impact on microtubule research and also offers an exciting broadening of the scope of photopharmacology in general.

9. Conclusion and Outlook

9.1 Conclusion

9.1.1 Research Summary

The success of a photopharmaceutical highly depends on the choice of the right photoswitch for the process under study. While no single ideal photoswitch exists, azobenzenes are the dominant scaffold of choice, for many reasons including synthetic accessibility, large structural changes between the two photoisomers, and bidirectionality and reversibility of photoswitching. For photopharmacology to succeed on a broad scope of targets, assay set-ups, and finally in transition to organisms, it would however be advantageous to expand the number of applicable photoswitches.

This thesis aimed at the systematic development of an alternative scaffold for photopharmacology. We based our work on the hemithioindigo photoswitch for which applications in photopharmacology had previously been only very scarce and far from systematic. We chose tubulin as a cellular target and investigated the suitability of HTIs as photoswitchable modulators of microtubule dynamics.

We considered HTIs as exceptionally well-suited since bidirectional photoswitching is (unlike for azobenzenes or SBTs) entirely powered by visible light. Planarity of both photoisomers is another peculiarity of HTIs unmatched by most other photoswitches. We showed that it is possible to harness these two unique features to create photoswitchable tubulin inhibitors with design control over which isomer is the more bioactive isomer.

We further demonstrated that HTIs can also be applied in cases where azobenzenes are known to be incompatible (*para*-substitution with tautomerizable electron-donating groups). This compatibility with a wider range of functional groups prominent in medicinal chemistry highlighted the suitability of HTIs in photopharmacology and their potential to complement the toolbox accessible to photopharmacologists.

Fine-tuning of spectral properties resulted in HTI-based tools which can be almost quantitatively toggled between the two isomers. This enabled us to study their biological effect in living cells, almost without background activity.

All HTI-based tubulin photopharmaceuticals share a mode of action: they light-dependently lead to cytotoxic effects, MT disruption and mitotic cell cycle arrest. For every study, we also designed a set of HTIs deviating from the expected SAR (permutation controls). Since these permutation controls proved to be non-cytotoxic (no unspecific toxicity caused by e.g., production of singlet oxygen), we conclude that HTIs are a generally well-tolerated scaffold for cellular photopharmacology. We also believe that HTI photopharmaceuticals, due to their

high functional group tolerance and synthetic accessibility, might be easily translated to other protein targets than tubulin.

In summary, this work systematically developed HTI-based tubulin photopharmaceuticals from an initial hypothesis and proof-of-concept study towards powerful tools for the investigation of MT dynamics in living cells.

9.1.2 General Conclusion

This thesis demonstrates that HTIs are a valuable addition to photopharmacology. While I believe that HTIs had been substantially underrepresented in literature and their potential had been underestimated, I personally do not expect that HTIs will entirely replace azobenzenes.

Instead, I hope that this work also shows that for a photopharmaceutical to succeed, thorough consideration of the target, the experimental set-up and the research question under study is necessary. Therefore, I would like to consider this thesis as an evaluation of a reliable photoswitch which is well-suited for photopharmacological research.

While the small changes in geometry and polarity between the two HTI isomers were advantageous in our hands (see Paper One), this probably hampers strategies which rely on installment of a photoswitch at the periphery of a drug. These ‘azoextension’ strategies (see chapter 2.2.2.2) are however often successful in producing a differential in activity and are usually rather facile to realize. I therefore expect that azobenzenes remain the ‘first-line approach’ for many applications in photopharmacology.

At the same time, I believe that HTIs and other indigoid photoswitches will be further developed and will find use in biological research. The following chapters contain some possible applications and ideas to overcome some challenges associated with HTIs.

9.2 Outlook

9.2.1 Towards HTI-based MT photopharmaceuticals for *in vivo* applications

In the previous chapters, it was shown that HTIs bear great potential for tubulin photopharmacology. In cell culture studies, **HOTubs**, **HITubs** and **PHTubs** were light-dependently cytotoxic, disrupted the MT network and arrested cells during mitosis.

However, a major obstacle en route towards more advanced *in vivo* applications is their limited aqueous solubility. To improve the solubility of indigoid photoswitches, I suggest (based on their chemical structures) two different approaches (Fig. 20).

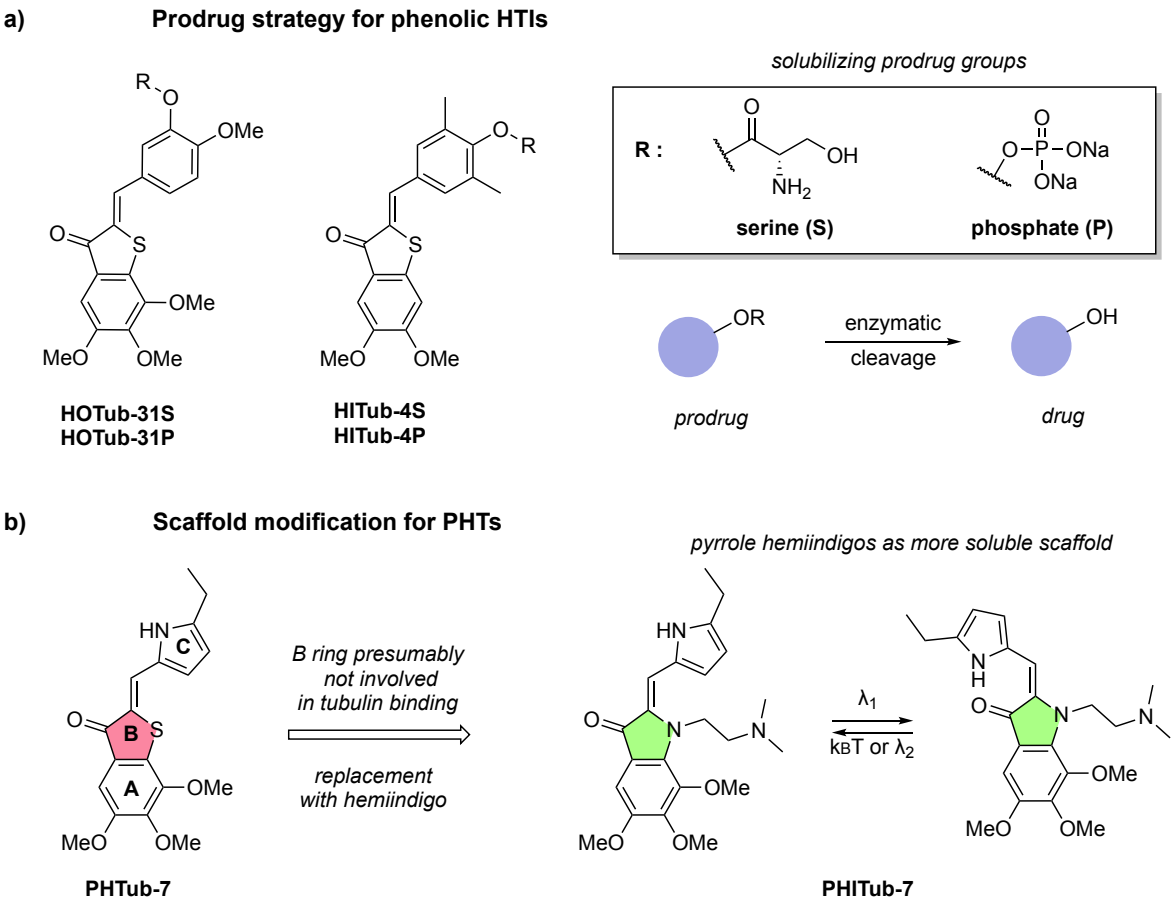

Fig. 20: Strategies to increase the solubility of indigoid (tubulin) photopharmaceuticals. a) For phenolic HTIs, prodrug strategies using esters of amino acids or phosphates are possibilities to increase the aqueous solubility. b) For PHTs, scaffold hopping to pyrrole hemiindigos seems desirable.

A standard way to increase solubility for phenolic drugs is capping with a solubility-enhancing group (like amino acids or phosphates, Fig. 20a).[24,48,49] These prodrugs undergo intracellular enzymatic cleavage releasing the active drug. This strategy seems feasible for phenolic HTIs, like **HOTubs** and **HITubs**. In a first attempt, I could envision synthesizing serine esters (S) and phosphates (P) of the most potent species, **HOTub-31,** and **HITub-4**.

For **PHTubs**, where no phenolic groups are available for derivatization, I suggest a different approach (Fig. 20b). According to the SAR of colchicine domain inhibitors (see chapter 2.3.1.3), I assume that the B ring of **PHTubs** is not involved in establishing contacts to tubulin but can be rather considered as 'space filler'. I therefore hope that isosteric replacement of PHTs with pyrrole hemiindigos is tolerated and that the resulting **p**yrrole **h**em**i**indigo **tub**ulin inhibitors (**PHITubs**) retain the cellular potency of **PHTubs**. This replacement seems advantageous because pyrrole hemiindigos are known to be near-quantitative photoswitches[159] which notably can be efficiently operated even in purely aqueous media.[160] To further increase the solubility, one could attach a basic tertiary amine which might allow administering **PHITubs** as fully water-soluble hydrochlorides; a strategy that was shown for HIs to be sufficient for efficient photoswitching in water.[78]

Approaches towards increasing the potency of HTI-based tubulin photopharmaceuticals by attachment on the periphery of highly potent tubulin inhibitors (as was done for SBTs[53] and azobenzenes[133]) are currently not planned since I believe that the small change in geometry between the two HTI isomers might not be sufficient for establishing a high differential in activity.

I hope that prodrug strategies or scaffold hopping will provide sufficient solubility to our HTI-based photopharmaceuticals allowing the first *in vivo* application of this scaffold in photopharmacology. I am convinced that the all-visible-light photoswitching, the high reversibility and fatigue resistance as well as the GSH resistance inherent to HTIs will prove a valuable addition to *in vivo* studies.

9.2.2 Tethered tubulin photopharmacology using hemiindigos

Halo fusion proteins consist of a POI and a Halo domain.[161] The Halo domain is a protein tag derived from a bacterial hydrolase which recognizes and selectively reacts with synthetic ligands carrying a specific terminal chloride. This reaction is irreversible and leads to covalent labeling ('tagging') of the POI-Halo fusion protein with the ligand. Tubulin-Halo fusion constructs are commercially available, and I suggest using these for optical control over tubulin biology (Fig. 21a).

I envision to build a tool comprised of a *lit*-active photoswitchable CDI which also contains the Halo-specific linker (**I**). This should lead to covalent attachment of the tool to the fusion protein without orthosteric binding to tubulin (**II**). Illumination with a suitable wavelength should then photoisomerize the CDI towards its bioactive isomer (**III**) which then binds tubulin and finally results in MT disruption (**IV**). My design approach is based on the hemiindigo scaffold and I thus term it **h**em**i**indigo-based **tub**ulin-**halo tag** (**HITubHaloTags**).

I choose this scaffold for three reasons: Firstly, due to structural similarity, I believe that the SAR requirements obtained for **HOTubs** (see Paper One) are equally valid for **HITubHaloTags**. This would result in a *lit*-active tool with construct **II** being inactive and construct **III** being active (Fig. 21b). Secondly, hemiindigos are described to be very efficient photoswitches that can be operated in highly aqueous media[77,78] and thirdly because the nitrogen atom of the indigo fragment appears to be a suitable site for linker attachment.

I propose a short reaction sequence towards **HITubHaloTag** (Fig. 21c): Liu described a broadly applicable method for C-H oxidation of indoles with PIDA.[162] I suggest to employ this method to introduce an acetate group at C3 of commercially available indole **1**. Attachment of the halo specific linker to **2** followed by aldol-type reaction with isovanillin should then afford ***Z*-HITubHaloTag** ready for conjugation to the tubulin-halo fusion protein.

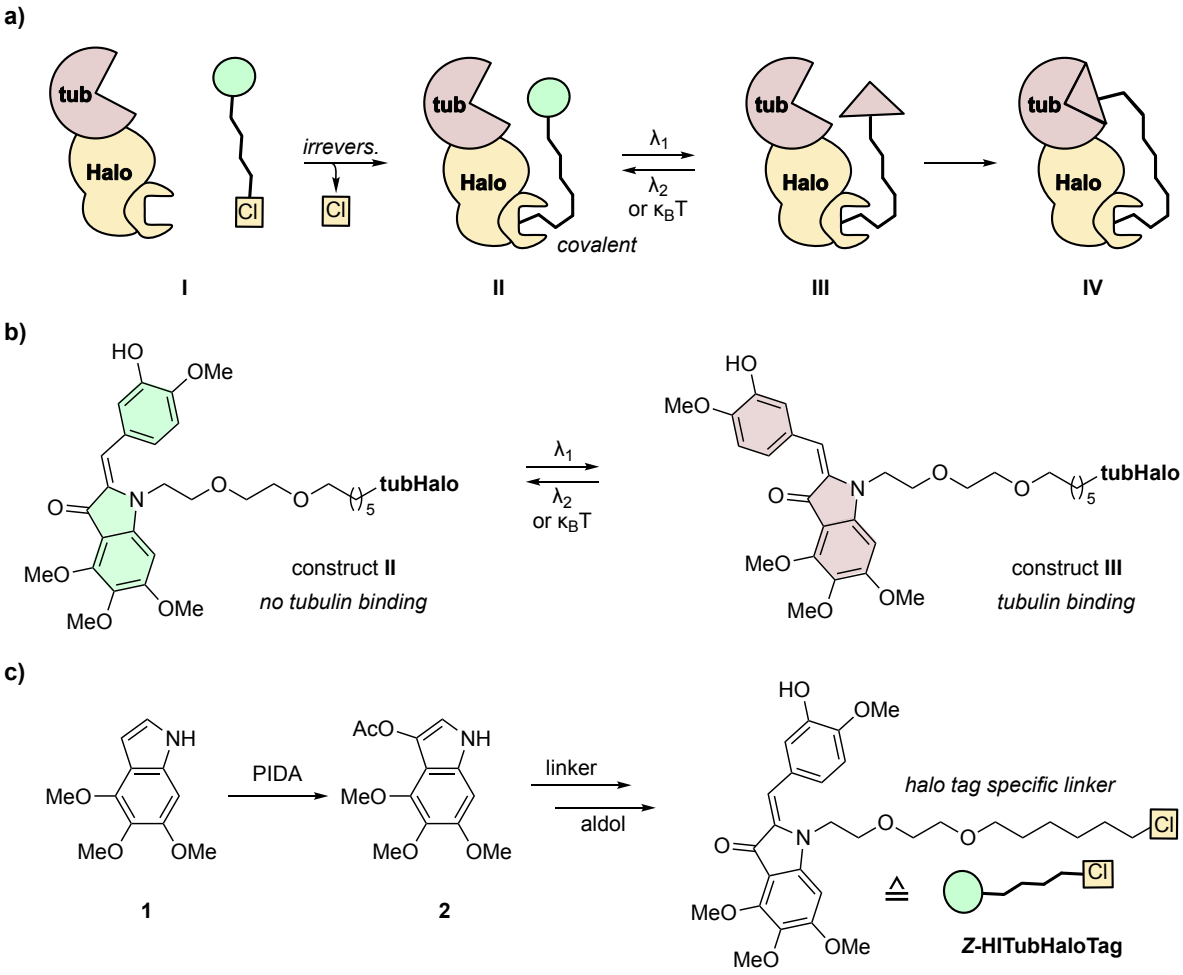

Fig. 21: Photoswitchable Halo tag tubulin constructs. a) **HITubHaloTag** irreversibly labels a tubulin-Halo fusion protein (**tubHalo**). b) Photoisomerization of construct **II** affords construct **III** and therefore activates tubulin binding. c) Proposed synthesis of **HITubHaloTag**.

Tubulin biology would benefit from such a system because inducing proximity (by covalent attachment to the fusion protein) between the ligand and tubulin would facilitate binding of the active photoisomer of the CDI and secure target selectivity. Covalent attachment would also direct biolocalization of the CDI to tubulin and prevent diffusion of the active photoisomer and therefore off-site reactivity. I also assume that photoisomerization already inside or close to the hydrophobic colchicine binding site might prove a valuable feature of the construct, in that the apolar environment enables efficient photoswitching and sufficiently high half-lives of the metastable isomer.

9.2.3 Isomer-specific coordinative bonds for sign inversion in PHTs

Recently, Doronina and coworkers[163] calculated optical band separations and isomer geometries for pyrrole hemiindigos for which the pyrrole hydrogen was replaced with a Lewis acid (Si and Ge) substituted with electron-deficient functional groups (Fig. 22a). For the *E*-isomers, they found very strong coordinative bonds from the carbonyl group towards the Lewis acid leading to high optical band separation (best case: ~ 70 nm) and substantial stabilization

of the *E*-isomer. According to their calculations, the *E*-isomer is thermodynamically favored over the *Z*-isomer by 8 and 13 kcal/mol for Si and Ge, respectively. Thus, introducing a Lewis acid to pyrrole hemiindigos leads to 'sign inversion' of the thermodynamic isomer, similar to the case of diazocines and azobenzenes.[164] I am interested in transferring this concept to PHT photoswitches and thereby creating **si**licon **p**yrrole **h**emi**t**hioindigo**s** (**SiPHTs**).

In general, **SiPHTs** might allow rational tuning of the isomer-activity relationship in a broader sense than **HOTubs** did. This approach might also allow sign inversion for **PHTubs** (see Paper Three) and especially transferring highly potent **PHTub-8** into a *lit*-active photopharmaceutical seems desirable.

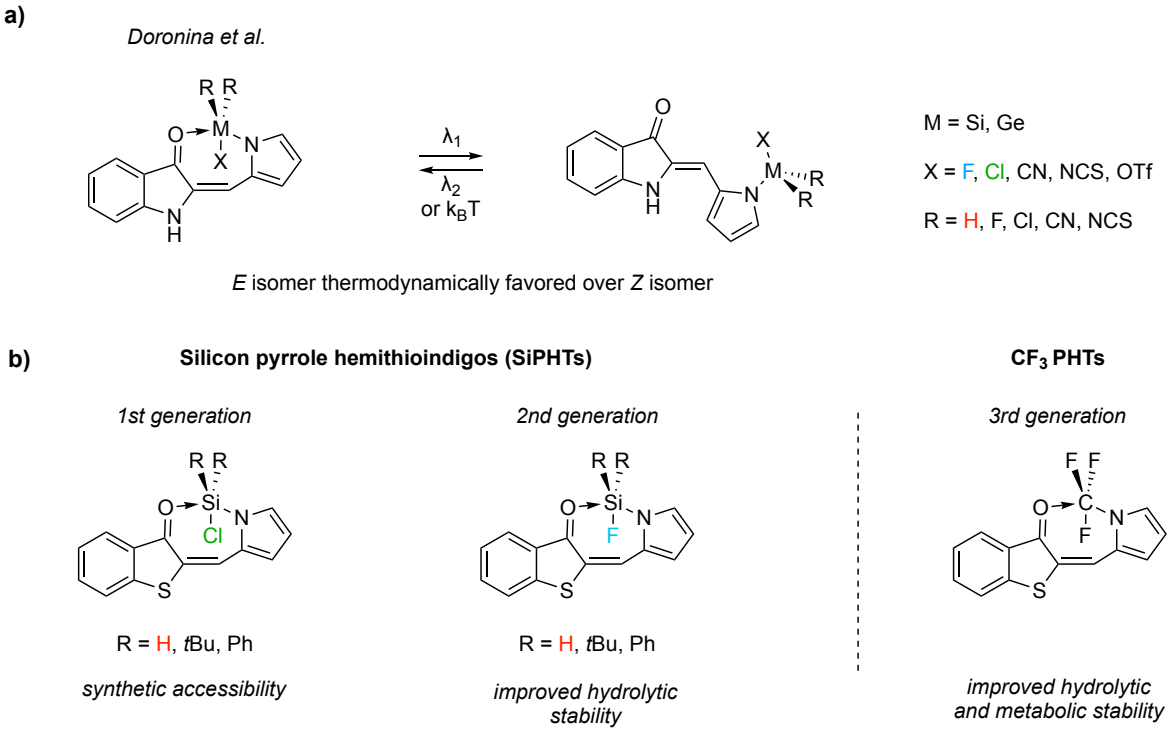

Fig. 22: Isomer-specific coordinative bonds in pyrrole hemiindigos and hemithioindigos. a) Replacement of the pyrrole N-H with an electron-deficient Lewis acid efficiently decouples the absorption spectra of pyrrole hemiindigos. b) Proposed structures of **SiPHTs** and **CF_3-PHTs**.

For the sake of synthetic ease, I suggest focusing on the more accessible silanes rather than on germylenes. I envision a first-generation series **SiPHTs** (Fig. 22b) which should be readily accessible from PHTs by deprotonation followed by quenching with commercial dichlorosilanes. These first-generation compounds could be used as proof of concept for the entire design rationale and to examine their photoswitching properties. Key emphasis should be put on optical band separation, solvent effects on photoswitching efficiency (quantitative bidirectional switching) and on examining whether the *E*-isomer would be indeed thermodynamically favored over the *Z*-isomer.

However, I assume that these first-generation **SiPHTs** might be labile towards hydrolysis which would limit their application to non-aqueous systems. Despite potential in material

science, I thus envision a second-generation series where we replace the silylchlorides with silylfluorides. It was shown that the hydrolytic stability of silylfluorides substantially increases with increasing steric hinderance around the Si and attachment to an aromatic system (half-lives > 300 h can be achieved[165]). Since Doronina and coworkers report the difference in optical band separation between chlorinated and fluorinated silanes to be non-substantial (55 vs. 51 nm), I believe that the fluorinated second generation **SiPHTs** could be valuable photoswitches for aqueous environments.

In order to create tools for photopharmacology, it would be highly desirable to secure metabolic stability. Therefore, I propose to replace the fluorosilane with a trifluoromethyl group which was shown to be resistant towards microsomal degradation[166] thereby creating **CF_3-PHTs**. The metabolic profile might also be increased by substituting the pyrrole for an indole system following the observation that indoles are important scaffolds in biology (for instance as tryptophane or serotonin derivatives) or drug discovery.[167]

While, unlike silicon, carbon does not form pentacoordinated species, I hope that the electron deficiency of the trifluoromethyl group would give rise to hyperconjugation effects which I hypothesize to be comparable to coordinative dative bonds.

I hope that **CF_3-PHTs** would combine the metabolic stability of trifluoromethyl groups with the exciting photochemistry of **SiPHTs**.

In general, I believe that sign inversion for the PHT scaffold can pave the way for further studies (like diazocines did in the field of azobenzenes) and can broaden the 'toolbox' accessible to photopharmacologists.

9.2.4 Indigoid switches for other targets: Optical control over RNA degradation

Recently, Costales and coworkers[168] reported a strategy for targeted degradation of oncogenic precursor microRNA 21 (pre-miR-21). Their system is comprised of an RNA binding domain that is linked to a recruiting molecule of a ribonuclease (RNAse, Fig. 23a). The resulting **RIBOTAC** is conceptually related to **PROTACs** (see chapter 8.2) and induces degradation of the microRNA upon simultaneous binding of pre-miR-21 and the RNAse.

The RNAse recruiter, which had previously been identified by high-throughput screening[169], contains a thiophenone ring conjugated to isovanillin (Fig. 23b). This structure is strikingly similar to HTIs and prompts the question whether photoswitching of it is possible. Since Costales discovered that swapping the position of hydroxy and methoxy groups abolished RNAse recruitment[168], I assume that photoswitching of the central double bond might enable optical control over RNAse recruitment and therefore RNA degradation. However, despite existing reports on their synthesis[170] and calculations on their DNA gyrase binding[171], to the best of my knowledge no attempts have been made to photoisomerize this scaffold.

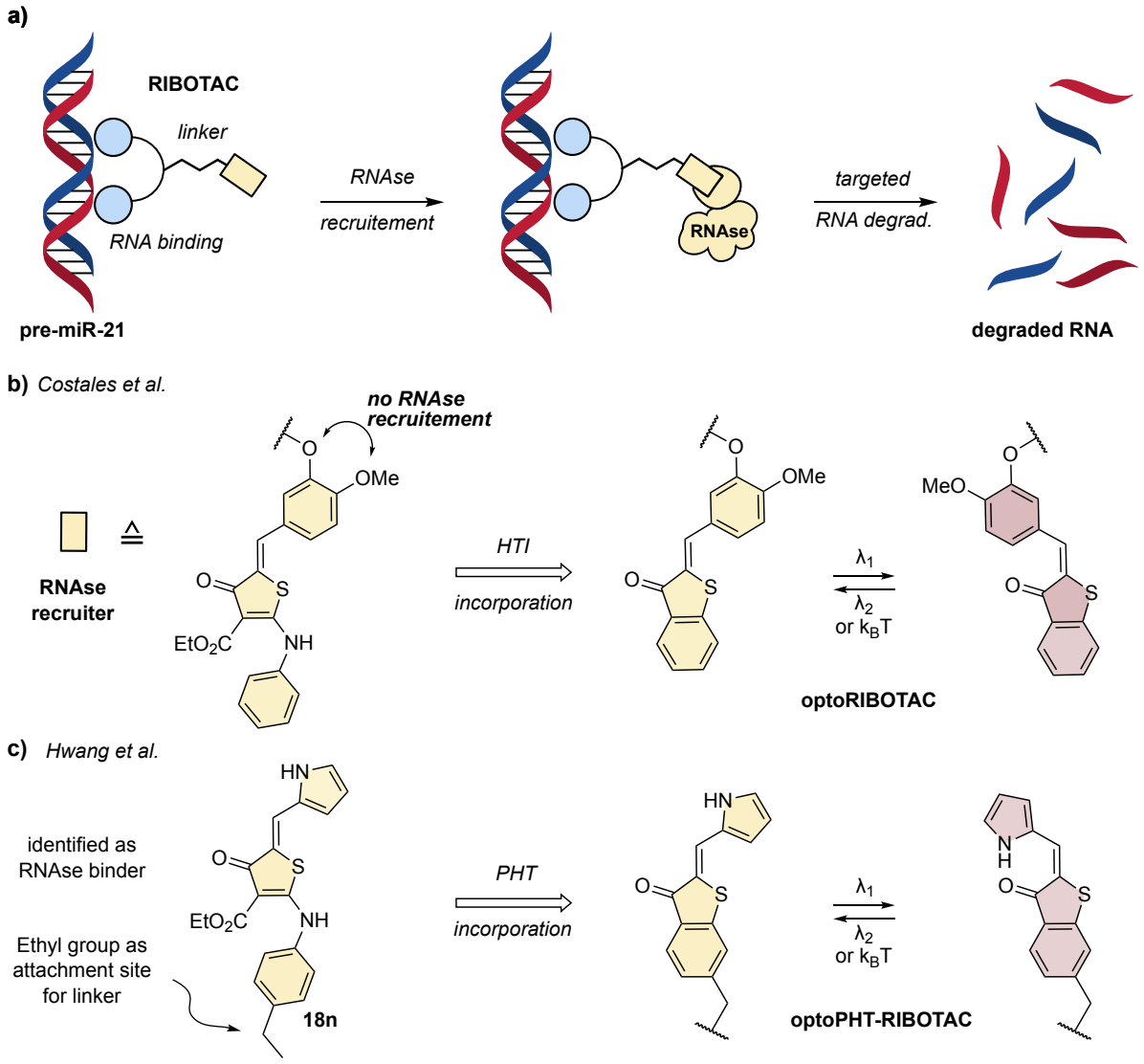

Fig. 23: RIBOTACs induce RNA degradation and optoRIBOTACs are photoswitchable derivatives thereof. a) **RIBOTACs** consist of an RNA binding domain that is linked to a ribonuclease recruiter. Simultaneous binding of pre-miR-21 and the RNAse induces degradation of pre-miR-21. b) The RNAse recruiter is structurally related to HTIs and incorporation of this photoswitchable motif (**optoRIBOTAC**) might lead to photocontrol over RNA degradation. c) Compound **18n** was identified to bind RNAse. The structural similarity to PHTs might be harnessed to create photoswitchable **RIBOTACs** with the advantageous properties of PHTs (**optoPHT-RIBOTAC**).

Encouraged by these observations, I could anticipate that optical control over **RIBOTAC** function can be achieved. For this, I would propose to firstly synthesize the RNAse recruiter following a known straightforward three-step procedure[170] and evaluate whether photoisomerization of this compound is possible. I then suggest synthesizing HTI derivatives of the RNAse recruiter and link these to the RNA binders resulting in **optoRIBOTACs**.

Hwang and coworkers[170] carried out a systematic SAR study on benzylidenthiophenone-based RNAse binder. They identified pyrrole containing **18n** (Fig. 23c) as hit which I consider to be a suitable starting point for the design of a second class of photoswitchable **RIBOTACs** (**optoPHT-RIBOTACs**) for two reasons. Firstly, the structural analogy to PHTs is overwhelming and I hope that the advantageous properties of PHTs (see **Paper Three**) will

prove valuable in the **RIBOTAC** context. Secondly, the ethyl group on the aniline might be used for straightforward attachment of the linker by nucleophilic substitution.

It is estimated that 100-fold more RNA targets exist than protein drug targets.[168] In addition to its modular approach, I thus believe that targeted RNA degradation will have a substantial effect not only in RNA biology but also in medicinal chemistry and drug development (very much like **PROTAC** approaches that have by now successfully been translated to clinical trials[172]). I also believe that optical control over this process can be achieved (by photoisomerization of the RNAse recruiter, or by photoswitchable indigoid RNAse recruiters). In my eyes, indigoid photoswitches are a good fit for **optoRIBOTACs** due to the structural similarity to the RNAse ligand and the avoidance of UV light which is known to damage RNA.[173]

9.2.5 Photopharmacology towards *in vivo* drug applications

Photopharmacology holds the potential for delivering spatiotemporally precise drugs. This would allow the global application of drugs, while very locally restraining their activity. This in turn would be a major leap towards overcoming side effects commonly associated with pharmacotherapy. To live up to this enormous potential, translation from purely *in vitro* or cell culture studies towards real *in vivo* applications must be realized. Major obstacles on this way include low penetration depths of light into biological tissue and strong absorption of endogenous biomolecules, like hemes and flavins. Extensive attempts[37,44] have thus been undertaken to shift the absorption maxima of photopharmaceuticals to a more biocompatible window ($\lambda \geq 600$ nm). At the same time, significant advances in technology have enabled endoscopic probes equipped with optical fibers for the precise on-site activation of photopharmaceuticals.[174] Both approaches can be considered milestones to real *in vivo* photopharmacology. However, another decisive parameter for the applicability of photopharmacology in living animals is metabolism of photopharmaceuticals. Regular azobenzenes have been shown to be labile towards reduction.[130] This reduction is indeed pronounced enough for azobenzenes to have been widely used as prodrugs of anilines (e.g., the azobenzene prontosil is a prodrug of the antibiotic sulfanilamide).[175] While some arylazopyrazoles are reported to be stable towards GSH-mediated reduction[176], I personally believe that real *in vivo* photopharmacology with azobenzenes is hard to realize.

9.2.6 General Outlook

Across these different strands of photopharmacology, there is a recurring need for alternative scaffolds in order to exploit opportunities and overcome challenges. Particularly, there is still much work to do before it will be evident whether HTIs or other indigoid photoswitches can hold true to their promising performance. The fact however that SBTs have

recently been applied for *in vivo* photopharmacology highlights the enormous potential for high-precision biological studies that distinguishes photopharmaceuticals. While it remains to be seen whether photopharmaceuticals will ever be applied in the clinic, I am convinced that photopharmacology will continue to emerge as a tool for biological research.

10. Acknowledgements

First and foremost, I would like to thank my supervisor Dr. Oliver Thorn-Seshold for giving me the opportunity to perform my PhD work in his group. Thank you for your trust, for enabling a stay abroad during my PhD and for collecting all the great colleagues I had the pleasure to work with over the years.

I would also like to thank Prof. Dr. Franz Bracher for agreeing to be the second reviewer of this PhD thesis and Prof. Dr. Ivan Huc, Prof. Dr. Daniel Merk, Prof. Dr. Oliver Trapp, and Dr. Pavel Kielkowski for being part of my scientific committee.

Additionally, I am very grateful for Prof. Dr. Dirk Trauner for giving me the unique opportunity to join his lab as a visiting scholar and the German Academic Exchange Service (DAAD) for granting me a research fellowship. The time in New York has been a formative experience for me, both scientifically and personally. I would like to thank all members of the Trauner group, especially Zisis, Peter, Chris, Tufan, Anna, Belinda, Gloria, Carolyn, Nynke, Ruiyang, Tom, Matt, and Bruno, my travel companion and Manhattan quarantine buddy. This time would have been nothing without the great people I met outside the lab, in particular Amanda and the HIMYM apartment. Thanks for showing me all the great places in Chelsea and beyond!

I would like to thank Prof. Dr. Klaus Wanner for his supervision early on in my thesis. Thanks to all the members of 'AKW', especially Janina, Heinrich, Tamara, Valentin and Jörg.

This work would not have been possible without the assistance of my great student interns Sebastian, Linda, Fabian, and Mikey. Thanks for your great work!

To all current and former members of the TS group (Adrian, Li, Ben, Philipp, Jan, Lukas, Markus, Carina, Constanze, Annabel, Julia, Nynke, Martin, Longhi, Franzi and Elena), and all the other great people on the campus, especially Christoph and Janni: Words can't express how grateful I am to have met, worked (out), travelled and partied with all of you!

I would like to express my deepest gratitude to all the lovely people I've met on my stints in Erlangen, Würzburg, Cracow, Munich, and New York. It's been ten amazing years!

My biggest and heartfelt thanks to Paul and Tobi for their great and unique friendship; no matter where I was, I could always rely on. I'm genuinely looking forward to seeing which paths you will tread and what the future might hold for us.

Lastly, I would like to thank my family and parents for their infinite trust and support throughout the years.

11. Appendix

11.1 Supporting information to chapter 8.1

Reagents and Conditions:

Unless stated otherwise: (1) all reactions and characterizations were performed with unpurified, undried, non-degassed solvents and reagents, used as obtained, under closed air atmosphere without special precautions. The use of dry solvents in this context is to be understood as using anhydrous solvents bought from Acros Organics which were stored and handled under an atmosphere of nitrogen; (2) “hexane” used for chromatography was distilled from commercial crude isohexane fraction on rotavap; (3) when not specified, “column” and “chromatography” refer to flash column chromatography performed on Merck silica gel Si-60 (40-63 µm); (4) procedures and yields are unoptimized; (5) yields refer to isolated chromatographically and spectroscopically pure materials (6) all eluent and solvent mixtures are given as volume ratios unless otherwise specified, thus “1:1 EA:Hx” indicates a 1:1 mixture (by volume) of ethyl acetate and hexanes.

Thin-layer chromatography (TLC):

TLC was run on 0.25 mm Merck silica gel plates (60, F-254). UV light (254 nm) was used as a visualizing agent. R_f values were usually determined in ethyl acetate : hexane (EA:Hx) eluents. TLC characterizations are thus abbreviated as per R_f = 0.09 (EA:Hx, 6:1).

Nuclear magnetic resonance (NMR) spectroscopy:

Standard NMR characterization was performed by 1D ^{1}H- and ^{13}C-NMR spectra with NOESY as needed. Known compounds were checked against literature data. The default spectrometer used was a Bruker Ascend 400 (400 MHz & 100 MHz for ^{1}H and ^{13}C respectively); NMR solvents are given individually for each compound. Chemical shifts (δ) are reported in ppm calibrated to residual non-perdeuterated solvent as an internal reference.[177] The following peak descriptions are used: singlet (s), doublet (d), triplet (t), quartet (q), multiplet (m), broad (br.), pseudotriplet (~t).

High-resolution mass spectrometry (HRMS)

Electron impact (EI) ionization was performed on a Thermo Q Exactive GC Orbitrap or Finnigan MAT 95 sector field mass spectrometer. The resolution was set to approximately 5000 (MAT95) or 50 000 (at m/z 200, Q Exactive GC). Depending on the used method, a span from 40 to 1040 u was detected. Ionization was performed at 250 °C source temperature and 70 eV electron energy. Electrospray ionization (ESI) was performed on a Thermo Finnigan LTQ FT Ultra Fourier Transform Ion Cyclotron Resonance Spectrometer. The resolution was set to 100 000 at m/z 400. Depending on the used method, a span from 50 to 2000 u was

detected. The current of the spray capillary at the IonMax ESI probe head was 4 kV, the temperature of the heating capillary 250 °C, N_2 flow of sheath gas 20 and the sweep gas flow 5 units.

Synthesis:

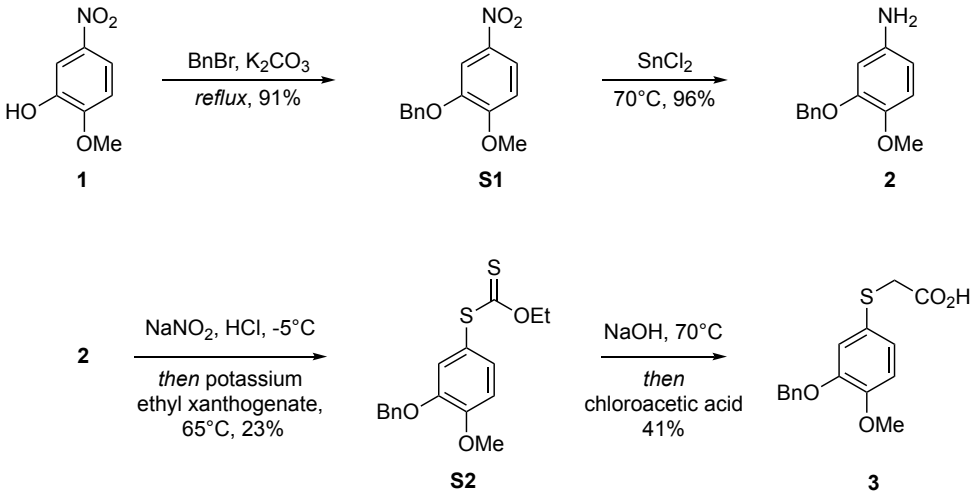

Scheme S1: Synthesis of carboxylic acid **3**.

2-(Benzyloxy)-1-methoxy-4-nitrobenzene (S1)

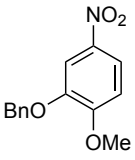

S1

To a suspension of **1** (500 mg, 2.96 mmol, 1.00 eq.) and K_2CO_3 (613 mg, 4.43 mmol, 1.50 eq.) in acetone (15 mL) was added benzyl bromide (607 mg, 3.55 mmol, 1.2 eq. 0.43 mL) at room temperature and the reaction mixture was heated to reflux for 3 h after which time the solvent was removed under reduced pressure. The residue was partitioned between water (15 mL) and DCM (20 mL), the phases were separated, and the aqueous layer was extracted with DCM (2 x 15 mL). The combined organic extracts were dried over Na_2SO_4, filtered, and evaporated. Column chromatography (EA:Hx, 1:4) of the crude product gave **S1** as yellow solid (697 mg, 2.69 mmol, 91%). The spectroscopic data is in agreement with literature.[178]

^{1}H-NMR ($CDCl_3$, 400 MHz): δ (ppm) = 7.90 (dd, *J* = 8.9 / 2.6 Hz, 1H), 7.78 (d, *J* = 2.6 Hz, 1H), 7.46 – 7.44 (m, 2H), 7.40 – 7.36 (m, 2H), 7.34 – 7.30 (m, 1H), 6.90 (d, *J* = 8.9 Hz, 1H), 5.18 (s, 2H,), 3.95 (s, 3 H, 3H); **^{13}C-NMR** ($CDCl_3$, 100 MHz): δ (ppm) = 155.2, 147.9, 141.4, 135.8, 128.9, 128.5, 127.7, 118.2, 110.2, 108.6, 71.3, 56.6; $\mathbf{R_f}$ = 0.63 on EA:Hx 1:4; **HRMS** (EI^+) for $C_{14}H_{13}NO_4^+$ = $[M^+]$: calcd. m/z 259.08446, found m/z 259.0838.

3-(Benzyloxy)-4-methoxyaniline (2)

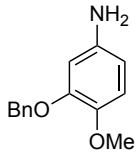

2

To a suspension of **S1** (500 mg, 1.93 mmol, 1.00 eq.) in MeOH (15 mL) were added tin (304 mg, 2.56 mmol, 1.33 eq.) and HCl (12M, 7 mL) and the suspension was heated to reflux for 30 min, then allowed to reach room temperature and stirred for 1 h. The solvent was removed under reduced pressure, the residue was suspended in DCM (100 mL) and washed with a saturated aqueous $NaHCO_3$ (100 mL) and brine (100 mL). The combined organic extracts were dried over Na_2SO_4 and evaporated. The crude product was dissolved in EtOAc and HCl was added until pH = 1. The precipitated white solid was dissolved in water and the aqueous phase was washed with EtOAc. The aqueous phase was treated with NaOH until pH = 12 and extracted with EtOAc (3 x 15 mL). The combined organic extracts were dried over Na_2SO_4 and evaporated to give the desired product as dark-brown tar (186 mg, 0.81 mmol, 42%). The spectroscopic data is in agreement with literature.[178]

^{1}H-NMR ($CDCl_3$, 400 MHz): δ (ppm) = 7.42 – 7.40 (m, 2H), 7.36 – 7.32 (m, 2H), 7.29 – 7.26 (m, 1H), 6.72 (d, *J* = 8.5 Hz, 1H), 6.30 (d, *J* = 2.6 Hz, 1H), 6.23 (dd, *J* = 2.6 / 8.5 Hz, 1H), 5.09 (s, 2H), 3.80 (s, 3H) **^{13}C-NMR** ($CDCl_3$, 100 MHz): δ (ppm) = 149.3, 142.9, 140.7, 137.4, 128.7, 127.9, 127.3, 114.1, 107.3, 103.3, 71.0, 57.1; **HRMS** (ESI^+) for $C_{14}H_{16}NO_2^+$ [M+H$^+$]: calcd. m/z 230.11756, found m/z 230.11773.

S-(3-(benzyloxy)-4-methoxyphenyl) O-ethyl carbonodithioate (S2)

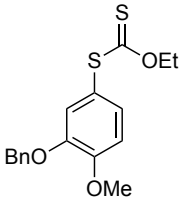

S2

To a solution of 3-(benzyloxy)-4-methoxyaniline **2** (186 mg, 0.81 mmol, 1.00 eq.) in MeOH (15 mL) was added an aqueous solution of $NaNO_2$ (2M, 0.48 mL, 1.19 eq.) and HCl (12M, 0.15 mL) keeping the temperature below -5 °C. The resulting solution was added to a solution of potassium ethyl xanthogenate (390 mg, 2.43 mmol, 3.00 eq.) in water (10 mL) and heated to 65 °C for 4 h and stirred overnight at room temperature. The solvents were removed under reduced pressure and the tarry residue was taken up in EtOAc (15 mL) and washed with brine (20 mL). The organic layer was evaporated and the crude product was purified by column chromatography (EA:Hx, 1:10) to give a yellow high-viscous oil (61 mg, 0.18 mmol, 23 %).

^{1}H-NMR ($CDCl_3$, 400 MHz): δ (ppm) = 7.43 – 7.41 (m, 2H), 7.37 – 7.33 (m, 2H), 7.31 – 7.28 (m, 1H), 7.08 (dd, *J* = 8.3 / 2.1 Hz, 1H), 7.03 (d, *J* = 2.0 Hz, 1H), 6.90 – 6.93 (m, 1H), 5.12 (s, 2H), 4.55 (q, *J* = 7.1 Hz, 2H), 3.90 (s, 3H), 1.28 (t, *J* = 7.1 Hz, 3H); **^{13}C-NMR** ($CDCl_3$, 100 MHz): δ (ppm) = 214.5, 151.4, 148.4, 136.6, 128.9, 128.7, 128.2, 127.5, 120.6, 111.8, 71.2, 70.4, 56.1, 13.8 **R_f** = 0.34 on EA:Hx 1:10, **HRMS** (EI^+) for $C_{17}H_{18}O_3S^+$ = $[M^+]$: calcd. m/z 334.0697, found 334.0688.

2-((3-(benzyloxy)-4-methoxyphenyl)thio)acetic acid (3)

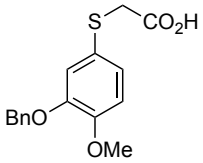

To a solution of S-(3-(benzyloxy)-4-methoxyphenyl) O-ethyl carbonodithioate **S2** (282 mg, 0.84 mmol, 1.00 eq.) in MeOH (5 mL) was added a solution of NaOH (370 mg) in water (5 mL) and the suspension was heated to 70 °C for 2.5 h after which time a solution of chloroacetic acid (80 mg, 0.84 mmol, 1.00 eq.) in NaOH (2M, 2 mL) was added. The reaction mixture was heated to 70 °C for 1.5 h, allowed to cool to room temperature and stirred for another hour. The organic solvent was then removed under reduced pressure followed by addition of HCl (2 M) until pH = 1 and the aqueous phase was extracted with EtOAc (3 x 10 mL). The organic phase was extracted with NaOH (2M, 3 x 25 mL) and the combined aqueous extracts were acidified with HCl (2 M) until pH = 1 and extracted with EtOAc (3 x 25 mL). The combined organic extracts were dried over Na_2SO_4 and evaporated. Trace impurities were removed by coevaporation with toluene (3 x 2 mL) and the orange crystalline product (106 mg, 0.35 mmol, 41%) was dried in high vacuum.

^{1}H-NMR (CD_3CN, 400 MHz): δ (ppm) = 7.47 – 7.36 (m, 5H), 7.11 (d, *J* = 2.2 Hz, 1H), 7.02 (dd, *J* = 8.4 / 2.2 Hz, 1H), 6.91 (d, *J* = 8.4 Hz, 1H), 5.08 (s, 2H), 3.80 (s, 3H), 3.58 (s, 2H); **^{13}C-NMR** (CD_3CN, 100 MHz): δ (ppm) = 171.1, 150.0, 148.8, 137.6, 129.1, 128.6, 128.6, 126.1, 124.7, 117.2, 112.9, 71.1, 56.0, 37.6; **HRMS** (ESI^-) for $C_{16}H_{15}O_4S^-$ = $[M-H]^-$: calcd. m/z 303.06965, found 303.06951.

Synthesis of dioxole 6

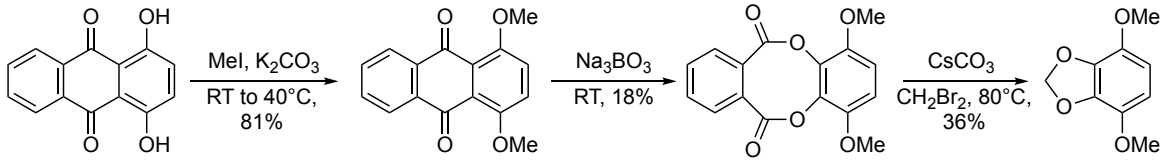

Scheme S2: Synthesis of dioxole **6**.

1,4-Dimethoxyanthracene-9,10-dione (S3)

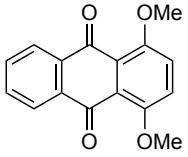

S3

Quinizarin **5** (3.00 g, 12.4 mmol, 1.00 eq.) and potassium carbonate (6.85 g, 49.5 mmol, 4.00 eq.) were suspended in dimethylformamide (50 mL) and methyl iodide (5.78 mL, 92.8 mmol, 7.48 eq.) was added at room temperature. The dark blue suspension was stirred at 40 °C for 2 d. The mixture was diluted with water (300 mL) and an aqueous solution of sodium hydroxide (2 M, 100 mL) was added. The mixture was extracted with dichloromethane (3 × 100 mL), the combined organic extracts were dried over sodium sulfate and the solvent was removed *in vacuo*. The crude product was purified by column chromatography (50% to 100% EA in Hex). An orange powder of **S3** (2.72 g, 10.1 mmol, 81%) was obtained.

The synthesis was performed as described in literature and the spectroscopic data is identical to those reported.[141]

^{1}H-NMR ($CDCl_3$, 400 MHz): δ (ppm) = 8.17 (dd, *J* = 5.8 / 3.3 Hz, 2H), 7.71 (dd, *J* = 5.8 / 3.3 Hz, 2H), 7.35 (s, 2H), 4.01 (s, 6H).

1,4-Dimethoxydibenzo[*b,f*][1,4]dioxocine-6,11-dione (S4)

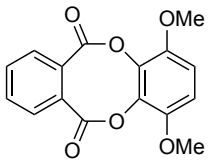

S4

To a stirred solution of **S3** (500 mg, 1.86 mmol, 1.00 eq.) in TFA (9 mL) was added sodium perborate tetrahydrate (1.72 g, 11.2 mmol, 6.00 eq.) under a stream of nitrogen. The reaction mixture was stirred over a water bath 90 min prior to quenching with ice-water (60 mL). DCM (20 mL) was added, the phases were separated, and the aqueous phase was extracted with DCM (2 x 20 mL). The combined organic layers were washed with water (20 mL) and brine (20 mL) and evaporated to give an orange crude product which was triturated from EtOAc to yield the product lactone **S4** as a white crystalline solid (101 mg, 0.34 mmol, 18%).

The synthesis was performed as described in literature and the spectroscopic data is identical to those reported.[141]

^{1}H-NMR ($CDCl_3$, 400 MHz): δ (ppm) = 7.53 (s, 4H), 6.65 (s, 2H), 3.80 (s, 6H).

4,7-Dimethoxybenzo[*d*][1,3]dioxole (6)

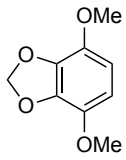

6

S4 (60.0 mg, 0.200 mmol, 1.00 eq.) was dissolved in dimethylformamide (10 mL, dried over 4 Å MS prior to use) and caesium carbonate (260 mg, 0.800 mmol, 4.00 eq.) as well as dibromomethane (139 mg, 0.800 mmol, 4.00 eq.) were added at room temperature. The reaction mixture was stirred at 80 °C for 12 h under a stream of nitrogen, after which time another portion of dibromomethane (139 mg, 0.800 mmol, 4.00 eq.) was added. The mixture was heated to 80 °C for another 12 h, diluted in an aqueous solution of sodium hydroxide (0.1 M) and extracted with dichloromethane (3 × 10 mL). The combined organic extracts were washed with water (10 mL) and brine (10 mL), dried over sodium sulfate and the solvent was removed *in vacuo*. A white solid of 4,7−dimethoxybenzo[*d*][1,3]dioxole (13.0 mg, 71.4 µmol, 36%) was obtained.

The synthesis was performed as described in literature and the spectroscopic data is identical to those reported.[141]

^{1}H-NMR ($CDCl_3$, 400 MHz): δ (ppm) = 6.42 (s, 2H), 5.97 (s, 2H), 3.83 (s, 6H).

NMR spectra

The following chapter includes the NMR spectra of all hitherto unknown compounds and those which were known but were not prepared using literature-known procedures.

2-(Benzyloxy)-1-methoxy-4-nitrobenzene (S1)

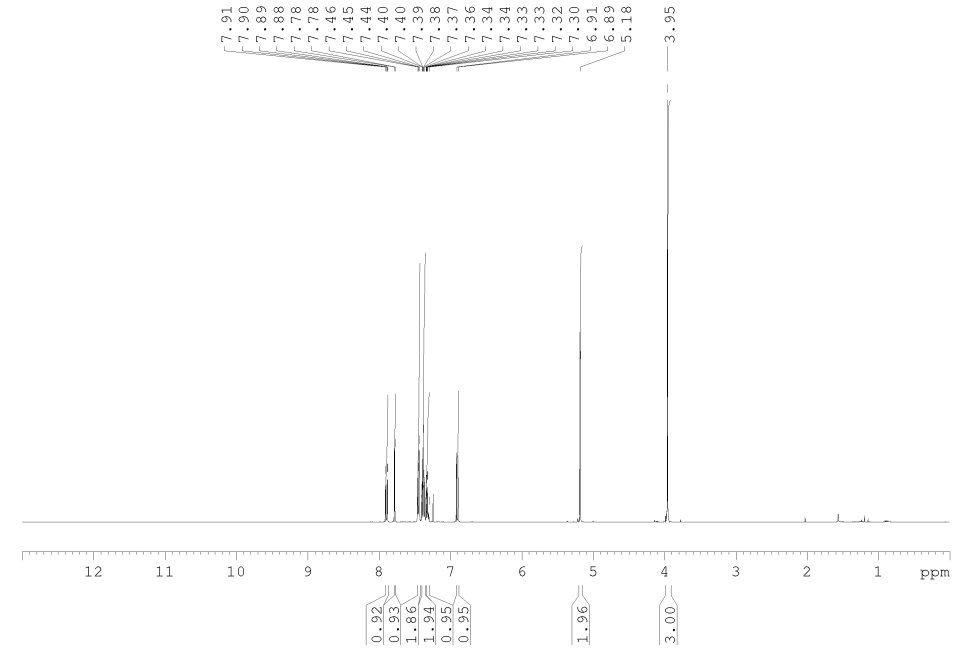

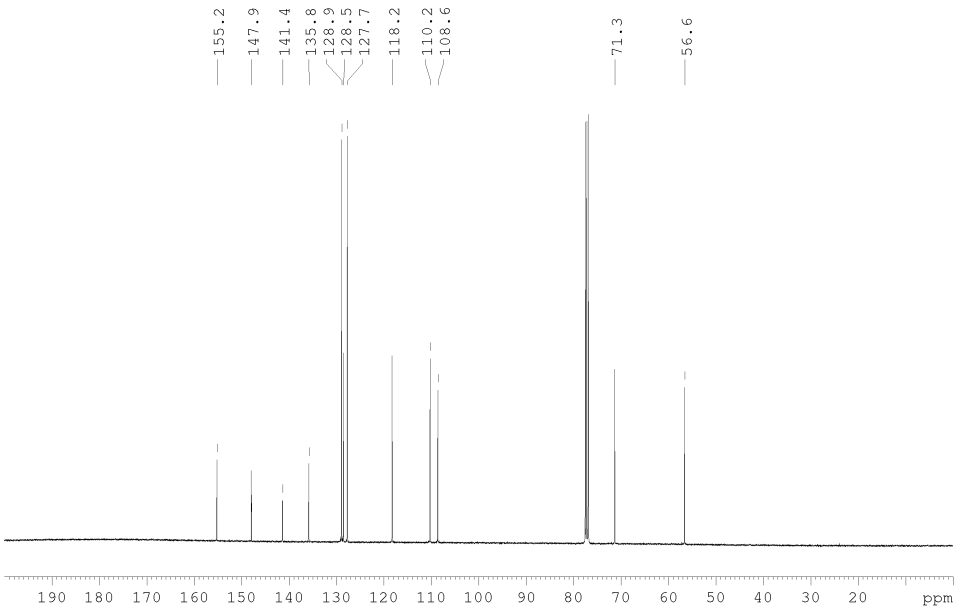

3-(Benzyloxy)-4-methoxyaniline (2)

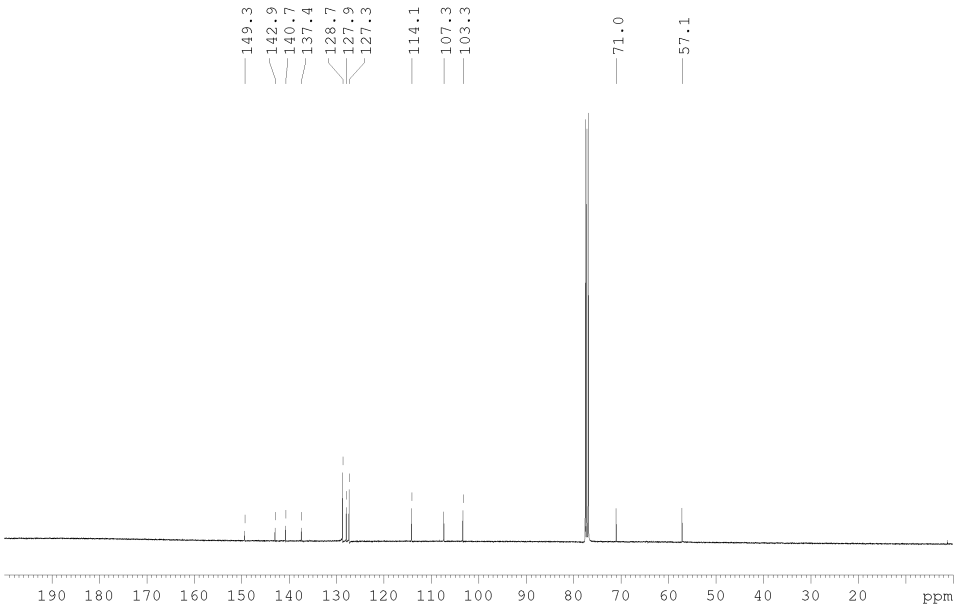

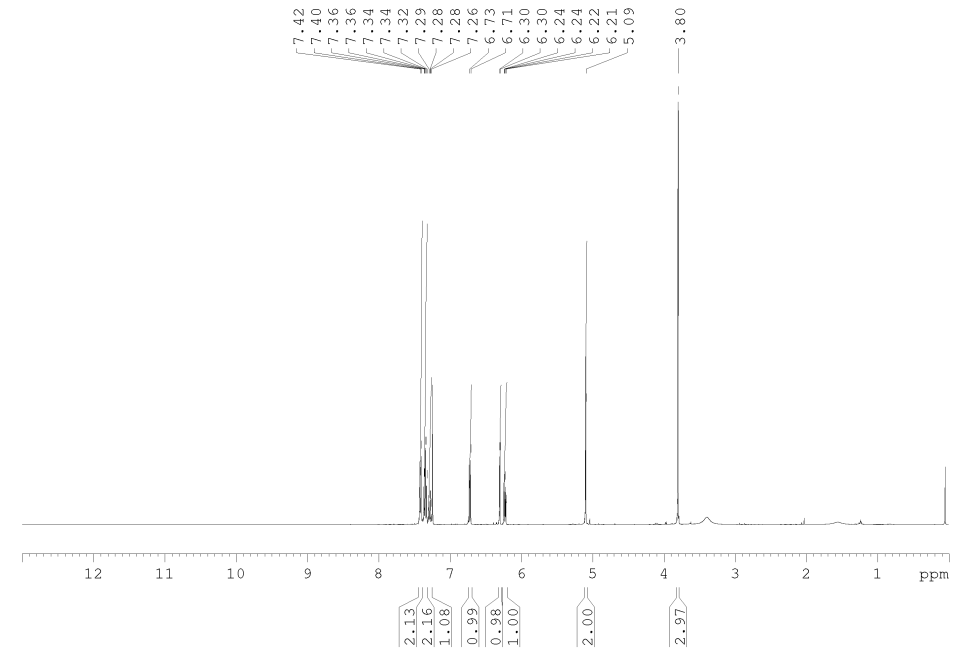

S-(3-(benzyloxy)-4-methoxyphenyl) O-ethyl carbonodithioate (S2)

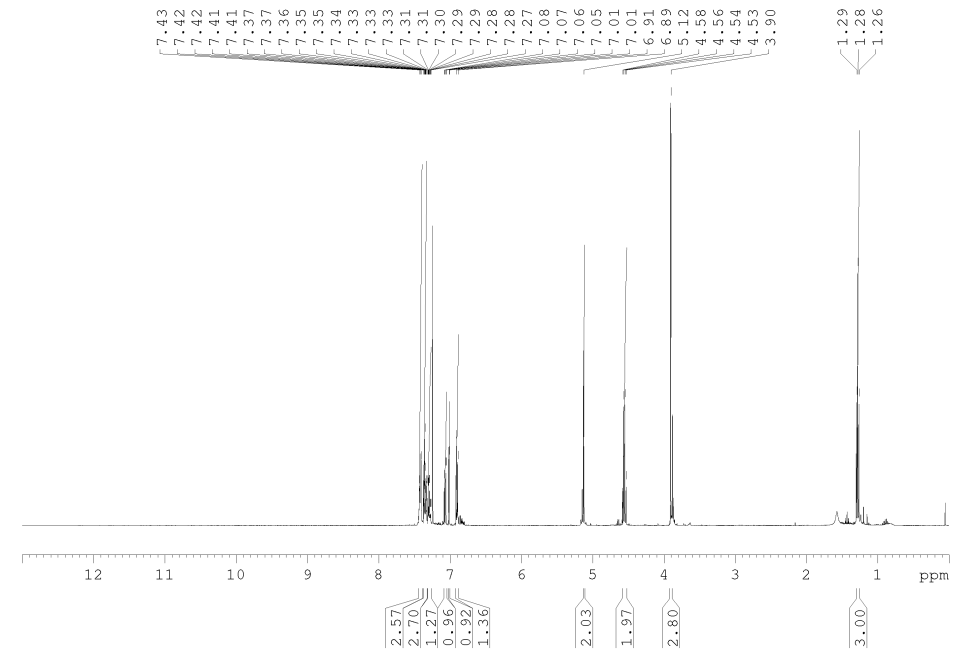

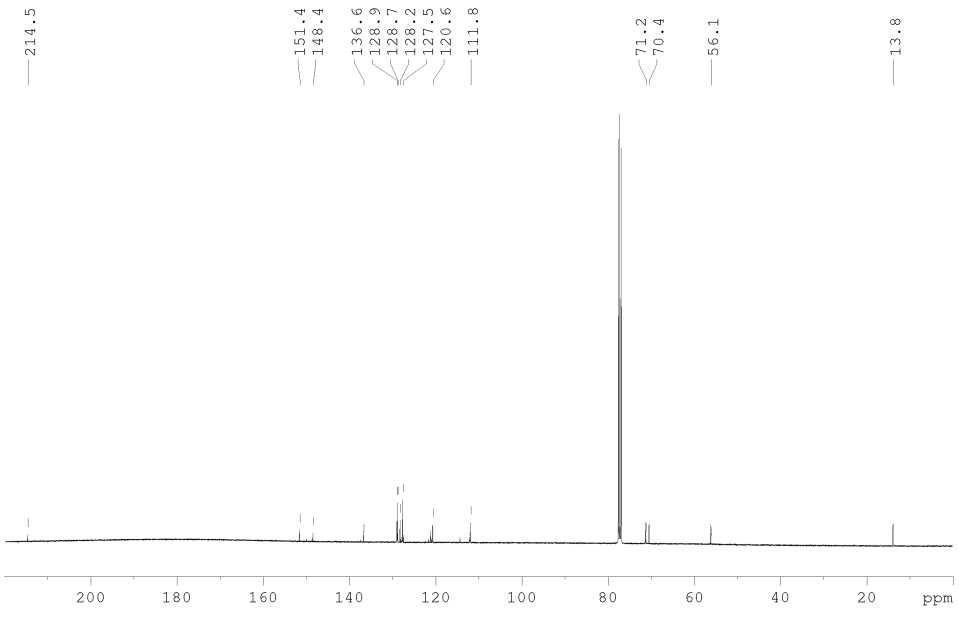

2-((3-(benzyloxy)-4-methoxyphenyl)thio)acetic acid (3)

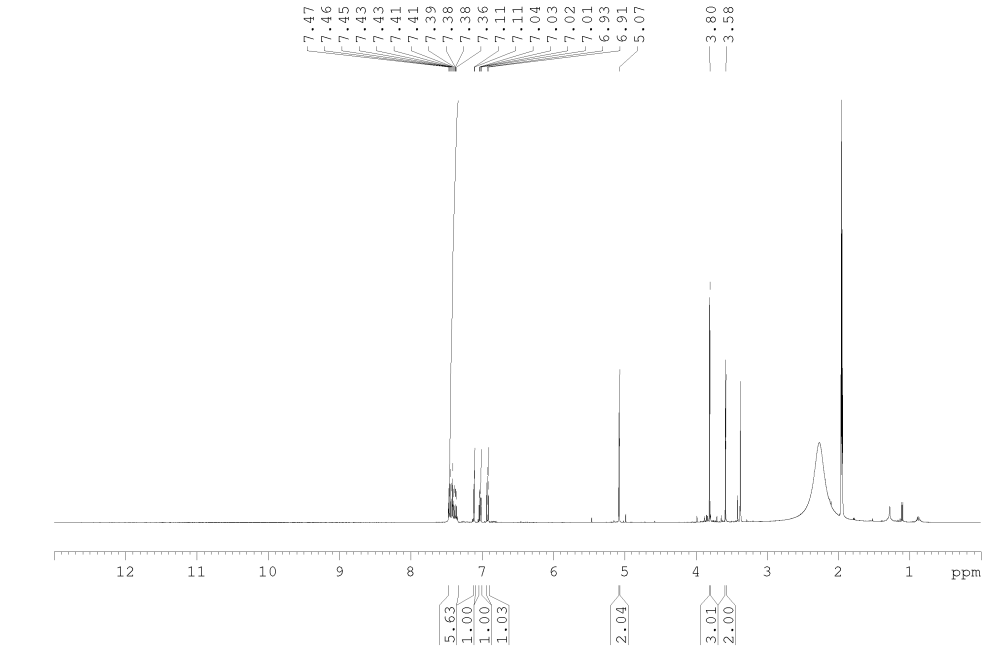

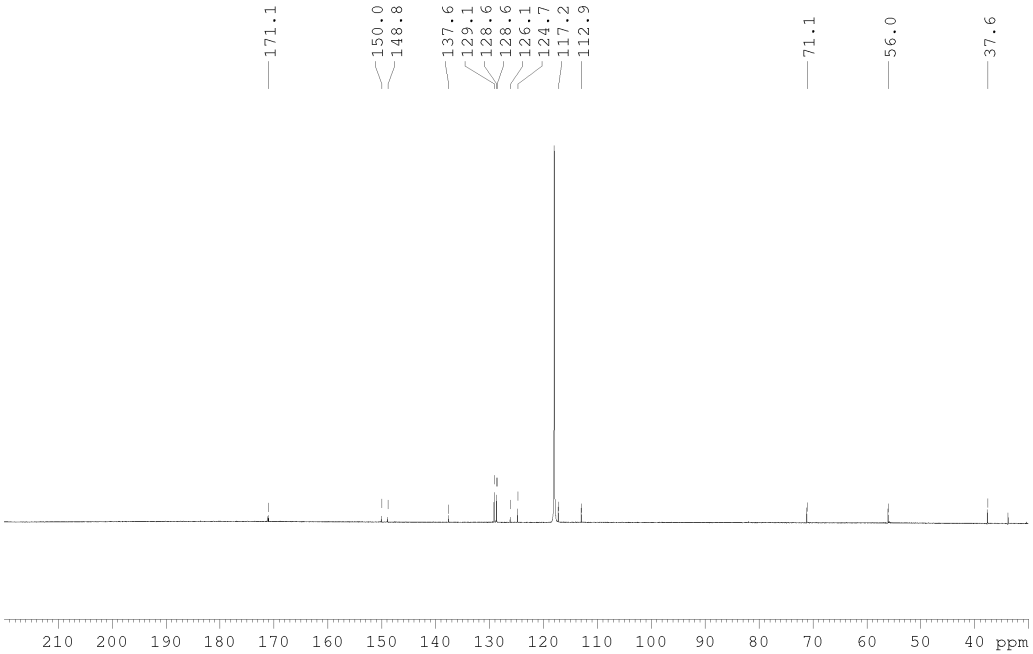

11.2 Supporting information to chapter 8.2

Reagents and Conditions:

Unless stated otherwise: (1) all reactions and characterizations were performed with unpurified, undried, non-degassed solvents and reagents, used as obtained, under closed air atmosphere without special precautions. The use of dry solvents in this context is to be understood as using anhydrous solvents bought from Acros Organics which were stored and handled under an atmosphere of nitrogen; (2) when not specified, “column” and “chromatography” refer to flash column chromatography performed on Merck silica gel Si-60 (40-63 µm); (4) procedures and yields are unoptimized; (5) yields refer to isolated chromatographically and spectroscopically pure materials (6) all eluent and solvent mixtures are given as volume ratios unless otherwise specified, thus “1:1 EA:Hx” indicates a 1:1 mixture (by volume) of ethyl acetate and hexanes.

Thin-layer chromatography (TLC):

TLC glass plates and visualized by ultraviolet light (UV)TLC was run on 0.25 mm Merck silica gel plates (60, F-254). UV light (254 nm) was used as a visualizing agent. R_f values were usually determined in MeOH: DCM eluents. TLC characterizations are thus abbreviated as per R_f = 0.09 (10% MeOH in DCM).

Automated flash chromatography:

Automated flash chromatography was performed on a Teledyne Isco CombiFlash.

Nuclear magnetic resonance (NMR) spectroscopy:

Known compounds were checked against literature data. The default spectrometer used was a Bruker Avance III (with TCI Cryoprobe; 400 MHz & 100 MHz for ^{1}H and ^{13}C respectively); NMR solvents are given individually for each compound. Chemical shifts (δ) are reported in ppm calibrated to residual non-perdeuterated solvent as an internal reference.[177] The following peak descriptions are used: singlet (s), doublet (d), doublet of doublets (dd), triplet (t), quartet (q), multiplet (m), broad (br.), pseudotriplet (~t).

General Procedure A (GP A): C10-modification of colchicine

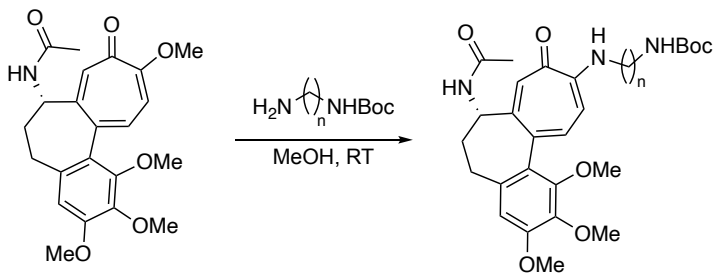

Scheme S1: C10-modification of colchicine.

To a solution of colchicine in MeOH (1.5 mL) was added the mono-N-*Boc*-protected bisamine and the mixture was stirred for 48h prior to evaporation of the solvent.

General Procedure B (GP B): Deprotection of Boc-protected amines

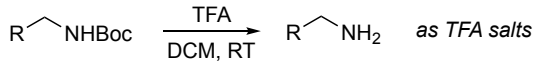

Scheme S2: TFA mediated Boc-deprotection.

To a solution of the protected amine in DCM was added TFA and the mixture was stirred at room temperature for the time indicated. The volatiles were removed *in vacuo* and the residue was dried in high vacuum to obtain the TFA salts of the desired free amines.

General Procedure C (GP C): HATU-mediated amide couplings

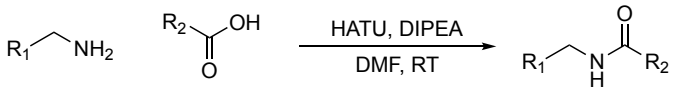

Scheme S3: HATU-mediated amide coupling.

A solution of the carboxylic acid (1 – 2 eq.), HATU (1.2 – 2 eq.) and DIPEA (excess) in DMF was stirred at room temperature for 10 min. prior to addition of a solution of the respective amine (1 – 2 eq.) in DMF. Upon completion of reaction (as indicated by TLC), NH_4Cl and EtOAc was added, the phases were separated, and the organic phase was extracted with EtOAc (3 times). The combined organic extracts were washed with 10% LiCl (3 times) and brine and dried over Na_2SO_4 or $MgSO_4$.

Synthesis of literature-known precursors

Carboxylic acid **1**, protected amides **2-4** and free amines **5-7** were prepared according to a procedure by Reynders et al. and all spectroscopic data matched those reported.[147]

Tubulin inhibitor **8** was synthesized according to a procedure by Chen et al. and all spectroscopic data matched those reported.[155]

***N*-(4-(2-(4-(-(2-(2,6-dioxopiperidin-3-yl)-1-oxoisoindolin-4-yl)diazenyl)-2,6-dimethoxyphenoxy)acetamido)butyl)-2-(3-hydroxy-4-methoxyphenyl)-3-(3,4,5-trimethoxyphenyl)acrylamide (CA-TubPHOTAC2)**

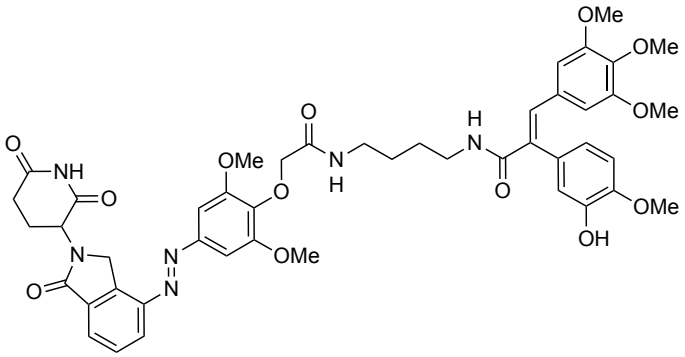

The compound was prepared by reacting **8**[155] (8 mg, 0.02 mmol, 1 eq), HATU (10 mg, 0.03 mmol, 1.5 eq.), DIPEA (100 µL, 80 mg, 0.60 mmol, 30 eq.) and **6**[147] (30 mg, 0.04 mmol, 2 eq.) in DMF (1 mL) according to GP C for 24h. Purification by automated flash chromatography (2 → 10% MeOH in DCM) yielded the desired product as orange solid (6 mg, 0.01 mmol, 30%).

^{1}H-NMR ($CDCl_3$, 400 MHz):δ = 8.17 (d, *J* = 8.1 Hz, 1H), 8.13 (s, 1H), 7.83 – 7.80 (m, 1H), 7.69 (d, *J* = 7.3 Hz, 1H), 7.66 (s, 1H), 7.28 (d, *J* = 7.3 Hz, 1H), 7.20 (s, 2H), 6.91 (d, *J* = 8.3 Hz, 1H), 6.84 (s, 1H), 6.74 – 6.68 (m, 1H), 6.28 (s, 2H), 5.72 – 5.69 (m, 1H), 5.24 (dd, *J* = 4.6 / 12.0 Hz, 1H), 4.85 (d, *J* = 18.0 Hz, 1H), 4.71 (d, *J* = 18.0 Hz, 1H), 4.60 (s, 2H), 3.97 (s, 6H), 3.89 (s, 3H), 3.77 (s, 3H), 3.54 (s, 3H), 3.35 – 3.29 (m, 4H), 3.22 (s, 2H), 2.91 – 2.78 (m, 2H), 1.54 – 1.52 (m, 6H); $\mathbf{R_f}$ = 0.26 (10% MeOH in DCM).

***tert*-butyl (*S*)-(2-((7-acetamido-1,2,3-trimethoxy-9-oxo-5,6,7,9-tetrahydrobenzo[*a*]heptalen-10-yl)amino)ethyl)carbamate (9)**

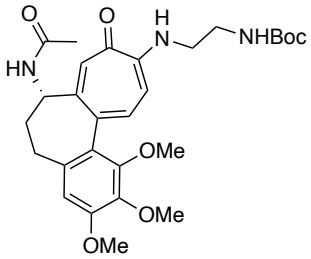

The compound was prepared from colchicine (50 mg, 0.13 mmol, 1 eq.) and N-*Boc*-ethylendiamine (79 µL, 80 mg, 0.50 mmol, 4 eq.) in MeOH (1.5 mL) according to **GP A** for 48h. Purification was accomplished by automated flash chromatography (0 → 10% MeOH in DCM, product eluting at 4% MeOH) yielding a yellow oil (66 mg, 0.13 mmol, 100%).

^{1}H-NMR ($CDCl_3$, 400 MHz):δ = 7.43 – 7.33 (m, 4H), 6.63 (d, *J* = 11.2 Hz, 1H), 6.50 (s, 1H), 4.91 (~s, 1H), 4.70 – 4.64 (m, 1H), 3.92 (s, 3H), 3.87 (s, 3H), 3.59 (s, 3H), 3.51 (t, *J* = 5.2 Hz, 2H), 3.46 (t, *J* = 5.5 Hz, 2H), 2.47 – 2.43 (m, 1H), 2.38 – 2.19 (m, 2H), 1.97 (s, 3H), 1.91 – 1.85 (m, 1H), 1.43 (s, 9H); **^{13}C-NMR** ($CDCl_3$, 100 MHz): δ = 175.4, 169.7, 156.1, 154.4, 152.9, 151.1, 150.9, 141.6, 139.1, 134.4, 130.7, 126.8, 123.3, 108.3, 107.2, 106.6, 79.9, 61.4, 61.3, 56.1, 52.5, 42.8, 39.3, 37.4, 30.1, 29.7, 28.4, 23.0; **R_f** = 0.19 (5% MeOH in DCM).

***tert*-butyl (*S*)-(4-((7-acetamido-1,2,3-trimethoxy-9-oxo-5,6,7,9-tetrahydrobenzo[*a*]heptalen-10-yl)amino)butyl)carbamate (10)**

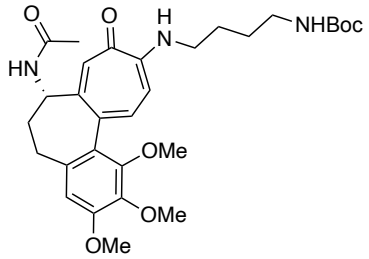

The compound was prepared from colchicine (50 mg, 0.13 mmol, 1 eq.) and *tert*-butyl (4-aminobutyl)carbamate (96 µL, 94 mg, 0.50 mmol, 4 eq.) in MeOH (1.5 mL) according to **GP A** for 48h. Purification was accomplished by automated flash chromatography (0 → 10% MeOH in DCM, product eluting at 4% MeOH) yielding a yellow oil (72 mg, 0.13 mmol, 100%).

^{1}H-NMR ($CDCl_3$, 400 MHz):δ = 7.41 – 7.38 (m, 2H), 7.33 (d, *J* = 6.9 Hz, 1H), 7.19 (t, *J* = 5.6 Hz, 1H), 6.57 – 6.53 (m, 2H), 6.50 (s, 1H), 4.69 – 4.65 (m, 1H), 4.57 (br. s, 1H), 3.92 (s, 3H), 3.87 (s, 3H), 3.59 (s, 3H), 3.36 (q, *J* = 6.6 Hz, 2H), 3.17 (q, *J* = 6.4 Hz, 2H), 2.48 – 2.43 (m, 1H), 2.39 – 2.19 (m, 2H), 1.97 (s, 3H), 1.91 – 1.84 (m, 1H), 1.81 – 1.74 (m, 2H), 1.66 – 1.57 (m, 2H), 1.42 (s, 9H); **^{13}C-NMR** ($CDCl_3$, 100 MHz): δ = 175.2, 169.7, 156.0, 154.2, 152.9, 151.1, 150.7, 141.6, 139.1, 134.5, 130.2, 126.9, 123.5, 122.9, 108.2, 107.2, 105.5, 70.1, 61.4, 61.3, 56.1, 52.5, 42.4, 37.4, 30.1, 28.4, 28.1, 27.8, 25.9, 23.0; **R_f** = 0.20 (2.5% MeOH in DCM).

***tert*-butyl (*S*)-(6-((7-acetamido-1,2,3-trimethoxy-9-oxo-5,6,7,9-tetrahydrobenzo[*a*]heptalen-10-yl)amino)hexyl)carbamate (11)**

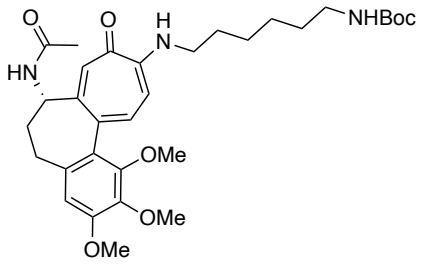

The compound was prepared from commercial colchicine (60 mg, 0.15 mmol, 1 eq.) and *tert*-butyl (6-aminohexyl)carbamate (130 µL, 130 mg, 0.60 mmol, 4 eq.) in MeOH (1.5 mL) according to **GP A** for 48h. Purification was accomplished by automated flash chromatography (0 → 10% MeOH in DCM) yielding a yellow oil (100 mg, 0.17 mmol, >99%).

^{1}H-NMR ($CDCl_3$, 400 MHz):δ = 8.31 (s, 1H), 7.49 (s, 1H), 7.38 (d, *J* = 11.2 Hz, 1H), 7.17 (t, *J* = 5.6 Hz, 1H), 6.54 (d, *J* = 11.4 Hz, 1H), 6.48 (s, 1H), 4.67 – 4.58 (m, 2H), 3.89 (s, 3H), 3.84 (s, 3H), 3.57 (s, 3H), 3.30 (q, *J* = 6.6 Hz, 2H), 3.16 – 3.06 (m, 4H), 2.44 – 2.40 (m, 1H), 2.35 – 2.17 (m, 2H), 2.11 (s, 3H), 1.74 – 1.69 (m, 2H), 1.48 – 1.43 (m, 6H), 1.38 (s, 9H); **^{13}C-NMR** ($CDCl_3$, 100 MHz): δ = 175.1, 170.0, 156.1, 154.3, 152.9, 151.3, 151.2, 141.6, 139.2, 134.7, 130.3, 127.0, 122.8, 108.4, 107.3, 79.1, 61.5, 61.4, 56.2, 52.7, 51.5, 42.8, 42.1, 40.5, 37.2, 33.7, 31.0, 30.1, 28.5, 26.9, 26.5, 22.9; **R_f** = 0.22 (5% MeOH in DCM).

(*S*)-2-((7-acetamido-1,2,3-trimethoxy-9-oxo-5,6,7,9-tetrahydrobenzo[*a*]heptalen-10-yl)amino)ethan-1-aminium 2,2,2-trifluoroacetate (12)

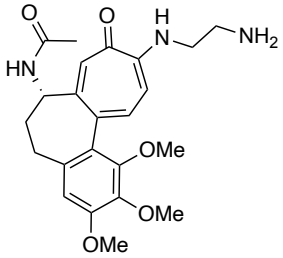

The compound was prepared by treatment of **9** (54 mg, 0.10 mmol, 1 eq.) with TFA (1 mL, excess) in DCM (2 mL) according to **GP B** for 3.5h. Removal of the volatiles and drying in high vacuum afforded desired product **12** as yellow solid in form of its TFA salt (55 mg, 0.10 mmol, 100%) with traces of residual TFA.

^{1}H-NMR (MeOD, 400 MHz):δ = 7.70 (d, *J* = 11.5 Hz, 1H), 7.56 (s, 1H), 7.21 (d, *J* = 11.6 Hz, 1H), 6.75 (s, 1H), 4.51 – 4.46 (m, 1H), 3.90 (s, 3H), 3.88 (s, 3H), 3.58 (s, 3H), 3.33 – 3.24 (m, 4H), 2.65 – 2.57 (m, 2H), 2.32 – 2.22 (m, 2H), 2.01 (s, 3H), 1.56 (s, 1H), **^{13}C-NMR** (MeOD, 100 MHz): δ = 172.9, 161.2 (q, *J* = 37.7 Hz), 155.9, 155.1, 153.8, 151.9, 142.9,

142.6, 136.4, 135.4, 127.1, 123.9, 117.4, 114.6, 108.8, 61.8, 61.7, 56.6, 54.2, 41.2, 38.8, 38.1, 30.5, 27.7, 22.4.

(*S*)-4-((7-acetamido-1,2,3-trimethoxy-9-oxo-5,6,7,9-tetrahydrobenzo[*a*]heptalen-10-yl)amino)butan-1-aminium 2,2,2-trifluoroacetate (13)

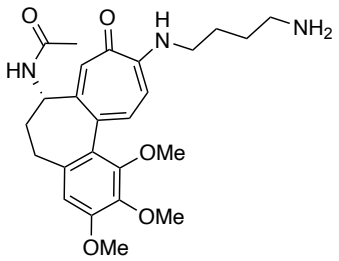

The compound was prepared by treatment of **10** (62 mg, 0.11 mmol, 1 eq.) with TFA (1 mL, excess) in DCM (2 mL) according to **GP B** for 3.5h. Removal of the volatiles and drying in high vacuum afforded desired product **13** as yellow solid in form of its TFA salt (76 mg, 0.13 mmol, >99%) with traces of residual TFA.

^{1}H-NMR (MeOD, 400 MHz):δ = 7.94 (d, *J* = 12.1 Hz, 1H), 7.79 (s, 1H), 7.53 (d, *J* = 12.2 Hz, 1H), 6.80 (s, 1H), 4.50 – 4.45 (m, 1H), 3.92 (s, 3H), 3.90 (s, 3H), 3.69 (t, *J* = 6.6 Hz, 2H), 3.62 (s, 3H), 3.02 (t, *J* = 7.0 Hz, 2H), 2.65 (dd, *J* = 12.6 / 5.5 Hz, 1H), 2.40 – 2.20 (m, 2H), 2.16 – 2.08 (m, 1H), 2.04 (s, 3H), 1.91 – 1.76 (m, 4H); **^{13}C-NMR** ($CDCl_3$, 100 MHz): δ = 171.5, 170.5, 168.8, 157.6 (q, *J* = 41.9 Hz), 154.8, 153.7, 152.9, 151.9, 150.5, 142.3, 141.2, 136.0, 135.1, 133.8, 125.7, 124.2, 121.1, 118.9, 117.6, 116.0, 114.7, 113.2, 113.0, 110.4, 107.4, 105.2, 87.0, 69.0, 60.4, 60.3, 59.5, 55.2, 55.2, 53.5, 53.3, 53.1, 52.8, 52.6, 52.4, 41.8, 38.9, 36.8, 29.7, 29.2, 26.3, 24.8, 24.7, 24.7, 21.0

(*S*)-6-((7-acetamido-1,2,3-trimethoxy-9-oxo-5,6,7,9-tetrahydrobenzo[*a*]heptalen-10-yl)amino)hexan-1-aminium 2,2,2-trifluoroacetate (14)

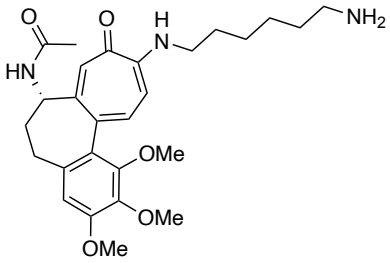

The compound was prepared by treatment of **11** (100 mg, 0.17 mmol, 1 eq.) with TFA (1 mL, excess) in DCM (2.5 mL) according to **GP B** for 3.5h. Removal of the volatiles and drying in high vacuum afforded desired product **14** as yellow solid in form of its TFA salt (124 mg, 0.21 mmol, >99%) with traces of residual TFA.

^{1}H-NMR (MeOD, 400 MHz):δ = 7.91 (d, *J* = 12.1 Hz, 1H), 7.77 (s, 1H), 7.49 (d, *J* = 12.3, 1H), 6.77 (s, 1H), 4.48 – 4.43 (m, 1H), 3.90 (s, 3H), 3.88 (s, 3H), 3.60 (s, 3H),

2.93 (t, *J* = 7.6 Hz, 1H), 2.64 – 2.60 (m, 1H), 2.37 – 2.20 (m, 2H), 2.14 – 2.05 (m, 1H), 2.02 (s, 3H), 1.83 – 1.76 (m, 2H), 1.73 – 1.70 (m, 2H), 1.49 – 1.42 (m, 6H), **^{13}C-NMR** (MeOD, 100 MHz): δ = 173.2, 161.4 (q, *J* = 36.7 Hz), 156.4, 155.6, 153.7, 151.9, 142.6, 136.7, 126.4, 120.3, 117.4, 114.6, 111.8, 108.9, 61.9, 61.7, 56.6, 44.1, 40.5, 38.4, 31.1, 30.4, 28.9, 27.5, 27.1,

***N*-(2-(((*S*)-7-acetamido-1,2,3-trimethoxy-9-oxo-5,6,7,9-tetrahydrobenzo[*a*]heptalen-10-yl)amino)ethyl)-2-(4-(2-(2,6-dioxopiperidin-3-yl)-1-oxoisoindolin-4-yl)diazenyl)-2,6-dimethoxyphenoxy)acetamide (Col-TubPHOTAC1)**

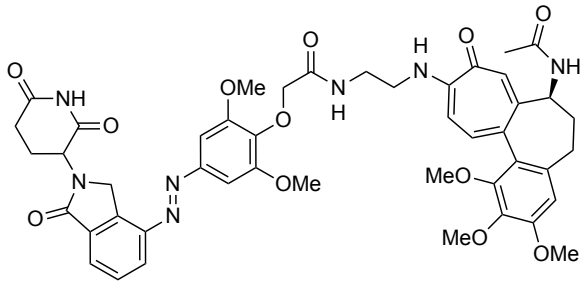

The compound was prepared by reacting the carboxylic acid **1** (32 mg, 0.05 mmol, 1 eq.), HATU (41 mg, 0.11 mmol, 2 eq.), DIPEA (350 µL, excess) and **12** (59 mg, 0.11 mmol, 2 eq.) in DMF (2 mL) according to **GP C** for 24h. Purification by automated flash chromatography (0 → 10% MeOH in DCM) yielded the desired product as orange solid (34 mg, 0.04 mmol, 70%).

^{1}H-NMR (DMSO-d_6, 400 MHz):δ = 11.03 (s, 1H), 8.33– 8.32 (m, 1H), 8,54 (d, *J* = 7.6 Hz, 1H), 8.21 (d, *J* = 7.7 Hz, 1H), 7.92 (d, *J* = 7.4 Hz, 1H), 7.81 – 7.77 (m, 2H), 7.33 (s, 2H), 7.17 (d, *J* = 11.1 Hz, 1H), 7.10 (s, 1H), 6.75 (d, *J* = 11.4 Hz, 1H), 6.73 (s, 1H), 5.75 (s, 2H), 5.16 (dd, *J* = 5.0 / 13.2 Hz, 1H), 4.81 (dd, *J* = 5.4 / 19.1 Hz, 1H), 4.69 (d, *J* = 19.1 Hz, 1H), 4.41 (s, 2H), 4.38 – 4.33 (m, 1H), 3.90 (s, 6H), 3.81 (s, 3H), 3.77 (s, 3H), 3.56 – 3.52 (m, 4H), 3.46 (s, 3H), 2.99 – 2.90 (m, 1H), 2.64 – 2.53 (m, 2H), 2.20 – 2.12 (m, 1H), 2.08 – 1.97 (m, 2H), 1.85 (s, 3H), **^{13}C-NMR** (DMSO-d_6, 100 MHz): δ = 174.8, 172.9, 172.9, 171.0, 168.7, 168.4, 167.2, 154.2, 152.8, 152.4, 150.3, 150.2, 148.4, 146.4, 140.7, 139.1, 137.9, 134.5, 134.4, 129.7, 128.7, 128.6, 126.6, 125.5, 122.8, 107.6, 107.0, 100.6, 71.7, 60.7, 60.5, 56.3, 55.8, 54.9, 51.9, 48.3, 42.0, 37.1, 36.6, 31.3, 29.4, 22.5, 22.3; **R_f** = 0.48 (10% MeOH in DCM).

***N*-(4-(((*S*)-7-acetamido-1,2,3-trimethoxy-9-oxo-5,6,7,9-tetrahydrobenzo[*a*]heptalen-10-yl)amino)butyl)-2-(4-(-(2-(2,6-dioxopiperidin-3-yl)-1-oxoisoindolin-4-yl)diazenyl)-2,6-dimethoxyphenoxy)acetamide (Col-TubPHOTAC2)**

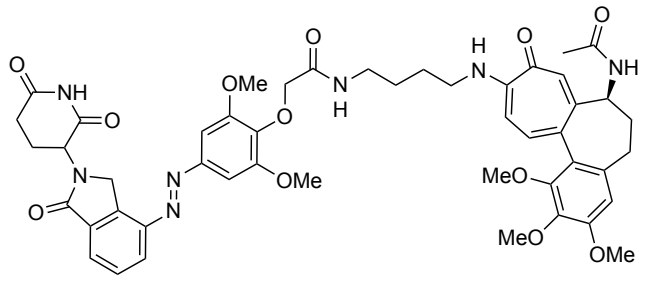

The compound was prepared by reacting carboxylic acid **1** (39 mg, 0.07 mmol, 1 eq.), HATU (50 mg, 0.13 mmol, 2 eq.), DIPEA (350 µL, excess) and **13** (75 mg, 0.13 mmol, 2 eq.) in DMF (2 mL) according to **GP C** for 24h. Purification by automated flash chromatography (0 → 10% MeOH in DCM, product eluting at 7% MeOH) yielded the desired product as orange solid (37 mg, 0.04 mmol, 61%).

^{1}H-NMR (DMSO-d_6, 400 MHz):δ = 11.03 (s, 1H), 8.54 (d, *J* = 7.7 Hz, 1H), 8.21 (d, *J* = 7.7 Hz, 1H), 8.01 – 7.98 (m, 1H), 7.92 (d, *J* = 7.5 Hz, 1H), 7.79 (t, *J* = 7.7 Hz, 1H), 7.68 – 7.65 (m, 1H), 7.34 (s, 1H), 7.17 (d, *J* = 11.1 Hz, 1H), 7.08 (s, 1H), 6.72 (s, 1H), 6.68 (d, *J* = 11.4 Hz, 1H), 5.75 (s, 2H), 5.15 (dd, *J* = 5.1 / 13.1 Hz, 1H), 4.84 – 4.77 (m, 1H), 4.71 – 4.66 (m, 1H), 4.42 (s, 2H), 4.39 – 4.32 (m, 1H), 3.92 (s, 3H), 3.90 (s, 3H), 3.81 (s, 3H), 3.76 (s, 3H), 3.46 (s, 3H), 3.41 – 3.38 (m, 2H), 3.25 (q, *J* = 6.4 Hz, 2H), 2.98 – 2.89 (m, 1H), 2.65 – 2.53 (m, 2H), 2.20 – 2.12 (m, 1H), 2.09 – 1.99 (m, 2H), 1.84 (s, 3H), 1.68 – 1.63 (m, 2H), 1.61 – 1.56 (m, 2H), **^{13}C-NMR** (DMSO-d_6, 100 MHz): δ = 174.6, 172.9, 171.0, 170.8, 168.4, 168.1, 167.2, 153.9, 152.6, 152.3, 152.1, 150.3, 150.1, 148.2, 146.4, 140.7, 139.3, 138.0, 134.5, 134.4, 134.4, 133.8, 129.7, 128.2, 126.7, 122.4, 107.6, 106.9, 100.6, 71.9, 60.7, 56.4, 56.2, 55.8, 54.9, 51.9, 51.4, 48.3, 36.7, 31.3, 29.5, 26.7, 25.2, 22.6; **R_f** = 0.17 (5% MeOH in DCM).

***N*-(6-(((*S*)-7-acetamido-1,2,3-trimethoxy-9-oxo-5,6,7,9-tetrahydrobenzo[*a*]heptalen-10-yl)amino)hexyl)-2-(4-(-(2-(2,6-dioxopiperidin-3-yl)-1-oxoisoindolin-4-yl)diazenyl)-2,6-dimethoxyphenoxy)acetamide (Col-TubPHOTAC3)**

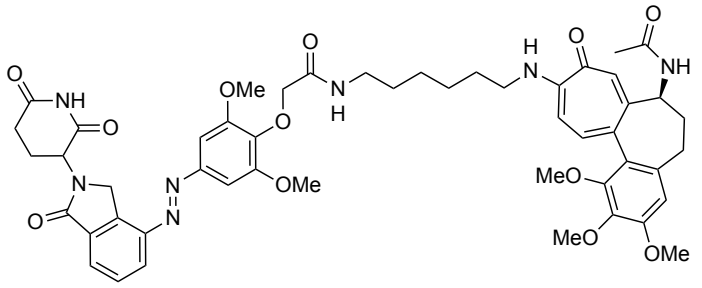

The compound was prepared by reacting carboxylic acid **1** (62 mg, 0.10 mmol, 1 eq.), HATU (79 mg, 0.21 mmol, 2 eq.), DIPEA (500 µL, excess) and **14** (124 mg, 0.21 mmol, 2 eq.) in DMF (2 mL) according to **GP C** for 24h. Purification by automated flash chromatography (0 → 10% MeOH in DCM) yielded the desired product as orange solid (52 mg, 0.05 mmol, 53%).

^{1}H-NMR (DMSO-d_6, 400 MHz):δ = 11.03 (s, 1H), 8.54 (d, *J* = 7.7 Hz, 1H), 8.20 (d, *J* = 7.6 Hz, 1H), 7.94 – 7.90 (m, 2H), 7.79 (t, *J* = 7.7 Hz, 1H), 7.60 (t, *J* = 5.9 Hz, 1H), 7.36 – 7.35 (m, 2H), 7.17 (d, *J* = 11.1 Hz, 1H), 7.08 (s, 1H), 6.72 (s, 1H), 6.64 (d, *J* = 11.4 Hz, 1H), 5.15 (dd, *J* = 5.1 Hz / 13.1 Hz, 1H), 4.81 (d, *J* = 19.2 Hz, 1H), 4.69 (d, *J* = 19.1 Hz, 1H), 4.43 (s, 2H), 4.39 – 4.32 (m, 1H), 3.94 – 3.93 (m, 6H), 3.81 (s, 3H), 3.76 (s, 3H), 3.46 (s, 3H), 3.91 (q, *J* = 6.5 Hz, 2H), 2.98 – 2.90 (m, 1H), 2.67 – 2.54 (m, 2H), 2.20 – 2.12 (m, 1H), 2.07 – 1.97 (m, 2H), 1.84 (s, 3H), 1.66 – 1.60 (m, 2H), 1.53 – 1.48 (m, 2H), 1.35 –1.31 (m, 6H); $\mathbf{R_f}$ = 0.50 (10% MeOH in DCM).

NMR spectra:

The following chapter includes the NMR spectra of all hitherto unknown compounds.

CA-TubPHOTAC2

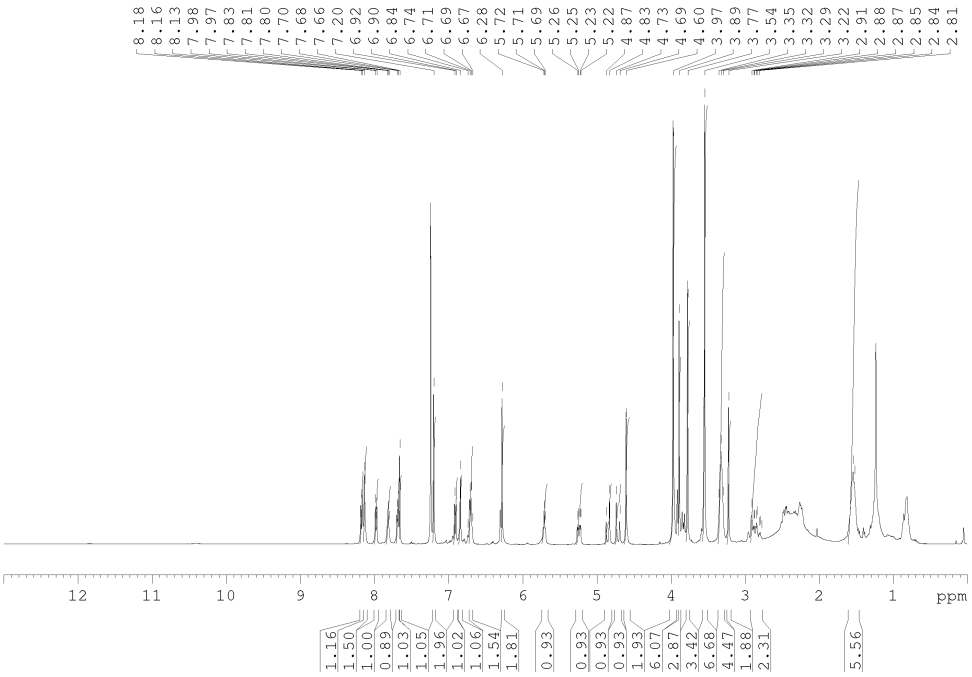

Protected colchicine amine 9

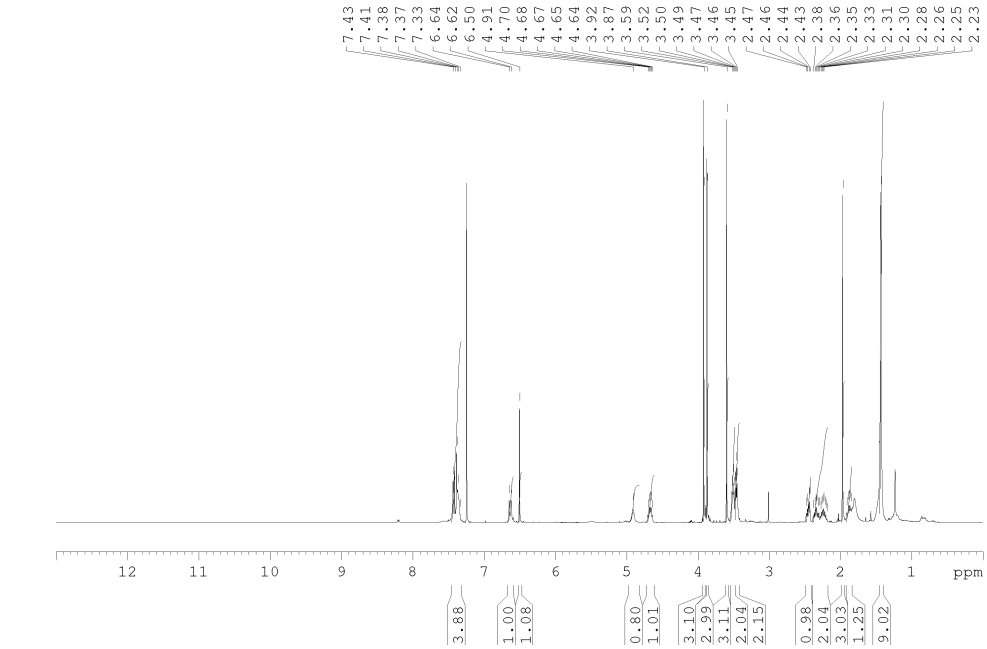

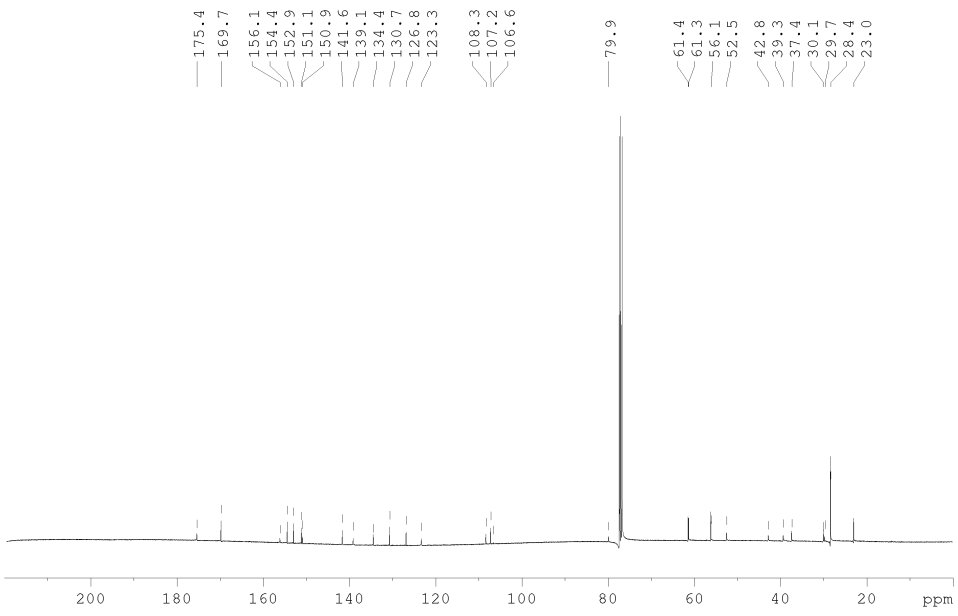

Protected colchicine amine 10

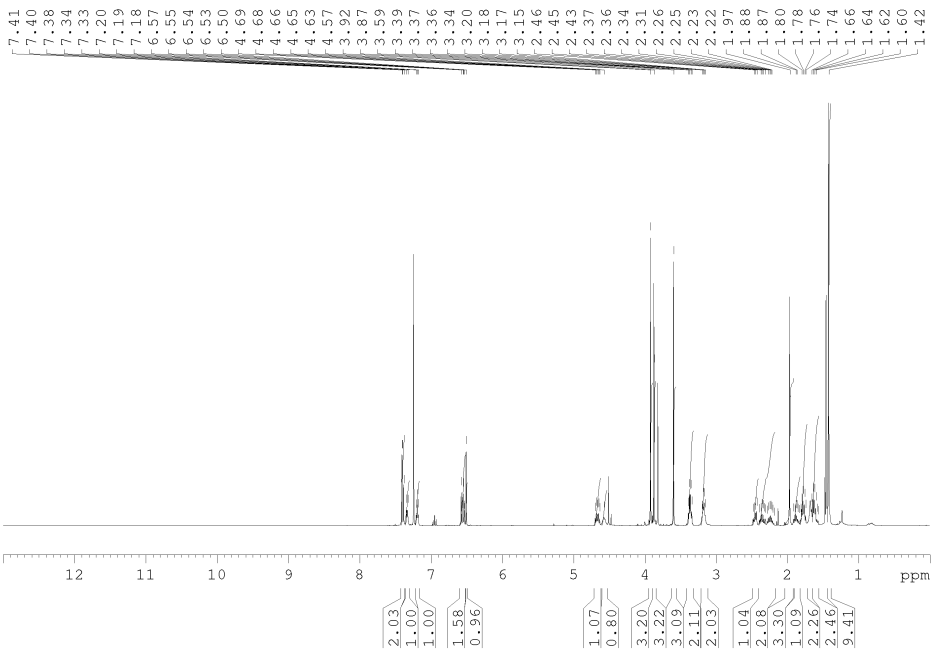

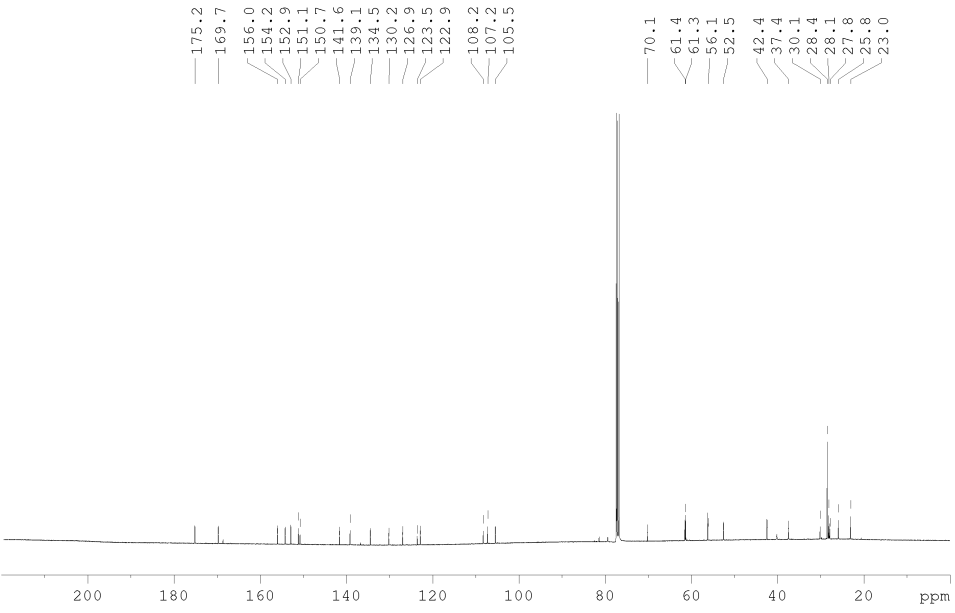

Protected colchicine amine 11

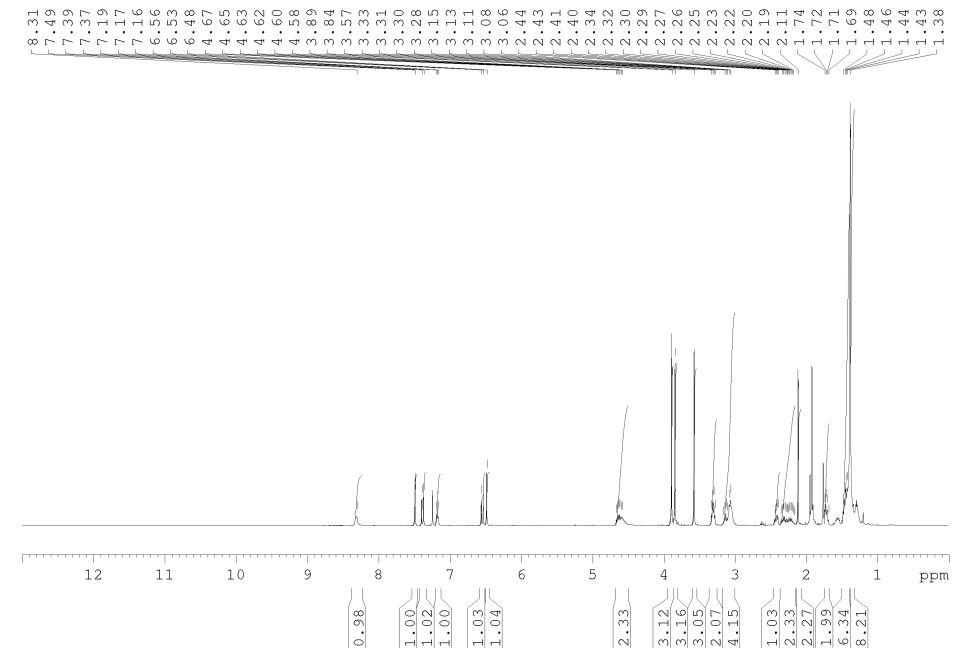

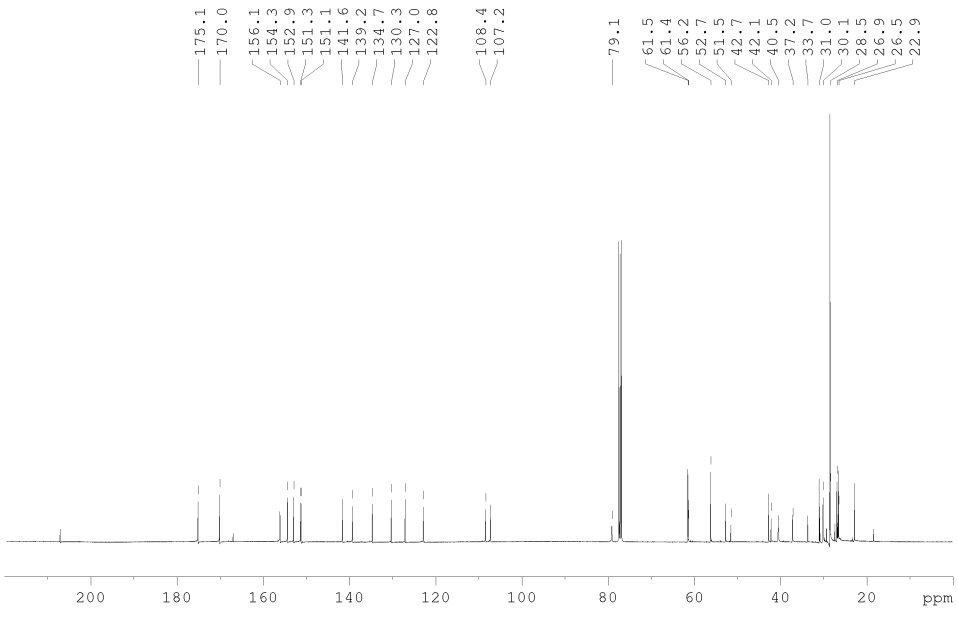

Free colchicine amine 12

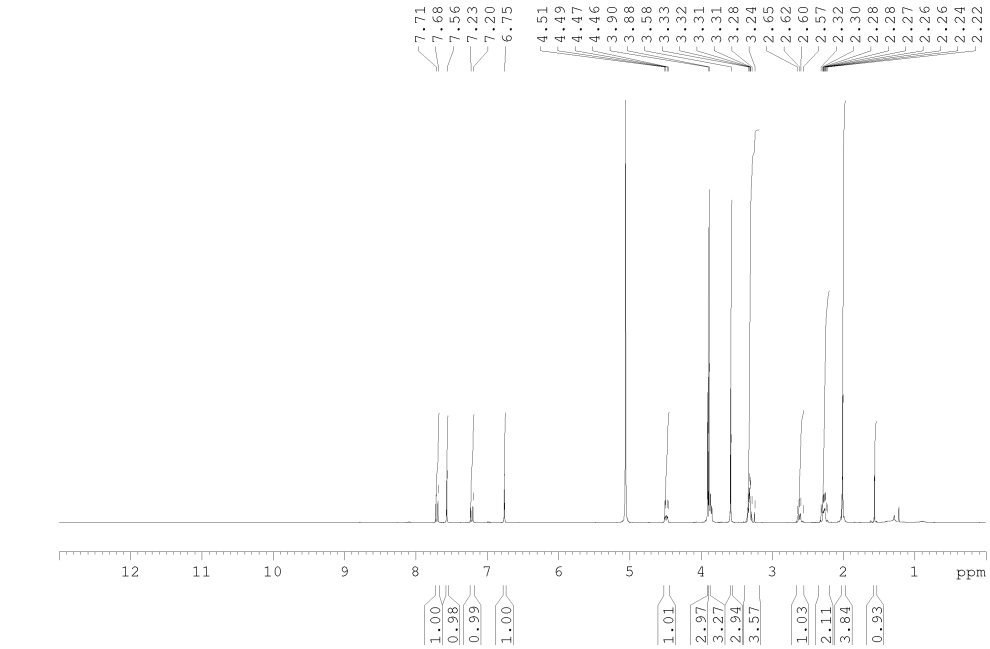

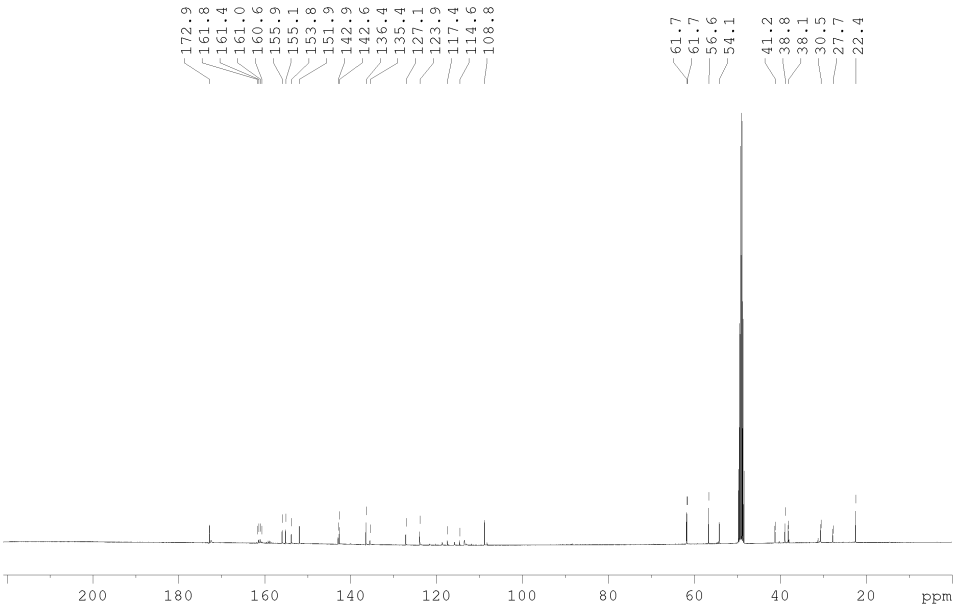

Free colchicine amine 13

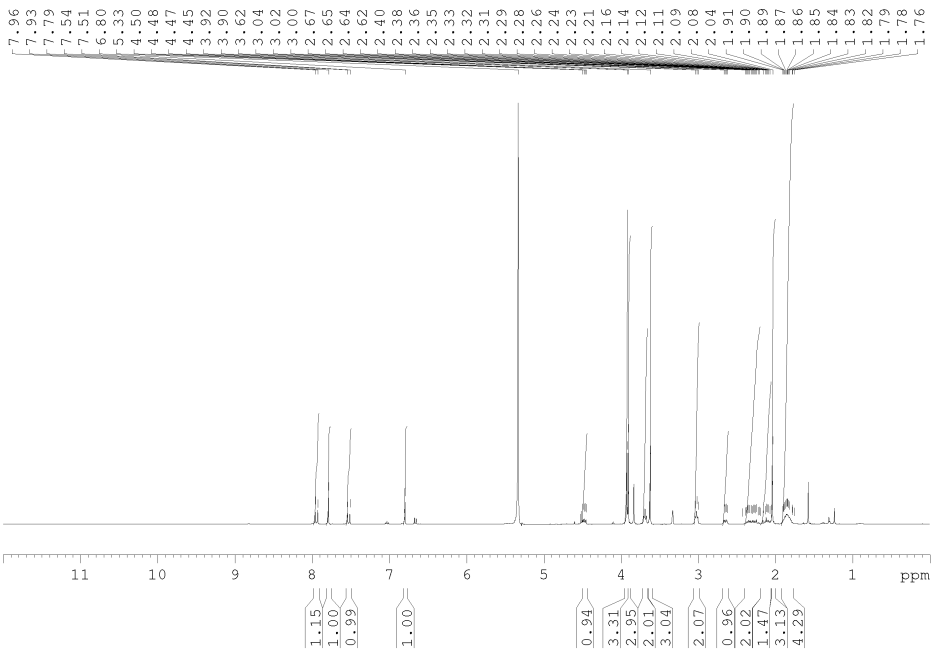

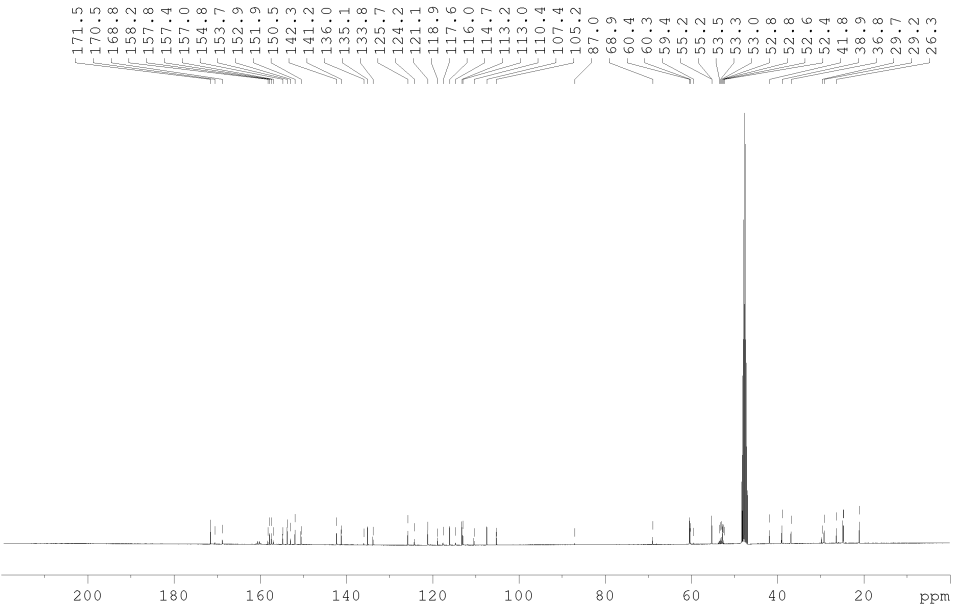

Free colchicine amine 14

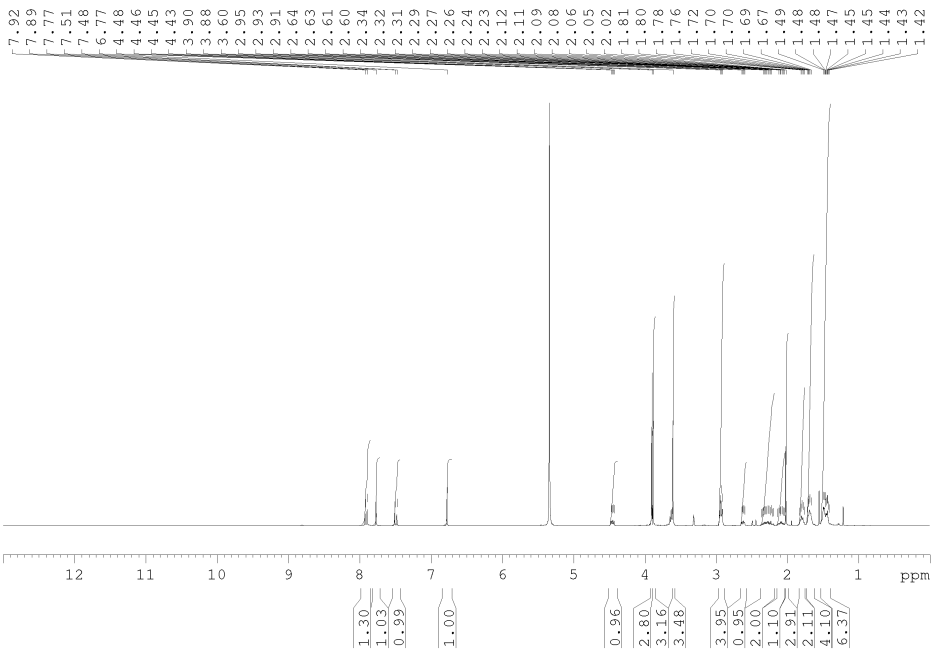

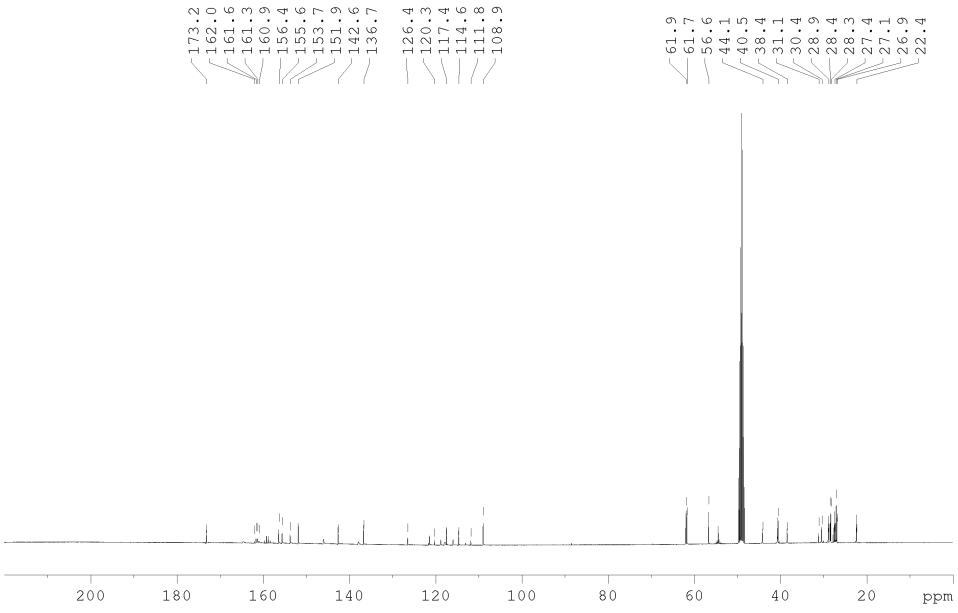

Col-TubPHOTAC1

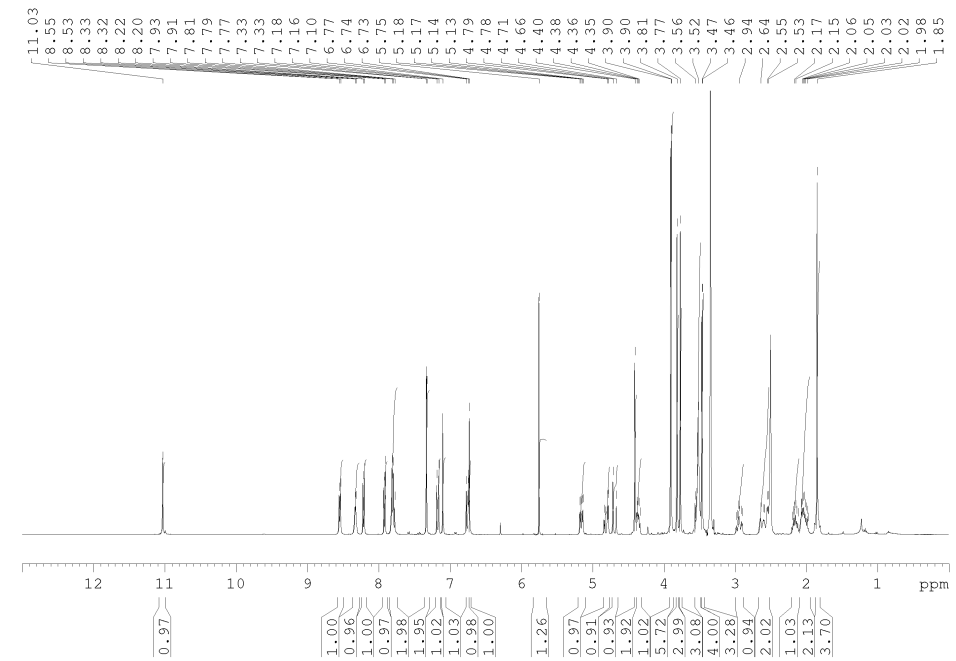

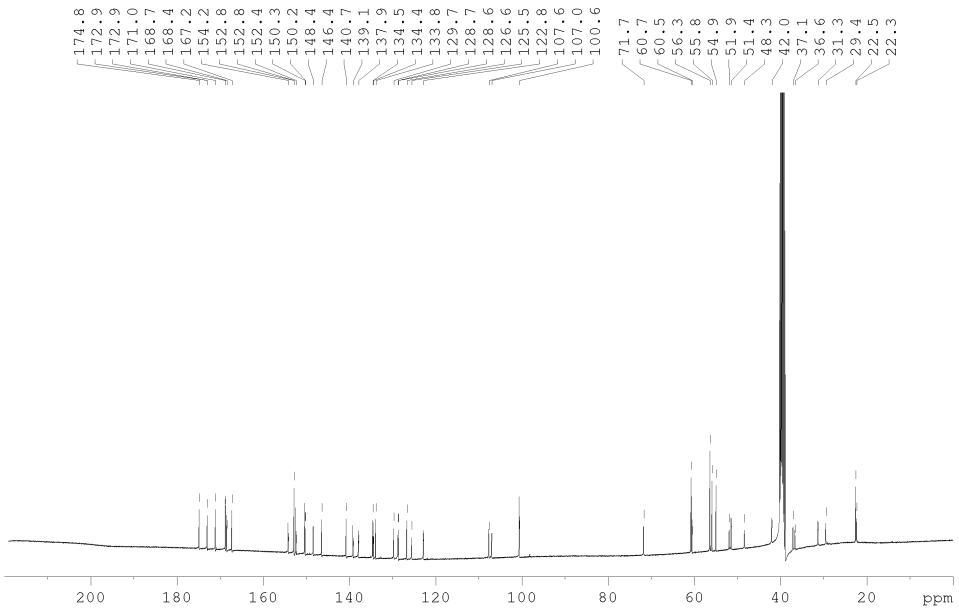

Col-TubPHOTAC2

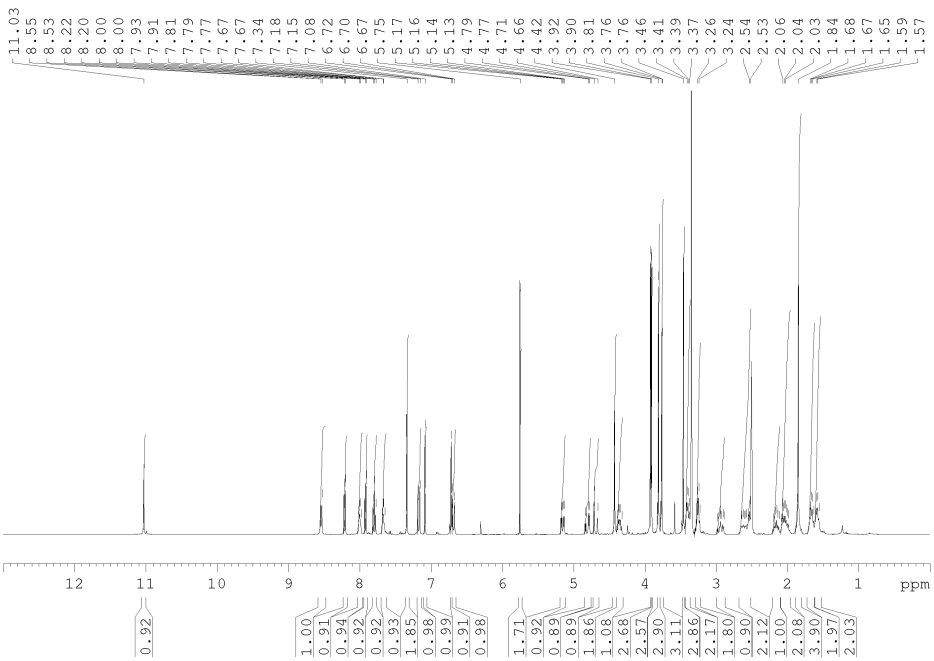

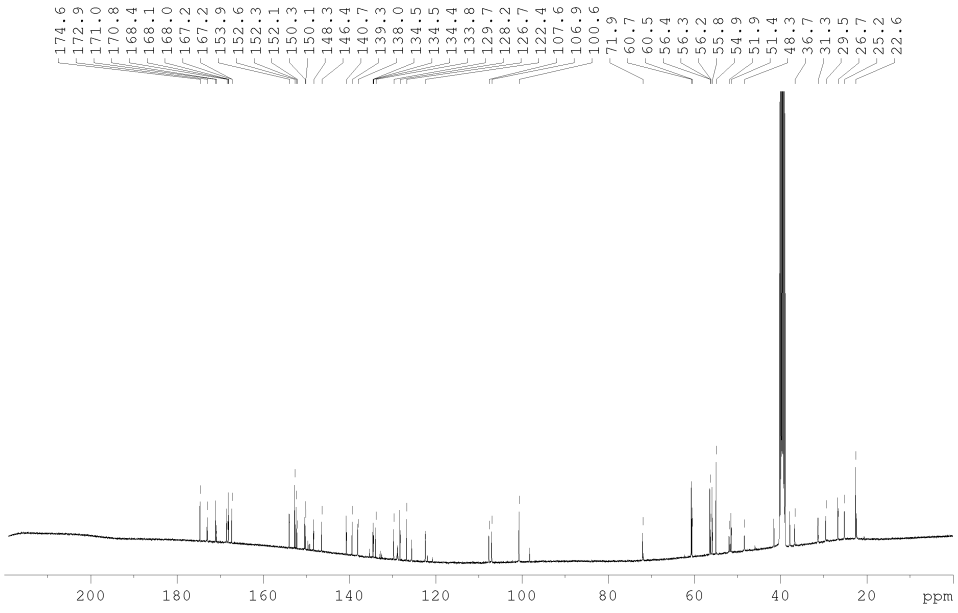

Col-TubPHOTAC3

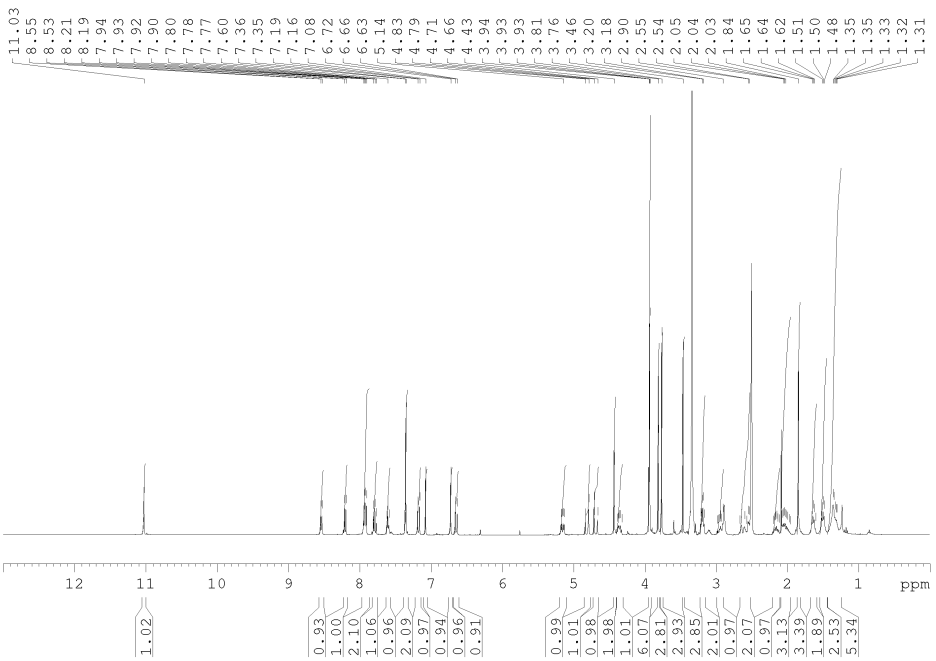

Light-dependent cytotoxicity assays:

Cells were seeded in 96 well-plates using 90 µL phenolred-free DMEM supplemented with 10% FBS 1% penicillin-streptomycin and a final concentration of 4 mM L-glutamine. After 24 h, cells were treated with compound stocks which were applied as 10x concentrations in 10 µL medium. As cosolvent, 1% DMSO and 2% MeCN final concentrations were used to ensure full solubility of all compounds at all concentrations and allow for comparability between all experiments. As reported previously, this did not alter cell growth and viability.[24,25] Light-dependent assays were performed as duplicates where one plate was kept in light-proof boxes, shielded from light (dark) and the second one was exposed to the irradiation protocol indicated using a cell DISCO as described previously.[24] Pulse program: 75 ms every 15 seconds: 96 well plates were placed on top of 24 LED arrays with a distance of ca. 1 cm. Pulse Program: 25 ms every 0.5 or 1 seconds, 96 well plates were placed 13 cm under 24 LED arrays to reduce toxicity due to overheating. LEDs were purchased from Roithner Laser Technik and operated as 24 LED arrays at 24 V input power (370 nm: XSL-370-5E, 380 nm: VL380-5-15, 390nm: VL390-5-15, 410 nm: VL410-5- 15, 440 nm: LED440-6-30, 475 nm: RLS-5B475-S, 505 nm: B5-433-B505, 525 nm B5-433- B525, 565 nm: LED565-03U). After 48 h of treatment, MTT (Invitrogen, Thermo Fischer Cat# M6494; 10 µL, 5 mg/mL in PBS) was added

to each well and incubated for 3 h (37 °C, 5% CO_2). The wells were emptied and the purple formazan crystals at the bottom of the wells were dissolved in 100 µL DMSO (incubated 10 minutes, 37 °C), followed by colorimetric read-out using a FLUOstar Omega microplate reader (BMG LABTECH) (120 sec. shaking, readout at 570 nm, blank corrected)

11.3 List of abbreviations

λ: Wavelength

Ac_2O: Acetic Anhydride

ADC: Antibody-Drug Conjugate

ATP: Adenosine Triphosphate

Boc: *tert*-Butyloxycarbonyl

BODIPY: 4,4-Difluor-4-bora-3a,4a-diaza-*s*-indacene

Bn: Benzyl

CA4: Combretastatin A4

Calcd.: Calculated

Cas: CRISPR Associated Protein

cAMP: Cyclic Adenosine Monophosphate

CDI: Colchicine Domain Inhibitor

ChR: Channelrhodopsin

CRISPR: Clustered Regularly Interspaced Short Palindromic Repeats

D: Debye

DAAD: Deutscher Akademischer Austauschdienst

DAMA-colchicine: N-deacetyl-N-(2-mercaptoacetyl)-colchicine

DCM: Dichloromethane

DIPEA: *N*,*N*-Diisopropylamine

DMEM: Dulbecco's Modified Eagle Medium

DMF: *N*,*N*-Dimethylformamide

DMSO: Dimethylsulfoxide

DNA: Desoxyribonucleic Acid

DTE: Dithienylethene

EA: Ethyl Acetate

EB protein: End-binding protein

EC_{50}: Half-maximal effective concentration

EI: Electron Ionization

EM: Electron Microscopy

ESI: Electrospray Ionization

Et: Ethyl

FBS: Fetal Bovine Serum

GDP: Guanosine-5'-diphosphate

GFP: Green Fluorescent Protein

GPCR: G-protein Coupled Receptor

GSH: Glutathione

GTP: Guanosine-5'-triphosphate

HATU: Hexafluorophosphate Azabenzotriazole Tetramethyl Uranium

HEK-293: Human embryonic kidney 293 (cells)

HI: Hemiindigo

HIV: Human Immunodeficiency Virus

HPLC: High-Performance Liquid Chromatography

HR: Halorhodopsin

HRMS: High Resolution Mass Spectrometry

HTI: Hemithioindigo

Hx: Hexanes

IC_{50} : Half-Maximal Inhibitory Concentration

ITI: Iminothioindoxyl

k_B: Boltzmann Constant

LED: Light-emitting Diode

LOV domain: Light-oxygen-voltage-sensing domain

LOX: Lipoxygenase

M: Molar

MDA: Microtubule Disrupting Agent

Me: Methyl

MSA: Microtubule Stabilizing Agent

MT: Microtubules

MTA: Microtubule Targeting Agent

MTT: 3,4-(Dimethylthiazol-2-yl)-2,5-diphenyl Tetrazolium Bromide

NMR: Nuclear Magnetic Resonance

NOESY: Nuclear Overhouser Effect Spectroscopy

NYU: New York University

PHOTAC: Photochemically Targeting Chimera

PHT: Pyrrole Hemithioindigo

PIDA: (Diacetoxy)iodobenzene

POI: Protein of Interest

PPG: Photolabile Protecting Group

Pre-miR-21: Precursor-microRNA-21

PROTAC: Proteolysis Targeting Chimera

PSS: Photostationary State

PST: Photostatin

R_f: Retention Factor

RIBOTAC: Ribonuclease Targeting Chimera

RNA: Ribonucleic Acid

RNAse: Ribonuclease

RT: Room Temperature

SAR: Structure-Activity Relationship

SBT: Styrylbenzothiazole

SBTub: SBT Tubulin Inhibitor

shRNA: Short Hairpin RNA

SPMC: Spiropyran-merocyanine

TFA: Trifluoroacetic Acid

TLC: Thin Layer Chromatography

γTuSC: γ-Tubulin Small Complex

UV: Ultraviolet

VDA: Vascular Disrupting Agent

YFP: Yellow Fluorescent Protein

11.4 Bibliography

(1) Vicente, J. J.; Wordeman, L. *Exp. Cell Res.* **2015**, *334*, 61–69. https://doi.org/10.1016/j.yexcr.2015.02.010.
(2) Lasser, M.; Tiber, J.; Lowery, L. A. *Front. Cell. Neurosci.* **2018**, *12*, 165. https://doi.org/10.3389/fncel.2018.00165.
(3) Velema, W. A.; Szymanski, W.; Feringa, B. L. *J. Am. Chem. Soc.* **2014**, *136*, 2178–2191. https://doi.org/10.1021/ja413063e.
(4) Khoshakhlagh, P.; Bowser, D. A.; Brown, J. Q.; Moore, M. J. *J. Biomed. Mater. Res. A* **2019**, *107*, 134–144. https://doi.org/10.1002/jbm.a.36540.
(5) Deisseroth, K.; Feng, G.; Majewska, A. K.; Miesenbock, G.; Ting, A.; Schnitzer, M. J. *J. Neurosci.* **2006**, *26*, 10380–10386. https://doi.org/10.1523/JNEUROSCI.3863-06.2006.
(6) Terakita, A. *Genome Biol.* **2005**, *6*, 213. https://doi.org/10.1186/gb-2005-6-3-213.
(7) Ernst, O. P.; Lodowski, D. T.; Elstner, M.; Hegemann, P.; Brown, L. S.; Kandori, H. *Chem. Rev.* **2014**, *114*, 126–163. https://doi.org/10.1021/cr4003769.
(8) Nagel, G.; Ollig, D.; Fuhrmann, M.; Kateriya, S.; Musti, A. M.; Bamberg, E.; et al. *Science* **2002**, *296*, 2395–2398. https://doi.org/10.1126/science.1072068.
(9) Matsuno-Yagi, A.; Mukohata, Y. *Biochem. Biophys. Res. Commun.* **1977**, *78*, 237–243. https://doi.org/10.1016/0006-291X(77)91245-1.
(10) Tan, N. G. A.; Wu, W.; Seifalian, A. M. Optogenetics: Lights, Camera, Action! A Ray of Light, a Shadow Unmasked. In *Applications of Nanoscience in Photomedicine*; Elsevier, 2015; pp 185–203. https://doi.org/10.1533/9781908818782.185.
(11) Murphy, C.; Matikainen-Ankney, B.; Chang, Y.-H.; Copits, B.; Creed, M. C. Optogenetically-Inspired Neuromodulation: Translating Basic Discoveries into Therapeutic Strategies. In *International Review of Neurobiology*; Elsevier, 2021; Vol. 159, pp 187–219. https://doi.org/10.1016/bs.irn.2021.06.002.
(12) Boyden, E. S.; Zhang, F.; Bamberg, E.; Nagel, G.; Deisseroth, K. *Nat. Neurosci.* **2005**, *8*, 1263–1268. https://doi.org/10.1038/nn1525.
(13) Huala, E.; Oeller, P. W.; Liscum, E.; Han, I.-S.; Larsen, E.; Briggs, W. R. *Science* **1997**, *278*, 2120–2123. https://doi.org/10.1126/science.278.5346.2120.
(14) Pudasaini, A.; El-Arab, K. K.; Zoltowski, B. D. *Front. Mol. Biosci.* **2015**, *2*. https://doi.org/10.3389/fmolb.2015.00018.
(15) Lehtinen, K.; Nokia, M. S.; Takala, H. *Front. Cell. Neurosci.* **2022**, *15*, 778900. https://doi.org/10.3389/fncel.2021.778900.
(16) Meiring, J. C. M.; Grigoriev, I.; Nijenhuis, W.; Kapitein, L. C.; Akhmanova, A. *Opto-Katanin: An Optogenetic Tool for Localized Microtubule Disassembly*; Cell Biology, 2021. https://doi.org/10.1101/2021.12.22.473806.
(17) Sahel, J.-A.; Boulanger-Scemama, E.; Pagot, C.; Arleo, A.; Galluppi, F.; Martel, J. N.; et al. *Nat. Med.* **2021**, *27*, 1223–1229. https://doi.org/10.1038/s41591-021-01351-4.
(18) Deal, W. J.; Erlanger, B. F.; Nachmansohn, D. *Proc. Natl. Acad. Sci.* **1969**, *64*, 1230–1234. https://doi.org/10.1073/pnas.64.4.1230.
(19) Lam, P.-Y.; Thawani, A. R.; Balderas, E.; White, A. J. P.; Chaudhuri, D.; Fuchter, M. J.; et al. *J. Am. Chem. Soc.* **2020**, *142*, 17457–17468. https://doi.org/10.1021/jacs.0c06811.
(20) Agnetta, L.; Kauk, M.; Canizal, M. C. A.; Messerer, R.; Holzgrabe, U.; Hoffmann, C.; et al. *Angew. Chem. Int. Ed.* **2017**, *56*, 7282–7287. https://doi.org/10.1002/anie.201701524.
(21) Morstein, J.; Impastato, A. C.; Trauner, D. *ChemBioChem* **2021**, *22*, 73–83. https://doi.org/10.1002/cbic.202000449.
(22) Broichhagen, J.; Jurastow, I.; Iwan, K.; Kummer, W.; Trauner, D. *Angew. Chem. Int. Ed.* **2014**, *53*, 7657–7660. https://doi.org/10.1002/anie.201403666.
(23) Szymanski, W.; Ourailidou, M. E.; Velema, W. A.; Dekker, F. J.; Feringa, B. L. *Chem. – Eur. J.* **2015**, *21*, 16517–16524. https://doi.org/10.1002/chem.201502809.
(24) Borowiak, M.; Nahaboo, W.; Reynders, M.; Nekolla, K.; Jalinot, P.; Hasserodt, J.; et al. *Cell* **2015**, *162*, 403–411. https://doi.org/10.1016/j.cell.2015.06.049.
(25) Borowiak, M.; Küllmer, F.; Gegenfurtner, F.; Peil, S.; Nasufovic, V.; Zahler, S.; et al. *J. Am. Chem. Soc.* **2020**, *142*, 9240–9249. https://doi.org/10.1021/jacs.9b12898.
(26) Broichhagen, J.; Frank, J. A.; Trauner, D. *Acc. Chem. Res.* **2015**, *48*, 1947–1960. https://doi.org/10.1021/acs.accounts.5b00129.
(27) Fuchter, M. J. *J. Med. Chem.* **2020**, *63*, 11436–11447. https://doi.org/10.1021/acs.jmedchem.0c00629.
(28) Norrish, R. G. W.; Bamford, C. H. *Nature* **1937**, *140*, 195–196. https://doi.org/10.1038/140195b0.
(29) Klán, P.; Šolomek, T.; Bochet, C. G.; Blanc, A.; Givens, R.; Rubina, M.; et al. *Chem. Rev.* **2013**, *113*, 119–191. https://doi.org/10.1021/cr300177k.
(30) Pirrung, M. C.; Lee, Y. R.; Park, K.; Springer, J. B. *J. Org. Chem.* **1999**, *64*, 5042–5047. https://doi.org/10.1021/jo982383d.
(31) Goswami, P. P.; Syed, A.; Beck, C. L.; Albright, T. R.; Mahoney, K. M.; Unash, R.; et al. *J. Am. Chem. Soc.* **2015**, *137*, 3783–3786. https://doi.org/10.1021/jacs.5b01297.

(32) Rubinstein, N.; Liu, P.; Miller, E. W.; Weinstain, R. *Chem. Commun.* **2015**, *51*, 6369–6372. https://doi.org/10.1039/C5CC00550G.
(33) Peterson, J. A.; Wijesooriya, C.; Gehrmann, E. J.; Mahoney, K. M.; Goswami, P. P.; Albright, T. R.; et al. *J. Am. Chem. Soc.* **2018**, *140*, 7343–7346. https://doi.org/10.1021/jacs.8b04040.
(34) Engels, J.; Schlaeger, E. J. *J. Med. Chem.* **1977**, *20*, 907–911. https://doi.org/10.1021/jm00217a008.
(35) Kaplan, J. H.; Forbush, B.; Hoffman, J. F. *Biochemistry* **1978**, *17*, 1929–1935. https://doi.org/10.1021/bi00603a020.
(36) Wieboldt, R.; Gee, K. R.; Niu, L.; Ramesh, D.; Carpenter, B. K.; Hess, G. P. *Proc. Natl. Acad. Sci.* **1994**, *91*, 8752–8756. https://doi.org/10.1073/pnas.91.19.8752.
(37) Sitkowska, K.; Hoes, M. F.; Lerch, M. M.; Lameijer, L. N.; van der Meer, P.; Szymański, W.; et al. *Chem. Commun.* **2020**, *56*, 5480–5483. https://doi.org/10.1039/D0CC02178D.
(38) Beier, M.; Hoheisel, J. D. *Curr. Protoc. Nucleic Acid Chem.* **2004**, *17*. https://doi.org/10.1002/0471142700.nc1203s17.
(39) Stutz, A.; Pitsch, S. *Synlett* **1999**, *1999*, 930–934. https://doi.org/10.1055/s-1999-3098.
(40) Barth, A.; Martin, S. R.; Corrie, J. E. T. *Photochem Photobiol Sci* **2006**, *5*, 107–115. https://doi.org/10.1039/B515469C.
(41) Gropeanu, R. A.; Baumann, H.; Ritz, S.; Mailänder, V.; Surrey, T.; del Campo, A. *PLoS ONE* **2012**, *7*, e43657. https://doi.org/10.1371/journal.pone.0043657.
(42) Hoorens, M. W. H.; Szymanski, W. *Trends Biochem. Sci.* **2018**, *43*, 567–575. https://doi.org/10.1016/j.tibs.2018.05.004.
(43) Banghart, M.; Borges, K.; Isacoff, E.; Trauner, D.; Kramer, R. H. *Nat. Neurosci.* **2004**, *7*, 1381–1386. https://doi.org/10.1038/nn1356.
(44) Dong, M.; Babalhavaeji, A.; Collins, C. V.; Jarrah, K.; Sadovski, O.; Dai, Q.; et al. *J. Am. Chem. Soc.* **2017**, *139*, 13483–13486. https://doi.org/10.1021/jacs.7b06471.
(45) Forman, H. J.; Zhang, H.; Rinna, A. *Mol. Aspects Med.* **2009**, *30*, 1–12. https://doi.org/10.1016/j.mam.2008.08.006.
(46) Broichhagen, J.; Schönberger, M.; Cork, S. C.; Frank, J. A.; Marchetti, P.; Bugliani, M.; et al. *Nat. Commun.* **2014**, *5*, 5116. https://doi.org/10.1038/ncomms6116.
(47) de Abreu Costa, L.; Henrique Fernandes Ottoni, M.; dos Santos, M.; Meireles, A.; Gomes de Almeida, V.; de Fátima Pereira, W.; et al. *Molecules* **2017**, *22*, 1789. https://doi.org/10.3390/molecules22111789.
(48) Gao, L.; Meiring, J. C. M.; Varady, A.; Ruider, I. E.; Heise, C.; Wranik, M.; et al. *J. Am. Chem. Soc.* **2022**, *144*, 5614–5628. https://doi.org/10.1021/jacs.2c01020.
(49) Volarić, J.; Szymanski, W.; Simeth, N. A.; Feringa, B. L. *Chem. Soc. Rev.* **2021**, *50*, 12377–12449. https://doi.org/10.1039/D0CS00547A.
(50) Hüll, K.; Morstein, J.; Trauner, D. *Chem. Rev.* **2018**, *118*, 10710–10747. https://doi.org/10.1021/acs.chemrev.8b00037.
(51) Schmidt, D.; Rodat, T.; Heintze, L.; Weber, J.; Horbert, R.; Girreser, U.; et al. *ChemMedChem* **2018**, *13*, 2415–2426. https://doi.org/10.1002/cmdc.201800531.
(52) Gao, L.; Meiring, J. C. M.; Kraus, Y.; Wranik, M.; Weinert, T.; Pritzl, S. D.; et al. *Cell Chem. Biol.* **2020**, S2451945620304700. https://doi.org/10.1016/j.chembiol.2020.11.007.
(53) Gao, L.; Meiring, J. C. M.; Heise, C.; Rai, A.; Müller-Deku, A.; Akhmanova, A.; et al. *Angew. Chem. Int. Ed.* **2022**, *61*. https://doi.org/10.1002/anie.202114614.
(54) Eggers, K.; Fyles, T. M.; Montoya-Pelaez, P. J. *J. Org. Chem.* **2001**, *66*, 2966–2977. https://doi.org/10.1021/jo0056848.
(55) Herre, S.; Schadendorf, T.; Ivanov, I.; Herrberger, C.; Steinle, W.; Rück-Braun, K.; et al. *ChemBioChem* **2006**, *7*, 1089–1095. https://doi.org/10.1002/cbic.200600082.
(56) Lachmann, D.; Studte, C.; Männel, B.; Hübner, H.; Gmeiner, P.; König, B. *Chem. - Eur. J.* **2017**, *23*, 13423–13434. https://doi.org/10.1002/chem.201702147.
(57) Nilsson, J. R.; Li, S.; Önfelt, B.; Andréasson, J. *Chem. Commun.* **2011**, *47*, 11020. https://doi.org/10.1039/c1cc13561a.
(58) Morstein, J.; Awale, M.; Reymond, J.-L.; Trauner, D. *ACS Cent. Sci.* **2019**, *5*, 607–618. https://doi.org/10.1021/acscentsci.8b00881.
(59) Beharry, A. A.; Woolley, G. A. *Chem. Soc. Rev.* **2011**, *40*, 4422. https://doi.org/10.1039/c1cs15023e.
(60) Bléger, D.; Schwarz, J.; Brouwer, A. M.; Hecht, S. *J. Am. Chem. Soc.* **2012**, *134*, 20597–20600. https://doi.org/10.1021/ja310323y.
(61) Weston, C. E.; Richardson, R. D.; Haycock, P. R.; White, A. J. P.; Fuchter, M. J. *J. Am. Chem. Soc.* **2014**, *136*, 11878–11881. https://doi.org/10.1021/ja505444d.
(62) Boulègue, C.; Löweneck, M.; Renner, C.; Moroder, L. *ChemBioChem* **2007**, *8*, 591–594. https://doi.org/10.1002/cbic.200600495.
(63) Garcia-Amorós, J.; Sánchez-Ferrer, A.; Massad, W. A.; Nonell, S.; Velasco, D. *Phys. Chem. Chem. Phys.* **2010**, *12*, 13238. https://doi.org/10.1039/c004340k.
(64) Dunn, N. J.; Humphries, W. H.; Offenbacher, A. R.; King, T. L.; Gray, J. A. *J. Phys. Chem. A* **2009**, *113*, 13144–13151. https://doi.org/10.1021/jp903102u.
(65) Friedländer, P. *Chem. Ber.* **1906**, *39*, 1060–1066.
(66) Wiedbrauk, S.; Bartelmann, T.; Thumser, S.; Mayer, P.; Dube, H. *Nat. Commun.* **2018**, *9*, 1456. https://doi.org/10.1038/s41467-018-03912-7.

(67) Guentner, M.; Schildhauer, M.; Thumser, S.; Mayer, P.; Stephenson, D.; Mayer, P. J.; et al. *Nat. Commun.* **2015**, *6*, 8406. https://doi.org/10.1038/ncomms9406.
(68) Ichimura, K.; Seki, T.; Tamaki, T.; Yamaguchi, T. *Chem. Lett.* **1990**, *19*, 1645–1646. https://doi.org/10.1246/cl.1990.1645.
(69) Réamonn, L. S. S.; O'Sullivan, W. I. *J Chem Soc Perkin Trans 1* **1977**, No. 9, 1009–1012. https://doi.org/10.1039/P19770001009.
(70) Izmail'skii, V. A.; Mostoslavskii, M. A. *Ukr. Khem. Zh.* **1961**, No. 27, 234–237.
(71) Wiedbrauk, S.; Dube, H. *Tetrahedron Lett.* **2015**, *56*, 4266–4274. https://doi.org/10.1016/j.tetlet.2015.05.022.
(72) Regner, N.; Herzog, T. T.; Haiser, K.; Hoppmann, C.; Beyermann, M.; Sauermann, J.; et al. *J. Phys. Chem. B* **2012**, *116*, 4181–4191. https://doi.org/10.1021/jp300982a.
(73) Zweig, J. E.; Newhouse, T. R. *J. Am. Chem. Soc.* **2017**, *139*, 10956–10959. https://doi.org/10.1021/jacs.7b04448.
(74) Zweig, J. E.; Ko, T. A.; Huang, J.; Newhouse, T. R. *Tetrahedron* **2019**, *75*, 130466. https://doi.org/10.1016/j.tet.2019.130466.
(75) Hoorens, M. W. H.; Medved', M.; Laurent, A. D.; Di Donato, M.; Fanetti, S.; Slappendel, L.; et al. *Nat. Commun.* **2019**, *10*, 2390. https://doi.org/10.1038/s41467-019-10251-8.
(76) Medved', M.; Hoorens, M. W. H.; Di Donato, M.; Laurent, A. D.; Fan, J.; Taddei, M.; et al. *Chem. Sci.* **2021**, *12*, 4588–4598. https://doi.org/10.1039/D0SC07000A.
(77) Petermayer, C.; Thumser, S.; Kink, F.; Mayer, P.; Dube, H. *J. Am. Chem. Soc.* **2017**, *139*, 15060–15067. https://doi.org/10.1021/jacs.7b07531.
(78) Berdnikova, D. V. *Beilstein J. Org. Chem.* **2019**, *15*, 2822–2829. https://doi.org/10.3762/bjoc.15.275.
(79) Meier, H. *Angew. Chem. Int. Ed. Engl.* **1992**, *31*, 1399–1420. https://doi.org/10.1002/anie.199213993.
(80) Irie, M. *Chem. Rev.* **2000**, *100*, 1685–1716. https://doi.org/10.1021/cr980069d.
(81) Waldeck, D. H. *Chem. Rev.* **1991**, *91*, 415–436. https://doi.org/10.1021/cr00003a007.
(82) Bisby, R. H.; Botchway, S. W.; Hadfield, J. A.; McGown, A. T.; Parker, A. W.; Scherer, K. M. *Eur. J. Cancer* **2012**, *48*, 1896–1903. https://doi.org/10.1016/j.ejca.2011.11.025.
(83) Kaupp, Gerd; Gründken, Eleonore; Matthies, Doris. *Chem. Ber.* **1986**, *119*, 3109–3120.
(84) Coelho, P. J.; Castro, M. C. R.; Raposo, M. M. M. *Dyes Pigments* **2015**, *117*, 163–169. https://doi.org/10.1016/j.dyepig.2015.02.015.
(85) Woodward, R. B.; Hoffmann, R. *Die Erhaltung Der Orbitalsymmetrie*, 1. Aufl., 2. Nachdr.; Verl. Chemie: Weinheim/Bergstr, 1972.
(86) Nakamura, S.; Yokojima, S.; Uchida, K.; Tsujioka, T.; Goldberg, A.; Murakami, A.; et al. *J. Photochem. Photobiol. Chem.* **2008**, *200*, 10–18. https://doi.org/10.1016/j.jphotochem.2008.05.005.
(87) Wilson, D.; Li, J. W.; Branda, N. R. *ChemMedChem* **2017**, *12*, 284–287. https://doi.org/10.1002/cmdc.201600632.
(88) Simeth, N. A.; Kneuttinger, A. C.; Sterner, R.; König, B. *Chem. Sci.* **2017**, *8*, 6474–6483. https://doi.org/10.1039/C7SC00781G.
(89) Berns, M. W.; Krasieva, T.; Sun, C.-H.; Dvornikov, A.; Rentzepis, P. M. *J. Photochem. Photobiol. B* **2004**, *75*, 51–56. https://doi.org/10.1016/j.jphotobiol.2004.05.002.
(90) Hammarson, M.; Nilsson, J. R.; Li, S.; Beke-Somfai, T.; Andréasson, J. *J. Phys. Chem. B* **2013**, *117*, 13561–13571. https://doi.org/10.1021/jp408781p.
(91) Stafforst, T.; Hilvert, D. *Chem Commun* **2009**, No. 3, 287–288. https://doi.org/10.1039/B818050D.
(92) Kohl-Landgraf, J.; Braun, M.; Özçoban, C.; Gonçalves, D. P. N.; Heckel, A.; Wachtveitl, J. *J. Am. Chem. Soc.* **2012**, *134*, 14070–14077. https://doi.org/10.1021/ja304395k.
(93) Gudimchuk, N. B.; McIntosh, J. R. *Nat. Rev. Mol. Cell Biol.* **2021**, *22*, 777–795. https://doi.org/10.1038/s41580-021-00399-x.
(94) Steinmetz, M. O.; Prota, A. E. *Trends Cell Biol.* **2018**, *28*, 776–792. https://doi.org/10.1016/j.tcb.2018.05.001.
(95) Mitchison, T.; Kirschner, M. *Nature* **1984**, *312*, 237–242. https://doi.org/10.1038/312237a0.
(96) Brangwynne, C. P.; MacKintosh, F. C.; Kumar, S.; Geisse, N. A.; Talbot, J.; Mahadevan, L.; et al. *J. Cell Biol.* **2006**, *173*, 733–741. https://doi.org/10.1083/jcb.200601060.
(97) Bates, D.; Eastman, A. *Br. J. Clin. Pharmacol.* **2017**, *83*, 255–268. https://doi.org/10.1111/bcp.13126.
(98) Gorbsky, G. J.; Sammak, P. J.; Borisy, G. G. *J. Cell Biol.* **1987**, *104*, 9–18. https://doi.org/10.1083/jcb.104.1.9.
(99) Mollinedo, F.; Gajate, C. *APOPTOSIS* **2003**, *8*, 413–450. https://doi.org/10.1023/A:1025513106330.
(100) McLoughlin, E. C.; O'Boyle, N. M. *Pharmaceuticals* **2020**, *13*, 8. https://doi.org/10.3390/ph13010008.
(101) Baudino, T. *Curr. Drug Discov. Technol.* **2015**, *12*, 3–20. https://doi.org/10.2174/1570163812666150602144310.
(102) Dumontet, C.; Jordan, M. A. *Nat. Rev. Drug Discov.* **2010**, *9*, 790–803. https://doi.org/10.1038/nrd3253.
(103) Gasic, I.; Mitchison, T. J. *Curr. Opin. Cell Biol.* **2019**, *56*, 80–87. https://doi.org/10.1016/j.ceb.2018.10.003.
(104) Gartz Hanson, M.; Aiken, J.; Sietsema, D. V.; Sept, D.; Bates, E. A.; Niswander, L.; et al. *Dev. Biol.* **2016**, *409*, 406–419. https://doi.org/10.1016/j.ydbio.2015.11.022.
(105) Yuba-Kubo, A.; Kubo, A.; Hata, M.; Tsukita, S. *Dev. Biol.* **2005**, *282*, 361–373. https://doi.org/10.1016/j.ydbio.2005.03.031.
(106) Anders, K. R.; Botstein, D. *Mol. Biol. Cell* **2001**, *12*, 3973–3986. https://doi.org/10.1091/mbc.12.12.3973.

(107) Yang, J.; Yu, Y.; Li, Y.; Yan, W.; Ye, H.; Niu, L.; et al. *Sci. Adv.* **2021**, *7*, eabg4168. https://doi.org/10.1126/sciadv.abg4168.
(108) Hearn, B. R.; Shaw, S. J.; Myles, D. C. Microtubule Targeting Agents. In *Comprehensive Medicinal Chemistry II*; Elsevier, 2007; pp 81–110. https://doi.org/10.1016/B0-08-045044-X/00205-4.
(109) Dark, G. G.; Hill, S. A.; Prise, V. E.; Tozer, G. M.; Pettit, G. R.; Chaplin, D. J. *Cancer Res.* **1997**, *57*, 1829–1834.
(110) Kamath, K.; Okouneva, T.; Larson, G.; Panda, D.; Wilson, L.; Jordan, M. A. *Mol. Cancer Ther.* **2006**, *5*, 2225–2233. https://doi.org/10.1158/1535-7163.MCT-06-0113.
(111) Xu, K.; Schwarz, P. M.; Ludueña, R. F. *Drug Dev. Res.* **2002**, *55*, 91–96. https://doi.org/10.1002/ddr.10023.
(112) Dong, M.; Liu, F.; Zhou, H.; Zhai, S.; Yan, B. *Molecules* **2016**, *21*, 1375. https://doi.org/10.3390/molecules21101375.
(113) Banwell, M.; Peters, S.; Greenwood, R.; Mackay, M.; Hamel, E.; Lin, C. *Aust. J. Chem.* **1992**, *45*, 1577. https://doi.org/10.1071/CH9921577.
(114) Sailer, A.; Ermer, F.; Kraus, Y.; Lutter, F. H.; Donau, C.; Bremerich, M.; et al. *ChemBioChem* **2019**, *20*, 1305–1314. https://doi.org/10.1002/cbic.201800752.
(115) Pettit, G. R.; Toki, B.; Herald, D. L.; Verdier-Pinard, P.; Boyd, M. R.; Hamel, E.; et al. *J. Med. Chem.* **1998**, *41*, 1688–1695. https://doi.org/10.1021/jm970644q.
(116) Tron, G. C.; Pirali, T.; Sorba, G.; Pagliai, F.; Busacca, S.; Genazzani, A. A. *J. Med. Chem.* **2006**, *49*, 3033–3044. https://doi.org/10.1021/jm0512903.
(117) Pettit, G. R.; Singh, S. B.; Hamel, E.; Lin, C. M.; Alberts, D. S.; Garcia-Kendal, D. *Experientia* **1989**, *45*, 209–211. https://doi.org/10.1007/BF01954881.
(118) Ji, Y.-T.; Liu, Y.-N.; Liu, Z.-P. *Curr. Med. Chem.* **2015**, *22*, 1348–1360. https://doi.org/10.2174/0929867322666150114163732.
(119) Graham, W.; Roberts, J. B. *Ann. Rheum. Dis.* **1953**, *12*, 16–19. https://doi.org/10.1136/ard.12.1.16.
(120) Li, Y.; Liu, Y.; Zhu, Z.; Yan, W.; Zhang, C.; Yang, Z.; et al. *J. Med. Chem.* **2022**, *65*, 2675–2693. https://doi.org/10.1021/acs.jmedchem.1c02159.
(121) Finkelstein, Y.; Aks, S. E.; Hutson, J. R.; Juurlink, D. N.; Nguyen, P.; Dubnov-Raz, G.; et al. *Clin. Toxicol.* **2010**, *48*, 407–414. https://doi.org/10.3109/15563650.2010.495348.
(122) Chen, H.; Lin, Z.; Arnst, K.; Miller, D.; Li, W. *Molecules* **2017**, *22*, 1281. https://doi.org/10.3390/molecules22081281.
(123) Gaspari, R.; Prota, A. E.; Bargsten, K.; Cavalli, A.; Steinmetz, M. O. *Chem* **2017**, *2*, 102–113. https://doi.org/10.1016/j.chempr.2016.12.005.
(124) Aronson, J.; Inoué, S. *J. Cell Biol.* **1970**, *45*, 470–477. https://doi.org/10.1083/jcb.45.2.470.
(125) Wühr, M.; Tan, E. S.; Parker, S. K.; Detrich, H. W.; Mitchison, T. J. *Curr. Biol.* **2010**, *20*, 2040–2045. https://doi.org/10.1016/j.cub.2010.10.024.
(126) Engdahl, A. J.; Torres, E. A.; Lock, S. E.; Engdahl, T. B.; Mertz, P. S.; Streu, C. N. *Org. Lett.* **2015**, *17*, 4546–4549. https://doi.org/10.1021/acs.orglett.5b02262.
(127) Eguchi, K.; Taoufiq, Z.; Thorn-Seshold, O.; Trauner, D.; Hasegawa, M.; Takahashi, T. *J. Neurosci.* **2017**, *37*, 6043–6052. https://doi.org/10.1523/JNEUROSCI.0179-17.2017.
(128) Kopf, A.; Renkawitz, J.; Hauschild, R.; Girkontaite, I.; Tedford, K.; Merrin, J.; et al. *J. Cell Biol.* **2020**, *219*, e201907154. https://doi.org/10.1083/jcb.201907154.
(129) Zenker, J.; White, M. D.; Gasnier, M.; Alvarez, Y. D.; Lim, H. Y. G.; Bissiere, S.; et al. *Cell* **2018**, *173*, 776-791.e17. https://doi.org/10.1016/j.cell.2018.02.035.
(130) Sheldon, J. E.; Dcona, M. M.; Lyons, C. E.; Hackett, J. C.; Hartman, M. C. T. *Org. Biomol. Chem.* **2016**, *14*, 40–49. https://doi.org/10.1039/C5OB02005K.
(131) Leoni, L. M.; Hamel, E.; Genini, D.; Shih, H.; Carrera, C. J.; Cottam, H. B.; et al. *JNCI J. Natl. Cancer Inst.* **2000**, *92*, 217–224. https://doi.org/10.1093/jnci/92.3.217.
(132) Rodríguez-Soacha, D. A.; Fender, J.; Ramírez, Y. A.; Collado, J. A.; Muñoz, E.; Maitra, R.; et al. *ACS Chem. Neurosci.* **2021**, *12*, 1632–1647. https://doi.org/10.1021/acschemneuro.1c00086.
(133) Müller-Deku, A.; Meiring, J. C. M.; Loy, K.; Kraus, Y.; Heise, C.; Bingham, R.; et al. *Nat. Commun.* **2020**, *11*, 4640. https://doi.org/10.1038/s41467-020-18389-6.
(134) Moritz, M.; Braunfeld, M. B.; Guénebaut, V.; Heuser, J.; Agard, D. A. *Nat. Cell Biol.* **2000**, *2*, 365–370. https://doi.org/10.1038/35014058.
(135) Chinen, T.; Liu, P.; Shioda, S.; Pagel, J.; Cerikan, B.; Lin, T.; et al. *Nat. Commun.* **2015**, *6*, 8722. https://doi.org/10.1038/ncomms9722.
(136) Plötner, J.; Dreuw, A. *J. Phys. Chem. A* **2009**, *113*, 11882–11887. https://doi.org/10.1021/jp903156j.
(137) Sailer, A.; Ermer, F.; Kraus, Y.; Bingham, R.; Lutter, F. H.; Ahlfeld, J.; et al. *Beilstein J. Org. Chem.* **2020**, *16*, 125–134. https://doi.org/10.3762/bjoc.16.14.
(138) Roostalu, J.; Thomas, C.; Cade, N. I.; Kunzelmann, S.; Taylor, I. A.; Surrey, T. *eLife* **2020**, *9*, e51992. https://doi.org/10.7554/eLife.51992.
(139) Kollman, J. M.; Zelter, A.; Muller, E. G. D.; Fox, B.; Rice, L. M.; Davis, T. N.; et al. *Mol. Biol. Cell* **2008**, *19*, 207–215. https://doi.org/10.1091/mbc.e07-09-0879.
(140) Leuckart, R. *J. F□r Prakt. Chem.* **1889**, *41*, 179–224. https://doi.org/10.1002/prac.18900410114.
(141) Newson, H. L.; Wild, D. A.; Yeung, S. Y.; Skelton, B. W.; Flematti, G. R.; Allan, J. E.; et al. *J. Org. Chem.* **2016**, *81*, 3127–3135. https://doi.org/10.1021/acs.joc.5b02861.

(142) Baeyer, A.; Villiger, V. *Berichte Dtsch. Chem. Ges.* **1899**, *32*, 3625–3633. https://doi.org/10.1002/cber.189903203151.
(143) Paddison, P. J.; Caudy, A. A.; Bernstein, E.; Hannon, G. J.; Conklin, D. S. *Genes Dev.* **2002**, *16*, 948–958. https://doi.org/10.1101/gad.981002.
(144) Jinek, M.; Chylinski, K.; Fonfara, I.; Hauer, M.; Doudna, J. A.; Charpentier, E. *Science* **2012**, *337*, 816–821. https://doi.org/10.1126/science.1225829.
(145) Sakamoto, K. M.; Kim, K. B.; Kumagai, A.; Mercurio, F.; Crews, C. M.; Deshaies, R. J. *Proc. Natl. Acad. Sci.* **2001**, *98*, 8554–8559. https://doi.org/10.1073/pnas.141230798.
(146) Verdine, G. L.; Walensky, L. D. *Clin. Cancer Res.* **2007**, *13*, 7264–7270. https://doi.org/10.1158/1078-0432.CCR-07-2184.
(147) Reynders, M.; Matsuura, B. S.; Bérouti, M.; Simoneschi, D.; Marzio, A.; Pagano, M.; et al. *Sci. Adv.* **2020**, *6*, eaay5064. https://doi.org/10.1126/sciadv.aay5064.
(148) Kargbo, R. B. *ACS Med. Chem. Lett.* **2019**, *10*, 1367–1369. https://doi.org/10.1021/acsmedchemlett.9b00397.
(149) Mohler, M. L.; Sikdar, A.; Ponnusamy, S.; Hwang, D.-J.; He, Y.; Miller, D. D.; et al. *Int. J. Mol. Sci.* **2021**, *22*, 2124. https://doi.org/10.3390/ijms22042124.
(150) Jones, L. H. *Cell Chem. Biol.* **2018**, *25*, 30–35. https://doi.org/10.1016/j.chembiol.2017.10.011.
(151) Yang, J.; Li, Y.; Yan, W.; Li, W.; Qiu, Q.; Ye, H.; et al. *J. Biol. Chem.* **2019**, *294*, 8161–8170. https://doi.org/10.1074/jbc.RA118.006325.
(152) Gasic, I.; Groendyke, B. J.; Nowak, R. P.; Yuan, J. C.; Kalabathula, J.; Fischer, E. S.; et al. *Cells* **2020**, *9*, 1083. https://doi.org/10.3390/cells9051083.
(153) Cyrus, K.; Wehenkel, M.; Choi, E.-Y.; Han, H.-J.; Lee, H.; Swanson, H.; et al. *Mol BioSyst* **2011**, *7*, 359–364. https://doi.org/10.1039/C0MB00074D.
(154) Cecchini, C.; Pannilunghi, S.; Tardy, S.; Scapozza, L. *Front. Chem.* **2021**, *9*, 672267. https://doi.org/10.3389/fchem.2021.672267.
(155) Chen, Y.; Zou, Y.; Sun, H.-Y.; Liu, X.-K.; Xiao, C.-F.; Sun, J.; et al. *Synthesis* **2011**, *2011*, 217–222. https://doi.org/10.1055/s-0030-1258358.
(156) Singh, B.; Kumar, A.; Joshi, P.; Guru, S. K.; Kumar, S.; Wani, Z. A.; et al. *Org. Biomol. Chem.* **2015**, *13*, 5674–5689. https://doi.org/10.1039/C5OB00406C.
(157) Wang, Y.; Tian, G.; Cowan, N. J.; Cabral, F. *J. Biol. Chem.* **2006**, *281*, 13628–13635. https://doi.org/10.1074/jbc.M513730200.
(158) Ducray, P.; Lebeau, L.; Mioskowski, C. *Helv. Chim. Acta* **1996**, *79*, 2346–2352. https://doi.org/10.1002/hlca.19960790821.
(159) Arai, T.; Ikegami, M. *Chem. Lett.* **1999**, *28*, 965–966. https://doi.org/10.1246/cl.1999.965.
(160) Ikegami, M.; Arai, T. *Chem. Lett.* **2005**, *34*, 492–493. https://doi.org/10.1246/cl.2005.492.
(161) Los, G. V.; Encell, L. P.; McDougall, M. G.; Hartzell, D. D.; Karassina, N.; Zimprich, C.; et al. *ACS Chem. Biol.* **2008**, *3*, 373–382. https://doi.org/10.1021/cb800025k.
(162) Liu, K.; Wen, P.; Liu, J.; Huang, G. *Synthesis* **2010**, *2010*, 3623–3626. https://doi.org/10.1055/s-0030-1258240.
(163) Doronina, E. P.; Jouikov, V.; Belogolova, E. F.; Sidorkin, V. F. *J. Organomet. Chem.* **2022**, *958*, 122189. https://doi.org/10.1016/j.jorganchem.2021.122189.
(164) Siewertsen, R.; Neumann, H.; Buchheim-Stehn, B.; Herges, R.; Näther, C.; Renth, F.; et al. *J. Am. Chem. Soc.* **2009**, *131*, 15594–15595. https://doi.org/10.1021/ja906547d.
(165) Höhne, A.; Yu, L.; Mu, L.; Reiher, M.; Voigtmann, U.; Klar, U.; et al. *Chem. - Eur. J.* **2009**, *15*, 3736–3743. https://doi.org/10.1002/chem.200802437.
(166) Diana, G. D.; Rudewicz, P.; Pevear, D. C.; Nitz, T. J.; Aldous, S. C.; Aldous, D. J.; et al. *J. Med. Chem.* **1995**, *38*, 1355–1371. https://doi.org/10.1021/jm00008a014.
(167) Sravanthi, T. V.; Manju, S. L. *Eur. J. Pharm. Sci.* **2016**, *91*, 1–10. https://doi.org/10.1016/j.ejps.2016.05.025.
(168) Costales, M. G.; Aikawa, H.; Li, Y.; Childs-Disney, J. L.; Abegg, D.; Hoch, D. G.; et al. *Proc. Natl. Acad. Sci.* **2020**, *117*, 2406–2411. https://doi.org/10.1073/pnas.1914286117.
(169) Thakur, C. S.; Jha, B. K.; Dong, B.; Das Gupta, J.; Silverman, K. M.; Mao, H.; et al. *Proc. Natl. Acad. Sci.* **2007**, *104*, 9585–9590. https://doi.org/10.1073/pnas.0700590104.
(170) Hwang, J.; Qiu, X.; Borgelt, L.; Haacke, N.; Kanis, L.; Petroulia, S.; et al. *Bioorg. Med. Chem.* **2022**, *58*, 116653. https://doi.org/10.1016/j.bmc.2022.116653.
(171) Brvar, M.; Perdih, A.; Hodnik, V.; Renko, M.; Anderluh, G.; Jerala, R.; et al. *Bioorg. Med. Chem.* **2012**, *20*, 2572–2580. https://doi.org/10.1016/j.bmc.2012.02.052.
(172) Békés, M.; Langley, D. R.; Crews, C. M. *Nat. Rev. Drug Discov.* **2022**, *21*, 181–200. https://doi.org/10.1038/s41573-021-00371-6.
(173) Wurtmann, E. J.; Wolin, S. L. *Crit. Rev. Biochem. Mol. Biol.* **2009**, *44*, 34–49. https://doi.org/10.1080/10409230802594043.
(174) Beaudette, K.; Baac, H. W.; Madore, W.-J.; Villiger, M.; Godbout, N.; Bouma, B. E.; et al. *Biomed. Opt. Express* **2015**, *6*, 1293. https://doi.org/10.1364/BOE.6.001293.
(175) Fouts, J. R.; Kamm, J. J.; Brodie, B. B. *J. Pharmacol. Exp. Ther.* **1957**, *120*, 291–300.
(176) Stricker, L.; Böckmann, M.; Kirse, T. M.; Doltsinis, N. L.; Ravoo, B. J. *Chem. Weinh. Bergstr. Ger.* **2018**, *24*, 8639–8647. https://doi.org/10.1002/chem.201800587.

(177) Gottlieb, H. E.; Kotlyar, V.; Nudelman, A. *J. Org. Chem.* **1997**, *62*, 7512–7515. https://doi.org/10.1021/jo971176v.
(178) Fukuda, T.; Anzai, M.; Nakahara, A.; Yamashita, K.; Matsukura, K.; Ishibashi, F.; et al. *Bioorg. Med. Chem.* **2021**, *34*, 116039. https://doi.org/10.1016/j.bmc.2021.116039.